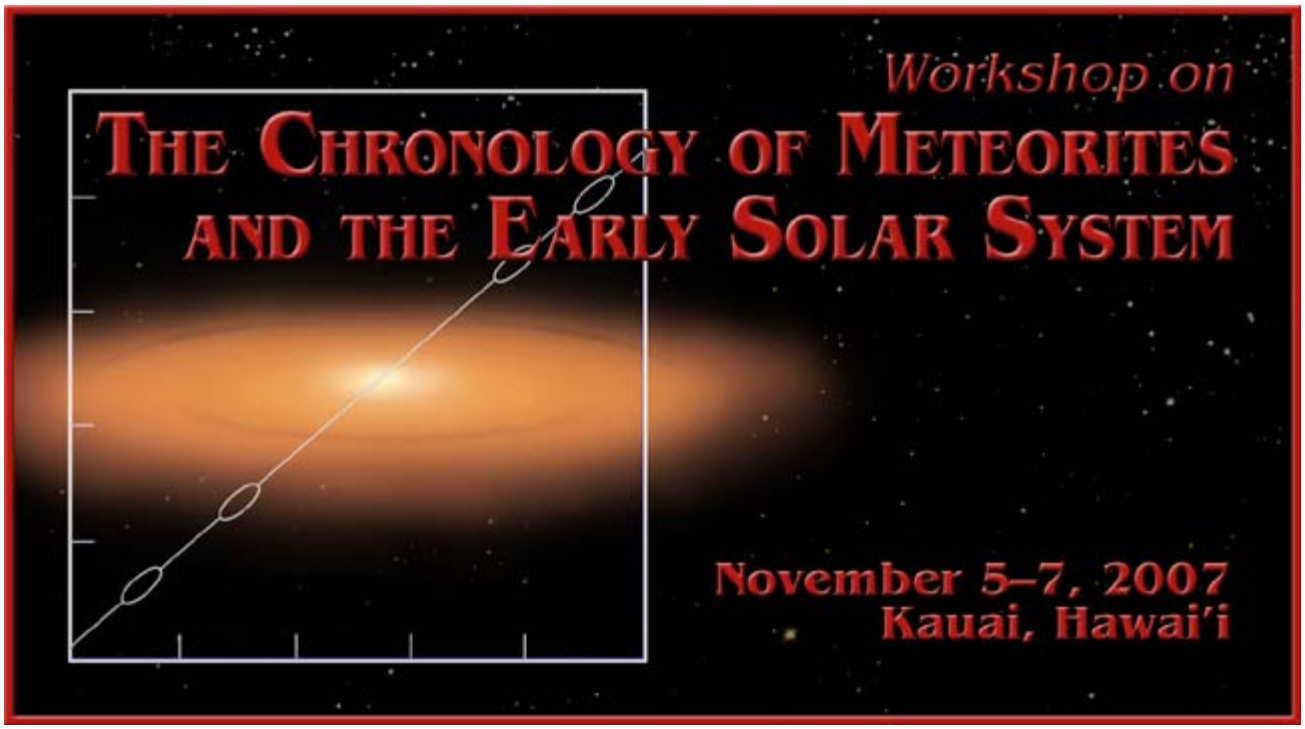

Workshop Program and Abstracts

LPI Contribution No. 1374

Workshop on
The Chronology of Meteorites and the Early Solar System

November 5–7, 2007 • Kauai, Hawai'i

Sponsored By

Lunar and Planetary Institute
National Aeronautics and Space Administration
University of Hawai'i at Manoa
NASA Mars Program Office
Barringer Crater Company

Hosted By

University of Hawai'i at Manoa
(Hawai'i Institute of Geophysics and Planetology,
School of Ocean and Earth Science and Technology,
and the Institute for Astronomy)

Conveners

Joel Baker, *Victoria University of Wellington, New Zealand*
Martin Bizzarro, *Geological Institute, Denmark*
Klaus Keil, *University of Hawai'i*
Alexander N. Krot, *University of Hawai'i*
Edward R. D. Scott, *University of Hawai'i*

Scientific Organizing Committee

Francis Albarede, *Ecole Normale Superieure, France*
Yuri Amelin, *Geological Survey of Canada*
Martin Bizzarro, *Geological Institute, Denmark*
Marc Chaussidon, *CRPG-SNRS, France*
Harold Connolly, *Kingsborough College- City College of New York*
Andrew Davis, *University of Chicago*
Gary Huss, *University of Hawai'i*
Klaus Keil, *University of Hawai'i*
Alexander Krot, *University of Hawai'i*
Frank Podosek, *Washington University*
Bo Reipurth, *University of Hawai'i*
Edward R. D. Scott, *University of Hawai'i*
Meenakshi Wadhwa, *Arizona State University*

Lunar and Planetary Institute 3600 Bay Area Boulevard Houston TX 77058-1113

LPI Contribution No. 1374

Compiled in 2007 by
LUNAR AND PLANETARY INSTITUTE

The Institute is operated by the Universities Space Research Association under Agreement No. NCC5-679 issued through the Solar System Exploration Division of the National Aeronautics and Space Administration.

Abstracts in this volume may be cited as

Author A. B. (2007) Title of abstract. In *Workshop on the Chronology of Meteorites and the Early Solar System*, p. XX. LPI Contribution No. 1374, Lunar and Planetary Institute, Houston.

This volume is distributed by

ORDER DEPARTMENT
Lunar and Planetary Institute
3600 Bay Area Boulevard
Houston TX 77058-1113, USA
Phone: 281-486-2172
Fax: 281-486-2186
E-mail: order@lpi.usra.edu

Mail orders requestors will be invoiced for the cost of shipping and handling.

ISSN No. 0161-5297

PREFACE

This volume contains abstracts that have been accepted for presentation at the Workshop on the Chronology of Meteorites and the Early Solar System, November 5–7, 2007, Kauai, Hawai'i.

Administration and publications support for this meeting were provided by the staff of the Publications and Program Services Department at the Lunar and Planetary Institute.

AGENDA

Sunday, November 4, 2007

4:00 p.m.	Poipu Ballroom Foyer	Registration
5:30 p.m.	Ocean Lawn	Welcome Reception

Monday, November 5, 2007

8:20 a.m.	Poipu Ballroom	Meteorite Chronology and Astrophysical Setting of Solar System Formation
12:15 p.m.	Shells Restaurant Sheraton Kauai Resort	Lunch
3:00 p.m.	Poipu Ballroom	Sources of Short-lived Radionuclides
6:30 p.m.	Koloa Room	Poster Session
	Poipu Ballroom Foyer	Poster Session Reception

Tuesday, November 6, 2007

8:30 a.m.	Poipu Ballroom	U-Pb, ^{53}Mn-^{53}Cr, ^{60}Fe-^{60}Ni, ^{182}Hf-^{182}W, and ^{129}I-^{129}Xe Isotopic Chronometers
12:15 p.m.	Shells Restaurant Sheraton Kauai Resort	Lunch
2:30 p.m.	Poipu Ballroom	^{26}Al-^{26}Mg Isotopic Systems and Dynamics of the Protosolar Disk
5:30 p.m.	Beach Lawn	Reception Honoring C. J. Allegre, G. W. Lugmair, L. E. Nyquist, D. A. Papanastassiou, and G. J. Wasserburg

Wednesday, November 7, 2007

8:30 a.m.	Poipu Ballroom	Stable Isotope Constraints; Chonologies of Chondritic and Igneous Meteorites
12:00 p.m.	Shells Restaurant Sheraton Kauai Resort	Lunch
3:00 p.m.	Poipu Ballroom	Chronology of Early Solar System: Consistency of Chronometers and Planetary Accretion
5:15 p.m.		Meeting Adjourns

CONTENTS

Monday, November 5, 2007
METEORITE CHRONOLOGY
AND ASTROPHYSICAL SETTING OF SOLAR SYSTEM FORMATION
8:20 a.m. – 12:15 p.m. Poipu Ballroom

Chairs: **K. Keil**
T. Lee

8:20 a.m. Dr. Brian Taylor, Dean
School of Ocean and Earth Science and Technology, University of Hawai'i at Manoa
Welcome

8:30 a.m. Lee T. * [INVITED] (15 minutes)
Introduction

8:45 a.m. Papanastassiou D. A. * [INVITED] (30 minutes)
Overview of Short-lived Nuclides: The Elusive Road to Consistency **[#4056]**

9:30 a.m. Davis A. M. * [INVITED] (30 minutes)
Recent Advances in Cosmochemistry **[#4081]**

10:15 a.m. BREAK

10:30 a.m. Hester J. J. * Bally J. Williams J. P. Desch S. [INVITED] (30 minutes)
The Role of the Astrophysical Environment **[#4086]**

11:15 a.m. Adams F. C. * [INVITED] (20 minutes)
Constraints on the Birth Environment of the Solar System **[#4001]**

11:45 a.m. Montmerle T. * Feigelson E. D. Ferreira J.
Glassgold A. E. Gounelle M. [INVITED] (20 minutes)
Magnetic and High-Energy Processes in Young Stars **[#4089]**

12:15 p.m. LUNCH

Monday, November 5, 2007
SOURCES OF SHORT-LIVED RADIONUCLIDES
3:00 p.m. – 6:30 p.m. Poipu Ballroom

Chairs: **K. D. McKeegan**
N. T. Kita

3:00 p.m. Huss G. R. * Goswami J. N. Meyer B. S.
Sahijpal S. Wasserburg G. J. [INVITED] (30 minutes)
Stellar Sources of Short-lived Radionuclides **[#4055]**

3:45 p.m. Ouellette N. * Desch S. J. Bizzarro M. Boss A. P.
Ciesla F. Meyer B. [INVITED] (30 minutes)
Injection Mechanism of Short-lived Radionuclides and Their Homogenization **[#4022]**

4:30 p.m. Gounelle M. * Meibom A. (10 minutes)
The Stellar Origin of Short-lived Radionuclides: Collateral Effects and Astrophysical Context **[#4030]**

4:45 p.m. Montmerle T. * Gounelle M. Güdel M. Meynet G. (10 minutes)
^{26}Al in the Early Solar System: A Stellar Wind Origin? **[#4090]**

5:00 p.m. BREAK

5:15 p.m. Chaussidon M. * Leya I. Gounelle M. Guan Y. McKeegan K. D.
Robert F. Srinivasan G. [INVITED] (30 minutes)
Irradiation Origin of Short-lived Radioactive Nuclides **[#4035]**

6:00 p.m. Liu M.-C. * McKeegan K. D. Davis A. M. Ireland T. R. (10 minutes)
Beryllium-10 in CM Hibonites: Implications for an Irradiation Origin **[#4037]**

6:15 p.m. Connelly J. N. * Amelin Y. Krot A. N. Bizzarro M. (10 minutes)
Difference in Pb Isotopic Ages of Chondrules and Ca, Al-rich Inclusions from the CV Carbonaceous Chondrite Allende **[#4028]**

Monday, November 5, 2007
POSTER SESSION
6:30 p.m. – 8:30 p.m. Koloa Room

Astrophysical Setting of Solar System Formation

Nittler L. R.
Presolar Grain Evidence for Low-Mass Supernova Injection into the Solar Nebula **[#4016]**

Sahijpal S. Gupta G.
The Nature of the Massive Star that Could Have Injected ^{26}Al in the Early Solar System **[#4017]**

Smith R. L. Pontoppidan K. M. Young E. D. Morris M. R. van Dishoeck E. F.
Detection of Rare CO Isotopologues in Protostellar Disks: An Infrared Investigation of Molecular Self Shielding **[#4073]**

Stellar Origin of Short-Lived Nuclides

Tachibana S. Takigawa A. Miki J. Yoshida T.
A Mixing-Fallback Supernova as a Possible Source of Short-lived Radionuclides in the Early Solar System **[#4079]**

Early Solar System Chronology Based on Short-Lived Nuclides

Andrews K. T. Schiller M. Bizzarro M. Baker J. A.
High Precision Nickel Isotope Measurements of Fe-Ni Metal in Meteorites **[#4021]**

Cosarinsky M. Taylor D. J. Liu M.-C. McKeegan K. D. Krot A. N.
Distribution of Aluminum-26 in Refractory Inclusions from CV Chondrites **[#4052]**

Filtness M. J. Crowther S. A. Gilmour J. D.
The I-Xe System and the Early History of the LL Chondrite Parent Body **[#4031]**

Ito M. Messenger S.
Thermal Metamorphic History of a CAI Constrained by High Spatial Resolution Mg Isotopic Measurements **[#4040]**

Jacobsen S. B. Chakrabarti R. Bogdanovski O. Ranen M. C. Petaev M. I.
High Resolution ^{26}Al-^{26}Mg Chronometry of CAIs from the Allende Meteorite **[#4070]**

Johnson T. V. Castillo-Rogez J. C. Matson D. L. Lunine J. I. Lunine J. I.
Searching for Constraints on the Chronology of the Outer Solar System from Satellite Geophysics **[#4043]**

Kurahashi E. Kita N. T. Nagahara H. Morishita Y.
^{26}Al-^{26}Mg Systems of Ferromagnesian and Aluminum-rich Chondrules in Primitive Carbonaceous Chondrites **[#4027]**

Matson D. L. Castillo-Rogez J. C. Sotin C. Johnson T. V. Lunine J. I.
Absolute Chronology and Implications from Geophysical Modeling of Iapetus **[#4049]**

McKibbin S. J. Ireland T. R. Amelin Y.
Solar System Isotopic Heterogeneity from ^{53}Mn-^{53}Cr **[#4026]**

Ranen M. C. Jacobsen S. B.
p-Process Samarium Isotopes in Solar System Materials: Implications for the ^{146}Sm-^{142}Nd Chronometer **[#4064]**

Schiller M. Bizzarro M. Baker J. A.
Development of Precise and Accurate Magnesium Isotope Measurements by Multiple-Collector Inductively Coupled Plasma Mass Spectrometry **[#4023]**

Thrane K. Bizzarro M. Nagashima K. Krot A. N. Connelly J. N.
Timing of Chondrule Formation: Constraints from High-Precision MC-ICPMS Measurements **[#4058]**

Town C. C. Schiller M. Bizzarro M. Baker J. A.
^{26}Al-^{26}Mg Dating Calcium-Aluminium-rich Inclusions **[#4024]**

Young E. D. Shahar A.
The Initial ^{26}Al/^{27}Al of the Solar System and Implications for the Duration of the Active Solar Protoplanetary Disk **[#4062]**

Long-Lived Nuclide Chronology

Avila J. N. Ireland T. R. Holden P. Gyngard F. Bennett V. Amelin Y. Zinner E.
Chronology of Presolar Silicon Carbide: Assessing the Viability of the U-Th-Pb System **[#4082]**

Edmunson J.
A Non-CHUR Initial Nd Isotopic Composition for the Bulk Moon: Evidence from Early Lunar Samples **[#4069]**

Sedaghatpour F. Sears D. W. G.
Re-Os Isotope Dating of Meteorites and Early Solar System Chronology: A Review **[#4012]**

Taylor D. J. McKeegan K. D. Harrison T. M.
^{176}Lu-^{176}Hf Zircon Evidence for Rapid Lunar Differentiation **[#4065]**

Chronology of Formation of Chondritic Components

Bouvier A. Wadhwa M.
An Appraisal of Pb-Pb and Al-Mg Chronologies in CAIs and Chondrules **[#4077]**

Itoh S. Yurimoto H.
Fluctuation Frequency of Oxygen Isotope Reservoirs in the Early Solar System **[#4057]**

Keller L. P. Messenger S.
Amorphous Silicates in Early Solar System and Presolar Materials **[#4071]**

Makide K. Nagashima K. Krot A. Huss G. Hutcheon I.
Magnesium Isotopic Composition of Calcium-Aluminum-rich Inclusions from CR Carbonaceous Chondrites **[#4087]**

Simon J. I. Young E. D.
Open-System Behavior of CAIs: A Key Component to Their ^{26}Al/^{26}Mg Chronologies **[#4080]**

Stroud R. M. Zega T. J. Cosarinsky M. McKeegan K. D.
FIB-TEM Investigation of an Allende Type A CAI Interior and the Associated Wark-Lovering Rim **[#4078]**

Yin Q.-Z. Jacobsen B. Moynier F. Hutcheon I. D.
Toward Consistent Chronology in the Early Solar System: High Resolution ^{53}Mn-^{53}Cr Chronometry Applied to Chondrules in Primitive Ordinary Chondrite **[#4045]**

Bland P. A. Howard L. E. Prior D. J. Wheeler J. Hammond S. M. Gordon S. H.
Petrofabrics in a Chondrule Rim — Evidence for a Nebula Origin **[#4091]**

Charles C. R. J. Davis D. W.
A New Approach to Pb Dating of Whole Meteoritic Phases by Thermal Extraction and Thermal Ionization in Silica Melt **[#4092]**

Chronology of Planetesimal, Protoplanet, and Planet Accretion

Castillo-Rogez J. C. Matson D. L. Sotin C. Johnson T. V. Lunine J. I.
Modeling the Thermophysical and Dynamical Evolution of Saturn's Satellites **[#4042]**

Irving A. J. Kuehner S. M.
Plutonic Angrite NWA 4801 and a Model for the Angrite Parent Body Consistent with Petrological and Chronological Constraints **[#4050]**

Moynier F. Yin Q.-Z. Jacobsen B.
Dating the First Stage of Planet Formation **[#4044]**

Righter K.
Outstanding Issues with Respect to the Timing of Differentiation and Mantle Oxidation: A Comparative Planetology Perspective — Earth, Mars and 4 Vesta **[#4083]**

Scott E. R. D. Sanders I. S. Goldstein J. I. Krot A. N.
Meteorite Constraints on the First 5 Myr of Planetary Growth in the Inner Solar System **[#4075]**

Touboul M. Kleine T. Bourdon B. Palme H. Wieler R.
The Age of the Moon and Lifetime of Its Magma Ocean: New Constraints from W Isotopes in Lunar Metals **[#4014]**

Chronology of Igneous and Metamorphic Processing in Asteroids

Sanders I. S. Scott E. R. D.
The Chronology of Basaltic Meteorites and the History of Their Parent Bodies **[#4048]**

Amelin Y. Irving A. J.
Seven Million Years of Evolution on the Angrite Parent Body from Pb-Isotopic Data **[#4061]**

Chronology of Alteration in Asteroids

de Leuw S. Rubin A. E. Schmitt A. K. Wasson J. T.
Timing of Aqueous Alteration on the CM Parent-Body: Mineral Chemistry and Mn-Cr Systematics for the CM Chondrites Y 791198 and QUE 93005 **[#4011]**

Ford R. L. Brearley A. J.
Timing and Location of CAI Alteration in Allende: Evidence from CAI-Matrix Interactions **[#4072]**

Inoue M. Nakamura N. Kimura M.
REE Fractionations in Chondrules from the CM Meteorites, Murchison and Yamato-793321 and Their Implications for Aqueous Alteration Processes in the Early Solar System **[#4013]**

Pravdivtseva O. V. Meshik A. P. Hohenberg C. M. Krot A. N.
The I-Xe Record of Metamorphism in CO3 Chondrites **[#4067]**

Inter-Calibration of Short-Lived and Long-Lived Chronometers

Debaille V. Brandon A. D. Yin Q.-Z. Jacobsen B.
Decoupled ^{182}Hf-^{182}W and ^{146}Sm-^{142}Nd Systematics of SNC Meteorites: Implications for Early Mars Evolution **[#4047]**

Quitté G. Markowski A.
Intercalibration of Short-lived and Long-lived Chronometers Based on Angrites and CB, CR Chondrites **[#4063]**

Stable Isotope Constraints on Early Solar System Chronology

Alexander C. M. O'D. Carlson R. W.
How Homogeneous was the Early Solar System? The Chromium Story **[#4046]**

Chen H-W. Lee T. Lee D-C. Iizuka Y.
In Situ Meteoritic Ti Isotopic Measurements by Laser Ablation MC-ICP-MS and the Homogeneity in Refractory Inclusions **[#4034]**

Hashizume K. Chaussidon M.
In Search for the Oxygen Isotopic Composition of the Solar Component Trapped in Lunar Metallic Grains — Evidence of at Least Two Extra-Selenial Components Accreting on the Moon **[#4009]**

Miscellaneous

Anderson F. S. Whitaker T. J. Young D. Peterson B.
Rb-Sr Dating Using LDRIMS **[#4084]**

Holland G. Gilmour J. D.
The I-Xe Record of Parent Body Processing in Meteoritic Nanodiamonds **[#4041]**

Kaito C. Kimura Y.
Crystallization of Forsterite from Amorphous Mg-bearing Silicate Grains **[#4007]**

Kimura Y. Nuth J. A. III Kaito C.
Laboratory Annealing Experiments of Refractory Silicate Grain Analogs Using Differential Scanning Calorimetry **[#4006]**

Knight K. B. Savina M. R. Davis A. M. Pellin M. J. Levine J. Grossman L. Simon S.
Application of RIMS to the Study of Beryllium Chronology in Early Solar System Condensates **[#4088]**

Mittlefehldt D. W.
A Tale of Three Asteroids: The Eucrite, Ureilite and Pallasite Parent Asteroids **[#4051]**

Miura H. Yasuda S. Nakamoto T.
Fragment-Collision Model for Compound Chondrule Formation: Estimation of Collision Frequency **[#4020]**

Nakamura N. Fujitani T. Okano O. Kimura M. Nyquist L. E. Ebihara M. Clayton R. N.
Chlorine Isotopic Fractionations in the Early Solar System: Correlation with Oxygen and Stable Chromium Isotope Anomalies **[#4029]**

Petaev M. I. Jacobsen S. B.
SJ101, a New Forsterite-bearing CAI from the Allende CV3 Chondrite: SEM and EPMA Studies **[#4036]**

Saito M. Kimura Y. Kaito C.
Laboratory Experiments of the Formation of PAH Clusters and Their Alteration with Inorganic Matter by Plasma, Ultraviolet and Electron Beam Irradiation **[#4008]**

Yasuda S. Miura H. Nakamoto T.
Compound Chondrule Formation in the Shock-Wave Heating Model: Three-Dimensional Hydrodynamic Simulation of Disruption of the Molten Dust Particle **[#4025]**

Tuesday, November 6, 2007
U-Pb, ^{53}Mn-^{53}Cr, ^{60}Fe-^{60}Ni, ^{182}Hf-^{182}W, AND ^{129}I-^{129}Xe ISOTOPIC CHRONOMETERS
8:30 a.m. – 12:15 p.m. Poipu Ballroom

Chairs: **M. Wadhwa**
Q. Z. Yin

8:30 a.m. Amelin Y. * Connelly J. Chen J. H. Göpel C. Zartman R. E. Wasserburg G. J. Allègre C. J. Bowring S. A. Jagoutz E. [INVITED] (30 minutes)
U-Pb Chronometry of Meteorites: New Opportunities, New Level of Complexity **[#4059]**

9:15 a.m. Lugmair G. W. * Birck J.-L. Nyquist L. E. Shukolyukov A. Trinquier A. Wadhwa M. Yin Q.-Z. [INVITED] (30 minutes)
The ^{53}Mn-^{53}Cr System **[#4038]**

10:00 a.m. BREAK

10:15 a.m. Bizzarro M. * Birck J.-L. Chen J. Huss G. Lugmair G. Mostefaoui S. Papanastassiou D. Shukolyukov A. Quitte G. Tachibana S. Wadhwa M. [INVITED] (30 minutes)
Nickel Isotope Anomalies in Meteorites and the ^{60}Fe-^{60}Ni Clock **[#4015]**

11:00 a.m. Kleine T. * Touboul M. Bourdon B. Mezger K. Palme H. Nimmo F. Jacobsen S. B. Yin Q. Z. [INVITED] (30 minutes)
^{182}Hf-^{182}W Chronometry and the Origin and Evolution of Planetary Bodies **[#4033]**

11:45 a.m. Gilmour J. D. * Pravdivtseva O. Busfield A. C. Hohenberg C. M. [INVITED]
The I-Xe System in the Early Solar System **[#4039]** (20 minutes)

12:15 p.m. LUNCH

Tuesday, November 6, 2007
^{26}Al-^{26}Mg ISOTOPIC SYSTEMS AND DYNAMICS OF THE PROTOSOLAR DISK
2:30 p.m. – 5:25 p.m. Poipu Ballroom

Chairs: **I. D. Hutcheon**
G. J. MacPherson

2:30 p.m. Watson D. M. * [INVITED] (30 minutes)
Sedimentation, Mineralization, Planet Formation and Dissipation in Protoplanetary Disks **[#4085]**

3:15 p.m. Ciesla F. J. * (10 minutes)
Two-Dimensional Dynamics of CAIs in the Solar Nebula **[#4005]**

3:30 p.m. MacPherson G. J. * (10 minutes)
^{26}Al: How Far We've Come, How Far To Go

3:40 p.m. Baker J. A. * [INVITED] (30 minutes)
^{26}Al-^{26}Mg Dating Solid Formation and Planetesimal Accretion and Differentiation in the Early Solar System **[#4074]**

4:25 p.m. BREAK

4:40 p.m. Jacobsen B. * Yin Q. -Z. Moynier F. Krot A. N. Amelin Y. Nagashima K. Hutcheon I. D. Palme H. (10 minutes)
^{26}Al/^{27}Al Ratio in the Early Solar System: Canonical or Supra-Canonical? **[#4066]**

4:55 p.m. Kita N. T. * Ushikubo T. Knight K. B. Mendybaev R. A. Davis A. M. Richter F. M. (10 minutes)
High Precision Al-Mg Internal Isochron Using Zoned Melilite in CAI **[#4068]**

5:10 p.m. Shahar A. * Young E. D. (10 minutes)
Timescales of CAI Formation in the Solar Protoplanetary Disk as Revealed by Si and Mg Isotopes **[#4019]**

5:30 p.m. RECEPTION

Wednesday, November 7, 2007
STABLE ISOTOPE CONSTRAINTS;
CHONOLOGIES OF CHONDRITIC AND IGNEOUS METEORITES
8:30 a.m. – 12:00 p.m. Poipu Ballroom

Chairs: **F. A. Podosek**
S. S. Russell

8:30 a.m. Lyons J. R. * Bergin E. Ciesla F Davis A. Desch S. Hashizume K. Ireland T. Lee J. E. Marcus R. A. Yurimoto H. [INVITED] (15 minutes)
Timescales for the Evolution of Oxygen Isotope Composition in the Solar Nebula **[#4076]**

8:53 a.m. Young E. D. * [INVITED] (15 minutes)
The Timing of Oxygen Isotope Variations in the Early Solar System: A Measure of Radial Transport in the Solar Protoplanetary Disk **[#4060]**

9:15 a.m. Albarede F. * Arnould M. Carlson R. W. Dauphas N. Fujii T. Jacobsen S. B. Yin Q. Young E. D. [INVITED] (30 minutes)
Stable Isotope Anomalies and Early Solar System Chronology **[#4032]**

10:00 a.m. Trinquier A. * Bizzarro M. Ulfbeck D. Krot A. N. Connelly J. N. (10 minutes)
Origin of Titanium Isotope Heterogeneity in the Protoplanetary Disk **[#4054]**

10:15 a.m. BREAK

10:30 a.m. Krot A. * Amelin Y. Bizzarro M. Bland P. Ciesla F. Connelly J. Connolly H. Cuzzi J. Davis A. Guan Y. Goswami J. Huss G. Hutcheon I. Ireland T. Kimura M. Kita N. Kurahashi E. Lin Y. MacPherson G. Mostefaoui S. Nagashima K. Nyquist L. Petaev M. Russell S. Scott E. Sugiura N. Tachibana S. Thrane K. Yin Q. Yurimoto H. Zinner E. [INVITED] (30 minutes)
Origin and Chronology of Chondritic Components **[#4018]**

11:15 a.m. Nyquist L. E. * Kleine T. Shih C.-Y. Kita N. Yamaguchi A. Reese Y. D. [INVITED] (30 minutes)
The Chronology of Early Asteroid Processes **[#4002]**

12:00 p.m. LUNCH

Wednesday, November 7, 2007
CHRONOLOGY OF EARLY SOLAR SYSTEM:
CONSISTENCY OF CHRONOMETERS AND PLANETARY ACCRETION
3:00 p.m. – 5:15 p.m. Poipu Ballroom

Chair: G. R. Huss

3:00 p.m. Wadhwa M. * Amelin Y. Bizzarro M. Kita N. Kleine T.
Lugmair G. W. Yin Q. [INVITED] (30 minutes)
Comparison of Short-lived and Long-lived Chronometers: Towards a Consistent Chronology of the Early Solar System **[#4053]**

3:45 p.m. Morbidelli A. * Bottke W. F. Jr. Chambers J.
Cuzzi J. Weidenschilling S. [INVITED] (30 minutes)
Accretion and Dynamical Evolution of Asteroids and Comets **[#4003]**

4:30 p.m. Allègre C. * [INVITED] (30 minutes)
Limitation on Solar System Chronology from Short-lived and Long-lived Radionuclides

5:15 p.m. MEETING ADJOURNS

Constraints on the Birth Environment of the Solar System

Fred C. Adams, University of Michigan

This talk outlines several ways in which the birth environment can affect the formation of the solar system. Since many solar systems form within star clusters, our first task is to understand the dynamical evolution of these systems. Cluster evolution depends on the pre-cluster initial conditions, the star formation efficiency, and the gas removal history. For clusters of intermediate size with $N = 100 - 3000$, roughly spanning the range expected for the solar birth cluster, the dynamics are highly chaotic and multiple realizations of equivalent cases ($\sim$100 simulations per initial condition) must be carried out in order to build up a robust statistical description of the results. From these dynamical calculations, we find the distributions of closest approaches and the distributions of radial positions of solar systems living within the cluster. In a separate set of Monte Carlo scattering calculations, we determine the cross sections for solar system disruption through stellar flybys. The closest approach distribution is then used in conjunction with the interaction cross sections to assess the disruptive influence of stellar scattering interactions and to thereby constrain the possible birth aggregate of our solar system. Similarly, the distributions of radial positions are used in conjunction with distributions of cluster FUV (and EUV) luminosities to determine the radiation exposure of the solar system during its planet forming phase. This assessment is then coupled with disk photoevaporation models to provide additional constraints on the solar birth aggregate.

STABLE ISOTOPE ANOMALIES AND EARLY SOLAR SYSTEM CHRONOLOGY. F. Albarède[1], M. Arnould[2], R.W. Carlson[3], N. Dauphas[4], T. Fujii[5], S.B. Jacobsen[6], Q. Yin[7], and E.D. Young[8], [1]Ecole Normale Supérieure, 69007 Lyon, France, [2]Univ. Libre de Bruxelles, 1050 Brussel, Belgium, [3]Dept of Terrestr. Magnetism, Carnegie Inst., Washington D.C. 20015, [4]Dept of Geophys. Sciences, Univ. Chicago, Chicago, IL 60637, [5]Research Reactor Institute, Kyoto Univ., Osaka 590-0494, Japan, [6]Dept of Earth and Planetary Sciences, Harvard Univ., Cambridge, MA 02138, [7]Depart. Of Geology, Univ. California, Davis, CA 95616, [8]Dept of Earth and Space Sciences, UCLA, Los Angeles, CA 90095

.

The initial isotopic variability of elements in the Solar System (SoS) becomes a serious chronometric concern as soon as it compares in extent to radiogenic ingrowth or dominates it. With the noticeable exception of oxygen, the stable isotopes of elements such as Fe [1], Zn [2], Ni [3], Cd [4], Te [5] each define, at least to a few tens of ppm, single smooth mass fractionation lines among different planetary objects. This suggests that most elements are derived from a single SoS reservoir or that if there were several contributing sources, the material was efficiently mixed down to a very small scale. More recently, high precision analyses have resolved isotopic anomalies on specific isotopes of chronometric relevance such as ^{54}Cr [6, 7], ^{62}Ni [8], Nd, Sm [9, 10], Mo [11, 12], Ru [13], and Os [14-16] at the whole rock scale in carbonaceous chondrites. Most if not all of these effects seem to oppose even and odd isotopes. Though some of these anomalies (Os) may reflect inadequate sampling of insoluble presolar grains during analysis, the remainder clearly are present at the whole-rock scale. Regardless of their origin, the occurrence of anomalous isotopic compositions in carbonaceous chondrites indicates that this class of meteorite samples a different elemental mixture compared to other chondrite groups, differentiated meteorites, Moon, Mars and Earth.

The implication of this observation for the chronology based on short-lived radionuclides is not yet clear. Some of these anomalies may be due to nuclear field shift effects (NFS) during chemical processing of materials in the solar nebula [17, 18]. Although the NFS effect itself is reasonably well-understood [19] and may be seen as a residual mass bias analogous to mass-dependent fractionation, the processes behind it and the site at which fractionation is most effective remain poorly understood. The implications of the NFS effect for the distribution of short-lived nuclides in the solar nebula may be minimal because, if generated by chemical processes occurring in the solar nebula, the NFS effects may have no connection with the input and mixing of short-lived radionuclides in the SoS. NFS affects, however, may produce artifacts in the internal normalization procedure used for radiogenic chronometers because the odd/even effect and the large deviations of nuclear radii away from magic numbers [17, 18] clearly affect the calculation of ^{53}Mn-^{53}Cr [20], U-Th-Pb [21], and possibly the ^{182}Hf-^{182}W ages, but their effect on the ^{146}Sm-^{142}Nd system can probably be neglected.

On the other hand, if these anomalies are nucleosynthetic in origin, they offer the exciting perspective of comparing abundance observations and nucleosynthesis models for a very limited number of stellar sources, even possibly a single one. The aspects of the p-, s-, and r-processes of most direct relevance to the interpretation of these anomalies will be briefly and critically discussed [22-24]. The situation is in marked contrast with the one encountered when trying to understand the bulk SoS composition, which results from the mixture of a large variety of nucleosynthesis events, and consequently requires the modeling of the chemical evolution of the Galaxy. Measured anomalies may relate to presolar grains that have survived the process of incorporation into meteorites. In principle, these grains may be of interstellar or circumstellar origins. Such anomalies were first discovered in CAIs, in the rare FUN inclusions. In contrast to the presolar grains, the CAIs are considered to have formed in the SoS itself, even if some aspects of their origins remain puzzling.

The carrier phases of these isotopic anomalies could be associated with the influx of material that also brought in the short-lived radionuclides: the stable isotope variation may track variations in the abundance of these radionuclides with implications for the chronology based on the assumption of a homogeneous parent/daughter ratio throughout the SoS. This issue has already been discussed for the ^{146}Sm-^{142}Nd system [9, 10], where it potentially is possible to track variations in the abundance of short-lived ^{146}Sm by examining variations in the abundance of the other p-process isotope, ^{144}Sm. Similar approaches could be used for other short-lived cosmochronometers that have multiple-isotope parent elements, for example Fe-Ni, Pd-Ag and Hf-W, but they are not applicable to systems with parent elements that are now monoisotopic (e.g. Al

and Mn). For systems with parent elements that are now monoisotopic (e.g. Al and Mn) this is not an option. Because isotopic variability is most prevalent in carbonaceous chondrites and their components, the most serious concern arises with comparisons of chronologies that relate to CAIs, where nucleosynthetic anomalies may play havoc with short-lived cosmochronometers.

References: [1] Zhu X. K. et al. (2001) *Nature, 412*, 311-313. [2] Luck J.-M. et al. (2005) *GCA, 69*, 5351-5363. [3] Moynier F. et al. (in press) *GCA.* [4] Wombacher F. et al. (2003) *GCA, 67*, 4639-4654. [5] Fehr M. A. et al. (2005) *GCA, 69*, 5099-5112. [6] Rotaru M. et al. (1992) *Nature, 358*, 465-470. [7] Trinquier A. et al. (2007) *ApJ, 655*, 1179-1185. [8] Bizzarro M. et al. (2007) *Science, 316*, 1178-1181. [9] Andreasen R. and Sharma M. (2006) *Science, 314*, 806-809. [10] Carlson R. W. et al. (2007) *Science, 316*, 1175-1178. [11] Dauphas N. et al. (2002) *ApJ, 565*, 640-644. [12] Yin Q. et al. (2002) *Nature, 418*, 949-952. [13] Chen J. H. et al. (2003) *LPSC XXXIV*, 1789. [14] Brandon A. D. et al. (2005) *Science, 309*, 1233-1236. [15] Reisberg L. C. et al. (2007) *LPSC XXXVIII*, #1177. [16] Yokoyama T. et al. (2007) *EPSL, 259*, 567-580. [17] Fujii T. et al. (2006) *EPSL, 247*, 1-9. [18] Fujii T. et al. (2006) *ApJ, 647*, 1506-1516. [19] Bigeleisen J. (1996) *J. Am. Chem. Soc., 118*, 3676-3680. [20] Lugmair G. W. and Shukolyukov A. (1998) *GCA, 62*, 2863-2886. [21] Amelin Y. et al. (2005) *GCA, 69*, A215. [22] Arnould M. and Goriely S. (2003) *Phys. Rep., 384*, 1-84. [23] Arnould M. et al. (2007) *Phys. Rep., 384*, doi:10.1016/ .physrep.2007. 06.002. [24] Herwig F. (2005) *ARAA, 43*, 435-479.

HOW HOMOGENEOUS WAS THE EARLY SOLAR SYSTEM? THE CHROMIUM STORY. C. M. O'D. Alexander and R. W. Carlson. DTM, Carnegie Institution of Washington, Washington D.C. 20015, USA (alexande@dtm.ciw.edu and carlson@dtm.ciw.edu).

Introduction: An isotopically homogeneous early Solar System is a prerequisite if short-lived radionuclides are to be used as chronometers. Shukolyukov and Lugmair [*1*] pointed out that there is a correlation between ε^{53}Cr and ε^{54}Cr excesses in bulk carbonaceous chondrites. Excesses in ^{53}Cr are generally ascribed to the decay of ^{53}Mn ($T_{1/2}$=3.7 Ma), while ^{54}Cr excesses are generally assumed to be nucleosynthetic in origin. Sequential leaching of bulk chondrites has shown that they are composed of several isotopically distinct Cr components, and that the ^{53}Cr and ^{54}Cr excesses are carried in separate components [*1-4*]. Hence this apparent correlation between the two Cr isotopes in the bulk compositions is a puzzle. In addition, correlations have also been reported between ε^{54}Cr and Mn/Cr ratio, and between ε^{54}Cr and Δ^{17}O [*2*]. A correlation between Δ^{17}O and ^{63}Cu excesses has also been reported [*5*]. The variations in O isotopes are not due to radioactive decay, but the ^{63}Cu excesses have been attributed to the decay of ^{63}Ni ($T_{1/2}$=100 yrs). Thus, in carbonaceous chondrites there appears to be a correlation between two possibly radiogenic nuclides (^{53}Cr and ^{63}Cu) with very different half-lives, a nucleosynthetically derived anomally (^{54}Cr excess), and what is generally thought to be a photochemical derived variation in Δ^{17}O.

The non-radiogenic anomalies point to significant nebular heterogeneity. The evidence for nebular heterogeneity is emphasized when the ordinary and enstatite chondrites, achondrites, Earth-Moon and Mars are included. They do not fall on the same correlation lines as the carbonaceous chondrites in plots of ε^{54}Cr vs. Mn/Cr, ^{63}Cu or Δ^{17}O. In the these bodies, but not the carbonaceous chondrites, it has been suggested that ε^{54}Cr and ε^{62}Ni are correlated [*6*]. The compositional distinction of carbonaceous chondrites is further displayed by their nucleogenic isotope anomalies in Ba, Nd and Sm compared to ordinary chondrites, differentiated meteorites, and Earth [*7, 8*].

The key to understanding the causes of the observed correlations in the bulk meteorites is to identify the various components responsible for the range of isotopic compositions observed. Several studies have shown that the ^{54}Cr carrier is resistant to acid attack at low temperatures [*1-4*]. Shukolyukov and Lugmair [*1*] suggested that the ^{54}Cr carrier may be a presolar grain preserved in the matrix, and that the range of ε^{53}Cr and ε^{54}Cr isotopes in carbonaceous chondrites is the result variable abundances of matrix and chondrules. Alexander [*9*] has suggested that the matrices of all chondrites are dominated by a CI-like component and that this component is responsible for the abundances of presolar grains and organic matter, as well as highly volatile elements, in chondrites – e.g., in the most primitive members of each chondrite class the matrix-normalized abundances of presolar grains [*10*] and organic matter are CI-like.

If all chondrites accreted the same presolar material in their matrix, the ε^{54}Cr carrier should have been present in all chondrites, including the ordinary chondrites and ECs. Since the ε^{54}Cr carrier is somewhat acid resistant, it should be possible to concentrate the carrier and determine whether it has the same composition in all chondrite classes. A common carrier in all carbonaceous chondrites is suggested by the results of Alexander [*11*] who reported similar ε^{54}Cr compositions for hot HCl (6N HCl, 80°C for ~12 hrs) leaches of acid residues of Orgueil, Tagish Lake and Murchison (201±23, 177±6 and 236±6, respectively). Ion probe mapping of the Orgueil residue failed to identify the ^{54}Cr carrier, but showed that it is not in ≥1μm grains with isotopically anomalous O (or S) compositions [*12, 13*], deepening the mystery about why there is an apparent correlation between ε^{54}Cr and Δ^{17}O in the bulk carbonaceous chondrites.

Methods: Following up on this, we have measured the Cr isotopic compositions of new residues for Murchison, the CVs Leoville and Mokoia, and the LL3.05s QUE97008 and MET00452. The residues were prepared using the relatively gentle CsF technique [e.g., *14*] at room temperature. Since almost all chondrule and CAI material is either destroyed or physically removed during the preparation of these residues, they are essentially concentrates of the acid-resistant matrix material, including the presolar grains. The residues were leached with 6N HCl at 80°C for ~12 hrs. A small aliquot of each solution was retained so that the amount of Cr in the leachates could be estimated by ICP-MS. The Cr was then isolated from the remainder of the solutions following standard column chemistry [e.g., *3, 4*], and analyzed by TIMS with the Carnegie's Triton.

Results: The results are given in Table 1. As can be seen, large ^{54}Cr anomalies were found in all the leachates, including the ordinary chondrites. The ^{54}Cr excesses for the new Murchison residue are not as large as previously reported by [*11*] for this meteorite, but it is possible that the new much larger residue is not as pure as the previous one. The ^{54}Cr excesses found in the CVs and ordinary chondrites are not as large as in Murchison, but they are larger than any previously reported values for meteorites from these

classes. As previously noted, the ^{54}Cr anomalies are accompanied by small, to not significant, ^{53}Cr anomalies.

Table 1. The isotopic compositions of 6N HCl leaches of acid residues and the estimated fraction of the bulk meteorite Cr in the leaches.

	% Cr	ε^{53}Cr	ε^{54}Cr
CM			
Murch 2	0.0075	-0.60±0.26	111.5±0.6
Murch 2b	0.0075	-0.28±0.21	103.0±0.5
CV			
Leoville	0.0171	-0.42±0.17	26.6±0.4
Mokoia	0.0140	0.15±0.15	9.1±0.4
LL			
MET00452	0.0075	-0.65±0.08	39.6±0.3
QUE97008	0.0077	-0.35±0.10	39.1±1.3

Discussion: Two factors may have caused the smaller excesses in the CV and ordinary chondrite leachates than in the Murchison leachates: the residues from these meteorites have more leachable isotopically normal Cr, and/or the metamorphism these meteorites have experienced has destroyed some of the ^{54}Cr carrier. Nevertheless, the most striking feature of our new results is that the two ordinary chondrite residues produced higher ^{54}Cr excesses than the two CVs despite the fact that, in bulk, the CVs have significant ^{54}Cr excesses and the ordinary chondrites have significant depletions [*1, 2*].

Table 2. Comparison of the predicted and measured bulk ε^{54}Cr compositions [*2*].

	Predicted	Measured
CM		
Murch 2	0.75	1.01
CV		
Leoville	0.67	0.86
Mokoia	0.54	0.86
LL		
MET00452	0.29	-0.44
QUE97008	0.30	-0.44

To test whether the leachates account for all the ^{54}Cr excesses in the bulk meteorites, it was assumed that the bulk meteorites are a mix of the leachate and material with a bulk ε^{54}Cr isotopic composition of 0. For the carbonaceous chondrites, this simple model is able to explain between 62 and 78% of the bulk ^{54}Cr anomaly. The ordinary chondrite bulk compositions cannot be explained by this simple model and require that the bulk of their Cr has a large ε^{54}Cr depletion (~-0.7). Nevertheless, these results are consistent with the bulk of the ^{54}Cr being carried in an acid-resistant phase that is concentrated in the matrix and is presolar. Supernova-derived Si_3N_4 is a possible candidate as in should be soluble in hot HCl.

The bulk of the Cr in ordinary chondrites is presumably in chondrules. Trinquier et al. [*2*] reported ε^{54}Cr compositions for two Chainpur chondrules of only -0.41±0.14 and -0.48±0.12, suggesting that there is an even more depleted component that has yet to be identified. The ε^{54}Cr composition of one chondrule from Qingzhen (EH3) is similar (-0.46±0.14) to those in Chainpur, but a chondrule from Allende has a composition that is significantly different (-0.08±0.11), suggesting that chondrules from different chondrites formed from different materials. Chondrules also exhibit a wide range of Δ^{17}O, wider than bulk meteorites, within and between chondrite classes that could also indicate a range of precursors. If, as seems possible from the reported ε^{54}Cr-Δ^{17}O correlation in bulk carbonaceous chondrites, these precursors had different Cr isotopic compositions, dating of chondrule formation based on bulk chondrule isochrons is questionable. If the CI composition is similar to that of the bulk Solar System, the fact that the chondrules are depleted in ^{54}Cr relative to CI suggests that at least one of their precursors formed from material that was depleted in the presumably presolar ^{54}Cr carrier.

Conclusions: Our results are consistent with the bulk of the ^{54}Cr excesses being carried in an acid-resistant presolar phase that is present in the matrices of all chondrites. The range of bulk Cr compositions and the reported correlations with Δ^{17}O, Mn/Cr ratio, ε^{62}Ni, and ε^{65}Cu requires at least 2 additional components in chondrites that are relatively depleted in ^{54}Cr. Thus, the Solar System was not isotopically homogeneous, potentially making the use of short-lived radionuclides as chronometers more difficult. Further studies of residues and other chondritic components are underway and will be presented at the meeting.

References: [1] Shukolyukov A. and Lugmair G.W. (2006) *EPSL,* 250, 200-213. [2] Trinquier A. *et al.* (2007) *ApJ,* 655, 1179-1185. [3] Podosek F.A. *et al.* (1997) *M&PS,* 32, 617-628. [4] Rotaru M. *et al.* (1992) *Nature,* 358, 465-470. [5] Luck J.M. *et al.* (2003) *GCA,* 67, 143-151. [6] Bizzarro M. *et al.* (2007) *Science,* 316, 1178-1181. [7] Carlson R.W. *et al.* (2007) *Science,* 316, 1175-1178. [8] Andreasen R. and Sharma M. (2007) *ApJ*, 665, 874-883. [9] Alexander C.M.O'D. (2005) *M&PS,* 40, 943-965. [10] Huss G.R. and Lewis R.S. (1995) *GCA,* 59, 115-160. [11] Alexander C.M.O'D. (2002) *LPS,* XXXIII, #1872. [12] Nittler L.R. and Alexander C.M.O'D. (2003) *M&PS,* 38, A129. [13] Zinner E. *et al.* (2005) *GCA,* 69, 4149-4165. [14] Cody G.D. *et al.* (2002) *GCA,* 66, 1851-1865.

U-PB CHRONOMETRY OF METEORITES: NEW OPPORTUNITIES, NEW LEVEL OF COMPLEXITY.
Y. Amelin[1,2], J. Connelly[3,4], J.H. Chen[5], C. Göpel[6], R.E. Zartman[7], G.J. Wasserburg[8], C.J. Allègre[9], S.A. Bowring[10], E. Jagoutz[11], [1]Geological Survey of Canada, 601 Booth Street, Ottawa, Ontario K1A 0E8, Canada (yamelin@nrcan.gc.ca), [2]Planetary Science Institute and Research School of Earth Sciences, The Australian National University, Canberra ACT 0200, Australia (yuri.amelin@anu.edu.au), [3]The Jackson School of Geosciences, The University of Texas at Austin, Austin, Texas, USA (connelly@mail.utexas.edu), [4]Geological Institute, Copenhagen University, Copenhagen, Denmark, [5]Science Division, 1M/S 183-601, Jet Propulsion Laboratory, Caltech, 4800 Oak Grove Dr., Pasadena, CA 91109-8099, (James.H.Chen@jpl.nasa.gov), [6]Laboratoire de Géochimie et Cosmochimie, IPGP, 4 Place Jussieu, 75252 Paris Cedex 05, France (gopel@ipgp.jussieu.fr), [7]EAPS, Massachusetts Institute of Technology, Cambridge, MA 02139, USA (rzartman@mit.edu), [8]The Lunatic Asylum, GPS Division, 170-25, Caltech, Pasadena, CA 91125 (gwasserburg@charter.net), [9]IPGP, Laboratoire de Géochimie et Cosmochimie, case 89, 4, place Jussieu, 75252 Paris cedex 05, France (allegre@ipgp.jussieu.fr), [10] EAPS, Massachusetts Institute of Technology, Cambridge, MA 02139, USA (sbowring@mit.edu), [11]Max-Planck-Institut für Chemie, P.O. BOX 3060, D-55020Mainz, Germany (jagoutz@mpch-mainz.mpg.de).

U-Pb, what's new? U-Pb was among the first (along with K-Ar) isotopic dating methods applied to meteorites. What makes the impact of today's U-Pb dating different?

First, the number of interesting meteorites that deserve a detailed study greatly increased, mainly due to meteorite recovery from Antarctica and deserts. In some cases, in place of a unique meteorite (e.g. AdoR during the consortium study of 1975-76), we have groups of meteorites with diverse compositions, structures and ages (e.g., 13 angrites are known today). Studying compositional and age patterns in such a group can tell us more about early solar system history. The number of meteorites studied with a variety of isotopic methods is also rapidly increasing.

Second, modern techniques of Pb isotopic analysis (plasma ionization mass spectrometry, and double-spike TIMS) give much improved precision and reproducibility, and can yield $^{207}Pb/^{206}Pb$ dates with precision as high as 0.1-0.2 Ma under favorable conditions. Better methods of common Pb removal help to improve precision and accuracy.

Third, improvements in the blanks and ionization efficiency using special reagents (e.g. high efficiency silicic acid emitter) in the last few years, allow analyses of much smaller samples to obtain high precision.

Many complexities in U-Pb systematics, which appeared insignificant compared to analytical errors in the past, are revealed at the new level of precision, and must be considered in order to turn $^{207}Pb/^{206}Pb$ dates into meaningful ages. Here are some of the questions we have to address:

Inter-laboratory standardization and other analytical issues. Ages of the same minerals from the same meteorite, determined using the same isotopic system but different techniques (e.g. TIMS vs. MC-ICPMS, dry plasma vs. wet plasma) or at different laboratories, vary in many instances well outside of the claimed error limits. Understanding and eliminating these variations by inter-laboratory standardization and calibration is essential for the progress of cosmochronology. A three-fold approach is required to achieve inter-laboratory reproducibility. First, we need to prepare standards that are both homogeneous and as close in composition to the samples as possible, and to make sure that the influence of all sources of errors on standard and sample analyses is the same. Second, we need to explore whether radiogenic $^{207}Pb/^{206}Pb$ ratios can be influenced by extensive leaching (such a possibility was suggested for zircons). Third, we have to revise our methods of data reduction to make certain that the total errors include all individual sources of errors, and account for their correlations.

Evolution of the protoplanetary disk - what are we dating? If Pb was completely lost from the system (e.g., a mineral) during, or after, formation, and the U-Pb system subsequently remained undisturbed, then we would date that episode of Pb loss. In a system cooling from hot gas, we would date the time at which Pb retention began. In a system being heated from cold dust to its melting point, we would date the time of volatile loss. If the Pb isotopic composition was completely homogenized between all minerals, then we would date the event that caused homogenization.

But what if there were multiple episodes of U-Pb fractionation, or separation and/or homogenization of Pb were incomplete? This is a likely situation for chondrules, which could have exchanged matter with nebular gas, and could include igneous material along with melted nebular condensates [e.g., 1, 2]. If the total duration of multi-episodic evolution was short compared to the dating error, then we can consider the integral chemical effect to all be of one episode, and use a conventional single-stage approach to age calculation. As precision of the dates increases, the single-stage approach becomes invalid. As the typical error of the dates becomes much shorter than the lifespan of the protoplanetary disk, consideration of a multi-stage

evolution becomes a standard requirement in U-Pb dating.

A related problem can affect dating of angrites and eucrites, which come from volatile-depleted asteroids. Even a short time period between volatile loss (during, or shortly after, accretion) and crystallization of angrite/eucrite parent bodies could have been sufficient to produce measurable amounts of radiogenic Pb with very high $^{207}Pb/^{206}Pb$ ratio. During subsequent magmatism and impacts, this anomalous Pb can be redistributed and embedded into other minerals, or deposited in grain boundaries. The excess, or deficit, of such Pb (tentatively called "aborted high-μ Pb", also referred to as "parentless Pb" in Lunar soils and breccias) can produce anomalously old, or anomalously young, $^{207}Pb/^{206}Pb$ single-stage dates. Possible uneven distribution of such Pb between minerals further complicates the situation.

Closed system behavior can be verified by comparing $^{207}Pb/^{206}Pb$ and $^{238}U/^{206}Pb$ dates, but we need to develop methods of removing damaged parts of crystals as efficient as air abrasion and chemical abrasion used for zircons.

Dating geological history of asteroids. In order to date asteroidal processes, such as cooling, metamorphism, aqueous alteration, and disruption by impacts, we need to separate the effects of volume diffusion, alteration, and shock on the U-Pb system in primary and secondary minerals. Interpretation of the data critically depends on the availability and quality of experimental data. The database of experimentally determined rates of Pb diffusion in minerals that contain U and radiogenic Pb in meteorites has been recently expanded [e.g. 3], but experimental data on alteration and shock effects on the U-Pb system are still scarce or non-existent.

Knowing the distribution of U between meteoritic minerals is equally important for understanding effects of diffusion, alteration, and shock. The current database of U distribution in meteorites is quite insufficient, both in quantity and quality. Detailed studies, using preferably high-sensitivity ion microprobes, are required.

Re-distribution of U and diffusion of Pb should be considered together. This is demonstrated by the meaning of U-Pb data from chondritic phosphates. Phosphates in many type 6 chondrites contain all the U of the sample, and the process we date is diffusion of Pb out of the phosphate crystals during high-temperature metamorphism. In contrast, phosphates in type 4 chondrites contain only a small part of the U of the sample, the rest is in silicate minerals. We are dating migration of U, or possibly growth of phosphate minerals. When we compare Pb-isotopic dates with the readings of other isotopic chronometers, in particular in meteorites that came from metamorphosed parent bodies, we need to be sure that we date the same event with both isotopic systems.

Possible heterogeneous $^{235}U/^{238}U$ in the early solar system may render $^{207}Pb/^{206}Pb$ dates inaccurate. Such heterogeneity may be caused by the presence of ^{247}Cm, or by addition of U with isotopic composition different from that in the nebula from a late supernova ejection (analogous to, and possibly brought in together with ^{60}Fe [4]). Precision of U isotopic analyses performed in the 1970's and early 1980's, which confirmed homogeneity of $^{235}U/^{238}U$ in the Solar System [e.g. 5], is not sufficient at the current level of precision of U-Pb dating (the $^{235}U/^{238}U$ ratio has to be determined with a precision of 0.01-0.02%). There are recent high-quality U isotopic determinations at this level of precision [6, 7], but many key meteorites and their components (e.g., CAIs) have not yet been studied.

Providing reliable age benchmarks for extinct nuclide chronometry of the early solar system is one of the main goals of U-Pb dating of meteorites. Having multiple "absolute" age reference points for each extinct nuclide chronometer allows direct testing of heterogeneous vs. homogeneous distribution of the parent nuclide, as well as detecting element migration and disturbance of extinct nuclide chronometers. The requirements of meteorites that can serve as age reference points are, however, very high. They are similar to the requirements of minerals for decay constant determination by age comparison [8]. Discovery of many new meteorites, together with development of analytical methods that combine high precision with improved throughput, improves our chances of establishing new, and better age benchmarks for the early solar system timescale.

At the MetChron 2007 meeting, we need to exchange information about methodology and the application of U-Pb geochronology to meteorites, to outline tangible goals for the coming several years, and find appropriate and acceptable tests to inter-calibrate extinct and extant nuclide chronometers. We also need to get our techniques ready for dating Lunar, Martian or asteroid samples, and materials such as those delivered by the Stardust mission, from future space programs.

References: [1] Libourel G. et al. (2006) *EPSL* 251, 232–240. [2] Libourel G. and Krot A.N. (2007) *EPSL* 254, 1-8. [3] Cherniak D.J. (2001) *Chem. Geol.* 177, 381–397. [4] Bizzarro M. et al. (2007) Science 316, 1178-1181. [5] Chen J.H. and Wasserburg G.J. (1981) *EPSL* 52, 1–15. [6] Stirling C.H. et al. (2005) *GCA* 69, 1059–1071. [7] Stirling C.H. et al. (2006) *EPSL* 251, 386–397. [8] Begemann F. et al. (2001) *GCA* 65, 111–121.

SEVEN MILLION YEARS OF EVOLUTION ON THE ANGRITE PARENT BODY FROM PB-ISOTOPIC DATA. Y. Amelin[1,2] and A. J. Irving[3], [1]Geological Survey of Canada, 601 Booth Street, Ottawa, Ontario K1A 0E8, Canada (yamelin@nrcan.gc.ca), [2]Planetary Science Institute and Research School of Earth Sciences, The Australian National University, Canberra ACT 0200, Australia (yuri.amelin@anu.edu.au). [3]Dept. of Earth and Space Sciences, University of Washington, Seattle, WA 98195 (irving@ess.washington.edu).

Introduction: Here we report preliminary Pb isotopic data for three angrites recently found in Northwest Africa: NWA 2999, NWA 4590 and NWA 4801. Petrologic data for NWA 4801 are presented in a companion abstract [1] and descriptions of the other two specimens were given previously [2].

Methods and results: Handpicked pyroxene separates from each angrite were washed in acids and analyzed by TIMS using ^{202}Pb-^{205}Pb double spike as described before [3]. A summary of the measured ages follows:

Meteorite	^{207}Pb/^{206}Pb date	2σ err	Pb-Pb isochron	2σ err
SAH 99555	4564.00	0.30	**4564.64**	**0.54**
D'Orbigny	**4564.42**	**0.12**		
NWA 2999	4561.39	0.40	**4561.79**	**0.42**
NWA 4590	4558.00	1.00	**4558.86**	**0.30**
LEW 86010	**4558.55**	**0.15**	4558.68	0.16
NWA 4801	4557.99	0.12	**4558.06**	**0.15**
Angra dos Reis	**4557.65**	**0.13**		

Dates for the angrites SAH 99555, D'Orbigny, LEW 86010 and AdoR were re-calculated with addition of new data points, and therefore differ slightly from the dates for the same meteorites reported at the LPSC-2007 [3]. Preferred dates (the weighted averages for the samples containing pure radiogenic Pb after washing and blank subtraction, and isochron dates for the samples containing common Pb) are highlighted with bold font.

NWA 2999 is unusual among the 13 known angrites in several ways. This specimen is unusually metal-rich, but also has a high abundance of spinel, a mineral that has low (but not negligible) solubility in HF under conditions of sample digestion. Spinel in NWA 2999 contains common Pb that cannot be removed by leaching. Furthermore, there is a pervasive brown coating (iron hydroxides) on all mineral grains, presumably due to terrestrial desert weathering. This coating is opaque and magnetic, obscuring both mineral picking and magnetic separation, and pure pyroxene was obtained from NWA 2999 only after additional washing cycles before mineral picking. The age obtained for NWA 2999 is intermediate between the ages of finer grained ("quenched") and coarser grained ("plutonic") angrites.

Two other new angrites have ages similar to those of two previously known "plutonic" angrites. NWA 4590 is coeval with LEW 86010, whereas NWA 4801 is slightly (but outside of the 2σ error limits) older than Angra dos Reis.

Age resolution of modern Pb-isotope chronometry: The age difference between the two youngest angrites, AdoR and NWA 4801, is probably close to the limit of age resolution of modern Pb-isotope chronometry. Pyroxenes from both angrites contain pure radiogenic Pb (two out of five fractions from NWA 4801 contain a very small amount of common Pb in excess of blank) - therefore the results are free from uncertainty in common Pb correction. The difference between weighted averages of ^{207}Pb/^{206}Pb is 0.34 ± 0.18 Ma, and appears to be resolved at 2σ level (Fig. 1).

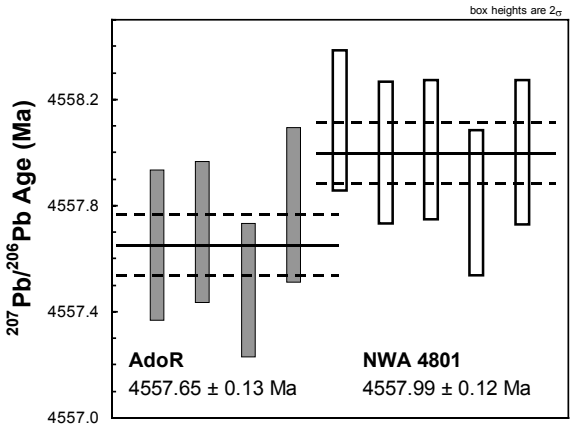

However, the age determinations on these meteorites were obtained in the same laboratory at GSC using identical techniques, and their comparison is free from inter-laboratory analytical biases. It remains to be seen whether such small age differences can be resolved if analyses are performed in different laboratories and by different techniques (e.g., TIMS vs. MC-ICPMS).

Th/U ratios vs. age: The model ^{232}Th/^{238}U values (κ values) in angritic pyroxenes (calculated from isotopic compositions of radiogenic Pb) vary with age in a systematic manner (see Fig. 2).

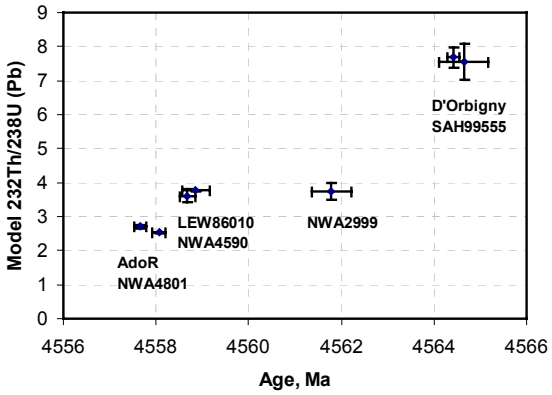

Three pairs of coeval (or nearly coeval) angrites have very similar κ values, which decrease with age: from 7-8 for D'Orbigny and SAH 99555, to 3.5-3.9 for LEW 86010 and NWA 4590, to 2.5-2.7 for AdoR and NWA 4801. In contrast, NWA 2999 yields a similar κ value to the younger angrites LEW 86010 and NWA 4590, and falls below the trend line. If the falling of Th/U with time reflects the evolution of the sources of magmatism in the angrite parent body, then the deviation of NWA 2999 from this trend may be related to the addition of a chemically different (e.g., chondritic) component, which also may be responsible for the unusually high concentration of metal in this particular angrite [4].

Conclusion: The angrite parent body underwent prolonged high temperature igneous (both volcanic and plutonic) activity and metamorphism for at least 7 Ma during a period very early in solar system history. It is difficult to conceive of a thermal mechanism by which this could be accomplished unless the parent body was a relatively large, differentiated planet.

References: [1] Irving A. J. and Kuehner S. M. (2007) this meeting [2] Irving A. J. et al. (2006) *EOS, Trans. AGU 87, Fall Mtg. Suppl.*, Abstract #P51E-1245; Kuehner S. M. and Irving A. J. (2007) *LPS XXXVIII,* Abstract #1522 [3] Amelin Y. (2007) *LPS XXXVIII,* Abstract #1669 [4] Humayun M. et al. (2007) *LPS XXXVIII,* Abstract #1221; Gellissen M. et al. (2007) *LPS XXXVIII,* Abstract #1612.

Rb-Sr Dating Using LDRIMS. F.S. Anderson[1], T.J. Whitaker[2], D. Young[3], B. Peterson[4], [1]University of Hawai'i at Manoa, HIGP, 1680 East-West Road, Honolulu, HI 96822 (anderson@higp.hawaii.edu), [2]Atom Sciences, TN, [3]Southwest Research Institute, TX, [4]Concepts Research Corporation, SC

Introduction: We are developing a miniature laser ablation resonance ionization system coupled with a time of flight mass spectrometer (LA-RI-MS) for in-situ rubidium and strontium (Rb-Sr) geochronology and geochemical measurements on Mars and other solid bodies. These measurements are critical for calibrating cratering statistics and constraining the age of planetary surfaces, in addition to measuring the geochemical and isotopic composition of surface rocks to provide insight into the formation and evolution of a planet's crust and mantle. The instrument has two modes, LA-RI-MS and LA-MS. The LA-RI-MS mode will be used to selectively ionize and precisely measure the abundance of Rb-Sr isotopes. The second mode, LA-MS (laser ablation mass spectroscopy), collects all ablated ions by turning off the RI subsystem, providing elemental abundance measurements of the surface to ~5%. Here we report on initial results from the lab version of the instrument.

Background: The chronology of geologic events is one of the most important questions of planetary science. The order and timing of events is usually constrained by superposition relationships and crater counting techniques, providing relative ages accurate to ~0.5-1 Ga for Mars [**1**]. However, a radiometric date would constrain the impact crater flux and thereby the absolute chronology of the entire planet. To significantly reduce the uncertainties of planetary geological periods it is desirable to measure ages to better than ±10% (relative), or ~<±250 Ma to perform an accurate calibration [**1-4**].

The relatively high abundance and simplicity of sampling and analysis strategies for ^{40}K-^{40}Ar and ^{87}Rb-^{87}Sr methods have been led to their proposal to flight programs and PIDDP [**1-4**]. An advantage of the LA-RI-MS approach is that samples require very little sample preparation, as the surface can be cleaned via laser ablation before measurements begin.

The growth of radiogenic ^{87}Sr in Rb rich minerals is described by $^{87}Sr = {}^{87}Sr_i + {}^{87}Rb(e^{\lambda t}-1)$, in which $^{87}Sr_i$ is the initial amount of ^{87}Sr in the sample, λ is the decay constant for ^{87}Rb ($1.42\times10^{-11}y^{-1}$ [**5**]), and t is the time elapsed in years since the formation of the minerals in the sample. Because mass-spectrometers are poor at measuring absolute abundances, but excellent at measuring relative abundance, this equation is usually expressed relative to the stable iostope ^{86}Sr:

$$\frac{^{87}Sr}{^{86}Sr} = \left(\frac{^{87}Sr}{^{86}Sr}\right)_i + \frac{^{87}Rb}{^{86}Sr}\left(e^{\lambda t}-1\right) \qquad (1)$$

In this equation, there are two unknowns, $(^{87}Sr/^{86}Sr)_i$ and t. The ^{87}Rb-^{87}Sr technique can be a difficult because one needs to 1) measure ^{87}Sr/^{86}Sr to a precision of better than 0.02% to achieve a time resolution < ±250Ma [**1**], despite isobaric interference by ^{87}Rb which is only different in mass of 0.00035%, requiring a mass resolution of 10^5+, and 2) measure ^{87}Rb/^{86}Sr to a precision of 1% [**1**].

We avoid these issues using LA-RI-MS, in which tunable lasers are used to selectively ionize ablated atoms of the chosen element [**6-11**]. The resulting ions are extracted into a mass spectrometer to obtain elemental & isotopic abundance, essentially eliminating isobaric and molecular interferences. This allows us to separate Rb from Sr, reducing the required MS resolution to ~500.

Because Sr requires a higher precision measurement, we use it to derive ablation requirements. The SNC meteorites provide insight into the abundance of Rb-Sr and size of mineral grains (100-300 μm) [**12**], however, because their provenance on the surface is unknown, radiometric ages do not help constrain cratering flux. Basaltic SNC's like Shergotty have abundant Sr in plagioclase (100-300 ppm), but lower values in pyroxenes (1-10 ppm) [**12**]. Plagioclase grains are common in Shergotty (**Fig. 1**), and fortuitously, the chemistry and mineralogy of the surface of Mars as seen by the MGS TES and MER rovers appears richer in K and plagioclase than implied by the SNC meteorites (**Fig. 2**). Assuming a sample with 1 ppm Sr (conservative compared to SNC's & Mars) and an overall measurement efficiency of 1%, a precision of 5000 and poission statistics suggest we need to measure ~10^{15} atoms, or a 20x20x20 μm^3 volume, given that most silicates have ~10^{11} atoms/μm^3. Given that Sr abundance on Mars may be more than 200

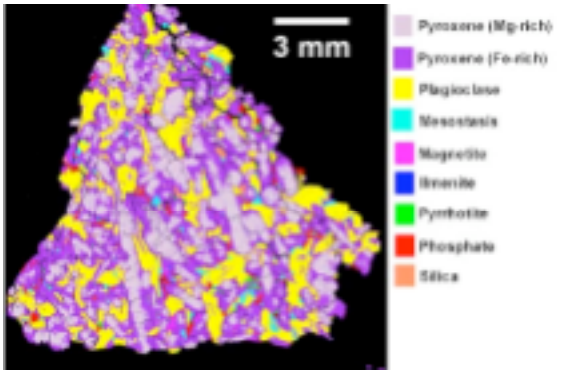

Figure 1: Microprobe map of minerals in Shergotty showing large size of Sr rich Plagioclase grains (courtesy [**13**]).

times larger, and that our ablation spot sizes will likely be 50 μm, this increases the accuracy of the measurement by a factor of $500^{1/2}$, suggesting dates accuracy better than 25 Ma may be possible.

Results: We have built a lab instrument from off-the-shelf components in order to demonstrate sufficient precision for Rb-Sr geochronology (**Fig. 3**). Building the lab instrument has provided us with insight into the requirements for a miniature system. For example, the initial measurements were made with much lower ablation and resonance ionization (RI) laser power levels than expected (<2-5mJ), and demonstrated the potential for using only two lasers for Sr (not three as anticipated). Sample preparation was done in 5-30 minutes from cutting of the sample with a Dremel tool to vacuum and measurement.

Current laser ablation and resonance ionization spectra have precision for $^{87}Sr/^{86}Sr$ of ±0.0008 (goal ±0.0002), however, several issues remain: (1) the RI system is not well aligned with the ablation plume causing losses of instrument efficiency, (2) ablation ions were not removed, saturating our detector & reducing our RI resolving power; these ions can be removed with simple modifications now underway, and (3) our high precision data collection system was under repair; all initial data were collected with a low precision oscilloscope. Nonetheless, all expected Sr peaks are evident (**Fig. 4**), suggesting a Rb-Sr date is possible. We anticipate that addressing these three issues will increase the measured precision to the required value. The current data suggest that the required number of shots will remain low, resulting in manageable power levels for an in-situ instrument.

Key parts of the miniaturization effort have begun, including the development of miniature (20x5x5 cm^3) tunable high power resonance and ablation lasers, as well as a miniature (50x20x10 cm^3) mass spectrometer. The lasers are based on a solid state diode pumped passively Q-switched Yb:YAG (**Fig. 5**) driving a miniature Ti-S etalon BBO back end, with initial delivery in mid-2007. The miniature, high resolution (20K+), multi-bounce time of flight mass focusing spectrometer is critical for making accurate LA-MS measurements; development is also on schedule for delivery in mid-2007.

References: [1] Anderson et al (2005), *LPS XXXVI,* Abs. #1843. [2] Swindle et al. (2003), *LPS XXXIV,* Abs. #1488. [3] Cardell et al. (2002), *LPS XXXIII,* Abs. #2407. [4] Stewart et al. (2001), *11th Ann. Goldschmidt Conf*., Abs. #3891. [5] Faure, Principles of Isotope Geology, 1986. [6] Arlinghaus et al. (1990), *J. Vac. Sci. Tech.* A8. [7] Arlinghaus et al. (1993), *J. Vac. Sci. Tech.* A11. [8] Arlinghaus and Joyner (1996) , *J. Vac. Sci. Tech*. B14. [9] Pappas et al. (1989) , *Science*, 243. [10] Pellin et al. (1990), *Phil. Trans. R. Soc. Lond*. A333. [11] Downey et al. (1990), *Inst. Phys. Conf.* Ser. No 114. [12] Borg et al. (2005), *Geochim Cos. Acta*, 69, 5819. [13] Pers. comm. G.J. Taylor, 2006. [14] Pers. comm. H. McSween, 2006.

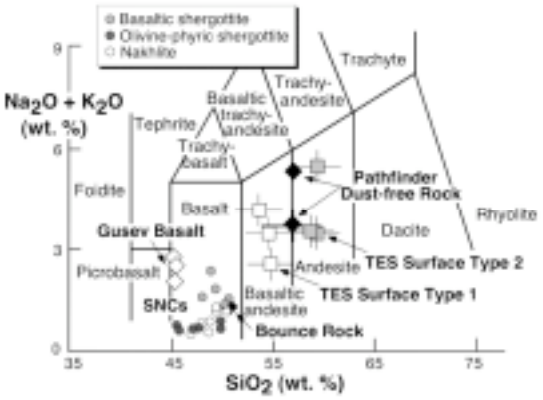

Figure 2: Mars as observed by MER, TES, and Pathfinder is richer in K and Si than implied by SNCs, suggesting that Sr concentration in Shergotty is conservative (courtesy [**14**]).

Figure 3. Lab version of LARIMS complete, ready to define requirements for miniature system.

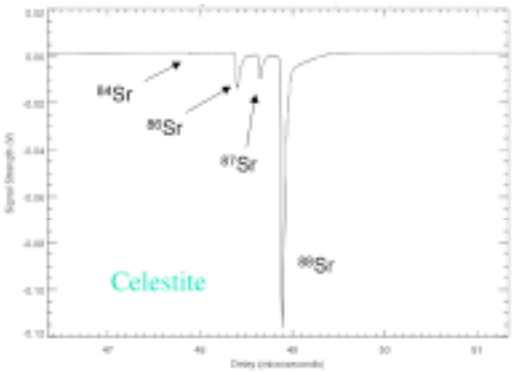

Figure 4. First light LARIMS spectrum of Sr. Left axis intensity, bottom time of flight (and hence mass).

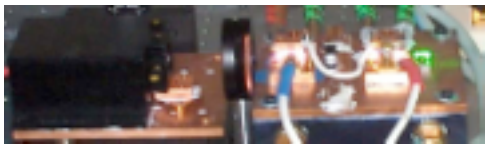

Figure 5: Ten inch prototype of Yb:YAG development for laser ablation; diode on left (black box) & 2 amplifiers on right; smaller package to be delivered in 2007.

HIGH PRECISION NICKEL ISOTOPE MEASUREMENTS OF FE-NI METAL IN METEORITES

K. T. Andrews[1], M. Schiller[1], M. Bizzarro[2] and J. A. Baker[1]
[1]School of Geography, Environment and Earth Sciences, Victoria University of Wellington, P.O. Box 600, Wellington, New Zealand (kimtandrews@gmail.com; joel.baker@vuw.ac.nz), [2]Axiom Laboratory, Geological Institute, University of Copenhagen, 1350 Copenhagen, Denmark (bizzarro@geol.ku.dk).

Introduction: Nickel has five isotopes (58, 60, 61, 62 & 64) and is potentially a powerful early Solar System chronometer and tool to identify the astrophysical setting in which our Solar System formed. Variations of ^{60}Ni abundances in meteorites can result from the decay of short-lived ^{60}Fe ($t_{1/2}$ = 1.49 Myr), if it was injected by a nearby supernova into the proto-Solar System shortly before or during its creation. Furthermore, variations in the abundances of neutron-rich isotopes, ^{62}Ni and ^{64}Ni, might trace different stellar nucleosynthetic inputs into the proto-Solar System and reveal time-scales of mixing of these nucleosynthetic components in the proto-planetary disc.

Recently published Ni isotope data for meteorites has produced somewhat conflicting results [1,2,3]. No evidence for measurable Ni isotopic anomalies in Fe-Ni metal of iron meteorites was found by Quitte et al. [1]. The study of [2] also found no resolvable ε^{60}Ni variations in irons and pallasites. In contrast, using somewhat higher precision techniques and different normalising isotopes to correct for instrumental mass bias, Bizzarro et al. [3] reported deficits in ε ^{60}Ni and ε ^{62}Ni in most classes of differentiated meteorites compared to Earth, Mars and chondrites. Uniform deficits in ε^{60}Ni in these early formed differentiated meteorite samples led Bizzarro et al. to conclude that ^{60}Fe was injected into the Solar System ca. 1 Myr after its formation and when the planetesimals from which these meteorites originate had already accreted. ^{62}Ni deficits in the irons and pallasites were interpreted to reflect preservation of nickel nucelosynthetic anomalies on a planetesimal scale in the Solar System as has been demonstrated for Cr isotopes [3,4].

Precise and accurate measurement of Ni isotope ratios by multiple-collector inductively coupled plasma mass spectrometry (MC-ICPMS) is hampered by two factors that largely result from the small size of three of the nickel isotopes (61, 62 and 64). This makes it difficult to: (a) precisely measure ratios involving, in particular, ^{61}Ni due to both analytical noise during analyses and also the need to very precisely measure baselines; (b) be confident that small isobaric interferences do not compromise the accuracy of the Ni isotope data. Here, we describe analytical developments intended to improve MC-ICPMS techniques for precise and accurate Ni isotopic analysis and report preliminary data for Fe-Ni metal from irons and pallasites.

Analytical Methods:

Chemical separation of Ni. Fe-Ni metal was digested in 6M HCl. After centrifugation, the supernatant was subjected to a two-step column chemistry on columns loaded with 4 mL of Eichrom TEVA spec resin following the methods of [3]. In the first step Ni is eluted with 6M HCl and in the second step Ni is eluted with concentrated HCl. This chemistry results in > 99% recovery of Ni and effectively separates Ni from major constituents in the Fe-Ni metal like Fe and Co. However, we note that this chemistry results in small but significant amounts of ^{31}P from the Fe-Ni metal remaining in the Ni cut. We have analysed Ni separated from pallasite metal samples Esquel and Brenham, as well as Ni cuts for Esquel, Arispe and Mundrabilla that were analysed and reported in the study of [3].

Ni isotopic measurements by MC-ICPMS. Ni isotope ratios were measured on a Nu Plasma MC-ICPMS at Victoria University of Wellington. The Faraday collector used to measure ^{58}Ni was equipped with a 10^{10} Ohm resistor that allows larger 61 and 62 ion beams to be measured during analysis. Ni is introduced into the plasma via a desolvating nebuliser. Each measurement comprises 10 min of baseline acquisition and 20 min of data acquistion that is acquired in two blocks. Samples are bracketed by analyses of standards and data are reported in the epsilon or per mil notation as the difference from the average values of the two bracketing standards. Uncertainties on each analysis are calculated by incorporating that on the sample run with those from the bracketing standards. Our preferred normalisation scheme uses the ^{61}Ni/^{58}Ni ratio to correct for instrumental mass bias, although all other possible correction schemes are monitored to assess data integrity. Using this approach, single Ni isotope analyses have uncertainties (2 se) on mass-bias-corrected ε^{60}Ni and ε^{62}Ni that are typically $\leq \pm 0.13$ and $\leq \pm 0.25$, respectively (Fig. 1). Multiple analysis of samples results in uncertainties that are $< \pm 0.05$ and $< \pm 0.10$, respectively (Fig. 1). Uncertainties (2 se) on ^{62}Ni/^{58}Ni mass-bias-corrected ε^{60}Ni and ε ^{61}Ni are also $\leq \pm 0.05$ and $\leq \pm 0.10$, respectively. Some analyses were also carried out in pseudo-high resolution mode at a resolution of *ca*. 4000, which permits complete resolution of all interferences with the exception of Ni and Fe hydrides.

Fig. 1. ε^{60}Ni and ε^{62}Ni values of repeated Ni isotopic measurements (n = 9) of the IIICD iron Mundrabilla.

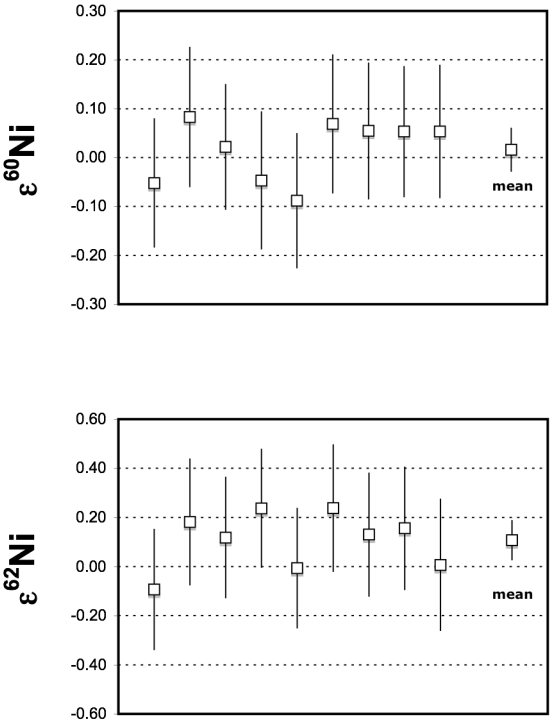

Preliminary Results: The meteorites studied here include Fe-Ni metal from two iron meteorites and two main group pallasites (PMG) (Table 1). The irons include examples that Hf-W isotopic systematics [5] suggest formed very early in the Solar System.

Selected Ni isotopic data are reported in Table 1. Nickel isotopes exhibit very limited variations compared to the terrestrial standard. ε^{60}Ni values range from +0.016 to -0.089 with Arispe having the most negative value that, given analytical uncertainties, is barely statistically resolvable from the analysis of Mundrabilla (+0.016). ε^{62}Ni values range from +0.107 to -0.042, although ε^{62}Ni values for all four irons and pallasites are identical within analytical uncertainty and yield a weighted average of all four samples of ε^{62}Ni = +0.060 ± 0.073. However, the two irons may have ε^{62}Ni values that are marginally higher (0.010 ε units) than the terrestrial standard.

Three separate digestions of metal from the pallasite Esquel including a sample prepared in Copenhagen whose results were published in [3] all produced statistically identical results. Several analyses of one of these digestions for Esquel were made in pseudo-high resolution mode with the results showing no significant difference from analyses made in low-resolution mode (Table 1).

Table 1 Preliminary Ni isotope data for irons and pallasites (# = measured at a mass resolution > 4000).

Sample	Type	δ^{61}Ni (± 2 se)	ε^{60}Ni (± 2 se)	ε^{62}Ni (± 2 se)	n
Arsipe	IC iron	-0.96 (0.07)	-0.089 (0.024)	+0.073 (0.035)	9
Mundrabilla	IIICD iron	+0.14 (0.03)	+0.016 (0.042)	+0.107 (0.077)	9
Brenham	PMG	-0.10 (0.18)	-0.021 (0.046)	-0.042 (0.128)	10
Esquel	PMG	0.21 (0.05)	-0.040 (0.037)	-0.005 (0.072)	24
Esquel#	PMG	0.09 (0.07)	+0.030 (0.044)	+0.046 (0.109)	6

Discussion: The preliminary results of this study differ from those for irons and pallasites recently published by [3], which reported a mean deficit for ε^{60}Ni = -0.024 and large negative ε^{62}Ni values up to -0.069 for irons and pallasites. Irrespective of which dataset is inaccurate or, indeed, whether both are inaccurate, it is clear given the levels of precision now obtainable that isobaric interferences during MC-ICPMS analysis can compromise the acquisition of accurate Ni isotope data and interpretations based on such data.

Taken at face value, the data produced in this study do not clearly reveal significant deficts in ^{60}Ni that might be attributed to a late (or early) supernova ^{60}Fe input into the young Solar System, or large ^{62}Ni variations in irons and pallasites that are significantly different from Earth that might represent preservation of Ni nucleosynthetic variability in these samples on a planetary scale in the Solar System. However, further work is necessary to assess if the accuracy of our data is comparable to the analytical precision, before such a simplistic interpretation can be considered.

References:

[1] Quitte G. et al. (2006) *Earth Planet. Sci. Lett. 242*, 16-25. [2] Cook D.L. et al. (2006) *Anal. Chem. 78*, 8477-8484. [3] Bizzarro M. et al. (2007) *Science 316*, 1178-1181. [4] Trinquier A. et al. (2007) *Ap. J. Lett. 655*, 1179-1185. [5] Markowski A. et al. (2006) *Earth Planet. Sci. Lett. 242*, 1-15.

CHRONOLOGY OF PRESOLAR SILICON CARBIDE: ASSESSING THE VIABILITY OF THE U-Th-Pb SYSTEM. J. N. Avila[1], T. R. Ireland[1], P. Holden[1], F. Gyngard[2], V. Bennett[1], Y. Amelin[1], E. Zinner[2]. [1]Research School of Earth Sciences and Planetary Science Institute, The Australian National University, Canberra ACT 0200, Australia. [2]Laboratory for Space Sciences and Physics Department, Washington University, St. Louis, MO 63130. janaina.avila@anu.edu.au; trevor.ireland@anu.edu.au; peter.holden@anu.edu.au; fmgyngar@artsci.wustl.edu; vickie.bennett@anu.edu.au, yuri.amelin@anu.edu.au; ekz@wustl.edu.

Introduction: Presolar grains are refractory phases that condensed at very high temperatures (1300-2000K) directly from the gas phase present in ancient stellar outflows, and thus became part of the interstellar medium from which our Solar System formed about 4.6×10^9yr ago. These grains can be recovered from primitive meteorites, and their study in the laboratory has provided new and complementary information to that commonly obtained by astronomers and astrophysicists on stellar nucleosynthesis, mixing in supernovae, galactic chemical evolution, dust formation in stellar environments, dust processing in the interstellar medium and formation of the Solar System [1; 2]. Constraints on the time of formation of presolar grains in stellar outflows before arriving in the solar nebula would be very useful, but obtaining chronological data on presolar grains is extremely difficult. This is because for many of the long-lived decay schemes, e.g. ^{87}Rb-^{87}Sr, the parent isotope does not condense at the high temperatures at which presolar grains form in stellar outflows. Secondly, the abundance of a particular radionuclide can be affected by a number of variables, such as the composition of the stellar outflows, the thermochemical behavior of the radionuclide under varying chemical and physical conditions of the stellar atmosphere, and its mechanism of incorporation into presolar grains. Finally, concentrations of potential chronometers are near the detection limit for most analytical techniques. However, depending on the stellar mass and metallicity of the grain's parent stars, presolar grains can incorporate trace amounts of U and Th, which can be used to trace r-process nucleosynthesis and serve as stellar chronometers. Once U and Th are incorporated into SiC grains, their isotope ratios will only be modified by their decay rates and their daughter isotopes of Pb build up in the grains and can potentially be detected. The utility of U-Th-Pb chronometry on presolar grains will depend on the concentration of the isotopes of these elements, precise measurements of their isotopic compositions, and the knowledge of their production ratios. Of prime importance is that measurable amounts of U, Th and Pb might exist in certain types of presolar grains.

X grains and supernovae: Type X SiC grains, which comprise ~1% of all presolar SiC [3], are believed to condense within expanding supernova ejecta [4]. The isotopic signatures of the X grains suggest deep and inhomogeneous mixing of matter from very different stellar zones in the SN ejecta [5]. The U and Th content of X grains will critically depend whether or not freshly synthesized r-process matter was available during grain formation. It is known that some isotopes formed only by r-process, such as ^{100}Mo, do not show the expected overabundance in X grains, a result that is not consistent with production in a canonical r-process [6]. The Mo isotopic pattern found by [6] in X grains can be successfully explained by a neutron-burst model [4]. However, there is still a possibility of incorporation of U and Th into type X SiC during their formation, and further ion implantation of heavy ions as the grains overtake the overlaying layers [7].

Mainstream grains and AGB stars: Mainstream grains, which comprise ~93% of all presolar SiC [8], are thought to have originated in the outflows of C-rich red giant stars during the asymptotic giant branch (AGB) phase of evolution [9]. Because U and Th are not synthesized in AGB stars, their content in mainstream SiC grains will reflect the composition of the precursor molecular cloud at the time of stellar formation, the decay of ^{238}U, ^{235}U and ^{232}Th during their stellar lifetime, and the time elapsed since grain formation. The U and Th isotopic compositions of AGB stars are not significantly modified by nucleosynthesis because most of the envelope material did not experience much neutron exposure.

Experimental considerations: U, Th and Pb are potentially present in measurable amounts in presolar SiC grains. However, the abundance of most heavy elements in presolar SiC is not known. The precise measurement of abundances and isotopic ratios of heavy elements in SiC grains presents a series of analytical challenges. First, SiC are usually very small (<20μm, with most of them being <1μm), hence single grain analysis is difficult. Secondly, the abundance of heavy elements, and in particular U, Th and Pb, in single grains is expected to be very low and close to the lower limit of detection of most current analytical methods. Third, background contributions from the substrate on which grains are analyzed, and also potential contamination of SiC acid residues by the meteorite matrix have to be considered. Finally, standards of SiC doped with heavy elements do not exist.

Here we propose to assess the potential of the U-Th-Pb system in presolar SiC grains using sensitive high-resolution ion microprobe (SHRIMP) measurements. SHRIMP is suitable for this task because: (i) it has high sensitivity, mass and spatial resolution, (ii) it enables a wide range of stable and radiogenic isotopes, plus trace elements, to be analyzed with precision, (iii) it has demonstrated capability in the measurement of U-Th-Pb systematics.

Our initial experiments will focus on "bulk" measurements of SiC grains. Depending on the results, single grain analysis of large SiC will also be attempted. Initial results will be presented at the meeting.

References:

[1] Zinner, E. (1998) *Annu. Rev. Earth Planet. Sci.*, 26, 147-188. [2] Nittler, L. R. (2003) *Earth Planet. Sci. Lett.*, 209, 259-273. [3] Amari, S., & Zinner, E.(1997) *in Astrophysical implications of the laboratory study of presolar materials*, eds. Bernatowicz, T., & Zinner, E., 287-305. [4] Meyer, B. S., Clayton, D. D., & The, L. S. (2000) *Astrophys. J.*, 540, L49-L52. [5] Zinner, E., Heinrich, D. H., & Karl, K. T.(2003) *in Treatise on Geochemistry* (Oxford: Pergamon), 1-33. [6] Pellin, M. J., et al. (2002) *Meteorit. Planet. Sci.*, 37, A115-A115. [7] Deneault, E. A. N., Clayton, D. D., & Heger, A. (2003) *Astrophys. J.*, 594, 312-325. [8] Meyer, B. S., & Zinner, E.(2006) *in Meteorites and the Early Solar System II*, eds. Lauretta, D. S., & McSween, H. Y. (Tucson: University of Arizona Press), 69-108. [9] Hoppe, P., & Ott, U.(1997) *in Astrophysical implications of the laboratory study of presolar materials*, eds. Bernatowicz, T., & Zinner, E., 27-58.

^{26}AL-^{26}MG DATING SOLID FORMATION AND PLANETESIMAL ACCRETION AND DIFFERENTIATION IN THE EARLY SOLAR SYSTEM

Joel A. Baker. School of Geography, Environment and Earth Sciences, Victoria University of Wellington, P.O. Box 600, Wellington, New Zealand (joel.baker@vuw.ac.nz).

Magnesium has three isotopes (24, 25, 26), one of which (^{26}Mg) can be produced by the short-lived decay of ^{26}Al ($t_{1/2}$ = 0.73 Myr; mean life = 1.05 Myr). Over 50 years ago, Urey [1] noted that ^{26}Al may have been an important heat source in the young Solar System. Some 20 years later, a series of reports documented the presence of ^{26}Mg excesses (and deficits) in calcium-aluminium-rich inclusions (CAIs), although it was not possible to unequivocally demonstrate that these were due to *in situ* decay of ^{26}Al and not the result of either natural mass fractionation or nucleosynthetic effects.

In 1977, Lee, Papanastassiou and Wasserburg [2] showed using thermal ionization mass spectrometry (TIMS) that excesses of ^{26}Mg in different minerals from an Allende CAI correlated with the Al/Mg ratios of the minerals. This yielded an initial ^{26}Al abundance of $(^{26}Al/^{27}Al_0) = (5.1\pm0.6)\times10^{-5}$ in CAIs, which are regarded as the oldest solids that formed in our Solar System. This work had three significant implications: (a) If ^{26}Al was distributed at levels comparable to CAIs throughout the young Solar System, any early formed planetesimals just a few km across would have rapidly melted, (b) It required a young nucleosynthetic event to have taken place in the vicintiy of the Solar System shortly before its formation and, (c) It provided the basic framework for the use of the ^{26}Al-^{26}Mg system as a chronometer to date meteoritic material. It is somewhat disconcerting that almost 30 years further on and despite the fact it is possible to measure the $(^{26}Al/^{27}Al_0)$ of CAIs with an order of magnitude better precision than [2], no consensus exists on the precise $(^{26}Al/^{27}Al_0)$ of CAIs. While the precise $(^{26}Al/^{27}Al_0)$ of CAIs has little bearing on the implications (a) and (b) above, it is an important consideration in establishing the age of meteoritic material with respect to CAIs.

Over the following two decades or so, most efforts to use the ^{26}Al-to-^{26}Mg chronometer focused on the application of *in situ* techniques (ion probe) to study CAIs and chondrules in undifferentiated or chondritic meteorites and, to a lesser extent, a search for the former presence of ^{26}Al in differentiated meteorites e.g., see reviews by [3,4]. While ion probe techniques (until recently) are inherently much less precise than TIMS and more recently applied multiple-collector inductively coupled plasma mass spectrometry (MC-ICPMS) techniques, they have the great advantage of being able to non-destructively analyse very small regions of high Al/Mg material (e.g., glass or feldspar) within chondrules and CAIs in chondrites.

These studies have shown that most CAIs from a range of chondrites contained live ^{26}Al at their time of formation with a so-called canonical abundance of ca. 4.5×10^{-5}, although some CAIs record no evidence for live ^{26}Al. Ion probe studies of chondrules from unequilibrated chondrites have generally shown that their initial $(^{26}Al/^{27}Al_0) \sim 1\times10^{-5}$, implying chondrule formation began ca. 1 Myr after the formation of CAIs and persisted for a further 2 Myr or more.

Despite the fact that ^{26}Al was postulated to be the dominant heat source for melting early formed planetesimals, most attempts to find excesses of ^{26}Mg in meteorites from differentiated planetesimals were fruitless. However, Srinivasan et al. [5] reported the presence of ^{26}Mg excesses in plagioclase from the eucrite Piplia Kalan, which yields an apparent age of ca. 4 Myr after CAI formation. However, the poor correlation between Al/Mg and δ^{26}Mg* indicated that this is a minimum age and that the Mg isotope system has experienced some degree of isotopic resetting. Using TIMS techniques, Nyquist et al. [6,7] subsequently demonstrated that ^{26}Mg excesses was present in both the unique eucrite Asuka 881394 and the angrites SAH99555 and D'Orbigny, corresponding to ages of ca. 4-5 Myr after CAI formation.

The advent of MC-ICPMS techniques in the past 10 years or so, has had the potential to revolutionize both the precision and breadth of application of the ^{26}Al-to-^{26}Mg chronometer to meteoritic material. Significant discoveries using MC-ICPMS technology in the past few years have included a highly precise isochron for bulk CAIs from CV chondrites, which apparently defines a $(^{26}Al/^{27}Al_0) = 5.85\times10^{-5}$ [8], which is somewhat higher than the "canonical" value. This value is consistent with less precise laser ablation MC-ICPMS studies of CAIs [9]. However, reinvestigation of CAIs from Allende has questioned [10] the revision of the Solar System initial ^{26}Mg abundance to this "super-canonical" value. I will present a substantial body of new ^{26}Al-^{26}Mg data for CAIs including that for aliquots of the CAIs studied in [10].

Importantly, the CAI isochron of [8] defined an initial ^{26}Mg abundance for CAIs that is lower than the terrestrial standard by an amount that is broadly consistent with the initial ^{26}Al abundance of CAIs and the Al/Mg ratio of the bulk Solar System. This apparently demonstrates that ^{26}Al was initially present in the material the Earth accreted from at levels broadly similar to that of CAIs.

MC-ICPMS studies of some bulk chondrules have shown that they have initial ^{26}Al values that approach those of CAIs [11,12], leading to the suggestion that at least some chondrule formation was contemporaneous with that of CAIs. However, in the absence of internal isochrons for such chondrules, it cannot be conclusively demonstrated that the initial ^{26}Al values recorded by such chondrules does not simply reflect inheritance of older material (e.g., remelting of CAI-like material during chondrule formation).

Further high-precision Mg isotope studies of basaltic meteorites from differentiated planetesials [13] identified small excesses in ^{26}Mg (ca. 0.01 to 0.05‰) that can be used to calculate model ages for the timing of planetesimal differentiation. This is based on the increase in ^{27}Al/^{24}Mg (ca. 2.0) that accompanies the formation of basaltic magmas as compared to the bulk Solar System ^{27}Al/^{24}Mg = 0.1. Samples of basaltic material from the eucrite, angrite and mesosiderite parent bodies have model ages that range from 2.5 to 4.0 Myr after CAI formation. In most cases, high Al/Mg phases like feldspar appear to record younger ages due to slow cooling and or thermal resetting after exinction of ^{26}Al. However, not all studies [14] have reproduced the small ^{26}Mg excesses reported by [13].

Using thermal modelling, these timescales for planetary melting or differentiation can be used to place constraints on planetary accretion, which can be shown to have occurred in the first million years of the Solar System. Thus ^{26}Al was the most plausible heat source for planetary melting in the young Solar System. These rapid timescales for accretion and differentiation of earliest formed planetesimals are broadly consistent with constraints from other short-lived chronometers like the ^{182}Hf-^{182}W system.

Most of these Mg isotope studies have been carried out using first-generation MC-ICPMS instruments. Recent analytical advances now make pseudo-high-resolution or true-high-resolution Mg isotopic analysis possible by MC-ICPMS. This enables resolution of potential isobaric interferences like CN^+ or doubly charged Ca, Ti or Cr that might otherwise potentially result in the acquisition of inaccurate data.

A variety of analytical tests using a new-generation MC-ICPMS instument are shown in Table 1 that demonstrate the potential accuracy and precision now obtainable for the Mg isotope system by MC-ICPMS. Analyses of standards with gravimetrically prepared ^{26}Mg excesses, and synthetic (Aristar) and natural standards (J11 olivine) subjected to ion exchange procedures show that it is possible to measure ^{26}Mg excesses and deficits with an accuracy and precision < 0.005‰. However, care is needed to avoid analytical artefacts that can produce inaccurate data [15].

Using this methodology we have measured Mg isotope ratios to high precision in olivine from four main group pallasites. These olivines have uniform ^{26}Mg deficits that can be used calculate a model age for olivine crystallization and diffusive isolation on the pallasite parent body of 1.05±0.12 Myr (^{26}Al/^{27}Al$_0$ = [2.16±0.24]x10^{-5}) after formation of calcium-aluminium-rich inclusions. ^{26}Mg deficit dating may open a plethora of high-precision dating opportunities of meteoritic material that formed in the first two million years of the Solar System. For example, it may be possible to precisely date differentiated meteorites with low Al/Mg like ureilites and aubrites, as well tiny fragments of olivine and orthopyroxene crystals from chondrites. Current sensitivities of MC-ICPMS instruments may allow dating of very small amounts of Mg-rich minerals (ca. 50 to 500 µg in size) and, if Mg isotope measurements on new generation TIMS instruments can achieve the type of precision obtainable for Sr isotopes, it may even be possible to reduce sample sizes by a further several orders of magnitude! However, application of ^{26}Mg deficit dating will require careful assessment of: (a) whether ^{26}Al was uniformly distributed and if Mg isotope heterogeneity existed in the young Solar System, (b) the potential cosmogenic effects on the Mg isotope system and, (c) the actual process(es) that the ^{26}Mg deficits might date.

Table 1 δ^{26}Mg*-δ^{25}Mg data of analytical experiments by high-resolution MC-ICPMS analysis.

Sample	δ^{26}Mg* (‰)	δ^{25}Mg (‰)	n
Aristar δ^{26}Mg* 0.01‰[1]	+0.0107±0.0052	-0.04±0.10	8
Aristar δ^{26}Mg* 0.03‰[1]	+0.0311±0.0069	-0.05±0.15	5
Aristar Mg anion-processed[1]	-0.0002±0.0062	-0.03±0.17	6
Aristar Mg cation-processed[1]	-0.0019±0.0049	-0.03±0.04	10
J11 anion-processed[2]	+0.0022±0.0040	-0.11±0.06	24
J11 cation-processed[2]	+0.0007±0.0053	-0.16±0.05	9
Main group pallasites[3]	-0.0155±0.0017		66

[1]measured vs pure Aristar Mg, [2]measured vs DSM-3, [3]measured vs J11 olivine (anion-processed)

References:

[1] Urey H.C. (1955) *PNAS 41*, 127-144. [2] Lee T. et al. (1977) *ApJ 211*, L107-110. [3] MacPherson G. et al. (1995) *Meteoritics 30*, 365-386. [4] McKeegan K.D. & Davis A.M. (2003) *Treatise of Geochemistry vol. 1*, 431-460. [5] Srinivasan G. et al. (1999) *Science 284*, 1348-1350. [6] Nyquist L. et al. (2003) *EPSL 214*, 11-25. [7] Nyquist L. et al. (2003) *LPS XXXIV*, Abstract #1338. [8] Thrane K. et al. (2006) *ApJ 646*, L159-L162. [9] Young E.D. et al. (2005) *Science 308*, 223-227. [10] Jacobson B. et al. (2007) *LPS XXXVIII,* Abstract #1491. [11] Galy A. et al. (2000) *Science 290*, 1751-1753. [12] Bizzarro M. et al. (2004) *Nature 431,* 275-278. [13] Bizzarro M. et al. (2005) *ApJ. 632,* L41-44. [14] Wiechert U. & Halliday A. N. (2007) *EPSL* 256, 360-371. [15] Schiller M. et al. (2007) *this conference.*

NICKEL ISOTOPE ANOMALIES IN METEORITES AND THE ^{60}Fe-^{60}Ni CLOCK. M. Bizzarro[1], J.-L. Birck[2], J. Chen[3], G. Huss[4], G. Lugmair[5], S. Mostefaoui[6], D. Papanastassiou[3], A. Shukolyukov[5], G. Quitté[7], S. Tachibana[8], M. Wadhwa[9].

[1]Geological Institute, University of Copenhagen, Copenahgen, Denmark. [2]Laboratoire de Géochimie et Cosmochimie, IPG, Paris, France. [3]JPL, Pasadena, CA 91109-8099, USA. [4]HIGP, University of Hawai'i at Manoa. [5]Scripps Institution of Oceanography, University of California, San Diego, La Jolla, CA 92093–0212, USA. [6]LEME, Muséum National d'Histoire Naturelle, Paris, France. [7]Laboratoire des Sciences de la Terre, ENS, Lyon, France. [8]Department of Earth and Planetary Science, University of Tokyo. [9]Center for Meteorite Studies, School of Earth and Space Exploration, Arizona State University, Tempe, AZ 85287, USA.

Introduction: With a half-life of ~1.5 Myr, the ^{60}Fe-^{60}Ni decay scheme is ideally suited for dating meteorites and planetary processes that occurred in the first 10 Myr of the solar system's evolution. Moreover, ^{60}Fe is efficiently produced only by stellar nucleosynthesis such that constraining the timing of its first appearance, intitial abudance and distribution can constrain models of solar system formation. Ni possesses two neutron-rich isotopes, ^{62}Ni and ^{64}Ni, believed to be produced through nuclear statistical equilibrium processes occurring in neutron-rich supernova ejecta [1]. Both excesses and deficits have been documented for iron-group neutron-rich isotopes (^{48}Ca, ^{50}Ti, ^{54}Cr, ^{62}Ni and ^{64}Ni) in normal and FUN Ca,Al-rich inclusions (CAIs) as well as in primitive and differentiated meteorites [2-4].

Initial solar system abundance of ^{60}Fe: Hints of ^{60}Fe in the solar system first came from excesses of ^{60}Ni (^{60}Ni*) in CAIs with an inferred initial solar system ^{60}Fe/^{56}Fe [$(^{60}Fe/^{56}Fe)_0$] value of ~1.5×10^{-6} [5]. However, the evidence that ^{60}Fe was present at time of CAI formation remains ambiguous, given the lack of correlation of ^{60}Ni* values with Fe/Ni ratios and the presence of anomalies in other Ni isotopes. The first clear evidence for live ^{60}Fe in the solar system was discovered in basaltic meteorites believed to have formed at the surface of the eucrite parent body (EPB; [6-7]). The inferred $(^{60}Fe/^{56}Fe)_0$ from these meteorites is low enough to be consistent with an initial solar system ^{60}Fe abundance resulting from long-term galactic nucleosynthesis [8]. However, this interpretation is hampered by the extended and complex thermal history of meteorites originating from the EPB [9]. Initial attempts to search for traces of ^{60}Fe in more pristine objects such as primitive chondrite meteorites using *in situ* methods (i.e., secondary ionization mass spectrometry; SIMS) were unsuccessful [10]. With continuous effort and improvement in analytical methods, clear evidence for the former presence of ^{60}Fe in chondritic components was reported in troilite and magnetite [11,12]. These minerals yielded inferred $(^{60}Fe/^{56}Fe)_0$ ratios ranging from (1-1.8) $\times 10^{-7}$ for sulfides from the Bishunpur and Krymka (LL3.1) chondrites [11] to ~10^{-6} for sulfides from Semarkona (LL3.0) [12]. Given that the ^{60}Fe-^{60}Ni systematics in sulfides can be easily disturbed by mild thermal metamorphism or aqueous alteration, recent attempts to determine the initial solar system abundance of ^{60}Fe have focused on silicate materials [13]. Ferromagnesian pyroxene-rich chondrules from Bishunpur and Semarkona yielded inferred $(^{60}Fe/^{56}Fe)_0$ ranging from $(2.2 \pm 1.0) \times 10^{-7}$ to $(3.7 \pm 1.9) \times 10^{-7}$. By applying the time difference of 1.5-2.0 Myr between formation of these chondrules and CAIs inferred from ^{26}Al-^{26}Mg systematics, a solar sytem $(^{60}Fe/^{56}Fe)_0$ of (5-10) $\times 10^{-7}$ is derived. This new estimate is inconsistent with the predicted steady state abundance of ^{60}Fe in the interstellar medium [8], and requires that a nearby stellar source interacted with the nascent solar system. Current models propose that either a supernova or a thermal pulsating asymptotic giant branch (AGB) star of intermediate mass produced and delivered ^{60}Fe to the solar system [13].

High-precision Ni isotopes measurements: With the advent of multiple collection inductively coupled plasma source mass spectrometry (MC-ICPMS) as well as second-generation thermal ionization mass spectrometry (TIMS), a number of laboratories have developed analytical protocols for high-precision measurements of Ni isotopes [14-18]. The precision and accuracy of these measurements, however, can be limited by the small size of three of the Ni isotopes, ^{61}Ni, ^{62}Ni and ^{64}Ni, with relative abundances of 1.1%, 3.6% and 0.9%, respectively. This is further exacerbated by the extensive number of potential isobaric interferences on the Ni mass array (~400) that may compromise the data. Currently, two approaches are taken to correct for instrumental mass bias during acquisition of the Ni isotope data. Some groups use the ^{62}Ni/^{58}Ni normalizing pair [14-16], while others use the ^{61}Ni/^{58}Ni ratio [17, 18]. Using the ^{62}Ni/^{58}Ni can provide better precision and accuracy given the higher natural abundance of ^{62}Ni, but the possible presence of nucleosynthetic anomalies at this mass may introduce biases in the ^{60}Ni/^{58}Ni data. Although the ^{61}Ni/^{58}Ni ratio may be potentially free of nucleosynthetic effects

[5], the intregrity of the data obtained using this normalization procedure is more easily compromised by the presence of any minor isobaric interferences, given the small natural abundance of ^{61}Ni.

Fossil ^{60}Ni* in CAIs? Re-investigations of Ni isotopes in CAIs [19] have confirmed the presence of correlated anomalies in ^{60}Ni and ^{62}Ni reported by [5]. Based on these data, a minimum solar system $(^{60}Fe/^{56}Fe)_0$ of 4.8×10^{-6} have been recently proposed [19], which is significantly higher than estimates derived from Bishunpur and Semarkona chondrules [13]. Two lines of evidence, however, suggest that the ^{60}Ni excesses present in CAIs may not record Fe/Ni fractionation at the time of CAI formation: (a) CAIs have subchondritic Fe/Ni ratios such that if these formed during the lifespan of ^{60}Fe, *deficits* in ^{60}Ni* should be observed, not excesses and (b) the ^{60}Ni* anomalies are not correlated with the Fe/Ni ratios. A tentative explanation is that ^{60}Ni excesses do not represent *in situ* decay of ^{60}Fe, but fossil ^{60}Ni* admixed to the CAI-forming reservoir. One of the required astrophysical environments for the nucleosynthesis of neutron-rich iron-group isotopes such as ^{48}Ca is the rare type Ia supernova having masses close to the Chandrasekar limiting mass [20]. These 'old' supernova sources produce ^{60}Fe, but no significant amount of ^{26}Al [21]. Therefore, admixing of this presolar component to the CAI-forming reservoir can generate correlated effects between ^{60}Ni* and neutron-rich iron group isotopes, without addition of ^{26}Al. In light of these caveats, we suggest that the CAI data may not accurately constrain the initial solar system abundance of ^{60}Fe.

Iron meteorites and pallasites: Recently published Ni isotope data for Fe-Ni metals and sulfides from iron meteorites and pallasites have yielded somewhat conflicting results. Using the ^{62}Ni/^{58}Ni for internal normalization, Quitté et al. [14] reported no ^{60}Ni anomalies at the ± 30 ppm level in Fe-Ni metals from iron meteorites, but significant correlated effects in ^{61}Ni and ^{60}Ni (up to ~1400 ppm) in co-existing sulfides, interpreted as nucleosynthetic anomalies. Cook et al. [15] and Chen et al. [16] reported no ^{60}Ni anomalies at the ± 20 ppm level for Fe-Ni metals. However, in contrast to [14], a normal Ni isotope composition was recently reported for sulfides from various irons by [16]. Using the ^{61}Ni/^{58}Ni for internal normalization, Bizzarro et al. [18] reported small deficits in ^{60}Ni of ~25 ppm with correlated effects on ^{62}Ni for Fe-Ni metals from iron meteorites and pallasites. Re-normalizing the data of [18] to ^{62}Ni/^{58}Ni yields a terrestrial ^{60}Ni composition to ±10 ppm and small resolvable ^{61}Ni excesses of ~30 ppm for these samples. We note that a preliminary report [17], using the same normalization procedure as [18] but with somewhat higher precision, also argues for the presence of widespread ^{62}Ni anomalies. Although there are contrasting systematics between the results obtained from several groups, the iron meteorite and pallasite data do not provide clear evidence for live ^{60}Fe at the time of Fe/Ni fractionation on their repective parent bodies.

Chondritic meteorites: Using the ^{62}Ni/^{58}Ni for internal normalization, Cook et al. [15] reported deficits in ^{60}Ni of ~25 ppm in metals separated from unequilibrated ordinary (OC) and carbonaceous chondrites (CC), including the well-dated Gujba chondrite [22]. If these reflect Fe/Ni fractionation from a chondritic reservoir during the lifespan of ^{60}Fe, the inferred $(^{60}Fe/^{56}Fe)_0$ at the time of Fe/Ni fractionation ranges from $(1.0\pm0.6) \times 10^{-6}$ to $(3.5\pm3.0) \times 10^{-6}$, which could be consistent with previous estimates based on Fe-Ni systematics in chondritic components [12,13]. Using the ^{61}Ni/^{58}Ni for internal normalization, Bizzarro et al. [18] reported a normal ^{60}Ni to ±15 ppm for bulk CC, OC and enstatite chondrites (EC), and small excesses in ^{62}Ni for CC, small deficits for OC, and normal ^{62}Ni for EC. These later results are in agreement with [17].

The SAH99555 angrite: With a well constrainted Pb-Pb age of 4564.55 ± 0.16 Myr [23], the SAH99555 angrite apparently provides a unique opportunity to anchor the ^{60}Fe-^{60}Ni system. Assuming a conservative solar system $(^{60}Fe/^{56}Fe)_0$ of 5×10^{-7}, crystallization of the SAH99555 angrite <5 Myr of CAIs would results in large excesses of at least 6 ε-units in the bulk samples. However, two different studies did not find the expected ^{60}Ni excesses, but reported either a terrestrial Ni isotope composition [24] or small ^{60}Ni and ^{62}Ni deficits [18]. Thus, these results are not consistent with estimates from Bishunpur and Semarkona chondrules.

Conclusion: Taken at face value, the currently available data for various meteorites does not provide compelling evidence for widespread distribution of ^{60}Fe in the early solar system and, therefore, does not support the chronological significance of the ^{60}Fe-^{60}Ni system. This could reflect either heteronegous distribution of ^{60}Fe in the solar system's parental molecular cloud or, alternatively, a late addition of ^{60}Fe to the protoplanetary disk.

References:: [1] Hartman, D. et al. (1985) *Apj* **297**: 837 [2] Birk, J.L. (2004) RMG 2, Vol. 55: 25. [3] Shukolyukov, A. & Lugmair, G. (2006) *EPSL* **250**:200 [4] Trinquier A. et al. (2007) *ApJ* 655:1179 [5] Birck, J-L. & Lugmair, G. (1989) *EPSL* **90**:141 [6] Shukolyukov, A. & Lugmair, G. (1993) *Science* **259**:1138 [7] Shukolyukov, A. & Lugmair, G. (1993) *EPSL* **119**:159 [8] Wasserburg, G. et al. (1996) *ApJ* **466**: L109 [9] Kleine, T. et al. (2005) *GCA* **231**: 41 [10] Kita, N. et al. (2000) *GCA* **64**: 3913 [11] Tachibana, S., & Huss, G. R. (2003) *ApJ* **588**: L41. [12] Mostefaoui, S. et al. (2005) *ApJ* **625**: 271 [13] Tachibana, S. et al. ApJ 639: L87 [14] Quitte , G. et al. (2006) *EPSL* **242**:16 [15] Cook, D.L. et al. (2006) *Anal. Chem.* **78**: 8477 [16] Chen, J. et al. (2007) *METSOC* #5165 [17] Regolous, M. et al. (2007) Goldschmidt conf. A815 [18] Bizzarro, M. et al. (2007) *Science* **316**: 1178 [19] Quitte , G. et al. (2007) *ApJ* **655**:678 [20] Clayton, D.D. (2003) Cambridge University Press, 314 p. [21] Meyer, B.S. & Clayton, D.D. (2000) *Space Science Reviews* **92**: 133 [22] Krot, A.N. et al. (2005) *Nature* **436**: 989 [23] Connelly, J.C. et al. (2007) *GCA* submitted [24] Quitte , G. et al. (2007) LPSC XXXVIII # 1900.

PETROFABRICS IN A CHONDRULE RIM – EVIDENCE FOR A NEBULA ORIGIN. P. A. Bland[1,2], L. E. Howard[2], D. J. Prior[3], J. Wheeler[3], S. M. Hammond[1] & S. H. Gordon[1], [1]Impacts & Astromaterials Research Centre (IARC), Department of Earth Science and Engineering, South Kensington Campus, Imperial College London SW7 2AZ, UK (p.a.bland@imperial.ac.uk); IARC, Department of Mineralogy, Natural History Museum, London SW7 5BD, UK; [3]Department of Earth Sciences, University of Liverpool, 4 Brownlow Street, Liverpool L69 3GP, UK.

Introduction: The description and interpretation of petrofabrics is a fundamental aspect of geology. Although chondritic meteorites are the most primitive rocks available to us, due to the abundance of fine-grained matrix they have largely resisted traditional fabric analysis. Magnetic susceptibility, natural remanent magnetisation, and X-ray pole figure goniometry studies of bulk meteorites *(1-4)* have revealed that many chondrites contain petrofabrics. But the fabrics themselves are only observed *in situ* in the preferred orientation of large (>100s µm) components e.g. non-spherical chondrules *(1,5-8)*, lithic fragments *(9)*, and large isolated grains *(10)*. We have used electron backscatter diffraction (EBSD) in a field emission gun scanning electron microscope to map the orientation of fine-grained materials in Allende, and quantify petrofabrics in this meteorite.

Results: We used automated EBSD maps (see *(11)* for details) with 50-200nm step sizes to reconstruct FGR microstructures around an Allende chondrule; grain orientation data (typically comprising several hundred thousand data points, and 300-1200 grains) were extracted from these maps. Earlier EBSD mapping has shown that matrix material in Allende possesses a planar fabric defined by a preferred orientation in the *a*-axis of fayalite grains 100nm - µm's in size *(11,12)*. This short-axis fabric is coherent over cm-scales *(11,12)*. The FGR also exhibits a short *a*-axis orientation in fayalite grains, but in this case the fabric is spherically symmetric, centred on the chondrule (Figure 1). Sub- µm to µm-scale fayalitic olivine laths effectively 'tile' the chondrule.

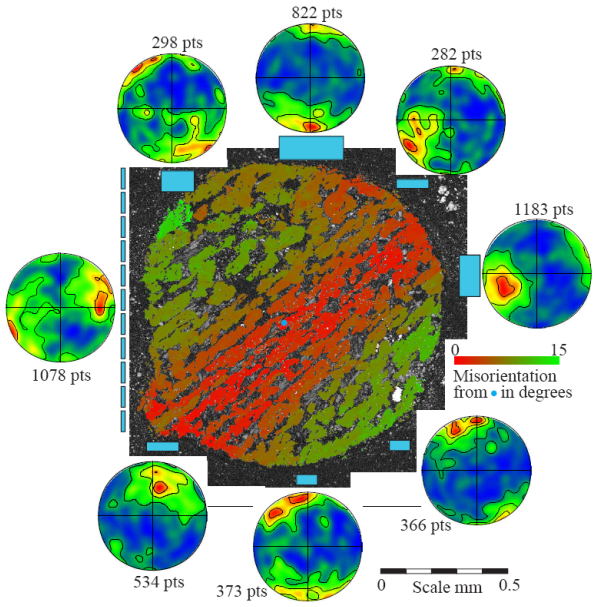

Within the mapped areas restoration of fabrics to give random orientations requires compaction by a factor of 2. In addition, the strength of the observed fabric varies by <9% over the entire rim, suggesting an absence of strain shadows.

Interpretation: Magnetic susceptibility anisotropy in Allende *(4)* was interpreted as arising from a preferred orientation of a matrix component, acquired during uniaxial compaction of matrix grains (either during accretion of the parent body, or through a subsequent impact). Our earlier observations of a sample-scale short-axis fabric are entirely consistent with uniaxial compression within a parent body *(11)*.

In contrast to the matrix petrofabric, the spherically symmetric chondrule rim fabric is not consistent with uniaxial compression within a meteorite parent body: both the known properties of chondrule rims, and the specific nature of the fabric we observe, indicate that the rim fabric was emplaced in a nebula setting. Chondrule rims are generally considered to have formed prior to the incorporation of chondrules in meteorite parent bodies, with rim particles accreting onto chondrules soon after their formation in the protoplanetary disk. Thus, rims are commonly referred to as 'accretionary rims'. In Allende, there is a clear relationship between the radius of the chondrule and the thickness of the FGR *(13)*, suggesting an accretionary origin. Oxygen isotopic studies of accretionary rims around CAIs in CV chondrites find substantial heterogeneity in rim materials, indicating that a pre-accretionary signature has survived subsequent parent body processing *(14)*. Similarly, analysis of trace element abundances in FGRs from Mokoia indicate an accretionary origin, and multiple dust reservoirs *(15)*. Finally, preliminary trace element analyses of chondrule and CAI FGRs in CVs by LA-ICP-MS suggests they have distinct compositions, supporting an accretionary origin *(16)*. If the FGR is accretionary, it is reasonable to conclude that the rim fabric may also have arisen during accretion of the rim.

We observe a fabric in fine-grained rim materials that is spherically symmetric around the chondrule. This would imply a spherically symmetric stress field acting on rim particles either before or after they accreted onto the chondrule. It is difficult to envisage how such a field could occur within an asteroid. Spherically symmetric fabrics have not been described in terrestrial rocks, where the most common principal stress field is uniaxial. However, they may well be present in situations where nodules, concretions, or porphyroblasts have grown in a mass of finer grained material – volume change during growth should produce a compaction fabric in the surrounding material. Clearly, this does not apply in the case of chondrules and rims. It has been sug-

gested that rims in CM chondrites were formed by compaction of high-porosity matrix against comparatively incompressible chondrules and CAIs during multiple impact events, followed by regolith gardening *(17)*. While we cannot comment on the CM chondrites, it would appear to be more difficult to apply this model to Allende. Allende possesses a uniform, planar, short-axis alignment fabric that is pervasive on a cm-scale and likely the result of a single major deformational shortening event *(12)*. Our chondrule+FGR (with a spherically symmetric fabric) is therefore embedded within a matrix that shows a fabric consistent with uniaxial compression. In addition, dark inclusions in Allende possess fabrics that are conformable with the broader matrix fabric, and strain shadows are observed in matrix close to parts of the inclusion margins - analogous to augen in terrestrial rocks *(12)*. Strain shadows are absent in our FGR. These observations suggest that the chondrule acquired a FGR, it was compacted prior to accretion, chondrule+FGR were accreted with high-porosity matrix (and DIs), and the whole was then subjected to a major uniaxial compressive event.

It is likely that chondrule rims initially accreted with extremely high porosity *(18)*. Yet, accretionary rims in primitive meteorites have rather low porosity (~20%). In addition, they were robust enough to survive accretion onto meteorite parent bodies, as well as any regolith processing that occurred prior to final burial and compaction. Modelling of collisions between fluffy aggregates *(19)* found that with low collision energies clusters will stick and attach at their first point of contact, just as two monomers would, forming a larger cluster. With larger collision energies, the aggregates restructure, and become more compact. This process proceeds to greater degree and density, until some disruption threshold energy is reached. In addition, triboelectric charging effects *(20,21)* might play a role, potentially increasing the disruption threshold. In modelling the process of rim formation, Cuzzi *(22)* found that restructuring of fluffy aggregate rims starts at impact velocities of ~10 cm⁄sec, with maximum compaction near ~50 cm⁄sec, and disruption beginning >300 cm⁄sec. Could our rim fabric have formed by compaction of a high-porosity rim in the nebula as new rim materials were accreted *(22)*? This mechanism would certainly be consistent with the observed rim fabric. While each individual impact on a porous rim would produce local uniaxial compression, the time-integrated result of multiple impacts would be spherically symmetric compression.

Conclusion: The origin of Allende matrix components remains a matter of debate. Certainly, analyses of Allende matrix chemistry do not provide evidence for a secondary origin *(23-25)*. But whether the fayalitic olivine that dominates matrix was formed in a nebula or asteroidal setting, the most straightforward interpretation of our data is that the fabric now delineated by rim fayalites was imposed in the nebula. This clearly favours a nebula origin for fayalitic olivine, but does not necessarily preclude asteroidal formation. If fayalitic olivine was produced by an asteroidal process, our data do place constraints on the nature of that alteration. It would suggest that alteration must have been topotactic – replacement of the primary mineral without substantially disturbing the original crystal structure, with widespread inheritance of structural polymers by the weathering product. This type of alteration is frequently observed in terrestrial samples *(26-29)*. In the context of Allende, such a process could allow a primordial fabric to be preserved by a secondary mineralogy. But whatever the origin of fayalitic olivine, the observation of a spherically symmetric chondrule rim fabric seems to require that primordial rim grains must have been crystalline and tabular - irregular amorphous materials would not be oriented by compaction

References: [1] D.S. Sneyd et al., *Meteoritics 23,* 139-149 (1988). [2] S.J. Morden, D.W. Collinson, *EPSL 109,* 185-204 (1992). [3] A. Fujimura (1983) *EPSL 66,* 25-32. [4] N. Sugiura et al., *Lunar Planet. Sci.* 16, 831-832 (1985). [5] R.T. Dodd, *Icarus 4,* 308-316 (1965). [6] P.M. Martin et al., *Nature 252,* 37-38 (1975). [7] P.M. Martin, A.A. Mills, *EPSL 51,* 18-25 (1980). [8] P.M. Cain et al., *EPSL 77,* 165-176 (1986). [9] R.C. Greenwood et al., *Meteoritics 28,* 357-358 (1993). [10] T.V.V. King et al., *Meteoritics 13,* (abstract) 517-518 (1978). [11] P.A. Bland et al., *MAPS* 38, A100 (2003). [12] L.E. Watt et al., *MAPS* 41, 989-1001 (2006). [13] J. M. Paque, J. N. Cuzzi, *Lunar Planet. Sci.* 28, 71 (1997). [14] M. Cosarinksy, L. A. Leshin, In *Workshop on Chondrites and the Protoplanetary Disk*, abstract #9025 (2004). [15] X. Hua et al., *GCA* 60*,* 4265-4274 (1996). [16] S. J. Hammond (unpublished data) (2007). [17] J. M. Trigo-Rodriguez et al., *GCA* 70, 1271-1290 (2006). [18] J. Blum, G. Wurm, *Icarus* 143, 138-146 (2000). [19] C. Dominik, A. G. G. M. Tielens, *Astrophys. J.* 480, 647-673 (1997). [20] S. Desch, J. N. Cuzzi, *Icarus 143*, 87–105 (2000). [21] J. Marshall, J. N. Cuzzi *Lunar Planet. Sci.* 32, #1262 (2001). [22] J. N. Cuzzi, *Icarus*, 484-497 (2004). [23] M. Inoue et al., *MAPS* 39, 599-608 (2004). [24] P. A. Bland et al., *PNAS* 102, 13755-13760 (2005). [25] S. H. Gordon et al., *Lunar Planet. Sci.* 32, #1338 (2007). [26] R. A. Eggleton, *Clays Clay Min.* 32, 1-11 (1984). [27] K. L. Smith et al., *Clays Clay Min.* 35, 418-428 (1987). [28] J. F. Banfield et al., *Contrib. Mineral. Petrol.* 106, 110-123 (1990). [29] M. F. Hochella Jr., J. F. Banfield, In *Chemical Weathering Rates of Silicate Minerals* (eds. A. F. White and S. L. Brantley), pp 353-406. Min. Soc. Am., Washington, D. C., USA (1995).

TRIGGERING PRESOLAR CLOUD COLLAPSE AND INJECTION OF SHORT-LIVED RADIOISOTOPES WITH AN OUTFLOW FROM A MASSIVE STAR. A. P. Boss[1], S. I. Ipatov[1], & E. A. Myhill[2], [1]DTM, Carnegie Institution, Washington DC [2]Marymount University, Arlington VA.

Short-lived radioisotopes (SLRI) such as ^{26}Al and ^{60}Fe were alive at the time that primitive meteorites formed and are often thought to have been synthesized in a supernova [1,2,3,4] and then either injected into the presolar cloud [5,6] or onto the surface of the solar nebula [7]. Recently it has been proposed that the outflow from a massive Wolf-Rayet star may have been the source of the ^{26}Al [8], and that the ^{60}Fe was the result of the subsequent supernova explosion of the massive star. We consider here triggering the collapse of the presolar cloud and simultaneously injecting SLRI with a shock front derived from either a Wolf-Rayet star wind or a supernova. Previous work on this problem [5,6,9,10,11] used either fixed grid or smoothed particle hydrodynamics (SPH) codes with a limited ability to resolve fine scale structure in the Rayleigh-Taylor fingers that form at the shock/cloud interface and are responsible for SLRI injection into the collapsing presolar cloud [10]. Here we study the same problem with a new code, FLASH.

FLASH is based on adaptive mesh refinement (AMR) by the block-structured adaptive grid approach. AMR techniques automatically insert new grid points in regions of strong physical gradients, and remove them in regions without strong gradients, in order to maximize the spatial resolution in the crucial regions while minimizing the computational burden. Advection is handled by the piecewise parabolic method (PPM). PPM includes a Riemann solver at cell boundaries that handles shock fronts exceptionally well. In FLASH, PPM is incorporated in a form that is second-order accurate in space and time. The Poisson equation for the cloud's gravitational potential is solved by either a multipole or multigrid technique. We have tested the FLASH code's ability to reproduce the results of several different test cases that are relevant to the problem of triggering cloud collapse, namely the Sod shock tube problem and the collapse of a pressureless sphere. We have also used FLASH to verify the long-term stability of the target cloud in the absence of a triggering shock front.

We have reproduced the main results of [9,10] in 2D cylindrical coordinates with isothermal thermodynamics and a range of shock speeds (2 to 40 km/s), finding that shocks with speeds in the range of 5 to 30 km/s are able to both trigger collapse and inject shock wave material. The figures on the next page show the results for a 30 km/sec shock. Given that Wolf-Rayet star winds and supernova shocks both are launched with shock speeds on the order of 10^3 km/sec, these shock fronts can only trigger collapse after they have travelled some distance (typically about 10 pc) and been slowed down to 30 km/sec or less by snowplowing intervening interstellar cloud gas and dust.

We have now extended these isothermal runs to 3D Cartesian coordinates to learn what happens in a fully 3D cloud. To date the 3D calculations are similar to the 2D calculations, though the enormously increased computational burden associated with adding the third dimension has limited the number of grid points that can be employed, even with the FLASH code. We next intend to study nonisothermal shocks. [11] found that when nonisothermal shocks were employed in SPH calculations, it was not possible for a shock wave to simultaneously trigger collapse and inject SLRIs, a potentially fatal flaw for the triggering and injection scenario. However, [12] found that improvements in the dust grain cooling model led to rapid post-shock cooling, closer to the isothermal assumptions used in [5,6,9,10]. Our ultimate goal is to use FLASH to determine if the triggering and injection scenario [13] is consistent with post-shock cooling processes.

The software used in this work was in part developed by the DOE-supported ASCI/Alliances Center for Astrophysical Thermonuclear Flashes at the University of Chicago.

References: [1] Mostefaoui, S., Lugmair, G. & Hoppe, P. 2005. Ap. J., 625, 271. [2] Tachibana, S. *et al.* 2006. Ap. J., 639, L87. [3] Limongi, M. & Chieffi, A. 2006. Ap. J., 647, 483. [4] Sahijpal, S. & Soni, P. 2006. MAPS, 41, 953. [5] Vanhala, H. A. T. & Boss, A. P. 2000. Ap. J., 538, 911. [6] Vanhala, H. A. T. & Boss, A. P. 2002. Ap. J., 575, 1144. [7] Ouellette, N., Desch, S. J., & Hester, J. J. 2007. Ap. J., 662, 1268. [8] Bizzarro, M. *et al.* 2007. Science, 316, 1178. [9] Foster, P. N. & Boss, A. P. 1996. Ap. J., 468, 784. [10] Foster, P. N. & Boss, A. P. 1997. Ap. J., 489, 346. [11] Vanhala, H. A. T. & Cameron, A. G. W. 1998. Ap. J., 508, 291. [12] Vanhala, H. A. T. & Boss, A. P. 1999. Abstract #1433. 30th LPSC. [13] Boss, A. P. 1995. Ap. J., 439, 224.

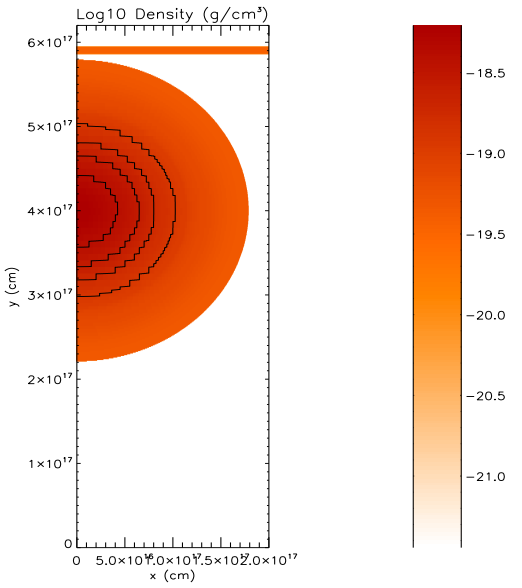

time = 0.000 ps
number of blocks = 1837, AMR levels = 5

/home/flash/FLASH2.5/objectp-combined-v30-5-bs/dustcoll_hdf5_chk_0000

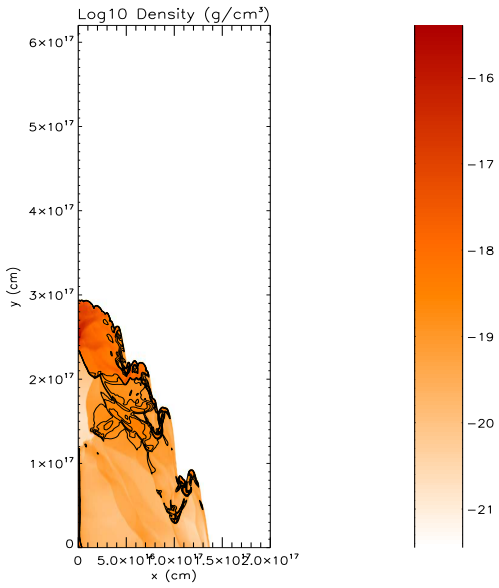

time = 73697.008 years
number of blocks = 2173, AMR levels = 5

/home/flash/FLASH2.5/objectp-combined-v30-5-bs/dustcoll_hdf5_chk_0075

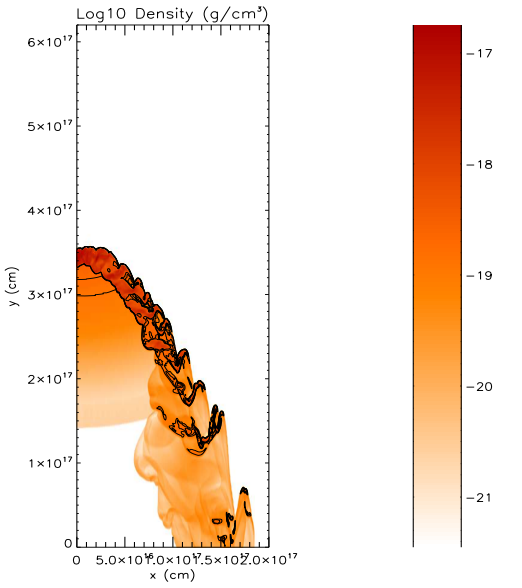

time = 49006.805 years
number of blocks = 2809, AMR levels = 5

/home/flash/FLASH2.5/objectp-combined-v30-5-bs/dustcoll_hdf5_chk_0050

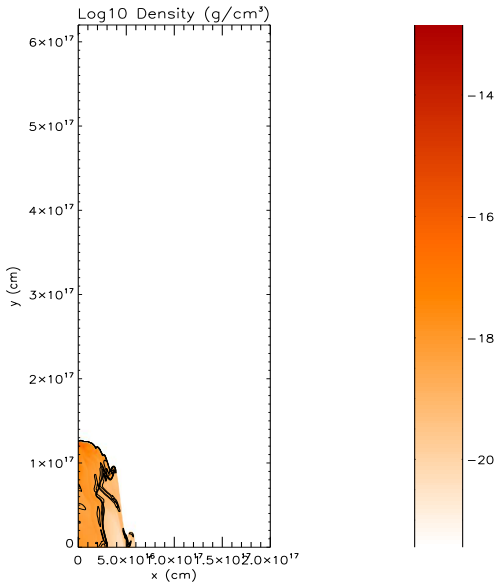

time = 118001.656 years
number of blocks = 553, AMR levels = 5

/home/flash/FLASH2.5/objectp-combined-v30-5-bs/dustcoll_hdf5_chk_0120

AN APPRAISAL OF ^{207}Pb-^{206}Pb AND ^{26}Al-^{26}Mg CHRONOLOGIES IN CAIs AND CHONDRULES. A. Bouvier and M. Wadhwa, School of Earth and Space Exploration, Arizona State University, Tempe, AZ, 85287, USA. Email: Audrey.Bouvier@asu.edu.

Introduction: Precise and accurate radiometric dating of chondrites and their components (CAIs, chondrules and matrix minerals) sheds light on the processes and timescales for events occurring in the protoplanetary disk. Analytical improvements associated with new laboratory procedures (i.e., ultra-low blanks, high yields) and mass spectrometry (MC-ICPMS, TIMS, SIMS) over the last decade have extended dramatically the capabilities for obtaining ages with high (typically, sub-My) precision with both long-lived (e.g., ^{207}Pb-^{206}Pb) and extinct (e.g., ^{26}Al-^{26}Mg, ^{53}Mn-^{53}Cr, ^{182}Hf-^{182}W) isotopic systems. While many precise and concordant dates have been obtained by using different clocks on similar objects, there are also some discrepancies [1]. Some possible explanations for such discrepancies may be as follows: (i) the parent radionuclide may not have been homogeneously distributed in the meteorite-forming region of the protoplanetary disk; (ii) the chronometers under consideration may have distinctly different closure temperatures such that some chronometers may have closed at resolvably different times than others in the same sample; (iii) secondary processes, such as thermal and/or shock metamorphism and aqueous alteration, may have disturbed the isotopic systematics to different degrees; (iv) uncertainties in the initial isotopic composition of the daughter element and in the decay constant may also introduce some discrepancies between high-resolution chronometers.

In the following we provide an appraisal of the high-resolution ages of CAIs and chondrules provided by the ^{207}Pb-^{206}Pb and ^{26}Al-^{26}Mg chronometers. In particular, we discuss some of the discrepancies that currently exist and how these may be resolved in the future.

CAI and chondrule dating: Some of the most important issues in cosmochronology relate to the age of the Solar System (estimated from the formation age of the oldest known solids, the CAIs) and the timescales of events occurring in the protoplanetary disk (estimated from the formation ages of chondrules).

While some of the extinct chronometers yield model ages as old as 4568 to 4570 Ma for the start of the Solar System [2-4], the first precise Pb-Pb age from two inclusions from the CV3 chondrite Efremovka gave a somewhat younger age of 4567.2 ± 0.6 Ma, recently revised to 4567.1 ± 0.2 Ma [5, 6]. New Pb isotope analyses of CV3 Allende CAIs, considered along with previous results for the Efremovka E60 inclusion [5], give an absolute age of 4568.5 ± 0.5 Ma for CAI formation [7]. There is therefore an apparent discordance of ~1.4 My between the estimates of Amelin [6] and Bouvier et al. [7] for the formation age of CAIs. In contrast, Al-Mg chronometry gives a relatively short time interval for CAI formation (i.e., on the order of a few 10s of Ky [8, 9]).

Most previous studies of Al-Mg systematics in chondrules of unequilibrated chondrites indicate that these were formed ~1-3 My after CAIs [10]. Nevertheless, Al-Mg model ages of bulk chondrules may indicate that chondrule formation may have begun contemporaneously with CAI formation [11]. Pb-Pb ages obtained thus far for chondrules vary from ~4567 to 4562 Ma [5, 12, 13], with the youngest age (for chondrules from the Gujba CB chondrite) possibly reflecting formation during impact between planetary embryos [13].

Pb-Pb systematics. The most precise CAI age of 4567.1 ± 0.2 Ma was obtained from radiogenic fractions of E60 (a forsterite-bearing type-2 CAI) with the highest measured ^{206}Pb/^{204}Pb ~2260 [6]. Such radiogenic Pb isotopic compositions were obtained by utilizating an extensive leaching procedure to remove terrestrial and chondritic common Pb. Small amounts of Pb (50-500 picograms) in the most radiogenic fractions were measured using the double-spike technique by TIMS [6]. However, since Efremovka is thought to have experienced a severe shock history [14], it is possible that the U-Pb system in some of the E60 fractions may have been affected by shock metamorphism.

The CAI age of Bouvier et al. [7] was obtained by isotope analyses of Pb (5-8 nanograms) in Allende CAI fractions by MC-ICPMS using the Tl doping method to correct for mass fractionation [15]. This study reported less radiogenic isotope compositions (^{206}Pb/^{204}Pb ~59-80) due to a milder leaching procedure employed (to avoid differential dissolution of CAI phases). The best estimate of the CAI formation age of 4568.5 ± 0.5 Ma in this study was obtained by considering the three Allende CAI fractions [7] along with the seven clear and white fragments of the Efremovka E60 (with ^{207}Pb*/^{206}Pb* ages between ~4567.2 and ~4569.0 Ma) [5]. This is consistent with the Hf-W age of Allende CAIs [4] and with model ages of Solar System formation from other extinct chronometers.

It is clearly important in Pb isotope analyses of CAIs to remove as much of the common Pb component as possible so as to minimize the uncertainties resulting from the subtraction of an assumed common Pb composition [16]. Nevertheless, the assumption that there is no isotope fractionation during leaching needs to be more rigorously evaluated, and we plan to test

this with further experiments. Furthermore, it is also recognized that the CAIs analyzed thus far are from chondrites (i.e., Efremovka and Allende) that have experienced a complex secondary alteration history. It will therefore be important to analyze CAIs from other primitive chondrites that are less severely affected by such secondary processing.

Al-Mg systematics. While it has been demonstrated that there were Cr and Ni isotopic heterogeneities in the protoplanetary disk which may complicate the interpretation of ages obtained from the ^{53}Mn-^{53}Cr and ^{60}Fe-^{60}Ni short-lived chronometers [17, 18], the ^{26}Al-^{26}Mg system appears to be free from such complications and there is evidence that ^{26}Al was homogeneously distributed in the meteorite-forming region of the protoplanetary disk [8]. However, estimations of the timescales over which CAIs and chondrules were formed are dependant of the initial value of ^{26}Al/^{27}Al for the Solar System, and this issue is currently under debate. Until recently, the best estimate for the initial ^{26}Al/^{27}Al ratio for the Solar System was the canonical value of ~5 × 10^{-5} [19]. However, more recent (high precision MC-ICPMS and SIMS) analyses indicate that this value may be higher (i.e., ~6 × 10^{-5}; [8, 9, 20]). It is possible that the higher initial value may represent the value for the solar system at the time of Al/Mg fractionation in CAI precursor materials, whereas the near-canonical value (commonly obtained from mineral phases within CAIs by SIMS) could represent the value at the time of isotopic closure of the Al-Mg system in CAIs. However, such an explanation may be problematic given more recently reported results. Specifically, MC-ICPMS analyses of microdrilled samples of CAIs (fine-grained and igneous) from four carbonaceous chondrites yielded a highly precise initial ^{26}Al/^{27}Al ratio of (5.85 ± 0.05) × 10^{-5} [8]. However, more recent analyses of fragments of Allende CAIs (also by MC-ICPMS) gave an initial ^{26}Al/^{27}Al ratio of (4.90 ± 0.28) × 10^{-5}, similar to the earlier canonical value [21]. While it is possible that sampling issues (i.e, whether the samples being analyzed represent true "bulk" compositions or if they are dominated by a particular mineral phase) may be the cause of this apparent discrepancy, it is clear than this cannot be resolved without further high-precision analyses of well-characterized CAIs (bulk samples and clean individual mineral phases) from relatively pristine primitive chondrites.

Conclusion: ^{207}Pb-^{206}Pb and ^{26}Al-^{26}Mg chronometers in CAIs and chondrules show a number of inconsistencies that need further investigation. These will be addressed with future high-precision analyses of both Pb-Pb and Al-Mg isotope systematics in the same bulk samples and mineral separates from CAIs and chondrules separated from primitive chondrites with minimal secondary alteration.

References: [1] Wadhwa M. et al. (2007) *Workshop on the Chronology of Meteorites and the Early Solar System,* submitted. [2] Lugmair G.W. and Shukolyukov A. (1998) *Geochim. Cosmo. Acta, 62,* 2863-2886. [3] Zinner E. and Göpel C. (2002) *Meteoritics & Planet. Sci., 37,* 1001-1013. [4] Burkhardt C. et al. (2007) *Meteoritics & Planet. Sci., 42,* Abstract #5189. [5] Amelin Y. et al. (2002) *Science, 297,* 1679-1683. [6] Amelin Y. et al. (2006) *LPS XXXVII,* Abstract #1970. [7] Bouvier A. et al. (2007) *Geochim. Cosmo. Acta, 71,* 1583-1604. [8] Thrane K. et al. (2006) *Astro. Phys. J., 646,* L159-L162. [9] Young E.D. et al. (2005) *Science, 308,* 223-227. [10] Kita N.T. et al. (2005) In *Chondrites and the Protoplanetary Disk,* Eds. A. N. Krot, E. R. D. Scott and B. Reipurth, pp. 558-587. [11] Bizzarro M. et al. (2004) *Nature, 431,* 275-278. [12] Amelin Y. et al. (2004) *Geochim. Cosmo. Acta, 68,* A759. [13] Krot A.N. et al. (2005) *Nature, 436,* 989-992. [14] Scott E.R.D. et al. (1992) *Geochim. Cosmo. Acta, 56,* 4281-4293. [15] Albarède F. et al. (2004) *Geochim. Cosmo. Acta, 68,* 2725-2744. [16] Amelin Y. (2006) *Meteoritics & Planet. Sci., 41,* 7-17. [17] Trinquier A. et al. (2007) *Astro. Phys. J., 655,* 1179-1185. [18] Bizzarro M. et al. (2007) Science, 316, 1178-1181. [19] MacPherson G.J. et al. (1995) *Meteoritics, 30,* 365-386. [20] Taylor D.J. et al. (2005) *LPS XXXVI,* Abstract #2121. [21] Jacobsen B. et al. (2007) *LPS XXXVIII,* Abstract #1491.

MODELING THE THERMOPHYSICAL AND DYNAMICAL EVOLUTION OF SATURN'S ICY SATELLITES. J. C. Castillo-Rogez[1], D. L. Matson[1], T. V. Johnson[1], C. Sotin[1,2], J. I. Lunine[1,3], (1) Jet Propulsion Laboratory, California Institute of Technology, 4800 Oak Grove Drive, Pasadena, CA 91109. (2) UMR – CNRS 6112 Laboratoire de planétologie et géodynamique de Nantes, 2, rue de la Houssinière, 44322 Nantes Cedex 3, France. (3) Lunar and Planetary Lab, 1629 E. University Blvd. Tucson, AZ 85721-0092.

This poster describes our methodology for modeling the simultaneous geophysical and dynamical evolution of the icy satellites of Saturn. For each of the model's modules we identify the relevant physical, chemical, mineralogical, and material science principals that are used. Then we present the logic of the modeling approach and its implementation. The main modules handle thermal, geological, and dynamical processes. Key parameters such as temperature, thermal conductivity, rigidity, viscosity, Young's modulus, tidal Love number k_2, and frequency-dependent dissipation factor $Q(\omega)$ are transmitted between the modules in the course of calculating an evolutionary sequence. Important initial conditions include volatile and nonvolatile compositions, formation time, rotation period and shape, orbital eccentricity and semimajor axis, and temperature and porosity profiles. The thermal module treats the thermal effects of accretion, melting of ice, differentiation and tidal dissipation. Heat transfer is by conduction only because in the cases thus far studied the criterion for convection is not met. The geological module handles the evolution of porosity, shape, and lithospheric strength. The dynamical module calculates despinning and orbital evolution. Chief outputs include the orbital evolution, the interior temperatures as a function of time and depth, and other parameters of interest such as k_2, and $Q(\omega)$ as a function of time.

FIGURE 1

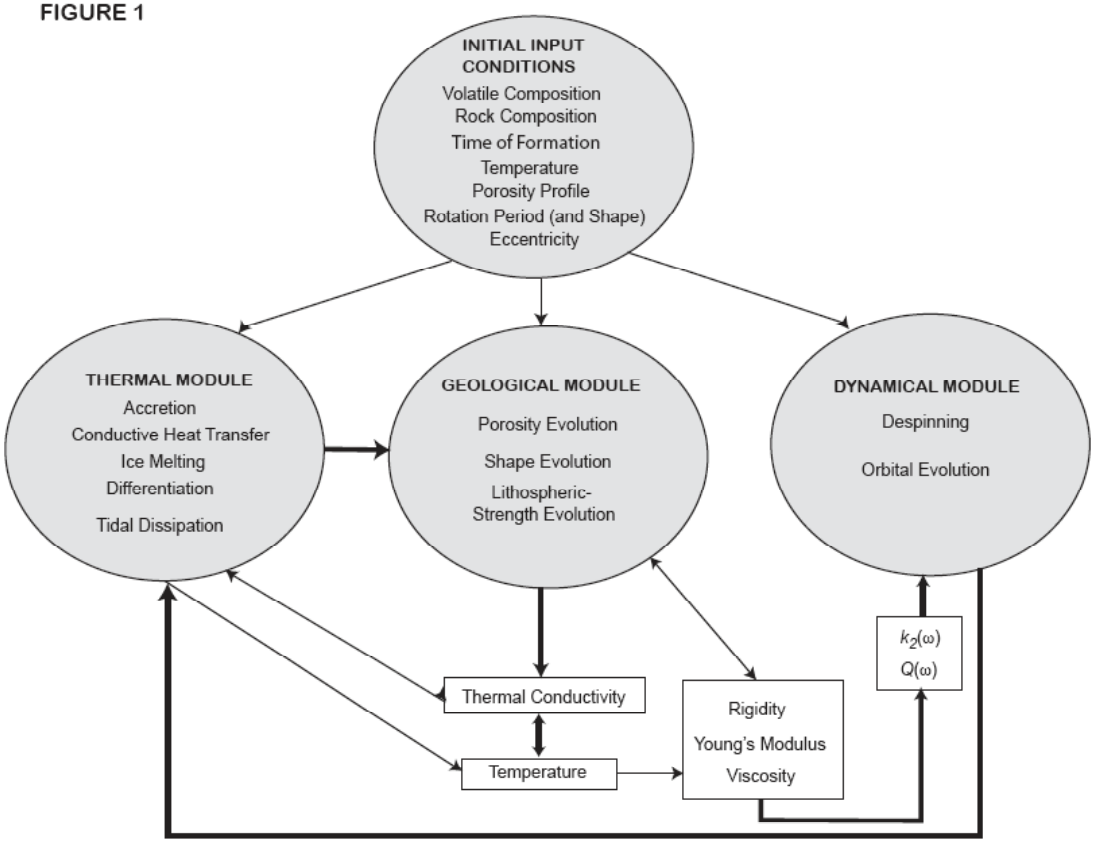

This work was carried out at the Jet Propulsion Laboratory-California Institute of Technology, under contract to NASA.

Reference: Castillo-Rogez, J. C., D.L. Matson, C. Sotin, T.V. Johnson, J.I. Lunine, P.C. Thomas, 2007. Iapetus' geophysics: Rotation rate, shape, and equatorial ridge. Icarus doi:10.1016/j.icarus.2007.02.018.

A NEW APPROACH TO Pb DATING OF WHOLE METEORITIC PHASES BY THERMAL EXTRACTION AND THERMAL IONIZATION IN SILICA MELT. Christopher R.J. Charles and Donald W. Davis, Jack Satterly Geochronology Laboratory, Department of Geology, University of Toronto (22 Russell Street, Toronto, Ontario, CANADA, M5S3B1. christopher.charles@utoronto.ca & dond@geology.utoronto.ca).

Introduction: A significant challenge to precise $^{207}Pb/^{206}Pb$ meteorite chronometry remains the removal of terrestrial lead. Presently this is done by leaching, dissolution and chromatographic separation in clean-lab environments followed by ID-TIMS [1,2] or MC-ICP-MS [3,4]. Here a novel thermal extraction (TE) procedure followed by thermal ionization mass spectrometry (TIMS) is described, where chemically untreated whole meteoritic phases are embedded in a silicate glass ionization enhancer (Figure 1). Radiogenic Pb from whole-samples is thermally extracted into the silicate melt and thermally ionized during TIMS analysis. $^{207}Pb/^{206}Pb$ ages for whole fragments of calcium-aluminum-rich inclusions (CAIs) from the Allende CV3 chondrite and for a pyroxene crystal from angrite SAH99555 were resolvable by this approach.

Method: Three CAI fragments ca. 200 µm in diameter (~0.01 mg) were obtained from Allende (#M29173; Royal Ontario Museum) by freeze thaw disaggregation and hand picking. One different Allende CAI fragment (#316/39) [5,6] of approximately the same weight and size was obtained by hand picking. One euhedral pyroxene crystal (800 µm diameter; 0.1 mg) from angrite SAH99555 was also obtained by crushing and hand picking. After rinsing with 3-4 cycles of clean acetone and MQ-H2O, all grains were washed several times with sub-boiling distilled HCl (0.1–3.0N) and HNO_3 (0.1–3.0N) under cleanroom conditions. Whole grains were covered with of clean Merck silicic acid "silica gel" & 9N H_3PO_4 emitter similar to [7]. All reagent blanks were ca. 0.1 pg Pb/mL as measured by ID-TIMS. The gel-fragment mixture for each individual sample was loaded in troughs (800 µm width) on separate zone-refined rhenium filaments (12 µm-thick × 1200 µm-wide; c.f. Figure 1). Filaments were previously moulded to this trough-shape and were spot-welded to standard Cathoedon #519 filament assemblies. Before sample loading all filaments were vacuum outgassed at 2000ºC for 1 hour. After loading each sample was fused to a glass in vacuum at 1400ºC over 30 min taking care to fully embed each fragment inside the glass. A VG354 thermal ionization mass spectrometer was used to measure all ratios in Daly-counting mode. Temperatures were recorded by a wire-pyrometer on the hottest part of each filament (typically around the folds of the trough). Mass fractionation corrections and data reductions were made under the UTILAGE software package (v060703; D.W. Davis). Results were fitted by IsoPlot/Ex (v3; K. Ludwig).

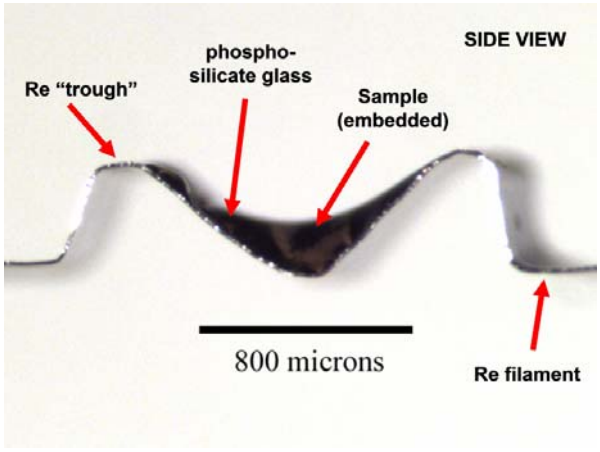

Figure 1: Trough-shaped Re filament showing a whole-sample fused into the phospho-silicate glass.

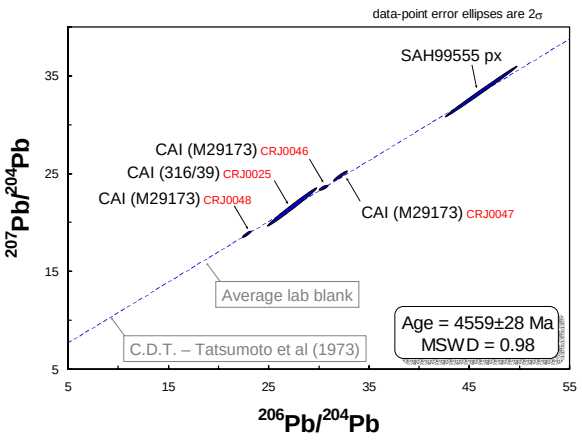

Figure 2: Pb-Pb plot of the four Allende CAIs and one px from angrite SAH99555. Primordial Canyon Diablo troilite & average lab blank are overlain but not included in this fit.

Observations – Allende CAIs: Interferences were seen on masses 204, 206, 207 and 208 for all fragments below 1590ºC. At 1630 – 1740ºC, lead ratios of the four fragments stabilized between $23 < {}^{206}Pb/^{204}Pb < 33$ (cf. Figure 2). Beam intensities ranged between 1.2 – 4 kcps on ^{206}Pb in this temperature interval showing the most radiogenic Pb. Three data blocks (30 ratios) were recorded for $^{206}Pb/^{204}Pb$ and $^{207}Pb/^{204}Pb$.

Observations – SAH99555 px: Interferences were observed until 1750ºC for this sample. Between 1770 – 1820ºC a beam intensity of 2.5 kcps on ^{206}Pb

was obtained giving an average ratio $^{206}Pb/^{204}Pb = 46$. This was the most radiogenic of all samples analyzed (cf. Figure 2). Three data blocks (30 ratios) for $^{206}Pb/^{204}Pb$ and $^{207}Pb/^{204}Pb$ were recorded.

Results: The data define a linear array within error in Pb-Pb space (Fig. 2) corresponding to an age of 4559±28 Ma (2σ). about the common Pb component is likely a mixture of initial Canyon Diablo troilite (CDT) lead[8] and laboratory blank (Fig. 2). If we include primordial CDT Pb and laboratory blank in the fit, an indistinguishable age of 4563±23 Ma (2σ; MSWD=3.5) is obtained.

Discussion & Conclusions: Results on two 0.1 mg samples of Allende CAIs (M29173) yielded mostly thorogenic Pb ($^{208}Pb/^{204}Pb$ = 160 and 260) [9]. ^{208}Pb emission began to increase at 1580ºC and attained between 16 – 30 kcps over about about 40 min. Given the small sample sizes and low concentrations of primary Pb in Allende CAI's (typically 0.3 – 0.01 ppm), the presence of a whole CAI in the melt does not appear to have significantly reduced the ionization efficiency of the Pb. Since Allende CAIs are known to contain primary Pb that is highly radiogenic, precise ratios should be measureable if sufficient sample can be embedded on the filament (comparible to [1] for example).

Potential limitations of TE include (a) degree of suppression of ionization from large samples; (b) influence of loading blank; and (c) practicalities of sample handling and loading – particularly the amount of silicic acid gel used. These will be investigated using a ^{202}Pb spike that is in preparation.

Aside from initial washing of the specimens, no clean chemical separation is required. In addition, thermal pre-treatment of CAI and angrite px fragments may prove useful for differential evaporation of contaminant Pb from meteoritic materials, as shown with zircon [10].

References: [1] Amelin Y. et al. (2002) *Science, 297,* 1678-1683. [2] Chen J. & Wasserburg G. (1981) *EPSL 52*, 1-15. [3] Albarede F. et al. (2004) *Geochim. Cosmochim. Acta 68*, 2725-2744. [4] Baker J. et al. (2005) *Nature 436*, 1127-1131. [5] Bogdanovski O. & Jagoutz E. (1997) *LPSC XXVIII*, 129. [6] Bogdanovski O. & Jagoutz E. (1999) *LPSC XXX*, 1891. [7] Gerstenberger H. & Haase G. (1997) *Chem. Geol. 136*, 309-312. [8] Tatsumoto M. et al. (1973) *Science 180*, 1279-1283. [9] Charles C.R.J. & Davis D.W. (2007) *Goldschmidt XVII,* Abstract #A161. [10] Davis, D.W. (2007) *Goldschmidt XVII,* Abstract #A206.

IRRADIATION ORIGIN OF SHORT-LIVED RADIOACTIVE NUCLIDES. M. Chaussidon[1], I. Leya[2], M. Gounelle[3], Y. Guan[4], K.D. McKeegan[5], F. Robert[6] and G. Srinivasan[7]. [1]CRPG-CNRS, BP 20, 54501 Vandoeuvre-lès-Nancy, France, (chocho@crpg.cnrs-nancy.fr), [2] Physikalisches Institut, Space Research and Planetary Sciences, Bern (ingo.leya@space.unibe.ch), [3]LEME-CNRS-MNHN, Paris (gounelle@mnhn.fr), [4]Geological and Planetary Sciences, Caltech, Pasadena (yunbin@gps.caltech.edu), [5]Earth and Space Sciences, UCLA, Los Angeles (mckeegan@ess.ucla.edu), [6] LEME-CNRS-MNHN, Paris (robert@mnhn.fr), [7]Department of Geology, University of Toronto, Toronto (srini@geology.utoronto.ca)

Introduction: The origin of short-lived radioactive nuclides (SLRs) which were present in the protosolar nebula is a central question related to the origin of the first solids and to the chronology of the events which occurred during the first few million years (Ma) of the Solar system. Some of these nuclides, ^{10}Be (and ^{7}Be) and ^{36}Cl, have indubitably an irradiation origin whereas ^{60}Fe, which is a neutron-rich nuclide, must be a stellar product [1,2]. The main questions which are actively studied, either from meteorite analysis or from theoretical modeling, are : (i) what is the fraction of other SLRs (essentially ^{26}Al but also ^{53}Mn, ^{41}Ca) which could be produced by irradiation together with Be and Cl isotopes, (ii) what is the distribution of the irradiation produced SLRs in the protosolar nebula, (iii) what are the physical conditions of the irradiation and the potential consequences on the evolution of gas and grains in the accretion disk and (iv) what are the consequences on the chronologies based on the SLRs ?

The case for Li-Be-B elements: The major nucleosynthetic source of Li-Be-B elements is spallation reactions which occur at energies typically higher than a few MeV [3]. CAIs and chondrules exhibit Li and B isotopic variations [4-9] that are indicative of the presence in the protosolar nebula of freshly nucleosynthesized isotopes of Li, B and of Be, including the two short-lived isotopes ^{10}Be ($T_{1/2}$=1.5Ma) and ^{7}Be ($T_{1/2}$=53 days). The strongest evidence is for ^{10}Be which was present at a level of ^{10}Be/^{9}Be$\approx 1\times10^{-3}$ when CAIs formed. The large Li isotope variations observed in several CAIs are best explained by the presence of ^{7}Be (with a ^{7}Be/^{9}Be$\approx 6\times10^{-3}$), though the evidence is at present not as strong as for ^{10}Be. Variations of the ^{10}Be/^{9}Be ratios seem present among CAIs and ^{26}Al and ^{10}Be are decoupled in hibonites [10]. The differences in Li and B isotopic ratio between CAIs, chondrules and bulk chondrites is a hint for an heterogeneous distribution of irradiation products in the protosolar nebula.

The case for ^{36}Cl: ^{36}Cl ($T_{1/2}$=0.3Ma) has a branched decay (98.1% to ^{36}Ar and 1.9% to ^{36}S) and, though hints for ^{36}Ar excesses were previously reported [11], very clear ^{36}S excesses positively correlated with the Cl/S ratios were only recently reported for secondary halogen-rich phases in CAIs and chondrules [12,13]. The best estimate of the ^{36}Cl/^{35}Cl at the time of formation of these Cl-rich phases (e. g. sodalite grains) is $\approx 4\times10^{-6}$. Because of (i) the short half-life of ^{36}Cl, (ii) the fact that ^{26}Al and ^{36}Cl are found decoupled in the Pink Angel CAI and (iii) the low production yields of ^{36}Cl by type II supernovae or by AGB stars, local irradiation by the young active Sun seems the only viable mechanism to produce the observed ^{36}Cl [13]. This would imply that these irradiation processes lasted for several Ma since the estimated age of formation of sodalite is ≈3.5Ma after the crystallization of CAIs. This is not inconsistent with the duration of high X-ray luminosity for YSOs of near solar mass [14].

Irradiation models: Several scenarios have been proposed for the origin of the irradiation produced SLRs : (i) production by trapping of galactic cosmic rays in the presolar cloud [15], (ii) irradiation by solar energetic particles of grains and gas of chondritic or solar composition [10,16,17] and (iii) irradiation, in the framework of the X-wind model, of protoCAIs in the reconnection ring [18,19]. These various models show the strong effect of the chemistry of the target, of the fluence and the energy spectra of the solar cosmic rays, on the production yields. They show that the co-production of ^{10}Be, ^{26}Al, ^{53}Mn, ^{36}Cl and ^{41}Ca is feasible at the levels observed in meteorites. The co-production of ^{7}Be at the observed level would require extremely short irradiation times (one to a few years) and high fluences.

References: [1] Mostéfaoui S. et al. (2004) *New Astron. Rev., 48*, 155-159. [2] Tachibana S. and Huss G.R. (2003) *ApJ., 588*, 41-44. [3] Reeves H. (1994) *Rev. Mod. Phys., 66,* 193-216. [4] Chaussidon M. and Robert F. (1995) *Nature, 374*, 337-339. [5] Chaussidon M. and Robert F. (1998) *EPSL, 164,* 577-589. [6] McKeegan K.D. et al. (2000) *Science, 289,* 1334-1337. [7] Sugiura N. et al. (2001) *Meteorit. Planet. Sci., 36,* 1397-1408. [8] MacPherson G.J. et al. (2003) *Geochim. Cosmochim. Acta, 67,* 3165-3179. [9] Chaussidon M. et al. (2006) *Geochim. Cosmochim. Acta, 70,* 224-245. [10] Marhas K.K. et al. (2002) *Science, 298*, 2182-2185. [11] Murty S.V.S. et al. (1997) *ApJ., 475,* 65-69. [12] Lin Y. et al. (2005) *PNAS, 102,* 1306-1311. [13] Hsu W. et al. (2006) *ApJ., 640,* 525-529. [14] Feigelson E.D. et al. (2002) *ApJ., 572*, 335-349. [15] Desch S.J. (2004) *ApJ., 602*, 528-542. [16] Goswami J.N. et al. (2001) *ApJ., 549,* 1151-1159. [17] Leya I. et al. (2003) *ApJ., 594,* 605-616. [18] Gounelle M. et al. (2001) *ApJ., 548,* 1051-1070. [19] Gounelle M. et al. (2006) *ApJ., 640,* 1163-1170.

In Situ Meteoritic Ti Isotopic Measurements by Laser Ablation MC-ICP-MS and the Homogeneity in Refractory Inclusions H-W. Chen[1], T. Lee[2], D-C. Lee[2], and Y. Iizuka[2], [1]Department of Geosciences, National Taiwan University, Taiwan (haart@earth.sinica.edu.tw), [2]Institute of Earth Sciences, Academia Sinica, Taiwan.

Introduction: Aiming for in situ analysis of small samples, we have been developing the laser-ablation multi-collecting inductively coupled plasma mass spectrometry (LA-MC-ICP-MS) [1]. Here we report the initial results for titanium isotopic analysis of 30 um spots on individual Ti-pyroxene grains from Allende CAIs.

Experimental Methods: A Ti composition standard solution with a concentration of 100 ppb was first prepared from high purity Merck CertiPUR grade Ti reagent. Then we diluted it to make a 25 ppb pure Ti solution standard that gave a ^{48}Ti ion beam of 40 pA. Moreover, a series of mixtures were prepared to cover the range of interferences on Ti from Cr, Ca, and Al-Mg. Our isotopic measurement of the pure Ti solution standards after normalizing ^{47}Ti/^{49}Ti to correct for isotopic fractionation yielded reproduced ^{46}Ti/^{49}Ti, ^{48}Ti/^{49}Ti, and ^{50}Ti/^{49}Ti ratios with two sigma external precision around 2-3 epsilon unit (εu). The same precision was achieved for the mixtures containing interfering neighboring elements thus demonstrating that our correction method worked to a large extent (Table 1). However, the absolute ratios for Ti isotopes are currently under dispute. Four groups have published Ti isotopic ratios that are inconsistent with one another [2,3,4,5]. Our values are closest to those of Heydegger et al. with differences less than the uncertainties (i.e. 2-3 εu) for all Ti ratios. Niemeyer's values were very different from any of the other groups. The most widely used ratios are those of Niederer et al. measured at Caltech'. They measured Ti as TiO which is more sensitive but requiring correction of contributions from other oxides (e.g. ^{48}Ti^{18}O on ^{50}Ti^{16}O). Comparing our data with the Caltech's, we found that after normalizing to ^{47}Ti/^{49}Ti, there are excellent agreements for ^{46}Ti/^{49}Ti and ^{48}Ti/^{49}Ti (i.e. difference < 2-3 εu) but there is a significant offset at ^{50}Ti/^{49}Ti of about 13 εu. Upon further examination, we found that the discrepancy decreases to 5± 3 εu if their measured oxygen isotope ratios were used for oxide correction rather than using that reported by Nier (1950) [6]. We thus believe that the ^{50}Ti isotope ratio published by the Caltech' group should be lowered by about 10 εu.

Our next step was to apply our method to four Ti-rich terrestrial mineral phases, metal, rutile (TiO_2), sphene ($CaTiSiO_5$), and perovskite ($CaTiO_3$) with laser ablation (using New Wave Nd-YAG 5X 213nm UV). All four phases yielded Ti compositions that were consistent with one another and also with our normal standard solution. The analytical precision of our LA-ICPMS technique was found to be about 3ε (2σ). This is an order of magnitude better than the performance of secondary ion mass spectrometry (SIMS), the traditional choice for in situ analysis. However, the spatial resolution of laser ablation in ICP-MS presently was about 30μm that is far less than the sub-μm capability of SIMS. Note that all four minerals show the same ^{50}Ti offset of around 12 εu relative to the Caltech' value. In the following we report our laser ablation results relative to the sphene standards analyzed in the same day. So offsets from the Caltech' value cancelled out and do not affect the data.

Table 1: Ti isotopic ratios of standard solution with different element mixtures and several terrestrial mineral standards.

Mass Bias Coefficient	ε ^{46}Ti/^{49}Ti	ε ^{48}Ti/^{49}Ti	ε ^{50}Ti/^{49}Ti
Ti Standard Solution—Ti~25ppb			
1.647±0.031	-1.4±2.4	-1.7±1.7	13.5±3.1
Ti-Cr Mixture (Ti/Cr~1300)—Ti~50ppb			
1.640±0.001	1.3±0.6	0.8±0.5	11.3±1.0
Ti-Cr Mixture (Ti/Cr~130)—Ti~70ppb			
1.609±0.010	0.9±1.0	0.9±0.4	10.2±1.4
Ca-Ti Mixture (Ca/Ti~5)—Ti~35ppb			
1.592±0.010	-1.7±2.8	1.0±0.7	11.2±2.6
Ca-Ti-Al-Mg-Cr Mixtures (6:2:3:2:0.0007)—Ti~30ppb			
1.610±0.015	-1.1±2.2	1.1±0.6	11.7±2.1
Titanium Metal (Ti)			
1.575±0.015	-0.1±1.7	0.9±0.9	11.6±2.5
Rutile (TiO_2)			
1.585±0.018	0.8±2.9	0.5±1.1	11.9±2.2
Sphene ($CaTiSiO_5$)			
1.568±0.018	0.5±2.3	0.7±1.6	12.8±2.3
Perovskite ($CaTiO_3$)			
1.559±0.017	-1.4±2.5	0.5±1.0	14.5±4.6

Results and Discussion: Following the procedures developed using the above terrestrial samples, we analyzed the titanium isotopic compositions of several fassaite grains from two large Ca-Al- inclusions of Allende meteorite whose titanium isotopic compositions were previously measured using TIMS on dissolved and chemically separated bulk samples. No titanium isotopic heterogeneity was found within different spots for single Ti-pyroxene crystal and all results were consistent with reported TIMS results (Fig.1). The search continues and we are exploring

ways to analyze smaller grains of minor phases that may be important to Ti. Examples are perovskite, hibonite, and rutile.

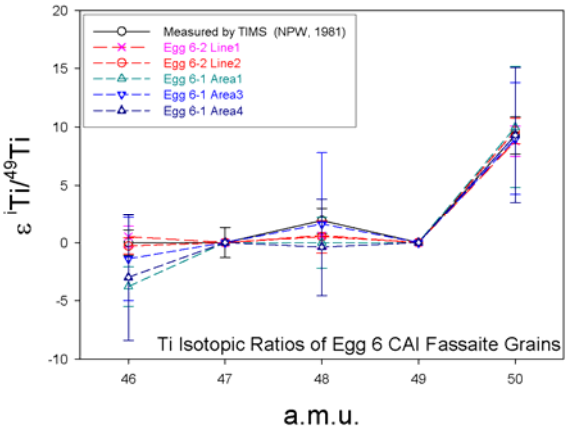

Fig.1: The titanium isotopic ratios of the Egg 6 fassaite grains measured by LA-MC-ICP-MS.

Acknowledgments: We thank G. J. Wasserburg for kindly providing his Egg3 and Egg6 samples for analysis.

References: [1] Chen H. and Lee T. (2002) *GCA, 66*, Supplement 1. [2] Heydegger H. R. et al. (1979) *Nature, 278*, 704-707. [3] Niederer F. R. (1981) *GCA, 45*, 1017–1031. [4] Niemeyer S. and Lugmair G. W. (1981) *EPSL, 53*, 211-225. [5] Niemeyer S. (1988) *GCA, 52*, 309-318. [5] Nier A. O. (1950) *Phys. Rev, 77*, 789-793.

TWO-DIMENSIONAL DYNAMICS OF CAIS IN THE SOLAR NEBULA. F. J. Ciesla[1], [1]Carnegie Institution of Washington, Department of Terrestrial Magnetism, 5241 Broad Branch Road NW, Washington DC 20015 (fciesla@ciw.edu).

Introduction: Among the challenges in reconciling our astrophysical models for the evolution of the solar nebula with the meteoritic record is understanding how Calcium-Aluminum-rich Inclusions (CAIs) were preserved for >1 million years prior to their incorporation into chondritic meteorite parent bodies [1,2]. Due to gas drag, these 0.1-1 cm sized objects are expected to spiral into the sun on timescales of ~10^5 years [3], yet CAIs are intimately mixed with much younger chondrules and matrix in chondritic meteorites and many appear to have experienced very little pre-accretionary alteration since their formation via condensation and evaporation processes in the nebula. Even more challenging is the identification of a CAI-like particle dubbed "Inti" in the Stardust samples collected from Comet Wild 2 whose mineralogy and oxygen isotopic compositions suggest that this particle formed in the same environment as chondritic CAIs and was then transported outward to ~20 AU [4,5]. Here I present a new model for radial transport in protoplanetary disks which investigates how CAIs could have been redistributed in the solar nebula in a manner that is consistent with what is observed in chondritic meteorites and comets.

Previous Work: One model recently proposed for transporting CAIs outward in the solar nebula and preserving them for longer thant 1 million years involves these objects diffusing outwards due to turbulence [6]. While the source of this turbulence remains an issue of debate, it is thought to be related to the mass and angular momentum transport associated with protoplanetary disk evolution [7]. The turbulence allows particles to diffuse along concentration gradients, and in this case, away from high concentrations near the sun to lower concentrations further away. While some CAIs would be able to avoid being lost to the sun as the outward diffusion would offset their movements due to the inward flows associated with mass transport and gas drag, the number is very low, with only a small fraction surviving for incorporation into chondritic meteorite parent bodies.

The turbulence model of Cuzzi et al [6], was one dimensional, tracking the concentration of CAIs relative to the *surface density* of hydrogen in the solar nebula. In this treatment, the dynamics of the CAIs are determined by allowing them to diffuse relative to the hydrogen gas and calculating the *net* advective flow of the disk due to mass transport and by determing the motions due to gas drag (which generally involves determing the motions that would occur at the midplane of the nebula and applying them to all particles).

Particle Dynamics in 2-D: I have recently begun to investigate the differences in radial transport rates as a function of height above the disk midplane. These differences arise due to the variation in the radial gas density and pressure gradients with height and impact all modes of transport for particles: gas drag, flows associated with mass transport, and diffusion.

In the case of gas drag, the radial velocities of the particles are proportional to the radial pressure gradients in the disk. In the case of negative gradients, such as at the disk midplane, the gas is partially supported against the central force of gravity due to the star and thus rotates at sub-Keplerian rates [3]. Particles thus feel a headwind in their orbits as they attempt to follow Keplerian orbits and move inwards over time. At higher altitudes, however, the pressure gradient switches directions (becomes positive). This is a result of the decrease in the vertical component of gravity pulling the gas toward the midplane at larger distances, resulting in greater pressure scale-heights. Due to the positive pressure gradients at these higher altitudes, the solids experience tailwinds in their orbits, allowing them to move outwards with time.

The large-scale flows associated with mass transport in the disk are driven by the viscous stresses that develop between neighboring annuli of gas. In the 1-D treatments, the calculated stresses are averaged over the vertical extent of the disk, allowing the *net* radial motions of the gas (and the particles suspended within) to be determined. In 2-D, however, the stresses can be determined as a function of height. When this is done [8-10], it is found that mass is driven rapidly inwards at high altitudes above the midplane due, in part, to the positive radial density gradients, wheras the flow decreases in magnitude closer to the midplane. In fact, around the midplane, where large negative radial density gradients can exist, the flows can also switch directions, resulting in the outward motion of materials around the disk midplane.

This outward transport of material at the disk midplane can be enhanced by diffusion. Outward diffusion is found to work most efficiently when the radial density gradient is negative, whereas inward diffusion occurs most easily when the radial density gradient is positive.

These variations in the radial transport rate with height above the midplane thus can lead to very different dynamical behavior than that found in the 1-D models often used. In essence, it is found that outward transport is much more efficient than previously be-

lieved, because particles will diffuse outwards along the midplane without having to battle any inward flow associated with mass transport (though gas drag may still be a factor). Thus the outward transport efficiency of materials will be determined by how long they reside in this region around the midplane—those particles that diffuse to high altitudes will be transported inward very rapidly by the large-scale flows present there. This leads to the surprising result that outward transport can be more efficient for larger particles due to the fact that vertical gravity (settling) will keep them closer to the midplane for longer periods of time as they will not diffuse upwards as easily as smaller particles. This result is counter to that expected from the 1-D models.

Application to CAIs: Due to the increase in the outward transport efficiency, a larger fraction of CAIs are able to preserved in the solar nebula than found in the previous work which employed a 1-D model to examine their dynamics. These CAIs are found to be transported as far outward as ~20-30 AU (results are sensitive to disk structure and level of turbulence), which is consistent with the observation of grains like Inti in the Stardust samples.

The redistribution of CAIs by this process would also be strong functions of the particle size, offering an explanation of the size sorting observed in chondritic meteorites [e.g. 11]. This sorting would be even further enhanced if the turbulence decays away or shuts off over time, as those particles that were transported out beyond the chondrite formation region (assumed to be 2-4 AU) would drift inward at a rate that depended on their size. In fact, if some CAIs were transported out to such large distances (>5 AU) and then drifted inwards again to be incorporated into chondritic meteorite parent body, this would explain how they avoided being processed in chondrule formation events and remain unmelted. This possibility and the dynamical relations of the different types of CAIs are the focus of ongoing work.

References: [1] Amelin Y. et al. (2002) *Science, 297*, 1678-1683. [2] Bizzarro M. et al. (2004) *Nature, 431*, 275-278. [3] Weidenschilling S. J. (1977) *Mon. Not. R. Astron. Soc., 180*, 57-70. [4] Zolensky M et al. (2006) *Science, 314,* 1735-1739. [5] McKeegan K. et al. (2006) *Science, 314, 1724-1728.* [6] Cuzzi J. N. et al. (2003) *Icarus, 166,* 385-402. [7] Sunyaev N. I. and Syunyaev R. A. (1973) *Astron. Astrophys., 24,* 337-355. [8] Urpin V. A. (1984) *Sov. Astron., 28*, 50-53. [9] Takeuchi T. and Lin D. N. C. (2002) *Astrophys. J., 5281*, 1344-1355. [10] Keller Ch. and Gail H.-P. (2004) *Astron. Astrophys. 415*, 1177-1185. [11] MacPherson G. J. (2005) in *ASPC 341: Chondrites and the Protoplanetary Disk* (Krot A. N. et al, Eds.), San Francicso:Astronomical Society of the Pacific. p.225.

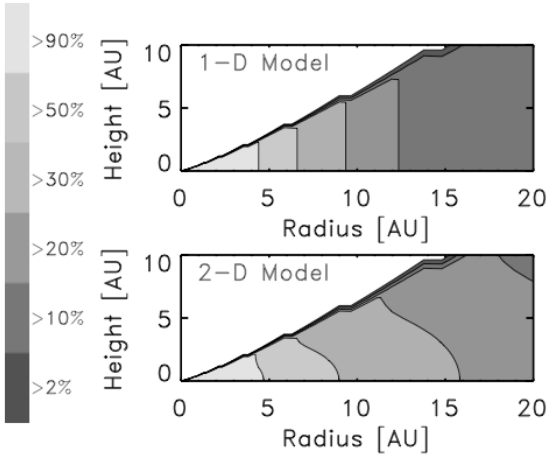

Figure 1: Comparison of the radial transport results for a 1-D disk model and the 2-D model described in the text. In this particular case, the disk is assumed to be in steady-state with a surface density distribution that goes as $3400(r/1\ AU)^{-1}$, a temperature distribution that goes ass $1400(r/1\ AU)^{-0.5}$, and a turbulence parameter given by $\alpha=3x10^{-3}$, giving a mass accretion rate through the disk of $\sim 5x10^{-7}\ M_{\odot}$/yr. The particles are all assumed to be 1 mm in size. The contours represent the fraction of materials processed at temperatures above 1000 K (appropriate for annealing amorphous precursors). While this temperature is lower than that needed for CAIs, this plot does demonstrate how accounting for the transport in 2-D leads to much more efficient outward redistribution of materials from the inner solar nebula.

DIFFERENCE IN PB ISOTOPIC AGES OF CHONDRULES AND CA, AL-RICH INCLUSIONS FROM THE CV CARBONACEOUS CHONDRITE ALLENDE. J.N. Connelly[1,2*], Y. Amelin[3], A.N. Krot[4], and M. Bizzarro[2,5]. [1]Jackson School of Geosciences, University of Texas at Austin, Austin, Texas, USA, *connelly@mail.utexas.edu. [2]Geological Institute, Copenhagen University, Copenhagen, Denmark, [3]Australian National University, Canberra, Australia, [4]University of Hawai'i at Manoa, Honolulu, Hawaii, USA. [5]Geological Museum, Copenhagen, Denmark.

Introduction. Chondrules and Ca,Al-rich inclusions (CAIs) are the major components of chondritic meteorites (chondrites) and are among the earliest solids formed in the solar nebula – the disk of dust and gas that surrounded the proto-Sun [1]. Compositions and textures of CAIs and chondrules indicate that they formed by high temperature processes that included condensation, evaporation, and, for chondrules and some CAIs, subsequent melting of the early condensates during multiple brief heating episodes, possibly induced by shock waves [e.g., 2]. The age relationship between CAIs and chondrules can provide important constraints on their origin and the chronology of the solar nebula [3]. This age relationship can be potentially established using the short-lived radionuclide ^{26}Al [$t_{1/2}$ = 0.73 million years (Ma)], which was present in the nebular regions where CAIs and chondrules formed [4-12]. Based on the observations that most CAIs in primitive (unmetamorphosed) chondrites appear to have formed with an initial ^{26}Al/^{27}Al ratio [$(^{26}Al/^{27}Al)_0$] of ~6×10^{-5}, whereas most chondrules apparently formed with a $(^{26}Al/^{27}Al)_I \leq 1.2\times10^{-5}$, it is commonly inferred that CAIs formed at least 1.5 Ma before the majority of chondrules [4-13].

This chronological interpretation is, however, model dependent: it is based on the assumption that ^{26}Al was homogenized in the solar nebula over a time scale that was short compared to its half-life [4]. Homogeneous distribution is readily achieved if ^{26}Al was produced by stellar nucleosynthesis in a supernova, an asymptotic giant branch star, or a Wolf-Rayet star, and was injected into the solar nebular [14]. The recent discovery of the short-lived radionuclide ^{60}Fe ($t_{1/2}$ = 1.5 Ma) in chondrites [15-17] at the level that can only be produced in massive (>10 $M_\odot$) stars, indicates that our Solar System must have formed near one or several massive stars, and most massive stars are thought to form in dense clusters [18]. However, the lack of ^{60}Fe in meteorites from several differentiated asteroids, which accreted early (~0.5-0.7 Ma after formation of CAIs with the canonical $(^{26}Al/^{27}Al)_0$) with high abundances of ^{26}Al, suggests that ^{60}Fe and ^{26}Al were decoupled; i.e., they either formed by different mechanisms or were injected into the Solar System at different stages of its evolution [19].

Based on the high precision whole-rock magnesium isotopic compositions of terrestrial samples, Martian meteorites and chondrites, it has been inferred that ^{26}Al was uniformly distributed at least in the inner Solar System [20, 21]. Although these observations support the chronological interpretation of ^{26}Al-^{26}Mg systematics, they do not prove it.

According to the alternative X-wind model, CAIs and chondrules formed contemporaneously in isotopically distinct and spatially separated nebular reservoirs and the observed differences in the $(^{26}Al/^{27}Al)_0$ reflects local formation of ^{26}Al by energetic particle irradiation near the proto-Sun [22, 23]. The abundances of ^{26}Al in this model have no direct chronological meaning. The X-wind model received significant attention after discovery of several short-lived radionuclides – ^{10}Be [24], ^{7}Be [25], and ^{36}Cl [26, 27] – that can be produced only by nuclear spallation reactions. In addition, theoretical calculations [e.g., 28] are able to reproduce within a factor of a few the initial abundances of most short-lived radionuclides reported in meteorites (^{10}Be, ^{26}Al, ^{36}Cl, ^{41}Ca, ^{53}Mn; ^{60}Fe is the only exception).

In contrast to the short-lived, relative isotope chronologies (e.g., ^{26}Al-^{26}Mg, ^{53}Mn-^{53}Cr), the long-lived Pb-Pb isotope chronology of CAIs and chondrules provides absolute ages, which can potentially test whether the age differences between these objects inferred from the extinct chronometers are correct. Amelin et al. [29] first reported a resolvable Pb isotopic age difference of CAIs from the CV chondrites Allende and Efremovka (4567.2 ± 0.7 Ma, revised to 4567.11 ± 0.16 [30]) and chondrules from the CR chondrite Acfer 059 (4564.7 ± 0.6 Ma). This result, however, does not preclude contemporaneous formation of chondrules and CAIs as suggested by X-wind model [22, 23, 28], since CAIs and chondrules analyzed by Amelin et al. [29] are from different chondrite groups. Here we report a resolvable ^{207}Pb-^{206}Pb age difference between CAIs and chondrules from the CV carbonaceous chondrite Allende. Previous attempts to resolve a Pb isotopic age difference between CAIs and chondrules from CV chondrites were unsuccessful [31-33].

Methods and Results. We extracted chondrules from two separate pieces of Allende and processed multichondrule fractions for Pb isotopic analyses

using two different approaches. Multiple fractions were aggressively leached at the Geological Survey of Canada, resulting in 15 highly-radiogenic Pb analyses from the residual portions. A single fraction was subjected to a progressive dissolution procedure at Copenhagen University that yielded 6 widely-spaced co-linear points in Pb-Pb space.

We have combined the two Pb-Pb data sets for chondrules from Allende to derive an integrated data array that defines an absolute Pb-Pb age of 4565.45 ± 0.45 Ma (Fig. 1). The precision reflects the highly-radiogenic nature of data set A (highly-leached residues, Geological Survey of Canada) combined with the large spread of points in data set B (progressive dissolution, University of Copenhagen). The robustness of this age is reinforced by the extrapolation of the line through the accepted estimate of the Solar System primordial Pb isotopic composition [34] indicating that terrestrial Pb contamination was successfully removed. This age is inferred to represent the time of final crystallization of the chondrules sampled from the CV chondrite Allende.

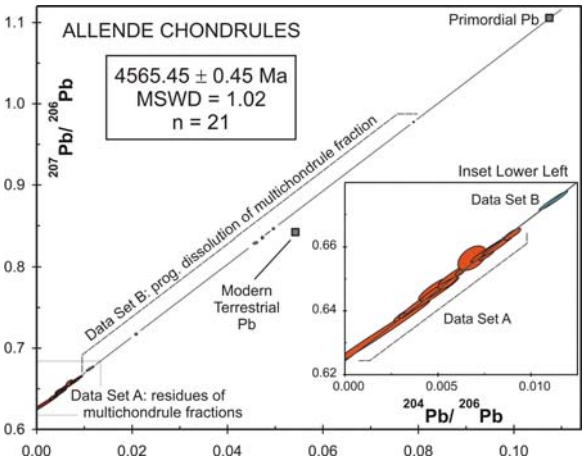

Fig. 1. Pb-Pb isochron for the Allende chondrules.

Discussion. Formation of chondrules after CAIs is supported by the presence of relict CAIs inside chondrules [4, 35], the presence of chondrule-like igneous rims around some CAIs [36], and the volatility fractionated (group II-like) trace element patterns exhibited by some chondrules [37]. The absolute age presented here indicates an age difference of 1.66 ± 0.48 Ma between CAIs and chondrules from CV chondrites. This age difference is consistent with their relative ages inferred from the differences in the initial $^{26}Al/^{27}Al$ ratios [6] and, therefore, supports a chronological significance of ^{26}Al-^{26}Mg systematics in general. We conclude that high-precision magnesium isotope measurements of CAIs and chondrules from primitive chondrites (e.g., CR2, CO3.0, Acfer 094) can be used to constrain the duration of CAI- and chondrule-forming events and the life-time of the protoplanetary disk.

References: [1] Krot A. N. et al. (2005) *Chondrites and the Protoplanetary Disk*, ASP Conference Series 341. [2] Scott E. R. D. and Krot A. N. (2005) in [1] pp. 15-54. [3] Russell S. S. et al. in [1] pp. 317-353. [4] MacPherson G. J. et al. (1995) *Meteoritics, 30,* 365-386. [5] Russell S. S. et al. (1996) *Science, 273,* 757-762. [6] Kita N. T. et al. in [1], pp. 558-587. [7] Kita N. T. et al. (2000) *Geochim. Cosmochim. Acta, 64,* 3913-3922. [8] McKeegan K. D. et al. (2000) *LPSC, XXXI*, Abstract #2009. [9] Mostefaoui S. et al. (2002) *Meteorit. Planet. Sci., 37,* 421-428. [10] Kunihiro T. et al. (2004) *Geochim. Cosmochim. Acta, 68,* 2947-2957. [11] Kurahashi E. et al. (2004) *LPSC, XXXV*, Abstract #1476. [12] Rudraswami N. G. and Goswami J. N. (2007) *Earth Planet. Sci. Lett., 277,* 231-244. [13] Young E. D. (2005) *Science, 308,* 223-227. [14] Boss A. P. (2007) *Astrophys. J., 660,* 1707-1714. [15] Tachibana S. and Huss G. R. (2003) *Astrophys. J., 588,* L41-L44. [16] Tachibana S. and Huss G. R. (2006) *Astrophys. J., 639,* L87-L90. [17] Mostefaoui S. et al. (2004) *New Astron. Rev., 48,* 155-159. [18] Hester J. J. and Desch S. J. in [1] pp. 107-131. [19] Bizzarro M. et al. (2007) *Science, 316,* 1178-1181. [20] Bizzarro M. et al. (2004) *Nature, 431,* 275-278. [21] Thrane K. et al. (2006) *Astrophys. J., 646,* L159-L162. [22] Shu F. H. et al. (1997) *Science, 277,* 1475-1479. [23] Gounelle M. et al. (2001) *Astrophys. J., 548,* 1051-1070. [24] McKeegan K. D. et al., (2000) *Science, 289,* 1334-1337. [25] Chaussidon M. et al. (2006) *Geochim. Cosmochim. Acta, 70,* 224-245. [26] Lin Y. et al. (2005) *Proc. Nat. Acad. Sci., 102,* 1306. [27] Hsu W. et al. (2006) *Astrophys. J., 640,* 525-529. [28] Gounelle M. et al. (2006) *Astrophys. J., 640,* 1163-1170. [29] Amelin Y. et al. (2002) *Science, 297,* 1678-1683. [30] Amelin Y. et al. (2006) *LPSC, XXXVII*, Abstract #1970. [31] Chen J. H. and Tilton G. R. (1976) *Geochim. Cosmochim. Acta, 40,* 635-643. [32] Tatsumoto M. et al. (1976) *Geochim. Cosmochim. Acta, 40,* 617-634. [33] Amelin Y. and Krot A. N. (2007) *Meteorit. Planet. Sci.*, in press. [34] Tatsumoto M. et al. (1973) *Science, 180,* 1279-1283. [35] Krot A. N. et al. (2002) *Meteorit. Planet. Sci., 37,* 155-182. [36] Krot A. N. et al. (2005) *Nature, 434,* 998-1001. [37] Misawa K. and Nakamura N. (1996) in *Chondrules and the Protoplanetary Disk*, R. H. Hewins, R. H. Jones, E. R. D. Scott, Eds. (Cambridge: Cambridge Univ. Press), pp. 99-105.

DISTRIBUTION OF ALUMINUM-26 IN REFRACTORY INCLUSIONS FROM CV CHONDRITES. M. Cosarinsky[1], D. J. Taylor[1], M.-C. Liu[1], K. D. McKeegan[1], and A.N. Krot[2]. [1]Dept. Earth & Space Sciences, University of California Los Angeles, Los Angeles, CA – 90095-1567; [2]HIGP/SOEST, University of Hawai'i at Manoa, HI – 96822. mariana@ess.ucla.edu

Introduction: The timing of formation and thermal processing of refractory Ca-, Al-rich inclusions (CAIs) plays an important role in models of early solar system evolution. The relative timing of those events can in principle be constrained from the abundance of ^{26}Al in CAIs [1]. High-precision Al-Mg isotope data have led to divergent answers regarding the periods of time over which CAIs could have formed, with bulk data indicating an extremely short period of ~20,000 years [2,3] and laser-ablation in situ data implying a much longer interval for the thermal processing (~300,000 years [4]). Other ICPMS data on bulk CAIs [5] suggest lower initial ^{26}Al/^{27}Al values, apparently in conflict with [2]. We have conducted an ion microprobe survey of 9 igneous and 3 non-igneous CAIs from the CV3 meteorites Efremovka, Vigarano and Allende in order to document the range of initial ^{26}Al/^{27}Al values preserved in these inclusions. We have also determined the initial ^{26}Al/^{27}Al abundances in the high-temperature Wark-Lovering rims (WLRs) around a subset of these CAIs to constrain the timing of rim formation processes. A set of these data has been previously reported [6,7].

Results: Analyses are obtained with the UCLA CAMECA ims1270 ion microprobe by high mass resolution multiple-collector Faraday cup measurements. Analyses on ~20 μm spots and have typical precision and accuracy, in a single spot, in the range ~0.2‰ (2σ) for Δ^{26}Mg* in the low Al/Mg phases (spinel and pyroxene). Δ^{26}Mg* values were calculated applying an exponential mass fractionation law with an exponent of 0.514 [8]. With the exception of melilite in the Allende and Vigarano CAIs, which has apparently undergone multiple reheating episodes resulting in internal redistribution of Mg isotopes, there is very good correlation between Al/Mg ratios and excess Δ^{26}Mg* in spinel, pyroxene and hibonite phases. Because of evidence for isotopic resetting in melilite, we only used spinel, pyroxene and hibonite, where available, to regress the data and calculate the initial ^{26}Al/^{27}Al values. Given the relatively low spread in Al/Mg ratios, isochron lines were forced through the origin in all cases. Uncertainties in the ^{26}Al/^{27}Al ratios are ~ 0.2×10^{-5} (2σ).

Two fluffy type A (FTA) samples (Vigarano 477-5 and Allende TS24) are composed of individual melilite+spinel+hibonite nodules, each surrounded by a WLR, whereas the third FTA studied (Allende TS25) consists of a single object overlain by a continuous WLR. The inferred initial ^{26}Al/^{27}Al ratios for the interiors of the FTAs range from 4.9×10^{-5} in V477-5 to 5.9×10^{-5} in TS24 and TS25 (Fig. 1). We also studied three igneous-textured compact type A CAIs (CTA): Vigarano 1623-2, and Efremovka E44L and E44N, which consist of melilite+ spinel±hibonite±fassaite and are also surrounded by WLR sequences. Well-correlated initial ^{26}Al/^{27}Al ratios for the interior phases range from 5.1×10^{-5} (E44N) to 6.1×10^{-5} (E44L) (Fig. 1). We measured the WLR spinel and pyroxene around each of the six type A CAIs and find that a range in ^{26}Al/^{27}Al ratios from 4.4×10^{-5} (TS24) to 5.6×10^{-5} (V1623-2) (Fig. 1). In all but one of these CAIs there are resolvable time differences between the formation of the CAI interiors and their surrounding WLRs. Six type B CAIs, Efremovka E38 and E107, and Allende TS23, TS34, 3712B and 181-129_1 have typical B1 igneous textures and consist of melilite+fassaite+ spinel±anorthite. These CAIs display a spread of inferred ^{26}Al/^{27}Al ratios at isotopic closure ranging from 3.8×10^{-5} for E107 to 5.5×10^{-5} for E38 as well as TS34 (Fig. 1).

Discussion: All CAI show a large range of initial ^{26}Al/^{27}Al ratios, as determined from spinel and pyroxene, which in principle are the phases least susceptible to secondary isotopic redistribution. Isotope resetting in spinel and pyroxene during melting and/or thermal processing can explain the low initial ^{26}Al/^{27}Al values for some (or all) of the type B CAIs. However the high initial values and also the spread in values seen in the FTA inclusions, which have not been melted [9], and in the CTA inclusions are not apparently compatible with a well-defined single CAI formation event, constrained by the ('supra-canonical') initial ^{26}Al/^{27}Al value of 5.85×10^{5} [3]. Alternatively, it is possible that even the FTAs may have undergone some degree of partial melting and evaporation, as suggested for the large ranges in Mg isotopic fractionation observed within each CAI [9], that resulted in isotopic resetting. In any case, our data suggest not only that the thermal recycling of CAIs lasted for a long time, in agreement with [4], but also that whatever nebular processes were responsible for the formation and thermal modification of CAIs, they continued for a period of time spanning at least 0.5 My. Our data on WLRs also suggest that WLR formation events occurred repeatedly in the solar nebula for a prolonged period of time (up to 2×10^{5}

years) and that these events alternated with CAI crystallization events.

References: [1] MacPherson G.J. et al. (1995) *Meteoritics* **30**, 365-386; [2] Bizzarro M. et al., (2004) *Nature* **431**, 275-278; [3] Thrane K. et al. (2006) *Astrophys. J.* **646**, 159-162; [4] Young E.D. et al. (2005) *Science* **308**, 223-227; [5] Jacobsen B. et al. (2007) *LPSC* **38**, #1491; [6] Taylor D.J. et al. (2005) *MAPS* **40**, #5282; [7] Cosarinsky M. et al. (2005) *MAPS* **40**, #5284; [8] Davis A.M. et al. (2005) *LPSC* **36**, #2334 ; MacPherson G.J. and Grossman L. (1984) *Geochim Cosmochim Acta* **48**, 29-46.

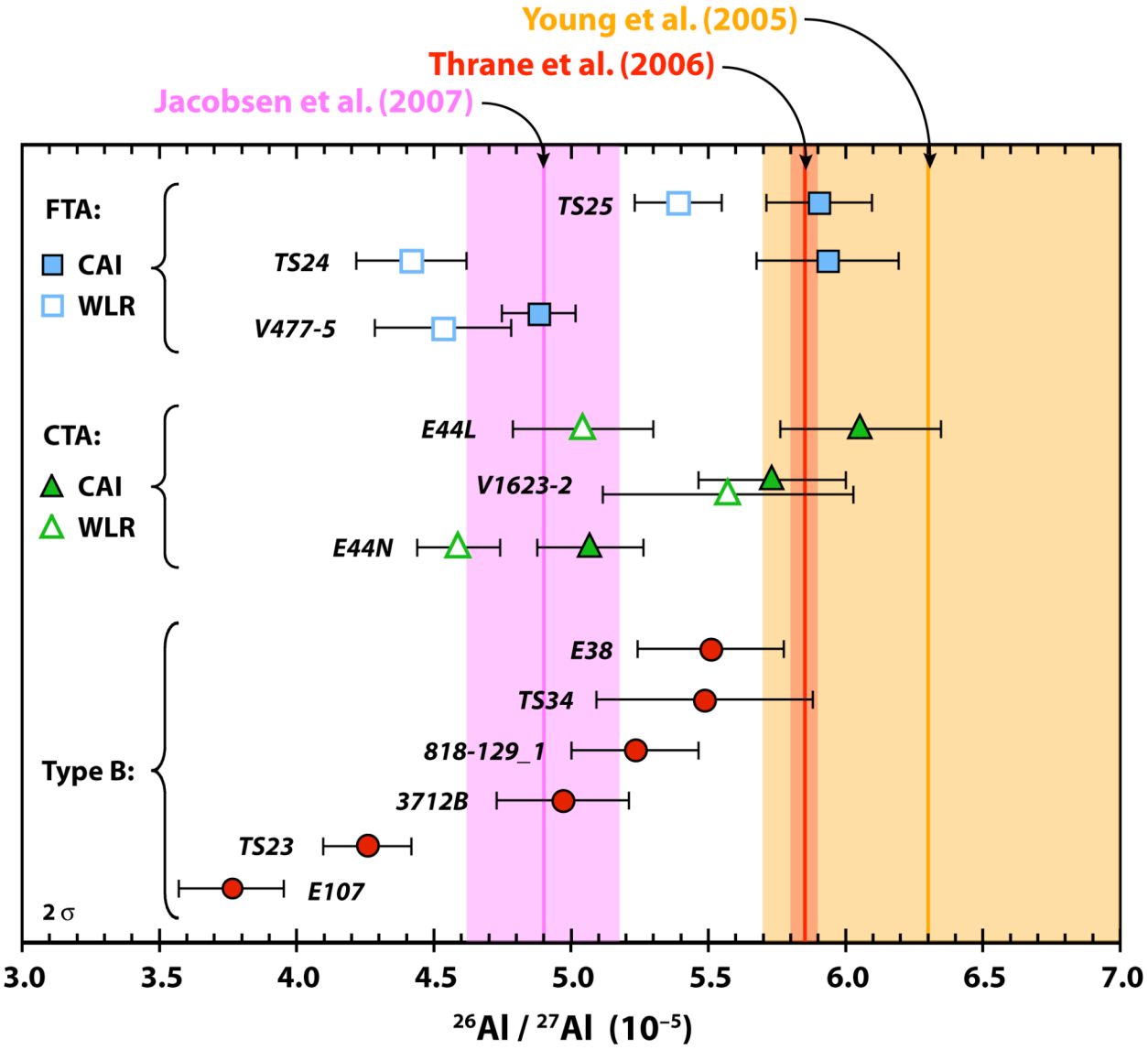

Fig. 1 Distribution of initial $^{26}Al/^{27}Al$ ratios in CV CAIs from Allende, Efremovka and Vigarano. Reference lines are shown for the initial $^{26}Al/^{27}Al$ ratios determined by [3,4,5] and the uncertainties are shown as shaded fields.

RECENT ADVANCES IN COSMOCHEMISTRY. A. M. Davis[1], [1]Department of the Geophysical Sciences, Enrico Fermi Institute, and Chicago Center for Cosmochemistry, University of Chicago, Chicago. IL 60637 (a-davis@uchicago.edu).

Introduction: New samples of solar system material, and a growing synergy with astrophysical theory and observation and significant technical advances are enabling rapid progress in cosmochemistry.

New Samples: For the first time since the Apollo era, new samples of solar sytem material have been returned to Earth by spacecraft.

Stardust. The Stardust mission has been a spectacular success, having returned to Earth dust from comet Wild 2 and, perhaps, contemporary interstellar dust. Although only the results of the preliminary examination have been published to date [1], the character of dust from the most primitive body sampled so far have deepened our understanding of the early system. The key result, surprising to some and anticipated by others, is that much of the dust was processed at high temperatures that can only be achieved in the inner solar system and transported by some means to the formation region of the comet, likely in the Kuiper Belt.

Genesis. The Genesis mission sampled the Sun via the solar wind. Although it returned to the surface of the Earth rather more abruptly than planned, much progress has been made in cleaning samples. Neon isotopic data from a metallic glass collector flown on Genesis have profoundly changed our view of solar noble gas components. Solar energetic particles are no longer needed to explain the lunar record of solar noble gases [2]. The most highly anticipated result of Genesis, the oxygen isotopic composition of the Sun, may be achieved within a year.

New Techniques: There has been significant progress in a number of analytical techniques in recent years.

Multicollector mass spectrometry. The development of multicollector inductively coupled plasma mass spectrometry has revolutionized early solar system chronology, leading to the development of new short-lived chronometers, such as ^{182}Hf-^{182}W, as well as extending ^{26}Al-^{26}Mg chronometry to samples with lower Al/Mg and greatly increasing precision of Mg isotopic analysis. Timescales as short as 20,000 years are now being discussed for CAIs formed >4.5 My ago [3]. The multicollector technique has had a similar impact on ion microprobe analyses, with high precision ^{26}Al-^{26}Mg internal isochrons now being obtained on minerals with Al/Mg<10 [e.g., 4]. Careful chemistry and the high precision allowed by multicollector thermal ionization mass spectrometry have now pinned the absolute age of CAIs, and, by extension, the solar system with spectacular precision, 4,567.11±0.16 Ma [5].

Ion microprobe. In addition to multicollection, improvements in spatial resolution through new instruments (NanoSIMS) and new imaging detectors ion microscope-type instruments have led to new discoveries, such as presolar silicates [6], early solar system water enriched in heavy oxygen isotopes [7], and other unusual oxygen isotope components [e.g., 8].

Resonant ionization mass spectrometry (RIMS). The use of lasers to resonantly ionize atoms sputtered or ablated from a surface allows very high sensitivity and practical elimination of isobaric interferences. This technique has mostly been applied to presolar grains and has led to: (1) the recognition of nearly pure s-process Zr, Mo, Ru and Ba [9,10]; (2) the inferred presence of 99Tc in presolar SiC, cementing their origin by s-process nucleosynthesis in low mass asymptotic giant branch stars [10]; and (3) recognition of a new nucleosynthesis mechanism likely caused by neutron bursts during supernova explosions [11,12].

Electron microscopy. The use of focused ion beam (FIB) sectioning techniques has allowed extension of transmission microscopy to samples not easily sectioned by ultramicrotomy. This technique has been used to study mineralogy and petrology of presolar grains and Stardust cometary dust.

Synchrotron x-ray sources. Synchrotron x-ray fluorescence has been particularly useful in studying interplanetary dust particles and is being widely applied to Stardust cometary samples [e.g., 13]. The synchrotron also is enabling studies of transition element valence in solar system materials, which can be used to infer oxygen fugacity in the early solar sytem [14].

Astrophysics: The fields of astrophysics and cosmochemistry are profoundly influencing one another. The detailed record of chronology and physicochemical conditions preserved in meteorites and their components is shaping models of events in the early solar system. New observations of young stellar stars and disks with the Spitzer spacecraft and other advanced instruments are becoming available. Presolar grains are not only deepening our understanding of stellar nucleosynthesis but their survival in the solar system constrains thermal histories in the solar nebula.

Summary: This is an exciting time in cosmochemistry, with new observations and ideas that are continually challenging the conventional wisdom on the early history of the solar sytem.

References: [1] Brownlee et al. (2006) *Science, 314,* 1711–1716. [2] Grimberg A. et al. (2006) *Science, 314,* 1133–1135. [3] Thrane K. et al. (2006) *Astrophys. J.*,

646, L159–L162. [4] Kita N. T. et al. (2007) this volume. [5] Amelin Y. et al. (2006) LPS XXXVII, Abstract #1970. [6] Messenger S. et al. (2003) *Science*, *300*, 105–108. [7] Sakamoto N. et al. (2007) *Science*, *317*, 231–233. [8] Aléon J. et al. (2005) *Nature*, *437*, 385–388. [9] Lugaro M. et al. (2003) *Astrophys. J.*, *593*, 486–508. [10] Savina M. R. et al. (2004) *Science*, *303*, 649–652. [11] Pellin M. J. et al. (1999) *LPS XXX*, Abstract #1969. [12] Mayer B. S. et al. (2000) *Astrophys. J.*, *540*, L49–L52. [13] Flynn G. J. et al. (2006) *Science*, *314*, 1731–1735. [14] Simon S. B. et al. (2007) *Geochim. Cosmochim. Acta*, *71*, 3098–3118.

TIMING OF AQUEOUS ALTERATION ON THE CM PARENT-BODY: MINERAL CHEMISTRY AND MN-CR SYSTEMATICS FOR THE CM CHONDRITES Y 791198 AND QUE 93005. Simone de Leuw[1], Alan E. Rubin[2], Axel K. Schmitt[1] and John T. Wasson[1,2], [1]Department of Earth and Space Sciences, University of California, Los Angeles, CA 90095-1567, USA (sdeleuw@ucla.edu), [2]Institute of Geophysics and Planetary Physics, University of California, Los Angeles, CA 90095-1567, USA.

Introduction: It is well-known that aqueous alteration occurred on the CM parent-body and that this process resulted in the formation of secondary phases such as carbonates, phyllosilicates, sulfides, sulfates, oxides, and hydroxides [1, 2]. Little is known about the timescale and location of these alteration processes. It is important to determine where and especially when and for how long the alteration took place. There is increasing evidence of a wide range of degrees of CM aqueous alteration. Rubin et al. [3] proposed a new alteration sequence that correlates with all of the major mineralogic and textural characteristics that change with progeressive alteration. They assigned petrologic subtypes ranging from 2.6 for the least-altered samples to 2.0 for the most highly altered CM chondrites. Alteration products such as carbonates can potentially provide a record of the timing of aqueous alteration on the parent-body. It is possible that the timescale of alteration is comparable to the half-life of ^{53}Mn (3.7 Ma) and that the degree of aqueous alteration is correlated with the age of carbonate formation.

Observations: In the new classification scheme of [3] for CM chondrites, QUE 93005 and Y 791198 are CM2.1 and CM2.4, respectively. The less-altered CM chondrite Y 791198 contains only calcite and/or aragonite ($CaCO_3$) in the fine-grained matrix, whereas the highly altered QUE 93005 chondrite contains both calcite/aragonite and dolomite ($CaMg(CO_3)_2$) grains. Calcite in Y 791198 occurs as single crystals and as irregularly shaped aggregates up to 80 μm in size. Calcite grains and aggregates in QUE 93005 range between 50 and 100 μm. Dolomite in this sample occurs as single crystals within the matrix and in rare cases as single grains within larger calcite grains. In general, dolomite grains are smaller and range between 10 and 30 μm.

Electron-probe analyses for both samples showed elevated Mn contents in several carbonate grains, indicating their suitability for Mn-Cr isotopic studies. Mn contents in calcite from Y 791198 range between 0.11 and 0.93 wt.%. EMPA in QUE 93005 showed that Mn contents in the dolomite grains are much higher than in the co-existing calcite grains. Mn contents range from 0.05 to 1.1 wt.% in calcite and from 1.8 to 5.0 wt.% in dolomite. In both CM samples, Cr contents in the secondary carbonates are below the detection limit of the electron probe.

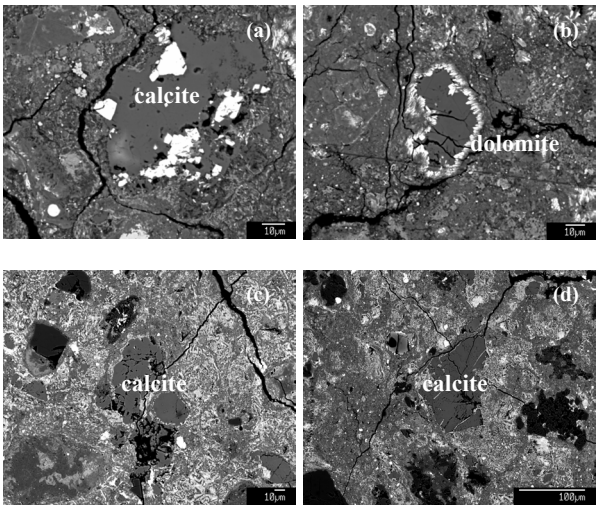

Figure 1: Backscattered electron images for typical grains of calcite (a) and dolomite (b) in QUE 93005 and for typical calcite grains in Y 791198 (c-d).

Results: Isotopic analyses were carried out on the high-resolution ims 1270 ion microprobe at UCLA. For our measurements, we used a $^{16}O^-$ primary beam, accelerated to 12.5 keV, to generate positive secondary ions. The secondary voltage was set to 10 kV with a 50 eV energy window. The mass resolving power was ~4000 and the beam size was approximately 10 μm. We used San Carlos olivine as our standard. $^{55}Mn/^{52}Cr$ ratios were calculated from $^{55}Mn^+/^{52}Cr^+$ using the sensitivity factor determined from San Carlos olivine (Mn/Cr = 10.93 [4]). Deviations in $^{53}Cr/^{52}Cr$ ratios are reported as $\delta^{53}Cr$ (‰).

We determined Mn-Cr systematics for a subset of 11 out of more than 60 characterized carbonates from the CM chondrite QUE 93005. We obtained replicate analyses on nine carbonate grains, getting a total of 22 measurements. Ten of the 22 measurements show excesses in $\delta^{53}Cr$ with the highest excess of ~1100‰, corresponding to a Mn/Cr ratio of more than 30,000. The ^{53}Cr excesses in QUE 93005 are linearly correlated with the $^{53}Mn/^{55}Mn$ ratio, indicating the *in-situ* decay of ^{53}Mn at the time of carbonate formation. The slope of the correlation line, determined by a weighted

least-squares fit, corresponds to an initial $^{53}Mn/^{55}Mn$ ratio of $(4.1 \pm 0.3) \times 10^{-6}$ (Fig. 2).

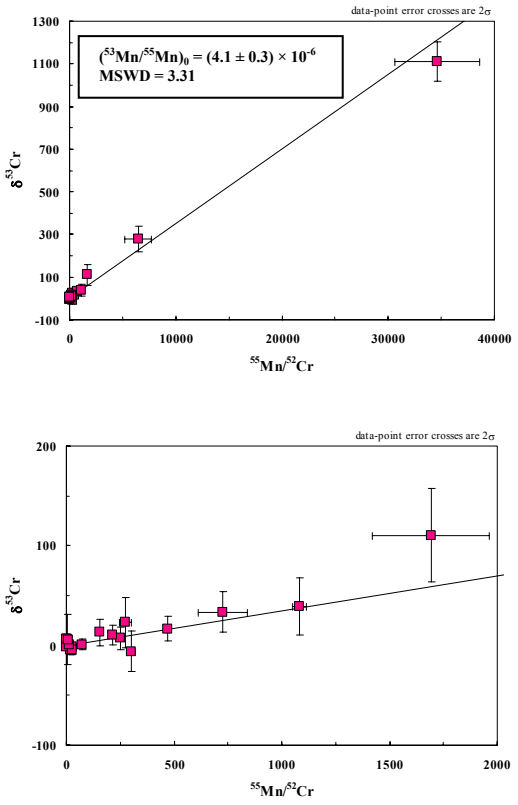

Figure 2: Mn-Cr evolution diagram for carbonates in QUE 93005. Deviations from the terrestrial $^{53}Cr/^{52}Cr$ ratio are plotted as δ values in ‰. An expanded-scale view of the lower left-hand corner of this plot is also shown (bottom).

Future work and conclusions: In order to constrain the time span of aqueous alteration on the CM parent body, we will further study the Mn-Cr isotopic systematics on the less-altered sample Y 791198 with the high-resolution ims 1270 ion microprobe. This sample was already studied by [5], using the LLNL ims 3f ion microprobe. The slope of their correlation line corresponds to an initial $^{53}Mn/^{55}Mn$ ratio of $(8.7 \pm 1.5) \times 10^{-6}$. In addition, we will examine other CM chondrites of different petrographic subtypes, preferentially of the CM end-members. It may also be possible that different initial $^{53}Mn/^{55}Mn$ ratios are present within the same meteorite. Previous work by [6] and [7] and our results already show that the most-altered samples have the lowest $(^{53}Mn/^{55}Mn)_0$ ratios. These results imply that the degree of aqueous alteration is correlated with the age of carbonate formation and that alteration occurred for an extended period of time on the CM parent body. Additional measurements of alteration phases in CM chondrites are needed in order to constrain the timeframe in which aqueous alteration occurred on the CM parent body.

References: [1] Zolensky M. E. and McSween H. Y. (1988) In: *Meteorites and the Early Solar System*, 114-143. [2] Brearley A. J. and Jones R. H. (1998) *Rev. Mineral., 36,* pp 398. [3] Rubin A. E. et al. (2007) *Geochim. Cosmochim. Acta, 71,* 2361-2382. [4] Hoppe et al. (2004) *LPS XXXV,* Abstract #1313. [5] Brearley A. J. and Hutcheon I. D. (2002) *Meteorit. Planet. Sci 37,* A23. [6] Brearley A. J. and Hutcheon I. D. (2000) *LPS XXXI,* Abstract #1407. [7] Brearley A. J. et al. (2001) *LPS XXXII,* Abstract #1458.

DECOUPLED ^{182}Hf-^{182}W AND ^{146}Sm-^{142}Nd SYSTEMATICS OF SNC METEORITES: IMPLICATIONS FOR EARLY MARS EVOLUTION. V. Debaille[1], A.D. Brandon[2], Q.-Z. Yin[3], B. Jacobsen[3], [1]Lunar and Planetary Institute, 3600 Bay Area, Houston TX 77058 (debaille@lpi.usra.edu); [2]NASA-Johnson Space Center, Mail code KR, Houston TX 77058 (alan.d.brandon@nasa.gov); [3]Department of Geology, University of California, One Shields Avenue, Davis, CA 95616-8605 (yin@geology.ucdavis.edu; jacobsen@geology.ucdavis.edu).

Introduction: The short-lived ^{182}Hf-^{182}W chronometer with a half-life of 9 My has previously been applied to constrain early metal-silicate differentiation (i.e., core formation) in planetary bodies [1-6]. In Mars, the ε^{182}W value of the primitive Martian mantle (PMM) (i.e., the silicate mantle after core segregation) was estimated using the short-lived ^{146}Sm-^{142}Nd chronometer, with a half-life of 103 My. The reasoning is that because the ^{146}Sm-^{142}Nd system is not influenced by core formation, considering samples with chondritic ε^{142}Nd should provide a direct estimate of the ε^{182}W of the PMM [4, 6].

However, this approach may be limited as a result of two factors. First, Hf/W fractionation is produced by two processes, metallic core formation, *and* silicate differentiation. In particular, the presence of garnet and majorite potentially can strongly fractionate Hf/W in early silicate differentiation [7]. Second, after the closure time of ^{182}Hf-^{182}W systematics, i.e. when ^{182}Hf became effectively extinct (~50 My after solar system formation), ^{146}Sm was still active and may have recorded later differentiation events in ε^{142}Nd not observed in ε^{182}W values.

New measurements for the chondritic ε^{142}Nd value [8, 9] raises several issues when determining the ε^{182}W of the PMM using ^{146}Sm-^{142}Nd systematics as a proxy. For example, Foley et al. [6] used the regression line observed between ε^{142}Nd and ε^{182}W systematics for the shergottite suite (both incompatible trace elements (ITE) depleted and enriched shergottites) to estimate that PMM is characterized by a ε^{182}W=0.34 for a ε^{142}Nd=0. Using the new chondritic value ε^{142}Nd=-0.18 [9], the ε^{182}W of the PMM is now estimated to be 0.29 using that line of reasoning. This new value is not resolvable from the previous one, but is very close of what is observed in ITE enriched shergottites Zagami and Shergotty. However, those meteorites are likely generated by mixing between ITE depleted and enriched end-members. As such their chondrite-like ε^{142}Nd is likely fortuitous and results from the mixing process instead of being representative of the PMM. Hence, observing a chondritic ε^{142}Nd in a SNC meteorite does not necessarily imply that such a sample is representative of the PMM.

To illustrate the discrepancy between ^{182}Hf-^{182}W and ^{146}Sm-^{142}Nd systematics, new ^{176}Hf/^{177}Hf, ^{143}Nd/^{144}Nd and ^{142}Nd/^{144}Nd have been obtained in three nakhlites (Nakhla, MIL03346 and Yamato000593). Nakhlites are characterized by high ε^{182}W among the SNC suite of approximately +3 [1, 4, 6] and an ε^{142}Nd similar to depleted shergottites of +0.6-0.9 [6, 10, 11]. It has hence been proposed that the source of nakhlites was established very early in Mars history (~8-10 My [4, 6]) in moderately fractionated source (Fig. 1). This time interval is during the time of live ^{182}Hf and thus constraining the origin of both Lu/Hf and Sm/Nd fractionation in the source of nakhlites will aid in interpreting the variation observed in ε^{182}W in the SNC's.

Discussion: The three nakhlites studied here are characterized by homogeneous isotope compositions with ^{176}Hf/^{177}Hf= 0.282998±31 to 0283108±10, ^{143}Nd/^{144}Nd= 0.512854±1 to 0.512873±1 and ε^{142}Nd= 0.61±0.02 to 0.67±0.03, with all errors at 2σ. The $\varepsilon_{Hf}/\varepsilon_{Nd}$ ratios of all nakhlites range from 0.8 to 1.2. This is consistent with melts derived from residues with ancient garnet segregation [12]. Nakhlites do not plot in a two-stage evolution diagram for ^{142}Nd/^{144}Nd versus ^{143}Nd/^{144}Nd ([10, 13], this study), indicating that their source has not always been a closed system. Thus, their source requires a more complex origin, which may be related to garnet/majorite segregation.

High ε^{182}W anomalies are predicted in a moderately fractionated source formed early in planet differentiation (Fig. 1). An alternative way to generate high ε^{182}W value is from crystallization of a more fractionated source (i.e., in presence of majorite, Fig. 1), but later in planetary differentiation. The presence of majorite will increase both Sm/Nd and Hf/W ratios (e.g., [7]). This could result in large excesses in ε^{142}Nd and ε^{182}W if fractionation occurs early in a planet's history (Fig. 1), in addition to Hf/W fractionation resulting from core formation affecting the ^{182}Hf-^{182}W system. Between 17 and 23.5 GPa, the Martian mantle is thought to be composed of

~45% of majoritic garnet [14]. A $\varepsilon^{182}W$ value of +3 is expected, with a $\varepsilon^{142}Nd$ of +1.1 for a nakhlite source formation in the majorite stability field at ~40 My after solar system formation (grey arrow, Fig.1). However, such a high $\varepsilon^{142}Nd$ value is not observed in nakhlites ([6], this study), indicating that their source did not remain a closed-system since its differentiation at ~40My, likely because of garnet/majorite has been removed. This observation is consistent with a scenario where the nakhlite source acted as a closed-system when ^{182}Hf was extant (~50 My), but then, garnet/majorite was removed from the source and the nakhlites source could never reach a $\varepsilon^{142}Nd$ value of +1.1.

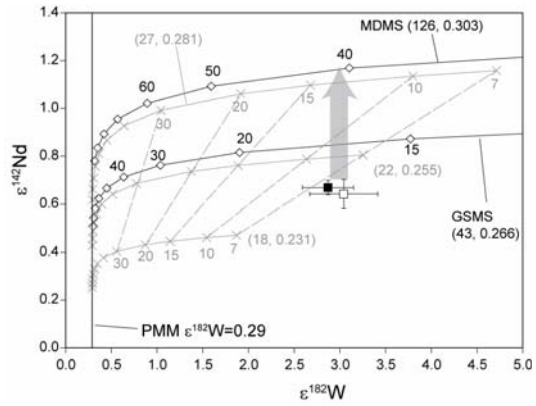

Figure 1: $\varepsilon^{142}Nd$ vs. $\varepsilon^{182}W$ in the nakhlites (adapted from [6]). Black square: Nakhla; white square: average value for all nakhlites ($\varepsilon^{142}Nd$: this study, $\varepsilon^{182}W$; [1, 6]). Error bars are 2σ. Symbols on the curves represent the present-day $\varepsilon^{182}W$ and $\varepsilon^{142}Nd$ attained in a source region for the age indicated in My. ($^{147}Sm/^{144}Nd$, $^{180}Hf/^{183}W$) pairs are indicated for each curves The black curves show the results for a majorite-bearing deep mantle source (MDMS) and for a garnet-bearing shallow mantle source (GSMS) [6]. Grey curves are three depleted mantle source compositions from [4]. The grey arrow indicates the $\varepsilon^{142}Nd$ vs. $\varepsilon^{182}W$ value that nakhlite source should have reached when crystallizing in the majorite stability field ~40 My after solar system formation if no garnet segregation has occurred after ^{182}Hf extinction.

Using an initial $^{147}Sm/^{144}Nd$ of 0.303 [6], and using the $^{147}Sm/^{144}Nd$ of majoritic garnet (~1.89) [15], mass balance indicates that 4% of majoritic garnet has to be removed from the nakhlites source to generate the observed $^{147}Sm/^{144}Nd$ in nakhlites (0.235).

If garnet segregation occurred as a single event, the nakhlite source can be modeled by a three-stage model, where T_0 = 4.567 Gy, t_1 is the time of differentiation in majorite stability field (closed-system), t_2 the time of garnet segregation (unknown) and t_3 is the crystallization age of the nakhlites (~1.3 Gy). Because garnet segregation is postulated from the discrepancy in $\varepsilon^{142}Nd$ (i.e. ~+0.63 versus predicted +1.1), but not in $\varepsilon^{182}W$, t_2 must lie between 50 My and 500 My after solar system formation. In Fig.1, t_1 is estimated at 40 My after T_0 for a $\varepsilon^{182}W$ of ~3 in the majorite stability field (grey arrow). Using time-integrated source ratios calculated from $^{143}Nd/^{144}Nd$ and $^{176}Hf/^{177}Hf$ measured in nakhlites (= source t_2; i.e., after majoritic garnet segregation) and source ratios before majoritic garnet segregation (= source t_1; closed-system in majorite stability field) estimating 4% of majoritic garnet loss, a value of t_2=100 My gives $\varepsilon^{143}Nd(t_3)$ = +17.1; $\varepsilon^{176}Hf(t_3)$ = +15.6 and $\varepsilon^{142}Nd$ = +0.61. These values can be compared to the average measured values in nakhlite, respectively +16.4, +15.3 and +0.63. Thus, a nakhlite source that first crystallized ~40 My after solar system formation in the majorite stability field and then experienced majoritic garnet segregation ~60 My later can reproduce values observed in nakhlites.

Conclusions: New $^{176}Hf/^{177}Hf$, $^{143}Nd/^{144}Nd$ and $\varepsilon^{142}Nd$ and previous $\varepsilon^{182}W$ measured in nakhlites are consistent with a three-stage model in their source. A first differentiation event occurred ~40 My after solar system formation in the majorite garnet field. Majoritic garnet was removed from the nakhlite source ~60 My later. These conclusions show that the ^{182}Hf-^{182}W and ^{146}Sm-^{142}Nd systematics are decoupled in nakhlites and hence, that a concomitant use of these systematics do not provide constraints on source crystallization timing. It also implies that the nakhlite source differentiation timing is longer than previously estimated. As demonstrated for shergottites, $\varepsilon^{142}Nd$ cannot necessarily be used to estimate the $\varepsilon^{182}W$ of the PMM. However, a SNC meteorite showing an "actual" chondritic $\varepsilon^{142}Nd$, i.e. not artificially acquired by mixing, could be the key-sample.

References

[1] Halliday A.N. and Lee D.-C. (1997), *Nature 388* 854-857; [2] Kleine T. et al. (2002), *Nature 418* 952-955; [3] Yin Q.-Z. et al. (2002), *Nature 418* 949-951; [4] Kleine T. et al. (2004), *GCA 68* 2935-2946; [5] Quitté G. and Birck J.L. (2004), *EPSL 219* 201-207; [6] Foley N.C. et al. (2005), *GCA 69* 4557-4751; [7] Righter K. and Shearer C.K. (2003), *GCA 67* 2497-2507; [8] Boyet M. and Carlson R.W. (2005), *Science 309* 576-581; [9] Andreasen R. and Sharma M. (2006), *Science 314* 806-809; [10] Harper C.L. et al. (1995), *Science 267* 213-216; [11] Carlson R.W. and Irving A.J. (2004), *LPS XXXV* #1442; [12] Vervoort J.D. and Patchett J. (1996), *GCA 60* 3717-3733; [13] Borg L.E. et al. (1997), *GCA 61* 4915-4931; [14] Bertka C. and Fei Y. (1997), *JGR 102* 5251-5264; [15] Draper D.S. et al. (2003), *PEPI 139* 149-169.

A NON-CHUR INITIAL Nd ISOTOPIC COMPOSITION FOR THE BULK MOON: EVIDENCE FROM EARLY LUNAR SAMPLES. J. Edmunson, Institute of Meteoritics, University of New Mexico (MSC03 2050, 1 University of New Mexico, Albuquerque, NM 87131-0001, Edmunson@unm.edu).

Introduction: Recent dating of Mg-suite troctolite 76335 has shed more light on early lunar chronology. Troctolite 76335 has an age of 4278 ± 60 Ma and an initial ε_{Nd}^{143} value of 0.06 ± 0.34 (Fig. 1). The relatively young age and near-Chondritic Uniform Reservoir (CHUR) initial ε_{Nd}^{143} value of 76335 prevent it from lying within error of the trend defined by Mg-suite norites with negative ε_{Nd}^{143} values relative to CHUR and younger KREEP samples [1,2]. There are three possible explanations for this unexpected result. The first reason is that the ^{147}Sm-^{143}Nd isotopic systematics of troctolite 76335 have been disturbed and do not accurately reflect the true age and initial ε_{Nd}^{143} value of this Mg-suite sample. The second is that the norites and troctolites are not isotopically related. The third involves the assumption that the bulk Nd isotopic composition of the Moon is equivalent to CHUR.

Discussion: The ^{147}Sm-^{143}Nd isotopic systematics of lunar materials, specifically those of highland rocks, are often scrutinized because of the effects of impact-induced thermal metamorphism [e.g., 3]. In the case of troctolite 76535, the ^{87}Rb-^{87}Sr age (4570 ± 70 Ma) [4] is much older than the ^{147}Sm-^{143}Nd age (4260 ± 60 Ma) [5] and the Ar-Ar age (4260 ± 20 Ma) [6]. The Ar-Ar age, and by default the ^{147}Sm-^{143}Nd age, is often considered the metamorphic age while the ^{87}Rb-^{87}Sr age is thought to be the crystallization age, despite the fact that the ^{87}Rb-^{87}Sr age of 76535 has yet to be reproduced [e.g., 7]. For 76335, the ^{147}Sm-^{143}Nd isotopic systematics yielded a six-point isochron, while the ^{87}Rb-^{87}Sr data held no determinable age significance. However, the 76335 ^{147}Sm-^{143}Nd isochron may have experienced rotation in response to thermal disturbance (i.e., a younger age and higher initial ^{143}Nd/^{144}Nd ratio will be produced as a rock undergoes isotopic resetting). If 76335 experienced isotopic resetting, the initial ^{143}Nd/^{144}Nd ratio would decrease as the age of 76335 increased. To evaluate the potential disturbance to the ^{147}Sm-^{143}Nd isochron, we assumed rotation about the whole rock and no loss of rare earth elements during the disturbance. Due to the sub-CHUR ^{147}Sm/^{144}Nd ratio of the whole rock, the initial ε_{Nd}^{143} value of 76335 actually increases relative to CHUR with greater age (Fig. 1). Thus, the difference between the ^{147}Sm-^{143}Nd isotopic systematics of 76335 and the KREEP evolution line of [1,2] cannot be explained by simple isochron rotation.

Given the established petrologic relationships between the Mg-suite norites and troctolites, it is expected that their sources should be isotopically related. However, the calculated initial ε_{Nd}^{143} value for the norites and troctolites differ. This may imply that KREEP in the troctolites formed in a later differentiation event. Conversely, the KREEP signature in the troctolites and norites may both define a single trend which does not have a CHUR-like bulk Moon starting composition.

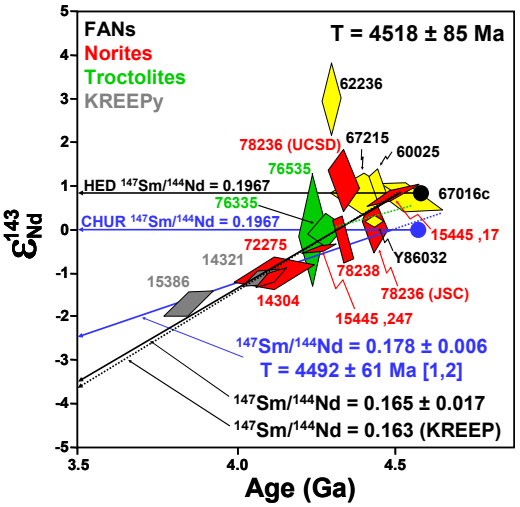

Figure 1. Time versus initial ε_{Nd}^{143} value calculated for the source of each highland and KREEP-rich sample relative to CHUR. FANs plotted in yellow, Mg-suite norites in red, Mg-suite troctolites in green, and younger samples with KREEP signatures in gray. The KREEP source trend (blue line) is defined by Mg-suite norites with negative ε_{Nd}^{143} values and younger KREEP-rich samples 14321, 15386, and NWA 773 [1,2]. Dashed blue line is an extension of this KREEP evolution line. This shows that the KREEP line of [1,2] does not intersect the HED parent body isotopic composition at a reasonable age. The green dashed line represents the calculated age and initial ε_{Nd}^{143} value of 76335 based on whole rock ^{147}Sm-^{143}Nd isotopic data assuming that the isochron rotated due to a disturbance. Note that rotation of the 76335 isochron would not intersect the KREEP line of [1,2]. This implies that the KREEP signature in the troctolite is different than the norite trend. However, if one uses the HED initial Nd isotopic composition for the Moon [12], and establishes a trend for the Mg-suite troctolites and norites, a calculated evolution line equivalent to a ^{147}Sm/^{144}Nd ratio of 0.165 ± 0.017 is produced. The calculated ratio is similar to that calculated for KREEP (0.163) from [14]. This indicates KREEP formation at 4518 ± 85 Ma.

The assumption that the bulk Nd isotopic composition of the Moon is equivalent to CHUR is problematic. First, multiple highland samples and ilmenite basalts indicate an originally positive ε_{Nd}^{143} value for the bulk Moon [e.g., 8]. Data from multiple labs indicate that ferroan anorthosites (FANs) crystallized early with positive ε_{Nd}^{143} values. Recent studies of meteorites and terrestrial samples show that the ε_{Nd}^{142} values of meteorites are negative relative to CHUR [9,10]. The differences between the initial ε_{Nd}^{143} value of CHUR and measured Precambrian terrestrial samples have also been investigated [11]. These samples show an apparent trend towards an initial ε_{Nd}^{143} value of approximately +1 for the bulk Earth.

The fact that FANs have positive initial ε_{Nd}^{143} values, as well as the uncertainties associated with using the CHUR Nd isotopic composition for the bulk Earth, allows the possibility of using a different initial Nd isotopic composition for the bulk Moon. In this case, we used the estimated bulk Moon Nd isotopic composition equivalent to that measured for the howardite-eucrite-diogenite (HED) parent body by [12] and proposed by [13]. A new KREEP evolution line was drawn using a linear regression of the Mg-suite samples (both norites and troctolites) with both positive and negative ε_{Nd}^{143} values. This line has a $^{147}Sm/^{144}Nd$ ratio of 0.165 ± 0.017, almost identical to that calculated for the KREEP composition proposed by [14]. This new evolution line intersects the HED parent body isotopic composition at 4518 ± 85 Ma, indicating the time of KREEP formation.

Implications: One benefit to using an HED initial Nd isotopic composition for the bulk Moon is that the ^{147}Sm-^{143}Nd isotopic systematics of the majority of the Apollo 16 FANs may now be explained by a lunar magma ocean model. The FANs may now also have a LREE-enriched source region, which is implied by their geochemistry. This indicates that 62236 is the only truly disturbed FAN measured to date. The new HED initial Nd isotopic composition accounts for the relatively old age and positive ε_{Nd}^{143} value of Mg-suite norite 15445 ,17. In addition, the age determined for KREEP formation is concordant with the ^{176}Lu-^{176}Hf isotopic systematics of lunar zircons [15].

There are a few disadvantages to using an HED initial Nd isotopic composition for the bulk Moon. For example, if the KREEP ^{147}Sm-^{143}Nd isotopic signature is uniform throughout the Mg-suite, this implies that any differences in the source region lithology that could have been reflected in the REE signature of the rocks is erased by the interaction with KREEP. In addition, the relationship shown between the Mg-suite norites and the younger KREEP-rich rocks in the KREEP line of [1,2] is not reinforced by this model. In fact, the new KREEP source evolution line ($^{147}Sm/^{144}Nd$ = 0.165 ± 0.017 in Fig. 1) does overlap the KREEP-rich samples 14321 and 15386, but does not overlap olivine cumulate NWA 773. This implies that the Mg-suite and other KREEP-rich rocks do not share the same evolutionary history. The new KREEP line is also not as constrained as the KREEP source evolution line proposed by [1,2].

Conclusions: The isotopic study of Mg-suite troctolite 76335 confirmed the CHUR-like initial ε_{Nd}^{143} value of troctolite 76535 [5]. This implies that (1) both troctolites 76335 and 76535 are disturbed, (2) KREEP in the troctolites differentiated later than for norites from a CHUR-like Moon, or (3) the assumption that the Moon has a CHUR initial Nd isotopic composition is in error. Rotation of the ^{147}Sm-^{143}Nd isochron for 76335 about the whole rock will not explain the differences between the isotopic compositions of the Mg-suite troctolites and norites. There is no geochemical evidence that the KREEP component found in troctolites is different from the KREEP component in norites. An initial Nd isotopic composition of the Moon equal to that of the HED parent body appears to be more likely than an initial bulk Moon composition equal to CHUR. A new KREEP evolution line can be drawn through the Mg-suite norites and troctolites with a slope equal to a $^{147}Sm/^{144}Nd$ ratio of 0.165 ± 0.017. This new evolution line corresponds to a KREEP reservoir formation age of 4518 ± 85 Ma, and explains the positive initial ε_{Nd}^{143} values of most FANs and norite 15445 ,17.

Acknowledgements: The author would like to thank L. E. Nyquist and L. E. Borg for their involvement in this work.

References: [1] Borg L.E. et al. (2005) *LPS XXXVI*, Abstract #1026. [2] Edmunson J. and Borg L.E. (2006) *Workshop on Early Planetary Differentiation*, Abstract #4034. [3] Nyquist L.E. et al. (1991) *LPS XXII*, 985-986. [4] Papanastassiou D.A. and Wasserburg G.J. (1976) *Proc. LPS VII*, 2035-2054. [5] Lugmair G.W. et al. (1976) *Proc. LPS VII*, 2009-2033. [6] Husain L. and Schaeffer O.A. (1975) *GRL, 2*, 29-32. [7] Bogard D.D. et al. (1975) *EPSL, 26*, 69-80. [8] Nyquist L.E. and Shih C.–Y. (1992) *GCA, 56*, 2213-2234. [9] Boyet M. and Carlson R.W. (2005) *Science, 309*, 576-581. [10] Rankenburg K. et al. (2006) *Science, 312*, 1369-1372. [11] Nagler Th.F. and Kramers J.D. (1998) *Precambrian Res., 91*, 233-252. [12] Nyquist L.E. et al. (2004) *Antarc. Met. XXVIII*, 66-67. [13] Nyquist L. et al. (2006) *GCA, 70*, 5990-6015. [14] Warren P.H. (1989) *Moon in Trans.*, 106-110. [15] Taylor D.J. et al. (2007) *MAPS, 42*, A147.

THE I-Xe SYSTEM AND THE EARLY HISTORY OF THE LL CHONDRITE PARENT BODY. M. J. Filtness, S. A. Crowther and J. D. Gilmour, , School of Earth, Atmospheric and Environmental Sciences, The University of Manchester, Oxford Road, Manchester, United Kingdom, M13 9PL. Michal.filtness@postgrad.manchester.ac.uk.

Introduction: The 16 Ma half life of ^{129}I makes the I-Xe chronometer ideal for investigating the evolution of planetesimals over the first 50-100 Ma of solar system history. Several previous studies have examined the I-Xe record of the primitive LL chondrites; results from Semarkona [1], Chainpur [2,3] and Parnallee [4] are available in the literature. In this study, we have focused on two other primitive LL chondrites, Bishunpur and Krymka. One goal of our study was to examine whether the I-Xe record of Bishunpur was consistent with the widespread evidence of extinct ^{26}Al in its chondrules [5], or if the I-Xe system has been reset. We also examined a clast from Krymka that may represent a fragment of a previous generation of planetesimals [6]. Overall, by extending the database of analyses we hope to better understand the evolution of the LL chondrite parent body.

LL chondrites: The LL chondrites Semarkona (3.0), Krymka (3.0/3.1), Bishunpur (3.1) and Chainpur (3.4) are among the most primitive ordinary chondrites [7]. Both Semarkona and Bishunpur appear to have suffered *in situ* hydrous alteration – this has resulted in the destruction of all but the most magnesian mafic minerals in Semarkona [7]. Primary sulphides such as troilite have been partially changed into phyllosilicates and Ni-rich pyrrhotite. The matrix of Krymka is primarily made of opaque silicates and its composition is uniform and significantly more oxidized than that of Bishunpur and Chainpur [8]. Chainpur is the most equilibrated of the four samples [8]. Based on thermoluminescence sensitivity, it was reported that Bishunpur is less primitive and unequilibrated than Krymka [9]. However, it was also noted that Krymka and Bishunpur contained some recrystallized matrix, but Chainpur did not [8]. It seems that classifying the samples according to a trend of increasing processing is non-trivial.

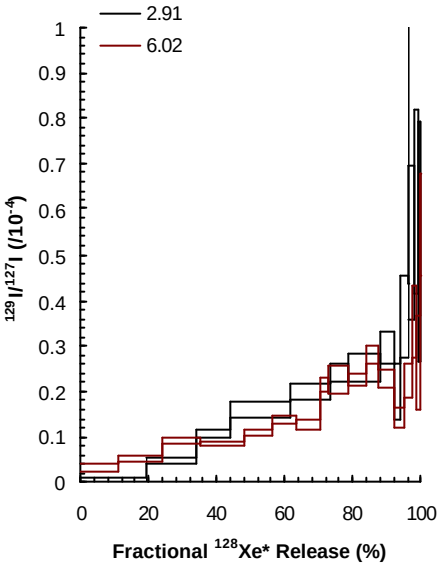

Fig. 1: Step release diagrams for two adjacent chondrules from a section of Bishunpur. Consistent ratios obtained after ~80% release of ^{128}Xe correspond to ages 40 Ma after Shallowater. Both show marginal evidence of an earlier event at higher release temperatures.*

Method: The principles of I/Xe analysis have been recently described [10] and are summarised in an accompanying abstract (Gilmour, Pravdivtseva et al.). Our samples (3 Bishunpur chondrules, 4 Krymka chondrules and 2 fragments of the Krymka clast) were loaded into a sealed tube alongside aliquots of the irradiation standard, Shallowater enstatite, and exposed to a thermal neutron fluence. Xenon was extracted using laser step heating [3] and isotopic analysis performed using the resonance ionization mass spectometer RELAX (Refrigerator Enhanced Laser Analyser for Xenon) at the Univeristy of Manchester [11]. Data analysis revealed some variation with tube location in the ^{128}Xe*/^{129}Xe* determined for Shallowater enstatite, so results reported here should be considered provisional within ~3 Ma pending analysis of the remaining aliquots of the Shallowater standard.

Results: All samples yielded a consistent ^{129}Xe*/^{128}Xe* ratios over a range of consecutive, high temperature releases that can be interpreted as corresponding to an initial iodine ratio.

Two Bishunpur chondrules exhibited a trend of increasing ^{129}Xe*/^{128}Xe* with temperature, ultimately converging on the same value. These samples were in close proximity in a parent section, suggesting that this records a parent-body process (Fig. 1). The third chondrule, from the same section, yielded no clear isochron, but reached a maximum ^{129}Xe*/^{128}Xe* ratio equivalent to an age ~8 Ma after Shallowater..

Krymka chondrules all yielded isochrons corresponding to -9.0 ± 1.6, -11.1 ± 3.0, -14.2 ± 0.9 and -27.7 ± 2.3 Ma (negative numbers denote ages later than Shallowater). One fragment of the clast yielded an isochron corresponding to resetting at -22.6 ± 3.2 Ma.

Discussion: In contrast to clear evidence for live ^{26}Al in LL chondrite chondrules, our data suggest that the I-Xe system has been reset relatively late in the history of the early solar system. In Fig 2, we summarise I-Xe data for the most primitive LL chondrites showing consistent evidence for late processing on this parent body. There is little evidence of a trend with increasing petrologic type, though such a trend may become more apparent if and when a wider range of samples have been analysed. In the light of the close agreement observed for our Bishunpur samples, it is possible that such variation as is apparent may reflect different sampling strategies, although 2 separate studies of Chainpur obtained similar results [2,3].

In Figure 3 we present accumulated data for the LL chondrites mapped against an absolute timescale based on assigning an age of 4563.3 Ma to closure of the I-Xe system in Shallowater [12]. It seems that 80% of the events recorded by the I-Xe system on the LL chondrite parent body occurred within the first 20-25 Ma of solar system evolution, with a declining rate over the ensuing 10s of Ma. This contrasts with the relatively sharp isochronism among chondrules of the enstatite [12] and ordinary [13] chondrites. In addition, it postdates the reasonable timescales over which radioactive decay can cause thermal resetting. We speculate that these primitive meteorites retained sufficient volatiles to remobilise iodine host phases during impact events.

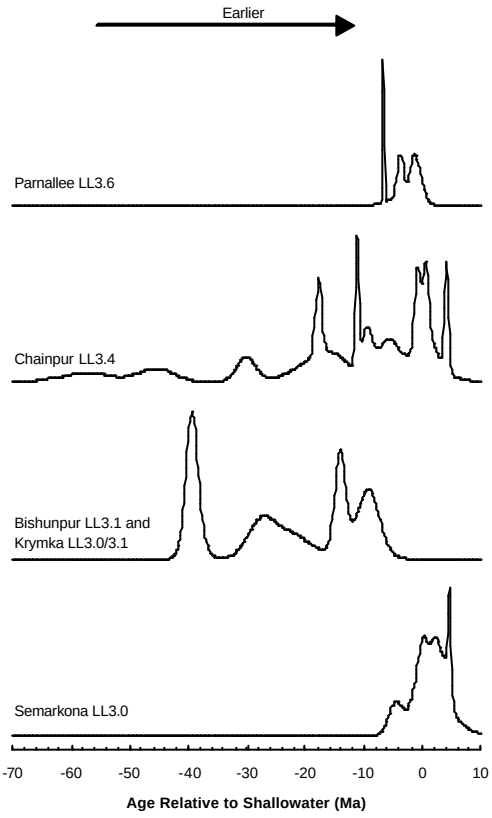

Fig. 2. Summary diagram of LL chondrite I-Xe data. Each age and associated error has been used to create a unit-area Gaussian, these have been summed together for each meteorite (curves are normalised to produce the same maximum value). Data from this work and refs [1] (Semarkona), [2,3] (Chainpur) and [4] (Parnallee).

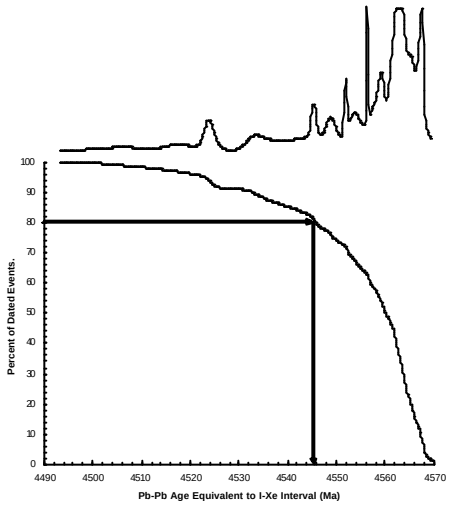

Fig.3. Summary diagram of equivalent Pb-Pb ages derived from I-Xe intervals for 5 separate studies of LL chondrites (top), and cumulative fraction of dated entities (bottom). The procedure adopted is as for Fig. 2, and each date has been assigned equal weight.

References: [1] Swindle T. D. *et al.* (1991) *GCA 55*, 3723- 3734. [2] Swindle T. D. *et al.* (1991) *GCA 55*, 861-880. [3] Holland G. *et al.* (2005) *GCA 69*, 189-200. [4] Gilmour *et al.* (2000) *MAPS 35*, 445-455. [5] Mostefaoui S. *et al.* (2000). *GCA 64*, 1945-1964. [6] Sokol A. K. *et al.* (2006) *MAPS 41*, A164 [7] Alexander, C, M, O'D. *et al.* (1989). *GCA 55*, 3045-3057. [8] Rambaldi, E. R. *et al.* (1984). *GCA 48*, 1885-1897. [9] Sears, D, W. *et al.* (1980). *Nature 287*, 791-795. [10] Gilmour J. D. *et al.* (2006) *MAPS 41*, 19-31. [11] Gilmour et al. (1994) *Rev. Sci. Instrum. 65*, 617-625. [12] Whitby J. A. *et al.* (2002) *GCA 66*, 347-359. [13] Gilmour J. D. *et al.* (1994) *MAPS 30*, 405-411.

TIMING AND LOCATION OF CAI ALTERATION IN ALLENDE: EVIDENCE FROM CAI-MATRIX INTERACTIONS R. L. Ford and A. J. Brearley, Dept. of Earth and Planetary Sciences, MSC03-2040, 1University of New Mexico, Albuquerque, NM 87131 (rford@unm.edu).

Introduction: The components of chondritic meteorites (CAIs, chondrules, matrix, etc) preserve a complex record of early solar system processes. CAIs, in particular, as the earliest surviving solar system solids, are of fundamental importance for understanding the earliest stages of protoplanetary disk evolution. However, many CAIs have experienced multistage formation and alteration histories that are challenging to interpret [1-5]. This is particularly true of CAIs in the oxidized CV3 chondrite, Allende which have been studied extensively. These CAIs have clearly experienced variable, but often extensive alteration that has overprinted their primary mineralogy [2, 3, 6]. Understanding the timing and location of this alteration is of fundamental importance for constraining conditions within the solar nebula. However, the complex alteration products in Allende CAIs have led to conflicting interpretations of the environment in which secondary processing occurred [4]. Both nebular and parent body processes been invoked to explain the alteration of CAIs in the Allende meteorite. Recent petrographic and isotopic studies of a variety of different characteristics of Allende have generally provided support for alteration within a parent body environment [1, 5, 7]. In order to gain additional insights into the location and timing of alteration of CAIs in Allende, we have undertaken a systematic study of the mineralogy of a large number of CAIs *in situ* in multiple thin sections of Allende. We have focused specifically on the style and degree of alteration of the CAIs as well as relationships between the CAIs and their associated matrix. Our results also suggest that alteration of most CAIs occurred in a parent body environment after accretion, but the extent of alteration of individual CAIs is variable. This variability is partially the result of differing primary mineralogical and textural characteristics of individual CAIs. However, other factors, such as local variations in the availability of fluid also appear to have been important.

Methods: We examined 16 type A CAIs *in situ* from 6 thin sections of the Allende meteorite. Several of the samples studied are from serial thin sections, and objects in one thin section are routinely found in the adjacent thin section. We used SEM, followed by electron microprobe WDS X-ray element mapping and quantitative microprobe analysis to characterize these CAIs.

Results: All CAIs observed in this study showed evidence of alteration to varying degrees. The alteration products of these CAIs are similar to those described previously [4, 6, 7], and their textural characteristics indicate that alteration of different primary CAIs phases occurred in a progressive sequence. Melilite clearly altered first followed later by Ca-pyroxene, and perovskite. In all the CAIs studied, regions of alteration are characterized by enhanced Na and Cl contents due to the presence of nepheline and sodalite alteration products. These regions also exhibit significant depletions in Ca, shown in figure 1, largely as a result of alteration of primary melilite. A notable feature of the CAIs is the presence of a distinct zone or aureole of Ca-enrichment in the matrix around the CAIs, that is generally complementary in shape to the depleted zone within the CAI itself. The aureoles range from nearly absent around some CAIs, to continuous zones of enrichment that entirely surround the CAI. This enrichment is caused by the presence of nodules of andradite and Ca-pyroxene within the matrix itself. These Ca enrichments are distinctly better developed around the most heavily altered CAIs and are reminiscent of Ca-rich rims seen around dark inclusions from Allende [7]. Examples of advanced and intermediate CAI alteration and associated Ca-rich aureole development are shown in figures 1 and 2.

Discussion: Collectively, these observations provide important clues as to the timing and environment of alteration of CAIs in Allende. First, there is clear evidence that systematic elemental exchange has occurred between CAIs and matrix, that is exactly analogous to that observed by [7] around Allende dark inclusions. Soluble Ca released by alteration of melilite has been mobilized from the interior of the CAIs and has precipitated in the matrix as Ca-rich pyroxene and andradite-rich aureoles. Such precipitation reactions are very likely driven by variations in the activities of different mobile species and pH as modeled by [7]. Conversely, Na and Cl are mobilized into CAIs and form feldspathoid minerals by reaction with immobile Al from primary melilite. There is also evidence of significant Si mobilization into CAIs during the alteration. These observations require that CAIs and matrix were assembled together within a parent body and required a fluid to transport soluble elements over the scale of 10s of microns.

Second, all CAIs have experienced similar styles of alteration, but to different degrees. Assessing the absolute degree of alteration of an individual CAI is somewhat complex, because many CAIs do show signifi-

cant internal variability in their extent of alteration. Nevertheless, it is clear that there are gross differences between the degree of CAI alteration observed in different thin sections. Based on the evidence presented above alteration clearly occurred *in situ*, after accretion and so the variation in the degree of alteration has to be explained by plausible factors, of which there are several possibilities. Differences in the primary mineralogical and textural characteristics of CAIs probably play at least some role in controlling the extent alteration. In addition, regolith processes may contribute to mixing of components which have experienced different degrees of aqueous alteration in different parts of the CV3 parent body. Finally, some of the differences might reflect local-scale variations in the fluid availability. We are currently examining the potential role of each of these factors.

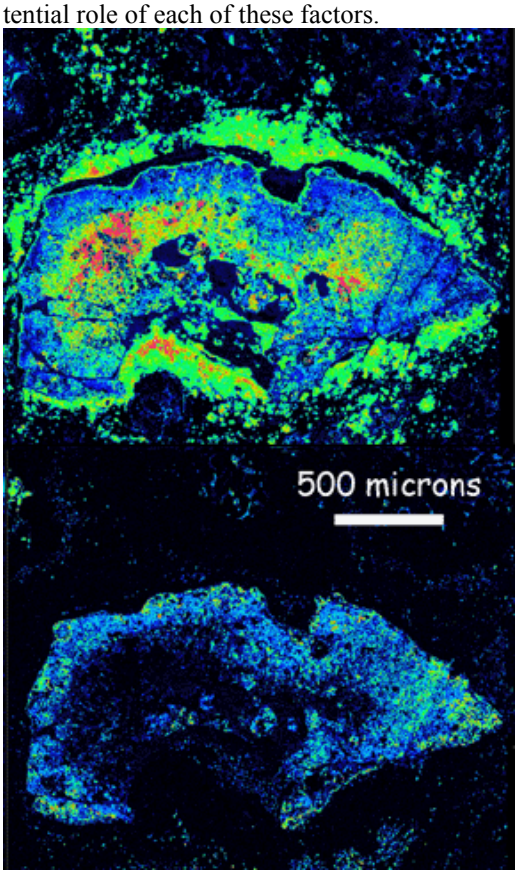

Figure 1. *Two X-ray maps of the same type a CAI are shown above, with Ca on top and Na on the bottom. These X-ray maps demonstrate the correlation between Na enrichment and a well developed Ca-rich aureole.*

Within each thin section, similar alteration is observed between the different CAIs. The more advanced aureoles are present on more than one CAI within a thin section. Likewise if a CAI has little or no aureole, then CAIs within that thin section are also lacking the aureole. The localization of alteration effects is a strong indicator that parent body processes were the cause of these Ca-rich regions immediately adjacent to some CAIs within Allende.

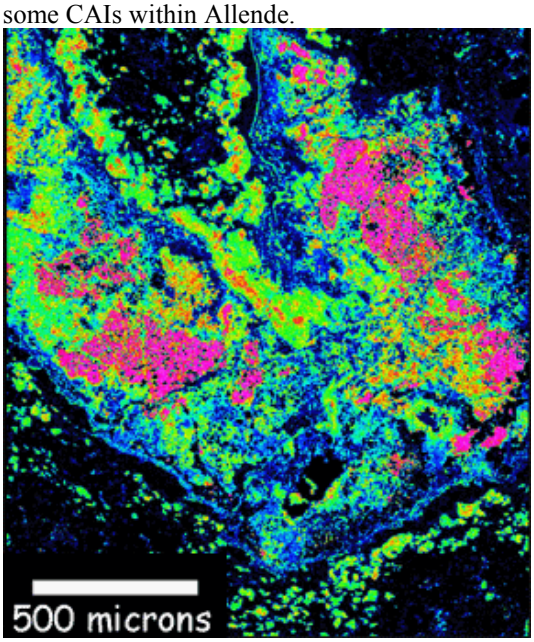

Figure 2. *Ca X-ray map of a Type A CAI with an intermediate Ca-rich ring.*

Conclusions: Element exchange between CAIs and adjacent matrix is pervasive in Allende and appears to correlate with the degree of alteration exhibited by each individual inclusion. These two lines of evidence are strong indicators that the CAIs altered *in situ* after accretion, consistent with other observations on Allende [4, 7]. The variable alteration displayed by these CAIs is probably the result of a combination of factors including the primary characteristics of the inclusions, mixing due to regolith processes and possible localized variations in the availability of water.

References: [1] MacPherson, G.J., et al. (2005) *ASP Conference Series*, Vol 341, pp. 225-250. [2] Meeker, G.P., et al (1983) *Geochim. Cosmochim. Acta.* Vol 47 pp. 707-721. [3] Simon, S.B., et al. (1998) *Meteoritics & Planet. Sci.* 33 pp 115-126. [4] Krot, A.N. et al. (1995) *Meteoritics*, vol 30, pp. 748-775. [5] Krot, A.N. et al. (1998) *Meteoritics & Planet. Sci.* 33, pp. 1065-1085 [6] Hashimoto, A., and Grossman, L., 1987, *Geochim. Cosmochim. Acta.* Vol 51, pp. 1685-1704. [7] Krot A. N. et al. 2000. *Geochemistry International.* 38 pp 351-368.

EXTINCT ^{26}AL FROM WOLF-RAYET STARS: ACCUMULATION, VARIATION, AND IMPLICATIONS. Eric Gaidos[1], Nicholas Moskovitz[2,3], Jonathan Williams[2], Daniel Rogers[3], [1]*Department of Geology & Geophysics,* [2]*Institute for Astronomy,* [3]*Department of Physics & Astronomy, University of Hawaii at Manoa, Honolulu HI 96822, USA, (gaidos@hawaii.edu).*

Primitive meteorites contain compelling evidence for the presence of short-lived radionuclides (SLRs) early in Solar System history. SLRs such as ^{26}Al ($\tau_{1/2}$ = 0.72 Myr) and ^{60}Fe ($\tau_{1/2}$ = 1.5 Myr) may have been important sources of internal heat for bodies that accreted within a few million years of the formation of calcium aluminum inclusion (CAIs), the oldest known Solar System solids. Isotopic ages and oxygen isotope data for the magmatic iron meteorites show that they derive from parent bodies that differentiated with 1-2 Myr years of the formation of CAIs and that intense heating did occur during the period [1,2]. The origin of SLRs is incompletely understood, and possible sources include irradiation of the solar nebula by high-energy protons from the T Tauri-phase Sun, AGB stars, massive stars, and supernovae. However, the source of at least one SLR (^{10}Be) seems to be central irradiation, whereas ^{60}Fe can only be produced in a massive star [3,4]. ^{26}Al could have been produced both by radiation from the early Sun as well as in massive stars. Recent high-precision measurements suggest that ^{26}Al was distributed homogenously in the inner Solar System, limiting the contribution from the proto-Sun [5]. (Boss has invoked a massive, gravitationally unstable disk to explain the heterogeneity [6]). Curiously, ^{60}Fe, which was unambiguously produced in a massive star, was not uniformly distributed, being present only in chondritic meteorites that formed 2-4 Myr after CAIs [7]. One explanation for this is a scenario where ^{26}Al originated in the wind of one or more massive Wolf-Rayet (WR) stars, and that ^{60}Fe (and perhaps a smaller amount of additional ^{26}Al) was injected during a subsequent supernova(e).

The supernova progenitor must have been within about 1 pc of the protosolar system [8,9], implying that the Sun formed in a dense stellar cluster [10]. Most stars form in such clusters, but most of those clusters disperse by 10 Myr [17], placing an upper limit on the main sequence lifetime of the source stars of the and hence a lower limit on its mass. SLRs were most likely transported in the form of grains rather than hot, low-density gas of winds or supernova ejecta: The latter could not have penetrated a cooler, higher density disk if one was present, or been incorporated into planets, if one was absent. Rather colliding, SLR-containing grains were vaporized in the gaseous disk of the primordial Solar System [8]. Williams & Gaidos [11] showed that because of cluster expansion and the finite lifetime of disks, the fraction of stars whose disks are contaminated by an inital Solar level of ^{60}Fe is at a most a few percent. A corollary, not explored by them, is that the abundance of SLRs, including ^{26}Al, will vary significantly between planetary systems. Several models describing the thermal and petrological evolution of meteorite parent bodies subjected to heating by ^{26}Al and ^{60}Fe have been published [11,12]. These illustrate the sensitivity of that evolution to the abundance of ^{26}Al (and to a much lesser extent, ^{60}Fe) at the time of accretion. Variation of planetesimal accretion time with semimajor axis may have produced the observed petrological stratification of the asteroid belt, with differentiated bodies in the inner belt, and relatively unaltered bodies in the outer belt [13]. Presumably, a different initial abundance of ^{26}Al in the protoplanetary disk would lead to changes in the thermal evolution and petrologic character of planetesimals and might effect the ultimate chemical composition of planets that accrete from them. The rough equality between the time scale for growth of embryos at 1 AU ($\sim$1 Myr [14]) and the period of maximum heating by ^{26}Al suggests that any effect might be particularly pronounced in the terrestrial planet region. Nevertheless, the requirement that Jupiter's core grow to at least a few $M_\oplus$ before the dissipation of nebular gas in a few Myr [15], means that a role for heating by ^{26}Al in giant planet formation is possible.

Improved stellar evolution models that include rotationally-induced mixing predict that the minimum initial mass for stars going through a WR phase is about 40 $M_\odot$ [16]. Thus planetary systems forming around stars in a cluster whose most massive member is less than 40 $M_\odot$ will be relatively depleted in ^{26}Al. This includes all clusters with a total membership less than about 4000 stars. Because the distribution of clusters with membership N obeys the power law N^{-2} [17], this means that the majority of stars have not experienced the proximity of a WR star and the concomitant injection of ^{26}Al. These objects will have ^{26}Al only from internal radiation and the SN event itself. However, if star-formation is co-eval in clusters (a proposition that is intensely debated) then many such stars will not even have a SN contribution because disks are observed to dissipate in about 6 Myr, shorter than the main sequence lifetime of stars with less than 30 $M_\odot$.

Even within a massive cluster like that most likely to have spawned the Sun, the abundance of ^{26}Al will vary significantly from star to star. We use N-body simulations and the results from recent nucleosynthesis calculations for WR stars to estimate the contribution of a WR wind to the ^{26}Al budget of planet-forming disks. We based a model of ^{26}Al injection by WR winds on a plausible scenario for the origin of SLRs in the Solar System. We consider the simplest case of a 9000-star cluster with a single 60 $M_\odot$ star that goes through the WR phase at 3.6 Myr and experiences core collapse at 4.6 Myr [16]. The cluster size is chosen because it maximizes the probability of contamination of a disk by ^{60}Fe to Solar System levels [11], and it will contain one star at least as massive as 60 $M_\odot$; that mass is chosen because the SN lifetime is about 4 Myr. That lifetime is significant because the parent bodies of chondritic meteorites formed up to 4 Myr after CAI formation; Jupiter could not have formed earlier than 4 Myr and thus the gas disk must have persisted for at least 4 Myr [18]. Disks are observed to dissipate in about 6 Myr, and thus a 60 $M_\odot$ star is a plausible progenitor of the SN that endowed the Solar System with ^{60}Fe.

The NBODY4 dynamical code running on the Cambridge

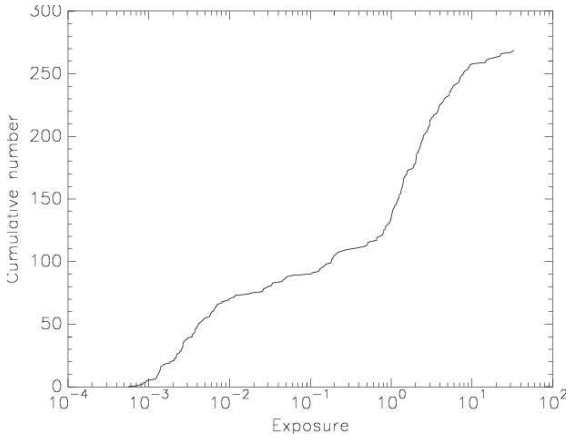

Figure 1: Cumulative distribution of ^{26}Al abundance in systems of solar-mass stars in a 9000-star cluster, normalized by the median value (see text for details)

University GRAPE-6a parallel architecture supercomputer card was used to simulate clusters. NBODY4 uses the Hermite scheme of dynamical integration; close two-body encounteres are handled using the Kustaanheimo-Stiefel regularization method and multiple systems are handled by chain regularization. Stellar evolutionp, including mass loss in winds and supernova events, is included. We assume an initial Plummer sphere distribution with a core radius of 0.2 pc and and a virial parameter (ratio of kinetic to absolute potential energy) of 1. The latter is equivalent to assuming 50% star formation efficiency and the removal of the remaining gas [19]. The simulation is run for 3.5 Myr and then the position of each star is recorded at an intervals of 3.4 kyr for an additional 800 kyr, the duration of the WN phase when the wind contains ^{26}Al. After each time t after the onset of the WN phase the distance r of the star from the WR star is calculated and the value of $\exp(-\log(2)t/t_{1/2})/(4\pi r^2)$ is calculated for each star. That is multiplied by the predicted total wind-ejected mass of ^{26}Al for a rotating 60 $M_\odot$ star with solar metallicity: 2.2×10^{-4} $M_\odot$ [20]. For familiarity, we normalize this by the surface density of ^{27}Al at 2.5 AU (the asteroid belt). Assuming a minimum mass solar nebula with total mass surface density of 7.1 g cm^{-2} at 1 AU, an $a^{-1.5}$ surface density profile, and a chondritic concentration (8680 ppm by weight). The surface density of ^{27}Al at 2.5 AU is 1.2×10^{-8} g cm^{-2}.

Figure 1 plots the distribution normalized by the 50% level of exposure. That value gives an ^{26}Al/^{27}Al ratio of 3.4×10^{-7}. Compared to the measured value of 5.8×10^{-5}, it suggests that the ^{26}Al was injected when the solar nebula was about an order of magnitude larger, i.e. in the T Tauri phase or before, and that it presented a larger cross-section to intercept material from the WR star. The range of exposures, interpreted here to represent the range of ^{26}Al contributions from the WR wind of a single star, spans 4 orders of magnitude, 3 below and 1 above the 50% level. The distribution relative to this mean shows two shoulders indicative of a bimodal distribution. This is the result of the presence of an inner core of stars closer to the WR star, and a halo of "ejected" stars farther out. Figure 1 does not include the contribution of the second most massive star in the cluster (45 $M_\odot$). However, other calculations show that this contribution will be much less because the total production of ^{26}Al will be less [20] and the star will enter the WR phase about 1 Myr later when the cluster has expanded further. We have also neglected the effect of tides by molecular clouds and the Galactic disk on the expanding cluster: This will probably only effect the stars that are already on orbits that take them far from the cluster center, and thus thus receive little ^{26}Al; the effect will likely be to move these stars further from the cluster and lengthen the low-abundance tail in the ^{26}Al distribution. We also have examined the effect of the motion of the WR star and find that simple subsitution of the origin for the location of the wind produces a nearly identical distribution.

Initial Solar values of ^{26}Al are sufficient to raise the temperature of even small (few km) bodies to the Fe-S eutectic and, in larger objects, to promote silicate-metal differentiation. Isotopic evidence suggests that this did indeed occur in the inner Solar System [1,2]. Our thermal models indicate that varying ^{26}Al by as little as a factor of 3, i.e. far smaller than the full variation suggested here, results in dramatically different thermal histories. We are investigating this effect, and its implications for the retention and processing of water and other volatiles.

References: [1] Greenwood, R. A., et al. 2005, *Nature* 435, 916 [2] Scherstén et al. (2006) *Earth Planet. Sci. Lett.* 241, 530 [3] Goswami et al. (2005) in A. N. Krot, et al. (eds.), *Chondrites and the Protoplanetary Disk*, ASP Conf. Ser. 341., p. 485 [4] Madhwa, M., et al. (2007) in B. Reipurth, et al. (eds.) *Protostars and Planets V*, Tucson, University of Arizona Press, p. 835 [5] Thrane, K., et al. (2006) *Astrophys. J.* 646, L159 [6] Boss, A. (2007) *Astrophys. J.* 660, 1707 [7] Bizzarro et al. (2007) *Science* 316, 1178 [8] Ouellette, N. et al. (2005) in A. N. Krot, et al. (eds.), *Chondrites and the Protoplanetary Disk*, ASP Conf. Ser. 341., p. 485 [9] Looney, L. W. et al. (2006) *Astrophys. J.* 652, 1755 [10] Hester, J. J., et al. (2004) *Science* 304, 1116 [11] Williams, J. P., Gaidos, E. (2007) *Astrophys. J.* 663, L33 [12] Ghosh, A., McSween, H. J., Jr. (1998) *Icarus* 134, 187 [12] Hevey, P. J., Sanders, I. S. (2006) *Meteorit. Planet. Sci.* 41, 95 [13] Ghosh, A., et al. (2006) in *Meteorites And The Early Solar System II*, D. S. Lauretta, et al. (eds.), Univ. Arizon Press, Tucson [14] Chambers, J., 2006, *Icarus* 180, 496. [15] Lissauer, J. J., & Stevenson, D. J., 2006, in *Protostars & Planets V*, B. Reipurth et al., Univ. Arizona Press, Tucson [16] Maeder, A., Meynet, G. (2000) *Annu. Rev. Astron. Astrophys.* 38, 143 [17] Lada, C. J., Lada, E. A. (2003) *Annu. Rev. Astron. Astrophys.* 41, 57 [18] Scott, E. R. D. (2006) *Icarus* 185, 72 [19] Bastian, N., Goodwin, S. P. (2006) *Mon. Not. R. Astron. Soc.* 369, L9 [20] Palacios, A., et al. (2005) *Astron. Astrophys.* 429, 613

Acknowledgements: E. G. is supported by NASA grants NNG04GL48G (TPF Foundation Science) and NNA04CC08A (Astrobiology); N. M. is is a NASA Graduate Student Research Fellow; D. R. is a UH/NASA Space Grant awardee.

THE I-Xe SYSTEM IN THE EARLY SOLAR SYSTEM. Jamie Gilmour[1], Olga Pravdivtseva[2], Alexis Busfield[1] and Charles Hohenberg[2] School of Earth, Atmospheric and Environmental Sciences, University of Manchester, Oxford Road, Manchester M13 9PL, United Kingdom. Jamie.gilmour@manchester.ac.uk, [2]McDonnell Center for the Space Sciences and Physics Department, Washington University, St Louis, Missouri 63130, USA. olga@wuphys.wustl.edu

Introduction: ^{129}I was the first decay product of a short-lived radionuclide to be identified in the early solar system[1] The methodology set the precedent for future identification of other extinct radioisotopes; excesses of the decay product, ^{129}Xe, were identified and the magnitude of these excesses was shown to correlate with iodine content.

It is unsurprising that ^{129}I was the first radioisotope identified – its decay product, xenon, is a noble gas so it is extremely depleted in solid phases. In fact, xenon is depleted by four orders of magnitude relative to elements of comparable mass in CI chondritic material (Fig. 1). Since the relative isotopic abundance of ^{129}I, like that of other extinct short-lived radioisotopes, is ~10^{-4}, this means that the atomic abundance of ^{129}Xe from ^{129}I decay is similar to that of stable isotopes of xenon in solid samples that have retained xenon from the early stages of the evolution of the solar system.

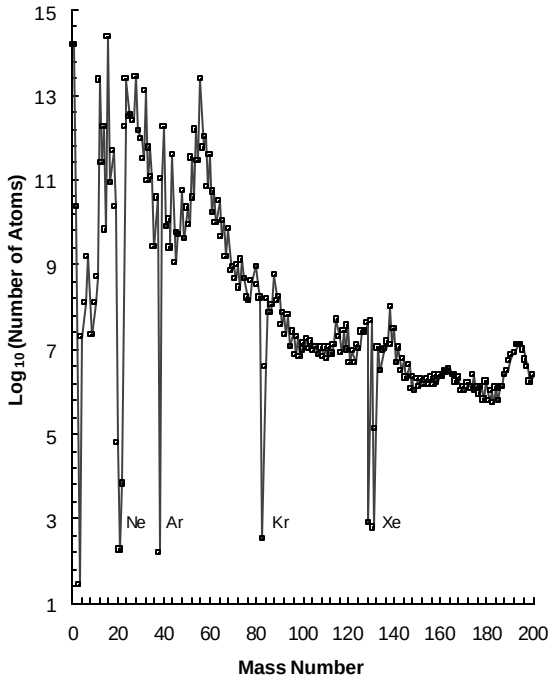

Fig. 1. Number of atoms at each mass number in a 10 micron sphere of CI material. Mass numbers corresponding only to a noble gas isotope exhibit severe depletion. Data from [2].

Methodology: The methodology of I-Xe analysis has recently been described in detail [3]. Briefly, samples are subject to neutron irradiation along with aliquots of pyroxene from the anomalous enstatite achondrite Shallowater. This is used as a monitor of the efficiency with which ^{127}I is converted to ^{128}Xe by neutron capture followed by beta decay, because it has a reproducible initial iodine ratio. Step heating analysis is usually employed; samples are heated in a sequence of increasing temperatures, the gas released at each temperature being analysed. The principle employed is that different sites release xenon at different temperatures. Where the same ratio of excess ^{129}I (from ^{129}I decay) to excess ^{128}Xe (from neutron capture on ^{127}I in the reactor) is observed across consecutive releases, this is identified as corresponding to a reproducible initial iodine ratio for the sample being analysed. Such ratios are compared to the same ratio obtained from analyses of the Shallowater aliquots irradiated at the same time as the sample. From this comparison, the time of closure to xenon loss relative to the closure age of Shallowater can be calculated directly. Strictly, the initial iodine ratio is deduced as a fraction or multiple of that in Shallowater – chronological interpretation of variations in initial iodine ratio assumes isotopic homogeneity across the region of the solar system under consideration, but there is no evidence of variation.

Relative I-Xe Chronology: Early studies of the I-Xe system focused on analyses of whole rock samples of meteorites [e.g. 4]. These proved hard to relate to macroscopic properties of the meteorites analysed, with the notable exception of enstatite chondrites [5]. When technological advances allowed finer scale examination the reason for this became apparent; many of the host phases of iodine that dominated whole rock analyses of ordinary and carbonaceous chondrites proved to be secondary[e.g. 6,7,8]. The case of enstatite chondrites can be understood because iodine trapped in enstatite dominates the high temperature releases in these meteorites.

To a significant extent, then, the I-Xe chronometer provides a record of the timing and nature of processing that occurred on parent bodies. In Fig. 2 we summarise the distribution of I-Xe ages of clasts, chondrules and single mineral phases from the recent literature. Each well defined I-Xe age with associated error has been used to generate a unit area Gaussian, and these have been summed together to provide a relative

frequency plot as a function of time relative to Shallowater. It is apparent that the earliest processes recorded by the chronometer (chondrules, igneous clasts and dark inclusions) predate Shallowater closure by around 5 Ma, while the rate of events recorded by the system declined by a factor of 10 within about 10Ma after Shallowater closure and by a factor of ~100 within a further 20 Ma.

Absolute I-Xe Chronology: A major advance in the field of I-Xe dating came when the closure age of Acapulco phosphates was determined relative to Shallowater enstatite [9,10]. Since the Pb-Pb age of Acapulco phosphates was known [11], this provided an absolute age of Shallowater enstatite – there is no need to replace the radiation monitor with one which can itself be directly dated. This calibration in turn provides absolute I-Xe ages for all samples referenced to Shallowater. Subsequent consideration of a variety of samples with I-Xe and Pb-Pb ages showed coherent evolution (Fig. 3) and led to refinement of the absolute age of Shallowater enstatite closure to 4563.3 ± 0.4 Ma[3] .

With this calibration, the highest initial I-Xe ages correspond to closure of clasts and the earliest chondrules at around 4568 Ga – adopting a 2 Ma offset for CAI formation based on the ^{26}Al system would lead to the earliest solar system ages being around 4570Ga. It is encouraging that this age, deduced on the assumption that the I-Xe system was a reliable chronometer[12], was subsequently verified by other means[13].

See also abstracts by Pravdivtseva *et al*., Filtness *et al*. and Holland *et al*. at this meeting.

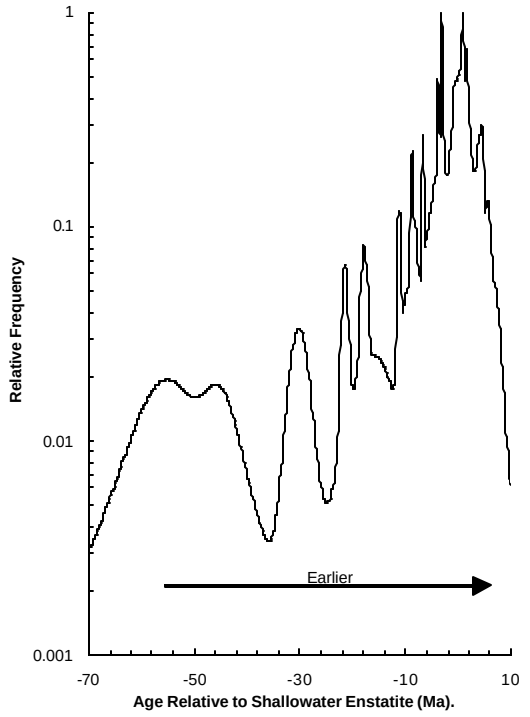

Fig. 2. Relative frequency of literature I-Xe ages relative to Shallowater ("whole rock" ages are not included) produced by summing unit-area Gaussian distributions.

References: [1] Jeffrey P. M and Reynolds J. H. (1961) *JGR, 66*, 3582-3583. [2] Anders E. and Grevesse N. (1989) *GCA 53*, 197-214. [3] Gilmour J. D. *et al*. (2006) *MAPS 41*, 19-31. [4] Hohenberg C. M. and Reynolds J. H. (1969) *JGR 74*, 6679-6683. [5] Kennedy B. M. *et al*. (1988) *GCA 52*, 101-111. [6] Swindle T. D. (1996) *MAPS 33*, 1147-1155. [7] Pravdivtseva O *et al*. (2003) *GCA 67*, 5011-5026. [8] Busfield A. C. *et al*. (2004) *GCA 68*, 195-202. [9] Nichols R. H. Jr *et al*. (1994) *GCA 58*, 2553-2561. [10] Brazzle R. H. *et al*. (1999) *GCA 63*, 739-760. [11] Göpel C. *et al*. (1994) *EPSL 121*, 153-171. [12] Gilmour J. D. and Saxton J. M. (2001) *Phil. Trans R. Soc. Lond. A 359*, 2037-2048. [13] Baker J. *et al*. (2005) *Nature 436*, 1127-1131.

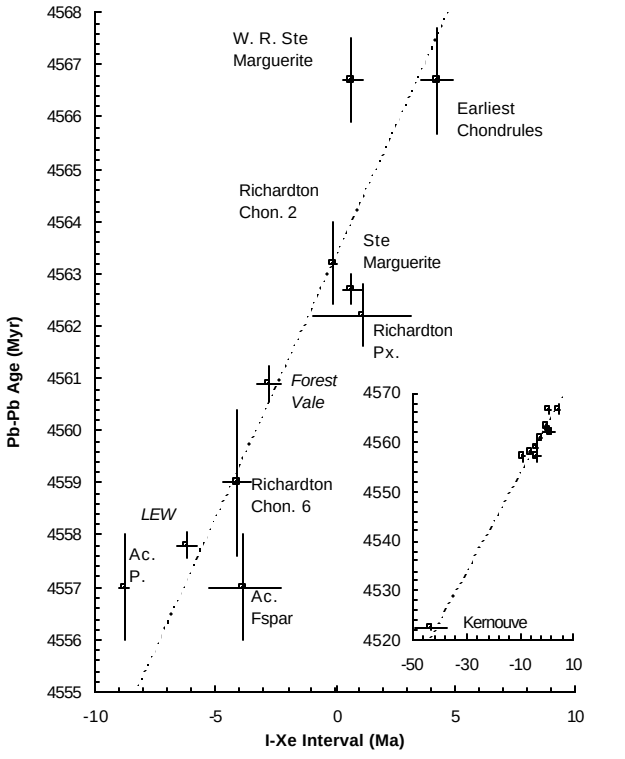

Fig. 3. Comparison of closure intervals relative to Shallowater in the I-Xe system with Pb-Pb data from the same or arguably similar samples. A gradient 1 line is a reasonable fit to the data, suggesting coherent evolution of these two isotopic systems and allowing a precise closure age for Shallowater in the Pb-Pb system to be determined. After reference [3] where data sources are listed.

THE STELLAR ORIGIN OF SHORT-LIVED RADIONUCLIDES: COLLATERAL EFFECTS AND ASTROPHYSICAL CONTEXT. M. Gounelle[1] & Anders Meibom[1] [1]Laboratoire d'Étude de la Matière Extraterrestre, Muséum National d'Histoire Naturelle, 57 rue Cuvier, CP52, 75005 Paris, France. (gounelle@mnhn.fr)

Introduction: Refractory silicates and oxides formed in the protoplanetary disk around the nascent Sun and have been preserved intact in primitive chondritic meteorites [1]. These minerals contain isotopic signatures of now extinct, short-lived radionuclides (SRs) that were present in the disk in abundances much higher than in the ambient interstellar medium [2]. The origin of short-lived radionuclides in the early Solar System remains one of the most intensely debated questions in cosmochemistry because it bears on fundamental problems such as early solar system chronology, thermal evolution of planetesimals and the astrophysical environment in which our Solar System was born [3]. If it often argued that a nearby supernova (SN) polluted our protoplanetary disk with freshly made SRs [4]. Here we discuss the collateral effects of SN material injection in the protoplanetary disk [5] and the likelihood of a protoplanetary disk – supernova association [6].

Shifting the oxygen isotopic composition of the Sun: ^{26}Al and ^{41}Ca share a common origin [7]. Assuming they were injected in the protoplanetary disk by a supernova, one can calculate for any SN nucleosynthetic model, mixing fractions (f) and time delays between the end of nucleosynthesis and their incorporation of CAIs (Δ) [5]. For the supernova models listed by [8], we calculate mixing fractions (*f*) in the range (1.9–7.6) 10^{-6} and Δ-values from 1.0 to 1.8 Myr, consistent with previous estimates [4].

Oxygen isotopes are injected together with ^{26}Al and ^{41}Ca in the protoplanetary disk, therefore shifting the disk oxygen isotopic composition. Using the f and Δ values found above and the nucleosynthetic models of [8], we calculate by mass balance the oxygen isotopic composition of the disk before injection. Depending on the SN model considered and assuming that dust only is injected, we find that δ^{17}O varies from 9 to 50 ‰ while δ^{18}O varies from -4 to 16 ‰. All calculated oxygen isotopic compositions are enriched in ^{17}O and are distinct from any measured meteoritic value.

SN injection does not change the oxygen isotopic compositionof the Sun. The Sun is roughly a factor of 100 times more massive than the protoplanetary disk and remains extremely well mixed by convection during ~10 Myr.Therefore, the Sun maintains an oxygen isotopic composition similar to the preinjection composition of the protoplanetary disk. Thus, if the protoplanetary disk was modified by injection of supernova material that co-delivered ^{26}Al and ^{41}Ca, the oxygen isotopic composition of the Sun should be enriched in ^{17}O. Forthcoming measurements of the oxygen isotopic composition in Genesis samples will help test the SN origin of ^{26}Al and ^{41}Ca.

The astrophysical context of Solar System formation: Based on the early solar system abundance of short-lived radionuclides, it is often asserted that the Sun was born in a large stellar cluster, with a massive star contaminating the protoplanetary disk with fresh nucleosynthetic products at the time of its supernova explosion [4]. To account for the inferred initial Solar System abundances of short-lived radionuclides, this supernova has to be close (~ 0.3 pc) to the young protoplanetary disk. We will show that massive stars evolution timescales are too long, compared to typical timescales of star formation in embedded clusters, for them to explode as supernovae within the lifetimes of disks. This is especially true in an Orion Nebular Cluster (ONC)-type of setting, where the most massive star will explode as a supernova (5 Myr after the onset of star formation) only when nearby disks have photoevaporated and/or formed large planetesimals. We will also quantitatively evaluate the probability of any star to be born close enough to a massive star to be polluted by its SN explosion and show that it is very low. We will conclude that the Orion-like setting is very improbable.

References: [1] G.J. MacPherson, et al., in: Chondrites and the Protoplanetary Disk, A.N. Krot, E.R.D. Scott, et al., Eds. 341, ASP Conference Series, San Francisco, 2005, pp. 225-250. [2] M. Wadhwa, et al., in: Protostars and Planets V, B. Reipurth, D. Jewitt, et al., Eds., University of Arizona Press, Tucson, 2007, pp. 835-848. [3] M. Gounelle, *New Astron. Rev.* 50 (2006) 596-599. [4] N. Ouellette, et al., in: Chondrites and the Protoplanetary Disk, A.N. Krot, E.R.D. Scott, et al., Eds. 341, ASP Conference Series, San Francisco, 2005, pp. 527-538. [5] M. Gounelle and A. Meibom, *Astrophysical Journal* 664 (2007) L123-L125. [6] M. Gounelle and A. Meibom, *Astrophysical Journal* Submitted (2007). [7] S. Sahijpal, et al., *Nature* 391 (1998) 559-561. [8] T. Rauscher, et al., *Astrophysical Journal* 576 (2002) 323-348.

In search for the oxygen isotopic composition of the solar component trapped in lunar metallic grains - Evidence of at least two extra-selenial components accreting on the Moon. Ko Hashizume[1] and Marc Chaussidon[2], [1]Dept. of Earth & Space Sciences, Osaka University, Toyonaka, Japan (kohash@ess.sci.osaka-u.ac.jp), [2]CRPG-CNRS, Nancy, France (chocho@crpg.cnrs-nancy.fr).

The knowledge of the protosolar oxygen isotopic composition bears a key importance in constraining the origin and the formation pathways of the building blocks of planetary materials. This knowledge is also essential in discussing the timescales for formation and preservation of oxygen anomalies. We report here our recent progress towards the identification of the oxygen isotopic composition of the solar wind implanted in lunar regolith samples.

The surface of the Moon has been exposed over billions of years to irradiation by solar ions and to contributions of various extraterrestrial sources. Potential contributors include interplanetary dust particles and micrometeorites which dominate the present-day mass flux of meteoritic matter to the Earth's surface, meteorites and comets. For example, from studies of nitrogen isotopes among various lunar soils sampled at different locations, a competition of at least two fluxes with different origins accreting onto the moon surface was clearly observed [1]. The proportions of these components differed largely among samples, or grain-by-grain within the same sample. These proportions appear to differ among different elements, depending on their relative abundances in the respective fluxes and on their trapping mechanism into lunar samples. It is important to note that our current knowledge of the oxygen fluxes reaching the surface of the Moon is very poor, mainly because of the sparse available data. The goal of this study is to better determine the proportion of the different fluxes - potentially, solar, asteroidal and cometary - recorded among lunar grains in the case of oxygen, and to decipher the endmember solar isotopic composition.

Hashizume & Chaussidon (2005) [2] have previously reported the presence among metallic grains from lunar sample 79035 of an oxygen component enriched in ^{16}O ($\Delta^{17}O$ (= $\delta^{17}O$ - 0.52 x $\delta^{18}O$) < -20 ± 4 ‰). Silicate grains from this sample were enriched in D-depleted hydrogen (δD < -930 ‰) [3] and solar noble gases [1], suggesting not only enrichment of the solar component in this sample, but a relatively low contribution of components that carry the D-rich hydrogen, like the asteroidal components. From this sample, we estimated the protosolar isotopic compositions of solar nitrogen [3] and carbon [4] and we interpreted that the observed ^{16}O-enriched component had a solar origin. However, Ireland *et al.* (2006) [5] came to a contrasting proposition from the finding of a ^{16}O depleted component ($\Delta^{17}O$ = +26 ± 3 ‰) at the surface of metallic grains from lunar regolith 10084, which they likewise argued to have a solar origin.

To untangle this contradictory situation, we performed further isotope measurements of oxygen residing at the surface of lunar metallic grains. We measured grains on the same mount than used for our previous analyses [2], >200 metallic 79035 grains embedded in an indium plate, this time mainly small ones which were not previously measured, and also several grains from soil 71501. The two samples 79035 and 71501 were often measured in pair [1,3] for comparison, because of their rather contrasting nature, respectively being exposed at ancient time (1-2 Ga), or recently exposed (100 Ma), and respectively being relatively enriched in ^{14}N and H, *i.e.*, the solar component, or in ^{15}N and D (planetary component), though both samples are enriched in solar noble gases. We were able to reproduce the two extreme O components previously found [2,5]. The range observed this time was $-11 \pm 4 < \Delta^{17}O < +33 \pm 3$ ‰ (1σ). The negative $\Delta^{17}O$ values were detected on grains from both 79035 and 71501 including one of the five grains for which we previously reported the negative values [2] and for which some part was left unsputtered. The positive values were observed among several newly measured 79035 grains. A marked difference discriminating these two components seems to be their concentrations. The maximum O concentration of the positive $\Delta^{17}O$ component was as high as 10 wt%, whereas those for the negative $\Delta^{17}O$ component were 1 wt% at most. From the solar ^{36}Ar concentrations of single grain analyses of size sorted (175-250 μm) 79035 silicate grains [1], the solar oxygen concentration among grains from this sample is expected to be of the order of 1 wt%, or less. Following our previous argument [1], our current results suggest that the solar composition is likely enriched in ^{16}O. Our results further confirm the supply to the Moon of two extra-selenial components with different origins.

References: [1] Hashizume *et al.* (2002) *EPSL*, 202, 201-216. [2] Hashizume & Chaussidon (2005) *Nature*, 434, 619-622. [3] Hashizume *et al.* (2000) *Science*, 290, 1142-1145. [4] Hashizume *et al.* (2004) *ApJ*, 600, 480-484. [5] Ireland *et al.* (2006) *Nature*, 440, 776-778.

The Role of the Astrophysical Environment. J. J. Hester[1], J. Bally[2], J. P. Williams[3,] and Steve Desch[1] [1]School of Earth and Space Exploration, Arizona State University, Tempe, AZ 85287; jhester@asu.edu, steven.desch@asu.edu, [2]Center for Astrophysics and Space Astronomy, University of Colorado, 389 UCB, Boulder, CO 80309; bally@casa.colorado.edu, [3]Institute for Astronomy, Univeristy of Hawaii, 2680 Woodlawn Dr., Honolulu, HI 96822; jpw@ifa.hawaii.edu

The astrophysical significance of studies of chondrites lies in what they can tell us about the Sun's birth environment, the early structure and evolution of the Solar System, and the effect of the one on the other. For much of the history of the study of chondrites, the assumption has been made that the Sun and Solar System formed in relative isolation in a dark cloud, such as that seen in Taurus Aurigae. With the discovery of the decay products of live ^{60}Fe in CAIs, however, this assumption became implausible. The only astrophysically sensible source for this short-lived radionuclide (SLR) is nucleosynthesis and subsequent mass loss from one or more nearby massive stars that must have formed close to (or probably somewhat before) the time of the Sun's formation. This result unambiguously places the origin of the Sun in the violent interior of a rich cluster, such as the Orion or Carina nebulae, where it was exposed to very rapidly evolving conditions characterized by high temperatures, strong shocks, intense ultraviolet radiation, stellar winds, supernovae, and other energetic phenomena associated with such environments.

With this change in basic understanding, there are a number of fundamental issues that must be addressed.

(1) Cosmochemical studies of meteorites provide a wealth of information about not only SLRs, but also a host of stable isotopes whose abundances might have been influenced by nearby massive stars. Interpretation of these meteoritic results requires a careful study of the various nucleosynthetic sites where these isotopes might form.

(2) How were newly synthesized nuclei transported from the interiors of massive stars into the young Solar System? Relevant issues here include the formation efficiency of dust in supernovae and Wolf-Rayet winds, the modes by which enriched gas or dust became mixed in with the Sun's protoplanetary disk, the relative time scales associated with enrichment and evolution of the solar nebula, and spatial inhomogeneity of supernovae ejecta and other products of stellar mass loss. It takes little more than reference to the extremely clumpy and chemically inhomogeneous enecta in the Cas A supernova remnant to make the point that arguments about environment based on the assumption of homogeneous isotropic ejecta must be viewed with caution.

(3) Having noted that meteoritic constraints on the details of the Sun's birth environment are poorly understood, there are still arguments that can be made about the richness of the cluster in which the Sun formed, the timing between formation of the Sun and formation of the massive stars, and how common systems like our own are likely to be. This is specifically relevant to the question of whether there were multiple injection events for SLRs, as suggested by recent analyses of ^{26}Al and ^{60}Fe data.

(4) How does low-mass star formation in rich clusters differ from isolated star formation, and what effects did that environment have on the evolution of the Sun's protoplanetary disk and the early Solar System? The rapid evolution of the region around massive stars can both trigger star formation and terminate infall onto stellar disks. Intense ultraviolet radiation truncates disks to a fraction of the size seen in regions such as Taurus, substantially shortens the lifetime of the gaseous component of the disk, but may actually promote planetesimal growth. Frequent encounters between young planetary systems in a cluster environment can have dramatic effects on the dynamics of those systems, and can even mix material from one system into another. Decay of SLRs provided the principle source of power to melt and bake out planetesimals in the early Solar System, suggesting that the properties of planets may depend sensitively on the amount and timing of injection of SLRs.

In this talk we will address a subset of these questions, specifically as they relate to establishing the chronology of the early Solar System.

THE I-Xe RECORD OF PARENT BODY PROCESSING IN METEORITIC NANODIAMONDS. Greg Holland[1] and Jamie Gilmour[1] School of Earth, Atmospheric and Environmental Sciences, University of Manchester, Oxford Road, Manchester M13 9PL, United Kingdom. Greg.holland@manchester.ac.uk, jamie.gilmour@manchester.ac.uk.

Introduction: In a recent study of xenon isotopes in size-separated nanodiamonds from the CV3 chondrite Efremovka (see [1]), it was shown that excesses of ^{129}Xe from ^{129}I decay are present in the P3 component [2]. Here we investigate the I-Xe system in nanodiamonds separates..

Systematics: In Fig. 1, we compare results of a simple model of the nanodiamond I-Xe system with literature data[3,4]. See also reference [2].

In our model, we assume that each meteorite parent body incorporated nanodiamonds from an initially homogeneous population. At some later time, the nanodiamonds were partially degassed of their Xe-P3 in a single event. During this event, such ^{129}Xe as had already been produced by ^{129}I decay was lost in the same proportion. To account for the data, this degassing must have taken place while ^{129}I was still alive.

After degassing, decay of the remaining ^{129}I drove up the ^{129}Xe/^{132}Xe ratio, the magnitude of the increase being higher for nanodiamonds that had been more degassed.

It is noticeable that many nanodiamond separates are consistent with degassing at about the same time, albeit to different extents. For instance, Bishunpur (LL3.1) appears to have lost more of its xenon than Semarkona, but the data are consistent with synchronous closure. Nanodiamonds from the primitive ordinary chondrite ALH77307 [5] are clearly distinct. Other nanodiamond separates closed to xenon loss about 3 half lives of ^{129}I (48 Ma) later. There is nothing inherently absurd about this conclusion – initial iodine ratios derived from isochrons from some chondrules from LL3 chondrites (and other meteorites) require similar late resetting (see Filtness et al., Gilmour et al., accompanying abstracts). In this respect, it is interesting that the "3 halflife" model line of Fig. 1 is close to the data from Colony (CO3), Mokoia (CV3), Tieschitz (H3.6), Renazzo (CR2), Vigarano (CV3) and Ragland (LL3.5), suggesting a similar response to a widespread decline in intensity of processing.

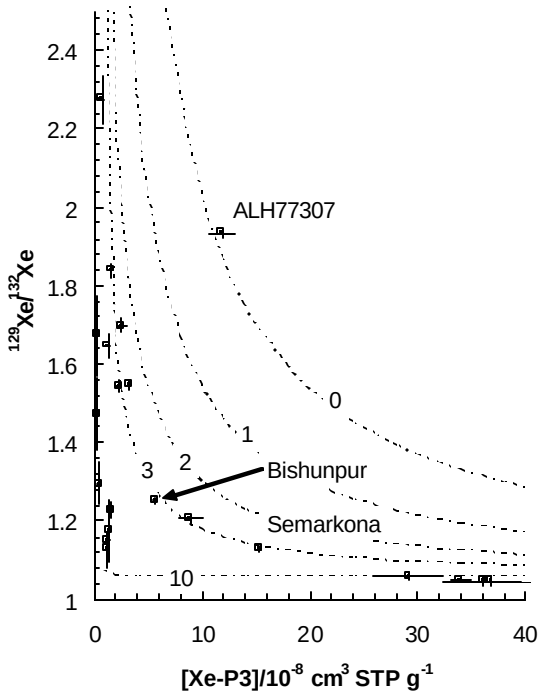

Fig. 1. Comparison of literature xenon data from nanodiamonds [3,4] with simple models of degassing an initially uniform nanodiamond population to different extents at times 1, 2, 3 and 10 half lives of ^{129}I after closure to degassing of the nanodiamond population in ALH77307.

Initial Iodine Ratio: Following on from our original work, we reported in abstract form the results of a con-

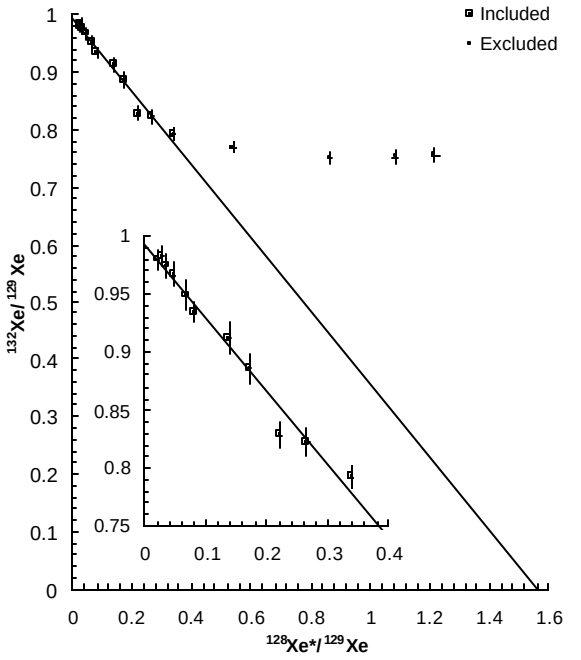

Fig.2. Low temperature data from analysis of a coarse grainsize separate of Efremovka nanodiamonds exhibit an isochron corresponding to closure 25.9 ± 0.9 Ma after closure of Shallowater enstatite.

ventional I-Xe analysis on the largest Efremovka grain size separate, ED12 [6]. Data yield an eleven point I-Xe isochron corresponding to an initial iodine ratio requiring ~26 Ma evolution from the Shallowater standard (Fig. 2).

There is a superficial disagreement between this result and that derived from the models shown in Fig 1, where >48Ma of evolution are required to account for the data from most separates. However, our model effectively treats the concentration of excess ^{129}Xe (^{129}Xe*) in a nanodiamond separate as a proxy for the ^{129}Xe*/I ratio, exploiting the fact that an initially homogeneous nanodiamond reservoir would have a well defined iodine concentration. Thus, rather than comparing our data with the isochron age, we should compare it with the integrated ^{129}Xe*/I ratio of the separate.

Figure 3 shows a step release diagram of the data used in Fig. 2's isochron plot with both isochron and average ratios plotted. The average ^{129}Xe*/I ratio for our analyses of this separate corresponds to closure 35-40 Ma after closure of Shallowater enstatite. Adopting the absolute age for Shallowater closure of 4563.3 Ma [7], this is broadly consistent with the interval deduced between closure of ALH77307 nanodiamonds and of those closing on around 3 half lives of ^{129}I later (Fig. 1), provided the I-Xe system in ALH77307 nanodiamonds closed very early in the evolution of the solar system. It is possible that an I-Xe analysis of ALH77307 matrix would reveal an unusually early elevated initial iodine ratio. The evidence strongly suggests, however, that the P3 content of most nanodiamond separates was set 10s of Ma after the nebula stage of the solar system. It is also interesting that the ^{129}I/^{127}I ratio of nanodiamonds appears to have evolved concordantly with that of the bulk solar system.

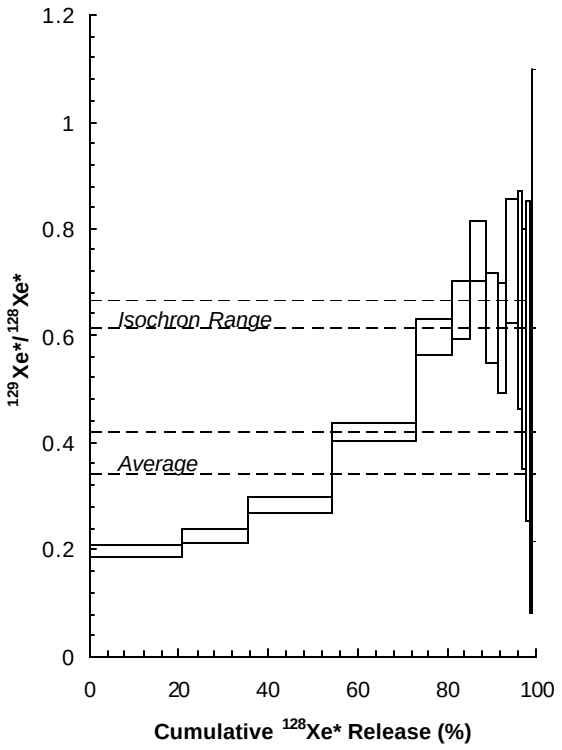

Fig. 3. A step release profile for the early temperature steps in analysis of coarse nanodiamond separate ED12. The average ^{129}Xe/I ratio is significantly lower than that of the isochron calculated in Fig. 2.

Note on Recoil. Recoil is not usually an issue in studies of the I-Xe system, but the exceptionally fine-grained nature of these samples suggested that it should be considered. Accordingly, our nanodiamond sample was irradiated in an evacuated vial and the contents analysed for the presence of excess ^{128}Xe*. Full details must await formal publication but the quantity observed does not negate the inferences made here.

References: [1] Verchovsky A. B. *et al.* (1998) *Science 281*, 1165-1168. [2] Gilmour J. D. *et al.* (2005) *GCA 69*, 4133-4148. [3[Huss G. R. and Lewis R. S. (1994) *MAPS 29*, 791-810. [4] Huss G. R. *et al.* (2003) *GCA 67*, 4823-4848. [5] Brearley A. J. (1993) *GCA 57*, 1521-1550. [6] Holland G. *et al.* (2003) *MAPS 38*, A123 (abstr.). [7] Gilmour J. D. *et al.* (2006) *MAPS 41*, 19-31.

Acknowledgements: This work is part of an ongoing collaboration with A. B. Verchovsky and A. V. Fisenko of the Vernadsky Inst., Moscow, whose patient work and skill led to the isolation of the size separates.

STELLAR SOURCES OF SHORT-LIVED RADIONUCLIDES. G. R. Huss[1], J. N. Goswami[2], B. S. Meyer[3], S. Sahijpal[4], and G. J. Wasserburg[5], [1]Hawai'i Institute of Geophysics and Planetology, University of Hawai'i at Manoa, 1680 East-West Road, Honolulu, HI, 96822, ghuss@higp.hawaii.edu. [2]Physical Research Laboratory, Ahmedabad 380009, India. [3]Department of Pysics and Astronomy, Clemson University, Clemson, SC 29634. [4]Deparetment of Physics, Panjab University, Chandigarh, India 160014. [5]The Lunatic Asylum, Division of Geological and Planetary Sciences, California Institute of Technology, Pasadena, CA 91125.

Introduction: Short-lived radionuclides (SLRs) are those for which the primordial abundance in the solar system has completely decayed away. Their presence in the early solar system provides information about the presolar and the early solar system environments and the plausible source(s) of the last nucleosynthetic material added to the solar system. They potentially provide high-resolution chronometers of early solar system events, and some of these radionuclides were also potential heat sources in planetary bodies.

There are three types of sources for the SLRs in the solar system: the galactic background abundance, stellar nucleosynthesis just before solar system formation, and irradiation. The galactic background can be a significant source of SLRs with half-lives longer than ~2-3 Myr. Recent work suggests that molecular clouds form in only a few Myr, and star formation is initiated within ~1 Myr after that [1]. Thus, SLRs with half-lives of a few Myr, if present in the material that becomes a molecular cloud, would survive to be incorporated into a newly forming stellar system.

Nuclides with half-lives ≤1 Myr require a source operating just before or during solar system formation. Irradiation as a source of SLRs will be discussed by Chaussidon et al. [2]. Our task is to discuss stellar sources. We review some possible stellar sources, discuss criteria by which to distinguish between them, and attempt to draw some tentative conclusions about the source for the SLRs in the solar system. SLRs produced in stars are listed in Table 1.

Table 1: Short-lived radionuclides in the solar system.

Nuclide	$t_{1/2}$ (Ma)	Nuclide	$t_{1/2}$ (Ma)
^{41}Ca	0.1	^{107}Pd	6.5
^{36}Cl	0.3	^{182}Hf	9.6
^{26}Al	0.73	^{129}I	16
^{60}Fe	1.5	^{247}Cm	23
^{53}Mn	3.7	^{244}Pu	80

Potential Stellar Sources: Stars from 1 to 120 $M_\odot$ are known to produce SLRs. Low- to intermediate-mass stars (1-8 $M_\odot$) end their lives by ejecting newly synthesized material via strong stellar winds. The mass-loss starts in the Red Giant stage and the rate increases through Asymptotic Giant Branch (ABG) phase and into the Planetary Nebula stage. Low-mass stars typically become carbon stars due to dredge-up of ^{12}C produced in the He-burning shell, and some experience additional CNO burning due to extra mixing (cool bottom processing). Intermediate-mass stars (4-8 $M_\odot$) experience additional CNO burning at the base of the convective envelope during the AGB (hot bottom burning) and typically fail to become C stars. Nucleosynthesis in these stars eventually ceases and they become white dwarfs. Stars of 8-10 $M_\odot$ also become white dwarf stars but proceed through C burning; thus, the core composition is dominated by O, Ne, and Mg.

Stars more massive than ~10 $M_\odot$ end their lives as core-collapse supernovae. In these stars, nuclear burning in the core proceeds all the way to Fe and Ni. Production of heavier nuclei requires input of energy, so the thermal pressure supporting the star disappears and it collapses. Solar metallicity stars with initial masses in the range 10 to ~(30-33) $M_\odot$ do not lose their entire H envelopes prior to explosion. The resulting supernova spectra thus show H, which classifies them as type II events. A shock wave, generated as the collapsing material reaches the incompressible core, ejects the outer layers of the star and explosive nucleosynthesis takes place. For very massive stars (> ~(30-33) $M_\odot$), the envelope may be completely ejected while nuclear burning is still going on in deeper layers, leaving material that has experienced extensive nuclear processing at the surface. Winds of these Wolf-Rayet stars can have extreme compositions. These stars end their lives as type Ib/Ic core-collapse supernovae.

Novae and type Ia supernovae, which occur in binary systems when a white dwarf accretes matter from its companion, are also potential sources of SLRs.

Criteria for Identifying the Stellar Source(s): To identify the stellar source(s) of the SLRs, we can ask the following series of questions: 1) Can the proposed source produce most of observed SLRs? 2) Can it produce the SLRs in the right relative abundances, allowing for dilution by solar system material, radioactive decay, and the dynamics of injection into the protosolar cloud? 3) Are there stable nuclide signatures accompanying the SLRs that can be identified? 4) What is the probability that the proposed source was in the right place at the right time to contribute to the solar system? 5) Was the stellar source also responsible for triggering the collapse of the presolar cloud?

Evaluating Two Likely Sources of SLRs: AGB stars have long been considered possible sources of solar system SLRs [3-5]. AGB stars can produce ^{41}Ca, ^{36}Cl, ^{26}Al, ^{60}Fe, and ^{107}Pd. They do not produce sig-

nificant ^{53}Mn, ^{182}Hf, ^{129}I, or the actinides. Model calculations done explicitly to evaluated 1.5-5 $M_\odot$ AGB stars as potential sources of solar system SLRs can approximately reproduce solar system abundances for ^{41}Ca, ^{26}Al, ^{60}Fe, and ^{107}Pd using a 3 $M_\odot$ star, assuming ~0.5% AGB material injected into the solar system material and ~0.7 million years to get the material into the solar system [5]. Lower-mass stars have trouble making enough ^{60}Fe, while higher-mass stars have trouble making enough ^{26}Al. The model does not produce enough ^{36}Cl, but this may not be a strong constraint because proton irradiation can make ^{36}Cl [2].

Type II supernovae produce all of the SLRs listed in Table 1. Several calculations have been done of nucleosynthetic yields for supernovae of different masses [e.g., 6-9]. Models based on these calculations that assume the canonical solar system initial ^{26}Al/^{27}Al (5×10^{-5}) and reasonable dilution factors and time delays can approximately match the abundances of ^{41}Ca and ^{26}Al, but the inferred abundance of ^{60}Fe is sometimes too high and ^{53}Mn is always much too high to match observations [e.g., 5, 10]. These studies use the bulk output of the supernova above a relatively deep mass cut (e.g., r ≈ 1.43 $M_\odot$ for a 25 $M_\odot$ star). However, the radionuclides are produced in different zones in the pre-supernova star, with ^{53}Mn produced in the deep interior, ^{60}Fe produced in intermediate zones, and ^{26}Al produced in an intermediate zone and in the outer regions. A 25 $M_\odot$ model with a mass cut at r ≈ 2.5 $M_\odot$ has very little ^{53}Mn in the ejecta [10, 11]. The 25 $M_\odot$ model of [11] was able to approximately match the abundances of ^{41}Ca, ^{36}Cl, ^{26}Al, ^{60}Fe, ^{129}I, and ^{182}Hf, with ^{53}Mn coming most from the galactic background. Higher mass cuts also minimize the size of predicted isotopic effects in stable isotopes [12].

Observations of the Cas-A supernova remnant show that layers in the ejecta mix during the supernova explosion. If mixing of adjacent zones is permitted prior to establishing the mass cut [9, 11], it is possible to produce supernova models that match solar system abundances of ^{41}Ca, ^{26}Al, ^{36}Cl, ^{60}Fe, and ^{53}Mn for a range of masses > 20 $M_\odot$ [13]. These models are very preliminary and do not address issues like synthesis of heavy radiogenic isotopes and the nature and expected magnitude of correlated stable-isotope anomalies.

It is worth noting that observed abundances of ^{182}Hf and ^{129}I in the solar system and in old stars appear to require two *types* of "r-process" sources [14, 15]. For these isotopes, background galactic synthesis may play the dominant role, leaving open the question of how much was provided by the last stellar input.

Is an AGB star or type-II supernova source more likely? The fraction of stars that form in clusters, such as the star-forming region in Orion, has been estimated at 70-90% [16]. In such regions, massive stars and low-mass stars form in close proximity over several Myr. The winds of early-formed massive stars and the supernova explosions that end their lives may both trigger star formation and disperse the cloud, ending star formation. If a cluster lasts long enough, the earliest-formed massive stars could explode as supernovae as the last stars are forming. Thus, one can envision a causal association between a supernova and a newly forming stellar system. However, once the protostellar system has formed, the probability that it will be enriched by supernova ejecta drops to ≤1% [17]. In contrast, low-mass stars live for billions of years, and by the time they reach the AGB phase, their spatial association with other stars that formed in the same cluster has long since disappeared. Thus, a chance encounter is required to put an AGB star close enough to the solar system to provide the SLRs. The probability that an AGB star would encounter a molecular cloud within a 4-million-year window is estimated at ~5% [18]. The probability is lower if the time window is shorter and lower still if only a fraction of AGB stars has ejecta of suitable composition. The probability that an AGB star could add SLRs to and already-formed protostellar system is infinitesimal.

Conclusions: Based on current understanding, both AGB and type-II-supernova sources are possible sources of SLRs in the early solar system, but a supernova source seems more probable. Both sources have problems, but other stellar sources have even more problems. Two different "r-process" sources are required to explain observed ^{182}Hf and ^{129}I abundances. Understanding of these processes and how they relate to the source of the last input of SLRs to the solar system is limited. Better models and better abundance data are resulting in significant progress in our understanding, but much remains to be done. The role of irradiation [2] must also be defined.

References: [1] Hartman L. et al. (2001) *Ap. J., 562*, 852-868. [2] Chaussidon et al., this volume. [3] Cameron A. G. W. (1984) *Icarus, 60,* 416-427. [4] Wasserburg et al., (1994) *Ap. J., 424*, 412-428. [5] Wasserburg et al. (2006) *Nucl. Phys. A, 777*, 5-69. [6] Woosley S. E. and Weaver T. A. (1995) *Ap. J. Supp., 101*, 181-235. [7] Rauscher R. et al. (2002) *Ap. J., 576*, 323-348. [8] Limongi M. and Chieffi A. (2006) *Ap. J., 647*, 647-500. [9] Nomoto et al. (2006) *Nucl. Phys. A*, 777, 424-458. [10] Meyer B. S. and Clayton D. D. (2000) *Space Sci. Rev., 92*, 133-152. [11] Meyer B. S. (2005) in *Chondrites and the Protoplanetary Disk, ASP Conf. Ser. 341*, 515-526. [12] Sahijpal S. and Soni P. (2006) *Meteorit. Planet. Sci., 41*, 953-976. [13] Takigawa et al. (2007) *LPS XXXVIII*, Abstract #1720. [14] Wasserburg G. J. et al. (1996) Ap. J. 466, L109-L113. [15] Qian Y.-Z. and Wasserburg G. J. (2007) *Physics Reports 442*, 237-268. [16] Lada C. J. and Lada E. A. (2003) *ARA&A, 41*, 57-115. [17] Williams J. P. and Gaidos E. (2007) *Ap. J., 663*, L33-L36. [18] Kastner J. H. and Myers P. C. (1994) *Ap. J., 421*, 605-614.

REE FRACTIONATIONS IN CHONDRULES FROM THE CM METEORITES, MURCHISON AND YAMATO-793321 AND THEIR IMPLICATIONS FOR AQUEOUS ALTERATION PROCESSES IN THE EARLY SOLAR SYSTEM. M. Inoue[1], N. Nakamura[2] and M. Kimura[3], [1]Kanazawa Univ., Ishikawa 923-1224, Japan, mutsuo@llrl.ku-unet.ocn.ne.jp, [2]Kobe Univ., Kobe 657-0059, Japan, noboru@kobe-u.ac.jp, [3]Ibaraki Univ., Mito 310-8512, Japan, makotoki@mx.ibaraki.ac.jp

Introduction: The CM chondrites as well as CV and CO contain significant amounts of chondrules together with CAIs, while CM chondrites have been subjected to aqueous alteration extensively [1]. Aqueous alteration process is one of most important events in the early solar system [2], and the chondrules from CM chondrites have preserved the abundant information about the evolution process of aqueously altered meteorites as well as the formation process. Many authors have studied the physico-chemical conditions of aqueous alteration by mineralogical and mineral-chemical approaches [3]. The abundances of rare earth elements (REE) in various meteoritic materials are expected to be a unique tool to constrain geochemical environments. In spite of cosmochemical importance, however, CM chondrules have rarely been analyzed for REE since Schmitt et al. [4], being due to difficulty caused by scarcity and tiny masses available for analysis. In this study, we analyzed REE (La, Ce, Nd, Sm, Eu, Gd, Dy, Er, Yb, Lu), Ba, Sr, Rb, K, Ca, Mg and Fe precisely by direct loading isotope dilution mass spectrometry (DL-IDMS) [5] for twenty-four chondrules from weakly altered CM chondrites, Murchison and Y-793321 along with petrographic examinations. Combining with REE data of chondrules from other carbonaceous (CV and CO group) chondrites previously reported [6, 7, 8], we discuss their formation and aqueous alteration processes.

Experimental setup: Ten Murchison and 14 Y-793321 chondrules (<~1.5 mm in diameter) were separated from Murchison and Y-793321 whole rock fragments. Individual specimens were broken into approximately two parts; One part (20-50wt.%) of a whole chondrule was used for preparation of a polished thin section for petrographic examinations and the rest (50-80wt.%) was used for analysis of DL-IDMS.

Results and Discussion: Twenty four chondrules show porphyritic (17), barred (5), radial (1) and granular (1) textures, and most of them (23 among 24) were subjected to various degrees of aqueous alteration. K and Rb in Murchison and Y-793321 chondrules are systematically depleted (0.06-0.94 X CI) compared to those of CV and CO chondrules (0.3-3 X CI) [6, 7] due to aqueous alteration. Abundances of Sr and Ba in CM chondrules are also variable and relatively lower (<0.1-2.2 X CI) than those of CV and CO chondrules (1-10 X CI) [6, 7]. As to REE patterns, the following two types were identified; Eight among 24 chondrules show unfractionated REE patterns with/without light/heavy-REE discontinuity and of Ce, Eu and Yb irregularities, which are indicative of high temperature nebular fractionations typically observed for CV and CO chondrules [6, 8]. On the other hand, other 16 chondrules indicate smoothly light-REE depleted patterns together with a large negative Eu anomaly (CI-normalized La/Sm ratio = 0.41-0.95; Eu/Eu* = 0.29-1.03) accompanying occasionally with nebular REE signatures. This type of REE pattern has not been observed in CV and CO chondrules, and are unique for aqueously altered CM chondrules. The light-REE depletion as observed here can not be explained as due to gas/solid fractionation in the nebula but are well understood as results of liquid/solid interation on the parent body. The REE features observed in CM chondrules imply that, like chondrules from other groups, refractory precursors of CM chondrules were formed as the high-temperature nebular condensates. After the agglomeration into CM parent bodies, light-REE and Eu have been selectively leached out from chondrules and incorporated into secondary alteration products such as Ca-rich minerals in matrix and/or chondrule mesostasis during aqueous alteration. Behaviors of REE (especially Eu and L-REE) in these CM chondrules provide valuable information about evolution processes, physico-chemical conditions and timing of aqueous alteration in the early solar system.

References:

[1] Bunch T. E. and Chang S. (1980) *Geochim. Cosmochim. Acta* 44, 1543-1577. [2] Brearley A. J. (2006) in *Meteorites and the Early Solar System II*, edited by Lauretta D. S. and McSween H. Y. Jr., 587-624. [3] Zolensky M. and McSween H. Y. Jr. (1988) in *Meteorites and the Early Solar System*, edited by Kerridge J. F. and Matthewa M. S., 114-143. [4] Schmitt R. A. et al. (1968) in *Origin and Distributions of the Elements*, edited by Ahrens L. H., 273-282. [5] Nakamura N. et al. (1989) *Anal. Chem.* 61, 755-762. [6] Misawa K. and Nakamura N. (1988) *Geochim. Cosmochim. Acta* 52, 1699-1710. [7] Misawa K. and Nakamura N. (1988) *Mem. Natl Inst. Polar Res. Spec. Issue* 1, 215-223. [8] Misawa K. and Nakamura N. (1988) *Nature* 334, 47-50.

PLUTONIC ANGRITE NWA 4801 AND A MODEL FOR THE ANGRITE PARENT BODY CONSISTENT WITH PETROLOGICAL AND CHRONOLOGICAL CONSTRAINTS. A. J. Irving[1] and S. M. Kuehner[2], [1]Dept. of Earth and Space Sciences, University of Washington, Seattle, WA 98195, irving@ess.washington.edu.

Introduction: The discovery of angrite NWA 4801 brings the total number of these enigmatic achondrites to 12, of which 6 have been found in the deserts of northwest Africa since 1999. One of the most remarkable aspects of this group of very ancient achondrites is the great variety among the specimens, ranging from rapidly quenched melts (with or without xenocrysts), ophitic "basaltic" rocks with prominent vesicles, and plutonic igneous rocks with cumulate textures to metamorphically-annealed, formerly brecciated plutonic rocks. This variety by itself tends to imply that the angrite parent body (APB) is or was a planet of sufficient size to undergo internal heating, differentiation, partial melting and metamorphism, and that it has or had a substantial regolith. The very ancient formation ages for angrites (4557-4564 Ga [1]) would then require that core formation, magmatism and regolith-forming collisions all occurred in a very short time (within ~4-11 Ma) after accretion. Given the very refractory bulk compositions of angrites, such a rapid and very high temperature process is not implausible.

Northwest Africa 4801: When found (probably in Algeria) this 252 gram, friable stone had broken into 4 pieces that fit together (Figure 1). This specimen (grainsize 0.1-1.2 mm) has an overall cumulus texture, but with evidence of subsequent annealing (see Figure 2). It is composed mostly of dark brown Al-Ti clinopyroxene ($Fs_{11.8}Wo_{56.9}$, Al_2O_3 = 10.6 wt.%, TiO_2 = 2.4 wt.%, FeO/MnO = 133) and pure anorthite (some as polycrystalline aggregates), with sporadic Cr-pleonaste grains (Cr_2O_3 = 6.3 wt.%), calcic olivine ($Fa_{45.5}Ln_{2.4}$, FeO/MnO = 88), pleonaste, poikilitic merrillite and minor troilite and altered metal. Some clinopyroxene and olivine are poikilitically enclosed in the pleonaste mantles around large Cr-pleonaste grains (Figure 3). Kirschsteinite is absent, and merrillite is more abundant than in most other known angrites.

Figure 1. Largest piece of NWA 4801 showing granular texture and anorthite aggregates (white).

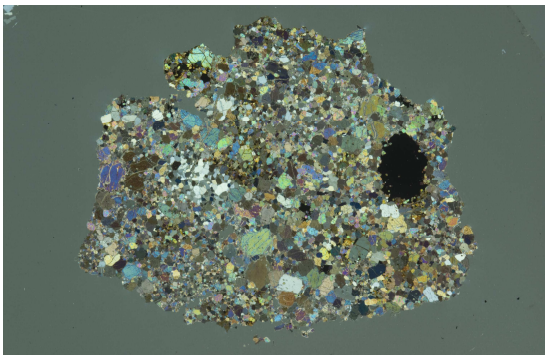

Figure 2. Partially cross-polarized light image (width 1.5 cm) showing clinopyroxene and olivine (colors), anorthite (white to gray) and spinels (black).

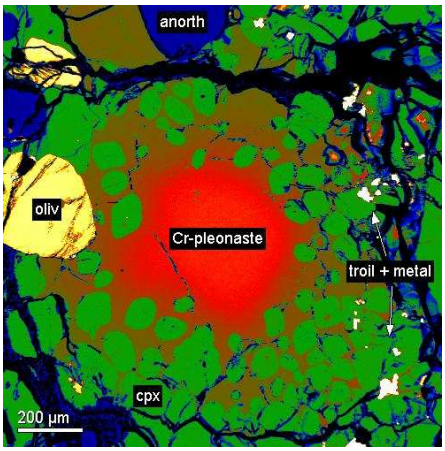

Figure 3. False-color, BSE image of an early-formed Cr-pleonaste grain (red) mantled by Cr-poor pleonaste containing Al-Ti diopside and olivine chadacrysts.

Metasomatism in Northwest Africa 2999: In comparison with other angrites, NWA 2999 is anomalous in several ways. It is an annealed breccia formed originally by disruption of a very coarse grained plutonic, igneous (olivine gabbroic) protolith, and it contains reaction textures [3] like those in exhumed terrestrial plutonic rocks. Although the symplectite and corona textures appear to represent high temperature solid-solid reactions, further modeling since our origi-

nal description [3] implies that the reactions are not isochemical, and may require the presence of metasomatic fluids or melts to add and remove Cr and Ti. The unexpectedly high sulfur contents of angrites (given their strong depletion in moderately volatile elements) suggest that an S-bearing fluid phase may be involved. NWA 2999 also is anomalous in its high content of metal (~8 vol.%), which may not be exotic to the APB [4]. This invites an analogy with mesosiderites and their presumed affinity with HED meteorites.

Age Systematics and Model: Based upon recent U-Pb and Hf-W isotopic studies [1, 5], the oldest angrites are the ophitic, vesicular specimens, with the quenched, xenocrystic specimens being up to 2 Ma younger. This permits the inference that the former may represent portions of early crust on the APB and the latter disrupted magma ocean samples ejected by penetrating impacts. Although it has been suggested that the vesicle-forming gas might be CO_2 or even rock vapor [6, 3], we propose that SO_2 or another S-rich phase may be more likely. The 4561.8 Ga age of NWA 2999 [5] is very significant in establishing that regolith formation, mixing with interior metal, burial, annealing and metasomatism all occurred in the evolving APB crust at a very early stage. The younger ages of NWA 4801, NWA 4590, LEW 86010 and Angra dos Reis [5] show that plutonic igneous intrusion, impact disruption and metamorphism continued to occur within the APB crust over at least the next 1.5-2 Ma.

We have illustrated a possible model in Figure 4. We propose that the ultimate source of the angrites was a fairly large differentiated planet that probably accreted relatively close to the Sun [2, 3], but whether this is related to present Mercury is difficult to prove. The evidence for a molten core on Mercury and the implication of its high S content [7] may argue for relatively high chalcophile element abundances in Hermean mantle and crustal rocks. If the angrite meteorites represent material ejected from such a planet by a lithosphere-stripping giant impact, then it must have resided for at least 4 Ga somewhere else to be resampled episodically and repeatedly over the last 55 Ma (based on available CRE ages [8]). The immediate source could be one or more relatively large spalled objects now within the main asteroid belt, or perhaps even objects in orbit around another planetary body (e.g., 'Vulcanoids' around Mercury?). The conspicuous lack of shock effects in angrites may not be inconsistent with this model, if the original spallation was on a sufficient scale and at sufficiently high temperatures.

References: [1] Amelin Y. (2007) *LPS XXVIII*, #1669; Zartman R. (2006) *LPS XXVII*, #1580; Markowski A. et al. (2007) *EPSL*, in press. [2] Irving A. et al. (2006) *EOS 87*, #P51E-1245; Kuehner S. and Irving A. (2007) *LPS XXVIII*, #1522 [3] Irving A. et al. (2005) *EOS 86*, #P51A-0898; Kuehner S. et al. (2006) *LPS XXVII*, #1344 [4] Gellissen M. et al. (2007) *LPS XXVIII*, #1612; Humayun M. et al. (2007) *LPS XXVIII*, #1221 [5] Amelin Y. and Irving A.. (2007) This conference [6] McCoy T. et al. (1999) *LPS XXXIII*, #1402 [7] Margot J. et al. (2007) *Science* **316**, 710-714 [8] Eugster O. (2003) *Chemie Erde* **63**, 3-30; Busemann H. et al. (2006) *GCA* **70**, 5403-5425.

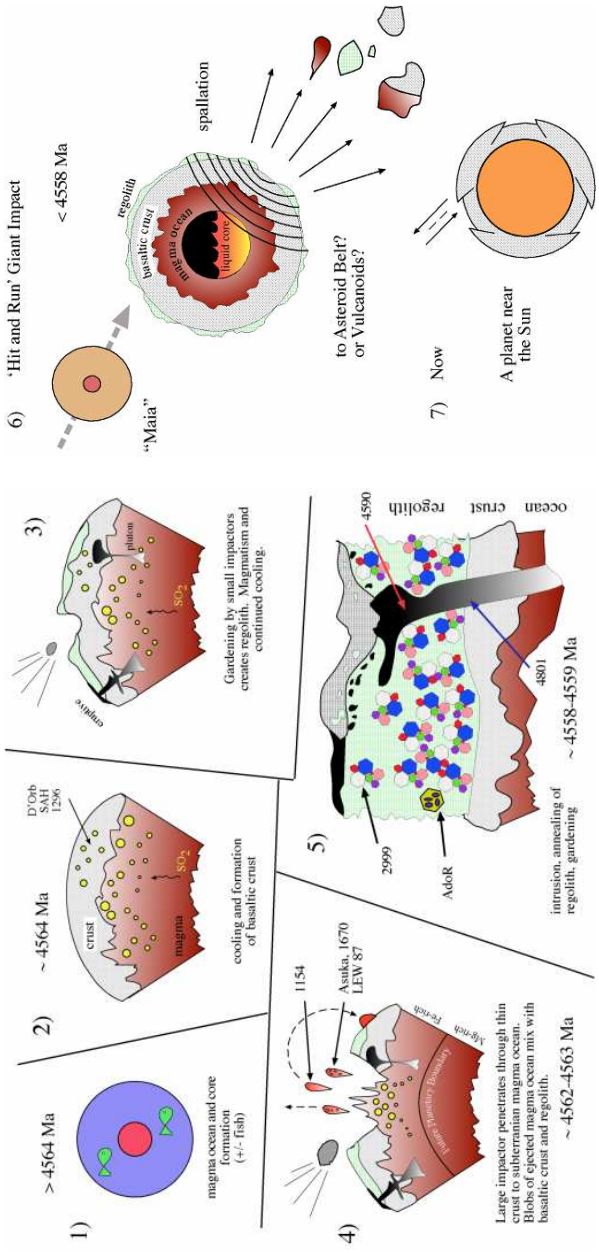

Figure 4. Schematic model for the evolution of the angrite parent body.

Thermal metamorphic history of a CAI constrained by high spatial resolution Mg isotopic measurements.
Motoo Ito and Scott Messenger. Robert M Walker Laboratory for Space Science, ARES, NASA Johnson Space Center. Mail code KR, 2101 NASA Parkway, Houston TX 77573, (motoo.ito-1@nasa.gov, scott.r.messenger@nasa.gov).

Introduction: The ^{26}Al-^{26}Mg decay system offers great potential for unraveling the sequence of events in the early solar system [e.g., 1]. However, widespread application of this system is limited by uncertainty in whether ^{26}Al was initially uniformly distributed in the early solar system. Parent body alteration introduces additional complications in the interpretation of Al-Mg studies because of the potential for redistributing Mg by diffusion during thermal metamorphism.

Here we present the results of high spatial resolution Al-Mg isotopic measurements of minerals within a type A CAI (EK1-6-3) from Allende (described in 2, 3). This is an extension of earlier studies in which we presented preliminary Al-Mg measurements and sub-μm scale O isotopic distributions of this object [3]. Here we show that heterogeneous Mg isotopic distributions in an anorthite crystal reflect a history of thermal alteration that has disturbed the original ^{26}Al-^{26}Mg systematics.

Experiments: Mg isotope measurements of fassaite, melilite, and anorthite crystals in EK1-6-3 were performed with the JSC NanoSIMS 50L. A 16 keV O^- primary beam was rastered over ~5μm regions and secondary $^{24}Mg^+$, $^{25}Mg^+$ and $^{26}Mg^+$ ions were measured in multicollection with electron multipliers, while $^{27}Al^+$ ions were detected with a Faraday cup by peak-switching. The measurements were performed with a mass resolving power of ~8000, sufficient to resolve Mg hydride interferences at mass 25 and 26. The integration time for each measurement was determined by the Mg and Al contents of each mineral. The data were corrected for EM dead time and QSA effect [4]. The instrumental mass fractionation and Al/Mg sensitivity factors were calibrated by terrestrial hibonite with known Mg isotope ratio, labradorite, augite and melilite (Åk50) glass standards.

Results: Al-Mg compositions of fassaite and melilite are shown in Fig 1a. The data for fassaite and melilite lie within errors on a straight line with an inferred initial $^{26}Al/^{27}Al$ ratio of (5.8 ± 2.4) (2σ) x 10^{-5}, equal to the canonical value. The analyses of anorthite are shown in Fig 1b. The $(^{26}Al/^{27}Al)_0$ for the anorthite scatters between 1.8 x 10^{-5} and 3.3 x 10^{-6}.

We found that the δ^{26}Mg value of the anorthite grain varied with distance from its core. Figure 2 shows the δ^{26}Mg value measured at points spaced ~15μm apart from core to rim of the anorthite grain (80-100μm). These data suggest that the Mg isotopic composition of the anorthite grain has been affected by diffusion, as discussed below.

Discussion: The large difference in the inferred $(^{26}Al/^{27}Al)_0$ values determined for the fassaite/melilite and the anorthite appear to show a difference in their formation ages of at least 1 Ma. Further, the varying

Fig 1. Al-Mg evolution diagram for EK1-6-3, a) melilite and fassaite and b) anorthite.

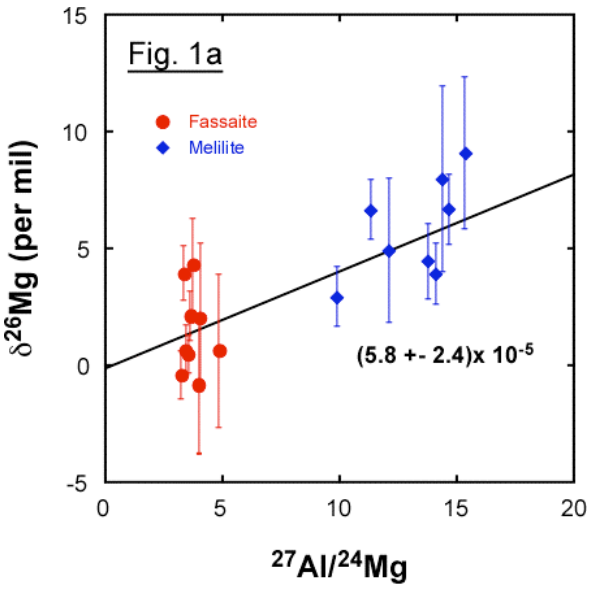

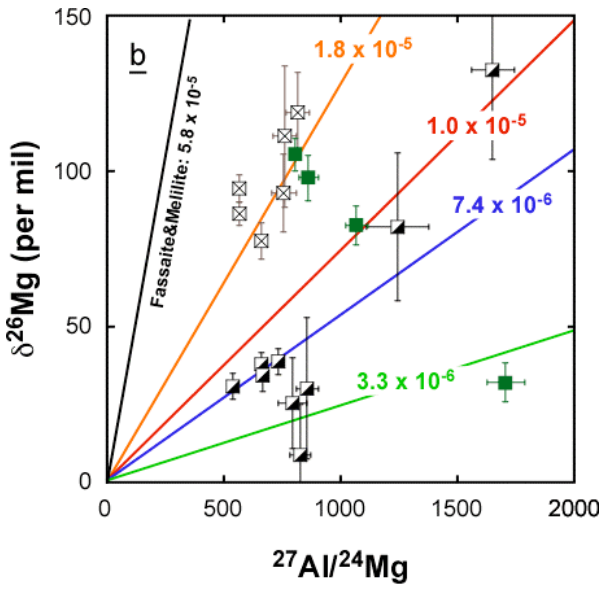

$(^{26}Al/^{27}Al)_0$ values obtained within the anorthite imply an additional 2 Ma time interval for its formation after the fassaite and melilite were crystallized.

It is possible that the $^{26}Mg^*$ heterogeneity is not due to differing formation times, but rather resulted from Mg diffusion during parent body thermal metamorphism. We modeled the Mg isotopic evolution of the (80 μm) anorthite grain, assuming that it was initially homogeneously enriched in $\delta^{26}Mg$ = +200 per mil ($^{26}Al/^{27}Al = 5 \times 10^{-5}$ and $Al/^{24}Mg = 560$), and experienced a temperature of 600˚C in its parent body [5, 6]. We find that the $^{26}Mg^*$ in the anorthite would partially homogenize with the adjacent fassaite grain and decrease by a factor of ~2 in the anorthite grain after 0.6-0.8Ma (Fig. 2), in good agreement with the observed $^{26}Mg^*$ distribution. The time scale at 450˚C increases to ~ 10^3Ma.

We calculated a numerical model of the evolution of the $^{26}Mg^*$ and Al/Mg ratio in anorthite affected by Mg diffusion kinetics in both directions (Fig. 3). Possible ranges of $^{26}Al/^{27}Al$ for certain time periods, 0.1, 0.5 and 1Ma, are shown in Fig. 3. The range for each bold-solid line represents the spatial heterogeneity toward to crystal boundary from 20μm depth to its core. If the anorthite was annealed at 600˚C for 1Ma, the $^{26}Al/^{27}Al$ slope will decrease to the observed values of ~0.3-0.6 x 10^{-5} from a canonical one. Thus Mg diffusion may be responsible for the apparent $(^{26}Al/^{27}Al)_0$ heterogeneity within the crystal, corresponding to 2-3Ma formation interval according to a chronological interpretation.

Thermal resetting is clearly important for interpreting the microscale distribution of $^{26}Mg^*$ in anorthite. This process may also affect other minerals, such as melilite, fassaite and spinel. The extent of Mg redistribution in refractory inclusions is expected to vary considerably with the grain size, geometry and composition of its mineral assemblages and the conditions of parent body alteration. Higher precision (sub per mil level) Mg isotopic measurements of low Al/Mg phases, melilite, fassaite and spinel may be required to fully resolve the formation and alteration histories of these objects.

References: [1] MacPherson G.J. et al. 1995. *Meteoritics* 30:365-377. [2] Ito M. and Messenger S. 2007. *Meteoritics & Planet. Sci.*, 42:A74. [3] Ito M. and Messenger S. 2007. 38th *LPS*, Abstract#1794. [4] Slodzian G. et al. 2004. *Applied Surface Science* 231-232:874-877. [5] LaTourrette T. and Wasserburg G.J. 1998. *EPSL* 158:19-108. [6] Ito M. and Ganguly J. *Meteoritics & Planet. Sci.* 39:1911-1919.

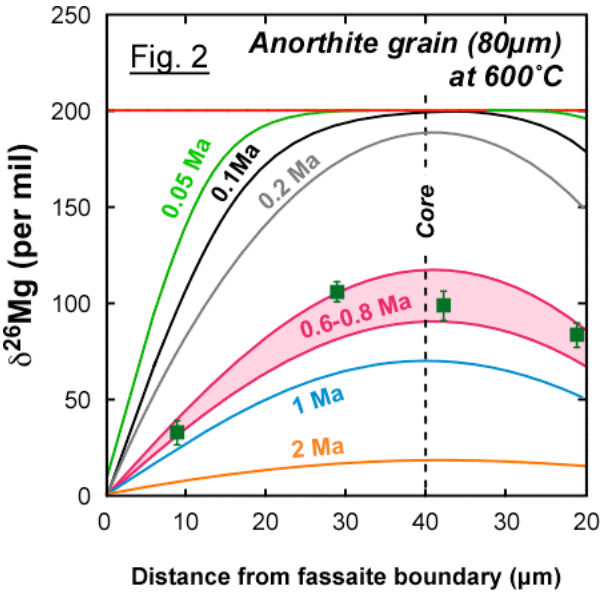

Fig 2. Numerical solutions to the initial $\delta^{26}Mg$ excess in anorthite using the Crank and Nicolson finite-difference technique. Curves indicate the $\delta^{26}Mg$ distributions as a function of distance at certain time intervals during metamorphic process.

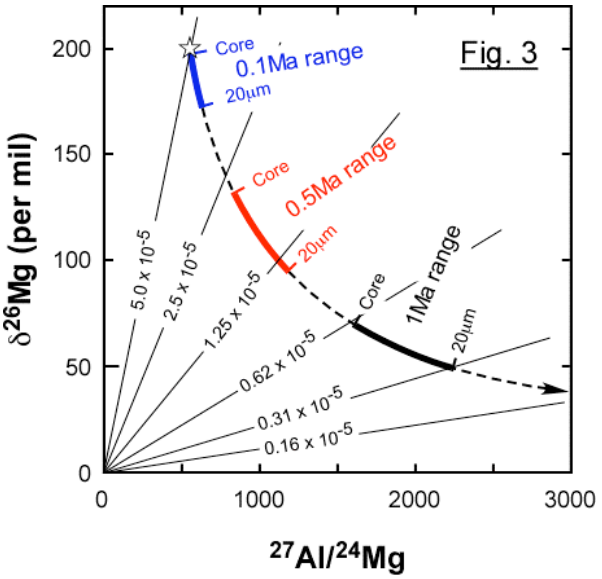

Fig 3. Al-Mg evolution diagram for 80μm anorthite grain calculated from Fig. 2. Dashed-line represents an Al/Mg evolution curve. Bold solid lines for 0.1, 0.5, and 1Ma represent a calculated range within a crystal during annealing. Thin solid lines represent different $^{26}Al/^{27}Al$ slopes at certain time periods corresponding to the half-life of ^{26}Al (0.72Ma).

FLUCTUATION FREQUENCY OF OXYGEN ISOTOPE RESERVOIRS IN THE EARLY SOLAR SYSTEM. S. Itoh[1]* and H. Yurimoto[1] [1]Department of Natural History Sciences, Hokkaido University, N10W8 Sapporo Hokkaido 060-0810 Japan (e-mail: sitoh@ep.sci.hokudai.ac.jp).

Introduction: The oxygen isotope distribution of coarse-grained Ca-Al-rich inclusion (CAI), in general, the ^{16}O-rich phases are spinel and fassaite and the ^{16}O-poor phases are melilite and anorthite [e.g., 1]. The crystallization sequence determined by experiment from CAI liquid [2] is the order of spinel, melilite, fassaite and anorthite. To explain the heterogeneous oxygen isotopic distribution among the minerals, isotopic exchange between ^{16}O-rich CAI liquid and ^{16}O-poor gas occurred in a single crystallization sequence during cooling stage is not applicable to account for the crystallization of ^{16}O-poor melilite precedes that of ^{16}O-rich fassaite, that is, fassaite must be also depleted in ^{16}O.

Recently, the following crystallization sequence has been proposed by the results of O isotopic petrography in type A 7R19-1 (a) CAI from Allende CV3 chondrite with the evidence of coexistence among ^{16}O-rich and ^{16}O-poor melilite crystals [3]. Initially, this CAI crystallized from ^{16}O-rich CAI liquid, which the crystallization sequence of the CAI minerals is the order of spinel, melilite and fassaite. Secondly, this CAI experienced partial melting in ^{16}O-poor gas. Following O isotopic exchange reaction between ^{16}O-rich liquid and ^{16}O-poor gas, melilite and fassaite recrystallized from the ^{16}O-poor liquid. The evidence for coexistence of ^{16}O-rich and ^{16}O-poor gaseous reservoirs in the CAI-forming region in the early solar system have been also confirmed by the O isotopic petrographic study of other coarse-grained CAIs and fine-grained CAIs [e.g., 4]. However, such O isotopic petrography has not been evaluated by chronology. The chronogical sequence for the O isotopic exchange events in the CAI-formation is unclear. In this study, we report a high precision Al-Mg isotopic study of coarse-grained CAIs from Y81020 CO chondrite and Allende CV chondrites, in order to evaluate the chronological sequence of ^{16}O-rich and -poor isotope exchange event using ^{26}Al-^{26}Mg internal isochron.

Analytical procedure: The sample used in this study is a fragment of type A Y20a CAI from Y81020 CO chondrite, a fragment of typeA 7R-19-1 (a) CAI [3] and a type B HN3-1 CAI [e.g., 5] from Allende CV chondrite. The study of O isotopic petrography of 7R-19-1 (a) and HN3-1 from Allende have been reported previously [3, 5].

Oxygen isotope measurement. The Hokudai isotope microscope system (Cameca ims 1270 SIMS system and SCAPS ion imager at Tokyo institute of technology (Titech) ; originally installed in TiTech and now in Hokkaido Univ. (Hokudai).) was used to obtain precise two-dimensional micro-distribution of isotope ratios on the solid surface called isotopography and in-situ O isotope analyses, which the detail analytical conditions described elsewhere [3, 6].

Al-Mg isotope measurement. The high precision Mg isotope analytical method of CAI minerals with the estimation of matrix effect by instrumental mass fractionation, performed by the Cameca ims-1270 SIMS instrument using four faraday cups of the multi-collection system is applied to determine the excess ^{26}Mg of low Al-Mg phases in CAI minerals (spinel, fassaite and melilite). A 13 keV O- primary ion beam for Al-Mg isotope analyses focused to a ~10-20 μm with 5-38nA. Analyses were done at the high mass resolving power of ~2000, sufficient to resolve all molecular ion interferences (e.g., ^{24}MgH, ^{48}Ca^{2+}). Secondary ions were collected by four faraday cups of the multi-collection system for ^{24}Mg for L'2, ^{25}Mg for C, ^{26}Mg for H1 and ^{27}Al for H'2. Total of 60 cycles are measured. After each sample measurement, we analyze the baseline of FC detectors to compensate the baseline drifts. The baseline drifts of the FC detectors are less than 0.1‰ relative to the secondary intensities within analytical session. Russian spinel (SPU), takashima augite (AUG), synthetic melilite-glass (åk$_{\sim 40}$) (Mel) and synthetic fassaite-glass (Fas) standards were used to correct instrumental mass fractionation for Mg isotopes and ^{27}Al/^{24}Mg ratios caused by different minerals. The internal and external error of δ^{25}Mg and δ^{26}Mg (2σ) for each standards is ~0.2‰ or less for SPU, Mel, AUG and Fas. The excess ^{26}Mg calculated using the exponential law with a slope of 0.5140 derived from evaporated CAI-like materials [7] after collecting instrumental mass frationation by matrx effect for CAI minerals. The internal and external error of excess ^{26}Mg is less than 0.1‰ for the standard minerals.

Results and discussion: *Y20a CAI*. Y20a CAI consists of a single crystalline melilite enclosed with fassaite, small patch of fassaite and tiny microstructure of spinels surrounded by a rim of Wark-Lovering rim. Fassaite are surrounded by åk-rich (30~50) melililte with fringe texture resulting from the partial melting. Fassaite has been enclosed by åk-rich melilite. Oxygen isotopic compositions of fassaite and Wark-Lovering rim are enriched in ^{16}O ($\delta^{17, 18}$O=~-40‰), in addition, those of melilite are distributed from ^{16}O-rich to ^{16}O-poor ($\delta^{17, 18}$O=~0 to -40‰) (Fig. 1). Remarkable, the

åk-rich melilites surrounding fassaite are likely to be ^{16}O-poor ($\delta^{17,18}$O=~0 ‰). We analyzed each phase in a Y20a CAI for magnesium isotopic compositions with different O isotopic compositions and petrologic texture. The constituent minerals are devided into ^{16}O-rich fassaite, ^{16}O-rich melilite interior, ^{16}O-rich melilite outer, ^{16}O-poor melilite and ^{16}O-rich Wark and Lovering (WL) rim. We calculate an initial ^{26}Al/^{27}Al ratio of each phase with different O isotopic compositions (Fig. 1). ^{16}O-rich Fassaite shows the highest δ^{26}Mg excess ((6.06±0.01) x 10^{-5} (2σ)), and followed as, inner ^{16}O-rich melilite ((5.25±0.19) x 10^{-5} (2σ)), ^{16}O-rich melilite outer ((4.60±0.01) x 10^{-5} (2σ)) and ^{16}O-poor melilite ((4.59±0.10) x 10^{-5} (2σ)), and WL-rim ((3.93±0.09) x 10^{-5} (2σ)), respectively (forced through the origin).

7R-19-1 (a). The constituent CAI-minerals in 7R-19-1 (a) type A CAI considering O isotopic compositions are divided into ^{16}O-rich spinel, ^{16}O-rich melilite, ^{16}O-rich fassaite, ^{16}O-poor melilite and ^{16}O-poor fassaite. The ^{16}O-rich minerals seem to be plotted to the straight line in the Al-Mg isotope diagram. The ^{16}O-poor minerals also seem to be plotted to the other straight line. We calculate an initial ^{26}Al/^{27}Al ratio followed as, ^{16}O-rich spinel, fassaite and melilite; (5.74±0.32) x 10^{-5} (2σ) and that of ^{16}O-poor melilite and fassaite; (4.61±0.38) x 10^{-5} (2σ) (forced through the origin). Al-Mg isotopic distribution in each phase of 7R-19-1 CAI indicates that the chronological sequence of crystallization is consistent with that of O isotopic petrography [3].

HN3-1. The constituent CAI-minerals in HN3-1 type B CAI considering O isotopic compositions are divided into ^{16}O-rich spinel, ^{16}O-poor melilite, ^{16}O-rich fassaite. We calculate an initial ^{26}Al/^{27}Al ratio followed as, ^{16}O-rich spinel, fassaite; (5.83±0.28) x 10^{-5} (2σ) and that of ^{16}O-poor melilite and fassaite; (5.49±0.03) x 10^{-5} (2σ) (forced through the origin).

The timing of O isotopic exchange event in the CAI-forming region. The Al-Mg model age in this study indicates that all of three CAIs having O isotopic heterogeneity has been experienced the short multiple heating events with fluctuation of O isotopic compositions in the early solar system. Remarkable fact from the result of Y20a shows that the dynamical O isotopic fluctuation from ^{16}O-rich to ^{16}O-poor, and then ^{16}O-rich WR-rim formation event occuurrd within just ~0.45Myr in the early solar system. In addition, the relative age of interior ^{16}O-poor melilite and ^{16}O-rich outer melilite in Y20a shows that the O isotopic exchange events occurred within analytical uncertainty (>0.01Myr). This shows that O isotopic flucutation in the early solar system sharply occurred from ^{16}O-rich to ^{16}O-poor and ^{16}O-poor to ^{16}O-rich.

The duration of CAI fomation and the beginning of ^{16}O-poor gaseous reservoir. If we assume the homogeneity ^{26}Al distribution in the early solar system, the comparison of each CAI with Al-Mg model age suggests that the CAI-formation starts before ~0.2 Myr relative to the canonical value (To=5 x 10^{-5}) and the duration of CAI formation less than 0.5 Myr. This is consistent with those of the bulk measurements [e.g., 9]. In addition, all of three CAIs indicate that the ^{16}O-rich gaseous reservoir exists firstly and at least ^{16}O-poor gaseous reservoir exists in the CAI-forming region less than ~0.1 Myr after ^{16}O-rich CAI formation occurred from the Al-Mg model age of HN3-1.

References: [1] Clayton R. N. (1993) *Ann. Rev. Earth Planet. Sci.* 21, 115. [2] Stolper (1982) *GCA* 46, 2159. [3] Yurimoto et al. (1998) *Science* 182, 1874. [4] Itoh and Yurimoto (2003) *Nature* 423, 728. [5] Ito, M. et al. (1998) *LPSC XXIX* No. 1556. [6] Yurimoto H. et al. (2003) *Appl. Surf. Sci.,* 203-204, 793. [7] Davis A. et al. (2005) *LPSC XXXVI* , No. 2334. [8] [9] Bizzaro et al. (2004) Nature 431, 275.

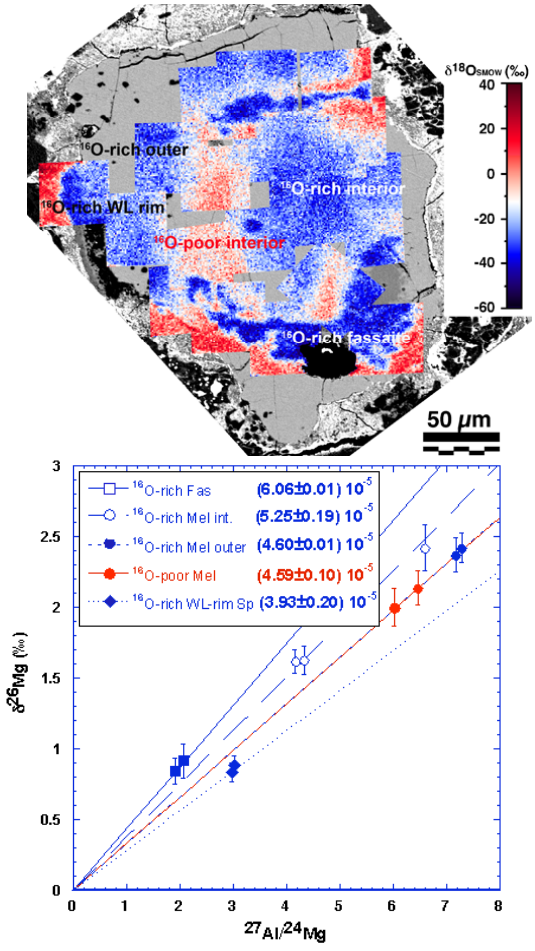

Fig. 1. O isotopograph and Al-Mg evolution diagram in Y20a. Color bar denote the scale of $\delta^{18}O_{SMOW}$. Blue means ^{16}O-rich. Red means ^{16}O-poor. Fas: fassaite. Mel int.: Melilite interior. WL: Wark-Lovering rim.

^{26}Al/^{27}Al RATIO IN THE EARLY SOLAR SYSTEM: CANONICAL OR SUPRA-CANONICAL? Benjamin Jacobsen[1], Qing-zhu Yin[1], Frederic Moynier[1] Alexander N. Krot[2], Yuri Amelin[3], Kazuhide Nagashima[2] Ian D. Hutcheon[4] and Herbert Palme[5]. [1]Department of Geology, University of California Davis, Davis, CA 95616, USA (jacobsen@geology.ucdavis.edu, yin@geology.ucdavis.edu) [2]HIGP, University of Hawai'i at Manoa, Honolulu, HI 96822, USA [3]Geological Survey of Canada, 601 Booth Street, Rm. 693, Ottawa, ON, Canada K1A 0E8, and Research School of Earth Sciences, Australian National University, 61 Mills Road, Canberra, ACT 0200, Australia. [4]Glenn T. Seaborg Institute, Lawrence Livermore National Laboratory, Livermore, CA 94551, USA [5]Institut für Geologie und Mineralogie, Universität zu Köln, 50674 Köln, Germany

Introduction: Ca-, Al-rich inclusions (CAIs) in primitive meteorites (chondrites) play a pivotal role in the high-resolution chronology of the early Solar System. They are the oldest solids formed within the Solar System and thus mark the beginning of Solar System evolution 4567.2±0.6 million years (Myr) ago 1. Over three decades of research using ^{26}Al-^{26}Mg chronometry (^{26}Al decays to ^{26}Mg with $t_{1/2}$ = 0.73 Myr) has revealed that most CAIs contain excess radiogenic ^{26}Mg* from the decay of ^{26}Al and define an initial ^{26}Al/^{27}Al ratio of ~5×10^{-5}, commonly referred to as the solar system "canonical" value [2,3]. The "canonical" ^{26}Al/^{27}Al ratio has recently been revised upwards to a "supra-canonical" value of $(5.8\text{-}7.0)\times10^{-5}$ [4-9]. Here we report new high precision ^{26}Al-^{26}Mg isotopic analyses of several coarse-grained, igneous CAIs and for mineral separates from one CAI from the Allende (CV) chondrite using multicollector inductively-coupled plasma mass-spectrometry (MC-ICP-MS). We show that our new results for both bulk CAIs and mineral separates are in excellent agreement with the data originally reported by Bizzarro et al. [4; Fig. 1a], but disagree with both the revised data presented in a corrigendum [5] as well as recent new data [6, Fig. 1b]. Our results do not support the supra-canonical ^{26}Al/^{27}Al ratio [4-9]; instead, they are consistent with the canonical value of 5×10^{-5} [2,3].

Suggested explanation for differences: Differences in slope on an Al-Mg evolution diagram may be due to (i) differences in age, (ii) spatial heterogeneity in ^{26}Al or (iii) systematic differences in analytical procedures. The first two possibilities are very unlikely, as both would posit two distinct populations of CAIs characterized by different ^{26}Al/^{27}Al ratios, one population analyzed by Bizzarro and co-workers and the other by us, with no intermingling. The third possibility, that the difference in slope is an artifact, due to analytical procedures and inadequate intercalibrations, must be critically evaluated.

The ^{27}Al/^{24}Mg ratios in [4] appear to have omitted the factor of At_{Mg}/At_{Al} = 0.9008 (or = 1/1.11, as in [5], where At_{Al} and At_{Mg} refer to the atomic weights of Al and Mg, respectively. This apparent error was corrected in a corrigendum [5], leading to an 11% increase in the inferred initial abundance of ^{26}Al. Our data, however, fail to reproduce the revised ^{26}Al/^{27}Al initial value (Fig. 1b). This discrepancy needs to be resolved through bilateral sample exchange and careful calibration against standards. We note that the Mg isotopic composition (δ^{26}Mg*) for one of the bulk CAI samples, A44A, has been reproduced by Bizzarro et al. to within 30 ppm (Fig. 1a); possible differences in ^{27}Al/^{24}Mg ratios await resolution

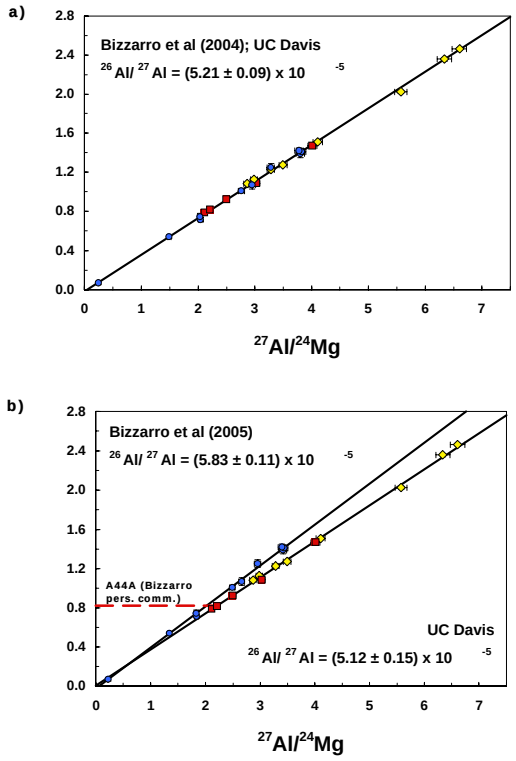

Fig. 1. ^{26}Al-^{26}Mg systematics in CAIs from the Allende CV3 carbonaceous chondrite. a) Summary of data from Bizzarro et al. [4] and the current study. The red squares (bulk CAIs) and yellow diamonds (mineral separates from the CAI, A44) are from this study. The blue dots are from [4]. The precision for both ^{27}Al/^{24}Mg and δ26Mg* (*denotes the radiogenic ^{26}Mg component, as deviations in parts per 1000 from a terrestrial standard) is comparable in both studies. The plot shows excellent agreement between the current study and the original data of Bizzarro et al [4]. b) Summary

of data from Bizzarro et al. [5], as reported in the corrigendum and the current study. In contrast to Fig. 1a, the systematic difference in slope is apparent. We provided A44, one of our CAI samples, to Bizzarro and co-workers to establish an inter-calibration between our laboratories. The Mg-isotopic composition (δ^{26}Mg*) of A44 measured by us and by Bizzarro et al. agrees to within 0.03‰; a comparison of ^{27}Al/^{24}Mg values is underway.

Discussion: In principle, Al-Mg isotope data can be used to constrain the timing of evaporation and condensation events, recorded in bulk CAI data, compared to melting and crystallization events, recorded in data for primary igneous minerals (e.g., whole rock vs. internal mineral isochrons). In addition to the bulk CAIs discussed above, we analyzed mineral separates for one coarse-grained Type B CAI (A44). While the full details will be published elsewhere given the space limitation of this short communication, the internal mineral isochron for A44 yields an initial ^{26}Al/^{27}Al ratio of $(5.12\pm0.18)\times10^{-5}$, indistinguishable within analytical uncertainty from the value inferred from our bulk Allende CAI measurements. Based on these observations, we infer that the formation of Allende CAIs, including processes of evaporation, condensation, melting and crystallization, occurred over a very short time interval (no more than 29 Kyr). These new data also underscore the need to understand more quantitatively the extent to which the deviations from an isochron often found with in situ measurement techniques (laser ablation MC-ICP-MS [7] and ion microprobe [8]) reflect spatially localized diffusion and transport of Mg isotopes.

Accurate knowledge of the Solar System initial ^{26}Al/^{27}Al ratio is crucial if we are to use CAIs as the "time zero" age-anchor to guide future work with other short-lived radio-chronometers, such as the ^{41}Ca-^{41}K system ($t_{1/2}$ = 0.1 Myr). Well established abundances of ^{26}Al and ^{41}Ca will significantly limit the possible sources of ^{41}Ca, ^{26}Al and other shortlived radionuclides in the early Solar System (e.g., energetic particle irradiation near the proto-Sun [10,11] vs. injection from nearby stars [12,13]). Differences between the canonical and supra-canonical ^{26}Al/^{27}Al ratios have led some authors to adjust the solar initial ^{41}Ca/^{40}Ca ratio by a factor of 26 to accommodate the ^{41}Ca overproduction problem encountered in the X-wind model [11]. However, the tightly constrained initial ^{26}Al/^{27}Al ratio reported here, with an age uncertainty of only 29 Kyr (Fig. 1), provides little support for this suggestion.

References: [1] Amelin, Y. et al. (2002) *Science* 297, 1678-1683. [2] Lee, T. et al. (1977) *ApJL* 211, L107-L110. [3] MacPherson, G.J. *in Meteorites, Comets and Planets (ed. Davis, A. M.) 201–246, Vol. 1 of Treatise on Geochemistry (eds Holland, H. D. & Turekian, K. K.) (Elsevier-Pergamon, Oxford, 2003).* [4] Bizzarro, M. et al. (2004) *Nature* 431, 275-278. [5] Bizzarro, M. et al. (2005) *Nature (Corrigendum)* 435, 1280. [6] Thrane, K. et al. (2006) *ApJL* 646, L159-162. [7] Young, E. et al. (2005) *Science* 308, 223-227. [8] Taylor, D. et al. (2005) *LPSC* 36, A2121. [9] Galy, A. et al. (2004) *LPSC* 35, A1790. [10] Shu, F. H. et al. (1996) *Science* 271, 1545-1552. [11] Gounelle, M. et al. (2006) *ApJ* 640, 1163-1170. [12] Wasserburg, G. J. et al. (2006) *Nuclear Physics* A 777, 5-69. [13] Sahijpal, S. et al. (1998) *Nature* 391, 559-561.

HIGH RESOLUTION ^{26}Al-^{26}Mg CHRONOMETRY OF CAIs FROM THE ALLENDE METEORITE S. B. Jacobsen, R. Chakrabarti, O. Bogdanovski, M.C. Ranen and M. I. Petaev, Department of Earth and Planetary Sciences, Harvard University, 20 Oxford St. Cambridge, MA 02138, USA (jacobsen@neodymium.harvard.edu).

Introduction: Most evidence for the presence of ^{26}Al ($\tau_{1/2}$ = 0.73 Ma) in the early Solar System comes from the study of CAIs, with most of them apparently having an initial ^{26}Al/^{27}Al of ~5x10^{-5} [1-3]. The recent comparison of ^{26}Al-^{26}Mg, ^{53}Mn-^{53}Cr and ^{207}Pb-^{206}Pb systems [4] seems to validate ^{26}Al as a chronometer and suggests that ^{26}Al was widely and uniformly distributed in the early Solar System and can be used as a fine-scale chronometer. This evidence suggests that (i) ^{26}Al was injected from a nearby stellar source and homogenized within the solar nebula in a short time period compared to its half-life and (ii) ^{26}Al must have been an important heat source for melting small planetesimals. The exact initial value is debated, with estimates ranging from ~4.5 to 7 x10^{-5} [5-10].

The MC-ICPMS measurements provide the most precise data for the Al-Mg system. [5-7] suggested that most CAIs formed within an extremely short time interval of ~ 20,000 years. However, two research groups have obtained similarly precise isochrons for CAIs, but quite different inferred initial ^{26}Al/^{27}Al values of 5.8x10^{-5} and 4.9x10^{-5} [7-8]. At this stage it is not clear what is the cause of this discrepancy: sample selection, interlaboratory calibration problems, or differences in data reduction procedures. We have initiated a study of ^{26}Al-^{26}Mg isotope systematics of CAIs by MC-ICPMS techniques aiming to resolve these problems and, in particular, to learn whether most CAIs formed over a very short time interval or not.

Samples: We selected one very large (~6.34 grams) potato-shaped CAI (SJ101) and several smaller CAIs from the Allende CV3 meteorite, with more CAIs to be added later. To obtain a representative "whole rock sample" of SJ101, the middle section (2.11 grams) was crushed to a fine powder, with one side of the CAI being used for a detailed petrologic and chemical study. This forsterite-bearing CAI is described in detail in an accompanying abstract [11]. Its Si isotope composition (δ^{29}Si = -0.30 ±0.05 and δ^{30}Si = -0.60 ±0.08) is close to the values of bulk chondrites [12], implying that this CAI experienced little or no evaporation and, as discussed below, is ideal for a chronological study. From a second ~ 1 cm irregular coarse-grained CAI (SJ103) we have extracted a small (8 mg) fragment for analysis.

Methods: The samples were dissolved with HF-HNO_3 mixture in a steel-jacketed Teflon bomb. The spinel residue left after the initial dissolution was dissolved separately and then recombined with the main sample. Mass spectrometric measurements were carried out using a GV Isoprobe P MC-ICPMS in conjunction with a desolvating nebulizer (Elemental Scientific APEX with SPIRO). The ^{24}Mg, ^{25}Mg, ^{26}Mg and ^{27}Al ion beams were measured simultaneously in low and high mass Faraday cups (L3, Ax, H4 and H6, respectively). The ^{27}Al/^{24}Mg as well as the preliminary Mg isotope compositions were determined on aliquots without any chemical processing. These measurements were interspersed with our gravimetrically determined ^{27}Al/^{24}Mg ratio (~1.09) standard as well as with DSM3 [13-14] to allow sample-standard bracketing for (i) preliminary determination of ^{25}Mg/^{24}Mg and ^{26}Mg/^{24}Mg isotope ratios relative to the DSM3 standard expressed as δ^{25}Mg and δ^{26}Mg values (DSM3 ~ the bulk Silicate Earth (BSE) Mg isotope composition [13]), and (ii) precise determination of the ^{27}Al/^{24}Mg ratios. Then the Mg was separated from the dissolved samples by cation exchange procedures (in 0.8N HNO_3 with AG50WX12 resin) to obtain ~99% pure Mg (~99% yield) for mass spectrometric analysis. The isotope composition of the chemically purified Mg was measured by MC-ICPMS. The mass spectrometric mass fractionation was cancelled out by the sample-standard bracketing method. The natural fractionation in a sample is then obtained with an uncertainty of ±0.05 per mil or better.

Data Evaluation: With MC-ICPMS it is possible to obtain very high precision Mg isotope data, but it is recognized that use of this precision to obtain precise estimates of the radiogenic excess of ^{26}Mg in a particular sample may be limited because of insufficient understanding of the fractionation laws both in the mass spectrometer measurements as well as in nature [15]. The radiogenic effect due to ^{26}Al decay is represented as

$$\varepsilon_{26Mg} = \left[\frac{\left(\frac{^{26}Mg}{^{24}Mg}\right)_{sample}}{\left(\frac{^{26}Mg}{^{24}Mg}\right)_{BSE}} - 1 \right] \times 10^4 \qquad (1)$$

where the ^{26}Mg/^{24}Mg ratios have been corrected for both instrumental and natural fractionation. The radiogenic effect in ε-units (ε_{26Mg}) can be calculated from the measured δ^{25}Mg and δ^{26}Mg values relative to the bulk Earth value:

$$\varepsilon_{26Mg} = \left\{ \left[1 + 10^{-3}\delta^{26}Mg\right]\left[1 + 10^{-3}\delta^{25}Mg\right]^{-(1/\rho)} - 1 \right\} \times 10^4 \quad (2)$$

where ρ is a fractionation coefficient that is, in general, not precisely known. In the exponential law commonly used for correcting for mass fractionation in TIMS measurements, the value of ρ is 0.51101 [for this law $\rho = \ln(m_{25Mg}/m_{24Mg})/\ln(m_{26Mg}/m_{24Mg})$ and the m_{iMg} are the masses for the Mg isotopes]. The raw $^{25}Mg/^{24}Mg$ and $^{26}Mg/^{24}Mg$ ratios measured with the Isoprobe-P yield a ρ value of ~0.52 which is substantially higher than the exponential law value and close to the equilibrium value [13]. Using our experimentally determined slope, we obtain fractionation corrected $^{26}Mg/^{24}Mg$ ratios for terrestrial samples and the standards that are essentially the same as the value of 0.139828 reported by [13-14] (when normalized to $^{25}Mg/^{24}Mg = 0.12663$). We can achieve an external reproducibility of 5 ppm for $^{26}Mg/^{24}Mg$ ratios if they are normalized this way. If, instead, we use the exponential law alone, then the reproducibility is substantially worse (10-15 ppm or worse) and we obtain a much lower $^{26}Mg/^{24}Mg$ ratio. It is clear that the exponential law is not correcting properly for mass spectrometric fractionation in the Isoprobe-P. We use the "law" determined by data obtained with this instrument. This is effectively done by first using a sample-standard bracketing method to obtain $\delta^{25}Mg$ and $\delta^{26}Mg$ values as explained above and then to apply a correction for non-instrumental (natural) mass fractionation to obtain a precise estimate of ε_{26Mg} (equation 2). Based on evaporation experiments an experimentally determined value of ρ = 0.514 was recommended by Davis et al. [15]. Since there is some ambiguity of what ρ value should be used for CAIs that have experienced substantial Mg isotopic fractionation from the average solar system value, one of our goals is to determine this value by analyzing CAIs with a large range of Mg isotope fractionations, rather than relying on the exponential law or the laboratory-determined evaporation coefficient. Until this is achieved it is best to base the chronology on samples with $\delta^{25}Mg \sim 0$.

Results: The forsterite bearing inclusion SJ101 has little or no excess ^{26}Mg. Thus, it does not appear to have had live ^{26}Al like FUN inclusions, however, it does not have the fractionation effects of such inclusions (both $\delta^{29}Si$ and $\delta^{25}Mg \sim 0$). It may thus appear to be an UN-inclusion. These data were all obtained with the low mass resolution mode (~500) of our Isoprobe P. This instrument has both true (for the axial channel) and pseudo (for all detectors) high mass resolution that is variable up to ~ 10,000. We will repeat these measurements using the high-resolution capabilities to verify that our measurements are not an artifact of unresolved interferences. At the meeting we will also present data for normal CAIs with the aim of having resolved the main issues about the high resolution chronology of CAIs.

References: [1] Lee T. et al. (1977) *ApJ, 211*, L107-L110. [2] Macpherson et al. (1995) *Meteoritics 30*, 365-386. [3] Hsu W. et al. (2000) *EPSL, 182*, 15-29. [4] Kita N. T. et al. (2005) *ASP Conference Series, 341*, pp.558-587. [5] Bizzarro M. et al. (2004) *Nature, 431*, 275-278. [6] Bizzarro M. et al. (2005) *Nature, 435*, 1280. [7] Thrane K. et al. (2006) *ApJ, 646*, L159-L162. [8] Jacobsen B. et al. (2007) *LPS, XXXVIII*, 1491. [9] Young E.D. et al. (2005) *Science, 308*, 223-227. [10] Cosarinsky M. et al. (2006) *LPS, 37*, 2357. [11] Petaev M.I. & Jacobsen S.B. (2007) this volume. [12] Georg R.B. et al. (2007) *Nature, 447*, 1102-1106. [13] Young E.D. & Galy A. (2004) *Reviews in mineralogy and geochemistry, 55*, 197-230. [14] Galy A. et al. (2001) *Intern. J. Mass Spectrometry 208*, 89-98. [15] Davis A.M. et al. (2005) *LPS, 36*, 2334.

SEARCHING FOR CONSTRAINTS ON THE CHRONOLOGY OF THE OUTER SOLAR SYSTEM FROM SATELLITE GEOPHYSICS. T. V. Johnson[1], J. C. Castillo-Rogez[1], D. L. Matson[1], J. I. Lunine[1,2], (1) Jet Propulsion Laboratory, California Institute of Technology, 4800 Oak Grove Drive, Pasadena, CA 91109. (2) Lunar and Planetary Lab, 1629 E. University Blvd. Tucson, AZ 85721-0092.

Introduction: Recent astronomical observations suggest that the lifetime of gas and dust sufficient for making giant planets around Sun-like stars may be typically only two to five million years [1, 2]. Thus if short-lived radioactive isotopes (SLRI) with half-lives of 10 My were present in the circumstellar disk, they would be included in any planets formed. These isotopes would supply heat as they decayed. The challenge is to search for observations that test the validity of this scenario. In the Solar System, we believe that models of medium-sized satellites can be used for this purpose. Initial results suggest that they can also yield constraints on the time of formation and chronology of the outer Solar system. We address the reasons supporting this suggestion, status of our understanding of this problem, and the outstanding issues.

Context: The SLRI that are most significant for modeling the thermal evolution of Solar system objects are ^{26}Al and ^{60}Fe. Their origin (^{26}Al from Solar X-Wind, [3]; or both from supernova injection, [4]), their distribution in the early Solar system, and their initial concentrations are still matters of some debate. The recent discovery of calcium-aluminum inclusions in samples of the comet Wild 2 [5] (*Stardust* mission) is the latest major development. We use the CAI formation date as the reference time for our satellite models discussed below and the initial concentrations of ^{26}Al and ^{60}Fe have been defined for that time on the basis of meteorite studies.

Small satellites in the outer solar system (less than 1000 km in radius) provide the right conditions for the heat from SLRI to express itself in terms of observable geophysical properties. Temperatures of accreting materials are low (less than 100 K), and the small satellites gain a negligible amount of heat during accretion compared to the larger icy satellites. It is difficult to heat them with long lived radioactive isotopes (LLRI) since they lose heat too fast. That is, the time scale required for LLRI decay to heat the interior up to water ice creep temperature is much longer than the time scale for these objects to cool. Whether or not tidal dissipation is a significant heat source is a crucial issue.

The possible geophysical significance of SLRI was first mentioned by [6]. The modeling of icy satellites that included SLRI was suggested by several authors [e.g., 7]. However these studies used the amount of SLRI included in the models as a free parameter. Also, they did not develop the relationship between SLRI content and accretion date. The abundance of SLRI in the rock fraction is now better known, except for a large uncertainty in ^{60}Fe. The models must include this range. Otherwise, the main variable is the date of accretion. Within the uncertainties of the ^{60}Fe abundance, that date and the rock fraction fix the amount of radioactive isotopes in the model.

We have been searching for evidence that SLRI were available in the early, outer Solar system, using coupled thermophysical-dynamical modeling of the icy satellites. If SLRI are present, then the main parameters determining the satellites' evolution are the silicate mass fraction x_s and the time of formation. Significant SLRI heating lasts no longer than the first 10 My after accretion. Depending on x_s, SLRI decay heat will affect the evolution of porosity, thus lithospheric properties, or also result (for large x_s) in rapid, and complete, melting of the ice, drastically affecting the long-term evolution of the satellite.

First Results: We have suggested [8] that Iapetus formed between 2.5 and 5 My after CAIs production. Our objective was to explain Iapetus' non-hydrostatic shape and current spin rate. We showed that heat from SLRI decay results in early porosity decrease, necessary to maintain the 33-km non-hydrostatic difference between the equatorial and polar radii. The presence of ammonia could have played a similar role in decreasing porosity. However, ice thermal conductivity (even with ammonia present) is large and promotes rapid cooling before despinning could happen. We found that SLRI are needed to promote conditions suitable for tidal dissipation that triggered Iapetus' despinning and brought it to its present, synchronous, spin rate.

This study highlighted a series of uncertainties in the current understanding of icy satellites. First, the importance of convection in satellites, which are small, cold, and volumetrically heated for most of their history is currently work in development by Sotin *et al.* and Barr and McKinnon. Also, most large icy satellites undergo significant melting during accretion have already partially differentiated by the end of accretion. In small satellites, the internal temperatures progress slowly to the ammonia-water eutectic. The fate of this ammonia hydrate melt as a function of initial ammonia content has not been modeled. Neither has been its role in tidal dissipation. As mentioned above, the conditions in which tidal dissipation can become a significant heat source is a major modeling issue. No data are available for dissipation under the conditions of forcing frequency and temperature that apply to these satellites.

An alternative approach to the latter issue consisted of constraining Mimas' dynamical evolution from its current, anomalously large free eccentricity [9]. We found that the dissipation factor of Mimas' ice between 80 and 220 K (the maximum temperature achieved in Mimas for times of formation longer than 6 My after CAIs), is greater than $3x10^3$

There is a need for experimental data on the dissipative properties of planetary materials at tidal forcing frequencies. This is the reason why this work has served as a rationale for developing a new laboratory at the Jet Propulsion Laboratory to measure, among other properties, the dissipation factor of various ices, for temperature as low as 80 K [10].

The Importance of Comparative Planetology: The concept that we can use the medium-sized Saturnian satellites to date the formation of the outer Solar system is viewed as "*an extraordinary claim that requires spectacular evidence*" (Steve Saunders, personal communication). We argue that the Mimas-Enceladus paradox is such evidence. It is the spectacular demonstration that tidal friction in a cold satellite is a marginal heat source. Both Mimas and Enceladus have the same, short, cooling time scale, and should follow a similar evolutionary path if they did not accrete SLRI. However, the warm temperatures reached in Enceladus' interior, necessary to explain the south pole geyser's content in molecular nitrogen and methane [11] cannot be explained by models that do not include SLRI. If we consider that Enceladus contains three times as much rock (in mass) as Mimas, then the solution to the paradox is obvious. SLRI heating results in early melting and differentiation of a rocky core in Enceladus [12].

More generally, comparative planetology and multidisciplinary studies are keys to progress in this research. Comparative planetology of satellites at the scale of the Saturnian system and between the Uranian and the Saturnian satellites is crucial because these objects cover a large range of densities and sizes (Figure 1). It is then possible to compare pairs of objects (e.g., Mimas and Enceladus, Rhea and Iapetus, Enceladus and Ariel, etc.) A multidisciplinary approach is also necessary to integrate available observational constraints in models. It might not be possible to find evidence of SLRI inclusion during accretion for all the satellites, considered individually, because in some cases there is little remaining evidence about their early history. Crater distribution, internal structure, current shape, hydrostatic equilibrium, geological activity can be symptomatic of early conditions. Extreme end-members, *e.g.*, rock-rich satellites, require special attention.

A rapid survey (Figure 1) indicates that several satellites share with Enceladus a relatively high x_s and dynamical properties favorable to significant tidal heat production over the long term. This is the case for example of Ariel. Could both Ariel and Enceladus have undergone a similar early history involving hydrothermal activity? Could Ariel currently exhibit intense geological activity? Can the difference in formation times of the Uranian and Saturnian satellites be assessed by studying these satellites?

In the same vein, could the fact that Callisto might be partially differentiated (i.e., late times, [13]), provide a further clue regarding the chronology of the outer solar system?

Figure 1. *Distribution of outer planet medium-sized satellites as a function of their rock mass fractions and the theoretical amount of tidal heating per kilogram of ice.*

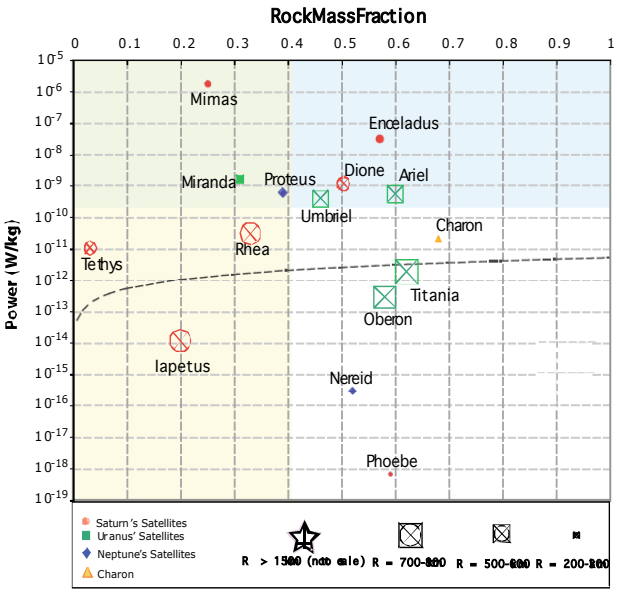

Summary: We propose a new research direction whose implications are many. First, evidence that ^{26}Al was present in the early history of the outer Solar system, would constrain the origin of this isotope, and as such the origin of the Solar system itself. This research would also open the door to coordinating the different chronological scales used by the different fields in planetary sciences: cosmochemical, dynamical, geochronology, crater counting, and now satellite geophysics. As such, it is crucial that efforts be undertaken to search for further evidence of the effects of SLRI on outer Solar system objects, or for alternative approaches to successfully model observations at these satellites.

References: [1] Najita and Williams (2005) *ApJ* 635, 625. [2] Calvet et al. (2005) *ApJ* 630, 185. [3] Shu et al. (1993) *Science* 271, 1545. [4] Vanhala and Boss (2005) *ApJ* 575, 1144. [5] McKeegan (2006) *Science* 314, 1724. [6] Urey (1955) *PNAS* 41, 127. [7] Prialnik and Bar-Nun (1991) *ApJ* 355, 281. [8] Castillo et al. (2007a) *Icarus* in press. [9] Castillo *et al.* (2007b) in preparation. [10] Hays *et al.* (2007) LPS 38. [11] Matson *et al.* (2007) *Icarus* 187, 569. [12] Matson *et al.* (2007), LPS 38. [13] McKinnon (2006) *LPS* 37, 2444.

Acknowledgements: This work was carried out at the Jet Propulsion Laboratory-California Institute of Technology, under contract to NASA.

CRYSTALLIZATIONS OF FORSTERITE FROM AMORPHOS Mg-BEARING SILICATE GRAINS. C. Kaito and Y. Kimura, Laboratory for Nano-Structure Science, Department of Physics, Ritsumeikan University, 1-1-1 Nojihigashi, Kusatsu-shi, Shiga, 525-8577, Japan. kaito@se.ritsumei.ac.jp, ykimura@se.ritsumei.ac.jp

Introduction: Magnesium-rich crystalline silicates have been discovered in some circumstellar shells [1], in disks around evolved stars [2], in protoplanetary accretion disks around young stars [3-5] and in comets [6] due to the observation of Infrared Space Observatory. The fact that part of the silicates produced around evolved stars are crystalline but that no crystalline silicates have been yet detected in the interstellar medium raises the question of the structural evolution of this crystalline dust during its life. Recently, abundant crystalline silicates in the disk of very low mass star have been reported [7]. In this paper, crystallization of Mg_2SiO_4 from amorphous Mg-bearing silicate grains due to the direct heating, electron beam irradiation and chemical reaction processes have been demonstrated by transmission electron microscope (TEM) based on the in-situ observation. Amorphous grain size and electron energy dependences on the crystallization have been presented as the one of the low-temperature crystallization.

Experimental setup: Amorphous Mg-bearing silicate grains with about 20-150 nm in diameter were produced by the coalescence between MgO and SiO smoke grains [8]. i) The direct observation of the crystallization process was carried out using transmission electron microscope equipped with a heating holder, which can be heated up to 800ºC. ii) The metamorphism of the carbon coated amorphous Mg-bearing silicate grains was directly observed using a Hitachi H-9000NAR TEM with a special holder, which can be heated up to 1500ºC. iii) Nonthermal crystallization was succeeded by preparing of the amorphous Mg-bearing silicate grains covered with a carbonaceous layer consisting of amorphous carbon, CH_4 and their derivatives. In order to observe the as-deposited structure of the sample before exposure to air, the sample was transformed to the TEM using special transfer holder and observed immediately. After that, it was exposed to air and then the same position was observed again. iv) By cooling amorphous Mg-bearing silicate grains in CH_4 gas at 80 Torr with liquid nitrogen, a lot of frosts of CH_4 were grown on the specimen surfaces. The frosts of CH_4 disappeared by taking out into air. The electron beam crystallization took place for the sample of the pre-treated CH_4 gas.

Results and Discussion: Typical crystallization samples by the four experiments are shown in Fig. 1. The direct heating method, the crystallization took place whole the particles, which can be clearly recognized Bragg reflection image. The size dependence was not observed. The crystallization temperature covered with carbon layer becomes 200ºC lower accompanying with the slight crystallization of an amorphous carbon layer.

Low temperature crystallization due to the exothermic chemical reaction [9] occurred concentrically beneath the carbon layer. The crystallization of amorphous carbon layer can be clearly observed. Therefore, chemical reaction energy with the oxygen gas in air introduced the crystallization of surface carbon layer and the reaction energy acted to the crystallization of the amorphous silicate. Electron beam crystallization by observing 90 minutes at the ordinary observation condition was observed as the crystallization of a few nanometers Mg_2SiO_4 crystal on the particle surface. The crystallization took place selectively for the 100 nm order amorphous silicate grains.

Direct heating crystallizations correspond to the thermal annealing model [10]. Last two experimental results correspond to the low-temperature crystallization. The chemical reaction based on Greenberg model and electron energy dependence on the crystallization were elucidated. The crystallization of amorphous dust started from the grain surface, the formation of a rim-like layer due to prenucleation was detected [11]. If the amorphous grain surfaces were covered with thin amorphous layer, the crystallization temperature decrement due to the graphitization of amorphous carbon layer becomes lower about 600ºC. The rim-like contrast was never observed. The crystallization process from some nucleuses at the surface layer was same for both experiments. As elucidated low-temperature crystallization of $MgSiO_3$ grains, the previous treatment by the irradiation of film by He+ ions indicated the crystallization at 300kV electron beam [12]. In the present grains, the electron beam crystallization hardly took place. If we adsorbed the CH_4 gas before the electron beam irradiation, the crystallization of 100 nm order amorphous Mg-bearing silicate grains predominantly took place at 100kV electron beam. The mean free path of the electron in the material was clearly observed. The crystallites of the order of 20 nm were distributed on the particle surface.

The nonthermal crystallization of the amorphous grains covered with carbon layer produced CH_4 gas atmosphere was directly observed accompanying with the alteration of carbonaceous layer to the graphitic structure due to oxidation at room temperature in air.

The differences of the crystallization processes for the four specimens were clarified by the present paper.

References: [1] Waters L. B. F. M. et al. 1996. *A&A* 315:L 361-364. [2] Molster F. J. et al. 1999. *Nature* 401:563-565. [3] Waelkens C. et al. 1996. *A&A* 315:L245-248. [4] Waelkens C. et al. 1998. *Astrophys. Space Sci.* 255:25-33. [5] Malfait K. Et al. 1998. *A&A* 332:L25-L28. [6] Crovisier J. et al. 1997. *Science* 275:1904-1907. [7] Merin B. et al. 2007. ApJ 661:361-367. [8] Kamitsuji K. et al. 2005. A&A 429:205-208. [9] Yamamoto T. et al. 2007. *ApJL* to be submitted. [10] Hallenbeck S. L.1998. *ICARUS* 131:198-209. [11] Kamitsuji, K. et al. 2005. *A&A* 436:165-169. [12] Carrez P. et al. 2002. *M&PS* 37:1615-1622.

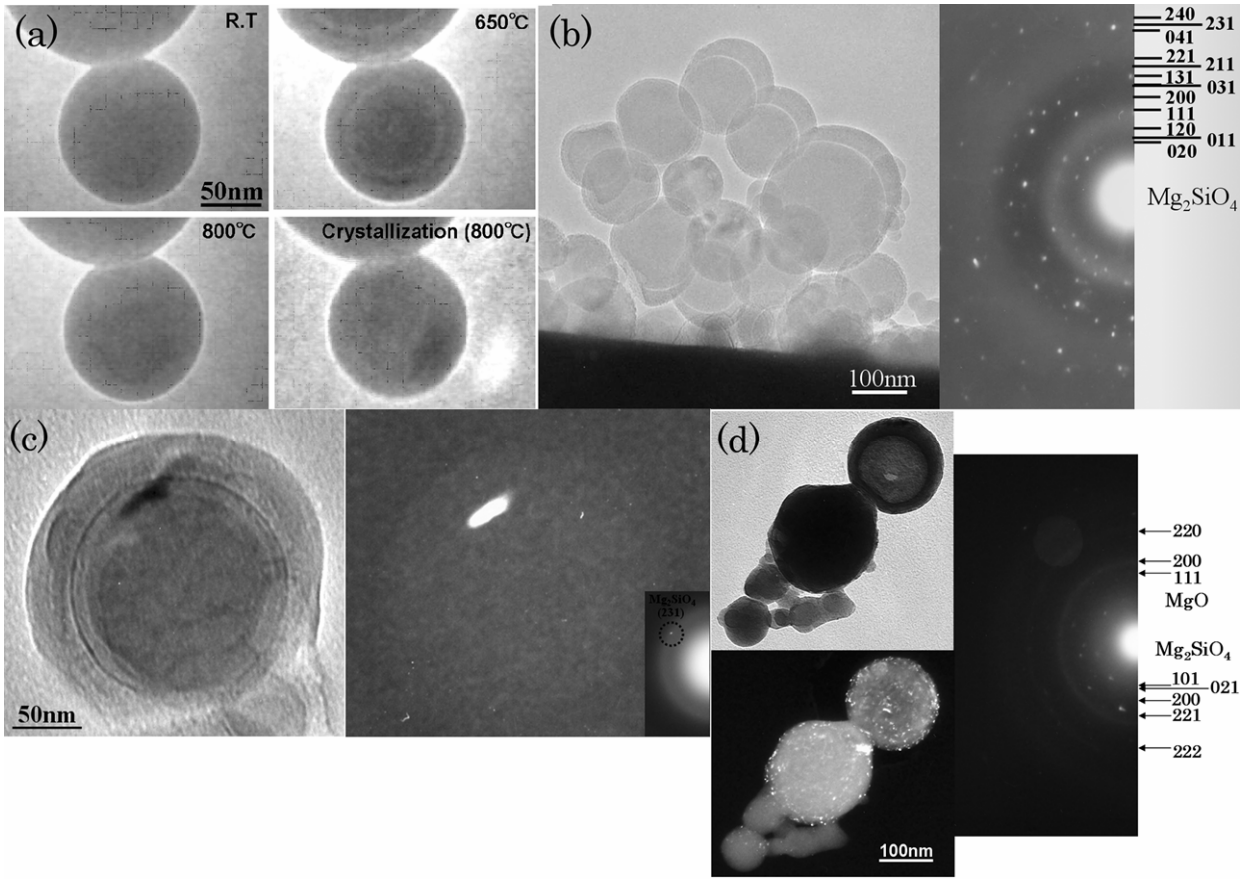

Fig. 1. (a) Alteration of an amorphous Mg-bearing silicate grain by heating in TEM. The appearance and disappearance of the white contrast ring are observed at 650 and 800°C. The Bragg reflection shows the crystallization of the grain. (b) Crystallization took place at 600°C. Electron diffraction pattern can be identified as the Mg_2SiO_4 crystal. Amorphous grains were crystallized lower temperature than (a). (c) Amorphous Mg-bearing silicate grains after adsorbed CH_4 gas. The grain was crystallized at room temperature from the surface. Large crystal formation on the part of Mg-bearing silicate grain can be seen. (d) Amorphous Mg-bearing silicate grains after adsorbed CH_4 gas. Electron beam irradiation at 100 kV induced the crystallization. In addition to Mg_2SiO_4 crystal, diffuse rings of MgO can be seen. The small crystallizations of MgO are also contained. The dark field image clearly shows the crystallization as light contrasts.

Amorphous Silicates in Early Solar System and Presolar Materials. Lindsay P. Keller and Scott Messenger, Robert M Walker Laboratory for Space Science, Astromaterials Research and Exploration Science Directorate, Mail Code KR, NASA Johnson Space Center, Houston, TX 77058. Lindsay.P.Keller@nasa.gov.

Introduction. Studies of early solar system processes have naturally focused on chondritic meteorites because they contain the oldest (dated) solar system solids. However, much of the earliest history of the solar system, predating the formation of CAIs and chondrules, is shrouded by extensive parent body hydrothermal alteration that has reworked the matrix mineralogy of all chondrites. Cometary materials have escaped significant parent body alteration, and thus may represent the most representative assemblage of the original solar system starting materials. Samples of cometary materials include chondritic-porous (CP) interplanetary dust particles (IDPs) and Stardust mission samples. Both of these sample sets are likely to have originated from the Kuiper belt, a collection of pre-cometary bodies residing in a fundamentally different regime of the solar system (>40 AU from the Sun) than meteorites (2.0 – 3.3 AU).

Typical CP "cometary" IDPs are highly porous particles that consist of fine-grained crystalline silicates, amorphous silicates, Fe-Ni sulfides, and minor refractory minerals all encased by an abundant organic-rich carbonaceous matrix. The constituent grains of IDPs are much finer-grained (100 nm ~ 1 μm) than typical meteorite matrix grains. Amorphous silicates in CP IDPs are highly abundant, accounting 30 – 60 wt % of their mass. Most of these amorphous silicates are classified as GEMS grains (glass with embedded metal and sulfides). GEMS grains are abundant in the least altered solar system materials, but apparently absent in meteorites. A clear understanding of their origins is central to understanding the origins of the first solar system solids.

Results and Discussion..GEMS grains are submicrometer, rounded grains that consist of nanophase inclusions of FeNi metal, FeNi sulfides, and numerous trace phases in a Mg-Al-Fe-Si-rich glassy matrix. Coordinated transmission electron microscope and ion microprobe measurements show that a few percent (<5%) of GEMS have non-solar O isotopic compositions and are thus demonstrably presolar (stardust). A systematic survey of the bulk elemental compositions of GEMS grains shows that their average S/Si, Mg/Si, Ca/Si, and Fe/Si ratios are approximately ~60% of solar values, although their average Al/Si ratio is solar. Compositional mapping reveals that most GEMS grains are aggregates composed of even smaller subgrains with diverse compositions. The subgrain compositions are dominated by two major components, silica-rich and FeS-rich grains that likely formed as late stage non-equilibrium condensates. The bulk compositions of GEMS grains can be explained largely by variable mixtures of these two subgrain compositions. We observe a continuum of GEMS morphologies from porous to solid GEMS to equilibrated (crystalline) aggregates that may in fact reflect a sequence of preaccretional thermal annealing at subsolidus temperatures (below the thermal stability limit of pyrrhotite).

These combined isotopic, bulk chemical, mineralogical studies show that GEMS grains are a collection of objects with different origins and histories. Differing explanations for their origins have been proposed, including direct condensation and extensive radiation processing (atomic scale sputtering and accretion) in the interstellar medium. The observed compositional heterogeneity in most GEMS is unlikely to have resulted from extensive radiation processing, which would tend to homogenize their elemental distributions *via* ion-mixing. GEMS grains and crystalline components in cometary IDPs have complementary elemental compositions that, taken together, nearly match solar composition [1]. This relationship suggests that most GEMS grains are also condensates (non-equilibrium) from a solar gas that had previously (at higher temperatures) fractionally condensed crystalline silicates and metal [1]. The elemental and isotopic data for GEMS grains suggest that most (>80 %) formed in the early solar nebula. A subset of GEMS grains (10-20%) has chemical and isotopic compositions that are consistent with models for homogenized interstellar silicates [1]. Since many GEMS grains

appear to be aggregates or partially annealed, these grains may have experienced variable degrees of processing after their formation.

An unexpected conclusion of this work is that the majority of cometary materials formed at high temperatures in the early solar system. However, the Kuiper belt is unlikely to have experienced the temperatures necessary to have formed silicates by condensation. We propose that large-scale radial dust transport within the protoplanetary disk is necessary to reconcile the intimate mixture of presolar, interstellar, and inner solar system materials that are observed in cometary IDPs [2]. A similar conclusion was reached to explain the occurrence of high temperature minerals (e.g. forsterite, melilite, osbornite) in Stardust samples from comet Wild-2 [3].

Astronomical IR spectra of comets [4] and young stars [5,6] are dominated by amorphous silicates that are generally considered unprocessed interstellar amorphous silicates. Here we propose that amorphous and crystalline silicates form in abundance in the inner regions of young stellar objects and are efficiently transported throughout protoplanetary disks. It is likely that only laboratory studies of these primitive materials can clearly identify the formation processes and origins of the most common constituents of the starting materials.

The presolar GEMS and the probable interstellar GEMS grains in IDPs predate the formation of CAIs, chondrules and matrix and may have been precursors to these meteoritic materials. Calculations show that average GEMS chemical compositions are highly normative for Fe-bearing olivine and so they also may have been a precursor component to the fine-grained fayalitic olivine common in the matrices of primitive carbonaceous chondrites.

Conclusions: Amorphous silicates were widespread constituents of the early solar system. Rare amorphous silicate stardust grains survived intact, but most were destroyed or heavily altered by shock and irradiation processes in the interstellar medium. Current evidence indicates that amorphous silicates were also efficiently produced in the early solar nebula.

References. [1] Keller, L. P. and Messenger, S. (2004) *LPS XXXV*, #1985. [2] Keller, L. P. and Messenger, S. (2005) The Nature and Origin of Interplanetary Dust: High-temperature Components, In *Chondrites and the Protoplanetary Disk* (Eds. Krot, Scott & Reipurth) *ASP Conf. Series* 341, 657-667. [3] Brownlee, D. E. *et al*. (2006) *Science*, 314, 1711-1716. [4] Hanner, M. (2003) The Mineralogy of Cometary Dust, In *Astromineralogy* (Ed. Henning), Springer, 171-185. [5] Meeus, G., Waters, L.B.F.M., Bouwman, J., et al. (2001) *A&A* 365, 476. [6] Bouwman, J., Meeus G., de Koter, A., (2001) *A&A* 375, 950.

.

LABORATORY ANNEALING EXPERIMENTS OF REFRACTORY SILICATE GRAIN ANALOGS USING DIFFERENTIAL SCANNING CALORIMETRY. Y. Kimura[1], J. A. Nuth III[2] and C. Kaito[1], [1]Laboratory for Nano-Structure Science, Department of Physics, Ritsumeikan University, 1-1-1 Nojihigashi, Kusatsu-shi, Shiga, 525-8577, Japan. ykimura@se.ritsumei.ac.jp, [2]Astrochemistry Laboratory, Code 691, NASA's Goddard Space Flight Center, Greenbelt MD 20771. Joseph.A.Nuth@nasa.gov, kaito@se.ritsumei.ac.jp

Introduction: Several comets show 10 μm emission features characteristic of a mixture of crystalline and amorphous Mg-rich olivine grains [1]. Since interstellar silicates are in an amorphous state, it has been considered simply that the amorphous silicates gradually crystallized via thermal annealing in the hot inner solar nebula over time and then were transported outward and incorporated in comets [e.g. 2,3]. Using this thermal annealing model, the chronology and formation age of comets in the early Solar System has been discussed based on laboratory experiments [4]. In this study, we will try to determine the crystallization temperature and the reaction energy of the silicate during thermal annealing using differential scanning calorimetry (DSC).

Experiment: Refractory silicate grains were produced in the laboratory by vapor phase condensation using the Condensation Flow Apparatus at NASA's GSFC [5]. The system produces well mixed amorphous grains that are several tens of nanometers in diameter. 2-7 mg of the analog grains are placed into a Pt pan, and then heated in vacuum or in air up to 1200 K at 1 or 5 K/min simultaneously with another Pt pan filled with the same mass of alumina powder using a commercial DSC system (DSC 8270; Rigaku Corp.). The alumina serves as a reference material and is inert. Since the temperature of the Pt pan with silicate varies depending on the reaction energy of the metamorphic processes caused by heating such as oxidation, crystallization or evaporation, we can measure the reaction energy by measuring the input thermal energy to keep the sample pan at equilibrium temperature, which is measured by thermocouple, with the reference pan. When it is an exothermic reaction, the spectrum goes to positive, i.e., in the case of an endothermic reaction, the slope declines. The reaction energy corresponds to the enthalpy of the reaction. The base line of the spectrum corresponds to the difference of the heat capacities between aluminum and Mg-silicate. In the case of the vacuum run, the sample chamber was continuously evacuated using a combination of mechanical and sorption pumps down to 0.1 Torr. At such pressures the thermal conductivity from the pans to the thermocouples is extremely poor. Therefore, we intend to build a new system using He flow. The DSC spectra in a He gas atmosphere will be presented on the poster.

Initial Results: We have performed annealing experiments on synthesized Mg silicate, Fe silicate and silica grains in the DSC at temperatures up to 1200 K. In the case of Mg silicate grains, several characteristic exothermic peaks were observed in both spectra of annealing in vacuum and air. Typical DSC spectra, which were measured in air for 5 and 1 K/min, are shown in Figs. 1 and 2. Five characteristic features were observed at about 590, 680, 740, 860 and 1060 K. When the scanning rate of annealing temperature is

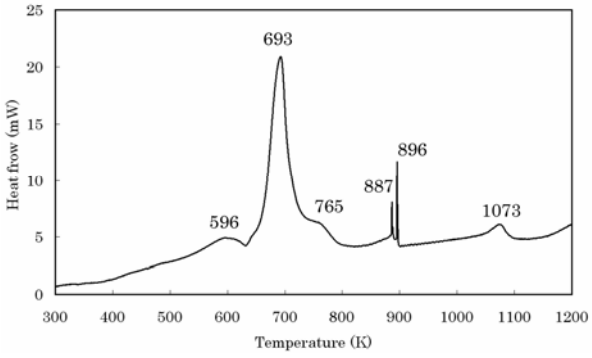

Fig. 1. DSC spectrum of Mg-silicate smoke particles (4.1 mg) heated at 5 K/min up to 1200 K in air. The numbers above the features indicate the peak temperatures. This spectrum has been corrected by subtracting the spectrum using blank Pt pans. The temperature of the feature at 1073 K corresponds to the crystallization temperature of forsterite.

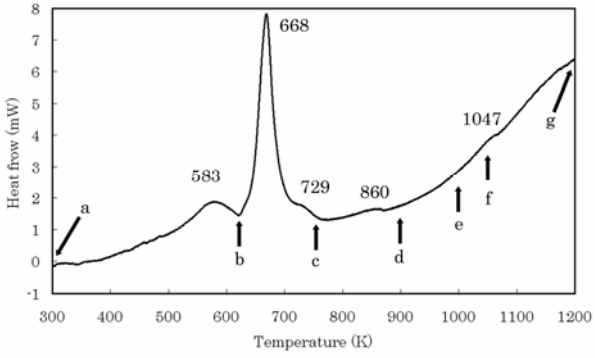

Fig. 2. DSC spectrum of Mg-silicate smoke particles (6.6 mg) heated at 1 K/min up to 1200 K in air. The numbers above the features indicate the peak temperatures. This spectrum has been corrected by subtracting the spectrum using blank Pt pans. The temperature of the feature at 1047 K corresponds to the crystallization temperature of forsterite.

decreased to 1 K/min, the peak positions are shifted about 10-30 K, which depends on the peaks, toward lower temperature. Namely, better reaction temperatures can be obtained from the spectrum obtained at 1 K/min. On the other hand, the peak heights of the spectrum become smaller as scanning speed decreases, because the reaction occurs slowly for a longer time, i.e., total reaction energies do not change. Please note the small value of the vertical axis in Fig. 2. As a result of heating at 5 K/min, although two significant sharp peaks at 887 and 896 K can be seen with the 860 K feature, those peaks disappeared in the spectrum heated at 1 K/min as shown in Fig. 2. The total exothermic energies of each peak at 590, 680, 740, 860 and 1060 K in Fig. 1 were roughly 174, 2118, 36, 104 and 105 J/g, respectively. In the case of the spectrum heated at 1 K/min in Fig.2, they were 348, 1970, 13, 30 and 35 J/g, respectively. These data will be verified and refined after further DSC experiments. Although the peak positions have been shown in the figure, starting temperatures are more important in a DSC spectrum, because reactions begin at the starting temperature.

Although it is difficult to decide the origin of each reaction feature, the energies (enthalpies) of each spectral change might be understood by the measurements of the infrared spectra before and after each feature. In order to observe the mid-infrared spectra of the samples over the several different temperatures, annealing experiments of Mg-silicate grains were performed up to 630, 750, 900, 1000 and 1050 K for 1 min/K. In addition to the spectra of as-prepared and annealed samples, the five infrared spectra just after the characteristic features have been measured as shown in Fig. 3. From these spectra, it is obvious that the feature at 1060 K corresponds to the energy of crystallization of forsterite. It was also found that the 10 μm feature attributed to silicate barely changes up to 900 K. The shape of the spectra after annealing up to 1000 K was close to that of the stall state, which is a stable intermediate spectral state of Mg-silicate grains during annealing [6]. The 10 μm feature of Mg silicate in the stall state corresponds to that of comets. Although the 10 μm feature shows less change up to 900 K, the 10 μm feature is drastically changed to the crystalline feature of forsterite as annealing temperatures approach the peak at 1047 K. Since, in the case of these silica experiments, only one broad feature was observed at 818 K in 5 K/min runs, those features in Figs. 1 and 2 should be attributed to the Mg rich silicate grains.

After annealing, the mass of the specimens always increased. For example, in the case of the experiment in Fig. 1, the initial mass of 4.1 mg increased to 4.8 mg. This result implies that oxidation occurred during annealing. By measurements of the mass of each annealed sample used for the infrared measurements, it was found that the exothermic reaction producing the feature at 680 K may be simple oxidation. As-prepared Mg-silicate smoke particles consist of moderate amounts of Mg_2Si, MgO, Mg_2SiO_4, and possibly amorphous SiO in addition to amorphous Mg silicate, which were analyzed using transmission electron microscope (TEM). Since the exothermic reaction at 680 K was not observed in the spectrum of silica smoke particles, the feature at 680 K could be due to oxidation of Mg_2Si and/or amorphous Mg silicate. Since the mass of the samples after annealing up to 630 K did not change, the peak at 590 K may be due to coagulation of the smaller grains, thus reducing the surface energy of the system. More detailed information will be available after TEM analysis.

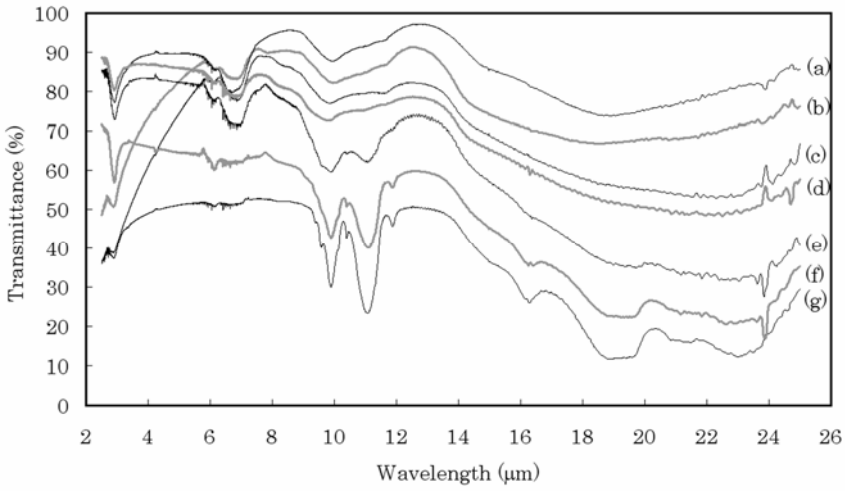

Fig. 3. Mid-infrared spectra of Mg-silicate smoke particles before and after DSC runs at 1 K/min up to 1200 K in air. Each spectrum corresponds to the points indicated in Fig. 2. (a) as-prepared. (b) 630 K. (c) 750 K. (d) 900 K. (e) 1000 K. (f) 1050 K. (g) 1200 K. Each spectrum has been shifted for clarity.

References: [1] Hanner M. S. 1999. *Space Science Reviews* 90:99-108. [2] Shu F. H. 1996. *Science* 271:1545-1552. [3] Boss A. P. 2004. *ApJ* 616:1265-1277. [4] Nuth III J. A. et al. 2000. *Nature* 406:275-276. [5] Nuth III J. A. et al. 2002. *Meteoritics & Planetary Science* 37:1579-1590. [6] Hallenbeck A. L. et al. 1998. *ICARUS* 133:198-209.

HIGH PRECISION AL-MG INTERNAL ISOCHRON USING ZONED MELILITE IN CAI. N. T. Kita[1], T. Ushikubo[1], K. B. Knight[2, 3], R. A. Mendybaev[2, 3], A. M. Davis[2, 3, 4], F. M. Richter[2, 3]. Department of Geology and Geophysics, University of Wisconsin-Madison, Madison, WI 53706 (noriko@geology.wisc.edu), [2]Department of the Geophysical Sciences, The University of Chicago, Chicago, Il 60637, [3]Chicago Center for Cosmochemistry, [4]Enrico Fermi Institute, The University of Chicago, Chicago, Il 60637

Introduction: The ^{26}Al-^{26}Mg decay system ($\tau_{1/2}$= 7.3×10^5 y) is a useful chronometer providing ~0.1 My time resolution for the formation of CAIs and chondrules in the earliest history of our solar system. Recent high precision MC-ICPMS bulk analyses of CAIs yield well-defined isochrons with initial ^{26}Al/^{27}Al of $(5.85\pm0.05)\times10^{-5}$ [1], slightly higher than the canonical value of $\sim5\times10^{-5}$ based on the peak value from the internal isochron of type B CAIs [2]. Furthermore, Laser MC-ICPMS and multicollector SIMS analyses of CAIs define internal isochrons with "supra-canonical" initial ^{26}Al/^{27}Al ratios of $(6–7)\times10^{-5}$, suggesting multiple events occurred to CAIs over time scales as long as 0.3–0.4 My [e.g., 3]. However, these data obtained from low Al/Mg phases are often scattered on the Al-Mg diagram, indicating the inferred higher initial ^{26}Al/^{27}Al could be an artifact caused by the redistribution of radiogenic ^{26}Mg during parent body metamorphism after most of the ^{26}Al had decayed. Also, the choice of isotopic mass fractionation correction law affects excess radiogenic ^{26}Mg (δ^{26}Mg*) by small amounts that can significantly affect initial ^{26}Al/^{27}Al ratios for CAIs with heavy Mg isotope enrichments and low Al/Mg [4].

Recently, we analyzed Mg isotopes in zoned melilite in a type B1 inclusion from Leoville (USNM 3535-1, 6×8 mm with a 500μm thick melilite mantle) using an ion microprobe CAMECA IMS 1280 (Wisc-SIMS Lab). We found nearly homogeneous δ^{25}Mg between 4.5 and 5.5‰ except for Geh-rich rims [5]. In this CAI, a single ^{26}Al-^{26}Mg isochron was obtained from melilite in both the core and the mantle with a slope corresponding to an initial ^{26}Al/^{27}Al ratio of $(5.68\pm0.34)\times10^{-5}$, implying melting and crystallization of this CAI within 0.1 My of the primary formation of refractory precursors inferred from the bulk CAI isochron [1].

To extend the high precision ^{26}Al chronology of CAIs, we report here preliminary results of additional Mg isotopic analyses from the same CAI with improved precision. Because of the relatively homogeneous δ^{25}Mg in the zoned melilite, the choice of mass fractionation law [4] will not affect the slope of the isochron for this CAI, though it may affect the intercept. The goal of this study is to achieve higher precision and accuracy of the ion microprobe Al-Mg dating, enabling us to better distinguish between well-defined and scattered internal isochrons in CAIs.

Method: We used primary O^- ion beam with a diameter of ~20 μm and an intensity of 20 nA. Multicollection detectors were used to simultaneously measure $^{24}Mg^+$, $^{25}Mg^+$, $^{26}Mg^+$ and $^{27}Al^+$. A single analysis consists of 60 s of presputtering, ~60 s for automated centering of the secondary optics, and 300 s of integration. We obtain ^{24}Mg signals of $(0.5–2.4)\times10^8$ cps for $Åk_{20}$–$Åk_{100}$. We used homogeneous melilite glass (~$Åk_{67}$) as a running standard. The fractionation-corrected δ^{26}Mg* values were calculated using an exponential law with slope of 0.514 from the evaporation experiment of [5]. Both internal errors and the reproducibility of fractionation-corrected δ^{26}Mg* values for the melilite glass standard were 0.1‰ (2SD). The reproducibility of the measured ^{27}Al/^{24}Mg ratios of the running standard was better than 2% (2SD).

Calibration of Standards: Synthetic zoned melilite crystals ($Åk_{20–70}$) were used to calibrate the matrix effect on both the ^{27}Al/^{24}Mg relative sensitivity, and on mass-fractionation-normalized δ^{26}Mg* values. We also made a small correction for negative bias on δ^{26}Mg* with decreasing Åk, as much as 0.1‰.

The relative sensitivity factor of the ion probe ^{27}Al/^{24}Mg ratios (RSF) was calculated by comparing the measured ^{27}Al/^{24}Mg with those converted from Al/Mg data obtained by SEM-EDS method, as shown in Fig. 1. We observed a systematic change of the RSF with Åk content as large as 7% from $Åk_{70}$ (0.93) to $Åk_{20}$ (1.00). Inaccurate calibration of RSF can be a potential artifact on the Al-Mg measurement, and can create a systematic bias on the corrected ^{27}Al/^{24}Mg ratios, changing the slope of the isochron.

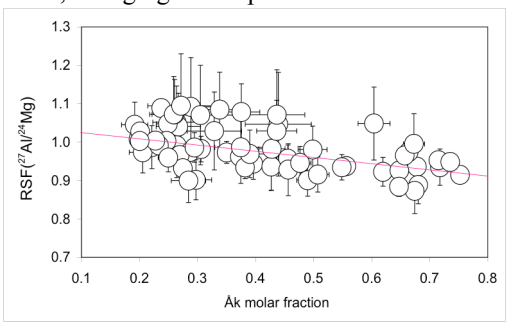

Fig. 1. Relative sensitivity factor of ^{27}Al/^{24}Mg ratios, as defined by $(^{27}Al/^{24}Mg)_{SIMS}/(^{27}Al/^{24}Mg)_{SEM\text{-}EDS}$.

Confirmation of the SEM-EDS analyses of the Al/Mg ratio of analyzed spots by WDS electron microprobe is needed.

Results: Fig 2a shows the isochron diagram for our previous analyses [5], which is revised by using the RSF shown in Fig. 1. The results of new analyses of melilite, 7 from the mantle ($^{27}Al/^{24}Mg \geq 2$) and 2 from the core ($^{27}Al/^{24}Mg$ ~1), are shown in the isochron diagram in Fig. 2b. The isochron obtained from these new data are consistent with our previous data, though they show small deviations from the regression line, having the MSWD (Mean Square Weighted Deviation) larger than 1.

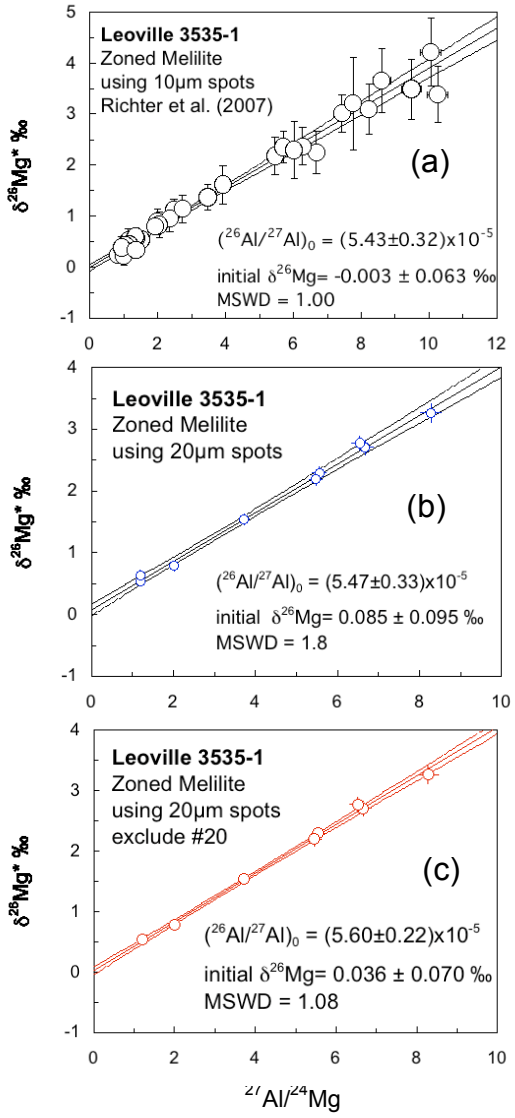

Fig. 2. The internal Al-Mg isochron diagram of zoned melilite from Leoville 3535-1 type B1 CAI. (a) Revised isochron from data obtained using 10 μm spots [4]. (b) New data obtained using 20 μm spots. (c) Isochron regression line without #20, which may have slightly overlapped nearby phases.

By omitting one of the core melilite analyses (#20, in Fig. 3), a less scattered isochron is obtained (MSWD~1) with an initial $^{27}Al/^{26}Al$ ratio of $(5.60\pm0.22)\times10^{-5}$ (Fig. 2c). The grain #20 is enclosed by plagioclase and contains abundant small grains of spinel, possibly affected by later isotopic exchange with other minerals. The initial $^{27}Al/^{26}Al$ ratio inferred from both isochrons (in Figs 2b and 2c) are significantly lower than the "supra-canonical value" ($\geq6\times10^{5}$), and only slightly lower than or indistinguishable to that of the bulk CAI by [1].

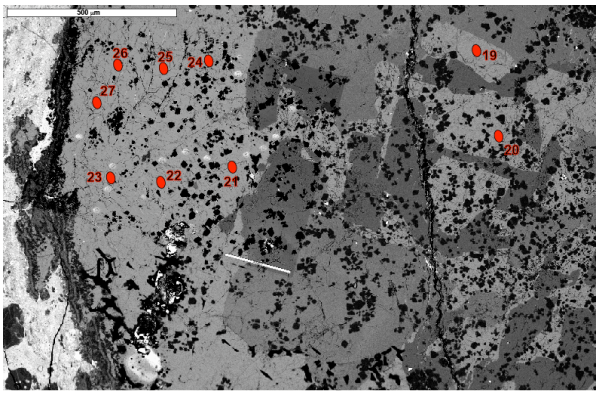

Fig. 3. The BSE image of Leoville 3535-1 CAI. Red oval spots are position of SIMS analyses. Scale bar; 500μm.

Discussion: Preliminary high precision analyses obtained here are mainly derived from mantle melilite with igneous zoning. The resulting isochron, therefore, corresponds to the final heating event experienced by this CAIs, within 0.1 My after the time that bulk isochron of the CAI [2] was established. More analyses from core melilite should be done to examine if the CAI recorded multiple events. Melilite is the common mineral phase in major types of CAIs (types A, B, and C), while anorthite, extensively used for the Al-Mg dating of CAIs in the past, is limited mainly to type B CAIs. Furthermore, anorthite has often lost radiogenic ^{26}Mg, resulted in disturbed isochrons [e.g., 6]. With the high precision melilite analyses we have achieved, we can evaluate a range of initial $(^{26}Al/^{27}Al)$ ratios among different groups of CAIs and examine the evidence for multiple heating events in a single CAI, corresponding to events occurred in the protoplanetary disk on a time scale of 0.1 My.

References: [1] Thrane K. et al. (2006) ApJ. 646, L159-L162. [2] MacPherson et al. (1995) Meteoritics 30, 365-386. [3] Young E. D. et al. (2005) Science, 308, 223-227. [4] Davis A. M. et al. (2005) LPS XXXVI, Abstract #2334. [5] Richter F. M. et al. (2007) LPS XXXVIII, Abstract #2303. [6] Podosek F.A. (1991) GCA 55, 1083-1110.

^{182}HF-^{182}W CHRONOMETRY AND THE ORIGIN AND EVOLUTION OF PLANETARY BODIES.

T. Kleine[1], M. Touboul[1], B. Bourdon[1], K. Mezger[2], H. Palme[3], F. Nimmo[4], S.B. Jacobsen[5], and Q.Z. Yin[6].
[1]IGMR, Dept. Earth Sci., ETH Zurich, CH-8092 Zurich (kleine@erdw.ethz.ch), [2]Inst. Min., Univ. Münster, D-48149 Münster, [3]Inst. Geol. Min., Univ. Köln, D-50674 Köln, [4]Dept. Earth Planet. Sci., UCSC, Santa Cruz, CA95064, USA, [5]Dept. Earth Planet. Sci., Harvard Univ., MA 02138, USA, [6]Dept. Geol., UCD, Davis, CA 95616, USA.

Introduction: In the past ~15 years ^{182}Hf-^{182}W chronometry has successfully been applied to provide time constraints for a variety of processes and events associated with the formation and earliest evolution of planetary bodies. The main interest in the Hf-W system was initially related to its potential for dating core formation [1-3] but Hf-W fractionations do not only occur during core formation but also during partial melting and fractional crystallization [4,5]. This allows the timescales of mantle differentiation (e.g., magma ocean crystallization) to be determined. Increasingly, Hf-W isochrons for meteorites are used to date Hf-W closure and to constrain the thermal evolution of asteroids. Here we review the chronology of early solar system processes as contrained by the ^{182}Hf-^{182}W system.

Accretion of the first planetesimals - iron meteorite parent bodies: Magmatic iron meteorites have ε_W values [6-9] similar to or below the initial ε_W of CAIs [10]. The ^{182}W/^{184}W in most iron meteorites has been lowered by burnout during prolonged exposure to cosmic rays [11, 12] and iron meteorites with the oldest exposure ages tend to show the most negative ε_W values [6]. However, iron meteorites with minor or no cosmogenic effects (e.g., Gibeon [13], Negrillos [6-8]) have ε_W values identical to the initial ε_W of CAIs, indicating that core formation in their parent bodies occurred within the first ~0.5 Ma of the solar system [6,8-10]. Such short timescales of accretion and differentiation contrast with the protracted formation of chondrite parent asteroids. Their accretion must have postdated the formation of chondrules, which in most cases did not end before ~2 Ma, as indicated by Al-Mg and Pb-Pb ages for chondrules [14-16,39]. These results indicate that the early thermal evolution and chemical differentiation of asteroids appears to be controlled by the energy produced by the decay of ^{26}Al. In the late-formed chondrite parent asteroids the decay of ^{26}Al could not raise the temperatures high enough to cause large scale chemical differentiation [6,15]. This model is supported by the relatively young Hf-W ages for chondrites and some primitive achondrites.

Accretion and thermal evolution of the parent asteroids of chondrites and primitive achondrites: Hf-W isochrons for several H chondrites yield ages of ~2 Ma for H4, ~6 Ma for H5, and ~10 Ma for H6 chondrites [17]. These ages are most consistent with an 'onion shell' model for the H chondrite parent body (but do not exclude later impact-driven disruption) and indicate that heating by ^{26}Al decay was the dominant heat source for the thermal metamorphism. Hf-W ages for acapulcoites and lodranites are ~6 Ma [18]. Comparison with ages obtained from other chronometers reveals that, although acapulcoites/lodranites were heated to much higher temperatures than H6 chondrites, they cooled faster than the H6 chondrites. This in conjunction with the higher peak temperatures of acapulcoites/lodranites indicates that their parent body was smaller and accreted earlier than the H chondrite parent asteroids. These results confirm that the early thermal evolution of asteroids was largely controlled by the amount of ^{26}Al present at the time of accretion.

Magmatism on the eucrite and angrite parent bodies: Eucrite whole-rocks define an isochron [19, 20] corresponding to an age of ~4 Ma [19], most likely dating differentiation in the mantle of their parent body. Chondrites do not plot on this isochron, indicating that core formation predated mantle differentiation [19]. Hf-W data for zircons from basaltic eucrites yield ages of ~7 Ma and date the crystallization of basaltic lavas on the eucrite parent body [21]. Internal isochrons for angrites yield crystallization ages of ~5 Ma for the quenched angrites Sahara 99555 and D'Orbigny. The slower cooled angrite Northwest Africa 2999, which is texturally similar to LEW86010 and Angra dos Reis, has a Hf-W age of ~10 Ma, which reflects metamorphism or more protracted cooling within the angrite parent body [22]. The timescales based on the Hf-W system in the eucrite and angrite parent bodies are consistent with results obtained from U-Pb, Mn-Cr and Al-Mg chronometry and also with ^{26}Al being an important heat source for differentiation of these asteroids.

Age and origin of Mars: Martian meteorites have elevated and variable ε_W values relative to chondrites, reflecting Hf/W fractionation due to core formation and early mantle differentiation [19,23,24]. The radiogenic ε_W of nakhlites is accompanied by relatively large ^{142}Nd anomalies [25], indicating that the radiogenic ε_W values of the nakhlites are largely due to Hf-W fractionation during mantle differentiation [19]. The shergotittes in contrast have lower ε_W and their ε^{142}Nd values range from chondritic to radiogenic [23]. The correlation of ε^{142}Nd and ε_W observed for Martian meteorites requires a major silicate differentiation event in the Martian mantle at ~42 Ma [23].

The constant ε_W of shergottites in spite of variable ε^{142}Nd indicates that the event that caused the fractionation of Sm from Nd occurred too late to cause significant variations in $^{182}W/^{184}W$. Given that some shergottites exhibit chondritic ε^{142}Nd, their W isotopic composition of ε_W~0.4 provide the currently best estimate for the W isotope composition of the Martian mantle [19,23]. The Hf/W ratio of the bulk Martian mantle, which is needed for calculating core formation ages, is poorly constrained. Th/W ratios of Martian meteorites are constant and thus can be used to determine the degree of W depletion in the Martian mantle but variations in the Hf/Th ratio among chondrite groups currently hamper a precise determination of the Hf/W ratio of the bulk Martian mantle [26]. Thus, estimates for the timing of Martian core formation are currently uncertain and range from ~0 to ~10 Ma [26].

The age of the Earth and its core: The $^{182}W/^{184}W$ of the Earth's mantle is elevated by 1.9 ε_W relative to chondrites, indicating that formation of the Earth's core at least in part occurred when ^{182}Hf was extant [27-29]. Determining an exact age of core formation from Hf-W chronometry, however, has proven difficult. If it is assumed that core formation occurred as a single event at a well-defined point in time, then the ^{182}W excess of Earth's mantle relative to chondrites would result from core formation at ~30 Ma [27-29]. A more realistic approach is to assume exponentially decreasing accretion with continuous core formation [1]. The calculated age of core formation in this model strongly depends on how much of the core material of newly accreted objects first equilibrated with Earth's mantle before entering its core [30-32]. It also depends on whether material from the Earth's core is involved in the re-equilibration process. For instance, if it is assumed that core and mantle of proto-Earth were completely equilibrated, then the age for complete formation of the Earth's core would be ~30 Ma [29,30]. If instead only material from the Earth's mantle is involved in the re-equilibration, this age would be ~50 Ma [29,32]. For a decreasing degree of re-equilibration the calculated core formation age becomes increasingly younger and is, for instance, ~70 Ma for 70% re-equilibration instead of ~50 Ma for complete equilibration.

Formation of the Earth most likely occurred by several distinct impacts that delivered large masses of core material at different times. The W isotope evolution of the Earth's mantle in this case depends on different parameters including the time of these impacts, the degree of re-equilibration during each impact, the differentiation history of each of the impactors, and the Hf/W ratios (and changes thereof) of the mantles of both proto-Earh and each impactor [33]. Determining an age for the Earth's core therefore requires these parameters to be determined independently. Such constraints are currently not available and would require the physical and chemical conditions during large impacts to be determined. Therefore, Hf-W ages for the Earth's core are strongly model-dependent, severly limiting the applicability of Hf-W chronometry to date the Earth. An alternative approach is dating the formation of the Moon, which most likely is the last major event during Earth's accretion [34].

The age of the Moon and lifetime of its magma ocean: Large variations in the $^{182}W/^{184}W$ of lunar whole-rock samples largely reflect cosmogenic production of ^{182}W mainly by neutron capture of ^{181}Ta during cosmic ray exposure of the lunar surface [35]. The cosmogenic ^{182}W production severly compromises application of Hf-W chronometry to lunar samples and several procedures were employed for determining indigenous $^{182}W/^{184}W$ (i.e., devoid of any cosmogenic ^{182}W) of lunar samples. Lee et al. [36] used the correlation of $^{182}W/^{184}W$ with Ta/W they obtained for mineral separates from several mare basalts to determine the $^{182}W/^{184}W$ at Ta/W=0. Kleine et al. [37] analyzed the W isotope composition of lunar metals that should not contain any Ta and hence cosmogenic ^{182}W. Both studies found variations in the $^{182}W/^{184}W$ among the different groups of lunar rocks, which apparently required formation and solidification of the Moon within the first ~60 Ma. More recently, however, Touboul et al. [38] determined the W isotope composition of metals from a comprehensive set of lunar samples with short exposure times (and hence potentially small cosmogenic ^{182}W components) and showed that there are no ^{182}Hf-induced $^{182}W/^{184}W$ variations within the lunar mantle. This indicates that solidification of the lunar magma ocean occurred later than ~60 Ma. The new data also reveal that the lunar and terrestrial mantles have identical $^{182}W/^{184}W$, indicating that core formation in the Moon and Earth occurred later than ~45 Ma.

References: [1] Harper C.L. and Jacobsen S.B. (1996), *GCA 60*. [2] Harper C.L. et al. (1991), *LPSC XXII*. [3] Lee D.C. and Halliday A.N. (1995), *Nature 378*. [4] Righter K. and Shearer C.K. (2003), *GCA 67*. [5] Shearer C.K. and Newsom H.E. (2000), *GCA 64*. [6] Kleine T. et al. (2005), *GCA 69*. [7] Lee D.C. (2005), *EPSL 237*. [8] Markowski A. et al. (2006), *EPSL 242*. [9] Schérsten A. et al. (2006), *EPSL 241*. [10] Burkhardt C. et al. (2007), *in prep.* [11] Leya I. et al. (2003), *GCA 67*. [12] Masarik J. (1997), *EPSL 152*. [13] Qin L.P. et al. (2007), *Anal. Chem. 79*. [14] Kita N.T. et al. (2000), *GCA 64*. [15] Kunihiro T. et al. (2004), *GCA 68*. [16] Russell S.S. et al. (1996), *Science 273*. [17] Kleine T. et al. in prep. [18] Touboul M. et al. in prep. [19] Kleine T. et al. (2004), *GCA 68*. [20] Quitté G. et al. (2000), *EPSL 184*. [21] Srinivasan G. et al. (2007), *Science 317*. [22] Markowski A. et al. (2007), *EPSL*. [23] Foley C.N. et al. (2005), *GCA 69*. [24] Lee D.C. and Halliday A.N. (1997), *Nature 388*. [25] Harper C.L. et al. (1995), *Science 267*. [26] Nimmo F. and Kleine T. (2007), *Icarus* [27] Kleine T. et al. (2002), *Nature 418*. [28] Schoenberg R. et al. (2002), *GCA 66*. [29] Yin Q.Z. et al. (2002), *Nature 418*. [30] Jacobsen S.B. (2005), *AREPS 33*. [31] Halliday A.N. (2004), *Nature 427*. [32] Kleine T. et al. (2004), *EPSL 228*. [33] Nimmo F. and Agnor C.B. (2006), *EPSL 243*. [34] Canup R.M. and Asphaug E. (2001), *Nature 412*. [35] Leya I. et al. (2000), *EPSL 175*. [36] Lee D.C. et al. (2002), *EPSL 198*. [37] Kleine T. et al. (2005), *Science 310*. [38] Touboul M. et al. (2007), *GCA 71*. [39] Amelin Y. et al. (2002), *Science 297*.

APPLICATION OF RIMS TO THE STUDY OF BERYLLIUM CHRONOLOGY IN EARLY SOLAR SYSTEM CONDENSATES. K. B. Knight[1,2], M. R. Savina[2,3], A. M. Davis[1,2,4], M. J. Pellin[2,3], J. Levine[1,2], L. Grossman[1,2,4], S. Simon[1,2]. [1]Department of the Geophysical Sciences, The University of Chicago, Chicago, Il 60637, [2]Chicago Center for Cosmochemistry, [3]Argonne National Laboratory, 9700 S. Cass Ave., Argonne, IL 60439, [4]Enrico Fermi Institute, The University of Chicago, Chicago, Il 60637.

Introduction: Resonant ionization mass spectrometry (RIMS) is a technique only recently applied to problems in cosmochemistry. Thus far, RIMS has been used to characterize isotopic compositions of select trace elements including Ba, Mo and Zr in presolar grains, allowing the detection of preserved nucleosynthetic signatures of parent stars (*r*- and *s*-processes), as well as supernovae signatures [e.g., 1-4]. Unambiguous evidence for the presence of extinct technetium has also been reported in presolar grains [5]. We are currently developing RIMS methods aimed at the determination of B, Be and Li in early solar system materials such as Ca-Al-rich inclusions (CAIs) using two RIMS instruments designed, built and optimized for the determination of trace element isotopic compositions with high spatial resolution [6] at Argonne National Laboratory.

Applications In Be Chronology: Using secondary ionization mass spectrometry (SIMS) techniques, several recent studies have focused on the short-lived decay of ^{10}Be to ^{10}B ($t_{1/2}$ ~1.5 Ma) [e.g. 7-11] in early solar system condensates. The presence of excess ^{10}B in these materials strongly suggests that CAIs and other highly refractory phases were witness to early system processes. ^{10}Be is likely to have formed in the solar system through energetic particle reactions, but steady state production in the interstellar medium by galactic cosmic ray spallation has also been suggested [12], with no stellar sources. The source of the initial ^{10}Be may be an active early sun (e.g., the x-wind model of [13]). Current data suggest that the inferred initial ^{10}Be/^{9}Be ratios in normal CAIs is ~1.0×10^{-3} and that the value in FUN CAIs is is ~0.5×10^{-3} [14, 15]. Also recently reported is the controversial detection of excess ^{7}Li resulting from the very short lived decay ($t_{1/2}$ ~53 d) of ^{7}Be [11]. In order to make this determination, the authors modeled lithium loss, and excluded analyses suggesting lithium mobility. While the ^{7}Be results have not yet been confirmed, they require that some CAIs recorded particle irradiation events from the earliest solar system.

SIMS analyses use relatively large analytical spot sizes (~50 um) and high primary beam currents in order to achieve adequate precision (±5%) on samples with low concentrations of Be, B and Li (generally in the range of 10^2 - 10^3 ppb). SIMS useful yields for these elements (atoms detected/atoms consumed) are generally in the 10^{-3}–10^{-4} range [16]. Pervasive terrestrial boron contamination and the high mobility of lithium create additional analytical complexity. RIMS may be able to contribute further to understanding the magnitude and extent of ^{10}B excesses, and possibly ^{7}Li excesses, in early solar system materials by achieving higher useful yields, thereby increasing the analytical precision at the current spot sizes or allowing one to analyze smaller or lower concentration spots at comparable precision. RIMS can also be used to ionize and detect isotopes from more than one element simultaneously, permitting analyses of the same sample volume for multiple elements (rather than through successive ablation or sputtering steps).

Resonant Ionization Mass Spectrometry: The advantages of RIMS lie in the ability to couple laser wavelengths with element-specific excited electronic states, combined with potentially small analytical spot sizes and generally large ion yields [6]. A primary beam from an Ar^+ or Ga^+ ion beam (which can be narrowly focused down to 30 nm) or a focused laser, is used to desorb neutral atoms from a sample surface. Atoms of interest in the resultant cloud of neutrals and ions are selectively excited by one or more laser photons tuned to intermediate (resonant) electronic states, followed by ionization from that state by an additional laser photon. This element-specific ionization greatly supresses isobaric interferences. The timing of each set of laser pulses sets the initial time for ions, which are then accelerated through a time-of-flight mass spectrometer. Instrumental mass fractionation is monitored by bracketed analyses of standards with similar elemental concentrations.

In addition to high spatial resolution and element-specific ionization, the Argonne RIMS instruments are optimized for high useful yields of 1-10%. Limitations include generally poor precision compared to SIMS. Isotopic differences smaller than ~10‰ are difficult to resolve. Additionally, if the lasers fail to saturate or nearly saturate the resonant steps in an excitation scheme, yields can be severely decreased and unstable isotopic fractionation can be introduced. While RIMS is in principle applicable to nearly all elements, appropriate laser ionization schemes can be challenging to develop and validate.

Developing RIMS-based Be Chronology: The CHARISMA instrument uses up to four Nd:YLF-pumped Ti:Sapphire lasers to generate tunable beams with wavelength ranges of ~700 nm to ~1000 nm. A nontunable Nd-YAG laser with a fundamental wavelength of 1064.16 nm is also available. Thus far, we have used this setup to develop resonant ionization

schemes for Be and B. The number of resonant states for light elements such as Be, B and Li is limited by their simple electronic structures.

Two resonant ionization schemes were investigated for Be. The first was a two-photon scheme, with excitation from the ground state to an intermediate level ($^1S \rightarrow {}^1P$) using a 234.93 nm photon (the 4th harmonic of the Ti:Sapphire fundamental at 939.73 nm), followed by photoionization at 306.70 nm (the 3rd harmonic of 920.09 nm). The laser power was insufficient to saturate the ionization step, however. We then developed a three-photon scheme using two resonant photons, the first exciting the Be atom to the ^1P state, and the second with a wavelength of 457.40 nm (2nd harmonic of 914.79 nm) exciting it to a ^1D state from which it was subsequently ionized by a 532.08 nm photon (2nd harmonic of the Nd-YAG laser). Saturation curves (signal intensity as a function of laser power) showed that the resonance steps were saturated.

Boron provides different resonant ionization challenges. These include a split ^2P ground state, with a low-lying $J = 3/2$ state a mere 15.29 cm^{-1} above the $J = 1/2$ ground state. The two states should be equally populated in laser-desorbed B. We have worked through several laser schemes to achieve initial success using a two-color ionization scheme. The first excitation is $^2P \rightarrow {}^2S$ at 249.75 nm (3rd harmonic of 749.26 nm), followed by ionization with a 371.91 nm photon (2nd harmonic of 743.82 nm). The isotopic reproducibility was stable within analytical error (±10%) at high laser powers, but we were unable to saturate the ionization transition for this laser scheme (Fig. 1).

Simultaneous ionization and detection of Be and B was achieved on a standard glass sample with ppm concentrations of both elements, using all five lasers at once. As in SIMS, the useful yields for these two elements are significantly different. The relative yield for Be was anywhere from 10 to 100 times higher than B. We speculate that this is due to B vaporizing as the oxide, in which case the desorption conditions will have to be adjusted to favor B atoms.

Development: We are continuing to develop the boron resonant ionization scheme. In particular, we will explore a three-photon scheme, exciting both the B ground state and the low-lying $J = 3/2$ state simultaneously. We expect this scheme to improve the B useful yield by a factor of two or more. Our goal is to maximize useful yields for all three elements, demonstrate isotopic reproducibility for Be-B and Be-Li determinations on crystalline and glass samples, begin determinations on Allende CAIs analyzed in previous studies, and extend the Be-B record to chondrules. RIMS techniques for Be decay products show potential for addressing questions in early solar system history.

References: [1] Nicolussi G. K. et al. (1998) *Geochim. Cosmochim. Acta*, 62, 1093-1104. [2] Nicolussi G. K. et al. (1997) *Science*, 277, 1281-1283. [3] Savina M. R. et al. (2003a) *Geochim. Cosmochim. Acta*, 67, 3201-3214. [4] Barzyk J. G. et al (2006) *New Astron. Rev.*, 50, 587-590. [5] Savina M. R. et al. (2004) *Science*, 303, 649-652. [6] Savina, M. R. et al. (2003b) *Geochim. Cosmochim. Acta*, 67, 3215-3225. [7] McKeegan K. D. et al. (2000) *Science*, 289, 1334-1337. [8] Sugiura N. et al. (2001) *Meteoritics & Planet. Sci.*, 36, 1397-1408. [9] Marhas K. K. et al. (2002) *Science*, 298, 2182-2185. [10] MacPherson G. J. et al. (2003) *Geochim. Cosmochim. Acta*, 67, 3165-3179. [11] Chaussidon M. et al. (2006) *Geochim. Cosmochim. Acta*, 70, 224-245. [12] Desch S. J. et al. (2004) *Astrophys. J.*, 602, 528–542. [13] Shu F. H. et al. (1997) *Science*, 277, 1475–1479. [14] McKeegan K. D. and Davis A. M. (2007) In *Meteorites, Comets and Planets* (ed. A. M. Davis), *Treatise on Geochemistry* (ed. H. D. Holland and K. K. Turekian), 2nd edition, in press. [15] Liu M.-C. et al. (2007) this volume. [16] Hervig R. L. et al. (2006) *Chem. Geol.*, 227, 83-99.

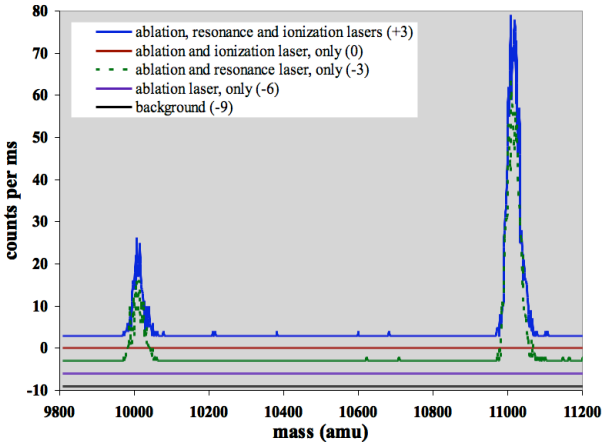

Fig. 1 Two-color RIMS spectra for boron showing different combinations of the desorption, resonance, and ionization lasers (arbitrarily offset from one another by multiples of three units). Backgrounds are zero. The boron ion yield is only slightly enhanced with the addition of the ionization laser (compared with two-photon resonance-only ionization), suggesting that the ionization step may not be saturated.

This work is supported, in part, by the U. S. Department of Energy, BES-Materials Sciences, under Contract W-31-109-ENG-38, and by the NASA Cosmochemistry Program.

ORIGIN AND CHRONOLOGY OF CHONDRITIC COMPONENTS. A. Krot[1], Y. Amelin[2], M. Bizzarro[3], P. Bland[4], J. Cuzzi[5], F. Ciesla[6], J. Connelly[3], H. Connolly[7], A. Davis[8], Y. Guan[9], J. Goswami[10], G. Huss[1], I. Hutcheon[11], T. Ireland[2], M. Kimura[12], N. Kita[13], E. Kurahashi[14], Y. Lin[15], G. MacPherson[16], S. Mostefaoui[17], K. Nagashima[1], L. Nyquist[18], M. Petaev[19], S. Russell[20], E. Scott[1], N. Sugiura[21], S. Tachibana[21], K. Thrane[3], Q. Yin[22], H. Yurimoto[23], E. Zinner[24]. [1]U. Hawaii, USA (sasha@higp.hawaii.edu). [2]ANU, Australia; [3]Geol. Inst., Denmark; [4]Imperial Coll., UK; [5]NASA Ames, USA; [6]Carnegie Inst., USA; [7]Kingsborough Coll., USA; [8]U. Chicago, USA; [9]CalTech, USA; [10]PRL, India; [11]LLNL, USA; [12]Ibaraki U., Japan; [13]U. Wisconsin, USA; [14]Geol. Survey, Japan; [15]Inst. Geol. Geophys., China; [16]Smithsonian Inst., USA; [17]MNHN, France; [18]JSC, USA; [19]Harvard U., USA; [20]NHM, UK; [21]U. Tokyo, Japan; [22]UC Davis, USA; [23]Hokkaido U., Japan; [24]Washington U., USA.

Summary: Evidence from short-lived (^{26}Al-^{26}Mg, ^{53}Mn-^{53}Cr) and long-lived (^{207}Pb-^{206}Pb) isotope systematics, oxygen isotopes, nuclear isotopic effects, mineralogy and petrography all suggest that Ca,Al-rich inclusions (CAIs) and amoeboid olivine aggregates (AOAs) were the first solids to form in the solar nebula, possibly within a period of <0.1-0.3 Myr, when the Sun was accreting rapidly as a class 0 or I protostar. CAIs and AOAs formed during multiple episodes either throughout the inner solar nebula (up to 4 AU) or in a localized nebular region (<0.1 AU) and were subsequently dispersed throughout the nebula. Most chondrules and meteorite matrix materials formed throughout the inner solar nebula 1-3 Myr after refractory inclusions, when the Sun was accreting more slowly. The majority of chondrules within each individual chondrite group may have formed over a much shorter period (<0.5-1 Myr). CAIs and AOAs were probably present in or near the chondrule-forming regions at the time of chondrule formation, but were largely unaffected by chondrule melting events. Chondrules and metal grains in CB chondrites formed during a single stage event ~4 Myr after CAIs, possibly from a vapor-melt plume generated by a collision between planetary embryos.

Chondritic components and their origin: The major chondritic components are CAIs, AOAs, chondrules, metal, and fine-grained matrix. CAIs are 0.1-20 mm-sized objects composed mostly of oxides and silicates of Ca, Al, Ti and Mg. AOAs are aggregates of mostly forsterite and Fe,Ni-metal, with small enclosed spinel-diopside-anorthite CAIs. Chondrules are igneous objects, 0.01-10 mm in size, composed largely of Fe,Mg-olivine and low-Ca Fe,Mg-pyroxene, Fe,Ni-metal and glassy mesostasis. Matrices of primitive (unmetamorphosed) chondrites consist largely of μm–sub-μm grains of crystalline Mg-olivine and low-Ca Mg-pyroxene, Fe,Ni-metal, sulfides, oxides and amorphous Fe,Mg-silicates. Evidence from mineralogical, chemical and isotopic studies suggest that CAIs and AOAs formed in an ^{16}O-rich ($\Delta^{17}O \leq -20‰$) but reducing environment of near-solar composition, at total pressure $\leq 10^{-4}$ bar and ambient temperature at or above condensation temperature of forsterite (~1300 K), possibly very near the protosun. In contrast, most chondrules and matrices formed in an ^{16}O-depleted ($\Delta^{17}O \geq -10‰$) nebular gas, under variable but generally more oxidizing conditions and lower ambient temperatures (<1000 K) than did CAIs and AOAs, and in regions with sufficiently high dust/gas ratios to stabilize silicate melts for perhaps hours, which can also satisfy the observed lack of mass-dependent isotopic fractionation in the vast majority of chondrules [1-3]. The apparent complementarity of chemical compositions of primitive chondrite chondrules and matrices [4], their similar oxygen isotopic compositions [5], and the high abundance of crystalline silicates in primitive chondrite matrices suggest that significant fraction of matrix materials was thermally processed during transient heating events that formed host chondrite chondrules [1], which is inconsistent with X-wind model of chondrule formation [6-8]

Absolute chronology of CAI and chondrule formation: ^{207}Pb-^{206}Pb isotopic ages of coarse-grained CAIs in CV chondrites Efremovka and Allende are 4567.11±0.16 and 4567.7±0.9 Myr, respectively [9-11], whereas ^{207}Pb-^{206}Pb ages of chondrules from CV, CR and CB carbonaceous chondrites are 4565.7±0.4 [12], 4564.7±0.6 [10] and 4562.7±0.5 Myr [13], respectively. These data indicate that chondrule formation lasted for several Myr, but the majority of chondrules within an individual chondrite group may have formed within ≤1 Myr. The resolved age difference (2±1 Myr) between CAIs and chondrules from Allende contradicts an X-wind hypothesis of contemporaneous formation of CAIs and chondrules in a single chondrite group [6-8].

Relative chronology of CAI and chondrule formation: Mineralogical and isotopic evidence indicates that, in each of the known chondrite groups, CAI formation predated chondrule formation [14]: (*i*) relict CAIs occur inside chondrules, and some CAIs are enclosed by chondrule-like igneous rims [14, 15], (*ii*) oxygen isotopic evidence indicates remelting of some CAIs in an ^{16}O-depleted nebular gas [16], and (*iii*) volatility fractionated, group II REE patterns in some chondrules indicate presence of CAIs among their precursors [17]. The similarities in mineralogy and isotopic compositions of CAIs inside and outside chondrules within an individual chondrite group suggest that CAIs were present in or near chondrule-forming regions at the time of chondrule formation, but were largely unaffected by chondrule melting events [18]. There is no unambiguous evidence that chondrules experienced re-melting in the CAI-forming region [19].

^{26}Al-^{26}Mg systematics: The use of the short-lived radionuclide ^{26}Al ($t_{1/2}$ = 0.73 Myr) as a high-resolution chronometer [specifically, inferred initial ^{26}Al/^{27}Al ratios $(^{26}Al/^{27}Al)_0$] for dating CAI and chondrule formation requires the assumption of ^{26}Al uniform distribution throughout the inner solar nebula, where CAIs and chondrules probably formed [20]. Cross-calibration of ^{26}Al-^{26}Mg and ^{207}Pb-^{206}Pb chronometers [21-23], and high-precision Mg isotope measurements of bulk chondrites, Earth and Mars [24], have validated the assumption and thus confirmed the chronological significance of ^{26}Al-^{26}Mg systematics.

Most CAIs, and few AOAs analyzed so far, define $(^{26}Al/^{27}Al)_0$ of ~5×10^{-5}, referred to as the "canonical" value [20, 25]. The canonical ratio has been recently revised upwards to a "supra-canonical" value of $(5.85\text{-}7)\times10^{-5}$ [24, 26-30]. Note the importance of Mg isotopic fractionation laws (exponential, equilibrium, or experimentally derived) in correction of Mg isotope data and in comparing isochrons for mass-fractionated CAIs [31]. High-precision Mg isotope measurements of bulk igneous Allende CAIs and their mineral separates using MC-ICPMS define $(^{26}Al/^{27}Al)_0$ of $(5.12\pm0.18)\times10^{-5}$ [32], which is inconsistent with $(5.85\pm0.05)\times10^{-5}$ value reported by [24] using the same analytical technique. Although this apparent discrepancy still needs to be resolved, both data sets suggest a very short (<20-30 Kyr) time difference between the formation of precursors of the igneous CV CAIs and their crystallization ages. To constrain the total duration of CAI formation, high precision measurements of internal Al-Mg isochrons in CAIs from primitive carbonaceous chondrites (e.g., CR2, CO3.0, Acfer 094, Adelaide) are required.

High-precision Al-Mg isotope measurements for chondrules from primitive chondrites are limited [33-40]. In CO3.0 chondrite Y-81020, the $(^{26}Al/^{27}Al)_0$ ranges from $(0.24\pm0.17)\times10^{-5}$ to $(1.4\pm0.3)\times10^{-5}$ [mean = $(8\pm4)\times10^{-6}$], which corresponds to an age difference of 1.3-3.2 Myr after CAIs with the canonical ^{26}Al/^{27}Al ratio [36, 37]. No systematic differences were found between the $(^{26}Al/^{27}Al)_0$ in chondrules from Y-81020 and those in chondrules from Semarkona (LL3.0) and Bishunpur (LL3.1) [$(^{26}Al/^{27}Al)_0$ ranges from $(0.46\pm0.21)\times10^{-5}$ to $(2.28\pm0.73)\times10^{-5}$; mean = $(1\pm0.5)\times10^{-5}$] [33-39]. In contrast, most chondrules in CR2 chondrites have $(^{26}Al/^{27}Al)_I$ <0.3×10^{-5} [40], consistent with their young ^{207}Pb-

^{206}Pb ages [10]. The young crystallization ages of primitive chondrite chondrules inferred from internal Al-Mg isochrons are in apparent conflict with the whole-chondrule Al-Mg isochrons [$(^{26}Al/^{27}Al)_0$ ~(3-5)×10^{-5}] inferred from bulk Mg-isotopic compositions of CV chondrules [26]. Note, however, that the whole-chondrule Al-Mg isochrons correspond to the formation time of chondrule *precursors*, not chondrule crystallization ages; the latter can be inferred only from internal Al-Mg isochrons. According to an X-wind model, chondrules formed in the disk and were well protected from irradiation by energetic particles. As a result, large excesses of ^{26}Mg reported in bulk CV chondrules are [26] in conflict with the X-wind model and its local irradiation origin for ^{26}Al [6-8].

^{53}Mn-^{53}Cr systematics: ^{53}Mn-^{53}Cr systematics of chondrules from Chainpur (LL3.4) define an initial ^{53}Mn/^{55}Mn of (5.1±1.6)×10^{-6} [41], which is similar to the value for Semarkona (LL3.0) chondrules (5.8±1.9)×10^{-6} [38]. Relative to the Solar System's initial ^{53}Mn/^{55}Mn of (8.5±1.5)×10^{-6} obtained from bulk carbonaceous chondrites [42, 43], chondrules in ordinary chondrites are 2.73 Ma younger than CV CAIs, which is in a good agreement with the ^{26}Al-^{26}Mg systematics of ordinary chondrite chondrules [38].

^{60}Fe-^{60}Ni systematics: Although ^{60}Fe ($t_{1/2}$ = 1.49 Myr) can potentially be a high-resolution early Solar System chronometer, its chronological implication for CAI and chondrule formation is still limited and controversial. The presence of ^{60}Ni excess due to decay of ^{60}Fe has been reported in chondrule silicates and sulfides, but the initial abundance of ^{60}Fe remains poorly constrained [44-49]. The initial ^{60}Fe/^{56}Fe ratio in Fe,Mg-silicates from Semarkona and Bishunpur chondrules ranges from (2.2±1.0)×10^{-7} to (3.7±1.9)×10^{-7} [46]. By applying the time difference of 1.5-2.0 Myr between formation of CAIs and chondrules, a Solar System initial ^{60}Fe/^{56}Fe of (5-10)×10^{-7} is estimated [46]. This estimate may be invalid, if ^{60}Fe and ^{26}Al were decoupled [47]. Note that although ^{60}Ni excesses have been reported in CAIs [48], these excesses are probably due to nucleosynthetic anomalies rather than decay of ^{60}Fe.

Chronology and O-isotopic compositions of chondritic components: If O-isotopic composition of the Sun (yet to be measured on Genesis samples) is similar to that of CAIs and AOAs from primitive chondrites ($\Delta^{17}O \leq -20‰$) [50, 51], then the differences in O-isotopic compositions between CAIs+AOAs and chondrules+matrices ($\Delta^{17}O \geq -10‰$) can be interpreted chronologically [52]. Note that the origin of ^{16}O-rich reservoir in the early Solar System and O-isotopic composition of the Sun remains controversial [53]. In addition, the evidence for coexistence of ^{16}O-rich and ^{16}O-poor gaseous reservoirs during early crystallization of igneous CAIs in CV chondrites [54, 55] and the lack of clear correlation between a degree of ^{16}O-enrichment in chondrules and their crystallization ages [56] may reduce chronological significance of oxygen isotopes.

Chronology of CB chondrites: Chondrules and metal grains in CB chondrites are mineralogically, chemically and isotopically unique. The CB chondrules coexist with Fe,Ni-metal condensates, have exclusively Mg-rich compositions and non-porphyritic (cryptocrystalline or skeletal) textures, flat REE patterns, similar O-isotopic compositions and young ^{207}Pb-^{206}Pb ages, and show no evidence for remelting [13]. Chondrules and metal grains show mass-dependent fractionation effects in Mg, Fe and Ni [57, 58]. It is suggested that chondrules and metal grains in CBs formed during a single-stage event, possibly from a gas-melt plume generated by a collision between planetary embryos; rare ^{16}O-depleted CAIs in CBs were remelted during this event [13]. If this is the case, chondrules and metal grains in CBs can potentially allow to link several relative chronometers to the absolute time scale.

Chronology of ^{26}Al-poor CAIs: A rare subset of CAIs (so-called FUN CAIs and some platy hibonite grains (PLACs) and corundum-rich CAIs) contain relatively large nucleosynthetic isotope anomalies, and had little or no ^{26}Al at the time of their formation. It has been suggested that such objects formed relatively early, prior to injection and homogenization of ^{26}Al in the Solar System [59, 60]. Measurements of ^{207}Pb-^{206}Pb ages of such CAIs are required to test this hypothesis. The common presence in CH chondrites of very refractory (grossite- and hibonite-rich), ^{16}O-rich and ^{26}Al-poor [$(^{26}Al/^{27}Al)_I$) < 10^{-6}] CAIs, which typically show no nuclear isotopic anomalies or mass-dependent fractionation effects, is intriguing [61-63]. These CAIs may have formed either very early, like is assumed for FUN CAIs and PLACs, or very late, after decay of ^{26}Al.

Presence of asteroidal material among chondrule precursors? If there is 1-2 Myr gap between CAIs and chondrules, and accretion and differentiation of planetesimals predated or overlapped with chondrule formation [63], fragments of these early differentiated bodies might be expected within chondrites or even among chondrule precursors. It has been recently shown that coarse-grained lithic clasts of forsteritic olivine with granoblastic textures inside magnesian porphyritic chondrules from CV chondrites are relict [65, 66]. Formation of the granoblastic textures requires sintering and prolonged, high-temperature (>1000°C) annealing [67] – conditions which are not expected in the solar nebula during chondrule formation, but could have been achieved on parent bodies. If these objects are indeed fragments of thermally processed planetesimals that were present among chondrule precursors, they will place important constraints on the early Solar System chronology. More work is required to establish this possibility, including whether they have trace element fractionation patterns indicative of igneous differentiation as opposed to volatility control.

References: [1] Scott & Krot (2005) in *CPD*, 15. [2] Cuzzi & Alexander (2006) *Nature* 441, 483. [3] Ebel & Grossman (2000) *GCA* 64, 339. [4] Bland et al. (2005) *PNAS* 102, 13755. [5] Clayton & Mayeda (1999) *GCA* 63, 2089. [6] Shu et al. (2001) *ApJ* 548, 1029. [7] Gounelle et al. (2001) *ApJ* 548, 1051. [8] Gounelle et al. (2006) *ApJ* 640, 1163. [9] Amelin et al. (2002) *LPS* 33, #1151. [10] Amelin et al. (2002) *Science* 297, 1678. [11] Amelin et al. (2005) *LPS* 37, #1970. [12] Connelly et al. (2007) in prep. [13] Krot et al. (2005) *Nature* 436, 989. [14] Russell et al. (2005) in *CPD*, 317. [15] Krot et al. (2005) *ApJ* 629, 1227. [16] Krot et al. (2005) *Nature* 434, 998. [17] Misawa & Nakamura (1988) *Nature* 334, 47. [18] Krot et al. (2007) *MAPS*, in press. [19] Itoh & Yurimoto (2003) *Nature* 423, 728. [20] MacPherson et al. (1995) *Meteoritics* 30, 365. [21] Zinner & Göpel (2002) *MAPS* 37, 1001. [22] Sanders & Taylor (2005) in *CPD*, 915. [23] Halliday & Kleine (2005) in *MESS II*, 775. [24] Thrane et al. (2006) *ApJL* 646, L159. [25] Weisberg et al. (2007) *LPS* 38, #1588. [26] Bizzarro et al. (2004) *Nature* 431, 275. [27] Bizzarro et al. (2005) *Nature* 435, 1280. [28] Young et al. (2005) *Science* 308, 223. [29] Taylor et al. (2005) *LPS* 36, #2121. [30] Richter et al. (2007) *LPS* 38, #2303. [31] Davis et al. (2006) *LPS* 37, #2334. [32] Jacobsen et al. (2007) *Nature*, submitted. [33] Kita et al. (2000) *GCA* 64, 3913. [34] McKeegan et al. (2000) *LPS* 31, #2009. [35] Mostefaoui et al. (2002) *MAPS* 37, 421. [36] Kunihiro et al. (2004) *GCA* 68, 2947. [37] Kurahashi et al. (2004) *LPS* 35, #1476. [38] Kita et al. (2005) in *CPD*, 558. [39] Rudraswami & Goswami (2007) *EPSL* 277, 231. [40] Nagashima et al. (2007) *MAPS*, in press. [41] Yin et al. (2007) *ApJ* 662, L43. [42] Shukolyukov & Lugmair (2006) *EPSL* 250, 200. [43] Moynier et al. (2007) *LPS* 38, #1401. [44] Tachibana & Huss (2003), *ApJ* 588, L41. [45] Mostefaoui et al. (2005) *ApJ* 625, 271. [46] Tachibana et al. (2006) *ApJ* 639, L87. [47] Bizzarro et al. (2007) *Science* 316, 1178. [48] Quitté et al. (2007) *ApJ* 655, 678. [49] Goswami et al. (2007) *LPS* 38, #1943. [50] Yurimoto & Kuramoto (2004) *Science* 305, 1763. [51] Hashizume & Chaussidon (2005) *Nature* 434, 619. [52] Krot et al. (2005) *ApJ* 622, 1333. [53] Yurimoto et al. (2006) in *PP V*, 849. [54] Yurimoto et al. (1998) *Science* 282, 1874. [55] Aléon et al. (2007) *EPSL*, submitted. [56] Krot et al. (2006) *Chem. Erde* 66, 249. [57] Gounelle et al. (2007) *EPSL* 256, 521. [58] Zipfel & Weyer (2007) *LPS* 38, #1927. [59] Sahijpal & Goswami (1998) *ApJ* 509, L137. [60] Simon et al. (2002) *MAPS* 37, 533. [61] Weber et al. (1995) *GCA* 59, 803. [62] Srinivasan et al. (2007) *LPS* 38, #1781. [63] Krot et al. (2007) *ApJ*, in press. [64] Bizzarro et al. (2005) *ApJ* 632, L41. [65] Libourel & Krot (2006) *EPSL* 254, 1. [66] Chaussidon et al. (2006) *LPS* 37, #1335. [67] Whattam & Hewins (2007) *LPS* 38, #1983.

^{26}Al-^{26}Mg systems of ferromagnesian and aluminum-rich chondrules in primitive carbonaceous chondrites.
E. Kurahashi[1,2], N. T. Kita[1,3], H. Nagahara[2], and Y. Morishita[1] [1]Institute of Geology and Geoinformation, Geological Survey of Japan, AIST, Centeral7, 1-1-1, Higashi, Tsukuba, 305-8567, JAPAN (kurahashi-erika@aist.go.jp), [2]Dep. of Earth and Planetary Science, The university of Tokyo, 7-3-1, Hongo, Bunkyo-ku, Tokyo, 113-0033, JAPAN, [3]Dep. of Geology and Geophysics, University of Wisconsin-Madison, Madison, WI 53706-1692, USA.

Introduction: Chondrites and chondrules have chemical and isotopic variations among chondrite chemical groups, such as oxidizing condition, chondrite bulk chemical compositions, abundance of chondrule chemical types, and oxygen isotopes [e.g. 1]. To clarify the origin of the diversities among chondrite and chondrule types, we have performed systematical investigations of formation ages and petrological properties of the early solar system materials.

The ^{26}Al-^{26}Mg systems of ferromagnesian chondrules in least equilibrated ordinary chondrites were investigated for two FeO-poor (Type I) chondrules and seventeen FeO-rich (Type II) chondrules from LL3.0-3.1 chondrites [e.g. 2, 3], and thirteen Type II chondrules from L3.0-3.1 chondrites [4], of which initial ^{26}Al/^{27}Al ratios were (0.5-2)×10^{-5} [2-4], corresponding to relative ages of 1.0-2.5 Myr after CAIs with assumption of homogeneous distribution of ^{26}Al in the early solar nebula. In carbonaceous chondrites (CC), six Type II chondrules in CO3.0 Yamato-81020 were studied and the initial ^{26}Al/^{27}Al ratios were from (0.24±0.17)×10^{-5} to (0.65±0.32)×10^{-5} [5, 6], corresponding to 2.0-3.0 Myr after CAIs. To determine formation timing of common Type I chondrules in CC (>90%), we measured Al-Mg systems for fourteen Type I chondrules from CO3.0 (Yamato-81020) and the initial ^{26}Al/^{27}Al ratios of the chondrules were from (0.71±0.19)×10^{-5} to (1.27±0.34)×10^{-5} [7], corresponding to 1.4-2.0Myr after CAIs, which show similar ranges of those of ordinary chondrites. The initial ^{26}Al/^{27}Al ratios of aluminum-rich (Al-rich) chondrules were obtained from some type3 chondrites (0.1-1×10^{-5}), but they contained data from slightly metamorphosed ones with large errors [8-12]. To determine chondrule formation timing among chemical chondrite groups, we have examined ^{26}Al-^{26}Mg systems of chondrules in primitive carbonaceous chondrites (CO and CR). In the present study, we focused the age studies of Type II and Al-rich chondrules, because less number of the age data was obtained.

Mineralogy and Petrography: Three Type II and two Al-rich chondrules in CO3.0 Yamato-81020 (Y-81020) have been measured for ^{26}Al ages up to now.

Type II chondrules: Chondrule Y56, 120×280μm in size, consists of olivine phenocrysts (Fo_{50-66}), plagioclase (An_{31-56}), high-Ca pyroxene ($Wo_{47}En_{30}$), and one large metal/sulfide with irregular outline. Porphyritic olivine chondrule Y58, 190μm in size, consists of olivine phenocrysts (Fo_{48-70}, 10-60μm) and interstitial plagioclase (An_{41-57}). Some olivine phenocrysts show strong compositional zoning from FeO-poor core (Fo_{81-90}) to FeO-rich rim. Fine olivine grains (< 10μm) occur at the rim of the chondrule. Rounded to irregular metal (3-20μm in size) and troilite (~20μm in size) are present. Chondrule Y46, 420×300μm in size, consists of euhedral FeO-rich olivine, high-Ca pyroxene, anorthite, and spinel. Some olivine grains show compositional zoning from FeO-poor core to FeO-rich rim. Rounded to irregular metal exists both inner region and periphery of the chondrule.

Al-rich chondrules: Chondrule Y23, 180μm in diameter, consists of fine (~10μm) euhedral anorthite (An_{99-100}) and anhedral high-Ca pyroxene ($Wo_{49-66}En_{30-60}$) in almost equal amounts with some rounded olivine (Fo_{97-99}) mostly in the periphery of the chondrule. No low-Ca pyroxene and only one metal are found. Y175 is a fragment of an Al-rich chondrule, 400×260μm in size, and consists of low-Ca pyroxene phenocrysts, subhedral to euhedral anorthite, high-Ca pyroxene. Mesostasis is intergrowing of plagioclase, high-Ca pyroxene and Si-rich glass. Low-Ca pyroxene contains round to oval metal grains (5-20μm). Fine grained (<5μm) euhedral FeO-rich olivine, pyroxene, and Si-Al-rich glass made a rim (10-40μm in thick) on the fragment periphery.

^{26}Al-^{26}Mg results: ^{26}Al-^{26}Mg measurements were performed by SIMS (IMS-1270) at Geological Survey of Japan, AIST [7, 13]. Fig. 1 and 2 show ^{26}Al-^{26}Mg isochron diagrams of Type II and Al-rich chondrules, respectively. Type II chondrules, Y56 and Y58, have clear ^{26}Mg-excesses, of which initial ^{26}Al/^{27}Al ratios are (0.75±0.18)×10^{-5} for Y56 and (0.71±0.36)×10^{-5} for Y58, respectively, corresponding to 2.00(-0.23/+0.29) and 2.06(-0.43/+ 0.75) Myr after CAIs on the assumption of homogeneous ^{26}Al distribution. For Y46, olivine or pyroxene was not analyzed, and the model isochron is (0.57±0.22)×10^{-5}, 2.28(-0.34/+0.51) Myr after CAIs. Revised ^{26}Al age data of Al-rich chondrule Y23 from the previous our results [13] show a scattered isochron (MSWD=1.6) with the slope of (0.50±0.14)×10^{-5}. The data is translated to relative age of 2.42(-0.26/+0.34) Myr after CAIs if the slope of the isochron represents the initial ^{26}Al/^{27}Al ratio. A model isochron of Y175 without olivine/pyroxene measure-

ments has the initial ratio of $(1.01\pm0.15)\times10^{-5}$, corresponding to 1.69(-0.15/+0.17) Myr after CAIs.

Discussions: The initial $^{26}Al/^{27}Al$ ratios of the chondrules including results of Type Is [7] in Y-81020 are summarized in Fig.3. The ranges of the initial $^{26}Al/^{27}Al$ ratios of Al-rich chondrules did not distinguish from those of Type I and Type II chondrules in the CO chondrite. Type I chondrules have peak initial $^{26}Al/^{27}Al$ ratios from 0.8×10^{-5} to 1.0×10^{-5}. The initial ratios of Type IIs are relatively lower $(0.6\text{-}0.8\times10^{-5})$ than Type Is $(0.7\text{-}1.3\times10^{-5})$. The present results of Type IIs are consistent with the upper limit of the initial $^{26}Al/^{27}Al$ ratios of Type IIs from the same chondrite (Y-81020) in literature $(0.2\text{-}0.7\times10^{-5})$ [5, 6], although the analytical errors are much larger than those in the present study. Thus, Type II chondrules in CO chondrites could be formed slightly later than Type I chondrules. Comparing to ferromagnesian chondrules in the CO chondrite, the initial $^{26}Al/^{27}Al$ ratios of Type Is in LL chondrites did not distinguish from those of Type IIs, although the number of Type I age data in LL chondrites are small [2, 3]. It is concluded that the formation age difference between Type I and Type II chondrules in the CO chondrite suggests a possibility that the redox states of the CO chondrule forming region had changed from reducing to oxidizing with time, but those of the LL chondrule forming region had not changed with time.

References: [1] Scott E. R. and Krot A. N. (2003) In *Meteorites, Comets, and Planets, Vol. 1*, 143-200. [2] Kita N. T. et al. (2005) In *Chondrites and the Protoplanetary Disk*, 558-587. [3] Mostefaoui et al. (2002) *Meteoritics & Planet. Sci.*, 37, 421-438. [4] Rudraswami N. G. and Goswami J. N. (2007) *Earth and Planet. Sci. Lett.*, 257, 231-244. [5] Yurimoto and Wasson (2002) *Geochim. Cosmochim. Acta*, 66, 4355-4363. [6] Kunihiro et al. (2004) *Geochim. Cosmochim. Acta*, 68, 2947-2957. [7] Kurahashi et al. (2007) submitted to *Geochim. Cosmichim. Acta*. [8] Russell et al. (1996) *Science*, 273, 757-762. [9] Srinivasan et al. (2000) *Meteoritics & Planet. Sci.*, 35, A151. [10] Hutcheon et al. (2000) *LPSXXXI*, 1869. [11] Marhas et al. (2000) *Meteoritics & Planet. Sci.*, 35, A102. [12] Huss et al. (2001) *Meteoritics & Planet. Sci.*, 36, 975-997. [13] Kurahashi et al. (2004) *LPSXXXV*, 1476.

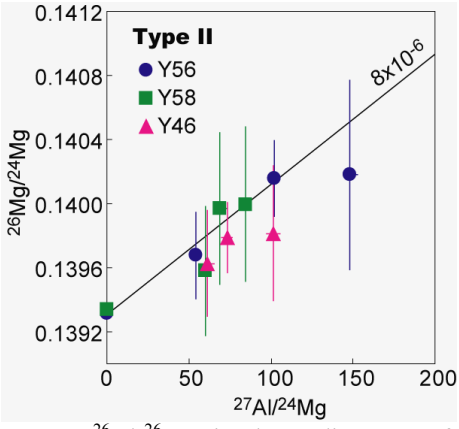

Figure 1. ^{26}Al-^{26}Mg isochron diagrams of Type II chondrules. The solid line is the initial $^{26}Al/^{27}Al$ ratio.

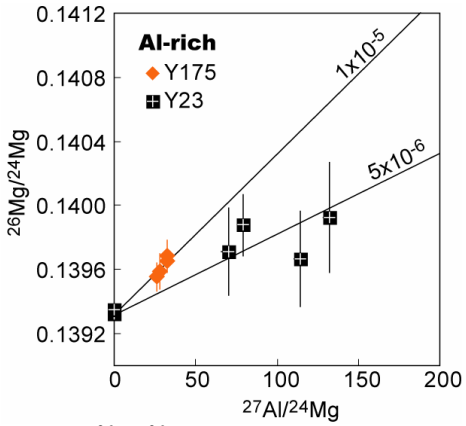

Figure 2. ^{26}Al-^{26}Mg isochron diagrams of Al-rich chondrules.

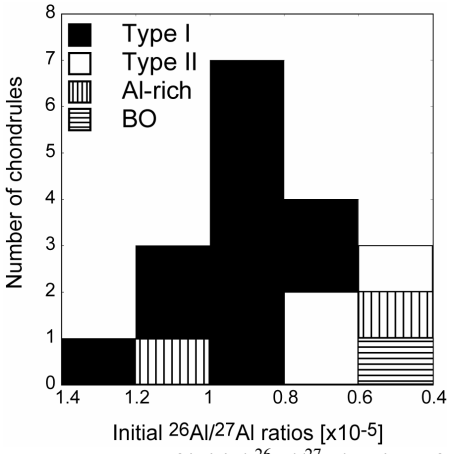

Figure 3. Summary of initial $^{26}Al/^{27}Al$ ratios of total 19 chondrules in CO3.0 Y-81020.

BERYLLIUM-10 IN CM HIBONITES: IMPLICATIONS FOR AN IRRADIATION ORIGIN. Ming-Chang Liu[1], Kevin D. McKeegan[1], Andrew M. Davis[2] and Trevor R. Ireland[3] [1]Department of Earth and Space Sciences, UCLA, Los Angeles, CA 90095 (mcliu@ess.ucla.edu), [2]Department of the Geophysical Sciences, Enrico Fermi Institute, and Chicago Center for Cosmochemistry, University of Chicago, Chicago, IL 60637, [3]Research School of Earth Sciences, ANU, Canberra, ACT, Australia.

Introduction: The origin(s) of short-lived radionuclides have been a long standing problem in cosmochemistry. Among all the most short-lived radionuclides ($t_{1/2} \leq 1.5$ My), ^{10}Be and ^{60}Fe require specific nucleosynthetic mechanisms. ^{60}Fe, due to its neutron-rich nature, has to be produced by stellar nucleosynthesis. On the other hand, ^{10}Be requires an origin that involves nuclear reactions with energetic particles since it is destroyed in stars. However, there has not been a consensus as to the true origin of solar system ^{10}Be.

The existence of ^{10}Be in the solar system was first proven by [1] in a CV3 CAI with an initial ^{10}Be/^{9}Be of ~9.5×10^{-4}. A re-examination of the same CAI by [2] yielded a more precise number of $(8.8\pm0.6)\times10^{-4}$. In addition to these studies, there have been other measurements in different refractory inclusions from various meteorites. Among all the measurements, the most interesting results are from [3-4], who revealed the abundance of ^{10}Be on the order of $5\times10^{-4}\times^{9}$Be in a suite of ^{26}Al-free but isotopically anomalous platy hibonite crystals, including the famous FUN inclusion HAL. MacPherson et al. (2003) [5] examined another FUN CAI, which lacks ^{26}Al, from Axtell and found that it also exhibits a lower ^{10}Be/^{9}Be ratio of ~ 3×10^{-4}.

McKeegan et al. (2000) [1], Gounelle et al. (2001, 2006) [6,7], Marhas et al. (2002) [2] and MacPherson et al. (2003) [3] assessed the irradiation contributions from both solar energetic particles and galactic cosmic rays (GCR) and concluded that an *in-situ* irradiation by the proto-Sun is the most likely origin for ^{10}Be as the steady state GCR contributions fall short by around an order of magnitude compared to the CAI initial. A potential implication of this origin is the heterogeneity of ^{10}Be in the solar nebula and ^{10}Be can not be used as a chronometer [5]. However, Desch et al. (2004) [8] challenged this view, on the basis of the "ubiquitous presence of ^{10}Be" at the level of $(0.45\text{-}1.8)\times10^{-3}\times^{9}$Be in refractory samples from meteorites, by considering the trapping of GCR-produced ^{10}Be nuclei in the progenitor molecular cloud core. From this view, ^{10}Be recorded in meteoritic materials does not require a local irradiation production and its spatial distribution in the solar nebula would have must been homogeneous. A consequence would be that ^{10}Be might be a good chronometer for the early solar system [8].

We are engaged in a study to evaluate ^{10}Be abundances in CM hibonite grains with higher precision with a goal of better understanding the origin and distribution of ^{10}Be and its chronological meaning, if there is any, in the early solar system. Some results are reported here.

Experimental: The isotope compositions of Li, Be, and B were analyzed and absolute concentrations estimated by following the procedures described in [1] and [3]. Samples were sputtered by a 22.5 keV $^{16}O^{-}$ primary beam of between 20 to 50 nA (depending on B concentration) to obtain sufficient count rates on Li, Be and B. Mass resolution (M/ΔM) was set at 2500 to separate Li-Be-B main peaks from all possible molecular interferences (hydrides and Al^{3+}, Si^{4+}). All secondary ions were collected by magnetic field peak switching onto an electron multiplier (EM) detector through the mass sequence 5.9^{+}, $^{6}Li^{+}$, $^{7}Li^{+}$, Al^{+++}, $^{9}Be^{+}$, $^{10}B^{+}$ and $^{11}B^{+}$. Counting time on each mass was optimized based upon Li-Be-B abundances and total analytical duration ranged from 45 minutes to two hours for each spot. Instrumental mass fractionation and relative sensitivity factors (RSF) were determined by analyses of NBS 612 glass (^{10}B/^{11}B = 0.2469114, ^{9}Be/^{11}B = 1.49; ^{7}Li/^{6}Li = 12.3917952; ^{9}Be/^{6}Li = 12.22). Matrix effects on B isotope compositions are not strongly dependent on sample chemistry [9] thus no additional correction is made mass fractionation of B (or Li). The contributions of spallogenic Li, Be and B from galactic cosmic ray exposures were also evaluated and corrected in the data reduction.

Results and Discussion: The results are shown in the Fig. 1. Resolvable ^{10}B excesses are detected in a suite of PLACs, in correlation with ^{9}Be/^{11}B of the grains. The slope yields ^{10}Be/^{9}Be ratio of $(5.1\pm1.4)\times10^{-4}$ (2σ) with the intercept of ^{10}B/^{11}B = 0.253±0.002. This initial ^{10}Be/^{9}Be is in very good agreement with the result found by [3-4] and the precision of the slope is improved by a factor of 2, confirming that the hibonite value is significantly lower than the best constrained ratio for a CV CAI of ^{10}Be/^{9}Be of 8.8×10^{-4}. The intercepts obtained from these two kinds of refractory inclusions are identical. Thus if these correlations are interpreted as isochrons, the implied time difference is ~1.2 Myr.

However, it is unlikely that platy hibonite crystals postdated CAIs by 1.2 My because they still record much larger magnitudes of stable isotope anomalies (in δ^{50}Ti and Δ^{17}O) than CAIs [10]. Moreover, 1.2 Myr is

not consistent with the total lack of ^{26}Al in PLACs, assuming CAIs obtained 26Al from an external stellar source. The implication is that ^{10}Be was not homogeneously distributed in the solar nebula. If PLACs formed prior to CAIs, as proposed by [10], and ^{10}Be was indeed homogeneously distributed, as what [8] suggested, we should have seen at least as high ^{10}Be/^{9}Be initial values in PLACs as it is in CAIs. Thus the origin of ^{10}Be is most likely due to the local irradiations of the proto-Sun rather than the trapping of ^{10}Be from GCR.

References: [1] McKeegan et al. (2000) *Science*, 1334-1337 [2] Chaussidon et al. (2006) *GCA*, 224-245. [3] Marhas et al. (2002) *Science*, 2182-2185 [4] Marhas et al. (2003) *LPSXXXIV*, Abstract 1303 [5] MacPherson et al. (2003) *GCA*, 3165-3179 [6] Gounelle et al. (2001) *ApJ*, 1051-1070 [7] Gounelle et al. (2006) *ApJ*, 1163-1170 [8] Desch et al. (2004) *ApJ*, 528-542 [9] Chaussidon et al. (1997) *Geostandard Newsletter*, 7-17 [10] Goswami et al. (2001) *ApJ*, 1151-1159

Additional Information: If you have any questions or need additional information regarding the preparation of your abstract, call the LPI at 281-486-2142 or -2188 (or send an e-mail message to publish@lpi.usra.edu).

Please DO NOT submit duplicates of your abstract, should you find it necessary to replace or repair your paper, please contact the numbers provided.

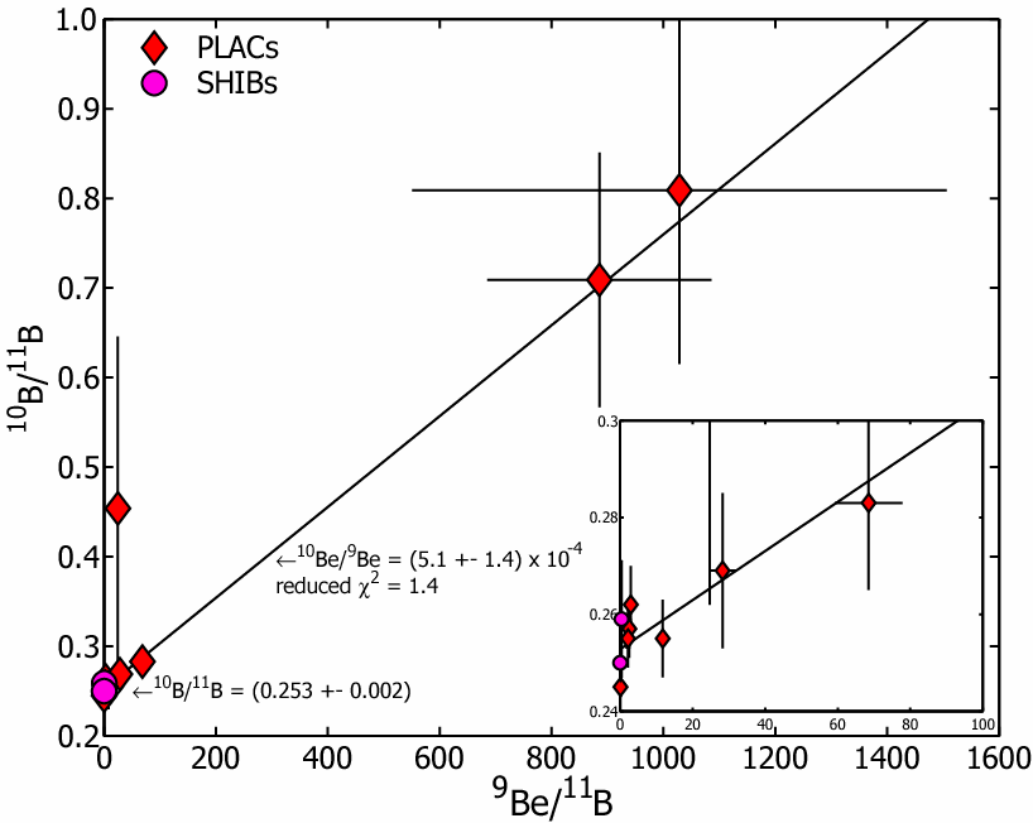

Fig. 1. CM hibonites on the ^{10}Be-^{10}B diagram. The best fit through all the data points gives rise to the slope of ^{10}Be/^{9}Be = (5.1±1.4)×10^{-4} with the intercept of ^{10}B/^{11}B = 0.253±0.002. Errors are 2 sigma.

THE ^{53}MN-^{53}CR SYSTEM. Lugmair G. W.[1], Birck J.-L.[2], Nyquist L E.[3], Shukolyukov A.[1], Trinquier A.[4], Wadhwa M.[5], Yin Q.-Z.[6]. [1] University of California, San Diego, 9500 Gilman Dv., La Jolla, CA 92093-0212, USA, glugmair@ucsd.edu. [2] Laboratoire de Geochimie et Cosmochimie, Institut de Physique du Globe, Paris, France, birck@ipgp.jussieu.fr. [3] Mail Code KR, NASA Johnson Space Center, Houston, TX 77058-3696, USA, laurence.e.nyquist@nasa.gov. [4] Axiom Laboratory, Geological Institute, Ãster Voldgade 10, 1350 Copenhagen K, Denmark, trinquier@geol.ku.dk. [5] School of Earth and Space Exploration Arizona State University, Box 871404, Tempe, AZ, 85287-1404, wadhwa@asu.edu. [6] Department of Geology, University of California at Davis, One Shields Avenue, Davis, CA 95616, qyin@ucdavis.edu.

In 1985, a year after the discovery of large relative excesses of ^{54}Cr in Allende inclusions (CAI), Birck and Allegre [1] reported from similar CAI the first evidence for relative ^{53}Cr variations that were correlated with the respective Mn/Cr ratios in mineral fractions. These ^{53}Cr variations were interpreted as being due to the in situ decay of ^{53}Mn ($T_{½}$ = 3.7 Ma, [2]) and, therefore, that live ^{53}Mn must have existed in the early solar system.

These first pioneering results were followed by the detection of ^{53}Cr excesses in various meteorites of different types. These include early results on carbonaceous chondrites [3 -9], enstatite chondrites [3, 10], ordinary chondrites and chondrules [11, 12], pallasites [3, 13, 14, 15], iron meteorites [16, 13, 18], angrites [19 -21], eucrites [21- 24, 15], mesosiderites [25], SNC meteorites [26, 15], and primitive achondrites Acapulco [27, 28], and Divnoe [29]. In most of these reports the relative ^{53}Cr variations were correlated with the Mn/Cr ratios in the respective samples, signifying the decay of live ^{53}Mn in these samples. From the slope of the best fit regression line the ^{53}Mn/^{55}Mn ratio in the samples at the time of system closure could be obtained. A comparison of the ^{53}Mn/^{55}Mn ratios then allows the derivation of relative times between these closure events, sometimes with a resolution of < 1 Ma.

Relative ages of early solar system materials are interesting and important in their own right. However, to compare these times on an absolute time scale with other absolute dating methods the ^{53}Mn/^{55}Mn ratios obtained from the angrites LEW86010 (LEW) and Angra dos Reis (AdoR) were mapped onto an absolute time scale by using the Pb-Pb ages of these two meteorites [30, 15]. Certain assumptions of ^{53}Mn homogeneity and fast closure of both the U-Pb and Mn-Cr systems are implicit in this endeavor and their validity had to be demonstrated.

In more recent years several of the previous results have been improved due to advances in mass spectrometric technology and further samples have been measured due also to the development of Cr measurement techniques in more laboratories. In addition, the improved mass spectrometric techniques allowed the resolution of not only positive ^{54}Cr anomalies in bulk samples of carbonaceous chondrites (e.g. [31] and references therein) but also deficits in most other meteorite types [32].

In terms of the chronological aspects of the ^{53}Mn-^{53}Cr system the improved precision of Cr isotopic measurements together with the refinements in Pb-Pb analytical technology (e.g. [33]) is leading to an ever improving concordance between the relative and absolute time scales. An attempt to illustrate this is shown in Fig. 1 (after [34]), where various relative ages derived from the Mn-Cr system are mapped on an absolute time line as defined by the Pb-Pb ages of the angrites LEW/AdoR and the CAI. However, on the fine scale that is currently resolvable, we may now be seeing small time differences (of the order of ~My or less) that may indeed be due to different closure times of the various isotope systems (e.g. Asuka 881394).

References: [1] Birck and Allègre (1985), *Geophys. Res. Lett.* **12**, 745-748. [2] Honda and Imamura (1971), *Phys. Rev. C* **4**, 1182-1188. [3] Birck and Allègre (1988) *Nature* **331**, 579-584.[4] Birck *et al.* (1990), *Meteoritics* **25**, 349 (abstr.). [5] Rotaru *et al.* (1989), *Meteoritics* **24**, 321 (abstr.). [6] Rotaru *et al.*, (1990), *LPS XXI,* 1037-1038. [7] Harper and Wiesmann (1992), *LPS XXIII,* 489-490. [8] Rotaru *et al.* (1992), *Nature* **358**, 465-470. [9] Endress *et al.* (1996), *Nature* **379**, 701-703. [10] Wadhwa *et al.* (1997), *MAPS* **32**, 281-292. [11] Lugmair and MacIsaac (1995), *LPS XXVI*, 879-880.[12] Nyquist *et al.* (1997) *LPS XXVIII,* 1033-1034. [13] Hutcheon and Olsen (1991). [14] Hsu *et al.* (1997), *LPS. XXVIII,* 609-610. [15] Lugmair and Shukolyukov (1998), GCA **62,** 2863-2886. [16] Hutcheon *et al.* (1985) *Meteoritics* **20**, 668 (abstr.). [17] Davis and Olsen (1990), *LPS XXI,* 258-259. [18] Hutcheon *et al.* (1992), *LPS XXIII,* 565-566. [19] Nyquist *et al.* (1991), *LPS XXII,* 989-990. [20] Nyquist *et al.* (1994), *Meteoritics* **29**, 872-885.[21] Lugmair *et al.* (1992), *LPS XXIII,* 823-824. [22] Lugmair *et al.* (1994), *LPS XXV,* 813-814. [23] Lugmair *et al.* (1994), *Meteoritics* **29**, 493 (abstr.). [24] Nyquist *et al.* (1996), *LPS XXVII,* 969-970. [25] Wadhwa *et al.* (1997), *LPS XXVIII,* 1487-1488. [26] Lugmair *et al* (1996), *LPS XXVII,* 785-786. [27] Harper *et al.* (1992), *LPS XXIII,* 491-492. [28] Zipfel *et al.* (1996), *MAPS* **31**, A160 (abstr.). [29] Bogdanovski *et al.* (1997), *MAPS* **32**, A16. [30] Lugmair and Galer (1992), *GCA* **56**, 1673-1694. [31] Shukolyukov and Lugmair (2006), *EPSL* 250, 200-213. [32] Trinquier *et al.* (2007), *ApJ* 656, 1179-1185. [33] Amelin and Davis (2002), JAAS 21, 1053-1061. [34] Yin *et al.* (2007), *ApJ.* 662, L43-L46.

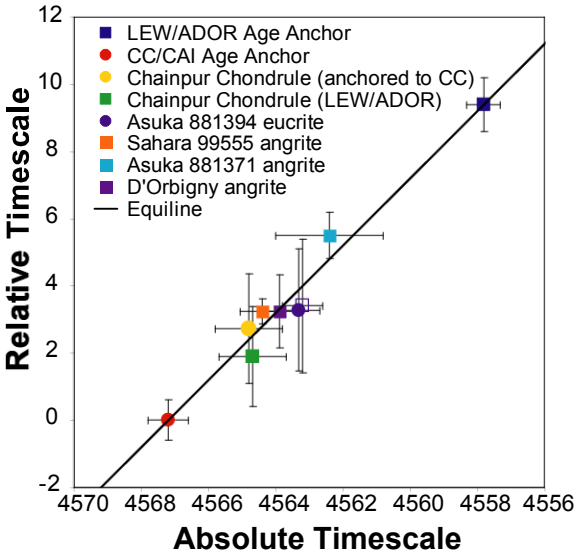

Fig. 1: Projection of relative ages onto an absolute timescale with the two age anchors LEW/AdoR and CC/CAI (after [34], see for details).

TIMESCALES FOR THE EVOLUTION OF OXYGEN ISOTOPE COMPOSITION IN THE SOLAR NEBULA. J. R. Lyons[1], E. Bergin[2], F. Ciesla[3], A. Davis[4], S. Desch[5], K. Hashizume[6], T. Ireland[7], J.-E. Lee[8], R. A. Marcus[9], H. Yurimoto[10]; [1]IGPP, UCLA, Los Angeles, CA 90095 , [2]Dept. Astronomy, Univ. of Michigan, Ann Arbor, MI 48109, [3]DTM Carnegie Inst. Washington, Washington, DC 20015, [4]Enrico Fermi Inst., Univ. of Chicago, Chicago, IL 60637, [5]Dept. Physics & Astronomy, Arizona State Univ., Tempe, AZ 85287, [6]Dept. Earth & Space Sciences, Osaka Univ., Osaka 560-0043, Japan, [7]Res. School of Earth Sciences, Australian National Univ., Canberra, ACT 0200, Australia, [8]Dept. Astronomy & Space Science, Sejong Univ., Seoul 143-747 Korea, [9]Noyes Lab. Of Chemical Physics, Caltech, Pasadena, CA 91124, [10]Dept. Natural History Sciences, Hokkaido Univ., Sapporo 060-0810, Japan.

Introduction: Given the variety of processes and nebula locations that have been proposed for creating the ^{16}O-depleted end member reservoir of the CAI mixing line, there are a large number of relevant timescales to be considered. Our focus here will be primarily on the physical and chemical timescales associated with CO self-shielding, with a short discussion of mass-independent fractionation (MIF) in high-temperature CAI-forming reactions.

The recent report [1] of poorly characterized minerals in chondritic matrix highly enriched in ^{17}O and ^{18}O along a slope-1 line lends credence to the idea that CO self-shielding formed a ^{16}O-depleted H_2O reservoir [2], and is consistent with recent model predictions [12,10]. However, the case made for self-shielding is not proven until both the size of the ^{16}O-depleted reservoir and the oxygen isotope composition of the Sun are known. Analyses of solar wind implanted in lunar grains are tantalizing but contradictory [3,4]. The implications for the chemical mass-independent mechanism [6] remain to be investigated.

A schematic view of the solar nebula is shown in Fig. 1. Region 1 is the hot, thermally ionized, low-dust, inner solar nebula, and is MRI (magneto-rotational instability) active. Region 2 is the MRI-dead zone [5], and is separated from region 1 by the dust front. Region 3 is the MRI-active nebular surface. Region 4 is the outer nebula which is generally MRI-active if the dust content is sufficiently low.

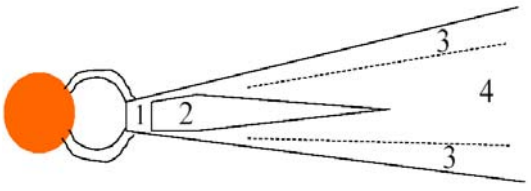

Fig. 1. Dynamical regions of the solar nebula.

The inner solar nebula: The hot, dense inner nebula (region 1 of Fig. 1) is the location for CO self-shielding suggested in [2], and the most likely place for proposed MIF-producing CAI/silicate reactions [6]. The chemical timescales here are rapid (<10^4 yrs) due the high temperature, density and photon flux.

For CO self-shielding, O liberated during CO photolysis reacts immediately (at temperatures > 1000 K) with H_2 to form H_2O. H_2O then passes the MIF signature to silicate precursors. However, at higher temperatures the magnitude of the MIF signature produced during self-shielding is reduced by H_2 absorption. Figure 2 illustrates this for the CO $E^1\Pi(1) - X^1\Sigma^+(0)$ band in which H_2 absorption has been included in the line-by-line calculation. The figure shows the δ-values for total H_2O (disk H_2O + H_2O derived from CO photolysis) at the disk midplane at 30 AU at a variety of gas temperatures. (A fixed distance of 30 AU was chosen to more clearly demonstrate the affect of temperature). At 1000 K the MIF signature of H_2O is not high enough to raise silicates from ~ -50 to ~ 0 ‰. Although the timescales for self-shielding are favorable in the inner disk, the self-shielding effect is diminished by H_2. (The unexpected slope at 1000 K appears to be a result of structure in the H_2 and $C^{18}O$ spectra, and is being investigated by one of us (JRL)).

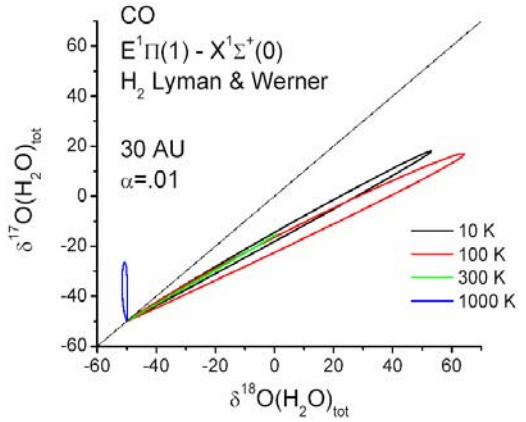

Fig. 2. CO self-shielding at various temperatures and with H_2 absorption [11].

Symmetry-dependent mass-independent chemical reactions proposed to occur on surfaces during grain growth [6] are also rapid, and need only process the total mass of CAIs rather than the entire mass of the

inner solar system. Surface MIF reactions may occur preferentially at high temperatures [7], but this requires experimental verification.

The surface nebula: CO self-shielding at the nebular surface (region 3 of Fig. 1) was proposed in [8] and [9], but was first treated quantitatively in [10]. As discussed in [10] self-shielding of surface CO can yield a significant fraction of ^{16}O-depleted H_2O at the midplane of a MMSN only if vertical mixing is rapid ($\alpha > 10^{-3}$). At 30 AU the shortest timescale ($t_{surf\ CO}$, Fig. 3) to produce sufficient ^{16}O-depleted H_2O to be a plausible end member is ~ 10^5 years. Surface shielding is a viable mechanism for introducing ^{16}O-depleted H_2O to the inner solar system (~1-3 AU), but only from the outer nebula (>20 AU). The diffusive radial transport timescale (t_{radial}, Fig. 3) is ~ 10^5 years at 30 AU for $\alpha = 10^{-2}$, comparable to $t_{surf\ CO}$ at 30 AU.

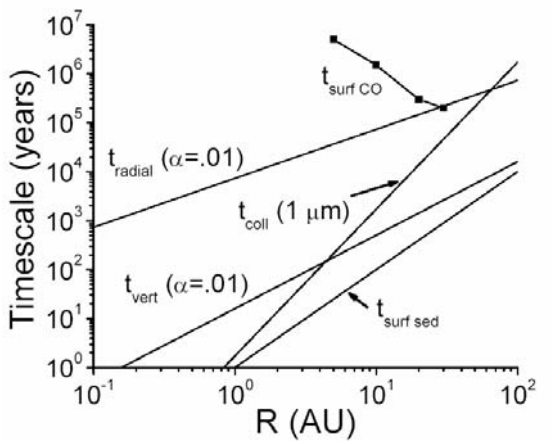

Fig. 3. Several timescales as a function of heliocentric distance in the solar nebula (MMSN).

Two additional points concerning self-shielding at the nebular surface must be made. First, dust provides a surface for condensation of H_2O vapor, with eventual sequestration of ice-coated dust at the midplane. Dust evolution by growth and sedimentation is intimately tied to the availability of surface area for condensation. In [10] dust was assumed to be static and uniformly distributed. One of us (JRL) is presently extending the model in [10] to include dust evolution. These results will be coupled to a radial transport model [14].

The second point is that the nebular surface (region 3, Fig. 1) is very likely to be MRI-active. Dust sedimentation here will be fast ($t_{surf\ sed}$, Fig. 3), and a reservoir of ^{16}O-enriched CO will be present. The ^{16}O-enriched reservoir will move inward with a smaller diffusive timescale than the bulk outer nebula because $\alpha_3 > \alpha_4$. Whether any of this ^{16}O-enriched reservoir can reach the probable region of CAI formation (region 1, Fig. 1) depends on how much mixing with the dead zone occurs.

Self-shielding in the parent cloud: Yurimoto and Kuramoto [12] suggested that CO self-shielding occurred in the parent cloud prior to formation of the solar nebula. Self-shielding in the parent cloud has a key advantage over nebular surface shielding in that CO self-shielding and H_2O formation can occur before the nebula even exists; dust evolution is not a concern.

A recent quantitative evaluation of the collapsing cloud scenario [13], modeled as inside-out collapse of an isothermal sphere, corroborates the suggestion of [12], and demonstrates the strong dependence of the resulting H_2O ice δ-values on the radiation field (and time) at the inner edge (~ 100 AU) of the collapsing cloud (Fig. 4). Very large H_2O ice δ-values, compareable to and larger than recent inferred δ-values for nebular water [1], are predicted.

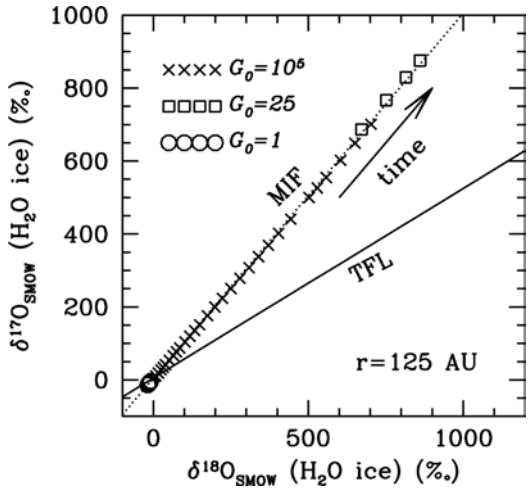

Fig. 4. δ-values for H_2O ice formed from CO in a collapsing cloud core. G_0 defines the magnitude of the radiation field. (Figure from [13])

References: [1] Sakamoto N. et al. (2007) *Science* 317, 231-233. [2] Clayton R. N. (2002) *Nature* 415, 860. [3] Hashizume K. and Chaussidon M. (2005) *Nature* 434, 619-621. [4] Ireland T. et al. (2006) *Nature* 440, 776-778. [5] Gammie C. (1996) *Ap. J.* 457, 355-362. [6] Marcus R. A. (2004), *J. Chem. Phys.* 121, 8201-8211. [7] Marcus R. A. (2007) *Adv. Quant. Chem.* (in press). [8] Thiemens M. H. and Heidenreich H. (1983) *Science* 219, 1073-1075. [9] Navon O. and Wasserburg G. (1985) *EPSL* 73, 1-16. [10] Lyons J. R. and Young E. D. (2005) *Nature* 435, 317-320. [11] Lyons J. R., Boney E., Marcus R. A., (in prep.) [12] Yurimoto H. and Kuramoto K. (2004) *Science* 305, 1763-1766. [13] Lee J.-E., Bergin E., Lyons J. R. (2007), *MAPS* (submitted). [14] Ciesla F. J. and Cuzzi, J. N. (2005), *Icarus* 181, 178-204.

MAGNESIUM ISOTOPIC COMPOSITION OF CALCIUM-ALUMINUM-RICH INCLUSIONS FROM CR CARBONACEOUS CHONDRITES. K. Makide[1], K. Nagashima[1], A. N. Krot[1], G. R. Huss[1], and I. D. Hutcheon[2]. [1]Hawai'i Institute of Geophysics and Planetology, School of Ocean and the Earth Science and Technology, University of Hawai'i at Manoa, Honolulu, HI 96822, USA (E-mail: makide@higp.hawaii.edu). [2]Lawrence Livermore National Laboratory, Livermore, CA 94551, USA.

Introduction: Calcium, aluminum-rich inclusions (CAIs) are the oldest solids formed in the solar nebula by condensation, evaporation and melting processes. High precision absolute, ^{207}Pb-^{206}Pb ages of CAIs (4567.2±0.7 Ma) have been reported only for coarse-grained, igneous CAIs from the CV carbonaceous chondrites [1]. The duration of CAI formation and thermal processing is largely based on Al-Mg isotope measurements and remains controversial[e.g., 2-11]. Most CAIs define the initial ^{26}Al/^{27}Al ratio [$(^{26}Al/^{27}Al)_0$] of 4.5×10^{-5}, referred to as the "canonical" value [2]. Based on the high precision Mg isotope measurements of CV CAIs using multicollector inductively-coupled mass-spectrometry (MC-ICP-MS) and secondary ionization mass-spectrometry (SIMS), the canonical ^{26}Al/^{27}Al ratio has been recently revised upwards to a "supra-canonical" value of $(5.5\text{-}7)\times10^{-5}$ [3-9]. In contrast, high-precision Mg isotope measurements of bulk igneous Allende CAIs and their mineral separates using MC-ICP-MS define $(^{26}Al/^{27}Al)_0$ of $(5.12\pm0.18)\times10^{-5}$ [10], which is inconsistent with $(5.85\pm0.05)\times10^{-5}$ value reported by [5] using the same analytical technique. Although this apparent discrepancy still needs to be resolved, both data sets suggest a very short (<20-30 Kyr) time difference between the formation of precursors of the igneous CV CAIs and their crystallization ages. The very short duration of the CV CAI formation is in conflict with the prolonged duration of the CV CAI thermal processing inferred from internal Al-Mg isochrons obtained by SIMS: e.g., the $(^{26}Al/^{27}Al)_0$ of $(6.44\pm0.27)\times10^{-5}$ and $(4.96\pm0.02)\times10^{-5}$ are inferred for ^{16}O-rich and ^{16}O-poor minerals, respectively, within a single coarse-grained igneous CAI from Allende [11]. We note, however, that internal isochrons of many CAIs from CV chondrites were disturbed during thermal metamorphism on their parent asteroid [2]. To constrain the duration of CAI formation and thermal processing, high precision measurements of internal Al-Mg isochrons in CAIs from primitive carbonaceous chondrites (e.g., CR2, CO3.0, Acfer 094, Adelaide) are required. Here we report Al-Mg systematics of nine CAIs from CR carbonaceous chondrites. The CR CAIs are mineralogically and isotopically pristine [12, 13] and appear to have preserved primary nebular signatures largely undisturbed. Oxygen isotopic compositions of some of these CAIs have been previously reported by [12] and are illustrated in Fig. 1.

Experimental: Nine CAIs identified by X-ray elemental mapping and studied in backscattered electron images from six CR chondrites (GRA 95229, EET 92042, EET 96286, El Djouf 001, Temple Bay, and Asuka-881828) were selected for *in situ* Al-Mg isotope measurements by the UH Cameca ims-1280. A 150–300 pA O^- primary ion beam was focused to ~5-7 µm. The secondary ion mass spectrometer was operated at +13 keV with a 50 eV energy window. ^{24}Mg, ^{25}Mg, and ^{26}Mg, and ^{27}Al were measured in 120 cycles on a monocollector electron multiplier and Faraday cup in a peak jumping mode (4, 10, 10, and 2 sec, respectively). The mass resolving power was set to ~3800, sufficient to separate interfering hydrides. Excess of radiogenic ^{26}Mg (^{26}Mg*) was calculated by normalizing to the terrestrial magnesium isotopic ratios (^{25}Mg/^{24}Mg = 0.12663; ^{26}Mg/^{24}Mg = 0.13932 [14]) according to a linear law. The sensitivity factors for melilite, anorthite, hibonite and spinel were calculated based on the measured $^{27}Al^+/^{24}Mg^+$ (SIMS) and Al/Mg (electron microprobe analysis) ratios in terrestrial standards. The sensitivity factor for grossite was assumed to be the same as for hibonite. ^{27}Al/^{24}Mg ratios in the samples were obtained by dividing the measured $^{27}Al^+/^{24}Mg^+$ ratios with the relative sensitivity factors for grossite, hibonite, and melilite.

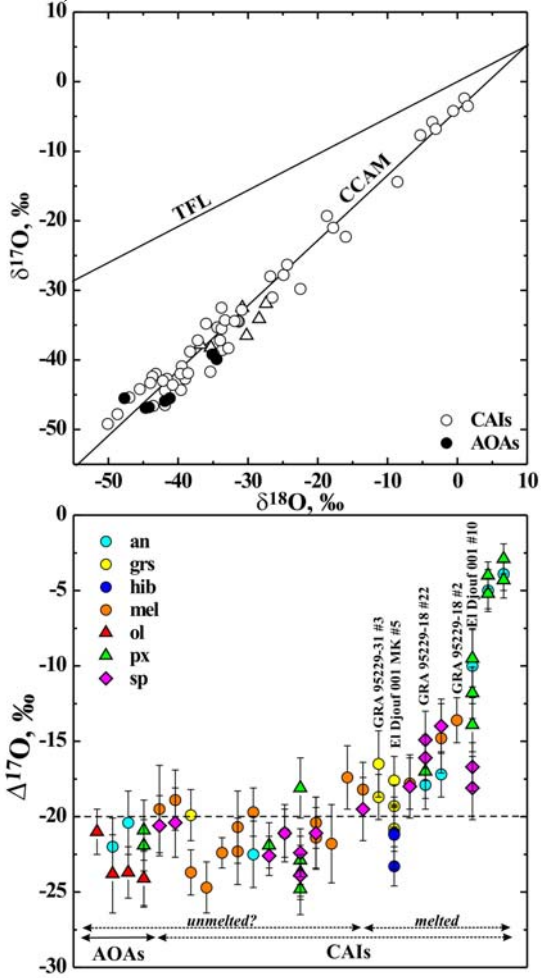

Fig. 1. Oxygen isotopic compositions of CAIs and amoeboid olivine aggregates (AOAs) from CR carbonaceous chondrites (data from [12]). CAI numbers with measured Mg isotopic compositions are indicated. an = anorthite; grs = grossite; hib = hibonite; mel = melilite; ol = olivine; px = Al,Ti-diopside; sp = spinel.

Results and Discussion: Eight out of nine CR CAIs analyzed show ^{26}Mg* corresponding to the $(^{26}Al/^{27}Al)_0$ of $(4.27\pm0.11)\times10^{-5}$ to $(5.63\pm0.46)\times10^{-5}$ (Fig. 2). The grossite-hibonite-rich CAI El Djouf 001 MK #5 shows no ^{26}Mg*: $(^{26}Al/^{27}Al)_0 = (-0.059\pm0.039)\times10^{-5}$. All CAIs analyzed are igneous and ^{16}O-enriched ($\Delta^{17}O = -15‰$ to $-20‰$), although to a lesser degree than AOAs and apparently unmelted CAIs in CR chondrites (Fig. 1). One of these CAIs, GRA 95229-18 #2, contains secondary sodalite replacing melilite; the CAI shows the largest depletion in ^{16}O ($\Delta^{17}O = -15‰$). Sodalite contains ^{26}Mg* that is comparable to the ^{26}Mg* in the melilite, suggesting that ^{26}Mg* in sodalite may have been inherited from melilite. Type C CAI El Djouf UH 154 #10 surrounded by an igneous diopside-forsterite rim is ^{16}O-depleted ($\Delta^{17}O$ up to $-10‰$) and has a small ^{26}Mg* corresponding to the $(^{26}Al/^{27}Al)_0$ of $(1.43\pm0.87)\times10^{-6}$ [15]. The CAI probably experienced late-stage melting in an ^{16}O-depleted nebular gas during chondrule formation [16]. Because El Djouf 001 MK #5 is ^{16}O-rich and surrounded by a multilayered Wark-Lovering rim sequence, the lack of ^{26}Mg* in it cannot be explained by late-stage remelting and must reflect the absence of ^{26}Al in its precursor. We note that ^{16}O-rich, ^{26}Al-poor grossite-rich CAIs are commonly observed in the CH carbonaceous chondrites [17-19]. It has been suggested that these CAIs formed prior to injection and homogenization of ^{26}Al in the solar nebula [18, 19].

Based on these observations, we infer that thermal processing of CR CAIs in an ^{16}O-rich nebular reservoir lasted for ~0.3 Myr after formation of CAIs with $(^{26}Al/^{27}Al)_0$ of $(5.85\pm0.05)\times10^{-5}$) (Fig. 3). Some CAIs were remelted 3-4 Myr later, during chondrule formation [15]. There is no clear evidence for CAIs with supracanonical $(^{26}Al/^{27}Al)_0$ ratio in CR chondrites yet.

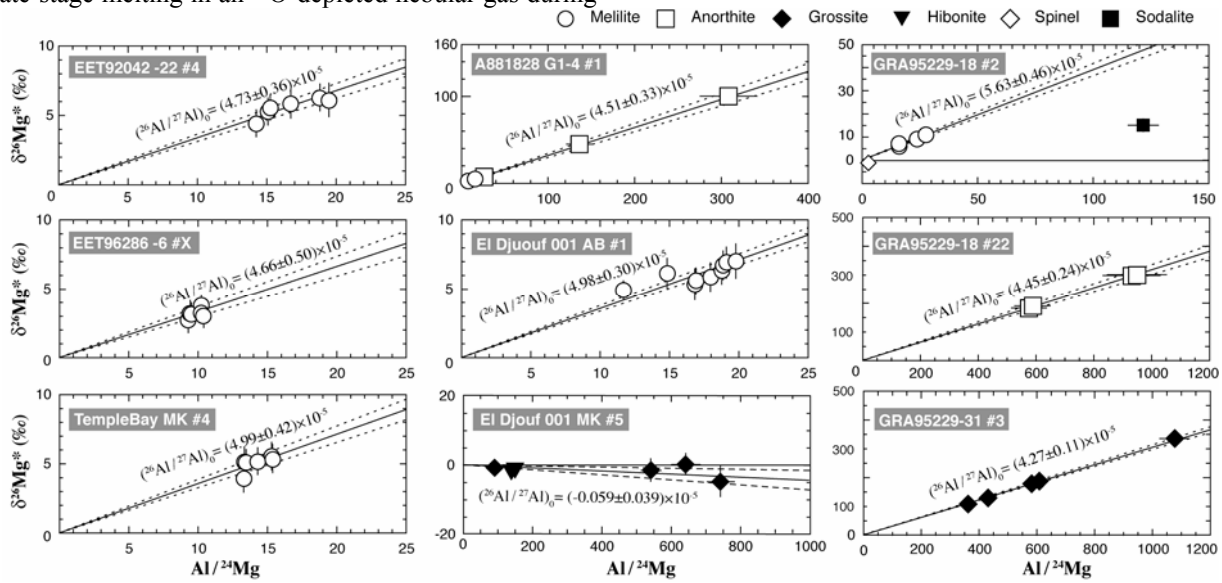

Fig. 2. Al-Mg isochron diagrams for individual CAIs from CR chondrites. All data are forced through the origin. Error bars are 2σ. Sodalite in GRA95229-18 #2 is a secondary phase and was not used for calculation of isochron.

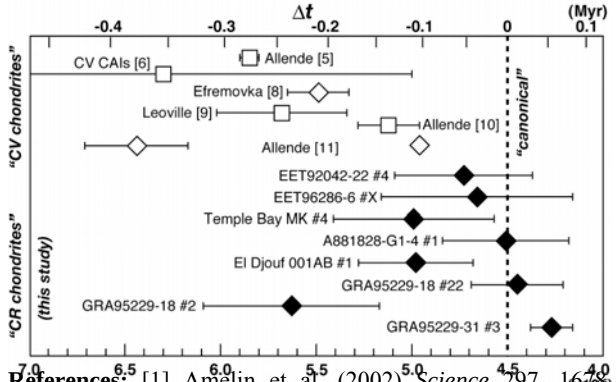

Fig. 3. ← The inferred $(^{26}Al/^{27}Al)_0$ in CR CAIs (this study). The canonical ratio of 4.5×10^{-5} (dashed line, [2]), "supracanonical" ratios of $(5.85\pm0.05)\times10^{-5}$ [5] and $(6.3\pm1.3)\times10^{-5}$ [6] in whole-rock CV CAIs measured by MC-ICP-MS, and several well-defined internal isochrons measured by SIMS [7-9, 11] and by MC-ICP-MS [10] are plotted for comparison. The $(^{26}Al/^{27}Al)_0$ ratios were calculated using linear (diamonds) and exponential (squares) law using kinetic (0.511 [5, 6, 19]) and experimentally defined (0.514 [9]) fractionation factor [20].

References: [1] Amelin et al. (2002) *Science* 297, 1678. [2] MacPherson et al. (1995) *Meteoritics* 30, 365. [3] Bizzarro et al. (2004) *Nature* 431, 275. [4] Bizzarro et al. (2005) *Nature* 435, 1280. [5] Thrane et al. (2006) *ApJL* 646, L159. [6] Young et al. (2005) *Science* 308, 223. [7] Taylor et al. (2005) *LPS* XXXVI, Abstract #2121. [8] Srinivasan et al. (2007) *LPS* XXXVIII, #1781. [9] Richter et al. (2007) *LPS* XXXVIII, #2303. [10] Jacobsen et al. (2007) this volume. [11] Itoh et al. (2007) *MAPS* 42, A75. [12] Aléon et al. (2002) *MAPS* 37, 1729. [13] Weber and Bischoff (1997) *Chem. Erde* 57, 1. [14] Catanzaro et al. (1966) *J. Res. Nat. Bur. Standrads* 71a, 453. [15] Nagashima et al. (2007) *MAPS* 42, A115. [16] Krot et al. (2005) *ApJ* 622, 1333. [17] Kimura et al. (1993) *GCA* 57, 2329. [18] Weber et al. (1995) *GCA* 59, 803. [19] Krot et al. (2007) *ApJ*, in press. [20] Davis et al. (2006) *LPS* XXXVIII, Abstract #2334.

ABSOLUTE CHRONOLOGY AND IMPLICATIONS FROM GEOPHYSICAL MODELING OF IAPETUS. D. L. Matson[1], J. C. Castillo-Rogez[1], C. Sotin[1,2], T. V. Johnson[1], J. I. Lunine[1,3], (1) Jet Propulsion Laboratory, California Institute of Technology, 4800 Oak Grove Drive, Pasadena, CA 91109. (2) UMR – CNRS 6112 Laboratoire de Planétologie et Géodynamique de Nantes, 2, rue de la Houssinière, 44322 Nantes Cedex 3, France. (3) Lunar and Planetary Lab, 1629 E. University Blvd. Tucson, AZ 85721-0092.

Iapetus has preserved evidence that constrains the modeling of its geophysical history from the time of its accretion until now. This evidence is (a) its present 79.33-day rotation rate, (b) its shape that corresponds to the equilibrium figure for a hydrostatic body rotating with a period of ~16 h, and (c) its sharp, equatorial ridge, which is unique in the Solar System.

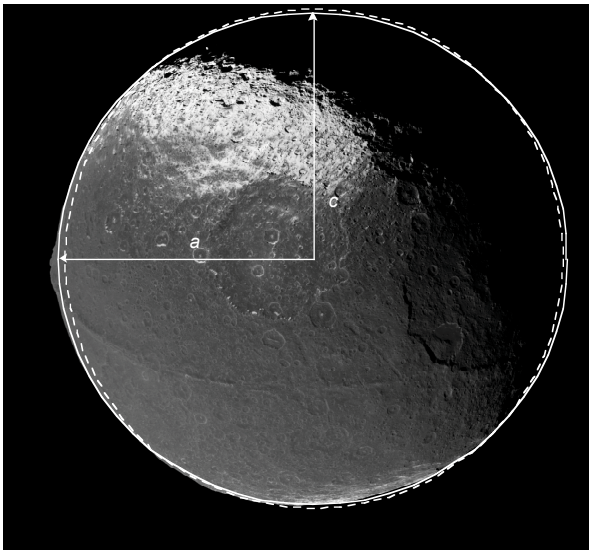

Fig. 1. Iapetus as seen by Cassini on December 31, 2004. The solid curve shows the shape of the satellite. The dashed curve indicates the shape the satellite would have if it were in hydrostatic equilibrium today. Given Iapetus' present rotation period and semi-major axis, a deviation from spherical of no more than 10 m is expected. The actual deviation is 33 km.

We have investigated the coupling between Iapetus' thermal and orbital evolution [1] for a wide range of conditions including the radial distributions with time of composition, porosity, short-lived radioactive isotopes (SLRI), and temperature. The thermal model uses conductive heat transfer with temperature-dependent conductivity. Only models with a thick lithosphere and an interior viscosity relatively close to the water ice melting point can explain both the observed shape and despinning to the current rotation period. Short-lived radioactive isotopes provide the heat that decreases porosity in Iapetus' early history. This increases thermal conductivity and allows the development of the strong lithosphere needed to preserve the 16-h rotational shape and the vertical relief of the topography. Long-lived radioisotopes and SLRI raise internal temperatures high enough that significant tidal dissipation can despin Iapetus to synchronous rotation. This occurred several hundred million years after Iapetus formed.

Such models also constrain the time when Iapetus formed because the successful models are critically dependent upon having just the right amount of heat added by SLRI decay in this early period. The amount of heat available from short-lived radioactivity is not a free parameter but is fixed by the time when Iapetus accreted, by the canonical concentration of ^{26}Al, and, to a lesser extent, by the concentration of ^{60}Fe. The needed amount of heat is available only if Iapetus accreted between 2.5 and 5.0 Myr after the formation of the calcium aluminum inclusions as found in meteorites. Models with these features allow us to explain Iapetus' present synchronous rotation, its fossil 16-h shape, and also provide a context for explaining why the equatorial ridge arose.

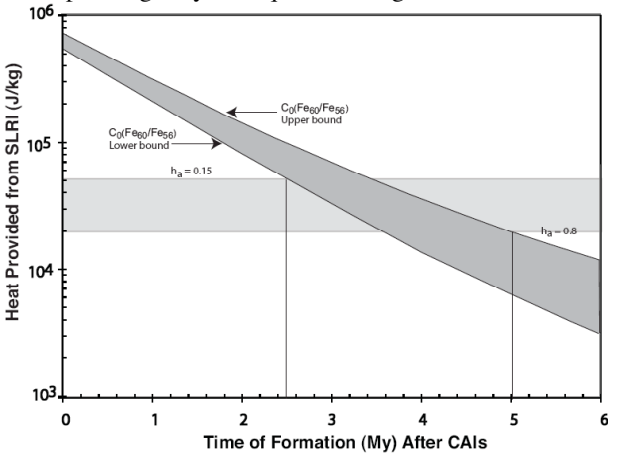

Fig. 2. The heat needed by Iapetus models (light grey band) compared with available heat after the formation of CAIs (curved band). Band widths show allowances made for the uncertainties in the Iapetus models and in the composition and initial isotopic ratios. The width of the available heat zone is chiefly due to the uncertainty in the initial abundance of ^{60}Fe. The light grey zone indicates the amount of heat needed for Iapetus to despin and yet preserve its non-hydrostatic shape until the present. The upper bound assumes little heat is provided by accretion and thus more is needed from SLRI. The lower bound assumes 80% of accretional energy is used to heat the satellite, and thus less heat is needed from SLRI. The intercept between the two zones yields the time of formation of Iapetus with respect to CAIs.

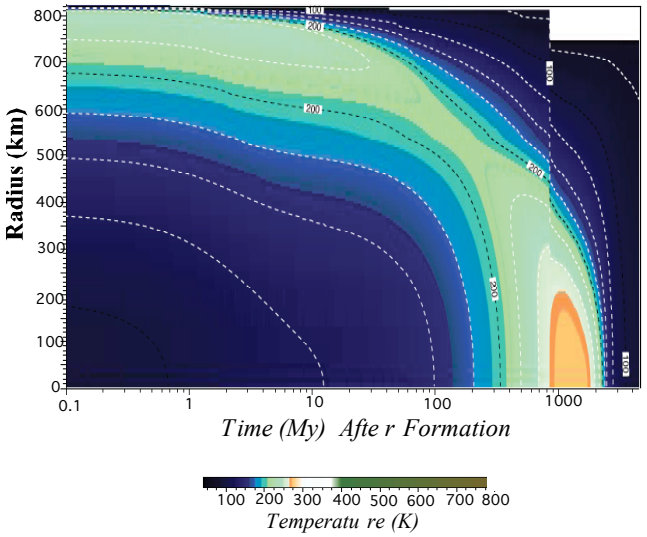

Fig 3. Thermal evolution model for Iapetus. Temperature is plotted as a function of equatorial radius and time (on a log scale) since accretion. The time at the extreme right is the present. Temperature is contoured every 25 K. The color scheme indicates geophysically significant temperatures. The time of formation with respect to CAIs is 5 My, The model assumes that 80% of accretional energy retained as heat. This model can successfully explain Iapetus' despinning to synchronous rotation. When despinning occurs, at about 700 My after formation, the spin period rapidly evolves while the lithosphere is thick enough to support large-scale non-hydrostatic topographic anomalies.

If we accept the Pb–Pb age of CAIs measured by [2] of 4567.2 ± 0.6 Myr, then the age of Iapetus is between 4562.2 and 4564.7 Myr.

Since Iapetus is almost certainly a regular satellite of Saturn, rather than a captured object [3], the absolute chronology obtained sets a limit of five million years to form Saturn. This is consistent with the independent evidence that the time scale for giant planet formation is millions, rather than tens of millions, of years. Recent astronomical observations suggest that the lifetime around Sun-like stars of sufficient gas to make giant planets may be typically two to five million years [4]. Models for the formation of giant planets by direct collapse can easily meet this time constraint [5]. The nucleated instability model of giant planet formation may be more relevant to the giant planets of our own Solar System, with their supersolar heavy element abundances and regular satellite systems, but only under certain restricted conditions do they seem able to produce gas giant planets within a few million years [6]. A somewhat weaker constraint on giant planet formation time scales comes from dynamical calculations that show the presence of Jupiter and Saturn to be important determinants of the final architecture of the terrestrial planet orbits and asses [7], coupled with the fact that much of the growth of the Earth was completed within 10–30 million years after CAIs based on the Hf–W isotopic system. Our time scale result provides an additional indication that giant planet formation was relatively rapid in our own Solar System and gives impetus to the further development and elaboration of the nucleated instability models for giant planet growth.

We will also report on the September 10, 2007 flyby that will provide observations of Iapetus obtained as close as 1600 km altitude

This work was carried out at the Jet Propulsion Laboratory-CalTech, under contract to NASA.

References: [1] Castillo-Rogez *et al*. 2007. Icarus doi:10.1016/j.icarus.2007.02.018. [2] Amelin *et al*. 2002. Science 297, 1678–1683. [3] Canup and Ward 2006. Nature 441, 834–839. [4] Najita and Williams 2005. Astrophys. J. 635, 625–635. [5] Mayer et al., 2002. Science 298, 1756–1759. [6] Lissauer and Stevenson, 2007. In: Reipurth, V.B., Jewitt, D., Keil, K. (Eds.), Protostars and Planets V. Univ. of Arizona Press, Tucson, pp. 591–606. [7] O'Brien et al. Icarus 184, 39–58.

SOLAR SYSTEM ISOTOPIC HETEROGENEITY FROM ^{53}Mn-^{53}Cr. S. J. McKibbin[1], T. R. Ireland[1] and Y. Amelin[1]. [1]Research School of Earth Sciences and Planetary Science Institute, Bldg 61 Mills Road Acton ACT 0200 Australia. Seann.McKibbin@anu.edu.au; Trevor.Ireland@anu.edu.au; Yuri.Amelin@anu.edu.au

Introduction: One of the requirements for the application of the short-lived nuclide chronometer ^{53}Mn (half-life of 3.7 My, anchored to angrite LEW86010) and short lived nuclides in general is that samples are derived from a common reservoir with a homogeneous distribution of the parent nuclide. Ideally, this should reflect the solar system abundances as a whole, but it requires that the solar nebula was well mixed after collapse of the molecular cloud. A more likely scenario is that the solar system is heterogeneous for many isotopes, but particular subsections (such as a specific parent body) will be homogeneous and suitable for short-lived nuclide chronometric studies. Short-lived radionuclide chronometry has been successfully applied and has produced useful information, but many assumptions about initial ratios and ages are involved because insufficient samples have had two or more chronometric systems applied to them. A few samples have been found to have isotope systematics that make them discordant in different systems, showing that a completely uniform distribution of short-lived nuclides in the solar system is not the case [1, 2].

Mn and Cr isotopic heterogeneity: A widespread and systematic chromium isotopic heterogeneity in the inner solar system was recognised by Lugmair and Shukolyukov [1] who found an apparent linear relationship between heliocentric distance and initial ^{53}Cr/^{52}Cr expressed in samples from Earth, Mars and those inferred to originate in the Asteroid Belt. With a few exceptions, meteorites from the Main-Belt have a common ^{53}Cr/^{52}Cr, which suggests that ^{53}Mn/^{55}Mn is homogeneous within the Asteroid Belt and the chronometric interpretation of ^{53}Mn/^{55}Mn for samples from this region is justified. An anomalous case is that of the enstatite chondrites: Shukolyukov and Lugmair [3] showed that they have Mn/Cr ratios that are chondritic, coupled with ^{53}Cr/^{52}Cr ratios that are lower than those of all other meteorites believed to come from the Asteroid Belt. Chondritic Mn/Cr shows that elemental fractionation has not suppressed the evolution of ^{53}Cr/^{52}Cr in enstatite chondrites, so either ^{53}Mn/^{55}Mn or ^{53}Cr/^{52}Cr must be heterogeneous in the solar nebula.

Simple explanations of the radial trend could involve a stellar-derived nucleosynthetic heterogeneity in ^{53}Cr/^{52}Cr, or heterogeneity in ^{53}Mn/^{55}Mn, with either ^{53}Cr or ^{53}Mn increasing with heliocentric distance. Shukolyukov and Lugmair [4] noted that ^{54}Cr anomalies were not observed in meteorites other than carbonaceous chondrites, so anomalies of ^{53}Cr were probably absent as well. Recent ^{54}Cr data does show heterogeneity in the solar system for this isotope [5], but it is not correlated with radial heliocentric distance. Elemental volatility leading to a depletion in Mn (and hence ^{53}Mn) must also be considered. Mn and Cr are approximately in the middle of the volatility range, with Cr being referred to as a *common element* (50% T_C 1296 K) and Mn a *moderately volatile element* (50% T_C 1158 K) [6]. Difference in volatilities is not a favoured explanation because the bulk compositions of the planets are not well known and few constraints can be put on such models.

Comparison with ^{26}Al and Pb-Pb timescales: Though CAIs are used as the reference point for ^{26}Al/^{27}Al, the ^{53}Mn/^{55}Mn ratios obtained from CAIs are inconsistent with the rest of the ^{53}Mn timescale [e.g. 7, 8] (Figure 1) and their generally anomalous isotopic composition suggests that they should not be used as anchors for short-lived nuclide chronometric systems. CAIs have average initial ^{53}Mn/^{55}Mn of 4.4×10^{-5} [9] although values as high as 14.8×10^{-5} have been reported [10]. As CAIs are known to have been isotopically disturbed, these values may represent a lower limit. Using the average ^{53}Mn/^{55}Mn value, this equates to a CAI age that is ~19 Ma older than LEW86010, implying a solar system timescale that is irreconcilably long. The Pb-Pb dates for Efremovka CAIs and LEW86010 [11, 12] give a much smaller age difference of 9.4 ±1.1 Ma, which is consistent with the ^{26}Al timescale, as well as theoretical models and astronomical observations of stellar system formation. The high initial ^{53}Mn/^{55}Mn may reflect an extreme early heterogeneity in the early solar system [1], which had been largely smoothed over by the time of chondrule formation.

Discrepancies between ^{26}Al and ^{53}Mn ages of some samples (D'Orbigny, Asuka 881394 and others; see [2] and Figure 1) are possibly expressions of solar system heterogeneity for these isotopes, or resolved differences in closure temperature. Placement of samples in the absolute timescale is also problematic, as Pb-Pb dates often have poor precision and different phases commonly return different ages. The most recent efforts at Pb-Pb dating of phases from D'Orbigny [13, 14] have yielded precise ages that are older than previously found, and make this meteorite discordant with the ^{26}Al-timescale. As such, a unique reconciliation of Pb-Pb, Al-Mg, and Mn-Cr isotope systematics is not possible with the data presently available.

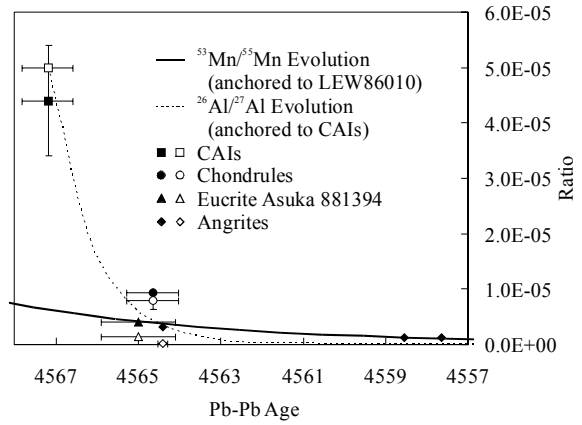

Figure 1. ^{53}Mn/^{55}Mn and ^{26}Al/^{27}Al in selected solar system objects. Filled symbols represent ^{53}Mn/^{55}Mn, open symbols represent ^{26}Al/^{27}Al. The evolution lines are calibrated to angrite LEW86010 and CAIs respectively. Data from [1, 9, 11, 14, 15, 16, 17, 18, 19, and 20].

References: [1] Lugmair G. W. and Shukolyukov A. (1998) *Geochim. Cosmochim. Acta, 62,* 2863-2886. [2] Gounelle M. and Russell S. S. (2005) *Geochim. Cosmochim. Acta, 69,* 3129-3144. [3] Shukolyukov A. and Lugmair G. W. (2004) *Geochim. Cosmochim. Acta, 68,* 2875-2888. [4] Shukolyukov A. and Lugmair G. W. (2000) *Space Sci. Rev., 92, 225-236.* [5] Trinquier A., Birck J-L. and Allègre C. J. (2007) *Astrophys. J., 655,* 1179-1185. [6] Lodders K. (2003) *Astrophys. J., 591,* 1220-1247. [7] Lugmair G. W., MacIsaac C. and Shukolyukov A. (1992) *LPS XXIII,* 823-824. [8] Nyquist L. E., Bansal B., Wiesmann H. and Shih C-Y. (1994) *Meteoritics, 29,* 872-885. [9] Birck J-L. and Allègre C. J. (1988) *Nature, 331,* 579-584. [10] Papanastassiou D. A., Wasserburg G. J. and Bogdanovski O. (2005) *LPS XXXVI,* Abstract #2198. [11] Amelin Y., Krot A. N., Hutcheon I. D. and Ulyanov A. A. (2002) *Science, 297,* 1678-1683. [12] Lugmair G. W. and Galer S. J. G. (1992) *Geochim. Cosmochim. Acta, 56,* 1673-1694. [13] Zartman R. E., Jagoutz E. and Bowring S. A. (2006) *LPS XXXVII,* Abstract #1580. [14] Amelin Y. (2007) *LPS XXXVIII,* Abstract #1669. [15] Glavin D. P., Kubny A., Jagoutz E. and Lugmair G. W. (2004) *Meteoritics & Planet. Sci.,39,* 693-700. [16] Kita N. T., Nagahara H., Togashi S. and Morishita Y. (2000) *Geochim. Cosmochim. Acta, 64,* 3913-3922. [17] Wadhwa M., Amelin Y., Bogdanovski O., Shukolyukov A., Lugmair G. W. and Janney P. (2005) *LPS XXXVI,* Abstract #2126. [18] Nyquist L. E., Shih C. Y., Wiesmann H. and Mikouchi T. (2003) *LPS XXXIV,* Abstract #1388. [19] Nyquist L., Lindstrom D., Mittlefehldt D., Shih C-Y., Wiesmann H., Wentworth S. and Martinez R. (2001) *Meteoritics & Planet. Sci.,36,* 911-938. [20] MacPherson G. J., Davis A. M. and Zinner E. K. (1995) *Meteoritics, 30,* 365-386.

A TALE OF THREE ASTEROIDS: THE EUCRITE, UREILITE AND PALLASITE PARENT ASTEROIDS. D. W. Mittlefehldt, NASA/Johnson Space Center, Houston, TX, USA (david.w.mittlefehldt@nasa.gov).

Introduction: Early in solar system history, some intense energy source heated asteroidal-sized bodies to the point where metal and silicate differentiation occurred. Asteroids provide us with only one datum point: 4 Vesta demonstrates that asteroids of mass ~10^{20} kg were sufficiently heated to produce basaltic crusts. However, 1 Ceres, with ~3.5x the mass of 4 Vesta, has a primitive, undifferentiated surface, indicating that while size does matter, it isn't everything. Achondrites provide records of the differentiation histories of their parent asteroids that can be used to evaluate how the heat source operated. Here I will contrast three achondrite groups – eucrites, ureilites and main-group pallasites – from the crust, mantle and core-mantle boundary of their respective parent asteroids. A widely held view is that ^{26}Al provided most of the energy, although ^{60}Fe may have contributed. This abstract is couched in terms of comparing meteoritical evidence against ^{26}Al, but a wider range in energy sources will be covered in the workshop.

Eucrites: Eucrites are brecciated pigeonite-plagioclase-silica basalts. Siderophile element contents of eucrites are very low. Cobalt contents are typically 3-6 μg g^{-1} while the best measurements of Ir contents are a few pg g^{-1} [1] (Fig. 1). High precision oxygen isotopic analyses have shown that eucrites have identical Δ^{17}O [2,3] (Fig. 2), implying either an isotopically homogeneous parent asteroid, or that any initial heterogeneity was homogenized during differentiation. Differentiation of the eucrite parent asteroid mantle occurred only ~3-4 Ma after formation of the oldest known objects in the solar system – CAIs [4].

Ureilites: Ureilites are shocked, but typically unbrecciated, olivine-pyroxene-carbon achondrites from the mantle of a differentiated asteroid. They are basalt-depleted compared to chondritic material; they lack plagioclase and have very low incompatible lithophile element contents, of particular significance is their Al content which averages ~3 mg g^{-1} [5]. One distinctive characteristic of ureilites is their relatively high siderophile element contents, with Co contents up to ~220 μg g^{-1} and Ir up to ~670 ng g^{-1} (Fig. 1). Ureilites are also characterized by very large range in Δ^{17}O – the largest range of any meteorite group [6] (Fig. 2).

Main-Group Pallasites: Main-group pallasites are olivine-metal rocks widely, though not universally, considered to represent mixing in the core-mantle boundary region of their parent asteroid. The non-metallic fraction is nearly pure magnesian olivine. The oxygen isotopic compositions of main-group pallasites are relatively uniform in Δ^{17}O [7] (Fig. 2), although there is variation outside analytical error [8]. There are also significant variations in Fe/Mn and Sc contents of olivine grains [9].

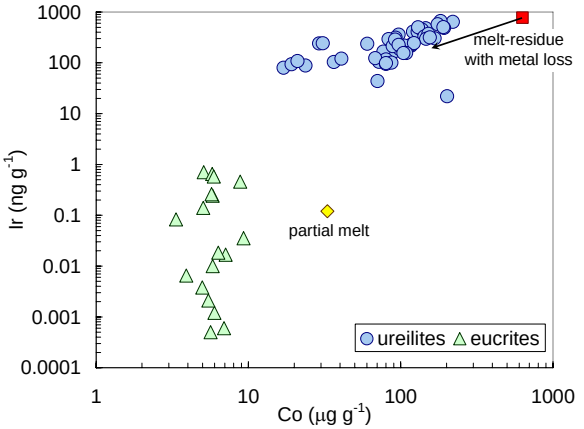

Figure 1. Ir vs. Co for ureilites compared to eucrites. A calculated partial melt of a chondritic source has a higher Co content than eucrites, and is higher in Ir for most. (For reference, 0.01% chondritic contamination in a eucrite breccia would contribute 0.06 ng g^{-1} Ir.). Ureilites can be matched as melt-residues that lost variable amounts of metal.

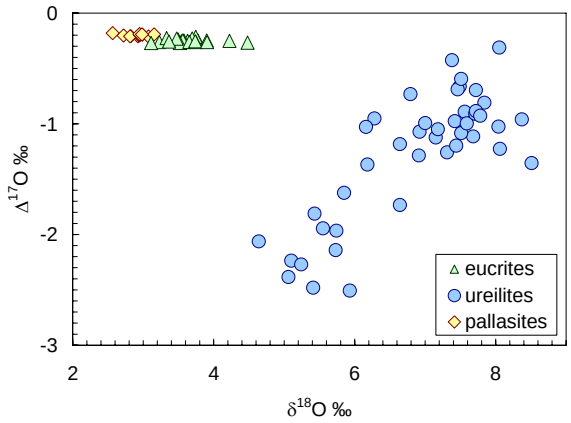

Figure 2. Oxygen isotopic data contrasting ureilites [6] with eucrites [2, 3] and pallasites [7].

Discussion: Although ureilites are among the most enigmatic achondrites, with many details of their formation still poorly understood, the first-order differentiation mechanism - partial melting to form a basalt-depleted residue - is well established. Their very large

range in $\Delta^{17}O$ obviates an origin as a suite of magma cumulates unless very many isotopically distinct magma bodies produced the ureilite suite. Their siderophile element contents are at levels consistent with partial melting and incomplete removal of residual metal (Fig. 1).

Olivine-pyroxene thermometry of ureilites, coupled with narrow reduction rims on olivine, indicate that these meteorite were rapidly cooled from high temperature [10], possibly peak magmatic temperature. Thus, ureilites give the clearest picture of the mantle of an asteroid during differentiation. Reduction rims on ureilite olivine grains were formed by a sudden pressure drop, possibly caused by impact, allowing graphite to reduce FeO in the silicate. Cooling rates estimated for this process from zoning profiles are 2-6º K/hr [11].

It is unlikely that, if magma had been present during the quenching event, it could have been lost with 100% efficiency before it would have solidified. More likely, the magma had been expelled from the residual mantle before hand. If ^{26}Al was the primary energy source, it would have been strongly partitioned into the magma. Removal of magma from the solid residue would then shut down igneous activity. The ureilites therefore provide strong evidence that on some differentiated asteroids, the rate of basalt eruption outpaced the rate of energy release. Chronologic evidenced summarized at this workshop [4] suggests ureilite ages are ~4 Ma younger than the age of eucrite parent asteroid mantle differentiation.

Dunites, as represented by the silicate portion of main-group pallasites, can form as cumulates from a mafic-ultramafic magma, or as residues of extensive melting of chondritic material. Either scenario implies a high degree of melting on the pallasite parent asteroid. Model simulations of chondrite melting at an appropriate oxygen fugacity suggest dunite residues with mg# of main-group pallasites require ~50-70% melting [12]. The uniform oxygen isotopic compositions of main-group pallasites have been taken to favor a cumulate origin [7]. However, variation in $\Delta^{17}O$ outside analytical error suggests rather that the pallasite parent asteroid was not homogenized [8], *i.e.* magma-ocean-type scenarios are untenable. This latter view is supported by variations in trace element contents of olivine grains that would require extensive amounts of fractional crystallization to produce the ranges observed [9]. A more plausible model is that pallasite silicates were formed by extensive melting (>50%) of a heterogeneous body that was not completely homogenized by this process. Differentiation of the pallasite parent asteroid was then more extensive than that experienced by the ureilites, and suggests that, if ^{26}Al was the energy source, heating outpaced magma eruption and allowed the production of more refractory residues.

The basaltic crust represented by eucrites could have been formed from partial melts of the solid chondritic precursor asteroid, or from residual melts from the crystallization of a highly melted asteroid. Melting experiments on eucrites were interpreted to indicate that these basalts were formed as primary partial melts of primitive chondritic source regions [13]. However, siderophile element contents of eucrites are too low for these melts to have been generated in source regions that included metal (Fig. 1); metal in the source region would buffer siderophile element contents of basalts at values much higher than observed [14]. This favors an origin as residual melts of an extensively melted parent asteroid [12].

The uniformity of $\Delta^{17}O$ in eucrites (Fig. 2) supports this view [2]. Ureilites demonstrate that melting to produce basalts doe not necessarily result in O isotopic homogenization of the asteroid, and thus basalts with differing $\Delta^{17}O$ could arise by a partial melting of a heterogeneous asteroid. (However, there is no *a priori* reason to suppose the eucrite parent asteroid was heterogeneous in O isotopic composition. For example, compare O isotopic data on ureilites with those on winonaites-IAB iron silicates [6]) The consensus view is that eucrites are residual melts, not primary partial melts. This implies, as is the case for main-group pallasites, that heating of the eucrite parent asteroid outpaced the rate of magma eruption, allowing the energy source to remain in the asteroid interior until the melt fraction was high enough to promote rapid separation of it from refractory solids.

References: [1] Warren P. H. (1999) *Antarct. Met. XXIV*, 185. [2] Greenwood R. C. et al. (2005) *Nature 435*, 916. [3] Wiechert U. H. et al. (2004) *EPSL 221*, 373. [4] Nyquist L. E. et al. (2007) this workshop. [5] Warren P. H. et al. (2006) *GCA 70*, 2104. [6] Clayton R. N. and Mayeda T. K. (1996) *GCA 60*, 1999. [7] Greenwood R. C. et al. (2006) *Science 313*, 1763. [8] Ziegler K. and Young E. D. (2007) *LPS XXXVIII*, 2021. [9] Mittlefehldt D. W. and Rumble D. III (2006) *Meteoritics & Planet. Sci. 41*, A123. [10] Singletary S. J. and Grove T. L. (2003) *Meteoritics & Planet. Sci. 38*, 95. [11] Miyamoto M. et al. (1985) *PLPSC 16, JGR 90 suppl.*, D116. [12] Righter K. and Drake M. J. (1997) *Meteoritics & Planet. Sci. 32*, 929. [13] Stolper E. (1977) *GCA 41*, 587. [14] Mittlefehldt D. W. and Lindstrom M. M. (2003) *GCA 67*, 1911.

FRAGMENT-COLLISION MODEL FOR COMPOUND CHONDRULE FORMATION: ESTIMATION OF COLLISION FREQUENCY. H. Miura[1,4], S. Yasuda[2,3,4], T. Nakamoto[3], [1]*Department of Physics, Kyoto Univ., Sakyo, Kyoto 606-8502, Japan, (miurah@tap.scphys.kyoto-u.ac.jp),* [2]*Pure and Applied Sciences, Univ. of Tsukuba, Tsukuba, Ibaraki 305-8577, Japan,* [3]*Department of Earth and Planetary Sciences, Tokyo Institute of Tech., Meguro, Tokyo 152-8551, Japan,* [4]*Research Fellow of the Japan Society for the Promotion of Science.*

Introduction: Compound chondrules are composed of two or more chondrules fused together. They are rare in all chondrules ($\sim 4\%$ [e.g., 1 – 5]), but occur in many classes of chondrites, so they o er crucial information regarding the physical and chemical state of solid materials during chondrule formation. One of the models for compound chondrule formation is the random collision model, in which totally or partially molten particles collided with appropriate relative velocity [1, 3]. However, the collision frequency in the solar nebula is too small to account for the observed compound fraction because of the low density of matter in the nebula [1 – 3].

In this paper, we propose a new scenario for compound chondrule formation. The shock-wave heating model is one of the most plausible models for chondrule formation [e.g., 6]. In this model, the dust particles are exposed to high-velocity gas ow and heated by gas frictional heating. Recently, we carried out three-dimensional hydrodynamic simulations of molten dust particle exposed to the gas ow and showed that molten cm-sized dust particle is disrupted into many small pieces in a typical setting of nebula shocks [7]. These pieces have many chances of mutual collisions to form compound chondrules because the local number density of them behind the disrupted particle is enhanced. We name this scenario "fragment-collision model" and believe that it can be a strong candidate for compound chondrule formation.

The purpose of this study is to estimate the collision frequency between these pieces by using a simple formulation. In this paper, we call the disrupted dust particle as "parent" and small pieces as "ejectors." For simplicity, we assume that all ejectors have the same radius of $r_{\rm e}$.

Formulation: The number of collision per unit time (collision rate) is given by $R_{\rm coll} \sim \sigma_{\rm coll} n_{\rm e} \Delta v$, where $\sigma_{\rm coll}$ is the collisional cross-section, $n_{\rm e}$ is the number density, and Δv is the velocity dispersion of ejectors [1, 3]. The original point of our model is to estimate $n_{\rm e}$ resulting from disruption of the parent. Considering the total number of ejectors torn away from the parent during a short period of time δt, δN, and the volume of the region in which these ejectors are scattered, δV, we obtain $n_{\rm e} = \delta N / \delta V$. Assuming that all ejectors just after ejection are parting from the parent with a velocity of $\sim \Delta v$, we obtain the volume in this phase as $\delta V_0 \sim 2\pi r_{\rm p}^2 \Delta v \delta t$, where $r_{\rm p}$ is the radius of parent (see Fig. 1a). After ejection, the motions of ejectors are a ected by the ambient gas ow. We simply assume that ejectors are accelerated with a constant acceleration a in the direction of the gas ow (z-axis), on the other hand, in the direction perpendicular to the gas ow (r-axis) they move with a constant velocity of $\sim \Delta v$ (see Fig. 1b). In this later phase, the region in which ejectors are scattered is getting wider steeply with time t and its volume is given by $\delta V_t \sim \pi (\Delta v t)^2 a t \delta t$. Approximating $\delta V \simeq \delta V_0 + \delta V_t$, we obtain the number density of ejectors

$$n_{\rm e} \sim R_{\rm eject} / (2\pi r_{\rm p}^2 \Delta v + \pi \Delta v^2 a t^3) \qquad (1)$$

and the collision rate

$$R_{\rm coll} \sim (2 r_{\rm e}^2 R_{\rm eject} / r_{\rm p}^2)[1 + (t/t_*)^3]^{-1}, \qquad (2)$$

where $R_{\rm eject}$ is the ejection rate de ned by $R_{\rm eject} \equiv \delta N / \delta t$ and $t_* \equiv (2 r_{\rm p}^2 / \Delta v a)^{1/3}$. Integrating Eq. (2) over t from 0 to ∞, we obtain the collision frequency

$$F_{\rm coll} \simeq \left(\frac{72 \rho_{\rm mat} r_{\rm e}^7 R_{\rm eject}^3}{r_{\rm p}^4 \Delta v p_{\rm fm}} \right)^{1/3}, \qquad (3)$$

where $p_{\rm fm}$ is the gas ram pressure and $\rho_{\rm mat}$ is the material density of parent and ejectors (we set $\rho_{\rm mat} = 3\,{\rm g\,cm^{-3}}$ in this paper). In Eq. (3), we substitute $a = 3 p_{\rm fm} / 4 r_{\rm e} \rho_{\rm mat}$.

Ejection from Liquid Layer: In order to estimate Δv and $R_{\rm eject}$ in Eq. (3), we have to model the ejection from molten parent. Since the cm-sized parent is too large to homogenize internal temperature due to the thermal conduction, it should melt from the surface facing the gas ow [8]. Fig. 2 shows the schematic picture of this situation. For simplicity, we assume that physical properties in the liquid layer is uniform. The surface of the liquid layer is forced to move with a velocity v_θ by the tangential component of ram pressure $\sim p_{\rm fm}/2$. In contrast, there is no motion at the surface of solid core. The tangential stress of viscosity is given by $T_{r\theta} \sim \mu v_\theta / h$, where μ is the viscosity and h is the width of the liquid layer. We obtain v_θ by considering the balance between $T_{r\theta}$ and $p_{\rm fm}/2$. Assuming that Δv is the same order of magnitude of v_θ, we obtain

$$\Delta v \sim (p_{\rm fm} r_{\rm p} / 2\mu) \lambda, \qquad (4)$$

where $\lambda \equiv h / r_{\rm p}$ is the normalized width of liquid layer. The total volume of liquid layer can be roughly estimated as λ times the volume of whole parent.

When the liquid layer fragments into ejectors, the total number of ejectors is $N_{\rm e} \sim \lambda(r_{\rm p}/r_{\rm e})^3$. Assuming that the fragmentation proceeds in a uid crossing time $t_{\rm cross} \sim r_{\rm p}/v_\theta$, we obtain the ejection rate as

$$R_{\rm eject} \sim \lambda^2 (r_{\rm p}/r_{\rm e})^3 p_{\rm fm}/2\mu. \quad (5)$$

Collision Frequency: We adopt a standard set of parameters as follows: $r_{\rm p} = 1\,{\rm cm}$, $r_{\rm e} = 300\,\mu{\rm m}$, $p_{\rm fm} = 3 \times 10^4\,{\rm dyne\,cm^{-2}}$, and $\mu = 10^2$ poise. We also nd that $\lambda \sim 0.05$ by considering the balance between the timescale of heat conduction and the uid crossing time. Substituting above values, we obtain $\Delta v \sim 7.5\,{\rm cm\,s^{-1}}$ and $R_{\rm eject} \sim 1.4 \times 10^4\,{\rm s^{-1}}$. Finally, the collision frequency is

$$F_{\rm coll} \sim 0.39. \quad (6)$$

Surprisingly, above estimation is about one order of magnitude larger than the observational compound fraction. It suggests that the fragment-collision model can account for the observational fraction if only $\sim 10\%$ of all chondrules formed via the fragmentation events of cm-sized parent dust particles.

We also substitute other sets of parameters in following ranges: $r_{\rm p} = 0.5-2.0\,{\rm cm}$, $r_{\rm e} = 100-1000\,\mu{\rm m}$, $p_{\rm fm} = 10^4 - 10^5\,{\rm dyne\,cm^{-2}}$, and $\mu = 10 - 10^3$ poise and nd that the collision frequency ranges about $\sim 0.1 - 1$.

Oxygen Isotopic Data: In the fragment-collision model we proposed in this paper, the constituent chondrules of compounds are likely to have similar compositions because ejectors originate the same parent. The oxygen isotopic compositions were measured for 3 sets of blurred-type compounds, 6 sets of adhering- or consorting-type compounds, and 2 sets of enveloping-type compounds [4]. It was found that in a three-isotopic diagram, all sets of blurred-, adhering-, and consorting-types fall in the typical range obtained for single chondrules from the same chondrites (CV3). These results suggest that the two constituent chondrules of these compounds originated from the same dust reservoirs as those single chondrules. These observations are consistent with our new model for compound chondrule formation.

In contrast, in one set of enveloping-type, the oxygen isotopic compositions di er between two constituent chondrules. This result might suggest that this enveloping-type compound has not formed by our new model but the relict grain model as suggested by [2, 9].

Summary: We proposed a new scenario for compound chondrule formation named as "fragment-collision model," in the framework of the shock-wave heating model. We modeled the disruption of molten cm-sized dust particle exposed to high-velocity gas ow in order to estimate the e ciency of mutual collisions between small fragments. The predicted collision frequency was $\sim 0.1 - 1$, which is about one order of magnitude larger than the observational compound fraction. We concluded that this new model can account for compound chondrule formation.

Refs.: [1] Gooding & Keil (1981) *Meteoritics* **16,** 17-43. [2] Wasson et al. (1995) *GCA* **59,** 1847-1869. [3] Sekiya & Nakamura (1996) *Proc. NIPR Symp. Antarct. Meteorites* **9,** 208-217. [4] Akaki & Nakamura (2005) *GCA* **69,** 2907-2929. [5] Ciesla et al. (2004) *MAPS* **39,** 531-544. [6] Connolly & Love (1998) *Science* **280,** 62-67. [7] Miura & Nakamoto (2007) *Icarus* **188,** 246-265. [8] Yasuda & Nakamoto (2005) *LPSC XXXI,* #1252 (abstract). [9] Wasson (1993) *Meteoritics* **28,** 14-28.

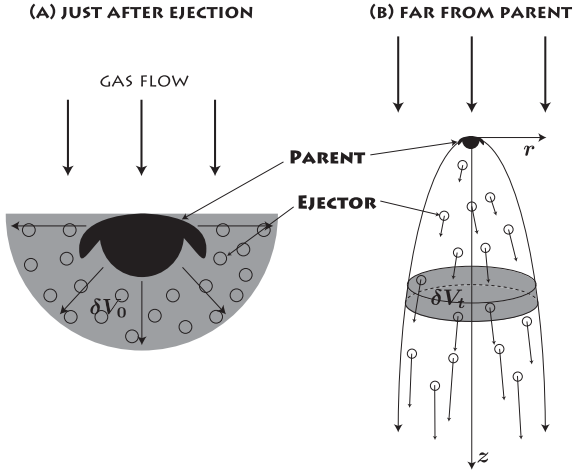

Figure 1: Schematic picture of disruption of molten parent dust particle exposed to high-velocity gas ow. When the gas ram pressure is too strong for the molten parent to keep its shape, many small ejectors are dispersed behind the parent. These ejectors have many chances of mutual collisions to form compound chondrules because the local number density of them behind the parent is enhanced.

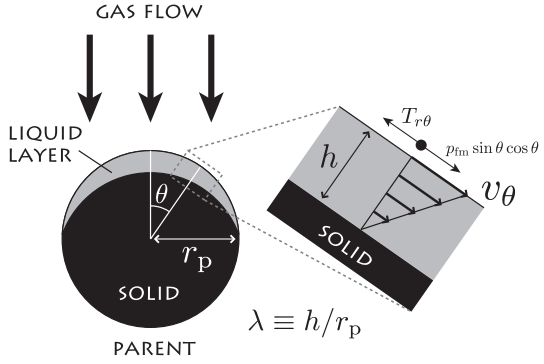

Figure 2: Schematic picture of liquid layer formed at the surface of parent particle.

MAGNETIC AND HIGH-ENERGY PROCESSES IN YOUNG STARS. T. Montmerle[1], E.D. Feigelson[2], J. Ferreira[3], A.E. Glassgold[4], M. Gounelle[5]
[1]Laboratoire d'Astrophysique de Grenoble, BP53, 38041 Grenoble Cedex, France, montmerle@obs.ujf-grenoble.fr, [2]Dept. of Astronomy & Astrophysics, Penn State University, PA 16802, USA, [3]Laboratoire d'Astrophysique de Grenoble, BP53, 38041 Grenoble Cedex, France, [4]Astronomy Department, University of California, Berkeley, CA 94720, USA, [5]Laboratoire d'Etude de la Matière Extraterrestre, Muséum d'Histoire Naturelle, 57, rue Buffon, 75005 Paris, France,

Ubiquitously in the case of low-mass stars, and also perhaps frequently in the case of massive stars, magnetic fields play a central role in their formation and early evolution (mediation of accretion flows, bipolar jets, confined winds, etc.). In the case of low-mass stars, their intrinsic magnetic activity (hot corona, flares) generates in addition high-energy processes, in the form of observed X-ray emission and particle acceleration. As a consequence, many phenomena, which may have left a record in the early solar system, result from the irradiation of the protoplanetary disks: heating and evaporation, ionization, nuclear reactions, etc. There is increasing observational evidence that such direct irradiation processes do occur in young stars.

^{26}AL IN THE EARLY SOLAR SYSTEM: A STELLAR WIND CONTRIBUTION ? T. Montmerle[1], M. Gounelle[2], M. Güdel[3], G. Meynet[4]
[1]Laboratoire d'Astrophysique de Grenoble, BP53, 38041 Grenoble Cedex, France, montmerle@obs.ujf-grenoble.fr, [2]Laboratoire d'Etude de la Matière Extraterrestre, Muséum d'Histoire Naturelle, 57, rue Buffon, 75005 Paris, France, [3]Paul Scherrer Institut, Würenlingen and Villigen, CH-5232 Villigen PSI, Switzerland, [4]Observatoire de Genève, CH-1290 Sauverny, Switzerland

Recent *XMM-Newton* observations of the Orion nebula have revealed the existence of a bubble of hot gas (1 MK) of mass ~ 0.1 Msol, pervading a wide cavity associated with the nebula, and therefore engulfing the famous *HST* "proplyds" (Güdel et al., submitted). The most likely origin for the observed soft X-ray emission is bremsstrahlung from the shocked, high-speed wind of the most massive star (Mstar = 45 Msol) of the exciting "Trapezium" cluster, θ^1 Ori C. One of the implications is that the nucleosynthetic products of this star, in particular ^{26}Al, must be carried into the wind-blown hot bubble and contaminate the proplyds. If, as is widely believed, the Sun was born in an Orion-like environment, then the forming solar system must have also been continuously contaminated during at least several Myr by "ambient" ^{26}Al nuclei carried by the shocked winds of nearby massive stars, before any of them explode as a supernova. We will discuss the possible contribution of this new mechanism to the extinct ^{26}Al observed in meteorites.

ACCRETION AND DYNAMICAL EVOLUTION OF ASTEROIDS AND COMETS.

A. Morbidelli[1] , W.F. Bottke[2], J. Chambers[3], J. Cuzzi[4], and S. Weidenschilling[5] .
[1]Observatoire de la Cote d'Azur (B.P. 4229, 06304 Nice Cedex 4, France, morby@oca.eu), [2] SWRI (1050 Walnut St, Boulder, CO 80302, bottke@boulder.swri.edu), [3]Dep. of Terrestrial Magnetism, Carnegie Inst. (5241 Broad Branch Road, N.W., Washington, DC 20015, chambers@dtm.ciw.edu), [4]Ames Research Center (Moffett Field, CA 94035-1000, jcuzzi@mail.arc.nasa.gov), [5]PSI (1700 E Ft. Lowell,Tucson, AZ 85719-2395, sjw@psi.edu)

Introduction: We review our understanding of the formation and evolution of the small bodies of the Solar System from the theoretical point of view. The goal is to provide a context for the interpretation of the chronological and cosmochemical data obtained from the analyses of samples returned from these small bodies.

Primary Accretion: The accretion of rocky and icy planetesimals (the asteroids and comets of today's Solar System) is one of the most mysterious and controversial phases of Solar System history. A key unknown factor, which dominates the evolution of particles in the pre-planetesimal stage, is the degree to which the nebula was turbulent. Surface forces help small dust grains stick to each other, forming macroscopic fractal aggregates, that are presumably made progressively more compact by collisions [1]. How far planetesimals can grow in this way is unclear. If the nebula is turbulent, collisions may become disruptive as particles grow larger and relative velocities increase [2], stalling accretion at around a meter in size. An additional severe problem is due to the drift of the growing particles towards the Sun, due to gas drag [3]. Bodies with sizes of order of a meter are removed from a region faster than they can grow up to sizes of a few kilometers, which are less sensitive to gas drag. This combination of problems is usually called the `meter-size barrier' problem. While making sticking more difficult, turbulence helps us understand observations which suggest widespread mixing in the early nebula, such as the recent finding of high temperature, crystalline minerals in samples of comet Wild II returned by STARDUST [4,5].

To overcome the meter-size barrier and avoid uncertainties about ‘sticking’, it has been suggested that planetesimals might form quickly by gravitational instability, in a dense particle layer close to the nebula mid-plane [6]. However, these dense layers themselves generate local turbulence which disperses the particles and prevents gravitational instability [7,8]. Although the idea of classical gravitational instability has been recently resurrected in the context of very small particles [9,10], this latter scenario is invalidated by even tiny amounts of nebula turbulence [2].

Recent numerical simulations indicate several new and complex ways that nonlinear outcomes in 3D turbulence might create opportunities for accretion that were unknown more than a decade ago. Global, 3D turbulence might be produced by the magneto rotational instability [11] or by other, less well understood processes. Under nebula conditions, chondrule-sized particles can be concentrated by orders of magnitude into dense zones with particle density approaching the classical (but not, as it turns out, actual) threshold for gravitational instability [12,2], the fate of which has only recently been explored [13]. Also, the localized gas density and pressure maxima created by large eddies attract meter-size particles, which drift rapidly towards these regions of high pressure under gas headwinds or tailwinds generated by the opposed radial pressure gradients. It is therefore possible that, at specific locations of the disk, the concentration of solids is temporarily high enough to allow the formation of a large planetesimal due to a `local' gravitational instability even in turbulence [14,15]. However, the role of inter particle collisions in this latter regime needs to be studied carefully.

Collisional growth: Once macroscopic planetesimals (tens of meters to kilometers) are formed, coagulation models [16,17] allow us to track the growth of the objects through their gravitational interactions and collisions. It should be noticed that these models fail to form a large number of Pluto-size bodies in the outer Solar System, whose past existence is inferred by a large number of constraints [18], as well as the cores of the giant planets. Therefore, some aspects of the growth of larger planetesimals and protoplanets are surely still missing in the theoretical models and numerical simulations. All models, however, agree in showing that the accretional process occurs faster at smaller distances from the Sun. Thus, it is likely that fully grown bodies existed in the inner Solar System, when the asteroid belt or the more distant disk where still dominated by dust particles. Because the differentiation of bodies is triggered by the decay of short-lived radioactive elements, it is likely that differentiated planetesimals were much

more numerous in the vicinity of the Sun than further out in the disk. Quantifying the distance at which planetesimals could differentiate, however, is beyond the capabilities of the current models.

Dynamical evolution of planetesimals: The population of small bodies is strongly dynamical affected by the growth of the planets. As Jupiter and Saturn grew in a gas disk, they dispersed by close encounter the planetesimals originally in their vicinities. The largest objects, insensitive to gas drag, were mostly ejected from the Solar System, but some (such as the newly discovered object Sedna) could be perturbed into orbits typical of the Inner Oort cloud [19] due to the dense galactic environment present at that early time. The comet-sized bodies, however, were presumably circularized by gas drag just outside of the Jupiter-Saturn region and participated in the subsequent formation of Uranus and Neptune [20]. The planetesimals from the Uranus-Neptune zone were dispersed by the ice giant planets on a longer time-scale, exceeding the gas disk lifetime. They formed the so-called scattered disk (the source of the current Jupiter-Family Comets) [21] and the outer Oort cloud (the source of the current Long Period Comets) [22]. In the framework of recent evolutionary models of the outer Solar System [23], both these two reservoirs of comets formed late, at the time of the so-called Late Heavy Bombardment (~700 My after planet formation), from planetesimals initially in the 15-30 AU region.

The asteroid belt was strongly affected during two evolutionary phases of the Solar System. First, during terrestrial planet formation, it underwent a substantial orbital excitation and dynamical depletion, due to the combined action of planetary embryos - originally formed in that region - and resonant perturbations exerted by Jupiter and Saturn [24-27]. During this phase, it is likely that fragments of differentiated planetesimals from the inner Solar System were implanted into the asteroid belt [28]. This may resolve the conundrum of the early differentiation age of some iron meteorite parent bodies [29]. It might be possible that some bodies of cometary nature from the Jupiter region were also trapped in the asteroid belt by a similar mechanism. Then, during the Late Heavy Bombardment of the terrestrial planets, the asteroid belt underwent a second dynamical excitation and depletion [23,30,31]. During this phase, some objects which originated in the trans-Neptunian disk could be captured in the outer part of the asteroid belt [32]. These objects are probably identified with the D and P type asteroids, which are numerous in the outer belt. In view of these results, the asteroid belt appears to be the reservoir of a population of planetesimals formed over a much larger range of heliocentric distances than its current radial extent would lead one to think. This has important implications for our understanding of the gradient of physical properties of planetesimals with heliocentric distance and for the nature of the planetesimal precursors of the terrestrial planets.

References:

[1] Dominik, C., J. Blum, J. Cuzzi, and G. Wurm (2007) in "Protostars and Planets V", 783 [2] Cuzzi, J. and Weidenschilling, S. (2006) in "Meteorites and the Early Solar System –II"; Univ. of Arizona Press, 353 [3] Weidenschilling S.J.(1977), MNRAS, 180, 57 [4] Brownlee D., et al. (2006), Science, 314, 1711 [5] Ciesla, F. and Cuzzi, J., (2007), 38th LPSC, paper # 1386 [6] Goldreich P. and Ward W.R. (1973), ApJ, 183, 1051 [7] Cuzzi J.N., Dobrovolskis A.R. and Champney J.M. (1993), Icarus, 106, 102 [8] Weidenschilling S.J. (1995), Icarus, 116, 433 [9] Sekiya, M. (1998) Icarus, 133, 298 [10] Youdin A.N. and Shu F.H. (2002), ApJ, 580, 494 [11] Stone, J. M., C. F. Gammie, S. A. Balbus, and J. F. Hawley (2000) in Protostars and Planets IV, 589 [12] Cuzzi, J. N. et al (2001) Astrophys, J. 546, 496 [13] Cuzzi J. N., R. C. Hogan, and K. Shariff (2007) 38th LPSC, paper #1439 [14] Johansen A., Klahr H. and Henning T. (2006), ApJ, 636, 1121 [15] H. Klahr, personal communication [16] Kenyon S.J. and Luu J.X. (1999), ApJ, 526, 465 [17] Weidenschilling S.J. (2004), Comets II, 97 [18] Stern, S.A. (1991), Icarus, 90, 271 [19] Brasser R., Duncan, M.J.,and Levison H.F. (2006), Icarus, 184, 59
[20] Brasser R., Duncan, M.J.,and Levison H.F. (2007), Icarus, in press. [21] Dones L., Weissman P.R., Levison H.F.and Duncan M.J. (2004), Comets II, 153 [22] Duncan M.J. and Levison H.F. (1997), Science, 276, 1670 [23] Gomes R., Levison H.F., Tsiganis K. and Morbidelli A. (2005), Nature, 435, 466 [24] Wetherill G.W. (1992), Icarus, 100, 307 [25] Chambers J. E. and Wetherill G.W. (2001), Meteoritics and Planetary Science, 36, 381 [26] Petit J.M., Morbidelli A. and Chambers J. (2001), Icarus, 153, 338. [27] O'Brien D., Morbidelli, A and Bottke W.F. (2007) Icarus in press. [28] Bottke W.F., Nesvorny D., Grimm R.E., Morbidelli A and O'Brien D.P. (2006), Nature, 439, 821 [29] Markowski A., Quitte G., Halliday A.N. and Kleine T. (2006), Earth and Planetary Science Letters, 242, 1 [30] Levison H.F., Dones L., Chapman C.R., Stern S.A.,Duncan M.J. and Zahnle K. (2001), Icarus, 151, 286 [31] Strom R.G., Malhotra R., Ito T., Yoshida F. and Kring, D.A. 2005, Science, 309, 1847 [32] Levison H.F. et al. (2007) in preparation.

DATING THE FIRST STAGE OF PLANET FORMATION. Frederic Moynier[1], Qing-zhu Yin[1]. and Benjamin Jacobsen[1]. [1]Department of Geology, University of California Davis, One Shields Avenue, Davis CA, 95616. moynier@geology.ucdavis.edu

Introduction: The "standard model" of planet formation established the following evolutionary stages in the protoplanetary disk: (I) coagulation of dust to km-sized planetesimals; (II) rapid "runaway" growth from planetesimals to planetary embryos, leading to ~20 Mars-sized bodies in the terrestrial planet region; (III) the planetary embryos perturb each other into crossing orbits and merge via giant impacts, eventually leading to full size planets [1]. Using planet wide metal-silicate segregation and core formation as a tool to monitor the rate of late stage accretion processes, the stage-II (Vesta to Mars) and stage-III (Earth-Moon system) formation timescales are now well established (e.g. 2-4).

Stage-I is the least understood among the three stages because there are very few observational constraints and the physics of grain growth in the solar nebula from micron-sized particles to kilometer-sized bodies is not well understood. Here we use ^{53}Mn-^{53}Cr isotopic records discerned from primitive meteorites to constrain the timescale of stage-I of planet formation.

The rationale for our approach is as follows: The asteroid belt is the cold storage warehouse for relicts from the stage-I of solar system development. Due to Jupiter's gravitational perturbation, we have free sample return of stony meteorites, chips off asteroid parent bodies created by impacts. The most pristine stony meteorites of our solar system, called carbonaceous chondrites, must have witnessed the initiation of planet formation. These samples hold key clues that allow us to view the processes inside our own protoplanetary disk 4567 Ma (million years) ago.

Primitive carbonaceous chondrites are cosmic sediments made of refractory materials such as Ca-Al-rich inclusions (CAIs), and chondrules (molten silicate droplets) that are "cemented" together by fine grained dust materials (dark matrix) rich in organics and presolar grains. The preservation of organic matter and pristine presolar grains in the matrix testifies that the parent bodies of the carbonaceous chondrites were never heated to high temperatures. This suggests that the parent bodies of the carbonaceous chondrites were on the order of a few kilometers to <20km at most in order to avoid heat insulation and melting by ^{26}Al heating [5]. Thus the parent bodies of carbonaceous chondrites can be regarded as products of stage-I of the planet formation. A key question is how and when did these diverse components come together? How can we devise a tool to date the formation of bulk carbonaceous chondrites (and their parent bodies)?

Mn is a moderately volatile element, and thus is concentrated in the low temperature matrices of the carbonaceous chondrites, whereas Cr is a relatively refractory element, concentrated in the refractory bits and pieces (chondrules and CAIs). It is well established that different carbonaceous chondrite groups show a systematic and progressive depletion pattern for moderately volatile elements (e.g. Mn/Cr) [6]; the Mn/Cr ratio is governed by the matrix fraction. This fact allows us to apply ^{53}Mn-^{53}Cr chronometry, where ^{53}Mn decays to ^{53}Cr with a half-life of 3.7 Ma, to constrain the timescale of accretion of the carbonaceous chondrites parent bodies.

Samples and analytical methods: We analyzed the Cr isotopic composition of the whole-rock samples of 6 carbonaceous chondrites from the different major groups: Orgueil (CI1), Dar al Gani 749 (CO3.1), Lancé (CO3.4), Ningqiang (CK3), Vigarano (CV3), Allende (CV3). The Cr purification is adapted from [3, 7, 8]. The Cr isotopes were run on a Nu Plasma HR multi-collector inductively-coupled plasma mass spectrometer with a desolvating nebulizer DSN-100 at UC Davis. "Pseudo-high resolution mode" is adopted to resolve polyatomic interferences on mass 52, 53 and 54. The ^{55}Mn/^{52}Cr ratios were measured directly on the Nu Plasma HR in multi-collection mode from a small aliquot of the initial dissolution and corrected against gravimetric standard of known ^{55}Mn/^{52}Cr ratio. An exponential law was used to correct for mass fractionation assuming ^{50}Cr/^{52}Cr=0.051859 [3]. ^{53}Cr/^{52}Cr is expressed as parts per 10,000 (ε^{53}Cr*) deviations relative to the terrestrial standard SRM 979. No "anomalies" of ^{53}Cr have been detected in the terrestrial olivines of San Carlos (ε^{53}Cr*=0.02±0.05).

Results and discussions: We demonstrate that all carbonaceous chondrites exhibit ^{53}Cr* anomalies that are correlated with ^{55}Mn/^{52}Cr ratio (Fig. 1). Our data are in very good agreement with [9]: similar results obtained in the same meteorite samples Allende and Orgueil, and for different samples from the same meteorite group (with the exception of Dar al Gani 749) .

Combining our new data with that of [9], we obtain the best estimate of the solar ^{53}Mn/^{55}Mn ratio of $(8.5\pm1.2)\times10^{-6}$ (slope in Fig. 1) at the time of formation of carbonaceous chondrite parent bodies. Assuming homogenous distribution of ^{53}Mn in the early solar nebula, the relative age between two objects 1 and 2 is:

$$\Delta T_{1\text{-}2} = 1/\lambda \times \ln[(^{53}Mn/^{55}Mn)_1/(^{53}Mn/^{55}Mn)_2] \quad (1)$$

where λ is the decay constant of ^{53}Mn. By comparing the initial $^{53}Mn/^{55}Mn$ ratio of $(8.5\pm1.2)\times10^{-6}$ with $(1.25\pm0.07)\times10^{-6}$ of angrite LEW86010 [3], a $\Delta T_{cc\text{-}angrites}$ of $10.2^{+0.87}/_{-0.75}$ Ma is deduced. The absolute Pb-Pb age of this angrite is 4557.8±0.5 Ma [10], thus an absolute age of $4568.0^{+0.91}/_{-1.17}$ Ma for the carbonaceous chondrite is derived. This age is very similar to Pb-Pb ages obtained on CAI fragments (4567.2 ± 0.6 Ma) from the CV3 chondrite Efremovka [11]. The age deduced from the initial $^{53}Mn/^{55}Mn$ ratio for the bulk carbonaceous chondrites is the same as that for the CAIs, therefore the formation of the first solid igneous objects as well as the accretion of the undifferentiated kilometer-sized carbonaceous chondrite parent bodies must have been complete within +0.91 to -1.17 Ma at 4568 Ma ago. This estimate conservatively includes both uncertainties of the Fig. 1 isochron and the absolute age anchor for angrite LEW86010 [10]. This is currently the best estimate for the stage-I planet formation timescale.

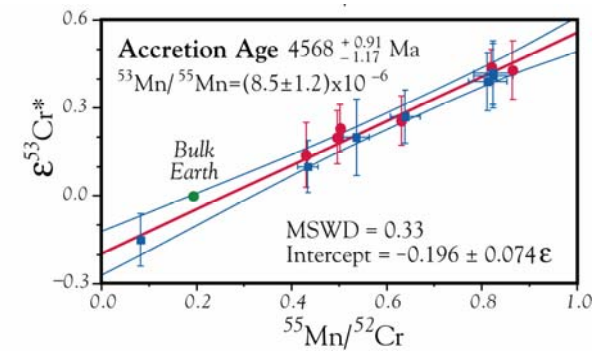

Fig. 1. ^{53}Mn-^{53}Cr fossil isochron diagram for bulk carbonaceous chondrites. Red solid circles are new data from UC Davis. Blue solid squares are from recent data of [9]. These data collectively suggest that carbonaceous chondrite parent bodies must have been accreted within -0.73 to +0.84 Myr, as defined by the uncertainty of this whole rock isochron. The maximum duration is thus <1.57 Myr.

The logical necessity that chondrules formed first in order to form chondrites means that the data also constrains chondrule formation (for carbonaceous chondrite) to be within +0.91 to -1.17 Ma at 4568 Ma ago. Since CAIs are just as old (4567.2±0.6 Ma) , we predict that a more precise dating of chondrules in carbonaceous chondrites in future studies will confirm the above conclusion. This would eliminate the longstanding puzzle known as the "storage problem" faced by the current prevailing chronological data, namely, how could mm- to cm-cized CAIs float in the solar nebula for over 2 Ma, relative to chondrules, without spiraling into the Sun?

Delayed chondrule formation for ordinary chondrites: Yin et al [12] report the chondrules from a primitive ordinary chondrite (Chainpur LL3.4) with $^{53}Mn/^{55}Mn = (5.1\pm1.6)x10^{-6}$. Compared to bulk carbonaceous chondrite initial $^{53}Mn/^{55}Mn = (8.5\pm1.2)x10^{-6}$, chondrules in ordinary chondrites are younger by $2.7^{-1.6}/_{+2.3}$ Myr.

Distinct Cr Isotopic Reservoirs in the Early Solar System: Importantly, the initial $\mu^{53}Cr_i$=8.7±9.1 ppm ($\mu = 100\varepsilon$) for Chainpur chondrules [12] is clearly higher than bulk carbonaceoous chondrites initial $\mu^{53}Cr_i$=-19.6±7.4 ppm (Fig. 1), strongly suggesting they are coming from two isotopically distinct reservoirs. This is consistent with the bulk ordinary chondrites ($\varepsilon^{53}Cr^*$=0.48±0.03, $^{55}Mn/^{52}Cr$= 0.76) [13] plotting above the bulk carbonaceous chondrite isochron. Bulk enstatite chondrites ($\varepsilon^{53}Cr^*$=0.16, $^{55}Mn/^{52}Cr$ = 0.76) [13], on the other hand, plot below the isochron in Fig. 1. Abee (EH4), the oldest among the three enstatite chondrites, is $5.6^{-1.0}/_{+1.2}$ Myr younger than carbonaceous chondrites based on its $^{53}Mn/^{55}Mn= (3.0\pm0.4)x10^{-6}$ and $\mu^{53}Cr_i$=-3±6 ppm. Bulk Earth with $(^{55}Mn/^{52}Cr)_{BE}$=0.19 [14] and $\varepsilon^{53}Cr^*$=0 plots on the bulk carbonaceous isochron within the error envelop of the regression line in Fig. 1 and given the uncertainty of $(^{55}Mn/^{52}Cr)_{BE}$ estimates. In contrast, Bulk Silicate Earth plots below the isochron, given the range of estimate for $(^{55}Mn/^{52}Cr)_{BSE}$ = 0.35-0.45 [14, 15], requiring substantial fraction of Cr must have been partitioned into the core. Mars also plots below the isochron, using $(^{55}Mn/^{52}Cr)_{Mars}$ = 0.76, and $\varepsilon^{53}Cr^*$=0.22 [3].

References: [1] J.E. Chambers, *Earth EPSL*, 223, 241 (2004). [2] Q.-Z. Yin et al., *Nature*, 418, 949 (2002). [3] G.W. Lugmair, A. Shukolyukov, *GCA*, 62, 2863 (1998). [4] S.B. Jacobsen, *AREPS.*, 33, 531 (2005). [5] I.S. Sanders, G.J. Taylor *ASPCP*, 241, 915 (2005). [6] J.T. Wasson, G.W. Kallemeyn, *PTRSL*, 325, 535 (1988). [7] J.L. Birck, C. J. Allègre, *GRL.*, 12, 745 (1984). [8] D. P. Glavin et al., *MAPS.* 39, 693 (2004). [9] Shukolyukov, G.W. Lugmair, EPSL, 250, 200 (2006). [10] G.W. Lugmair, S.J.G. Galer, *GCA*, 56, 1673 (1992). [11] Y. Amelin et al., *Science*, 297, 1678 (2002). [12] Q.-Z. Yin et al., ApJL, 662, L43. [13] A. Shukolyukov and G.W. Lugmair (2004) *GCA*, *68*, 2875-2888. [14] W.F. McDonough, (2003) *TOG*, *2*, 547-568. [15] S.R. Hart. And A. Zindler,. (1996) *CG,. 57*, 247-267.

CHLORINE ISOTOPIC FRACTIONATIONS IN THE EARLY SOLAR SYSTEM: CORRELATION WITH OXYGEN AND STABLE CHROMIUM ISOTOPE ANOMALIES IN CHONDRITES. N. Nakamura[1], T. Fujitanin[1,2], O. Okano[3], M. Kimura[4], L. E Nyquist[5], M. Ebihara[6] and R. N. Clayton[7], [1]Kobe University, Kobe 657-0059, Japan, noboru@kobe-u.ac.jp, [2]Marine Technical College, Ashiya 659-0026, Japan, fujitani@mail.mtc.ac.jp, [3]Okayama University, Okayama 700-8530, Japan, ookano@cc.okayama-u.ac.jp, [4]Ibaraki University, Mito 310-8512, Japan, makotoki@mx.ibaraki.ac.jp, [5]NASA Johnson Space Center, Texas 77058, USA, laurence.e.nyquist@nasa. gov, [6]Tokyo Metropolitan University, Tokyo 192-0397, Japan, ebihara-mitsuru@c.metro-u.ac.jp, [7]Enrico Fermi Institute, University of Chicago, Illinoi 60637, USA, rclayton@uchicago.edu.

Introduction: Stable chlorine isotope analyses for bulk chondrites provide a potentially unique record of isotopic behaviors of volatiles in the early solar system. We have established TIMS technique of chlorine isotope analyses and reported preliminary results for different types of chondrites (1-4). We discuss here analytical problems of Cl isotopes, implications of isotopic fractionations observed and their timing in the early solar system.

Analytical Problems: Mainly two methods (5), gas-source mass spectrometry using CH_3Cl^+ (IRMS) and thermal ionization mass spectrometry using Cs_2Cl^+ (TIMS), have been used for analysis of stable Cl isotopes for silicate materials. The IRMS provides a better precision (~0.05‰) compared to TIMS (~0.2‰) but requires large amounts of sample (Cl= ~1mg). The TIMS provide reasonably good precision, precise enough for most planetary materials, and need only small amounts of materials (Cl= ~2 μ g). It has thus advantages for small planetary materials with low Cl contents (≤ a few hundreds ppm). The two methods have been reported to be consistent with each other in isotopic compositions (6), although some authors (7) have argued that the δ^{37}Cl (deviation in 10^3 from seawater) obtained by TIMS are too high compared to those by IRMS.

A literature search shows that only a few standard rocks and chondrites are available for comparison. The δ^{37}Cl values obtained by IRMS are mostly close to zero or smaller while our TIMS values are about 1.5‰ higher than IRMS values. It seems likely that some unknown systematic errors (and/or partly a sampling problem) may be responsible for the observed shift between both methods. Due to the negative δ^{37}Cl as small as –2‰ in the laboratory environments (1), the lower δ^{37}Cl potentially arise by laboratory contaminations. In general, however, the higher δ^{37}Cl are possible for TIMS, if analytical conditions of sample to standard are not sufficiently controlled.

Correlation of δ^{37}Cl with Δ^{17}O and ε^{54}Cr: We have reported preliminary results of Cl abundances and isotopic compositions for 23 bulk (and one chondrule) samples from several groups of chondrites [4].

We presented evidence for Cl isotopic fractionation within several groups of chondrites that correlates with the Cl abundance in individual meteorites within a given subgroup. In particular, δ^{37}Cl in carbonaceous chondrites correlates positively with the abundance of Cl (ppm) in individual group members. These observations are analogous to the correlation of ε^{54}Cr with O-isotope group (8), leading to expectation of a correlation between ε^{54}Cr and δ^{37}Cl. Although the current data are incomplete Cl concentrations are in the order CI>CM>CV~CK. The order of δ^{37}Cl enrichments is in the same order if the correlation of δ^{37}Cl with Cl (ppm) is used to predict δ^{37}Cl for CI. In view of Cl- and Cr-bearing phases in the least metamorphosed chondrites (9), this is suggestive of partial resolution of one of the most puzzling features of the stable chromium isotopic composition of carbonaceous chondrites.

The positive correlations of δ^{37}Cl with Δ^{17}O and ε^{54}Cr suggest that there exist at least two Cl isotope reservoirs in the early solar system. It is, therefore, considered that stable chlorine isotope fractionations as observed in chondrites occurred as the same timing when the Δ^{17}O–ε^{54}Cr correlation had been established. We suggest that the Cl isotope variations and their correlation with isotopic anomalies of some elements may provide new insight into origins and processes of the early solar system materials**.**

References: [1] Numata M. et al. (2001) *Geochem. J.,* 35, 89-100. [2] Fujitani T. & Nakamura N. (2006) *Geostandard & Geoanal Res.* 30, 113-120. [3] Fujitani T. & Nakamura N. (2006) *Antarct Meteor* XXX 11-12; [4] Nakamura N. et al. (2007) *LPS. XXXVIII,* #1929. [5] Kaufmann R.S. et al (1984) Nature 309, 338-340; Xiao Y. K. & Zhang C. G. (1992) *Int. J. Mass Spectrom. Ion Proc.* 116, 183-192. [6] Godon A. et al. (2004) *Chem. Geol.* 207, 1-12; Rosenbaum J. M. et al. (2000) *Anal. Chem.* 72, 2261-2264. (7) Bonifacie M. et al. (2007) *Chemical Geology* 242, 187-201; Sharp Z. D. et al. (2007) *Nature* 446,1062-1065. [8] Trinquier A. et al. (2007) Astrophys. J. 655, 1179-1185. [9] Kimura M. & Ikeda Y. (1997*) Meteo. Planet. Sci.,* 32, A72.

PRESOLAR GRAIN EVIDENCE FOR LOW-MASS SUPERNOVA INJECTION INTO THE SOLAR NEBULA. Larry R. Nittler, Department of Terrestrial Magnetism, Carnegie Institution of Washington, Washington, DC 20015, lnittler AT ciw.edu

The inferred presence of short-lived radionuclides in the early Solar System suggests that the Sun formed close in time and space to a supernova (SN) explosion. Early ideas focused on the triggered-collapse scenario, where the SN shock wave initiated collapse of the protosolar cloud core and injected radioactivities into it [1]. More recently, an alternative scenario has been proposed [2], namely that a nearby SN injected material directly into an already-formed protoplanetary disk. Possible support for this model has been reported based on Ni isotopes in meteorites [3]. Here I argue that a sub-class of presolar silicate and oxide grains found in meteorites and interplanetary dust particles (IDPs) likely originated in a single SN, perhaps the same one that provided the radioactivities to the early Solar System.

The O isotopic ratios of several hundred presolar oxide and silicate grains are shown in Fig. 1 [4-15], along with the Group designations of [4]. The vast majority of the grains (Groups 1-3) are understood as having formed in low-mass red giants and asymptotic giant branch (AGB) stars [4]. In contrast, the origin of the ^{18}O- and ^{17}O-rich Group 4 grains (10-20% of presolar oxides and silicates, [11]) has been enigmatic. Original suggestions included high-metallicity AGB stars and unusual AGB stars in which very early third dredge-up episodes enriched the surface in ^{18}O from partial He-burning [4]. However, there are major difficulties with both of these suggestions, making an AGB origin highly unlikely [5].

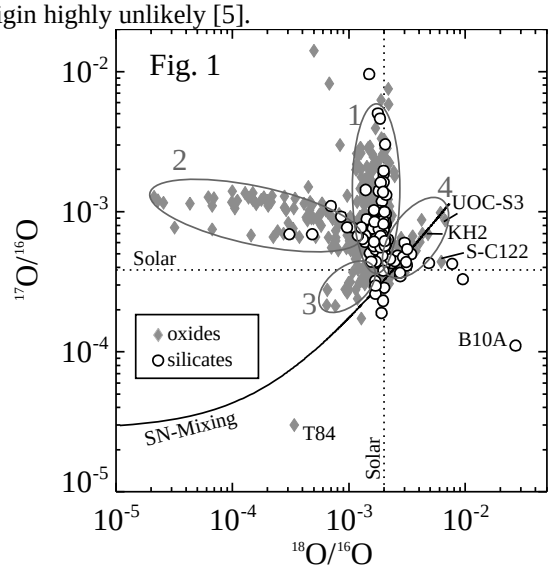

On the other hand, [7] suggested an origin in a Type II SN for a highly ^{18}O-enriched presolar Al_2O_3 grain (S-C122) and a SN is certainly required to explain a few other similar grains [13, 15] and an ^{18}O-rich and ^{17}O-poor olivine grain (B10A) reported by [9]. All of these grains differ from the main Group 4 O isotopic trend, in that they do not show ^{17}O excesses. There is little isotopic data for Group 4 grains besides O, but the extant data argue in favor of a SN origin for these grains. The strongest case comes from a presolar hibonite grain, KH2 (originally named 110-1, [6]). This grain has a typical Group 4 composition, very high inferred ^{26}Al/^{27}Al and ^{41}Ca/^{40}Ca ratios (0.01 and 4×10^{-4} respectively), a 30% ^{25}Mg depletion, 4% depletions in ^{42}Ca and ^{43}Ca and a 6% excess in ^{44}Ca. We have also recently identified a Group 4 presolar spinel grain, UOC-S3, which also exhibits high ^{26}Al/^{27}Al=0.015 and a 24% ^{25}Mg depletion [5]. These compositions are inconsistent with an origin in AGB stars, but can be easily understood in the context of Type II SNe.

Figure 2 shows the O isotopic compositions of several zones of a 15$M_\odot$ Type II SN [16], along with the presolar grain data. Clearly, mixing of these zones in variable proportions could produce almost any composition one would desire. Nonetheless, the very high ^{18}O/^{16}O ratio of the partially He-burnt He/C zone provides a natural explanation for presolar grains with large ^{18}O excesses [17]. The Group 4 grains lie along a linear trend that is well explained by mixing (Mix-2) of variable amounts of material from the inner ^{16}O-rich zones with a single mixture (triangle) of the H envelope and the He/C zone (Mix-1). Moreover, simple mixing models of the various zones can quantitatively reproduce 7 of the 8 isotopic ratios measured in KH2 and the 4 ratios measured in UOC-S3. Only the ^{43}Ca/^{40}Ca ratio of KH2 is missed, but nucleosynthesis models are known to under produce ^{43}Ca [18]. The mixtures that explain the two grains are similar and require close to a 50:50 mix of the envelope and He/N zone (to provide ^{26}Al), mixed with small amounts of the He/C (to provide ^{18}O and ^{41}Ca) and the innermost zones (to provide ^{16}O, ^{24}Mg, ^{40}Ca and ^{44}Ti). There is little O in the He/N zone, so this component does not significantly affect the O isotopes. Also, because the contribution from inner zones is small, one does not expect large isotopic anomalies in other elements like Si or Fe in these mixtures. Moreover, we note that the mixing line explaining the Group 4 O data also passes near several ^{16}O-rich grains (outside the Group 3 ellipse on Fig. 1) that are not well-explained by AGB stars, suggesting these might also have formed in SNe. Note also that ^{16}O-rich grain T84 [14] is well ex-

plained by a mixture of the inner zones with the He/C zone (Mix-3).

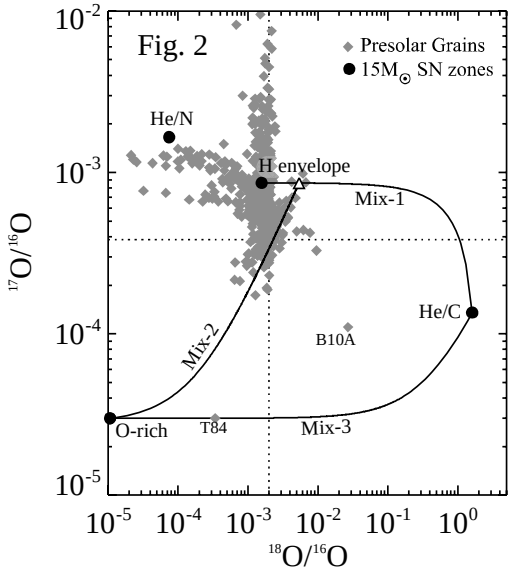

These results argue strongly for a SN origin for most or all Group 4 (and possibly some Group 3) grains. However, an intriguing aspect of this conclusion is the rather narrow range of mixing conditions required to explain the grain data. Mixing in SN ejecta is observed to be highly heterogeneous and variable from remnant to remnant [19, 20]. This is consistent with the wide range of isotopic compositions observed in single presolar SiC and graphitic grains from SNe [21, 22], requiring a range of mixing conditions and probably many different parent SNe. Given the extreme diversity in SN compositions and mixing details, it is difficult to envision a realistic scenario in which different SNe ended up producing grains primarily along a single mixing line as observed in the O-rich grains. The most likely explanation is that these grains formed in a single SN. If so, the observed mixing line might reflect a jet of ^{16}O-rich material from the inner part of the explosion passing through and mixing with the outer partially mixed ejecta, followed by grain formation as the material expands and cools.

An obvious explanation for a preponderance of grains in the Solar System from a single SN would be if they formed in the same SN postulated to have injected radioactivities into the disk. The model of [2] requires that the radioactivities be injected in the form of pre-condensed dust, as gaseous ejecta passes around the disk. Moreover, recent calculations [23] suggest that grains in the size range of the observed presolar grains (0.1-10μm) are preferentially injected and many of these are expected to survive. If the Group 4 grains were indeed injected into an already-formed solar nebula, one might expect to see a heterogeneous distribution of them in the Solar System. In fact, the limited dataset so far suggests a significantly higher fraction of Group 4 grains in IDPs and Antarctic micrometeorites (AMMs), compared to meteorites [8-10, 12]. Since IDPs and possibly AMMs are believed to originate preferentially in comets, this would support a heterogeneous distribution of SN grains in the Solar System. Note that the SN that provided the Group 4 grains apparently did not provide any significant number of SiC or graphite grains as no obvious single source is implicated by their isotopic data (and note that presolar Group 4 silicates are more than 100 times more abundant than SiC X-grains in meteorites). This is also qualitatively consistent with the proposed scenario of a single O-rich jet from the SN intersecting the disk.

We have thus far only considered the 15M$_\odot$ model of [16], and it is likely that other SN models could also reproduce the isotopic compositions of the Group 4 grains. We plan to investigate additional SN models to better constrain the nature of the source (e.g., the initial mass) of Group 4 grains and to investigate whether this scenario can simultaneously explain the short-lived nuclide data. In any case, the necessity of mixing material from advanced nuclear burning stages with the stellar envelope constrains the progenitor mass to be less than about 30M$_\odot$, since more massive stars lose their entire envelopes due to strong Wolf-Rayet winds prior to the SN explosion. Therefore, if the Group 4 presolar grains indeed were injected into the early Solar System by the same SN that provided the short-lived nuclides, this would argue strongly against the suggestion of [3] that the ^{26}Al was provided in a Wolf-Rayet wind followed by injection of ^{60}Fe from the explosion of a very massive star.

References: [1] Cameron A. G. W. and Truran J. W. (1977). *Icarus, 30,* 447-461. [2] Ouellette N., et al. (2007). *ApJ, 662,* 1268-1281. [3] Bizzarro M., et al. (2007). *Science, 316,* 1178-1181. [4] Nittler L., et al. (1997). *ApJ, 483,* 475-495. [5] Nittler L. R., et al. (2007). *ApJ, in prep*. [6] Nittler L. R., et al., (2005), *LPS XXXVI,* Abstract #2200. [7] Choi B.-G., et al. (1998). *Science, 282,* 1282-1289. [8] Floss C., et al. (2006). *GCA, 70,* 2371-2399. [9] Messenger S., et al. (2005). *Science, 309,* 737-741. [10] Messenger S., et al. (2003). *Science, 300,* 105-108. [11] Nguyen A. N., et al. (2007). *ApJ, 656,* 1223-1240. [12] Yada T., et al., (206), *LPS XXXVII,* Abstract #1470. [13] Bland P. A., et al. (2007). *M&PS, in press.* [14] Nittler L. R., et al. (1998). *Nature, 393,* 222. [15] Mostefaoui S. and Hoppe P. (2004). *ApJ, 613,* L149-L152. [16] Rauscher T., et al. (2002). *ApJ, 576,* 323-348. [17] Amari S., et al. (1995). *ApJ, 447,* L147-L150. [18] Woosley S. E. and Weaver T. A. (1995). *ApJ Supplement, 101,* 181-235. [19] Hwang U., et al. (2004). *ApJ, 615,* L117-L120. [20] Park S., et al. (2004). *ApJ, 602,* L33-L36. [21] Hoppe P., et al. (2000). *M&PS, 35,* 1157-1176. [22] Travaglio C., et al. (1999). *ApJ, 510,* 325-354. [23] Ouellette N. and Desch S. J., (2007), *LPS XXXVIII,* Abstract #1909.

THE CHRONOLOGY OF EARLY ASTEROID PROCESSES. L. E. Nyquist[1], T. Kleine[2], C.-Y. Shih[3], N. Kita[4], A. Yamaguchi[5], Y. D. Reese[6], [1]Mail Code KR, NASA Johnson Space Center, Houston, TX 77058-3696, USA, laurence.e.nyquist@nasa. gov, [2]Inst. Isotope Geochemistry and Mineral Resources, ETH Zurich, Switzerland, [3]Mail Code JE-23, ESCG/Jacobs Sverdrup, P.O. Box 58477, Houston, TX 77258-8477, USA, [4]Dept. Geology and Geophysics, UW-Madison. [5]Antarctic Meteorite Research Center, National Institute of Polar Research, 1-9-10 Kaga, Tokyo 173-8515, Japan. [6]Mail Code JE-23, ESCG/Muniz Engineering, Houston, TX 77058, USA.

Introduction: We examine the chronology of differentiated asteroids as obtained by applying the ^{26}Al-^{26}Mg ($t_{1/2}$ = 0.73±0.03 Ma), ^{53}Mn-^{53}Cr ($t_{1/2}$ = 3.7±0.4 Ma), ^{182}Hf-^{182}W ($t_{1/2}$ = 8.90±0.09 Ma), and ^{146}Sm-^{142}Nd ($t_{1/2}$ = 103 Ma) chronometers in combination with ^{207}Pb-^{206}Pb ages.

Planetary Differentiation: Fig.1 shows ^{26}Al/^{27}Al ratios (Log_{10}) vs ^{207}Pb/^{206}Pb (Pb-Pb) ages. Pb-Pb ages from [1] and mineral separate isochron values of ^{26}Al/^{27}Al for angrites and the oldest eucrite, Asuka 881394 [2,3,4] (red squares and blue hexagons, resp.)

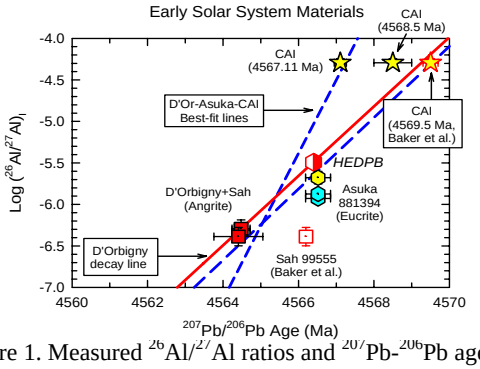

Figure 1. Measured ^{26}Al/^{27}Al ratios and ^{207}Pb-^{206}Pb ages in D'Orbigny, Sah99555, A881394, and CAI.

imply some heterogenity in ^{26}Al/^{27}Al between the Angrite Parent Body (APB), the HED Parent Body (HEDPB, i.e., Asteroid 4 Vesta?), and the Efremovka E60 CAI dated at ~4567.11 Ma [1]. This problem is relieved for the SIMS ^{26}Al/^{27}Al data for A881394 [5] (yellow hexagon), and more for the highest "model ^{26}Al/^{27}Al" calculated for eucrites by [6] (HEDPB, half-filled hexagaon). These data imply an age of ~4569.5 Ma [7] for the solar system.

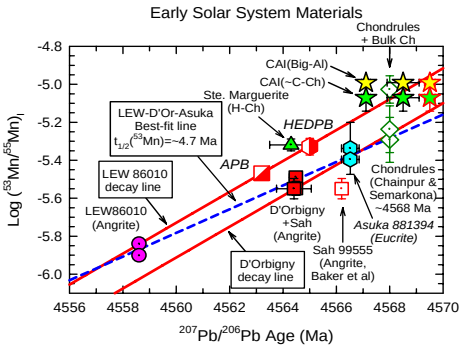

Figure 2. Measured ^{53}Mn/^{55}Mn ratios and ^{207}Pb/^{206}Pb ages in some early solar system materials. The Pb-Pb age for Ste. Marguerite are for ol and px residues [18].

Because of the longer halflife of ^{53}Mn, the "young" LEW86010 angrite can be included in Fig. 2. A curious feature of Fig. 2 is that the mineral isochron data for the two angrite groups and A881394 are collinear along a line corresponding to an apparent ^{53}Mn decay halflife of ~4.7 Ma.

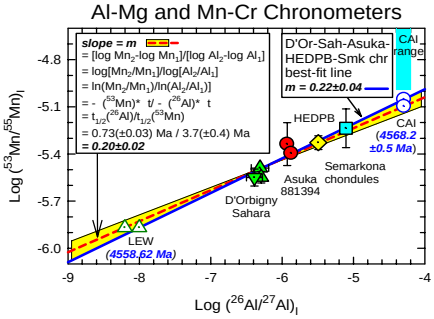

Figure 3. Al-Mg and Mn-Cr data for two angrites, the HEDPB, and Semarkkona chondrules.

Alternatively, a relative chronology from the short-lived chronometers can be anchored to the Pb-Pb age of a single reference. Fig. 3 shows Mn-Cr and Al-Mg data for D'Orbigny and Sah 99555, A881394, HEDPB, and Semarkona chronrules. The good linear correlation of these data allows an "absolute" age to be calculated for the time when the solar system had the canonical ^{26}Al/^{27}Al ratio relative to the initial ^{53}Mn/^{55}Mn and revised Pb-Pb age of LEW86010 [1]. The result obtained from the ^{53}Mn/^{55}Mn intercept of the best fit (blue line; slope = 0.22±0.04) averaged with that from a line of slope 0.20±0.02 calculated from the relative decay constatnts (red line) gives a "best estimate" of 4568.2±0.5 Ma for the solar system.

As shown in Fig. 4, the T_{LEW} Mn-Cr model ages

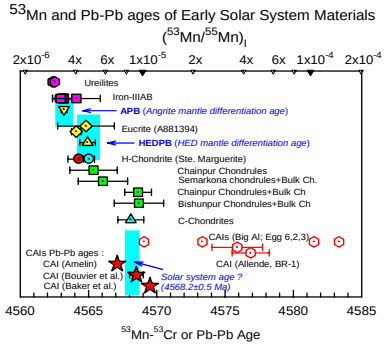

Figure 4. T_{LEW} ^{53}Mn/^{55}Mn ages and measured Pb-Pb ages (red symbols) in early solar system objects and materials.

for mantle differentiation of the APB and HEDPB are, respectively, ~4563 and ~4565 Ma. Mn-Cr model ages for other differentiated meteorites suggest similar time scales for differentiation of other asteroidal bodies (Fig. 4). Magmatic iron meteorites have unradiogenic $^{182}W/^{184}W$ ratios that are identical to or slightly below the initial $^{182}W/^{184}W$ of Allende CAIs [8]. $^{182}W/^{184}W$ of iron meteorites having short exposure times indicate that core formation in their parent bodies occurred < ~1 Ma after formation of CAIs [8].

Magmatism on the HEDPB: T_{LEW} Mn-Cr ages and zircon Pb-Pb ages (red circles, [9]) show that several eucrites crystallized as basaltic rocks within a few million years of differentiation of the HEDPB (Fig. 5). The Hf-W zircon age of A881388 [10] and the Hf-W mantle differentiaton age (Fig. 5) also suggest very early initiation of magmatism on the HEDPB.

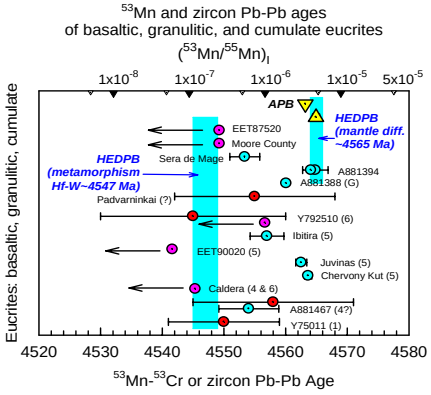

Figure 5. $^{53}Mn/^{55}Mn$ ages (rel. LEW86010) and zircon Pb-Pb ages [9] (red symbols).

Thermal Metamorphism on the HEDPB: Metamorphic grades based on the pyroxene equilibration criteria of [11] are shown in parentheses in Fig. 5. $^{53}Mn/^{55}Mn$ appears to have been completely equilibrated in the Type-6 eucrite, Y792510, for example. The zircon Pb-Pb age of this eucrite also hints at an age slightly lower than for the other eucrites. The time of thermal metamorphism inferred from Hf-W chonometry for 5 of 6 eucrites was 4547±2 Ma [12]. Upper limits to the Mn-Cr ages of most of the eucrites shown in Fig. 5 are consistent with reequilibration at that time. However, both the Mn-Cr and Hf-W zircon ages of EET90020 indicate later isotopic equilibration. Fig. 7 shows T_{LEW} model ages for ^{146}Sm-^{142}Nd data for some of the same eucrites included in Figs. 5 and 6. The longer halflife of ^{146}Sm allows the ^{146}Sm-^{142}Nd model age of 4484±26 Ma of EET90020 to be well-defined. The EET90020 age may be attributable to formation of a single large crater on the surface of 4

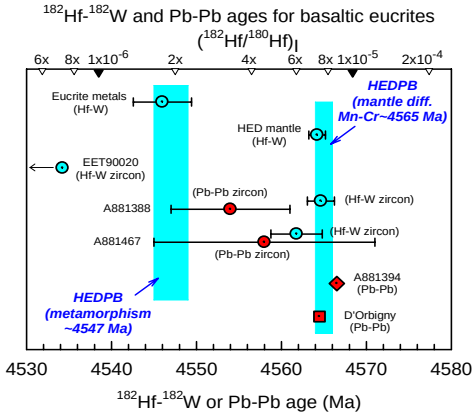

Figure 6. ^{182}Hf-^{182}W and Pb-Pb ages.

Vesta [13]. Other eucrites. may have been involved in the same event [14] (*cf*. Fig. 7).

Conclusions: Short-lived chronometers define a mostly-consistent chronology for events in the early solar system. An age of the solar system near 4569 Ma seems to be implied by combining Al-Mg and Mn-Cr data with available Pb-Pb data, but an age of 4568.2±0.5 Ma relative to 4558.62 Ma for LEW86010 [1] also can be derived from Al-Mg and Mn-Cr data. Space limitations preclude consideration here of the effect of additional asteroidal processes.

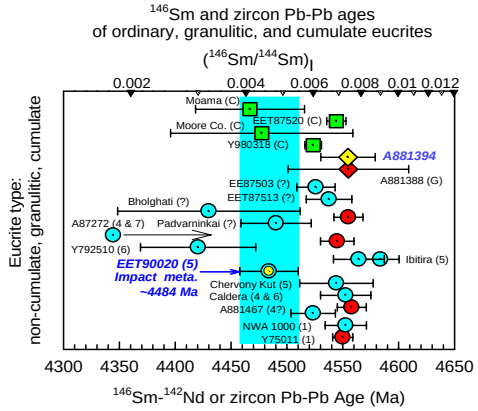

Acknowledgement: Data for figures from references [15-18].

References: [1] Amelin Y. (2007) *LPS XXXVIII*, Abstract #1669. [2] Nyquist L. et al. (2003) *EPSL 214*, 11-25. [3] Wadhwa M. et al. (2005) *LPS XXXVI*, Abstract #2126. [4] Spivak-Birndorf L. et al. (2005) *MAPS., 40*, A145. [5] Srinivasan G. et al. (2002) *LPS XXXIII*, Abstract #1489 [6] Bizzarro M. et al. (2005) *Ap. J.* 632, L41-L44. [7] Baker J. et al. (2005) *Nature* 436, 1127-1131. [8] Kleine T. et al. (2005) *GCA 69*, 5805-5818. [9] Misawa K. et al. (2005) *GCA 69*, 5847-5861. [10] Srinivasan G. et al. (2007) *Science 317*, 345-347. [11] Takeda H. and Graham A. L. (1991) *Meteoritics* 26, 129-134. [12] Kleine T. et al. (2005) *EPSL. 231*, 42-52. [13] Yamaguchi A. et al. (2001) *GCA 65*, 3577-3599. [14] Bogard D. and Garrison D. H. (2003) *MAPS 38*, 669-710. [15] Papanastassiou D. A. et al. (2005) *LPS XXXVI*, Abstract #2198. [16] Shukolyukov A. and Lugmair G. (2006) *EPSL 250*, 200-213. [17] Nyquist L. et al. (2001) *MAPS, 36*, 911-938. [18] Bouvier A. et al. (2007) *GCA 71*, 1583-1604.

Injection Mechanism of Short-Lived Radionuclides And Their Homogenization. N. Ouellette[1], S. J. Desch[2], M. Bizzarro[3], A. P. Boss[4], F. Ciesla[4], and B. Meyer[5] [1](Department of Physics, Arizona State University, Nicolas.Ouellette@asu.edu), [2](School of Earth and Space Exploration, Arizona State University). [3](Geological Institute, University of Copenhagen) [4](Department of Terrestrial Magnetism, Carnegie Institution of Washington) [5](Department of Physics & Astronomy, Clemson University)

Introduction: The presence of ^{60}Fe in the early Solar System strongly suggests the Solar System formed in close proximity to a supernova [1,2]. Besides ^{60}Fe, this supernova probably also injected other SLRs, too [3]. Matches to the meteoritic abundances are possible if the supernova injected SLRs into a molecular cloud core a few pc away, or into a protoplanetary disks a few x 0.1 pc away [3,4]. However the injection occurred, SLRs were homogeneously distributed by the time the first meteoritic solids formed [5], implying efficient mixing. Here we discuss mechanisms of SLR injection and mixing.

Meteoritic Evidence: In recent years, evidence from meteorites for the presence of many SLRs in the early solar system has been discovered. In addition to ^{60}Fe, the presence of ^{10}Be, ^{26}Al, ^{36}Cl, ^{41}Ca, ^{53}Mn, ^{107}Pd and ^{182}Hf has been confirmed [6]. Their initial solar system abundances [6] are given in Table 1; some bulk isotopic analyses suggest ^{26}Al/^{27}Al was initially as high as 6 x 10^{-5} [7]. All of these SLRs can be explained by injection from a supernova, except ^{10}Be which can be attributed to the trapping of ^{10}Be cosmic rays in the Sun's molecular cloud [8]. It has been proposed that ^{53}Mn and ^{182}Hf were also inherited from the Sun's molecular cloud [9], and either injection or inheritance could account for these isotopes. The presence of refractory inclusions devoid of ^{26}Al and ^{41}Ca suggests that the injection occurred after the first solids had already formed [10]; this has been dubbed the "late injection" scenario. In addition, recent work by Bizzarro et al. [11] suggests that ^{26}Al was well mixed in the presolar disk before ^{60}Fe was injected. Their ^{60}Fe-^{60}Ni isotope data show that most meteorites originating from differentiated planetesimals that accreted within 1 million years of the Solar System's formation have a lower ^{60}Ni/^{58}Ni ratio than samples from Earth, Mars and chondrite parent bodies. This indicates that the oldest planetesimals in the Solar System formed in the absence of ^{60}Fe, and that this isotope was injected within 1 million of the Solar System formation, when ^{26}Al was already homogeneously distributed.

Supernova Trigger: As supernovae are rare, a causal link must exist between the supernova and the birth of the Solar System. The "supernova trigger" model describes one possible link, wherein the shock wave from a supernova triggered the collapse of the presolar cloud [12]. The SLRs were injected when ejecta lagging the shock mixed into the presolar cloud via Rayleigh-Taylor fingers at the shock/cloud interface [13,14]. Computer simulations have shown that a range of shock speeds between 5 and 30 km/s are able to trigger the collapse of the disk and inject radioactive material in it without shredding the cloud.

Aerogel Model: The "aerogel model" describes a second possible link. Observations of star-forming regions such as the Orion Nebula, the Carina Nebula and NGC 6611 show protoplanetary disks commonly form within a few tenths of a parsec of massive stars doomed to explode as supernovae [15-17]. The ejecta of these supernovae, and the SLRs they contain, will hit the nearby protoplanetary disks. Previous work has shown that disks are not destroyed by the ejecta, even as close as 0.1 pc away [18]. Little gaseous ejecta makes it into the disk (~1% of the intercepted ejecta), but dust grains that condense out of the ejecta are efficiently injected. The majority of the SLRs will have condensed into such grains and enter the disk. Simulations show that > 90% of dust grains > 0.1 um, containing > 90% of the mass of SLRs, will penetrate to within 3 scale heights of the protoplanetary disk midplane [19,20]. Supernova dust grains penetrate and lodge in the disk in a manner reminiscent of how aerogel captures interplanetary dust particles.

Late injection: Both injection models described above are compatible with "late injection" of SLRs, after the first refractory solids form in the disk. In the supernova trigger model, there is a lag of a few x 10^4 yr between the compression of the presolar cloud core and the arrival of the SLRs behind the shock wave material [14]. This delay may be long enough for the first solids to form in a SLR-free environment. In the aerogel model, the disk has already formed when the SLRs arrive; hence there is ample opportunity for the first solids to form. The aerogel model is further compatible with a gap in time between injection of ^{26}Al and ^{60}Fe if the supernova progenitor was massive enough to enter a Wolf-Rayet phase before exploding [11]. During this phase, powerful winds from the star will eject large amounts of ^{26}Al (and possibly other SLRs like ^{41}Ca and ^{107}Pd); later, during the supernova proper, ^{60}Fe and other SLRs are injected

Mixing: The initial abundance of ^{26}Al/^{27}Al is taken to be ~4.5 x 10^{-5}, and thought to be homogeneous throughout the disk [5]. Meteoritical components with lower values are attributed to crystallization times a few Myr later, after some ^{26}Al has decayed. Neither of

the above two scenarios predicts an *initially* homogenous distribution of SLRs in the disk. In the supernova trigger model, the injection occurs via narrow Rayleigh-Taylor fingers, spiking the disk with SLRs non-uniformly, on 10-AU scales [14]. In the aerogel model, supernova ejecta explode non-isotropically, and injection is complicated by disk orientation. Even if the ejecta are isotropic and injected into a face-on disk, the final distribution of SLRs in the disk could not be homogeneous, because the column density of disk material is lower farther from the Sun. Hence the concentration of SLRs with respect to disk material will be higher in the outer parts. In either model, a mechanism must be present in the disk to rapidly homogenize the SLRs before the majority of the solids form. Computer simulations have shown that mixing in a marginally gravitationally unstable disk can transport and disperse SLRs within the disk. Although perfect homogeneity cannot be achieved throughout the disk, the dispersion approaches a value of ~10% on timescales of ~1000 yr [21]. In addition, SLRs injected at the surface of the disk, where the gas is easily ionized and unstable to the magnetorotational instability [22], may be mixed by turbulent diffusion. In this turbulent layer, marked by turbulent diffusivity $\nu = \alpha H^2 \Omega$ (where H is the disk scale height, Ω the orbital frequency and $\alpha \approx 0.01$), the injected dust grains can be mixed across the entire disk on timescales of only $r^2/\nu < (r/H)^2 \alpha^{-1} \Omega^{-1}$. Assuming $r/H \approx 10$, this is $< 10^5$ years at 20 - 30 AU. Other dynamical effects may also be important. As the radial pressure and density gradients vary with height above the midplane, differences arise in the rates at which materials are redistributed by large-scale flows associated with mass transport and gas drag [23]. These effects will further serve as a way of mixing freshly injected material both inward and outward within the disk [24].

Injected SLRs: A supernova has been well established as the source of ^{60}Fe [6]. However many other SLRs, like ^{26}Al, ^{36}Cl, ^{41}Ca and ^{53}Mn are formed in massive stars and ejected during their explosions. These isotopes would all be injected in the early Solar System, by direct dust injection or Rayleigh-Taylor fingers. Taking the ejecta of a 25 $M_\odot$ supernova from Woosley and Weaver [25] and mixing it into a "minimum-mass disk" [26], assuming a dilution ratio of ~1.7 x 10^{-7} (caused by either geometric dilution or mixing with the presolar cloud), enough SLRs are injected to explain the abundance of ^{60}Fe, ^{26}Al, ^{36}Cl, ^{41}Ca and ^{53}Mn (Table 1).

Some complications must however be considered in this simple injection model. First, the ratios from Table 1 assume the ejecta are well mixed during the supernova explosion, which will probably not be the case. Certain shells of the pre-supernova star should be sampled more than others, which would alter the predicted ratio. In addition, if there is a delay between the injection and the formation of the majority of the solids, the SLRs with the shorter half-lives, (e.g., ^{41}Ca and ^{36}Cl), will decay proportionally more than longer-lived ones (e.g., ^{60}Fe). Table 1 demonstrates nevertheless that a single supernova is capable of supplying the early Solar System with the meteoritic abundances of SLRs.

Ratio	Measured	Predicted
^{26}Al/^{27}Al	4.5×10^{-5}	4.4×10^{-5}
^{36}Cl/^{35}Cl	$1.4 - 3.0 \times 10^{-6}$	3.4×10^{-5}
^{41}Ca/^{40}Ca	1.5×10^{-8}	6.2×10^{-6}
^{53}Mn/^{55}Mn	1.4×10^{-5}	5.6×10^{-4}
^{60}Fe/^{56}Fe	$3 - 10 \times 10^{-7}$	3.7×10^{-7}

Table 1: Measured meteoritic ratios of various SLRs and the ratios expected when the average composition of the ejecta of a 25 $M_\odot$ supernova explodes isotropically and is injected into a "minimum-mass" protoplanetary disk [26].

References: [1] Hester J.J. et al. (2004) *Science 304*, 1116. [2] Hester J.J. & Desch S.J. (2005) in *Chondrites and the Protoplanetary Disk (CPPD)*, ASPC 348, 107. [3] Ouellette N. et al. (2005) *CPPD*, 527. [4] Looney L.W. et al. (2006) *ApJ, 652*, 1755. [5] MacPherson et al. (1995) *Meteoritics, 30*, 365. [6] Wadhwa et al. (2007) in *Protostars and Planets V*, 835. [7] Young, E et al. (2005) *Science* 308, 223. [8] Desch S.J. et al. (2004) *ApJ, 602*, 528. [9] Jacobsen, S (2005), *CPPD*, 548. [10] Sahijpal S. and Goswami J.N. (1998), *ApJ, 509*, 137. [11] Bizzarro M. et al. (2007), *Science, 316*, 1178. [12] Cameron A.G.W. and Truran J.W. 1977, *Icarus,* 30, 447. [13] Vanhala H.A.T. and Boss A.P. (2000) *ApJ, 538*, 911. [14] Vanhala H.A.T. and Boss A.P. (2002) *ApJ, 575*, 1144. [15] McCaughrean M.J. and O'Dell C.R. (1996) *AJ, 111*, 1977. [16] Smith N. et al. (2003) *ApJ, 587*,105. [17] Oliveira J.M. at al. (2007) in *Triggered Star Formation in a Turbulent ISM, 237*, 460. [18] Ouellette N. et al. (2007) *ApJ, 662*, 1268. [19] Hoppe P. et al. (2000) *MAPS 35*, 1157. [20] Amari S. et al. (1994) *GCA, 58*, 459. [21] Boss A.P. (2007) *ApJ, 660*, 1707. [22] Gammie C.F. (1996) *ApJ, 462*, 725. [23] Haghighipour N. and Boss A.P. (2003) *ApJ, 598*, 1301. [24] Ciesla F.J. and Cuzzi J.N. (2007) *LPSC 38, 1386* [25] Woosley S.E. and Weaver T. (1995) *ApJS, 101*, 181. [26] Hayashi C. (1985) in *Protostars and planets II*, 1100

OVERVIEW OF SHORT-LIVED NUCLIDES: THE ELUSIVE ROAD TO CONSISTENCY.

D. A. Papanastassiou, Science Division, Jet Propulsion Laboratory, Caltech, M/S 183-335, 4800 Oak Grove Drive, Pasadena, CA 91109-8099 (Dimitri.A.Papanastassiou@jpl.nasa.gov).

This workshop has been organized with planned, detailed presentations of specific parent-daughter systems, as well as with serious attempts to correlate the chronology extracted from individual systems, with the general aim of achieving a self-consistent chronology for the early solar system. There is a parallel effort to establish a set of consistent stellar production mechanisms and sources, to account for the introduction in the solar system of short-lived nuclides. However, there is a sufficiently wide range in mean lives among the various short-lived nuclides, that exponential decay intervals can wreak havoc with the implied production ratios and required number of diverse stellar sources.

The purpose of an introduction is to recognize the advances in the field as well as to remind us of the complexities of the individual parent-daughter systems. A driving force has been the attempt to define a consistent chronology. This driving force can be taken to extremes, where the desire for different systems to be concordant results in minimizing the importance of the complexities of individual systems and of limitations of specific data or of data on specific samples.

It is clear from a plethora of robust data that many short-lived parent nuclides were introduced (live) in the early solar system and that evidence for their existence has been preserved. It is less clear that a specific parent-daughter, short-lived system provides a well-defined chronology and it is much less clear that chronologies from different systems are correlated or can be considered to be consistent or "forced" into being consistent with judicious, rather than arbitrary choices.

The primary considerations are: a) Did the radioactive parent(s) get mixed uniformly, within the early solar system, prior to solid body formation, or at least in the regions of the solar system from where samples that are being dated originate? and b) Were the requirements met for internal isochron determinations, for individual parent-daughter systems and specific samples?

To a large extent, the answer to (a) is the last thing to determine, based on whether consistent chronologies can be defined. The requirements for (b) are an initial state of uniform isotopic compositions among coexisting mineral phases, with sufficient (chemical) dispersion in parent-daughter ratios. For multistage evolution, there may also be a correlation of initial isotopic compositions and time. If the analytical techniques involve leaching, the key question is whether the parent-daughter ratios of the leaches and/or residues preserve the parent daughter ratios of the mineral phases. If, for specific parent-daughter systems, there are only two minerals that dominate, then establishing the distinction between an internal isochron and a mixing line, with no time significance, becomes a serious concern, and especially so when leaching is used.

When it comes to leaching, the case of the U-Pb system is of paramount importance. This system allows the precise calculation of $^{207}Pb/^{206}Pb$ model ages as well the determination of more complex evolution. However, if all samples have to be leached to remove potential terrestrial contamination, the question becomes whether U-Pb ages on the residual samples are compromised. For example, if leaching removes 98% of the terrestrial contamination and 25% of the natural/radiogenic Pb, can a sensible age be obtained? If such ages are compromised, then the ability to establish concordant U-Pb ages becomes inherently limited. Should Pb-Pb ages be viewed as true ages, with the extremely high precision inherent in determining a model age, based on the intermediate mean life of ^{235}U, if U-Pb ages are not concordant? What processes would allow Pb-Pb ages to give a precise age (or ages) for refractory inclusions, when we know that the long-lived Sm-Nd and Rb-Sr systems are significantly disturbed? Clearly, a zero-age (very recent) disturbance for the U-Pb system is allowed, but the nature of the disturbance for meteorites observed to be falls is unclear as it is unclear why we should be so lucky.

When it comes to other systems, for refractory inclusions, we know (from ion microprobe work) that, for ^{26}Al-^{26}Mg individual mineral plagioclase grains show disturbances. What then is the meaning of the "canonical" $^{26}Al/^{27}Al$ initial ratio or of "super-canonical" ratios, obtained on bulk mineral separates? We also know that for ^{53}Mn-^{53}Cr, in Allende, the system is disturbed and that there is no correlation between Al-Mg and Mn-Cr ages. We also know that for individual inclusions when a ^{53}Mn-^{53}Cr age can be determined from coexisting spinel and pyroxene, the $^{54}Cr/^{52}Cr$ ratios of the same coexisting minerals are not uniform. This implies migration of Mn, Cr (and Fe) and would invalidate any internal isochron determination. For this system, the limitation of the measurements to only two mineral phases can definitely lead to mixing lines

which are not valid as isochrons. Similarly, for the Al-Mg system, because only limited attention has been paid to obtaining data on melilites, with sufficient precision, the internal isochrons are not necessarily robust. One should keep in mind that mixtures of two minerals can generally give collinear data and do not resolve the issue of a mixing line *vs*. an isochron with age significance.

These are but few of the considerations to keep in mind during the workshop and beyond. Such considerations may also help us temper the push for data and sample selection towards a consistent chronology for the early solar system.

And finally, a statement of caution about new and old techniques, when modern analytical improvements appear to result in highly improved precision at the ppm level. At this level, many interferences and artifacts that could be safely neglected at the 100 ppm (1 part in 10^4) level may become dominant. Similarly, chemical separation techniques which are adequate for thermal ionization techniques (with selective ionization conditions, for individual elements) may become totally inadequate for plasma ionization, with uniformly high ionization efficiency. These analytical issues reflect the importance and danger of living in "interesting times".

SJ101, A NEW FORSTERITE-BEARING CAI FROM THE ALLENDE CV3 CHONDRITE: SEM AND EPMA STUDIES. Michail I. Petaev[1,2] and Stein B. Jacobsen[1], [1]Department of Earth & Planetary Sciences, Harvard University and [2]Harvard-Smithsonian Center for Astrophysics, Cambridge MA 02138, USA.

Introduction: The forsterite-bearing Type B CAIs (FoBs) are rather rare but important members of the CV chondrite CAI's suite because of (1) their intermediate chemistry and mineralogy between the 'classic' CAIs and forsterite-rich AOA's and (2) rather high proportion of FUN CAIs among FoBs [1]. Only half a dozen FoBs are described in the literature [1] so far. In our recent search of the Allende CV3 chondrite for CAIs large enough for comprehensive petrologic, chemical, and isotopic studies [2] we found a large (6.34 g, ~2.5×1.5 cm), potato-shaped intact CAI labeled SJ101. The CAI was cut perpendicular to its longest axis into two pieces weighing 2.41 and 3.83 g. Here we report preliminary results of SEM and EPMA studies of a thick polished section made from the smaller piece. Isotopic measurements of the same CAI are discussed in the accompanying abstract [2].

Petrography and Mineralogy: The overall texture of SJ101 is shown in an Al X-ray mosaic of the CAI's complete cross-section (Fig. 1). SJ101 is dominated by an Al-rich spinel-clinopyroxene (Sp-Cpx) lithology which forms rather large, contorted islands separated by sinuous bands and/or pockets of a forsterite-clinopyroxene (Fo-Cpx) lithology. The inclusion lacks the Al-enriched mantle typical of other FoBs [1]. No 'classic' Wark-Lovering rim was observed so far. Instead, the peripheral portions of SJ101 contain rather large, discontinuous anhedral masses of spinel in a reaction relationship with the Al_2O_3-poor and SiO_2-rich (up to 55 wt.%) clinopyroxene which, in many cases, is in direct contact with the Allende matrix. No perovskite or hibonite was found in these spinel masses so far. The inclusion contains cavities and was cross-cut by several more or less straight cracks extended to its very periphery.

Both the Sp-Cpx and Fo-Cpx lithologies display igneous textures (Fig. 2A) with Sp and Fo being poikilitically enclosed in clinopyroxene. A few grain boundaries observed in BSE images of the Sp-Cpx lithology suggests that the Cpx is polycrystalline and rather coarse-grained; this may also be the case of the Fo-Cpx lithology. The boundary between these lithologies is rather smooth and gradational, suggestive of their interaction during a late melting episode.

In addition to spinel and clinopyroxene the Sp-Cpx lithology typically includes irregular patches of Al-poor melilite (Åk ~82) with poikilitic inclusions of spinel. The melilite is partially replaced by grossular-monticellite intergrowths. In a few occurrences anorthite laths were observed at the melilte-clinopyroxene interfaces (Fig. 2B). All three silicates contain numerous poikilitic spinel grains of the same habits. In general, the melilite-clinopyroxene relationships are consistent with the melilite being a relict of the precursor material rather then a product of co-crystallization with clinopyroxene.

Essentially each band or pocket of the Fo-Cpx lithology contains a rather large number of Ni-rich metal grains, with some of them being completely or partially replaced by magnetite.

Secondary alteration of SJ101 is rather minor. Secondary minerals observed so far include grossular, monticellite, magnetite, and a few grains of wollastonite and nepheline.

Mineral and bulk chemistry: The chemical compositions of all minerals except for Cpx are rather constant. Forsterite, spinel, anorthite, grossular, monticellite, and wollastonite are essentially pure end-members. Cpx shows a wide range of compositional variations apparently independent of lithology. Some elemental X-ray maps display polygonal areas with different Al contents consistent with the sector-zoning described in other FoBs [*e.g.*, 1,3,4]. In general, there are two compositional varieties of cpx with low and high concentrations of Al_2O_3 and TiO_2.

The bulk composition of SJ101, calculated by averaging 484 50-μm DBA spot analyses equally spaced along 4 traverses crossing the whole CAI, is as follows (wt%): SiO_2 35.90, TiO_2 0.96, Al_2O_3 24.86, Cr_2O_3 0.10, FeO 0.60, MgO 17.83, CaO 19.83, V_2O_3 0.08.

Discussion: Mineralogically and chemically SJ101 is a rather typical FoB [*e.g.*, 1,3,4]. The lack of an Al-rich mantle and the unfractionated Si isotopic composition [2] suggests that it is the only known FoB that did not experience substantial evaporation and, therefore, has retained its primary texture, mineralogy, and chemistry. The textural and mineralogical relationships between the Al-rich Sp-Cpx and Al-poor Fo-Cpx lithologies suggest that the latter formed by remelting of a forsterite and metal-rich precursor (AOA-like) that might represent accretionary rims around individual Sp-Cpx (Type B) CAIs. Such a scenario is consistent with the ideas expressed in [5].

References: [1] MacPherson G. J (2005) *Treatise on Geochemistry, vol. 1,* 201-246. [2] Jacobsen S. B. et al. (2007) *this volume*. [3] Wark D. A. et al. (1987) *GCA 51,* 607-622. [4] Davis A. M. et al. (1991) *GCA 55,* 621-637. [5] Bullock E. S. et al. (2007) *MAPS 42,* A26.

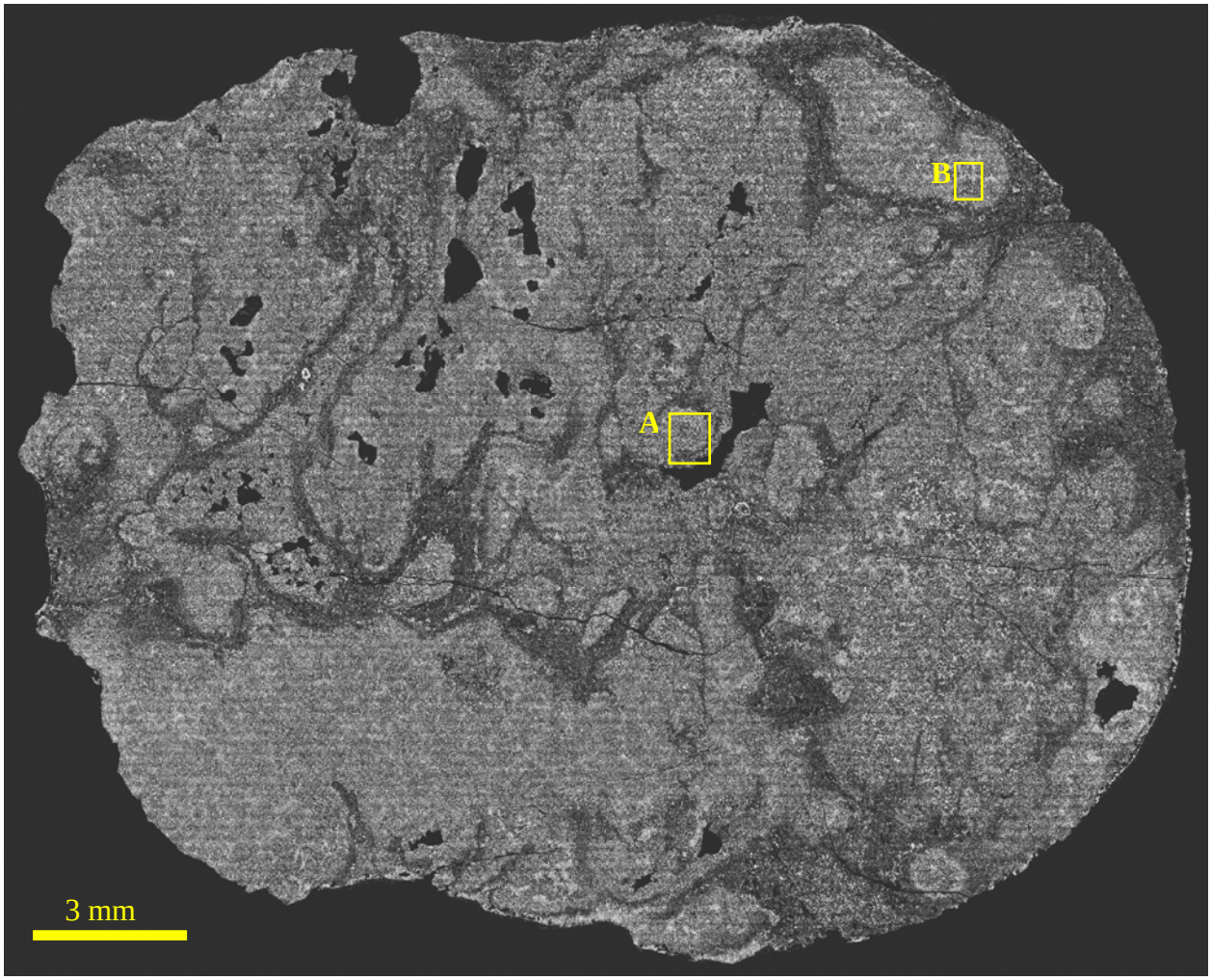

Fig. 1. Al X-ray map of SJ101. White - Al-rich Sp-Cpx lithology, gray - Al-poor Fo-Cpx lithology, black - epoxy. The horizontal streaking is an artifact of imperfect stitching of 14720 individual tiles.

Fig. 2. BSE images of areas A and B of Fig. 1 rotated 90° counterclockwise. Black – epoxy, tiny white spots – Fe,Ni metal. Dark gray are forsterite (small euhedral grains) and spinel (clusters of tiny grains). Light gray – melilite and its alteration products. Medium gray are clinopyroxene and anorthite (An, laths shown by arrows in B). White contour in A outlines Sp-Cpx lithology.

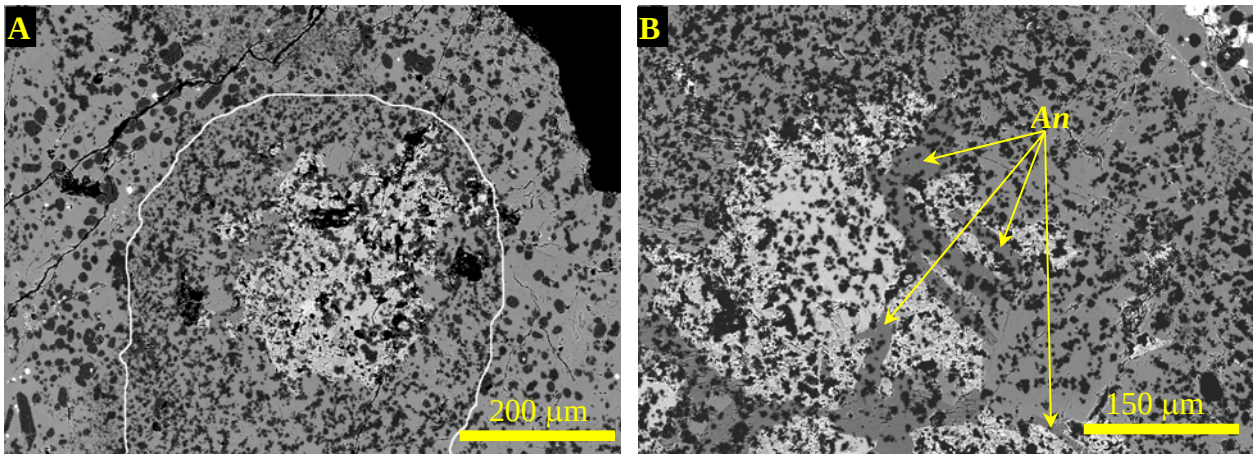

The I-Xe record of metamorphism in CO3 chondrites. O. V. Pravdivtseva[1], A. P. Meshik[1], C. M. Hohenberg[1], and A. N. Krot[2], McDonnell Center for the Space Sciences and Department of Physics, Washington University, St. Louis, MO 63130, USA, (olga@wuphys.wustl.edu). [2]Hawai'i Institute of Geophysics and Planetology, University of Hawai'i at Manoa, Honolulu, HI 96822, USA.

Introduction: McSween presented the first strong case that CO3 chondrites represent a metamorphic sequence [1]. It was demonstrated later that the matrix of CO3 chondrites changes markedly during metamorphism. With increasing petrologic type, the range of olivine composition decreases [2] as well as the mean fayalite content of matrix olivine [3]. Abundances of presolar grains also decrease systematically with increasing petrologic type [4, 5], while abundance of secondary nepheline in chondrules and CAIs increases.

Magnetite is one of the first alteration products formed in carbonaceous chondrites during aqueous alteration. Although CO3 chondrites mainly experienced changes induced by heating on the meteorite parent body over a long timescale, presence of phyllosilicates indicates that water must have played an important role in the alteration history of matrices of some CO3 chondrites. Thus magnetites in CO3 chondrites could provide a timeline for the metamorphic changes on their parent body.

Results: Here we present I-Xe data for 11 magnetite-rich samples from CO3 meteorites of different petrologic type (Table). Magnetites were chemically separated following the LiCl procedure developed by Lewis and Anders [6]. LiCl could potentially contaminate magnetite with iodine and after irradiation produce non-correlated ^{128}Xe and perhaps spurious I-Xe ages. To evaluate this possibility, in our previous work we separated magnetites from two aliquots of Orgueil using the LiCl procedure, one before and another after irradiation. Only the before procedure would affect the I-Xe age. Both samples yielded I-Xe ages that agree within experimental uncertainties [7], confirming that chemical separation could not compromise I-Xe system.

Each CO3 meteorite studied was finely ground and stirred with a saturated LiCl solution for 8 days at 60°C to remove possible silicate-magnetite intergrowth. After further separation in NaOH and washing [8], the samples were dried and weighted, small amounts of resulting separates were saved for the later study of the magnetites morphologies. The purity of resulting magnetite was confirmed for Lancé by x-ray diffraction analysis. For the Orgueil CI chondrite this chemical separation procedure previously yielded magnetic fractions that were at least 90% pure [6]. The abundances of magnetites in this set of samples differ by more than order of magnitude (Table) and do not correlate with meteorites petrologic type.

All samples had masses of less than 1 gram before the chemical separation. Thus, if magnetites were distributed heterogeneously in the matrices, it would be difficult to obtain representative magnetite abundances.

The magnetite samples were sealed under vacuum in separate fused quartz ampoules and irradiated with thermal neutrons in the package designated SLC-16 at the Missouri University Research Reactor along with Shallowater, the usual reference standard and irradiation monitor. Xenon isotopic compositions were measured in 9 samples.

I-Xe system in bulk samples of Felix (3.3), Ornans (3.4), Lance (3.5) and Warrenton (3.7) have been previously studied [9]. Relative I-Xe ages in these meteorites correlated with their metamorphic sequence with most metamorphosed Warrenton being "undatable owing to homogenization of radiogenic and trapped Xe" [9]. I-Xe isochrons were well defined and formed by temperature points starting from 1100 ºC, indicating one iodine host phase [9].

If magnetite were the major iodine carrier phase in previous studies of bulk meteorites, chemical separation would result in higher observed iodine concentrations. But this is not the case. Iodine concentrations in pure magnetites of Felix, Ornans, Lancé and Warrenton are ~ 4 – 8 times smaller than in bulk samples, indicating the presence of at least two iodine-host phases in these CO3 chondrites. Indeed, when results are presented as three-isotope plots ^{128}Xe/^{132}Xe versus ^{129}Xe/^{132}Xe, three meteorites Colony, Lancé and Y-82094 yield double isochrons, where the low-temperature correlation lines indicate later closures of the I-Xe system, than the lines formed by the high-temperature extraction steps. The low-temperature iodine host phase most probably is magnetite. Previous studies [6], as well as our three independent measurements of Orgueil magnetite (from different irradiations and measured few years apart) all produce isochrons starting from 1100-1200 ºC [7, 10]. The high-temperature iodine host phase is most likely pyroxene. ALHA 77307 (3.0) is known to contain enstatite grains that are probably primary [11]. If so, pyroxene is a major iodine-host phase, and is responsible for the isochrons in the bulk samples of Felix, Ornans and Lancé. Small addition of this phase in Lance magnetite separate, that is at least 90% iron oxide, could be re-

sponsible for the high-temperature isochron in this sample.

Iodine concentrations (Table, column 5) do not correlate with petrographic type of the CO3 meteorites studied, while the radiogenic ^{129}Xe content seems to decrease with increasing petrographic type.

I-Xe ages are shown in column 8 of the Table. Three meteorites Y-81020, Kainsaz and Y-790992 had all their ^{129*}Xe released in only one experimental point within 3σ of the ordinary chondrites (OC) value. Experimental points for the Warrenton magnetite all cluster within 1σ of OC point. I-Xe ages for bulk Felix, Ornans and Lancé are shown in column 7 relative to the Shallowater. Negative I-Xe age values indicate I-Xe closure after Shallowater (4563.2 ± 0.6 Ma [12]). Two magnetites, Felix and Ornans, yielded single correlation lines, although Felix I-Xe isochron is defined with somewhat lesser precision. Both I-Xe ages agree within experimental uncertainties with the previous I-Xe age data for the bulk samples [9].

Colony, Lance, and Y-82094 high-temperature isochrons are in good agreement with I-Xe ages for the bulk samples as well as with Felix and Ornans data reported here. Low-temperature correlation lines indicate later closure for the I-Xe system in less refractory magnetite phase in Colony, Lance and Y-82094, that seems to correlate with their petrographic type.

The I-Xe system in CO3 meteorites reflects a complex metamorphic history. At least two iodine-host phases are present in these meteorites. The refractory phase, most probably pyroxene, closed about 2 Ma later than Shallowater. The I-Xe system in low-temperature magnetite closed 12 Ma after Shallowater in 3.0 Colony, and ~30 Ma after Shallowater in 3.5 Lance and Y-82094.

References: [1] McSween H. Y. Jr. (1977) *Geochim. Cosmochim. Acta*, 41, 1777–1790. [2] Brearly A. J. and Jones R. H. (1998) In *Planetary Materials, Reviews* in Mineralogy, 36, 3–1 to 3–398. [3] Scott E. R. D. and Jones R. H. (1990) *Geochim. Cosmochim. Acta*, 54, 2485–2502. [4] Huss G. R. (1990) *Nature*, 347, 159–162. [5] Huss G. R. et al. (2003) *Geochim. Cosmochim. Acta*, 67, 4823–4848. [6] Lewis R. S. and Anders E. (1975) *Proc. Nat. Acad. Sci., V.72, 1*, 268–273. [7] Pravdivtseva O. V. et al. (2003) *LPSC XXXIV*, Abstract #1863. [8] Herzog G. F. et al. (1973) *Science 180*, 489-491. [9] Crabb J. et al. (1982) *Geochim. Cosmochim. Acta*, 46, 2511–2525. [10] Hohenberg C. M. et al. (2000) *Geochim. Cosmochim. Acta*, 64, 4257–4262. [11] Huss G. R. et al. (2006*) In: Meteorites and the Early Solar System*, Ed.Lauretta D. S., McSween H. Y. Jr., 587–586. [12] Gilmour J. D. et al. (2006) *Meteoritics & Planetary Science*, 41, 19–31.

Acknowledgements: Supported by NASA grants #NNG06GE84G and NAG5-11591.

CO3 meteorite, sample	type	Starting weight, mg	Separated magnetite %	Iodine >800 ºC ppb	^{129*}Xe ×10^{-12} cm^3 STP/g	I-Xe age Ma [9]	I-Xe age, Ma	
							High T	Low T
Y-81020,101	3.0	349	0.34	0.3	1.38		—	—
Colony	3.0	706	1.40	7.3	18.10		-6.1 ± 3.1	-12.3 ± 2.9
Kainsaz	3.2	691	0.98	28	7.34		—	—
Y-82050,115	3.2	384	0.10	*to be measured*				
Felix	3.3	500	0.97	6.8	15.9	1.2 ± 2.1	-2.0 ± 1.5	
Ornans	3.4	556	0.40	14	47.1	-1.0 ± 0.7	-1.3 ± 0.5	
Y-790992,80	3.5	369	0.12	294	11.4		—	—
Lancé	3.5	531	0.14	10	7.07	-4.0 ± 1.9	-6.7 ± 6.0	~ -28
Y-82094,110	3.5	446	0.82	21	1.10		-2.2 ± 3.6	~ -30
ALHA77003,117	3.6	445	0.91	*to be measured*				
Warrenton	3.7	320	1.76	9.3	4.56	—	—	—

INTERCALIBRATION OF SHORT-LIVED AND LONG-LIVED CHRONOMETERS BASED ON ANGRITES AND CB, CR CHONDRITES. G. Quitté[1] and A. Markowski[2], [1]Laboratoire de Sciences de la Terre, CNRS-ENS Lyon-Université de Lyon, France (Ghylaine.Quitte@ens-lyon.fr), [2]IGMR, ETH Zurich, Switzerland.

Introduction: While different short-lived chronometers are commonly used to refine the chronology of the earliest events in the solar system, a clear intercalibration of all those systems is still missing despite recent efforts in this field. The best samples that can be used as anchor for a possible intercalibration are those that formed early, from an isotopically homogeneous reservoir, cooled quickly and remained afterwards undisturbed so that all chronometers closed at the same time even if they do not date the same event or have different closure temperatures. Refractory inclusions were possibly the most obvious choice to intercalibrate chronometers. They have been successfully used to map ^{26}Al-^{26}Mg and ^{182}Hf-^{182}W ages onto an absolute timescale as defined by Pb-Pb but revealed unsuitable for ^{53}Mn-^{53}Cr and probaby also ^{60}Fe-^{60}Ni due to the presence of nucleosynthetic anomalies and/or heterogeneity of the parent isotopes. Three other possible anchors are represented by angrites, chondrules and metal nuggets from metal-rich CR and CB chondrites. Angrites are among the earliest igneous rocks that formed in the solar system and they cooled rapidly. CBs are also of great interest: indeed, if they crystallized from an impact-melt as suggested by Krot et al. [1], all chondrules as well as the metal formed at the same time. Determining the ^{53}Mn-^{53}Cr , ^{182}Hf-^{182}W and ^{60}Fe-^{60}Ni age of these objects may then make it possible to map these chronometers and to anchor them onto an absolute timescale.

Angrites: The intercalibration of chronometers based on angrites has been undertaken for several years in different laboratories. For instance, the precise ^{207}Pb-^{206}Pb age of 4557.8±0.5 Ma for the angrite LEW 86010 [2] in conjunction with its initial ^{53}Mn/^{53}Mn [3-6] has been used to obtain absolute Mn-Cr ages. Similarly, the ^{207}Pb-^{206}Pb age of angrite SAH 99555 has been used to infer absolute ages based on ^{26}Al-^{26}Mg chronometry [7]. To expand the intercalibration to other isotopic systems, we recently completed a detailed ^{182}Hf-^{182}W and ^{60}Fe-^{60}Ni study of three angrites (Sahara 99555, D'Orbigny, Northwest Africa 2999). Different mineral fractions were separated by hand-picking and sieving. Tungsten and nickel were then extracted from the matrix using a multi-step procedure on ion-exchange resins. Isotopic measurements were finally performed using a MC-ICPMS (Nu Plasma instrument).

^{182}Hf-^{182}W systematics. Data obtained for SAH 99555 plot on a well-defined Hf-W isochron, with a ^{182}Hf/^{180}Hf of $(7.2\pm0.2) \times 10^{-5}$ and an initial of -2.2 ± 0.2 ε_W [8]. Similarly, fractions from D'Orbigny and NWA 2999 also define Hf-W isochrons with slopes of $(7.5\pm0.8)\times10^{-5}$ and $(5.1\pm1.2)\text{x}10^{-5}$, respectively. SAH 99555 and D'Orbigny thus formed at roughly the same time, ~5 Ma after CAIs, while NWA2999 formed ~5 Ma later according to the Hf-W systematics [8]. The ^{182}Hf-^{182}W ages are consistent with most of the other chronological data for angrites. At high chronological precision, the ^{182}Hf-^{182}W data are in excellent agreement with some ^{26}Al-^{26}Mg and ^{53}Mn-^{53}Cr data, even if slight discrepancies exist in the Mn-Cr and Al-Mg data reported from different laboratories resulting in uncertainties in the intercalibration of the three chronometers. The coherent chronology for quenched and slowly cooled angrites obtained from ^{182}Hf-^{182}W, ^{53}Mn-^{53}Cr and ^{26}Al-^{26}Mg systematics, and the consistency of these ages with most ^{207}Pb-^{206}Pb ages, provide nonetheless compelling evidence that this chronometry is accurate and that angrites are a good anchor for these isotopic systems.

^{60}Fe-^{60}Ni systematics. The picture is more complex for the ^{60}Fe-^{60}Ni chronometer. NWA 2999 shows no resolvable Ni isotopic anomaly while the Fe/Ni of the different fractions spreads up to ~80. As this meteorite belongs to the slowly cooled angrite group, it is supposed to have formed ~10 Ma after the start of the solar system and the expected excesses may not be detected. In this respect, the Fe-Ni data are not incompatible with the other chronometers [9] and the results are inconclusive as far as the intercalibration is concerned. In SAH 99555, only the pyroxene separate has a slight ^{60}Ni* excess for a Fe/Ni of about 15000. This excess is much smaller than the ex-

pected anomaly if the meteorite formed ~5 Ma after the start of the solar system as inferred from other chronometers, taking a value of 10^{-6} as the initial $^{60}Fe/^{56}Fe$ of the solar system [10]. The different mineral fractions in D'Orbigny plot on a regression line in a ε_{Ni} vs. Fe/Ni diagram with a slope of $(8.0\pm2.6)\times10^{-9}$ and an initial of -1.2 ± 0.6 ε_{Ni}. If this line is interpreted as an isochron, the Fe-Ni age of D'Orbigny is 10.4 Ma after CAIs, in disagreement with the other chronometers. To sum up, Ni isotopic data in angrites indicate that only very small amounts of live ^{60}Fe were present when these meteorites formed. As Ni data are inconsistent for the three angrites studied here and also disagree with Al-Mg, Mn-Cr, Hf-W and Pb-Pb results, it is clear that the ^{60}Fe-^{60}Ni system cannot be intercalibrated with other chronometers nor anchored onto an absolute timescale using angrites. In fact, if we consider these data together with other Ni data ([9] and references therein), it looks like ^{60}Fe was probably heterogeneously distributed in the early solar system and that the ^{60}Fe-^{60}Ni cannot be used as an ubiquitous reliable chronometer. To check this hypothesis and to look for a second anchor to intercalibrate chronometers, we decided to study metal-rich chondrites.

Metal-rich chondrites: Together with CH chondrites, CBs and CRs belong to the CR clan whose members are among the most pristine early solar system materials. As such, they can be very helpful to intercalibrate chronometers. These meteorites contain abundant free metal in the form of iron-nickel and iron sulfides. Contrary to angrites, they formed in a reduced environment and contain reduced silicates. CRs are primitive chondrites that largely escaped thermal processing in the asteroidal setting but were subjected to the process of aqueous alteration. Hence anchoring the ^{182}Hf-^{182}W to the other chronometers should be possible but the ^{60}Fe-^{60}Ni system may be disturbed. CBs are probably a better choice for our purpose: they are characterized by large (mm-sized) metal globules which will permit to precisely constrain the initial of a potential isochron and all belong to petrologic type 3 which means they are not altered. CBs experienced thermal processing as they are thought to be issued from impact melting in a planetary environment [11], but this formation process makes them an excellent choice as an anchor since all isotopic systems were reset at the same time.

Two CRs (NWA 721 and NWA 801) and five CBs (Gujba, Bencubbin, GRO 95551, MIL 05082, PCA 91452) were selected for this study. MIL 05082 resembles Gujba and contains very large chondrules (several mm-size). It it thus one of the best sample to get very precise Ni data as the available amount of silicate material is relatively large. Among the three paired meteorites (PCA 91467, PCA 91452 and PCA 91328), PCA 91452 is less weathered. As Ni is highly mobile, it is highly preferable to study the least weathered sample.

Absolute Pb-Pb ages already exist for some of these samples and will be determined for the others. Tungsten and nickel isotopic measurements are currently under progress; the results will be discussed at the workshop.

References: [1] Krot A. et al. (2005) *Nature, 436,* 989-992. [2] Lugmair G. W. and Galer S. J. G. (1992) *GCA, 56,* 1673-1694. [3] Lugmair G. W. and Shukolyukov A. (1998) *GCA, 62,* 2863-2886. [4] Nyquist L. et al. (2003) *LPS XXXIV,* Abstract #1388. [5] Glavin D.P. et al. (2004) *MAPS, 39,* 693-700. [6] Sugiura N. et al. (2005) *Earth Planet. Space, 57,* E13-E16. [7] Baker J.A. et al. (2005) *Nature, 436,* 1127-1131. [8] Markowski A. et al. (2007) *EPSL,* in press, doi: 10.1016/j.epsl.2007.07.035. [9] Quitté G. et al. (2007) *LPS XXXVIII,* Abstract #1900. [10] Mostefaoui S. et al. (2005) *ApJ, 625,* 271-277. [11] Krot A.N. et al. (2005) *Nature, 436,* 989–992.

Acknowledgments: We would like to tank M. Bizzarro, T. Irving, M. Wadhwa, Y. Amelin, the NASA and the MNHN Paris for kindly providing the samples and I. Ivanov for the careful mineral separation.

P-PROCESS SAMARIUM ISOTOPES IN SOLAR SYSTEM MATERIALS: IMPLICATIONS FOR THE ^{146}Sm-^{142}Nd CHRONOMETER. M. C. Ranen[1] and S. B. Jacobsen[1], [1]Dept. of Earth and Planet. Sci., Harvard Univ., 20 Oxford St., Cambridge, MA 02138 (ranen@fas.harvard.edu).

Introduction: The Sm-Nd system is one of the most powerful tools for constraining Solar System processes. Sm has two radioactive isotopes, the long lived ^{147}Sm which decays to ^{143}Nd with a half life of 106 Ga and the now extinct ^{146}Sm which decayed to ^{142}Nd with a half life of 106 Ma. Coupling these two systems can enable the ^{147}Sm-^{143}Nd to give a precise age as well as a tracer for Sm/Nd fractionation while ^{142}Nd/^{144}Nd variations can trace early silicate differentiation. In order to use radioisotope systems to compare fractionation processes in the solar nebula and on planetary bodies it is imperative to know the initial conditions for the object as well as to know bulk reference values. Ideally the initial conditions for all Solar System bodies will be equal. Small variations in initial conditions of either the ^{143}Nd/^{144}Nd ratio or the Sm/Nd ratio will not affect our interpretation of the ^{147}Sm-^{143}Nd system since differences in ^{143}Nd/^{144}Nd are usually large enough (>1ε) that small uncertainties (<50 ppm) in Sm/Nd or initial ^{143}Nd/^{144}Nd are trivial. However, variations seen in the ^{142}Nd/^{144}Nd ratio in terrestrial rocks (the Isua supracrustal belt in Greenland [1]) and differences between different classes of meteorites and the Earth [2] are all less than 50 ppm. In order to interpret the cause of these variations as Sm/Nd fractionation and subsequent decay of ^{146}Sm while it was still alive it is necessary to be certain that the Earth and all planetary bodies had both the same initial ^{142}Nd/^{144}Nd ratios and the same ^{146}Sm/^{144}Sm ratios. Here we examine the initial ^{146}Sm/^{144}Sm ratio of the Solar System, whether this ratio is homogenous throughout the Solar System, how heterogeneities could originate, and finally what these variations in ^{146}Sm/^{144}Sm mean for interpretation of the ^{142}Nd/^{144}Nd ratio.

Nucleosynthetic Components: Most isotopes of heavy elements are made by the s-process (slow neutron capture in an Asymptotic Giant Branch star) or the r-process (rapid neutron capture associated with a supernovae explosion. Another smaller process also associated with a supernova is the p-process which is thought to occur through photo-disintegration reactions. These p-process isotopes are enriched in protons unlike the r- and s-process isotopes. Sm has 7 isotopes, 1 that is p-only (144), 2 s-only (148,150), 1 r-only (154) and 3 having contributions from both the r- and s-process (147,149,152). The now extinct ^{146}Sm was also a p-only isotope. ^{149}Sm and ^{150}Sm both have high neutron capture cross sections and their composition in an object is influenced by the neutron fluence received.

Estimating initial ^{146}Sm/^{144}Sm ratio: ^{146}Sm has been proven to be live during the formation of the Solar System in a number of different meteorites including primitive meteorites such as carbonaceous chondrites as well as in various classes of differentiated meteorites including basaltic meteorites such as the eucrites. Table 1 lists a compilation of coupled ^{146,147}Sm-^{142,143}Nd data for a variety of meteorites [3-9]. The most recent high resolution ^{207}Pb-^{206}Pb ages of CAIs give an age of the Solar System to be 4.567 Ga [10]. All meteorite ^{146}Sm/^{144}Sm ratios were back calculated to an age of 4.567 Ga by using the formula $(^{146}Sm/^{144}Sm)_o = (^{146}Sm/^{144}Sm)_{CHUR,t}e^{\lambda 146 t}$. Each sample shows evidence for live ^{146}Sm in the solar system. The only ancient meteorite that had no live ^{146}Sm at the time of closure is D'Orbigny, a relatively newly found angrite [11]. Figure 1 graphically presents these data along with model ^{146}Sm evolution curves for initial Solar System ^{146}Sm/^{144}Sm values of 0.007 – 0.011 at 4.567 Ga. There is wide scatter in these data but it appears that the average ^{146}Sm/^{144}Sm value is at least 0.009 at 4.567 Ga. This is in contrast with [2,12] who both cite a value of 0.008.

P-process heterogeneities: [12] measured all isotopes of Sm in a variety of planetary bodies. in two carbonaceous chondrites studied, Murchison and Allende, they found an average deficit of 118 ppm in the ^{144}Sm/^{154}Sm ratio compared to the terrestrial upper mantle. This will lower the ^{146}Sm/^{144}Sm ratio in carbonaceous chondrites by 1-2% by changing the ^{146}Sm/^{144}Sm production ratio. No deficits in ^{144}Sm were found in an ordinary chondrite and a eucrite studied. This study concluded that r- and s-process isotopes in Sm were homogenously distributed. Somehow the p-process must have become decoupled from the r-process even though both nucleosynthetic processes are believed to take place in a supernova.

Implications for ^{142}Nd/^{144}Nd: [2] found deficits in the ^{142}Nd/^{144}Nd ratio compared to the terrestrial upper mantle in a variety of planetary materials, with the larger differences being seen in carbonaceous chondrites. [13] also noticed this difference and suggested four possible reasons. (i) nuclear variation of initial ^{142}Nd/^{144}Nd; (ii) nuclear variation of (^{146}Sm/^{144}Sm); (iii) variation in Sm/Nd; and (iv) radiogenic evolution

of $^{142}Nd/^{144}Nd$ in an Sm/Nd-fractionated "parental" reservoir before ^{146}Sm is extinct. [2] focuses on possibility (iv) concluding that the Earth had a very early silicate differentiation where an early enriched reservoir and an early depleted reservoir were formed prior to the Moon forming impact. [12] shows that the p-process heterogeneities seen in Sm isotopes of carbonaceous chondrites compared to Earth will affect the $^{142}Nd/^{144}Nd$ ratio. Figure 2 presents two scenarios that could explain the differences in $^{142}Nd/^{144}Nd$ seen in the literature. Fig. 2a assumes constant $^{146}Sm/^{144}Nd$ of 0.009 but with a 50 ppm difference in initial $^{142}Nd/^{144}Nd$. Fig. 2b presents $^{142}Nd/^{144}Nd$ evolution assuming that there is a range of initial $^{146}Sm/^{144}Nd$ values from 0.007-0.011. This allows for a difference in $^{142}Nd/^{144}Nd$ of 140 ppm. We know that there is a real variation in $^{142}Nd/^{144}Nd$ of up to 50 ppm. Figure 2 shows that the variation can be explained by either the uncertainties in the initial $^{146}Sm/^{144}Sm$ ratio or by incomplete mixing of ^{142}Nd in the solar nebula. In spite of large possible variations of 20% in ^{146}Sm, it appears to still be the best mixed of all extinct nuclides (more variation is seen in ^{26}Al for ex.). For a precise chronometry to be valid at the 5 ppm level in $^{142}Nd/^{144}Nd$ it is necessary to know $^{146}Sm/^{144}Sm$ to within an uncertainty of 1.4%. Currently there is a 20% spread in this ratio. We need new and better data to help constrain what the initial $^{146}Sm/^{144}Sm$ ratio of the Solar System was and whether or not these p-process nuclides were heterogeneously distributed.

Table 1. Compilation of Meteorite data

meteorite	Age (Ga)	$(^{146}Sm/^{144}Sm)_i$	$^{146}Sm/^{144}Sm$ at 4.567 Ga	Ref.
Divnoe	4.62	0.0116±16	0.0116	[3]
Caddo IAB	4.53	0.0086±21	0.0110	[4]
Acapulco	4.6	0.0067±19	0.0067	[5]
Ibitra	4.46	0.009±10	0.0185	[5]
Morristown	4.47	0.0075±11	0.0144	[5]
ADOR	4.56	0.0118±32	0.0119	[6]
V.M. Pebble 12	4.48	0.0058±15	0.0104	[7]
V.M Pebble 16	4.48	0.0059±4	0.0106	[7]
V.M Pebble 5	4.42	0.0042±17	0.0113	[7]
Mt. Padbury	4.52	0.0056±9	0.0077	[7]
Caldera	4.54	0.0075±10	0.0088	[8]
Moama	4.46	.0041 ± 13	.0084	[6]
LEW	4.553	0.0071 ± 17	.0078	[9]

References: [1] Harper C.L. and Jacobsen S.B. (1992) *Nature, 360*, 728-733. [2] Boyet M. and Carlson R.W. (1995) *Science, 309*, 576-581. [3] Bogdanovski O. and Jagoutz E. (1996) *LPS XXVII*, 129-130. [4] Stewart B. et al. (1996) *EPSL, 143*, 1-12. [5] Prinzhofer A. et al. (1992) *GCA, 56*, 797-815. [6] Jacobsen S.B. and Wasserburg G.J. (1984) *EPSL, 67*, 137-150. [7] Stewart B.W. et al. (1994) *GCA, 58*, 3487-3509. [8] Wadhwa M. and Lugmair G.W. (1995) *MAPS, 30*, 592. [9] Lugmair G.W. and Galer S.J.G. (1992) *GCA, 56*, 1673-1694. [10] Amelin Y. et al. (2002) *Science, 297*, 1678-1683. [11] Tonui E.K. et al. (2003) *LPS XXIV*, Abstract #1812. [12] Andreasen R. and Sharma M. (2006) *Science, 314*, 806-809. [13] Harper C.L. and Jacobsen S.B. (1993) *LPS XXIV*, 607-608.

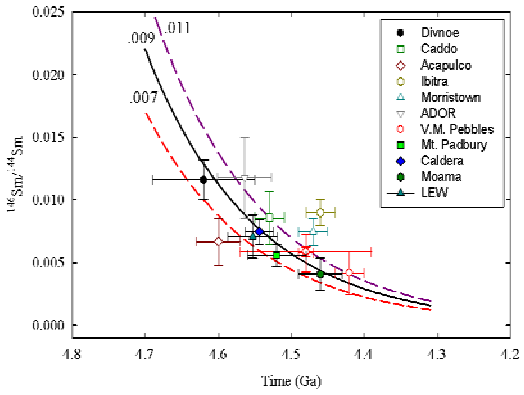

Fig. 1

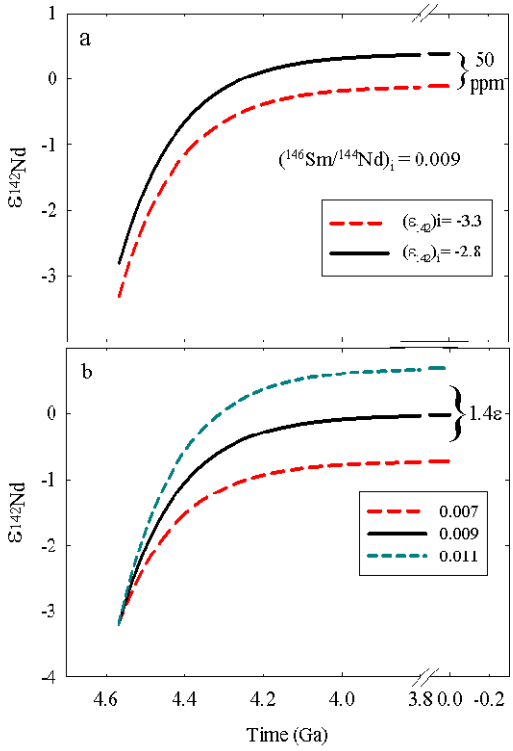

Fig. 2

Outstanding issues with respect to the timing of differentiation and mantle oxidation: a comparative planetology perspective – Earth, Mars and 4 Vesta. K. Righter[1], [1]NASA Johnson Space Center, Mailcode KT, 2101 NASA Pkwy., Houston, TX 77058; kevin.righter-1@nasa.gov.

Introduction: Detailed chronologic and petrologic information available for Earth, Mars and Vesta reveal several outstanding problems concerning our understanding of their formation. This contribution aims to define what we know for each body, compare the similarities and differences and suggest future pathways for resolution. In particular, focus will be on the timing and mechanisms for mantle oxidation.

4 Vesta: The HED clan of achondrites is most likely from asteroid 4 Vesta or a similar differentiated body [1]. As such we have samples of a small, dry, ancient planetsesimal in our collections. This small body should have a straightforward explanation given the simple array of factors controlling its formation. Nonetheless, many aspects remain elusive. A satisfactory explanation for depletion of volatile elements in the HED parent body/Vesta does not yet exist. New timing constraints on the differentiation of the HED parent body have requiring re-thinking the origin of the body. Petrogenetic scenarios are based on just a few low pressure phase equilibria; more experimental constraints would be useful. Recent discoveries have shown that there may be multiple parent bodies for the HED clan. And finally, the origin of this small body cannot be modeled adequately, even despite its simplicity; a model that includes metal and silicate together is not yet available. Clearly there are many aspects to the origin and evolution of the HED parent body that remain to be studied.

With respect to mantle oxidation state, we have a conundrum that core formation models result in conditions of IW-2.5, but basalt melting models require conditions of IW-1. When and how did the oxidation take place?

Mars

Based on studies of Martian meteorites, we know that Mars differentiated early, faster than Earth, but slower than Vesta. And we also know that the meteorites record evidence of several Martian interior reservoirs [2].

Calculations of fO_2 in the Martian meteorites result in a 5 log fO_2 unit range in values relative to the FMQ buffer (Fig. 1). In the absence of plate tectonics and recycling mechanisms, oxidation of the mantle is difficult to explain. However, if graphite is present in a planetary mantle, the effect of pressure on C-CO-CO_2-CH_4 equilibria is such that oxygen fugacity would become very high as pressure increases. Given the range of fO_2 estimates for martian meteorites, it is worthwhile considering whether this could be achieved by polybaric C-CO-CO_2-CH_4 equilibria in the martian mantle. Only 40-80 ppm C is required to keep peridotite mantle buffered at the C-O surface. Indeed, studies of Martian meteorites have shown that Mars is a volatile-rich planet, and C may be an important constituent of the volatile budget. If C buffering at variable pressure is controlling oxygen fugacity in the Martian mantle, it would require formation of ALH84001 at lowest pressures, shergottites at intermediate pressures, and nakhlite and Chassigny parent melt formation at high pressures, all of which is consistent with what we know.

Earth: Earth accreted the slowest of all planets studied, between 20 and 45 Ma after T_0. In addition, the terrestrial mantle is much more oxidized than the conditions at which the core separated (Fig. 1). Earth is different from Vesta and Mars in that its internal heat has provided driving energy for vigorous mantle convection and associated plate tectonic on the surface. As a result the Earth's mantle has had plenty of time and opportunity for transformation over time. No secular changes in mantle redox state have been detected, but there is ~300 Ma of missing rock record for Earth, so it is not clear on what timeframe mantle oxidation could have occurred. A recent suggestion that Earth's mantle was oxidized by the breakdown of MgFe perovskite to Fe^{3+} and Fe metal [3] is an interesting solution to this old problem, but is not without additional questions. Mars is just as oxidized as Earth (maybe even more so), but MgFe perovskite (small or non-existent in the martian mantle) is not available for oxidation in the Martian mantle.

Discussion

A viable mechanism for oxidation of the Martian mantle remains elusive; water as an oxidant is possible, but there is not much water available from the interior given what we know from Martian meteorite samples, and the stability of hydrous phases. An alternative explanation is that the Martian mantle is buffered by C-CO-CO_2 equilibria, and the broad range is caused by normal magmatic polybaric processes in the deep and shallow mantle. If this works for Mars, then why couldn't it for Earth? An elaborate MgFe

perovskite dissociation mechanism may be unnecessary for the Earth as well.

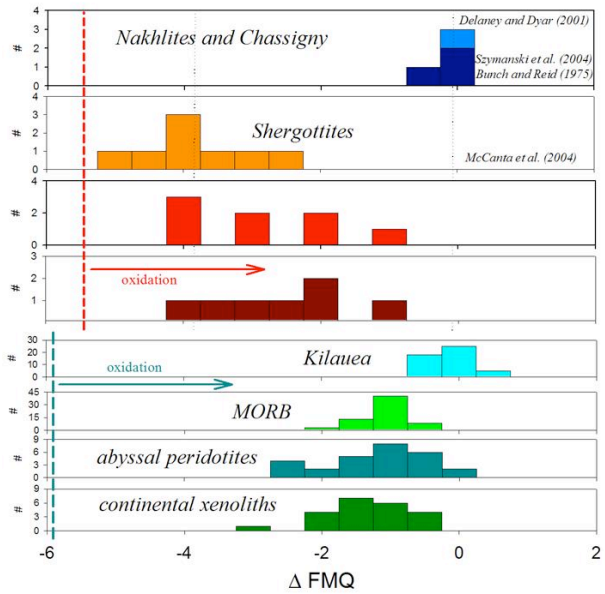

Figure 1: (Top) Histogram of Martian meteorite values of oxygen fugacity compared to the conditions proposed for Martian core formation (dashed red vertical line). (Bottom) histogram of terrestrial sample values of oxygen fugacity compared to the conditions proposed for terrestrial core formation (dashed vertical green line). A similar relation exists for samples from the HED parent body (or 4 Vesta).

References:

[1] Drake, M.J. (2001) MAPS 36, 501.

[2] Righter, K. (2007) 31st Antarctic Meteorite Symposium (NIPR, Tokyo) meeting abstract.

[3] Frost, D. J. et al. (2004) Nature 428, 409–412.

THE NATURE OF THE MASSIVE STAR THAT COULD HAVE INJECTED ^{26}AL IN THE EARLY SOLAR SYSTEM. S. Sahijpal and G. Gupta, Department of Physics, Panjab University, Chandigarh, 160014, India (sandeep@pu.ac.in)

Introduction: We make an assessment of the irradiation contributions of the now extinct ^{26}Al and other short-lived nuclides (SLRs) to the early solar system (ESS) within the X-wind irradiation formulation. Furthermore, we explore the nature of the massive star that probably synthesized the bulk inventory of the ^{26}Al.

Numerical simulations: Based on the numerical code of the irradiation of protoCAIs in the magnetic reconnection ring within the X-wind irradiation formulation [1] along with the recent refinements [2], we present the results of the various simulations with a wide range of parameters (fig. 1). Within the framework of the numerous physico-chemical processes operating in the reconnection ring over the repeated x-wind cycles and the wide range of parameters it would be difficult to obtain the canonical value of ^{26}Al/^{27}Al along with the yields of other SLRs in a self consistent manner. In case the gradual flares dominated the early solar system as in the case of modern sun, we anticipate ~1% X-wind irradiation contribution to the initial ^{26}Al to match the requisite amount of ^{10}Be. A massive star probably contributed the bulk [2,3]. We now make an attempt to understand the environment associated with the formation of the massive star and the solar system.

The astrophysical settings: Stars are mostly formed in embedded stellar clusters [4-6]. Whether a cluster of low-mass stars alone (e.g., the Taurus-Auriga complex) or a cluster of low-mass and massive stars together (OB associations, e.g., the Trapezium cluster) is formed depends primarily upon the cluster mass [5]. In a broad sense, two distinct astrophysical settings can be envisaged that can lead to the contribution of SLRs by a massive star to the ESS: **Case A)** the massive star and the solar system were formed in the same cluster [e.g., 6], **Case B)** the two were formed either in the different regions of the molecular cloud or in distinct stellar clusters, e.g., the Scorpius-Centaurus complex [7].

Case A: There need not be any casual relationship between the formation of the massive star and the formation of the solar system in this scenario. Apart from the hypothesis that the ionizing front and winds from the massive star can trigger low-mass star formation, an alternative hypothesis also requires discussion. It is quite likely that within a cluster the formation of low-mass stars occur spontaneously as a result of local density fluctuations in the self gravitationally contracting pre-cluster cores [5,7]. Subsequently, the massive stars are formed at the cluster core by either rapid accretion scenario or stellar mergers during the embedded dense phase [5,8,9]. The ionizing fronts and the winds of the newly formed massive stars terminate the local star formation. This star formation scenario explains the empirical relationship between the mass of the most massive star within a cluster and the estimated stellar cluster mass by forming stars in an ordered fashion, starting with the lowest-mass stars [5]. Within this star formation scenario the formation of the massive star might have occurred a little latter after the initiation of the formation of the solar system. The massive star will eventually undergo core collapse supernova (SN) and eject SLRs into the proto-planetary disc [10]. Several issues regarding this scenario need to be addressed. These are;

1) The mass of the most massive O star within the cluster. This massive star would be the earliest to evolve, explode and eject SLRs. The mass of the stellar cluster would probably determine the mass of this massive star [5]. A single massive star (M_{ZAMS} >30 $M_\odot$;$Z_\odot$) or a primary massive star (M_{ZAMS} >15 $M_\odot$;$Z_\odot$) within a close interacting binary system goes through Wolf-Rayet stage followed by SNIb/c [11-13]. One of these stars could be a potential source of SLRs [3]. For example, the most massive stellar system in the Trapazium cluster, the θ^1 Orionis C is presumably a close interacting binary with an estimated stellar masses of ~34 & ~15 $M_\odot$ [14]. This would probably go through WR+SNIb/c stages. Apart from this, in general, a single massive star >40 $M_\odot$ explodes within an interval of 3-5 Myr after its formation compared to ≥ 7 Myr required by the ≤ 25 $M_\odot$ single stars to explode as SNII. Since in the case of proto-planetary disc scenario [10] the ejection of SLRs should occur early prior to significant evolution of the disc, the massive stars (>40 $M_\odot$) would be favorable.

2) The probability of the massive star against its dynamical ejection from the cluster as a runaway star prior to SN [15,16]. The dynamical ejection of O stars seems to be quite predominant. During the last ~1 Myr the Trapazium cluster could have suffered significant losses in terms of even more massive stars than presently observed and could be presently in a state of further decay [17]. In order to be a source of SLRs, the massive star has to survive the runaway status. In this regard, the Upper Scorpius OB association probably represents an ideal case of an evolved cluster [17] with an age of ~5 Myr and a spatial spread of ~25 pc [7,18]. The progenitor of the pulsar PSR J1932+1059, with an estimated mass of 40-60 $M_\odot$ [17] could have injected SLRs during SN into the proto-planetary discs of the cluster stars within a short period of ~3.5 Myr. This could be a more realistic analog for the solar system,

along with our assumed formation sequence of the low- and massive stars within the cluster.

3) In order to avoid perturbations to the evolving planetary system it would be essential for the solar system, formed within a cluster, to avoid close encounters with the companion stars [18]. The cluster should disperse prior to the major planetary formation, otherwise highly eccentric planetary orbits would result.

Case B: This is a conventional scenario involving the triggered formation of the solar system by a distant massive star. Due to the various isotopic and dynamical constraints, the massive star contributing ^{26}Al to the presolar cloud should be <10 pc away [3]. This would place the SN right within the evolved stellar cluster as in the case of Upper Scorpius. The chances of a SN to trigger star formation within these shorter distances would be less than the chances of a SN injecting SLRs into an already existing proto-planetary disc as the former scenario could lead to the disruption of the presolar cloud rather than its gravitational collapse. The distant SN >10 pc can contribute ^{60}Fe without ^{26}Al along with triggering the gravitational collapse [3].

Conclusions: The bulk of the ^{26}Al in ESS was probably synthesized by a massive star. Further, we have explored the feasibility of the initiation of the formation of the solar system followed closely by the formation of the massive star with in a single stellar cluster. As the cluster dynamical evolves and the massive star eventually explodes, the SLRs are injected into the proto-planetary disc. The cluster is eventually dispersed prior to the major planetary formation.

Acknowledgement: This work is supported by the PLANEX grant.

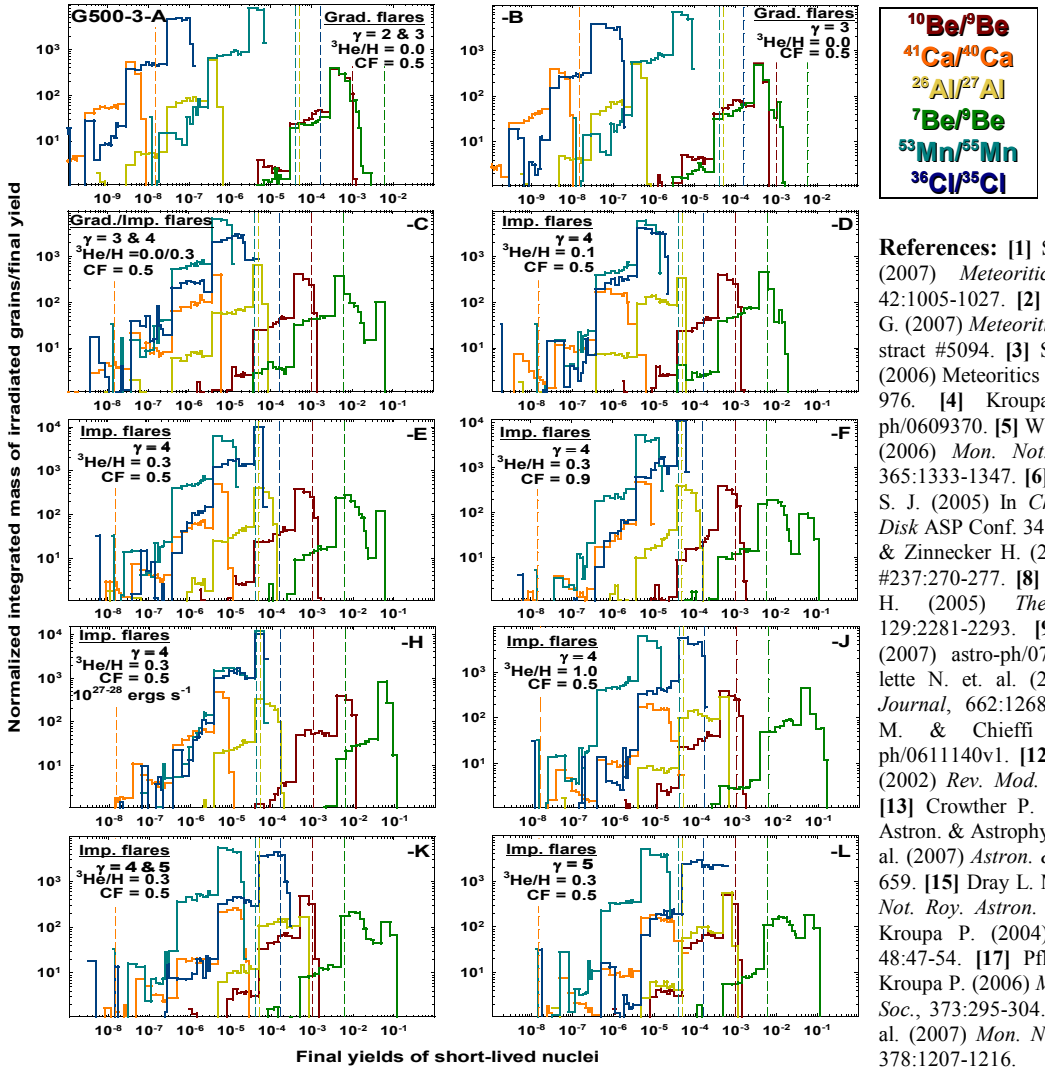

References: **[1]** Sahijpal S. & Soni P. (2007) *Meteoritics & Planet. Sci.* 42:1005-1027. **[2]** Sahijpal S. & Gupta G. (2007) *Meteoritics & Planet. Sci.,* Abstract #5094. **[3]** Sahijpal S. & Soni P. (2006) Meteoritics *& Planet. Sci.* 41:953-976. **[4]** Kroupa P. (2006) astro-ph/0609370. **[5]** Weidner C. & Kroupa P. (2006) *Mon. Not. Roy. Astron. Soc.*, 365:1333-1347. **[6]** Hester J. J. & Desch S. J. (2005) In *Chond. & Protoplanet. Disk* ASP Conf. 341:107. **[7]** Preibisch T. & Zinnecker H. (2007) *IAU Symposium* #237:270-277. **[8]** Bally J. & Zinnecker H. (2005) *The Astron. Journal*, 129:2281-2293. **[9]** Garry G. et. al. (2007) astro-ph/0706.2171. **[10]** Ouellette N. et. al. (2007) *The Astrophys. Journal*, 662:1268-1281. **[11]** Limongi M. & Chieffi A. (2006) astro-ph/0611140v1. **[12]** Woosley S.E et. al. (2002) *Rev. Mod. Phys.*, 74:1015-1071. **[13]** Crowther P. A. (2007) Ann. Rev. Astron. & Astrophys. 45: **[14]** Kraus S. et al. (2007) *Astron. & Astrophys.* 466:649-659. **[15]** Dray L. M. et. al. (2005) *Mon. Not. Roy. Astron. Soc.*, 364:59-68. **[16]** Kroupa P. (2004) *New Astron. Rev.*, 48:47-54. **[17]** Pflamm-Altenburg J. & Kroupa P. (2006) *Mon. Not. Roy. Astron. Soc.*, 373:295-304. **[18]** Malmberg D. et al. (2007) *Mon. Not. Roy. Astron. Soc.*, 378:1207-1216.

Figure 1. The normalized differential mass spectra of the final yields of the short-lived nuclides for the core-mantle ensemble of grains at the end of various simulations [1,2]. ***Grad***ual flares: ^{4}He/^{1}H = 0.01; ***Imp***ulsive flares: ^{4}He/^{1}H = 0.1. The energy spectra: dN α E $^{-\gamma}$dE. The dashed vertical lines represent the various empirical estimates of the SLRs.

LABORATORY EXPERIMENTS ON THE FORMATION OF PAH CLUSTERS AND THEIR ALTERATION WITH INORGANIC MATTER BY PLASMA, ULTRAVIOLET AND ELECTRON BEAM IRRADIATION. M. Saito, Y. Kimura, and C. Kaito, Laboratory for Nano-Structure Science, Department of Physics, Ritsumeikan University, 1-1-1 Nojihigashi, Kusatsu-shi, Shiga, 525-8577, Japan. rp010027@se.ritsumei.ac.jp, ykimura@se.ritsumei.ac.jp, kaito@se.ritsumei.ac.jp

Introduction: Polycyclic aromatic hydrocarbons (PAHs) have been considered most plausible candidates of the unidentified infrared bands observed from various astronomical objects including young stars [1,2]. PAHs consist of carbon atoms arranged in benzene rings terminated by hydrogen atoms. They have C-C and C-H bonds, which show the vibration modes at mid-infrared region. In order to elucidate the behavior of the PAHs in the early Solar Nebula, I have performed experimental studies on the formation of PAH clusters with and without inorganic elements, alteration by ultraviolet irradiation and plasma field, and measured their infrared spectra in the laboratory. If the mechanisms of formation and growth of PAH clusters via experimental studies were elucidated, it will be able to discuss the behaviors of PAH clusters including interaction with inorganic grains in the early Solar Nebula. Indeed, recently, it has been reported the crystallization temperature of the amorphous Mg-bearing silicate grains is decrease to 300 K from thermal annealing crystallization temperature at ~1000 K, when the amorphous silicate grains have an amorphous carbonaceous layer [3]. Generally, it has been considered that amorphous silicates gradually crystallize via thermal annealing in the hot inner solar nebula over time and then were transported outward and incorporated in comets [e.g. 4,5]. Using this thermal annealing model, the chronology and formation age of comets in the early Solar System has been discussed based on laboratory experiments [6]. The experimental results imply that the crystallization of cometary silicates has been occurred in the coma of comets at each time comet approach the Sun, i.e., not 4.5 billion years ago. As a result, it can be explain how cometary silicate crystallize yet still preserve volatile interstellar ices in their parent comets. Thus, organic materials will strongly affect to the behavior of inorganic materials. The abundances of oxygen, nitrogen and carbon are more than 10 times of that of silicon, magnesium and iron. Indeed, as a result of recent observation, the presence of significant amount of organic materials in the primitive solar nebula has been found. Since we assume that the organic materials affect to the nucleation, growth and crystallization of inorganic cosmic dust, the behavior of organic materials and interaction to the inorganic materials such as silicates, oxides and carbides in primitive solar nebula should be considered. In the present study, laboratory experiments of nucleation and growth of Si in PAHs gas atmosphere will be also shown. Si interacts with both oxygen and carbon and become a component of many kinds of minerals. In addition, PAHs are widely presented in the universe. Therefore, experiment using Si and PAHs were performed, initially. In the primitive solar nebula, dust particles would be undergone plasma environments and irradiation of cosmic ray during formation and growth. Therefore, growth of PAHs with or without Si in a plasma field and irradiation of ultraviolet or electron beam to the grown particles are also shown.

Experiment: Pyrene and coronene were used as the materials of PAHs clusters. The structures of both PAHs have been shown in Fig. 1. They have a molecular structure constructed by four and seven benzene rings in compact, respectively. Pyrene has two duo C-H bonds and two trio C-H bonds, and coronene has six duo C-H bonds. C-H out-of-plane deformation mode make bands in 11-15 μm region depending on the number of directly adjacent H atoms, because of the coupling between the vibrating H atoms bonded to neighboring C atoms on a ring. PAH clusters were produced by evaporation of commercial powder in He gas of 80 Torr using an experimental setup as shown in Fig. 2. Commercial PAH (pyrene or coronene) and Si powders were charged on upper and lower tantalum boats. A boat with Si was electrically heated at about 2000 K. Then, the other boat with a PAH was heated by the convection of He gas. As a result, PAH was simultaneously evaporated with Si. In the case of the experiment in Fig. 2(a), Si should be condensed and growth in the PAH vapor, because the sublimation temperature of PAHs are quite lower compared with Si. In the case of the experiment in Fig. 2(b), Si particles could be produced before it contact with PAH vapor. Therefore, sublimated PAH molecules may condense on the Si particles in addition to the homogeneous nucleation, when Si smoke particles were cooled below the sublimation temperature of the PAH. These experiments are supposed reprocessing of original interstellar materials in the solar nebula. The produced clusters collected on a glass plate placed 8 cm above the upper boat for measurements of infrared spectra and on a standard Cu transmission electron microscope (TEM) grid supported with amorphous

carbon film for observation of the size and the structure of the grains.

Initial Results: Figure 3 shows mid-infrared spectra of (a) Si-coronene, which is corresponding to Fig. 2(a), (b) coronene-Si, which is corresponding with Fig. 2(b) and (c) coronene without Si. In the spectrum (b), a significant feature at 9 μm can be seen in addition to the sharp peaks at 7.6, 11.8 and 18 μm attributed to coronene. The 9 μm feature is caused by the asymmetric stretching vibration mode of Si-O. The appearance of the feature at 9 μm shows production of SiO particles. Namely, although Si particles were produced and passed in the vapor of sublimated coronene, the deposition of coronene on the pre-nucleated Si particles may be insufficient or not occurred. As a result, Si surface was oxidized by taking out the specimen into air. In the case of the experiment in Fig. 2 (a), since Si is grown in the coronene vapor, Si may incorporate in the coronene clusters. Therefore, there is no chance to form SiO. As a result, 9 μm feature does not appear in the spectrum in Fig. 3(a). Since the 11-12 μm feature by silicon carbide did not show up in the both spectra, Si does not react with coronene molecules, even if Si is nucleated and growth in coronene vapor. Slight difference of the feature of coronene is visible in the spectra. The intensity of a characteristic double peak at 11.8 μm caused by duo of C-H vibration mode is changing by the existence of Si. In the case of Pyrene, the mid-infrared spectrum did not change.

Although ultraviolet at 254 or 365 nm was irradiated to the samples of coronene and pyrene with Si, which were produced by the method of Fig. 2(a), the infrared spectra did not change for the duration of 15 hours, which is corresponding to the total flux of 4.3×10^{21} and 7.5×10^{21} photons/cm^2, respectively. On the other hand, when electron beam of 300 KeV for 10^{-3}-10^{-2} A/cm^2 was irradiated to the samples of pyrene with Si, which was produced by the method in Fig. 2(a), formation of silicon carbide nanoparticles were appeared after about 15 minutes during TEM observation. We will show further experiments including experiments of formation in a plasma field and discussion on the expanding to the environment in the early Solar Nebula on the poster.

References: [1] Boersma C. et al. 2006. *A&A* 447:213-220. [2] Acke B. and van den Ancker M. E. 2004. *A&A* 426:151-170. [3] Kaito, C. el al. 2007. *ApJL* in press. [4] Shu F. H. 1996. *Science* 271:1545-1552. [5] Boss A. P. 2004. *ApJ* 616:1265-1277 [6] Nuth III J. A. et al. 2000. *Nature* 406:275-276.

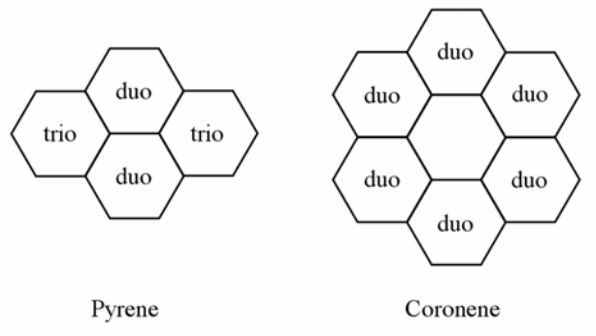

Fig. 1. Molecule structures of PAHs.

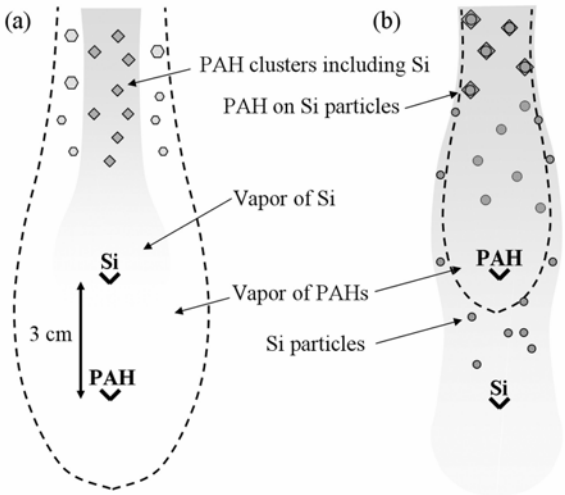

Fig. 2. Schematic drawing of the experimental setup to produce PAH clusters and Si particles. The break lines show the expected region of the PAH vapr.

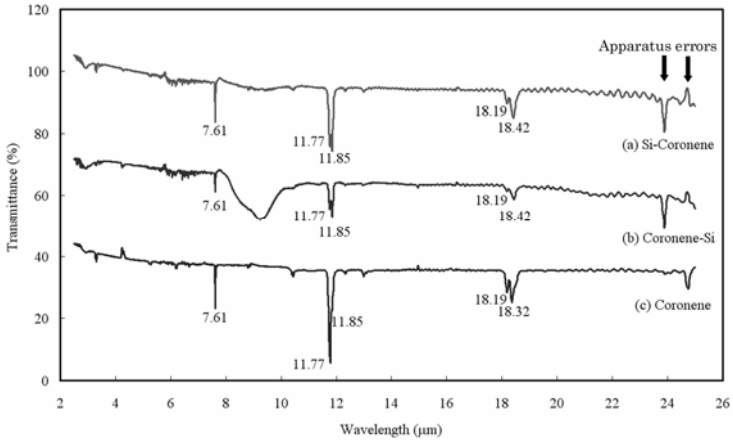

Fig. 3. Mid-infrared spectra of PAH clusters with Si.
(a) Produced by the method shown in Fig. 1(a).
(b) Produced by the method shown in Fig. 1(b).
(c) Coronene clusters without silicon.

THE CHRONOLOGY OF BASALTIC METEORITES AND THE HISTORY OF THEIR PARENT BODIES. Ian S. Sanders[1] and Edward R. D. Scott[2] [1]Department of Geology, Trinity College, Dublin 2, Ireland (isanders@tcd.ie) [2]Hawaii Institute of Geophysics and Planetology, University of Hawaii at Manoa, Honolulu, Hawaii 96822, USA

Basaltic meteorites probably sample at least six different asteroidal parent bodies, based on oxyen isotope [1] and geochemical signatures. They comprise two main groups (the eucrites and angrites), a suite of basaltic clasts in mesosiderites and three apparently unique examples, namely Asuka 881394, Ibitira, and Northwest Africa 011. Published ages of these meteorites, based on four high-resolution chronometers (^{207}Pb-^{206}Pb, ^{26}Al-^{26}Mg, ^{53}Mn-^{53}Cr and ^{182}Hf-^{182}W) are summarised in Fig. 1. The ages are of two types, whole-rock (W-R) and mineral isochron ages.

W-R ages include ^{53}Mn-^{53}Cr and ^{182}Hf-^{182}W bulk meteorite isochrons [2-4] and also ^{26}Al-^{26}Mg model ages which are two point isochrons passing through bulk meteorite and an inferred chondritic source [5, 6]. W-R ages, regardless of parent body, are about 3 to 4 Myr after CAIs and correspond to an idealized stage when the basalts in a given parent body were chemically heterogeneous but isotopically homogeneous. We suggest that the W-R ages may date the local extraction of melt fractions with differing degrees of partial melting from a homogeneous parent body source.

Mineral isochrons are in many cases close to, or up to 1 or 2 Myr younger than, W-R ages (4 to 5 Myr after CAIs) [e.g. 2, 7-14]. They date the last time of isotopic equilibration between minerals, and can provide good estimates of crystallization ages of rapidly cooled basalts. In the latter case, to account for the slightly younger ages, we suggest the magma may have remained trapped for a while within the parent body after it segregated but before it erupted and crystallized.

Younger ages of 9 Myr characterise a sub-set of texturally equilibrated angrites, presumably reflecting their slow cooling [e.g. 2, 7, 12]. A wide range of still younger ages in eucrites probably result from late isotopic disturbance or resetting, perhaps related to slow cooling or impact heating [2].

Sahara 99555 [6] and Asuka 881394 [8] have anomalously old ^{207}Pb-^{206}Pb ages < 1 Myr after CAIs. Sahara 99555 now has a revised younger age, close to that of D'Orbigny [9], casting doubt on a claim that CAIs were formed about 3 Myr earlier that this, at 4569.5 Myr ago [6]. Asuka 881394 remains enigmatic, and is the subject of ongoing investigation.

The tight clustering of mineral isochron ages between 4 and 5 Myr demonstrates concordance, within error, between the four chronometers, and it implies uniform distribution in the accretion disk of the parent nuclides, ^{26}Al, ^{53}Mn and ^{182}Hf. Age concordance has been reinforced by recent ^{182}Hf-^{182}W isochrons for angrites, not plotted on Fig. 1 [7]. This, along with independent evidence for the uniform distribution of ^{26}Al in the disk [15], is very significant because it implies widespread and inevitable meltdown of early-accreted bodies due to ^{26}Al heating.

Knowing that parent bodies of iron meteorites had melted within just 0.5 Myr after CAIs [14, 16] the segregation of basalt, at 3 to 4 Myr after CAIs, is a little puzzling. A solution may be found in simple thermal modelling of the parent bodies, assuming an ^{26}Al heat source. Our calculations, based on assumptions in [17] suggest that where a parent body accreted very early (< 1 Myr after CAIs) it would quickly have overheated and become a global magma ocean undergoing convection. The dense metal would evidently have segregated quickly, accounting for the highly unradiogenic tungsten in magmatic irons. By 3 to 4 Myr, after substantial crystallization of the magma ocean, basalt would, we predict, have remained as a *residual* interstitial melt, in a locked-up crystal mush. In some way, the basalt would then have been drawn off in batches and migrated upwards. On the other hand, where a parent body accreted later, at say 1.5 Myr, (Fig. 2) then *partial melting* would have yielded basaltic magma, by 3 to 4 Myr, in a straightforward way. Thus the consistent ages of basaltic meteorites may be purely a function of the decline in heating power of ^{26}Al, regardless of how early accretion occurred. After all, while tungsten anomalies imply very early core formation they tell us nothing of when continued heating and melting in the overlying silicate mantle finally ended.

Basaltic meteorites show large depletions in moderately volatile elements . We suggest that this cosmochemical signature is inherited from their parent bodies that perhaps accreted, as 'second-generation' bodies, from the volatile-depleted ejecta of early giant impacts, in the manner inferred by [18-20]. This kind of two-stage accretion model is also consistent with Hf-W isochrons of eucrites [4] and angrites [7], both of which pass above the position of primitive chondrites. These basalts could not, therefore, have a chondritic source, but require instead a source with a pre-accretion history giving inflated (supra-chondritic) Hf/W such as being in the mantle of a first generation body.

Returning to the issue of very old ^{207}Pb-^{206}Pb ages, we proposed earlier [21] that these recorded Pb loss during early impact-induce volatile depletion. This

now appears doubtful since ^{207}Pb-^{206}Pb ages are strictly isochron ages that date fractionation of Pb and U between pyroxene and other minerals at the time of crystallization.

References: [1] Greenwood R. (2005) *Nature* 435, 916-918. [2] Lugmair G. W. and Shukolyuklov A. (1998) *GCA* 62, 2863 - 2886. [3] Shukolyuklov A. and Lugmair G. W. (2007) *LPS* 38, abstract #1423. [4] Kleine T. et al. (2004) *GCA* 68, 2935-2946. [5] Bizzarro M. et al. (2005) *ApJ* 632, L41-L44. [6] Baker J. A. et al. (2005) *Nature* 436, 1127-1131. [7] Markowski A. et al. (2007) *EPSL* in press. [8] Amelin Y. et al. (2006) *LPS* 37, abstract #1970. [9] Amelin Y. (2007) *LPS* 38, abstract #1669. [10] Nyquist L. E. et al. (2001) *M&PS* A151-A152 [11] Wadhwa M. et al. (2005) *LPS* 36, abstract #2126. [12] Lugmair G. W. and Galer S. J. G. (1992) *GCA* 56, 1673-1694. [13] Srinivasan G. et al. (1998) *M&PS* 33, A148-A149. [14] Kleine T. et al. (2005) *GCA* 69, 5805-5818. [15] Thrane K., Bizzarro M. and Baker J. A. (2006) *ApJ* 646, L159-L162. [16] Burkhardt C. et al. (2007) *M&PS* 42, 5189.pdf [17] Sanders I. S. and Taylor G. J. (2005) *ASP Conference Series* 341, 915-932. [18] Bland P. A. and Benedix G. K. (2006) *M&PS* 41, A22. [19] Halliday A. N. and Porcelli D. (2001) *EPSL* 192, 545-559. [20] Yang J., Goldstein J.I. and Scott E. R. D. (2007) *Nature* 446, 888-891. [21] Sanders I. S. and Scott E. R. D. (2007) *LPS* 38, abstract #1910. [22] Amelin Y. et al. (2002) *Science* 297, 1678-1683.

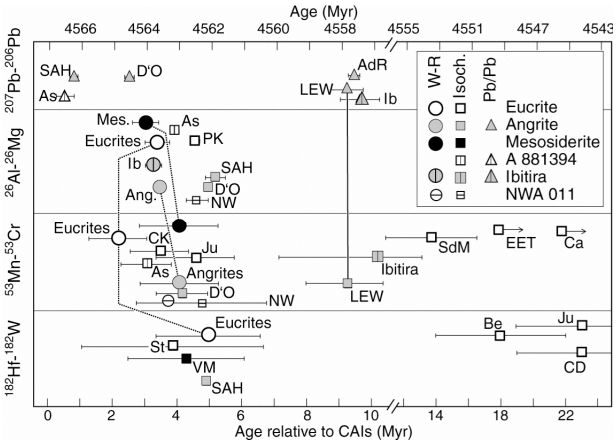

Fig. 1 Compilation of published ages of meteoritic basalts. ^{53}Mn-^{53}Cr relative ages are tied to ^{207}Pb-^{206}Pb ages using LEW 86010 [2, 12]; ^{26}Al-^{26}Mg, and ^{182}Hf-^{182}W relative ages are tied to ^{207}Pb-^{206}Pb ages using CAIs as an anchor [14, 22]. Abbreviation: SAH – Sahara 99555, D'O – D'Orbigny, AdR – Angra dos Reis, LEW – LEW 86010, As – Asuka 881394, Ib – Ibitira, Mes. – basalt clasts in mesosiderites, PK – Piplia Kalan, Ang. – angrites, NW – NWA 011, CK – Chervony Kut, Ju – Juvinas, SdM – Serra de Magé, EET – EET87520, Ca – Caldera, Be – Bereba, CD – Camel Donga, St – Stannern, VM – Vaca Muerta. Not all data sources have been cited in the reference list.

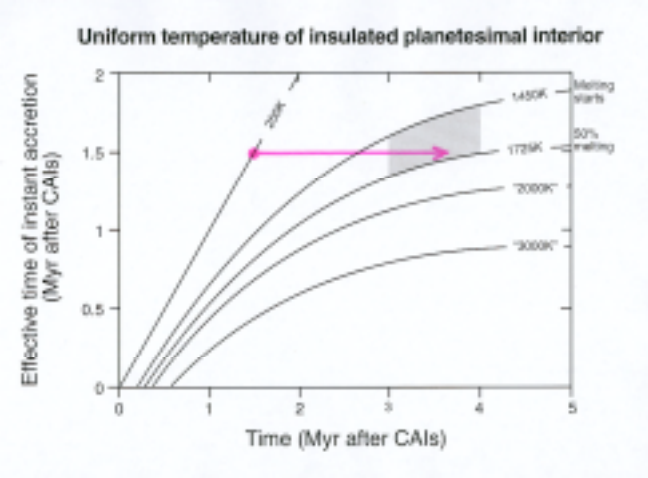

Fig. 2 . Time (in Myr after CAI formation) when a particular uniform temperature is reached throughout the insulated interior of a planetary body of dry chondritic composition, as a function of the time when accretion takes place. ^{26}Al is the only heat source, and the starting temperature is 250 K. Planetesimals up to a few hundred km across are envisaged. Thermal parameters are those used in [17] but with a decay energy of 3 MeV per atom. Partial melting and basalt production occurs in the shaded area between 1450 K (the solidus) and 1725 K (corresponding to 50% melting). Accretion at 1.5 Myr leads to partial melting between about 3 and 4 Myr, marked by an arrow. Accretion at 2 Myr will not lead to any melting. Accretion at 0.5 Myr would theoretically lead to temperatures exceeding 3000 K by 2 Myr, but in practice a global magma ocean is predicted to develop [17] and will lose heat rapidly by convection, keeping its temperature below the liquidus (1850 K). Once ^{26}Al has largely gone, the ocean will gradually freeze and basalt will remain for a while as a residual liquid between the solid silicate grains. This stage is estimated to occur, again, between about 3 and 4 Myr.

DEVELOPMENT OF PRECISE AND ACCURATE MAGNESIUM ISOTOPE MEASUREMENTS BY MULTIPLE-COLLECTOR INDUCTIVELY COUPLED PLASMA MASS SPECTROMETRY

M. Schiller[1], M. Bizzarro[2] and J. A. Baker[1]
[1]School of Geography, Environment and Earth Sciences, Victoria University of Wellington, P.O. Box 600, Wellington, New Zealand (martin.schiller@vuw.ac.nz, joel.baker@vuw.ac.nz); [2]Axiom Laboratory, Geological Institute, University of Copenhagen, 1350 Copenhagen, Denmark (bizzarro@geol.ku.dk).

Introduction: Magnesium has three isotopes (24, 25 & 26), one of which can be produced by the short-lived decay of ^{26}Al ($t_{1/2}$ = 0.73 Myr). Since the demonstration of the former presence of ^{26}Al in calcium-aluminium-rich inclusions (CAIs) [1], the ^{26}Al-to-^{26}Mg chronometer has been used to date the relative timing of CAIs and chondrules as well as the formation of some basaltic meteorites [e.g., 2,3]. Recent application of multiple-collector inductively coupled plasma mass spectrometry (MC-ICPMS) to Mg isotope analysis has potentially opened up a new range of dating opportunities. In particular, small excesses or deficits in meteorites and their constituents should now be resolvable that might allow isochron or model age dating of material that was previously impossible to date. For example, the presence of small ^{26}Mg excesses in bulk basaltic meteorites might be used to date the increase in Al/Mg ratio associated with the formation of basaltic magmas. Conversely, Al/Mg ratios of essentially zero in some types of differentiated meteorites and their minerals should allow ^{26}Mg deficits to place age constraints on their formation if this took place within 2 million years of CAI formation.

The δ^{26}Mg* excesses and deficits expected from such processes will be ca. < ±0.050‰ and require both the precision *and* accuracy of Mg isotope measurements to be ca. ±0.005‰ if the full potential of the ^{26}Al-to-^{26}Mg dating system is to be utilised. Here, we describe analytical developments intended to assess whether MC-ICPMS techniques can really produce Mg isotope data at these levels of precision and accuracy.

Analytical Methods:

Chemical separation of Mg. We explored Mg separation from silicate meteoritic material using a number of methods, primarily based around the elution of Mg on cation exchange resins in dilute HNO_3 media. While this method can satisfactorily remove most Na, Cr, Al, Ti, and Ca from Mg, several percent of other elements may remain in the Mg solution even after several column passes (e.g., [4,5]). These contaminants could potentially preclude the acquisition of very accurate δ^{26}Mg* excess and deficit data. We have developed procedures designed to achieve Mg yields of > 99.5% with > 99.5% purity. For most samples we now routinely apply a 4-step column separation procedure to produce high purity Mg separates.

Samples are taken fully into solution after normal HF-HNO_3 digestion techniques. An aliquot of this solution containing 2 mg of dissolved sample is then processed as follows:

(1) Fe is removed by eluting Mg in conc. HCl through a 0.5 ml AG-1 X8 anion exchange resin bed.

(2) Ca is removed by eluting Mg in 3M HNO_3 through a 0.25 ml DGA (Eichrom) resin bed. This step is repeated at least twice for high Ca samples (e.g., CAIs).

(3) Na, Al, Ti and Cr are eluted in 6 ml of 1M HNO_3-0.1M HF on a AG50W-X8 cation exchange resin (200-400 mesh). Mg is then collected by eluting >10 ml of 1M HNO_3-0.1M HF. This step is repeated for high Al samples.

(4) Mn is removed from Mg by elution in dilute HCl-acetone through AG50W-X8 cation exchange resin.

Mg isotope measurements by MC-ICPMS. Mg isotope ratios are measured on a Nu Plasma MC-ICPMS at Victoria University of Wellington. The Faraday collector used to measure ^{24}Mg is equipped with a 10^{10} Ohm resistor that allows larger 25 and 26 ion beams (3-9 V) to be measured during analysis. Mg is introduced into the plasma via a desolvating nebuliser as dilute HCl solutions. Each measurement typically comprises 8 min of baseline and 26.67 min of data acquistion acquired in four blocks. Sample analyses are bracketed by analyses of standards and data are reported in the per mil (‰) notation as the difference from the average value of the two bracketing standards. Uncertainties on each analysis are calculated by rigorously incorporating that on the sample run with those from the bracketing standards. δ^{26}Mg* is calculated from the offset of a sample's mass-bias corrected ^{26}Mg/^{24}Mg (using the exponential mass fractionation law and ^{25}Mg/^{24}Mg = 0.12663) compared to the average value obtained from bracketing standards. Implicit in this approach is the assumption that any natural stable isotope differences between the sample and standard are the result of kinetic processes. Using this approach, single Mg isotope analyses have uncertainties (2 se) on mass-bias-corrected δ^{26}Mg* that are ≤±0.016‰ and as low as ±0.012‰. Multiple analysis of samples routinely results in weighted means with uncertainties that are ≤ ±0.005‰. Analyses are carried out in pseudo-medium resolution mode at a resolution of 2000, which permits complete resolution of all interferences with the exception of hydrides and Cr^{++}, Ti^{++} and Ca^{++}.

Results: A number of tests were conducted to examine the veracity of Mg isotope data obtainable by MC-ICPMS (Table 1). Analyses were made of:
- an ICPMS Mg standard (Aristar) gravimetrically spiked with pure ^{26}Mg to produce solutions with 10, 20 and 30 ppm excesses
- an ICPMS Mg standard (Aristar) doped with 2 mol % of a range of contaminant elements
- a range of Mg standard solutions against a Bulk Earth Mg composition as represented by Mg separated from mantle olivine (J11)
- aliquots of Mg collected during the elution of Mg through AG50W-X8 cation exchange resin
- a Mg standard solution processed through both anion and cation exchange chemistry
- mantle olivine (J11) subjected to differing levels of chemical separation i.e., just anion exchange removal of Fe and the complete separation procedure through anion, DGA and cation exchange chemistry

Table 1 δ^{26}Mg*-δ^{25}Mg data of analytical experiments.

Sample	δ^{26}Mg* (‰)	δ^{25}Mg (‰)	n
Aristar δ^{26}Mg* 0.01‰[1]	+0.0107±0.0052	-0.04±0.10	8
Aristar δ^{26}Mg* 0.03‰[1]	+0.0311±0.0069	-0.05±0.15	5
Aristar Ca/Mg = 2.0[1]	+0.2425±0.0240	+0.76±0.18	1
Aristar Ca/Mg = 0.2[1]	+0.0294±0.0142	+0.80±0.13	1
Aristar Ca/Mg = 0.02[1]	+0.0102±0.0080	+0.67±0.15	4
Aristar Mn/Mg = 0.02[1]	-0.0022±0.0089	+0.64±0.05	3
Aristar Ti/Mg = 0.02[1]	+0.0074±0.0094	+0.30±0.01	3
Aristar Ni/Mg = 0.02[1]	-0.0008±0.0074	+0.16±0.03	5
Aristar Fe/Mg = 0.02[1]	+0.0095±0.0081	+0.24±0.05	4
Aristar Cr/Mg = 0.02[1]	-0.0036±0.0096	+0.35±0.20	3
Aristar Al/Mg = 0.02[1]	-0.0072±0.0083	+0.27±0.01	3
Aristar Na/Mg = 0.02[1]	-0.0002 ± 0.012	+0.05±0.01	2
Aristar Mg[2]	+0.0161±0.058	-0.81±0.12	5
Alfa Aesar Mg[2]	+0.0153±0.0071	-1.72±0.10	5
DSM-3 Mg[2]	-0.0014±0.0065	+0.14±0.10	9
SRM-980 Mg[2]	+0.0030±0.0063	-2.33±0.09	7
Column cut 60-70 ml[3]	-0.0149±0.0084	+0.51±0.17	3
Column cut 70-80 ml[3]	+0.0010±0.0220	+0.16±0.07	3
Column cut 80-90 ml[3]	+0.0145±0.0078	-0.44±0.09	3
Column cut 90-100 ml[3]	+0.0260±0.0210	-0.67±0.11	3
Aristar Mg anion-processed[1]	-0.0002±0.0062	-0.03±0.17	6
Aristar Mg cation-processed[1]	-0.0019±0.0049	-0.03±0.04	10
J11 anion-processed[4]	+0.0022±0.0040	-0.11±0.06	24
J11 cation-processed[4]	+0.0007±0.0053	-0.16±0.05	9

[1]measured vs pure Aristar Mg, [2]measured vs J11 olivine (anion-processed), [3]measured vs bulk Mg standard, [4]measured vs DSM-3

Discussion: The results presented in Table 1 illustrate a number of important points. Repeated analyses of Mg standards with gravimetrically prepared ^{26}Mg anomalies can be reproduced with an accuracy and precision of ≤ ±0.005‰. Similarly, replicate analyses of Mg standard (Aristar) and mantle olivine (J11) subjected to anion and cation chemistry show no significant deviation from the expected δ^{26}Mg* (i.e., 0.000‰).

Our data also illustrate some potential difficulties in attempting to obtain highly precise and accurate Mg isotope data by MC-ICPMS. Some ICPMS Mg standards with fractionated stable isotope compositions have experienced some part of this fractionation by equilibrium processes that produces apparent δ^{26}Mg* excesses in isotopically light standards. In contrast, despite the fact that SRM980 is the lightest isotopically standard we have analysed, most of this fractionation was induced by a kinetic process. Given that DSM-3 is slightly isotopically heavier than mantle olivine and terrestrial basalts, we prefer to use matrix-matched olivine and basalt standards as bracketing standards for analyses of unknowns.

Small amounts of contaminant elements remaining after chemistry can be seen to variably bias sample stable Mg isotope data to heavier values, suggesting that discussions regarding small stable isotopic variations amongst planetary materials are premature [4,5], given the levels of contaminants reported by these studies to be present in their analysed Mg cuts. However, the presence of most elements appear to have little effect on δ^{26}Mg* if the Mg cut is >99% pure. Care must be taken that recovery of Mg is high as the stable isotopic fractionation associated with incomplete recovery on ion exchange resins is controlled by an equilibrium process that introduces analytical artefacts on the δ^{26}Mg* when this is calculated using the approach adopted here.

In summary, our results indicate that it is possible to resolve δ^{26}Mg* anomalies to high precision and accuracy (≤ ±0.005‰) in meteorites, which should allow extension of ^{26}Al-to-^{26}Mg dating to meteorite materials with small anomalies. We will present new high-precision Mg isotope data for meteorites where small δ^{26}Mg* excesses (angrites, eucrites) and deficits (pallasite olivines, ureilites, aubrites) have previously been reported [e.g., 6], and used to constrain rapid timescales of planetesimal melting, differentiation and accretion in the young Solar System. For example, 66 new analyses of olivine from four main group pallasites have a weighted mean δ^{26}Mg* = -0.0155± 0.0017‰, that can be used to calculate a model age for olivine crystallization and diffusive isolation on the pallasite parent body of 1.05±0.12 Myr (^{26}Al/^{27}Al$_0$ = [2.16±0.24]x10^{-5}) after formation of calcium-aluminium-rich inclusions.

References:

[1] Lee T. et al. (1976) *GRL 3*, 109-112. [2] Kita N.T. et al. (2000) *GCA 64*, 3913-3922. [3] Srinivasan G. et al. (1999) *Science 284*, 1348-1350. [4] Wiechert U. & Halliday A. N. (2007) *EPSL* 256, 360-371. [5] Teng F. et al. (2007) *EPSL*, in press. [6] Bizzarro. M. et al. (2005) *ApJ 632,* L41-44.

METEORITE CONSTRAINTS ON THE FIRST 5 MYR OF PLANETARY GROWTH IN THE INNER SOLAR SYSTEM. Edward R. D. Scott[1], Ian S. Sanders[2], Joseph I. Goldstein[3], and Alexander N. Krot[1]. [1]HIGP, University of Hawaii at Manoa, Honolulu, HI 96822, USA; [2]Dept of Geology, Trinity College, Dublin 2, Ireland; [3]Dept. of Mechanical and Industrial Engineering, University of Massachusetts, Amherst, MA 01003, USA. Email: escott@hawaii.edu.

Introduction: Growing evidence indicates that CAIs are the oldest objects with Pb-Pb ages that date solar system formation 4567 Myr ago and provide the best reference point (t_0) for early solar system chronologies [1, 2]. The overall consistency between chronometers based on long-lived ^{235}U and ^{238}U isotopes and the short-lived isotopes, ^{26}Al, ^{53}Mn, ^{182}Hf and ^{129}I, coupled with improved understanding of secondary geological processes such as alteration and impact heating have provided a coherent geological history of early high temperature events [e.g., 3, 4]. This geological history is strengthened by its consistency with thermal models for asteroidal bodies based on the inferred initial concentration of ^{26}Al in CAIs being uniformly distributed throughout the solar system and the assumption that meteorite parent bodies were large enough (>40 km in radius) so that surface zones that lost heat by conduction during ^{26}Al decay were relatively small [5-8].

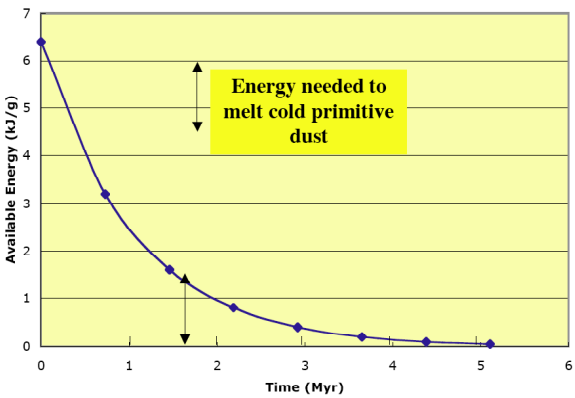

This plot shows how the available energy for heating dry asteroids decreases according to the half-life of ^{26}Al of 0.73 Myr [see 6]. Bodies that were melted would have accreted <1-1.5 Myr after CAI formation; metamorphosed bodies accreted ~1-3 Myr, and unmetamorphosed bodies accreted after 3 Myr. Below we summarize the meteorite constraints on planetesimal and protoplanetary accretion at these three stages during the first 5 Myr of solar system evolution. Parent body sizes are inferred from cooling rate measurements and thermal modeling.

0-0.1 Myr: CAIs probably formed close to the protosun in <0.1 Myr [7, 8, 17] and were dispersed throughout the solar disk so that they accreted over the next 5 Myr with other nebular materials.

0.1-1 Myr: Evidence for accretion in this period comes from magmatic iron meteorites. After correction for cosmic-ray effects, these irons have ^{182}W/^{184}W ratios that are indistinguishable from the initial ratio derived from the CAI isochron [9, 10]. This implies that magmatic irons come from differentiated bodies in which the metallic cores formed <0.5-1 Myr after CAI formation. The parent bodies of irons were traditionally inferred from metallographic cooling rates to be 10-200 km in size, assuming that the cores cooled inside insulating silicate mantles [11]. However, 50-fold variations in the cooling rates in group IVA iron meteorites and smaller ranges in other groups can only be explained by cooling in metallic bodies with little or no silicate mantle [12]. The cooling rates of IVA irons are compatible with a hot metallic body 300±100 km in diameter that developed significant thermal gradients on cooling [12]. Because impacts cannot efficiently strip mantle material from cores, the original differentiated body from which IVA metal was derived was probably much larger than 600 km in size.

Protoplanetary collisions provide a plausible mechanism for generating metal-rich asteroidal bodies. Asphaug et al. [13] found that Moon-to-Mars sized protoplanets are eviscerated by hit-and-run collisions which generate strings of metal-rich bodies from the smaller body. Thus the 150 km radius metallic IVA body was plausibly derived from a protoplanet that accreted <1 Myr after CAI formation. These studies imply that protoplanets ~1000 km in size accreted and differentiated 0.1-1 Myr after CAI formation [12].

According to Bottke et al. [14], differentiated meteorites come from bodies that accreted inside 2 AU and broke up early generating debris that was perturbed by protoplanets into the asteroid belt.

We do not know when the IVA protoplanetary impact occurred, but collisional disruption of protoplanets probably started in the first few Myr, as IIIAB irons record Mn-Cr isotopic closure only 4±1 Myr after CAIs [15]. Protoplanetary collisions may also be responsible for the extremely low volatile concentrations in IVA irons [16], eucrites [24], and angrites.

1-3 Myr: Most chondrite groups (~90%) have chondrule ages of 1-3 Myr after CAIs. The range of chondrule ages within a group could be <1 Myr [27]. During this period chondrules formed episodically and were accreted into diverse asteroidal bodies along with CAIs, stardust, planetary debris, and solar nebula dust.

The earlier bodies to accrete at 1-3 Myr were strongly metamorphosed, e.g., CV and O chondrites. Bodies accreting 2-3 Myr after CAIs, like CR chondrites, were only mildy metamorphosed (<300°C) consistent with thermal models (Fig. 1).

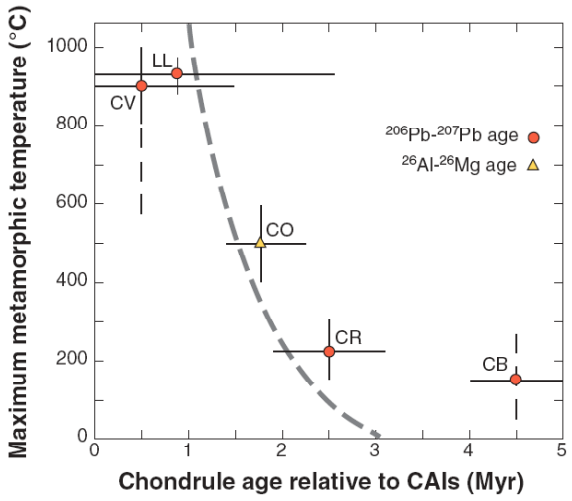

This figure (reprinted with permission from the Annual Review of Earth and Planetary Sciences, Volume 35 ©2007 [4]) shows how maximum metamorphic temperatures decline with increasing chondrule formation age, consistent with theoretical calculations assuming immediate accretion after chondrule formation [7]. For data see refs [4, 17].

Assuming that H chondrites have typical thermal histories, the chondritic parent bodies that formed at 1-3 Myr were ≈200 km in size [18]. Since protoplanets prevented adjacent planetesimals from accreting [28], chondritic planetesimal growth may have been confined to a region between ~2 AU and the snowline.

3-5 Myr: The few chondrites with chondrules that formed at 3-5 Myr accreted into bodies that show the lowest degrees of metamorphism, as ^{26}Al heating was minimal after 3 Myr. Thus parent body sizes have not been inferred from meteorite thermal histories. CB chondrules, may have formed from a protoplanetary collision that created an impact plume of vapor and droplets that was mixed with CAIs and carbonaceous clasts, presumably in a still dusty disk [19]. CH chondrites, which have some CB-like features and clasts that probably come from other asteroids, probably also formed in this period.

Basalts from Vesta and several other disrupted, presumably Vesta-sized asteroids record two kinds of igneous processes at 3-5 Myr. Whole-rock ages for eucrites, angrites, mesosiderites, and ungrouped basalts (Ibitira, Asuka 881394, and NWA 011) of ~3-4 Myr after CAIs record global igneous processes that created chemical heterogeneous but isotopically homogeneous reservoirs [20-22]. At least for Vesta, this process was probably crystallization of a magma ocean, rather than partial melting, as Hf-W data show that core formation preceded eucrite whole-rock ages by 1 Myr [22, 23]. Rare Vestan basalts and several basalts from other sources have crystallization ages of 4-5 Myr; most Vestan basalts were probably reheated later by impact burial [29].

It is commonly inferred that Vesta accreted at ~1.5 Myr after CAIs so that basaltic reservoirs formed at 3-5 Myr by partial melting, e.g. [7], but magma oceans could have formed in bodies that accreted earlier and cooled rapidly by convection until crystal lock-up [22]. Low concentrations of volatiles like Na and K in all asteroidal basalts suggest that volatile loss by protoplanetary impacts may have been prevalent prior to 3 Myr [22, 24)]. Thus even Vesta may be a "second-generation" body.

Implications: Meteorites show that planetesimals did not accrete simultaneously throughout the inner solar system. Instead planetesimals appear to have been accreting in the asteroid belt long after protoplanets had formed and collided in the terrestrial region. This 5 Myr record of planetesimal and protoplanet accretion recorded in meteorites is not consistent with planetary accretion and disk evolution models and appears to require that planetesimal formation spread across the nebula from regions where the differentiated bodies formed [25]. Numerical modeling is needed to understand the meteorite constraints [26].

References: [1] Amelin et al. (2002) *Science* 297, 1678. [2] Amelin et al. (2006) *LPS* 37, #1970. [3] Kita et al. (2004) in *CPD*, 558. [4] Scott (2007) *Ann. Rev. Earth Planet. Sci.* 35, 577. [5] Hevey & Sanders (2006) *MAPS* 41, 95. [6] Sanders & Taylor (2004) in *CPD*, 915. [7] Bizzarro et al. (2005) *ApJ* 632, L41. [8] Thrane et al. (2006) *ApJ* 646, L159. [9] Kleine et al. (2005) *GCA* 69, 5805. [10] Burkhardt et al. (2007) *MAPS* 42, #5189. [11] Chabot & Haack (2006) in *MESS II*, 747. [12] Yang, Goldstein, & Scott (2007) *Nature* 446, 888. [13] Asphaug et al. (2006) *Nature* 439, 155. [14] Bottke et al. (2005) *Nature* 439, 821. [15] Sugiura and Hoshino (2003) *MAPS* 38, 117. [16] Wasson et al. (2006) *GCA* 70, 3149. [17] Krot et al., this vol. [18] Trieloff et al. (2003) *Nature* (2003) 422, 502. [19] Krot et al. (2005) *Nature* 436, 989. [20] Wadhwa et al. (2006) in *MESS II*, 715. [21] Nyquist et al., this vol. [22] Scott & Sanders, this vol. [23] Kleine et al. (2004) *GCA* 68, 2935. [24] Halliday & Porcelli (2001) *EPSL* 192, 545. [25] Scott (2006) *Icarus* 185, 72. [26] Haghighipour & Scott (2007) *DPS abst*. [27] Rudraswami & Goswami (2007) *EPSL* 257, 231. [28] Wetherill & Inaba (2000) *Space Sci. Rev.* 92, 311. [29] Bogard (1995) *MAPS* 30, 244.

Re-Os Isotope Dating of Meteorites and Early Solar System Chronology: A Review F. Sedaghatpour[1] and D. W. G. Sears[2], [1, 2]Arkansas Center for Space and Planetary Sciences, and [2]Department of Chemistry and Biochemistry, University of Arkansas, Fayetteville, AR 72701, USA

Introduction: The Re-Os isotopic system is the most recent of a series of long-lived radiogenic isotope systems used for the study of early solar system materials and several proerties of the system make it particularly valuable [1, 2]. The half life of ^{187}Re is comparable to the age of the solar system, making it suitable for dating soilar system events. The siderophilic nature of the Re and Os causes them to concentrate in metal phases, so the system is useful to address the chronology of of core formation [3], the crystallization path and ages of asteroidal cores [4, 5], and the age of different types of metal-rich meteorites and, consequently, the chronology and early history of the solar system [1, 6]. Since Os is highly compatible element and enriched in the residual solid, while Re is moderately incompatible and enriched in the melt, the system is suitable for studying igneous processes, and thus Re/Os is a factor of ~100 higher in basalts than in the mantle. Finally, the system contains nucleosynthetic information since ^{187}Re is an r-process nuclide, ^{186}Os is an s-process nuclide, and ^{187}Os contains radiogenic and s-process components.

On the other hand, precise and accurate determination of the Re decay constant has been a challenge (the value 1.64×10^{-11} y^{-1} with a 3% uncertainty is most widely used [8, 9]), and measurement of ^{187}Re and ^{187}Os in meteorites is difficult because of very low concentrations (3-0.3 ppm). However, within the past twenty years the Re-Os system has achieved a degree of success in geology and cosmochemistry, particularly with reghard to chronology. Our present objective is to review the Re-Os isotopic dating of different groups of meteorites, especially iron and chondritic meteorites.

Iron Meteorite: Measurements of iron meteorite ages in the 1960s using the Re-Os method reported ages of ~4000 My [10, 11]. In 1980 Luck et al. [1] determined the ^{187}Re/^{186}Os and ^{187}Os/^{186}Os ratios of five iron meteorites. Using $1.52 \pm 0.04 \times 10^{-11}$ y^{-1} for λ^{187}Re, Luck et al [6] obtained the age of 4250 ± 50 My as the first precise age of this type of meteorite which is consistent with the value reported from Rb-Sr measurements on silicate fraction (4350 ± 100) [12]. Pernica's and Wasson's [13] investigation of the Re/Os fractionations in the iron meteorites showed no significant change in Re/Os ratio with Ni content in nonmagmatic groups. However, the Re/Os ratio increases by a factor 3 from low-Ni to high-Ni members of the magmatic groups IIA and IIIAB. Therefore, the Re/Os ratio change is large enough to allow Re-Os age determination for each of those groups. Horan et al. [14] showed that the Re-Os isotopic systematics of group IIA closed near the age of solar system (between 4444 - 4560 My), and their initial ^{187}Os/^{186}Os ratio was the same as that of carbonaceous chondrites. Data for IA, IIB and IIIA irons all plotted above the IIA isochron in this study (Fig.1).

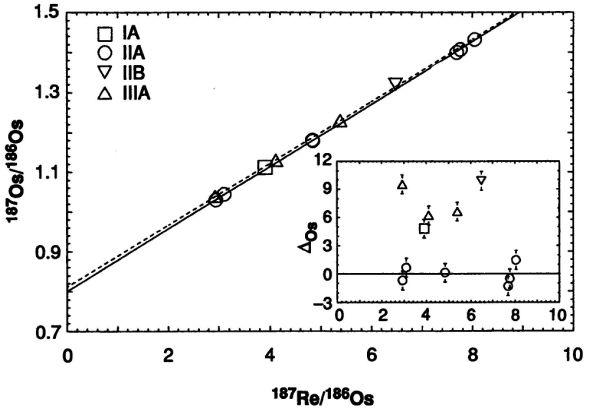

Fig.1 Plot of ^{187}Os/^{186}Os versus ^{187}Re/^{186}Os for iron meteorites in different groups. Isochron are regressed trough the IIA data (solid line) and IIIA data (dashed line). The inset shows the per mil deviation in ^{187}Os/^{186}Os from the IIA isochron, ΔOs, versues ^{187}Re/^{186}Os [14].

The data implied that the parent body of the IIIA iron meteorite melted and cooled 100 My after the oldest portions of chondrites. The other interpretation is that, if all those irons closed to Re and Os at the same time, their parent bodies would either form with different Os isotopic composition or change to different Os isotopic composition before core formation.

Morgan et al. [15] reported the age of 4584 ± 43 My for five meteorites of group IIA and eight meteorites of IIB, which is well within error of the canonical age of solar system. Most IIB irons are plotted on or within error of the IIA isochron, and their data gave an age of 4577 ± 37 My for this group. The younger age of 4430 ± 0.05 My for group IIB than group IIA was reported by Smoliar et al. [16], which is consistent with previous work. Their results are consistent with rapid core segregation, differentiation and crystallization in the IIAB parent. Using improved analytical techniques, Chen et al. [17] reported Re-Os data for low Re and PGE pallasites and IIIAB irons, which shows an age of 4560 ± 0.01 My for IIIAB and an age of 60 My younger for pallasites.

Chondrites: Chondrites probably represent one of the most primitive samples of the primordial solar nebula. They consist of materials agglomerated during the early solar system evolution. Therefore, chondrite me-

teorites provide the initial composition of Os in the early solar system. However, contrary to magmatic irons, chondrites show a relatively minimal spread in Re/Os ratios. Therefore, obtaining precise isochrons for chondrite groups is a challenge. Despite this, Re-Os isotopic studies of chondrites are of interest [2]. First, as pointed out by Walker et al. [18], "the precise determination of the initial $^{187}Os/^{188}Os$ ratio of the solar system may prove critical for ultimately utilizing the system to date refractory components in chondrites". Second, the characterization of the long-term evolution of ^{187}Os in different chondrite groups may provide constraints on the behavior of their highly siderophile elements during the early solar system [2], and also help to characterize the materials added to planetary mantle through the late accretion. Third, differences in the modern Re/Os and the time-integrated $^{187}Os/^{188}Os$ of whole-rock chondrites may reflect fractionations resulting from high-temperature nebular condensation processes in precursor materials. Therefore, this system can provide a robust method to compare the nebular histories of refractory phases within chondrite components.

Luck et al. [1, 6] reported the first Re-Os isotopic data for metal phases separated from ordinary chondrite. Re-Os isotopic reported for the whole rock samples of carbonaceous chondrites (group CI, CM, CV and CO) and an ordinary chondrite (Semarkona, LL3) [19] showed a significant difference between irons and chondrites. A younger age for iron meteorites was reported in this study. Most chondrites plotted 1 - 2% above the iron meteorites. They suggested that either irons have significantly younger Re-Os closure ages than chondrites or that chondrites were formed from precursor materials with different chemical histories from the precursors of irons. Being plotted 4 – 6% above the iron meteorite isochron, Semarkona (LL3) and Murray (C2M) may have lost Re by aqueous alteration. However, since there is an evidence for only slight aqueous alteration in Semarkona, the Re-Os isotopic composition can reflect the isotopically heterogeneous components in the primordial solar nebula.

Calcium-Aluminium-rich Inclusions: Calcium-Aluminium-rich Inclusions (CAIs) are inclusions in chondritres that are thought to be either the first minerals to condense in the solar nebula or the high temperature residues of flash heating. The Re-Os systematics of CAIs in chondrite clarify the Re-Os system's behavior in bulk chondrites and the timing of chemical fractionation in primitive chondrites [20]. Re-Os systematic of CAIs in carbonaceous meteorites has been investigated by Becker et al. [20]. It was shown that differences in Re/Os early established in solar system history are the major cause of the observed variability of $^{187}Os/^{188}Os$ in CAIs. No overlapping between the abundance of group II CAIs and the other groups was reported. This suggests that the group II CAIs have lost the bulk of their highly refractory elements in a previous condensation event. In this study, some bulk CAIs and CAI splits plotted on the IIIA iron meteorite isochron reference resulting in 4558 My age. Whereas, eight samples plotted off the isochron. This deviation could have reflected either chemical differentiation in the early solar system or primitive heterogeneities in $^{187}Os/^{188}Os$. However, there are neither evidences for such a fractionation nor resolvable anomalies in other Os isotopic ratios for thes CAIs to prove the primordial heterogeneities. The most likely explanation for this deviation is late-stage movement of Re or Os in CAI samples.

Conclusion: The Re-Os isotopic has allowed unique advances in the precise chronology of meteorites, this is despite experimental difficulties and uncertainty in Re decay constant. The Re-Os age dating has accomplished for the iron groups and their initial isotopic ratio determined. High- precision analysis of chondrites and refractory components has been achieved.

References: [1] Luck. J. M. et al (1980) *Nature* **283**, 17, 256. [2] Shirey S. B. et al (1998) *Anuu. Rev. Earth Planer. Sci.* **26**, 423. [3] Walker R. J. et al (1995) *Science* **169**, 819. [4] Shen. J. J. et al (1996) *Geochim. Cosmochim. Acta* **60**, 2887. [5] Smoliar M. I. et al (1996) *Science* **271**, 1099. [6] Luck J. M. et al (1983) *Nature* **302**, 130. [7] Clayton D. D. (1964) *Astrophys. J.* **139**, 637. [8] Selby D. et al. (2007) *Geochim. Cosmochim. Acta* **71**, 1999. [9] Linder M. et al. (1989) *Geochim. Cosmochim Acta* **53**, 1597. [10] Herr W. et al (1961) *Naturforschung* **16a**, 1053. [11] Hirt B. et al (1963) *Radioactive dating*, 35. [12] Murthy V. R., Coscio, M. R. and Sabelin T. (1997), *Geochim. Cosmochim. Acta* **8**, 177-186. [13] Pernica E. et al (1987) *Geochim. Cosmochim Acta* **51**, 1717. [14] Horan M. F. et al. (1992) *Science* **255**, 1118. [15] Morgan J. W. et al (1995) *Geochim. Cosmochim Acta* **59**, 11, 2331. [16] Smoliar M. I. et al *LPS XXVIII*, 1341. [17] Chen J. H. et al (2002) *Geochim. Cosmochim Acta* **66**, 21, 3793. [18] Walker R. J. et al. (2002) *Geochim. Cosmochim Acta* **66**, 23, 4187. [19] Walker R. J. and Morgan J. W. (1989) *Science* **243,** 519. [20] Becker H. et al. (2001) *Geochim. Cosmochim Acta* **65**, 19, 3379.

TIMESCALES OF CAI FORMATION IN THE SOLAR PROTOPLANETARY DISK AS REVEALED BY Si AND Mg ISOTOPES. A. Shahar[1] and E. D. Young[1, 2], [1]Department of Earth and Space Sciences, University of California Los Angeles, 595 Charles Young Dr. E., Los Angeles, CA 90095 (ashahar@ess.ucla.edu), [2]Institute of Geophysics and Planetary Physics (eyoung@ess.ucla.edu).

Introduction: While it is well known that igneous CAIs tend to have high $^{29}Si/^{28}Si$ and $^{25}Mg/^{24}Mg$ relative to chondritic values, there have been few systematic studies that relate observed isotopic fractionations in CAIs to their conditions and timescales of formation. Together with a wealth of information about the physical chemistry associated with evaporation and condensation of CAI-like liquids, a recent study [1], constructed a P_{H2}-time curve unique to a CAI (Leoville 144A) that constrains the astrophysical setting of CAI melting. This study builds on that previous one by analyzing more CAIs by LA-MC-ICPMS and modeling the results to deduce the thermal histories of igneous CAIs in general.

Analytical Methods: Silicon and magnesium stable isotope ratios were measured using UV laser ablation MC-ICPMS. Corrections for instrumental mass bias were performed by sample-standard bracketing with an in-house standard (San Carlos olivine). We used a 193 nm excimer laser operated with a pulse rate of 2 to 6 Hz. *In situ* analyses were acquired from spots measuring 100 um in diameter for Si, and 55 um in diameter for Mg. Precision of the LA-MC-ICPMS analyses is on the order of +/– 0.2‰.

Modeling: We modeled the isotopic evolution of CAIs, including rates of mass loss, time-dependent variations in isotope ratios, and time-dependent variations in elemental concentrations. The models consist of numerical solutions to the problem of elemental and isotopic fractionation at the moving surface of an evaporating sphere coupled with diffusive transport within the sphere. In order to validate our calculation scheme we compared models for the measured changes in Mg and Si isotope ratios with laboratory experiments [2] and [3].

Astrophysical Implications: The Si and Mg isotope data place important constraints on where in the solar protoplanetary disk CAIs may have been melted and subsequently heated. If melting occurred in shockwaves, the likely pressure was between 10^{-5} to 10^{-3} bar for a cumulative time of up to a few days (Fig. 1). On the other hand if melting occurred in solar flare events the timescale could have been a few weeks.

Number Density: The substantial Si and Mg isotopic fractionation in CAIs suggest that their number densities were too low to permit an overall elevation in background partial pressure of Mg and SiO that would have prevented fractionation. We quantified this effect by estimating the pressure of gas molecules or atoms produced by a population of evaporating CAIs. The result is a linear spacing of > 8 meters, which corresponds to a number density that is four orders of magnitude lower than that for chondrules [4].

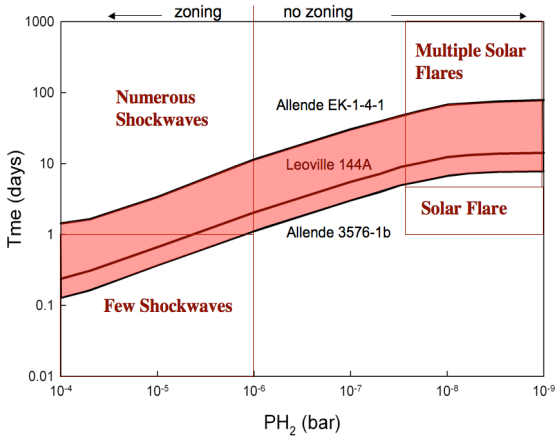

Fig. 1 Calculated P_{H2}-time curves for evaporation of two CV igneous CAIs and a FUN inclusion (latter from published data.

Conclusions: Silicon and magnesium isotope ratios obtained in situ by laser ablation MC-ICPMS in igneous CAIs reveal a detailed picture of the astrophysical setting of CAI melting and subsequent heating. Models for the chemical and isotopic effects of evaporation of molten CAIs, validated by published evaporation experiments, are used to produce a unique univariant relationship between P_{H2} and time during melting. These stable isotope data point to a two-stage history for some igneous CAIs involving melting for days to months followed by subsolidus heating for years to hundreds of years. The thermobarometric history deduced from combining Si and Mg isotope ratio data implicates thermal processing in the disk, perhaps by passage through shockwaves, following melting. This study underscores the direct link between the meaning of stable isotope ratio zoning, or lack thereof, and the inferred astrophysical setting of melting and subsequent processing of CAIs.

References: [1] Shahar, A. and Young E. D. (2007) *EPSL, 257,* 497-510. [2] Richter F. M. et al. (2002) *GCA, 66,* 521-540. [3] Janney P. E. et al. (2005) *LPS XXXVI,* Abstract #2123. [4] Cuzzi J. N. (2006) *Nature, 441*, 483-485.

OPEN-SYSTEM BEHAVIOR OF CAIs: A KEY COMPONENT TO THEIR $^{26}Al/^{26}Mg$ CHRONOLOGIES. Justin I. Simon[1,2] and Edward D. Young[3,4], [1]Earth & Planetary Science, University of California Berkeley (simon@eps.berkeley.edu), [2]Berkeley Geochronology Center, [3]Earth & Space Sciences, University of California Los Angeles, [4]Institute of Geophysics and Planetary Physics, University of California Los Angeles.

Introduction: Refractory calcium- aluminum-rich inclusions (CAIs) are comprised of high temperature minerals and record the oldest age of any solid material formed in our solar system. Constraining the duration and timing of CAI formation is important because it governs astrophysical models for the solar nebula. Magnesium isotopes have proven particularly useful for reconstructing the history of the solar system. Under favorable circumstances the abundance of the short-lived nuclide ^{26}Al (half-live = 0.73 Ma) that decays to $^{26}Mg^*$ is undisturbed, providing a high-resolution relative chronometer. Techniques to analyze $^{27}Al/^{24}Mg$, $^{25}Mg/^{24}Mg$, and $^{26}Mg/^{24}Mg$ isotope ratios in solution by MC-ICPMS and *in situ* by both MC-SIMS and laser ablation MC-ICPMS have greatly improved our ability to extract information from the ^{26}AL-^{26}Mg system over the last ~5 years (e.g., [1-3]).

For over ~30 years $^{26}Al/^{26}Mg$ chronometry indicated that many CAIs had initial $^{26}Al/^{27}Al$ ratios of 4-5x10^{-5} and for this reason ~5x10^{-5} has been referred to as the "canonical" value of the solar system. Its common occurrence was assumed to reflect a uniform initial distribution of ^{26}Al within the solar system. The canonical value has been recently revised upwards to the "supra-canonical" $(^{26}Al/^{27}Al)_0$ value of ~6-7x10^{-5} [4-7]. The absolute time difference corresponding to the different $(^{26}Al/^{27}Al)_0$ values is ~200 to 400 ka. The debate regarding the significance of canonical values, given the existence of a supra-canonical value, is heightened by additional investigations reporting highly precise canonical and supra-canonical measurements [8, 9]. The ubiquity of measured canonical $(^{26}Al/^{27}Al)_0$ values compelled Young and others [4] to model the difference between their evidence for canonical and supra-canonical $(^{26}Al/^{27}Al)_0$ values as closed system resetting of the Al-Mg system by transient heating events while ^{26}Al was actively decaying to $^{26}Mg^*$. Following the evidence and logic of Simon and others [10] that most (perhaps all) CAIs have experienced some degree of open system nebular processing, next we describe how the complexities of CAI $^{26}Al/^{26}Mg$ chronometry might be reconciled.

Discussion: Based on our detailed core-to-rim traverses across CV3 CAIs by LA-MC-ICPMS we suggest a general model for the formation of end-member Mg isotope zoning profiles and $^{26}Al/^{26}Mg$ chronologies [11]. It considers the effect of isotopic exchange with a chondritic gas as a mechanism to explain the observed differences. Mg isotope zoning profiles and $^{26}Al/^{26}Mg$ chronometry reported by others [12-15] can also be explained by such a model. Accurate determination of the $^{26}Al/^{27}Al_0$ values of CAI fragments are subject to the vagaries of sampling if they contain internal heterogeneity. Understanding the origin and extent of isotopic zoning in CAIs may help explain the apparent discrepancy between supra-canonical and canonical $^{26}Al/^{27}Al_0$ values.

We assume that the measured zoning profiles reflect modification of the Mg isotopic composition recorded by CAIs due to condensation and evaporation (e.g., [16], and references therein). Following Simon and others [11] the measured Mg isotope zoning profiles can be modeled with a set of simple numerical solutions considering radial diffusive Mg transfer in a solid sphere. These models depict CAIs at subsolidus temperatures and consider the effect of Mg isotopic exchange with surrounding chondritic gas. Mg diffusivities, isotopic compositions, and abundances are known for CAI interiors. The isotopic composition of the Wark-Lovering rims along with the Mg abundance in a 10^{-3} bar chondritic gas complete the set of initial boundary concentrations in these calculations. Model calculations fit to Mg isotope measurements can be seen in Figure 1. They are consistent with variable effects of reheating and isotopic exchange with a chondritic gas, resulting in a variety of modifications to original isotopic profiles (compare 3576 "b", right panel with144A, left panel). We suggest that this reheating and partial isotopic exchange of CAIs with a chondritic gas occurred contemporaneously with their internal Al-Mg isotopic resetting (i.e., [4]), both contributing to the observed canonical $(^{26}Al/^{27}Al)_0$ values. Collectively these models provide a logical explanation for the existence of CAIs with supra-canonical $(^{26}Al/^{27}Al)_0$ values and the preponderance of CAIs with canonical $(^{26}Al/^{27}Al)_0$ values.

Simple isotope exchange results in "dilution" of supra-canonical $^{26}Mg^*$. Therefore the Al/Mg ratio of bulk objects and that of their constituents are unaffected by this process (Al is stoichiometrically controlled by the tschermak substitution mechanism). For this reason bias produced by distinct sampling procedures might be expected. Bizzarro and others [9, 17] sample "bulk" CAIs by microdrilling whereas others dislodge isolated CAI fragments [4, 7, 8]. Neither approach likely produces a truly representative bulk CAI measurement. In the former, "coring" out the åkermanite-rich interiors is consistent with the very low "bulk" Al/Mg ratios in [9, 17]. These "cores" that come from the interior of CAIs, would be shielded by their outer margins, and would be therefore less susceptible to $^{26}Mg^*$ dilution by Mg isotope exchange. On the other hand, analysis of bulk CAIs fragment would include more (or entirely) CAI margin material (spherical volume goes to the radius cubed) and would be therefore preferentially diluted by canonical $^{26}Mg^*$ (e.g., [8]). The elevated $^{26}Mg^*$ intercept value (+0.039±0.055) of the potentially "diluted" data of Jacobsen and others [8] as compared to the $^{26}Mg^*$ value (-0.0317±0.0038) of the CAI "cores" of Thrane

and others [9] is consistent with the downward bulk $^{26}Mg^*$ and subbulk CAI Al/Mg of the "diluted" whole fragments and microdrilled samples, respectively, as predicted by our model. If the CAIs sampled by microdrilling exclude portions that have been penetrated by open system exchange processes then a ~$6x10^{-5}$ supra-canonical value may represent the solar system initial, otherwise it may be higher still. Furthermore if some CAI "cores" have not experienced $^{26}Mg^*$ dilution, but are lower than their true bulk Al/Mg compositions then an even lower intercept would be expected. A lower intercept is also consistent with the possibility of a higher supra-canonical $^{26}Al/^{27}Al_0$ value and might explain the apparently low initial Al/Mg value of CAIs as compared to chondrites (and the apparently higher $^{26}Mg^*$ abundance of Earth, Mars, and chondrites, cf. [9]). Regardless of the actual initial $^{26}Al/^{27}Al$ value of the solar system it follows that the canonical value represents a younger event(s), common to many CAIs, that likely involved episodic thermal processing (e.g.,[4]).

Conclusion: Despite the antiquity and refractory nature of CAIs many are clearly not pristine nebular condensates but have undergone significant reprocessing, including episodes of partial to complete remelting, partial evaporation [18], recrystallization [19], and open system chemical exchange [10] in the solar nebula prior to chondrite accretion. For these reasons it is possible that no reported CAI preserves a primary record of nebula condensation and that if more precise measurements could be made of the least modified cores of CAIs that the apparent supra-canonical values may need to be revised upwards still.

References: [1] Galy, A., et al., *JAAS*, 2003. **18**: p. 1352-1356, [2] McKeegan, K.D., et al. *Met. Soc.*, 2004, [3] Young, E.D., et al., *GCA,* 2002. **66**: p. 683-689, [4] Young, E.D., et al., *Science*, 2005: doi. 1108140, [5] Bizzarro, M., J. Baker, and H. Haack, *Nature Corrigendum*, 2005. **435**: p. 1280, [6] Taylor, D.J., et al. *Met. Soc.* 2005, [7] Galy, A., I.D. Hutcheon, and L. Grossman, *LPSC*. 2004, [8] Jacobsen, B., et al. *LPSC*. 2007, [9] Thrane, K., M. Bizzarro, and J. Baker, *The Astro. J.*, 2006. **646**: p. 159-162, [10] Simon, J.I., et al., *EPSL*, 2005. **238**: p. 272-283, [11] Simon, J.I., et al. *LPSC*. 2006, [12] Richter, F.M., et al. *LPSC*. 2007, [13] Fahey, A.J., et al., *GCA*, 1987. **51**: p. 3215-3229, [14] Caillet, C., et al., *LPSC,* 1997, [15] Lui, M.-C., et al. *LPSC*. 2005, [16] Davis, A.M. and F.M. Richter, in *Meteorites, Comets, and Planets*, A.M. Davis, Editor. 2004. p. 407-430, [17] Bizzarro, M., J.A. Baker, and H. Haack, *Nature*, 2004. **431**: p. 275-278, [18] Grossman, L., et al., *GCA*, 2000. **64**: p. 2879-2894, [19] Podosek, F.A., et al., *GCA*, 1991. **55**: p. 1083-1110.

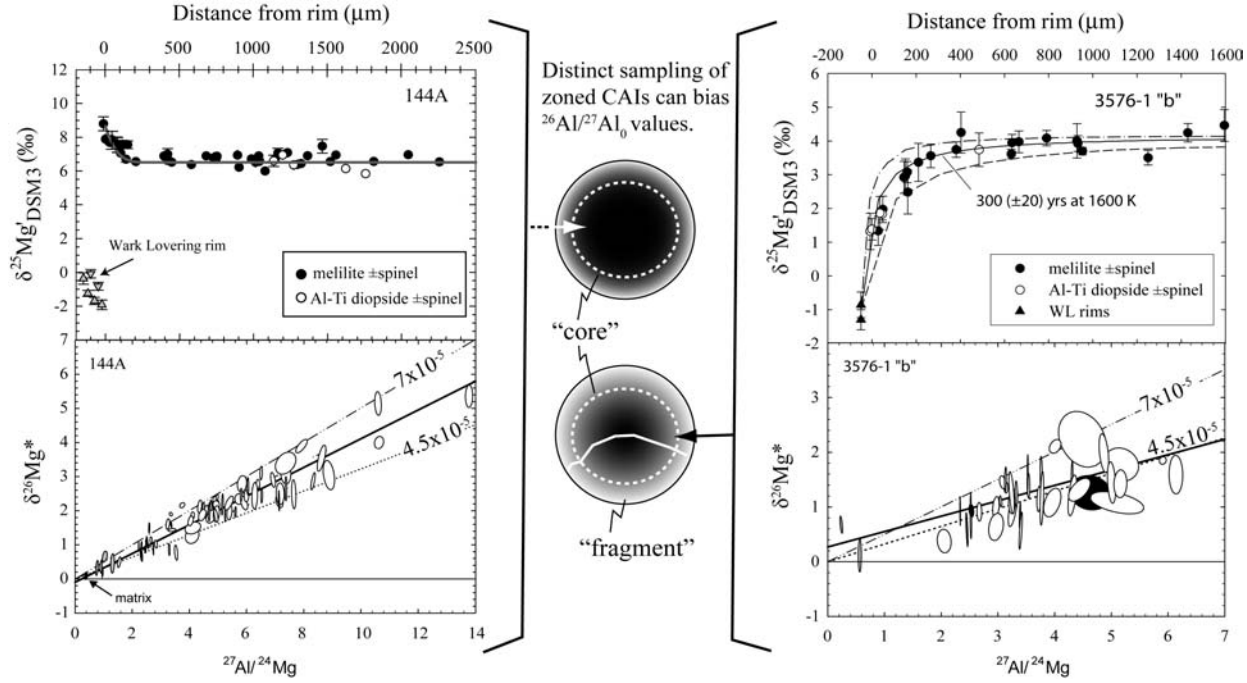

Supra-canonical $(^{26}Al/^{27}Al)_0 = (5.74\pm0.32)x10^{-5}$
intercept = -0.14±0.08; MSWD = 3.5 (β=0.514)

Canonical $(^{26}Al/^{27}Al)_0 = (3.81\pm0.75)x10^{-5}$
intercept = 0.24±0.20; MSWD = 1.6 (β=0.514)

Figure 1. 144A and 3576 "b" CAIs show endmember Al-Mg systematics. Upper panels: Mg isotope zoning profiles for CAIs with little (left) to significant (right) evidence for open system isotopic exchange likely leading to $^{26}Mg^*$ dilution of the $^{26}Al/^{26}Mg$ chronometer. Model calculations of [11] for reference. Lower panels: corresponding Al-Mg internal isochrons defined by LA-MC-ICPMS data. Heavy line is best fit regression; also included are dah-dot line = $7x10^{-5}$ and dotted line = $4.5x10^{-5}$ (canonical) for reference. Two sigma error ellipses are shown.

DETECTION OF RARE CO ISOTOPOLOGUES IN PROTOSTELLAR DISKS: AN INFRARED INVESTIGATION OF MOLECULAR SELF SHIELDING. R. L. Smith[1], K. M. Pontoppidan[2], E. D. Young[1,3], M. R. Morris[4] & E. F. van Dishoeck[5]. [1]Dept. of Earth & Space Sciences, University of California Los Angeles (UCLA) (rsmith@ess.ucla.edu), [2]Division of Geological & Planetary Sciences, California Institute of Technology, Pasadena, CA, Hubble Fellow (pontoppi@gps.caltech.edu), [3]Institute of Geophysics & Planetary Physics, UCLA (eyoung@ess.ucla.edu), [4]Dept. of Physics & Astronomy, UCLA (morris@astro.ucla.edu),[5]Leiden Observatory, Huygens Laboratory, NL- 2300 RA Leiden, The Netherlands (ewine@strw.leidenuniv.nl)

Introduction: Here we report an astronomical approach toward investigating molecular self shielding by CO on the surfaces of circumstellar disks. We have detected the fundamental vibrational band of four stable CO isotopologues, including the rare species, $C^{17}O$, in the protostellar object IRAS 19110+1045 with NIRSPEC on the Keck II Telescope. We also report detection of at least 3 of the more abundant CO isotopologues in the solar-type young stellar object, RNO 91, using first-run, high-resolution data obtained with the European Southern Observatory's (ESO) CRIRES spectrograph on the Very Large Telescope (VLT).

Molecular self shielding by CO: The mass-independent variation of oxygen abundances, $^{18}O/^{16}O$ and $^{17}O/^{16}O$, is a pronounced and intriguing feature among rocky bodies in the solar system. One plausible explanation for this phenomenon is self shielding by $C^{16}O$ against photodestruction by far-UV from the central star. Known to be important in the interstellar medium [1,2], molecular self shielding refers to the blocking of photodissociating wavelengths of light by optically thick molecular species. CO absorbs far ultraviolet (FUV) wavelengths in proportion to column densities of the constituent oxygen isotopologues, $^{12}C^{16}O$, $C^{17}O$ and $C^{18}O$. Because interstellar $^{16}O/^{18}O$ and $^{16}O/^{17}O$ ratios are ~ 500 and ~ 2600, respectively, $^{12}C^{16}O$ will be more optically thick and thus photodissociate at a lesser rate (i.e. "self shield" to a greater degree) than $C^{17}O$ and $C^{18}O$ [3].

Our goal is to use infrared spectroscopy to search for $C^{16}O/C^{18}O$ and $C^{16}O/C^{17}O$ excesses in protostellar disks around young stellar objects (YSOs) — environments believed to be similar to the early solar nebula — to test the plausibility of the self shielding phenomenon as a cause for oxygen isotope anomalies. This study will test the viability of the Lyons & Young [4] model for isotope-specific CO photodissociation in disk surface layers (Figure 1). This model predicts that the surfaces of circumstellar disks around YSOs should exhibit high $C^{16}O/(C^{18}O,C^{17}O)$ relative to the surrounding interstellar environment.

Motivation: A recent study reported detection of a high $C^{16}O/C^{18}O$ ratio (800 +/– 500) in the disk surrounding HL Tau, based on high-resolution measurements of IR absorption by gas in the outer disk at ~ 100 K [5]. This offers tantalizing evidence that CO self shielding of stellar UV may be a feature of the chemical evolution of disks, and provides motivation for further study.

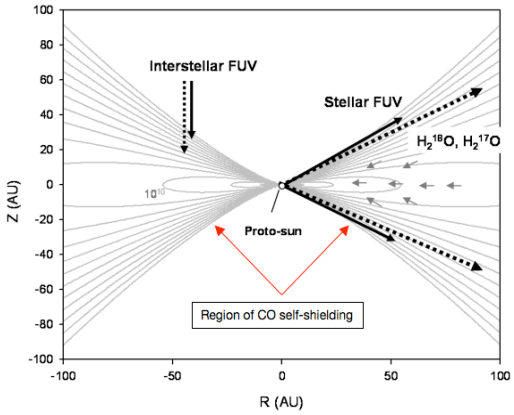

Figure 1. Contour map of a circumstellar disk viewed edge-on, as described for the accretion disk surrounding DM Tau [6]. FUV originates from a central star or interstellar sources. Contours are hydrogen number density, increasing inward at decade increments. Dashed lines are optically thin FUV wavelengths that dissociate $C^{18}O$ and $C^{17}O$ [4].

Methods, results & discussion:

IRAS 19110+1045: We analyzed spectra of the CO 4.7 μm fundamental band in the protostellar object IRAS 19110+1045. These data were collected with the NIRSPEC spectrograph at Keck II Telescope in a 15 minute integration by Geoff Blake's research group at the California Institute of Technology. Spectral resolution is $R = \Delta\lambda/\lambda$ = 25,000 (~12 km/s). Of particular interest is the detection of $C^{17}O$, appreciable signals of which have not been detected in the near IR. Column densities were obtained using the equivalent widths for optically thin species $C^{18}O$ and $C^{17}O$. A rotational excitation plot was used to estimate the temperatures for these molecules (Figure 2). The ^{13}CO and $C^{17}O$ lines are best fit with a two-temperature model. The apparent break in slope for these species could be due to a temperature gradient in the disk or, in the case of

^{13}CO, a large optical depth (τ). We cannot rule out a temperature gradient from these data.

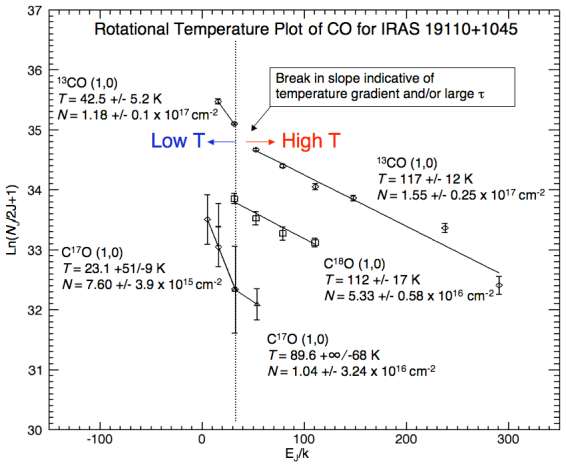

Figure 2. Rotational plot for presumed optically-thin CO isotopologues. Each point represents a separate absorption line from the fundamental ro-vibrational band. One-sigma error bars are from the continuum fit [7].

A curve of growth analysis was used to obtain column densities for optically thick species, ^{13}CO and ^{12}C^{16}O, and final abundance ratios (Figure 3).

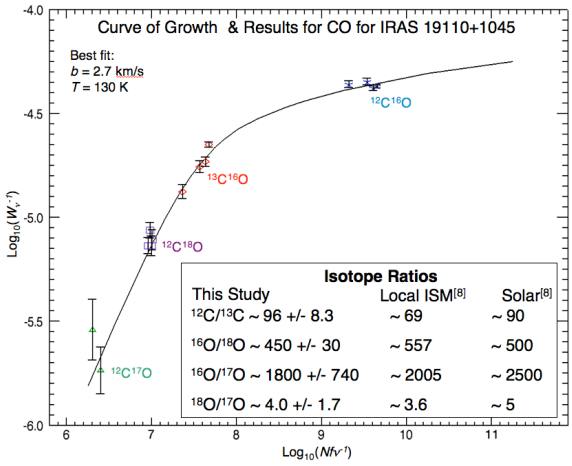

Figure 3. Curve of growth for IRAS 19110+1045. Isotope ratios, determined from inferred column densities, are shown for this study in comparison with local ISM and solar abundances. Errors are 1 se [7].

We found a best-fit temperature of ~130 K and isotope ratios consistent with solar/ISM compositions, albeit with large errors: ^{12}C/^{13}C ~ 96 +/– 8.3 (1 se), ^{16}O/^{18}O ~ 450 +/– 30, ^{16}O/^{17}O ~ 1800 +/– 740, ^{18}O/^{17}O ~4.0 +/– 1.7. No evidence for molecular self shielding by CO (an effect expected to be possibly as large as tens of percent) was found for this object.

RNO 91: We have recently begun analyzing very high-resolution (R = Δλ/λ = 100,000) spectra for the young stellar object, RNO 91. These first-run data were collected by Pontoppidan and collaborators using the CRIRES spectrograph on the Very Large Telescope (VLT) at Paranal Observatory. The superior resolving capability of the CRIRES spectrograph allows us to resolve the CO absorption lines, which should ultimately enable us to use their profiles for accurate isotope ratio determinations.

Preliminary results include unequivocal detection of ^{12}C^{16}O, ^{13}CO and C^{18}O (C^{17}O is not yet detected at a significant level). Emission features were also visible. We found a slight trend toward increased line broadening for the less abundant isotopologues: average FWHM = 5.1, 5.4 and 5.8 (km/s) for ^{12}C^{16}O, ^{13}CO and C^{18}O, respectively, suggesting that a multi-component disk model may be needed to explain these data.

Conclusions and future work: Our analysis of IRAS 19110+1045 indicates that all four CO isotopologues are detectable in the infrared ro-vibration lines. No evidence for CO self shielding was found for this object. However, because observations to date have been made with relatively short integration times, we are confident that CO self shielding at disk surfaces is a testable hypothesis using deeper integrations. We anticipate more conclusive results using high-resolution data sets and forthcoming collection runs tailored to our project goals.

References: [1] Bally J. & Langer W. D. (1982) *ApJ 255*, 143-148. [2] Sheffer Y. et al. (2002) *ApJ* 574, L171-L174. [3] van Dishoeck E. & Black J. H. (1988) *ApJ 334*, 771-802. [4] Lyons J. R. & Young E. D. (2005) *Nature 435*, 317-320. [5] Brittain S. D. et al (2005) *ApJ 626*, 283-291. [6] Aikawa Y. & Herbst E. (2001) *A&A 371*, 1107-1117. [7] Smith et al. (2007) *LPS XXXVIII,* Abstract #2293. [8] Wilson T. L. (1999) *Rep. Prog. Phys. 62,* 143-185.

FIB-TEM INVESTIGATION OF AN ALLENDE TYPE A CAI INTERIOR AND THE ASSOCIATED WARK-LOVERING RIM. Rhonda M. Stroud[1]. Thomas J. Zega[1], Mariana Cosarinsky[2] and Kevin D. McKeegan[2], [1]Code 6366 Naval Research Laboratory, Washington DC, 20375 (stroud@nrl.navy.mil). [2] Dept. Earth & Space Sciences, UCLA, Los Angeles, CA – 90095-1567.

Introduction: The outer boundaries of calcium aluminum rich inclusions (CAIs) typically consist of concentric layers of oxide and silicate minerals, known as Wark-Lovering rims (WLRs). These WLRs are thought to have formed by either flash heating [1] or condensation [2]. In the case of a type A CAI (G4a TS#25) from the Allende CV3 meteorite, isotopic analyses show that WLR formed $1.3x10^5$ years after the interior, based the well-correlated isochrons in Al-Mg evolution diagrams [3]. In order to further constrain the relationship between the CAI interior and WLR, and the formation conditions of each, we are conducting FIB-enabled, correlated isotope-structure studies. We present herein results of transmission electron microscopy (TEM) studies of interior and WLR sections.

Methods: We used an FEI Nova 600 focused ion beam-scanning electron microscope (FIB-SEM) equipped with an Ascend Extreme Access lift-out tool to produce site-specific sections of the CAI and WLR for TEM analysis [4]. The extracted rim section spanning the entire WLR, is approximately 20 μm across by ~ 6.5 μm deep. The interior section is 21 μm by 7.4 μm. The TEM analysis was carried out with a JEOL 2200FS microscope equipped with a Thermo Noran NSS energy-dispersive spectrometer (EDS), and bright and dark field scanning transmission electron microscopy detectors. The mineral identifications are based on selected area diffraction and EDS results.

Results and Discussion: The interior section contained three grains: one each of spinel, hibonite and gehlenite. The grain boundary between the hibonite and spinel is flat, whereas the gehlenite shows round grain boundaries. The is no sign of replacement phases at any of the boundaries. The direction of curvature of these boundaries indicates that the gehlentite was the last to form. Although it is typical for melilite (of which gehlenite is the Al-rich end member) to enclose spinel in type A CAIs, this is inconsistent with the condensation sequence predicted equilibrium thermodynamic calculations [5]. However, it was previously suggested that the kinetics of epitaxial growth of spinel on hibonite can result in spinel condensation temperatures higher than melilite [6], as appears to be the case here.

Figure 1. Bright field STEM image of the CAI interior. Sp= spinel, Hib= hibonite, Geh= gehlenite.

Scanning electron microscopy of the WLR shows three layers: an innermost layer of spinel intergrown with hibonite blades and minor perovskite; an intermediate layer of melilite, pervasively replaced by anorthite; and an outermost layer of Ti-Al-rich pyroxene grading outwards to Al-diopside. The TEM analyses of the extracted section (Figure 2) reveal that the layers contain a complex mixture of polycrystalline material. Identified primary phases at increasing distance from the interior include: melalite, anorthite, wollastonite (tentative) and diopside. The grains are primarily subhedral in texture with grain sizes of a few microns. However, some grains, e.g., melilite, exhibit triple junctions with surrounding material. Inclusions occur both in and between the melilite and anorthite. Two aqueous alteration products [7], grossular and sodalite, also appear. The sodalite shows abundant radiation tracks. The origin of these tracks could be an important constraint on the timing and location of the aqueous alteration event that produced the sodalite. A solar flare origin would indicate that the hydration most likely occurred in the solar nebula, prior to accretion of the CAI onto the Allende parent body, possibly by mechanism similar to that described by Cielsa et al [8].

References:

[1] Wark D. and Boynton W.V. 2001 *Meteoritics and Planetary Science* 36:1135-1166. [2] Simon J.I. et al. 2005 *Earth and Planetary Science Letters* 238:272-283. [3] Cosarinsky M. et al. 2005. *Meteoritics and Planetary Science* 40: A34. [4] Zega T.J. et al. (2007) *Meteoritics and Planetary Science* in press. [5] Ebel D. 2006 in *Meteorites in the Early Solar System II*, 253-277. [6] Beckett J.R. et al. 1994 *Metoritics* 29:41-65. [7] Krot A. et al. 1995. *Meteoritics and Planetary Science* 30:748-775. [8] Ciesla F.J.et al. 2003 *Science* 200:549-552.

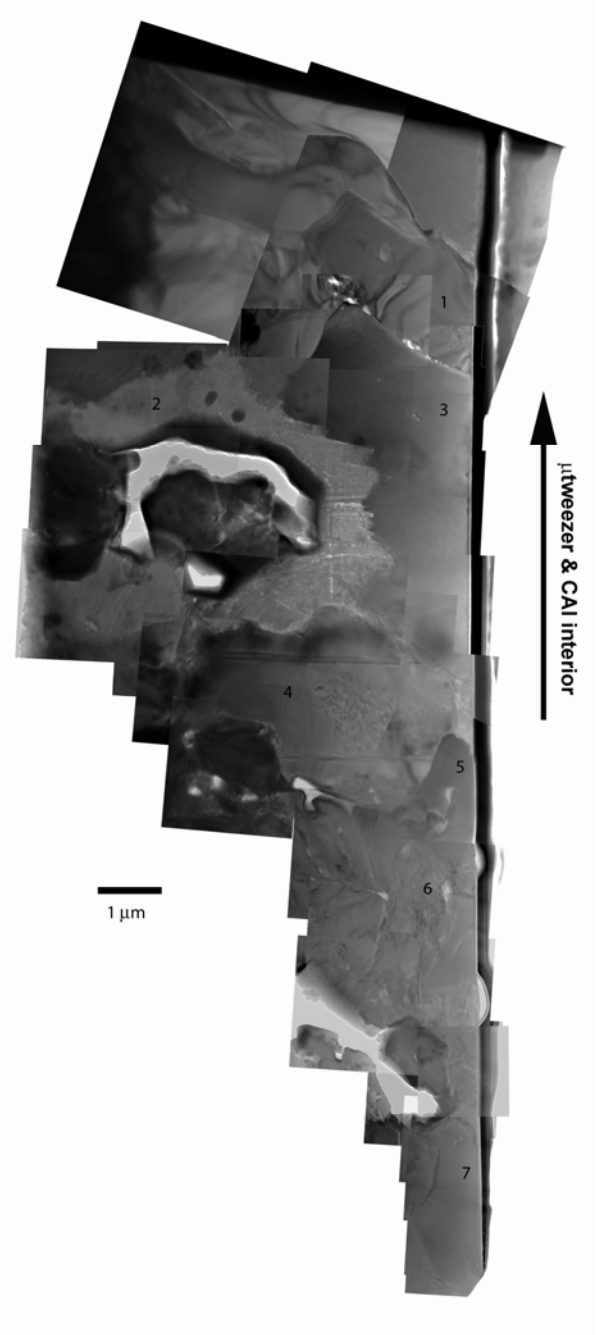

Figure 2. TEM mosaic of the Wark-Lovering RIM. The image is a composite of bright field images taken with the individual grains oriented along a crystal zone axis to highlight diffraction contrast features. The phases are: (1) melilite; (2) sodalite; (3) anorthite; (4) anorthite / pyroxene; (5) grossular; (6) wollastonite and (7) diopside. Note the track features (white stripes) in the sodalite.

A MIXING-FALLBACK SUPERNOVA AS A POSSIBLE SOURCE OF SHORT-LIVED RADIONUCLIDES IN THE EARLY SOLAR SYSTEM. S. Tachibana[1], A. Takigawa[1], J. Miki[1], and T. Yoshida[2], [1]Department of Earth and Planetary Science, University of Tokyo (7-3-1 Hongo, Tokyo 113-0033, Japan. E-mail: tachi@eps.s.u-tokyo.ac.jp), [2]National Astronomical Observatory of Japan (2-21-1 Osawa, Mitaka, Tokyo, 181-8588, JAPAN).

It has been known that several short-lived radionuclides were present in the early solar system from excesses in the abundances of their daughter nuclides in meteorites. Short-lived radionuclides with half lives of <5 Myr, such as ^{10}Be, ^{26}Al, ^{36}Cl, ^{41}Ca, ^{53}Mn, and ^{60}Fe, can be produced either by energetic-particle irradiation in the early solar system or by stellar nucleosynthesis just prior to or shortly after the solar system formation.

The estimated initial abundance of ^{60}Fe in the solar system [1-3], which is produced efficiently only by stellar nucleosynthesis, implies that stellar nucleosynthesis prior to or shortly after the birth of the solar system contributed to the inventory of the solar-system short-lived radionuclides.

A low-mass AGB (Asymptotic-Giant-Branch) star has been proposed as a suitable stellar source for the short-lived radionuclides in the early solar system, but it cannot produce sufficient amounts of ^{60}Fe [e.g., 4]. Intermediate-mass AGB stars may explain the abundances of ^{26}Al, ^{41}Ca and ^{60}Fe [4], but astronomical observation shows that encounters between molecular clouds and AGB stars are extremely rare [5], which makes it implausible for an AGB star to be a source of short-lived radionuclides in the solar system. Models for type II supernovae (SNe II) [e.g., 6-9] indicate that the abundance of ^{53}Mn inferred for SNe II is 10-100 times larger than that estimated for the early solar system. If a SN II occurred with less kinetic energy, most of ^{53}Mn would have undergone fallback onto a collapsing stellar core [10]. If this is the case, ^{53}Mn in the solar system should have been derived from another source. Moreover, ^{60}Fe may have been overproduced if all the ^{26}Al and ^{41}Ca in the solar system were provided by a SN II.

[11] proposed a SN II with mixing-fallback, where the inner region of the exploding star experienced mixing, some fraction of mixed materials is ejected, and the rest undergoes fallback onto the core. The mixing-fall back model that reproduces the abundance pattern of hyper metal-poor stars well [e.g., 9] explains the abundances of ^{26}Al, ^{41}Ca, ^{53}Mn, and ^{60}Fe in the solar system.

In this study, we evaluate effects of a mixing-fallback supernova on the isotopic abundances of light elements in the solar system such as C, N, O and ^{10}Be. Bellirium-10 would have formed mainly by solar energetic-particle irradiation in the early solar system. However, neutrino processes in the supernova, which produces Li, Be, and B via interactions between neutrinos and C, may have contributed the inventory of ^{10}Be in the early solar system. We calculated the yield of ^{10}Be for neutrino processes based on newly calculated reaction cross sections related to ^{10}Be formation, and evaluated the abundance of ^{10}Be mixed to the solar system materials with a mixing ratio and a time interval that explain the abundances of ^{26}Al, ^{41}Ca, ^{53}Mn, and ^{60}Fe. We found that ^{10}Be is synthesized as much as ^{9}Be by neutrino processes during supernova explosion but ^{10}Be injected to the solar system would be much less than its inferred abundance in the early solar system [e.g., 12].

We also evaluated injection of stable isotopes of C, N, and O from a nearby mixing-fallback supernova to the solar system materials. Most of presolar silicates are considered to have formed around AGB stars and have oxygen isotopic compositions enriched in ^{17}O compared to the solar system material [e.g., 13], implying that there are missing components depleted in ^{17}O to explain the solar system oxygen isotopic compositions. We found that the injection of light elements from a nearby mixing-fallback supernova may have changed the isotopic compositions of pre-solar system materials slightly (at most several percent), but not as large as to explain the gap in oxygen isotopic compositions between presolar silicates and solar system materials.

References: [1] Tachibana, S., and Huss, G. R. (2003) *ApJ 588*, L41. [2] Mostefaoui, S. et al. (2005) *ApJ 625*, 271 [3] Tachibana, S. et al. (2006) *ApJ 639*, L87 [4] Wasserburg G. J. et al. (2006) *Nuclear Physics A, 777*, 5. [5] Kastner J. H. and Meyers P. C. (1994) *ApJ, 421*, 605. [6] Woosley S. E. and Weaver T. A. (1995) *ApJ, 101*, 181. [7] Rauscher T. et al. (2002) *ApJ, 576* 323. [8] Chieffi A. and Limongi M. (2004) *ApJ, 608*, 405. [9] Nomoto K. et al. (2006) *Nuclear Physics A (Special Issue on Nuclear Astrophysics) 777*, 424. [10] Meyer B. S. and Clayton D. D. (2000) *Space Science Reviews, 99*, 133. [11] Takigawa A. et al. (2007) *LPS XXXVIII*, #1720. [12] McKeegan, K. D. et al. (2000) *Science 289*, 1334. [13] Nagashima K. et al. (2004)

^{176}LU-^{176}HF ZIRCON EVIDENCE FOR RAPID LUNAR DIFFERENTIATION. Dianne J. Taylor[1], Kevin D. McKeegan[1] and T. Mark Harrison[1,2] [1]Dept. of Earth and Space Sciences & IGPP, UCLA, Los Angeles, CA, 90095, dtaylor @ess.ucla.edu. [2]Research School of Earth Sciences, Australian National University, Canberra, A.C.T. 0200

Introduction: The most accessible record of the earliest phases of planetary formation and evolution is preserved in rocks returned from the surface of the Moon by the Apollo missions. Examination of their mineralogy and chemical compositions suggests that a large portion of the Moon was initially completely molten due to the high temperatures associated with its formation [1]. A timescale for the cooling and solidification (and accompanying chemical differentiation) of this planetary-sized magma body has not been firmly established, with estimates based on various isotope systems (both short-lived and long-lived) ranging from ~30 to 300 million years after Solar System formation (e.g. [2, 3, 4, 5, 6]). Here we report a coupled U-Pb and ^{176}Lu-^{176}Hf isotope study of individual lunar zircons from the KREEP-rich Apollo 14 landing site. As the final layer of the lunar magma ocean (LMO) to solidify, a closure age for the so-called KREEP reservoir would establish an upper bound for the duration of LMO crystallization. The zircon crystallization ages and $\varepsilon_{Hf(T)}$ values from our study yield a separation age of the KREEP source region of 4505^{+36}_{-24} Ma (1σ, Fig. 1b), implying that primary differentiation of the Moon was complete within 60 million years of the formation of CAIs [7].

Samples and technique: The lunar zircons analyzed in this study were isolated from the clast-rich polymict breccias 14304, 14305 and 14321. We utilized ion microprobes to obtain crystallization ages (^{207}Pb-^{206}Pb and U-Pb ages) in ~20 μm spots of each zircon as well as rare earth element (REE) and Ti concentrations on select samples (ages, REE and Ti crystallization temperatures were previously reported in [8]). Lu and Hf isotope analyses were undertaken by using laser ablation inductively-coupled plasma mass spectrometry (LA-ICPMS) according to the techniques described by Harrison et al. [9].

The Apollo 14 zircons show a distribution of crystallization ages ranging from 3.9 Ga to 4.4 Ga. With the exception of 4 zircons, all U-Pb ages are concordant at the 4% level or better, which we take as evidence that the ^{207}Pb-^{206}Pb ages correspond to original crystallization ages. The lack of zoning and core-rim relationships in the zircons give us confidence in relating the Hf isotope composition to the ^{207}Pb-^{206}Pb age used to calculate $\varepsilon_{Hf(T)}$.

Results and discussion: Our ^{176}Hf/^{177}Hf data for 29 zircons (Fig. 1) show $\varepsilon_{Hf(T)}$ values ranging from -7 to +0.3. The lunar zircon results extend the age range over which Hf isotope data are available for the Moon back to 4.35 Ga and represent the least radiogenic Hf results thus far in lunar materials. Although there is some scatter toward less negative $\varepsilon_{Hf(T)}$, which is not unexpected given the likelihood of some reservoir mixing, the data show a clearly defined trend in negative $\varepsilon_{Hf(T)}$ vs. age with a distinct lower bound (which, however, does not transgress into the 'forbidden region' corresponding to Lu/Hf < 0). Such a correlation testifies to the existence of a coherent enriched source region which was isotopically isolated from mantle sources and continued to evolve independently over time. The well-resolved negative $\varepsilon_{Hf(T)}$ values, in conjunction with the REE concentrations in these zircons [10], clearly point toward a KREEP source for the magmas from which the zircons crystallized.

We can derive a two-stage model age for the isotopic closure of the KREEP source region from the intersection of the linear trend with the chondritic evolution line (CHUR). We assume that the Moon formed with a chondritic Lu/Hf ratio, which steadily decreased as the LMO cooled and crystallized until a minimum Lu/Hf ratio is attained in the ITE-enriched KREEP reservoir. If the KREEP reservoir remains chemically isolated after formation, then later-crystallizing minerals containing a KREEP component will reflect a time-integrated subchondritic ^{176}Hf/^{177}Hf signature. An estimate for the formation of the KREEP reservoir is provided by a fit to the 23 least radiogenic data points, yielding a model age of 4505^{+36}_{-24} Ma (1σ) and corresponding ^{176}Lu/^{177}Hf = 0.014 ± 0.002 (given by the slope of the fit line). The scatter of the data about this evolution line is roughly commensurate with analytical uncertainties (MSWD = 1.29), and the error on the intersection with CHUR is determined from the 1σ error envelope propagated around the regression line. Notably, the ^{176}Lu/^{177}Hf inferred from this fit is within uncertainty of the lower bound for ^{176}Lu/^{177}Hf of KREEP estimated by Warren [11] (= 0.01420) thus lending confidence that these zircons represent the KREEP source region. An absolute lower limit on the closure age of KREEP can be obtained from the intersection of the Lu/Hf = 0 evolution line with the least radiogenic $\varepsilon_{Hf(T)}$ zircon data; our data require a closure age no younger than 4.45 Ga.

The zircon $\varepsilon_{Hf(T)}$ data are not consistent with the younger magma ocean crystallization age determined by using the coupled ^{147}Sm-$^{143}Nd/^{146}Sm$-^{142}Nd system (4.352±0.023 [5]) but are consistent with ^{182}Hf-^{182}W data suggesting an LMO crystallization age of 4.527±0.010 Ga [4] (although that result has recently been called into question [12]) and with the requirement that the lunar mantle be shielded from accretion of highly siderophile elements prior to 4.4 Ga [13]. The younger ^{142}Nd age may indicate resetting of the Sm-Nd system and/or component mixing in bulk analyses. Thermal models of magma ocean evolution which suggest that it may have taken up to 200 million years for a magma layer insulated by a plagioclase crust to cool [14] also do not appear to be viable, according to our estimate. More recent thermal models [15, 16] suggest that LMO cooling can proceed quite rapidly if the crust is fractured by repeated impacts during this early period in the Moon's history.

Our results do not strictly require that the entire magma ocean had completely crystallized by 4.50 Ga. However, in order for the enriched signature seen in the Apollo 14 zircons to have evolved, the LMO must have proceeded to greater than 99% crystallization by this time. Once formed, this KREEP reservoir must have remained isolated from any depleted Hf-isotope signature originating from the lower part of the lunar mantle. At 4.50 Ga, the KREEP layer could still have been a mush of liquid and crystals which did not communicate with the lower mantle or the over-riding plagioclase crust, at least not in the Procellarum KREEP terrain region of the Moon sampled by the Apollo 14 mission. Other regions of the Moon's crust, during this time, could still have experienced some remelting through interaction with the upper mantle, leading to the formation of new crustal rocks, either Mg-suite rocks or ferroan anorthosites. Thus, the <4.50 Ga ages found for some ferroan anorthosites [6], are not inconsistent with an early crystallization age of the magma ocean. Our data indicate that geophysical models of magma ocean crystallization should be revised to account for a short timescale of differentiation of no more than a few tens of millions of years following the Moon-forming impact.

References: [1] Wood J.A. et al. (1970) *Science,* 167, 602-604. [2] Lugmair G.W. and Carlson R.W. (1978) *Proc. LPSC IX,* 689-704. [3] Nyquist L.E. and Shih C.Y. (1992) *GCA*, 56, 2213-2234. [4] Kleine T. et al. (2005) *Science,* 320, 1671-1674. [5] Rankenburg K. et al. (2006) *Science*, 312, 1369-1372. [6] Norman M.D. et al. (2003) *Meteoritics & Planet. Sci.,* 38, 645-661. [7] Amelin Y. et al. (2002) *Science,* 297, 1678-1683. [8] Taylor D.J. et al., (2007) *LPSC XXXVIII,* Abstract #1338. [9] Harrison T.M. et al. (2005) *Science*, 310, 1947-1950. [10] Taylor D.J. et al. (2007) *Meteor. & Planet. Sci.,* 42, A147. [11] Warren P.H. (1989) *Workshop on Moon in Transition: Apollo 14,* 149-153. [12] Touboul M. et al. (2007) *LPSC XXXVIII,* Abstract #2385. [13] Day J.M.D. et al. (2007) *Science,* 315, 217-210. [14] Solomon S.C. and Longhi J. (1977) *Proc. LPSC VIII,* 583-599. [15] Shearer C.K. and Newsom H.E. (2000) *GCA,* 64, 3599-3613. [16] Righter K. and Shearer C.K. (2003) *GCA,* 67, 2497-2507. [17] Patchett P.J. and Tatsumoto M. (1981) *LPS XII, 819*. [18] Unruh D.M. et al. (1982) *LPS XIII,* 815. [19] Unruh D.M. and Tatsumoto M. (1984) *LPS XV,* 876. [20] Beard B.L. et al. (1998) *GCA*, 62, 525-544.

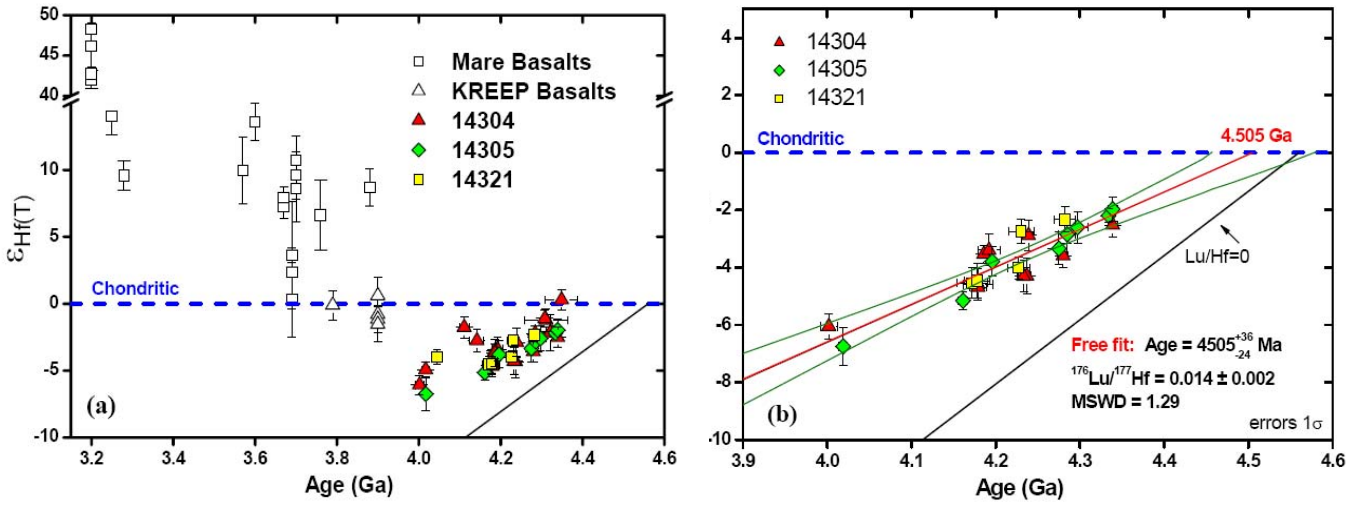

Figure 1. $\varepsilon_{Hf(T)}$ **vs. T** (a) LA-MC-ICPMS *in situ* data for lunar zircons from this study along with bulk TIMS data for mare and KREEP basalts from the literature [17-20] (grey data points). (b) Subset of the 23 least radiogenic data points. A weighted least-squares fit yields a closure age of KREEP of 4505^{+36}_{-24} Ma (1σ), $^{176}Lu/^{176}Hf = 0.014 \pm 0.002$. Also plotted is the $^{176}Lu/^{177}Hf = 0$ evolution line which marks the boundary of the "forbidden zone." Datapoint errors are 1 sigma; the confidence interval on the fit is 95%.

TIMING OF CHRONDRULE FORMATION: CONSTRAINTS FROM HIGH-PRECISION MC-ICPMS MEASUREMENTS. K. Thrane[1], M. Bizzarro[1], K. Nagashima[2], A. N. Krot[2] and J.N. Connelly[1,3]. [1]Geological Institute, University of Copenhagen, Denmark (kthrane@geol.ku.dk), [2]Hawai'i Institute of Geophysics and Planetology, University of Hawai'i at Manoa, Honolulu, USA, [3]The Jackson School of Geosciences, The University of Texas at Austin, USA.

Introduction: High-precision Al-Mg isotope measurements for chondrules are limited [1-11], with the majority performed by secondary ionization mass-spectrometry (SIMS) [1-9]. In these cases, phases with high (>20) Al/Mg ratio (plagioclase and/or glassy mesostasis) are typically analyzed to construct isochrons. The results consistently show that the chondrules formed >1 Ma after CAIs [e.g., 9]. We have attempted to test these results using higher precision multicollector inductively coupled mass spectrometer (MC-ICPMS) with material drilled out of the chondrules. Material derived from holes ~500 µm in diameter was collected as representative of the "bulk chondrule". Chondrule regions with high and low Al/Mg ratios (as defined by X-ray elemental mapping technique using electron microprobe) were sampled using smaller drill bits (200 µm) with hopes of generating internal Al-Mg isochrons.

Results: Fourteen chondrules from the CV/CR-like carbonaceous chondrite SAH 00182 and CV carbonaceous chondrite NWA 779 were sampled and analysed. Only 4 out of 14 chondrules had high enough bulk $^{27}Al/^{24}Mg$ ratios to determine a sufficiently precise model age, three of these chondrules showed $\delta^{26}Mg$ excess ($\delta^{26}Mg^*$) > 0.3‰; no $^{26}Mg^*$ was detected in the fourth chondrule. The bulk analyses of the remaining 10 chondrules had $^{27}Al/^{24}Mg$ ratios < 0.5, two had small resolvable $^{26}Mg^*$ of 26 ± 9ppm and 54 ± 29ppm, but in the rest of the chondrules, no resolvable excesses were detected. Model isochrons using the bulk analyses of the three chondrules with the highest $^{26}Mg^*$ yield initial $^{26}Al/^{27}Al$ ratios [$(^{26}Al/^{27}Al)_0$] ranging from (4.2±0.3) x 10^{-5} to (2.7±0.1) x 10^{-5} corresponding to model ages from 0.24 to 0.71 Ma after formation of CAIs with the inferred $(^{26}Al/^{27}Al)_0$ of (5.85±0.05) x 10^{-5} [12] (hereafter T_0) when forced through the solar $^{27}Al/^{24}Mg$ ratio of 0.101 [13].

Analyses of material using the smaller drill bit were made from two of the Al-rich chondrules (SAH 00182-A3 and NWA 779-A3) and internal isochrons were generated. The chondrule SAH 00182-A3 yielded $(^{26}Al/^{27}Al)_0$ of (1.07±0.15) x 10^{-5} (MSWD = 1.3), corresponding to 1.79 Ma after T_0 and a $\delta^{26}Mg^*$ initial value of 0.236±0.013‰. The "bulk analysis" for this chondrule plots on the isochron.

The chondrule NWA 779-A3 yielded $(^{26}Al/^{27}Al)_0$ of (3.13±0.46) x 10^{-5} corresponding to 0.66 Ma after T_0 and a $\delta^{26}Mg^*$ initial value of 0.137±0.016‰ (MSWD = 1.2). The "bulk analysis" for this chondrule falls slightly below the isochron defined by the material from the smaller drill holes.

Elemental maps of the third chondrule yielding a bulk $^{26}Mg^*$ of 547 ± 24ppm, SAH 00182-B5, had a very homogeneous elemental distribution such that a spread in Al/Mg ratio would be difficult to obtain by microdrilling. Instead, four different plagioclase grains from this chondrule were analysed by the cameca ims-1280 at University of Hawai'i. The measured $^{27}Al/^{24}Mg$ ratios in plagioclase range from 154 to 15,085 but none of the analyses showed any resolvable $^{26}Mg^*$. Two plagioclase grains from chondrule SAH00182-A3 were also analysed by SIMS. Their $^{27}Al/^{24}Mg$ ratios varied from 89 to 123 but none of these analyses showed any resolvable $^{26}Mg^*$.

Discussion: Model ages of three chondrules from NWA 779 and SAH 00182 range from 0.24 to 0.71 Ma after T_0. This age range overlaps the model ages of the Allende chondrules reported by Bizzarro et al. [11] and, taken at face value, indicates that the chondrule precursor materials formed early. The validity of these bulk model ages depends on the assumptions that (*i*) the sample is representative of the bulk chondrule, (*ii*) the source of the precursor material had a bulk solar system Al/Mg ratio, and (*iii*) the precursor/chondrule acted as closed system during subsequent remelting and thermal metamorphism.

Two internal isochrons have been generated for chondrules from NWA 779 and SAH 00182 corresponding to ages of 0.66 Ma and 1.79 Ma, respectively. Both isochrons have positive intercepts. These ages must reflect timing of the last melting and crystallization of the chondrules. The ages require that reprocessing ceased for some chondrules as early as 0.66 Ma after T_0, whereas other chondrules were formed or reprocessed as late as 1.79 Ma after T_0. The younger age agrees well with the many ages derived by SIMS analyses [1-9]. However, it is clear from the older age and an even older internal Al/Mg isochron age of 0.25 Ma by Bizzarro et al. [11] that some chondrules were formed and that reprocessing ceased very early.

An explanation for at least some of the very young chondrule ages derived by SIMS analyses may lie in

the analyses of plagioclase in this study. Contrary to what we expected, SIMS data of the plagioclase grains from two chondrules with unambiguous $^{26}Mg^*$ in the MC-ICPMS bulk analyses showed no $^{26}Mg^*$. The internal isochron obtained by drilling for chondrule SAH00182-A3 predicts that the plagioclases, yielding $^{27}Al/^{24}Mg$ ratios of 89-123 should have an $\delta^{26}Mg^*$ of ~7-10‰, which should be easily resolvable by SIMS analyses, even with the large uncertainties. Instead, $\delta^{26}Mg$ "excess/deficits" of (–1.6 to 0.4) ± 4‰ were measured. Chondrule SAH00182-B5 yielded the highest bulk $^{26}Mg^*$ of 547 ± 23 ppm yet no resolvable $^{26}Mg^*$ was detected in any of these plagioclase grains. This data requires that either the original Al/Mg ratio was very low (<50) making the $^{26}Mg^*$ correspondingly low and undetectable within the uncertainly, or $^{26}Mg^*$ has diffused out of plagioclase.

It has been previously proposed that short scale diffusion of Mg takes place in plagioclase, during asteroidal metamorphism [14]. Short scale diffusion would result in some areas in the plagioclase with high concentration of Mg and other areas with low concentration of Mg. This chemical diffusion would account for the Al/Mg ratio being driven from normal ratios of 100-300 in plagioclase to ratios >1000, However, if purely chemical diffusion were taking place, the remaining Mg would retain the original $^{26}Mg^*$. Assuming that original Al/Mg ratios were > 70 and seeing no excess, we propose that $^{26}Mg^*$ may have preferentially diffused relative to bulk Mg. This may be due to $^{26}Mg^*$ being the decay product of ^{26}Al such that it resides in the Al site where it is less stable than the bulk Mg. Therefore, metamorphism or other alteration processes may cause $^{26}Mg^*$ to diffuse out of the Al-site of the plagioclase resulting in a preferential loss of $^{26}Mg^*$ over non-radiogenic Mg. Regardless of whether the $^{26}Mg^*$ in plagioclase is lower than predicted (by the MC-ICPMS analyses) due to elevated Al/Mg ratios and/or preferential loss of $^{26}Mg^*$, the data clearly suggests that in situ analyses may not provide accurate ^{26}Al-^{26}Mg ages in metamorphosed samples.

If diffusional length scales are short enough, larger volumes of drilled samples may, on average, return isotopic and elemental analyses representative of the pre-diffusional state. Clearly, if $^{26}Mg^*$ diffuses out of the chondrule, then drilled samples will not contain the full inventory of the original $^{26}Mg^*$, and will also yield incorrect ages.

References: 1] MacPherson G. J. et al. (1995) *Meteoritics, 30,* 365-386. [2] Russell S. S. et al. (1996) *Science, 273,* 757-762. [3] Kita N. T. et al. (2000) *Geochim. Cosmochim. Acta, 64,* 3913-3922. [4] McKeegan K. D. et al. (2000) *LPSC, XXXI,* Abstract #2009. [5] Mostefaoui S. et al. (2002) *Meteorit. Planet. Sci., 37,* 421-428. [6] Kunihiro T. et al. (2004) *Geochim. Cosmochim. Acta, 68,* 2947-2957. [7] Kurahashi E. et al. (2004) *LPSC, XXXV,* Abstract #1476. [8] Rudraswami N. G. and Goswami J. N. (2007) *Earth Planet. Sci. Lett., 277,* 231-244. [9] Kita N. T. et al. in *Chondrites and the Protoplanetary Disk*, ASP Conference Series 341, pp. 558-587. [10] Young E. D. (2005) *Science, 308,* 223-227. [11] Bizzarro M. et al. (2004) *Nature, 431,* 275-278. [12] Thrane K. et al. (2006) *Astrophys. J., 646,* L159-L162. [13] Palme H. and Jones A. (2004) in *Treatise in Geochemistry*, vol. 1, Meteorites, Comets and Planets, A. M. Davis, ed., Elsevier-Pergamon, pp. 41-63. [14] LaTourrette T. and Wasserburg G. J. (1998) *EPSL,158,* 91-108.

THE AGE OF THE MOON AND LIFETIME OF ITS MAGMA OCEAN - NEW CONSTRAINTS FROM W ISOTOPES IN LUNAR METALS. M. Touboul[1], T. Kleine[1], B. Bourdon[1], H. Palme[2], and R. Wieler[1]. [1]Institute for Isotope Geochemistry and Mineral Resources, Department of Earth Sciences, ETH Zürich, Clausiusstrasse 25, 8092 Zürich, Switzerland (touboul@erdw.ethz.ch), [2]Institut für Mineralogie und Geochemie, Universität zu Köln, Zülpicherstr. 49b, 50674 Köln, Germany.

Introduction: ^{182}Hf-^{182}W chronometry is well suited to constraining the timescales of lunar differentiation because large Hf-W fractionation occurred during crystallization of the lunar magma ocean [1-3]. Variations in the ^{182}W/^{184}W of lunar whole-rock whole-rock samples were interpreted to indicate formation and differentiation of the Moon during the effective life-time of ^{182}Hf (i.e., within the first ~60 Ma of the solar system) [1-4]. This time constraint, however, is inconsistent with results from ^{146}Sm-^{142}Nd chronometry that indicate a much longer lifetime of the lunar magma ocean [5, 6]. The ^{182}W/^{184}W of lunar whole-rock samples does not only reflect ^{182}Hf-decay but also cosmogenic production of ^{182}W, mainly by neutron capture of ^{181}Ta during cosmic-ray exposure of the lunar surface [7]. The dominant ^{182}W component in most lunar rocks is cosmogenic, compromising a reliable interpretation in terms of ^{182}Hf-^{182}W chronometry. Here we present W isotope data for lunar metals from a comprehensive set of lunar rocks and show that these metals do not contain any measurable Ta-derived ^{182}W. These data are used to better constrain the Hf-W record of early lunar differentiation.

Results: We separated metals from 5 high-Ti basalts, 4 low-Ti basalts and 2 KREEP-rich samples. The purity of the metal separates was checked under the binocular. The metals were dissolved in 6 M HCl-0.06 M HF and W was separated from its sample matrix using standard ion exchange techniques. All isotope measurements were performed using the Nu Plasma MC-ICPMS at ETH Zurich. The ^{182}W/^{184}W ratios of the samples are determined relative to a terrestrial W standard and are expressed as ε_W, which is deviation in parts per 10^4. ^{183}W/^{184}W ratios were used as a monitor of accurate measurements. They agree for all samples analyzed here to within ±0.2 ε units (ε is parts per 10^4) with the terrestrial standard. Ta/W ratios of metal separates are estimated using their Hf/W ratios, determined by isotope dilution on 5% aliquots, combined with Ta/Hf ratios of whole rocks. Cosmogenic corrections of ε_W, calculated using these Ta/W ratios and exposure ages, were applied to all samples and were usually below ~0.1 ε units.

All samples analyzed here have identical ^{182}W/^{184}W ratios within ±0.32 ε units (2 SD) and agree with previously reported data for metals from KREEP-rich samples [1]. These data combined average at ε_W=0.09±0.10 (2 SE, n=15). In contrast to earlier reports [1, 2, 4] we do not find elevated ^{182}W/^{184}W ratios for low- and high-Ti mare basalts.

Discussion: The identical ^{182}W/^{184}W ratios for pure metal separates reported here indicates that are no ^{182}Hf-induced W isotope variations among KREEP and the mare basalt sources. Elevated ^{182}W/^{184}W ratios in low- and high-Ti mare basalts reported earlier likely reflect the presence of small cosmogenic ^{182}W components in the analysed fractions.

The homogeneous ^{182}W/^{184}W ratios of all lunar samples in spite of strongly fractionated Hf/W ratios in their source areas [3, 8] indicates that the equilibration of W isotopes within the lunar magma ocean continued for more than ~60 Ma after the start of the solar system. This is no longer in conflict with Sm-Nd constraints regarding the lifespan of the lunar magma ocean. The rapid crystallization required by the earlier W isotope data [1, 2, 4] implied that some ^{147}Sm–^{143}Nd ages for ferroan anorthosites [9, 10] and the ^{146}Sm-^{142}Nd model age [5, 6] of the lunar mantle reflect events that were not associated with the primordial differentiation of the Moon. With the revised Hf-W time constraint pesented here, however, this is no longer required and the aforementioned Sm-Nd ages could possibly date processes associated with the primordial differentiation of the lunar mantle. This would suggests that the lunar magma ocean was largely solidified as late as ~215 Myr, as given by its ^{146}Sm-^{142}Nd model age [5, 6].

The apparent presence of ^{182}Hf-induced ^{182}W variations within the Moon was used as an argument that the Moon formed within the first ~60 Ma of the solar system [1, 2, 4]. Our new data, however, indicate that there are no ^{182}W/^{184}W variations within the lunar mantle, such that formation of the Moon during the lifespan of ^{182}Hf is no longer required, although it can not be excluded. An alternative approach to date the formation of the Moon uses the Hf/W and ^{182}W/^{184}W ratios of the bulk lunar and terrestrial mantles. The best current estimates for the Hf/W ratios of the lunar and terrestrial mantles are 26.4±1.5 (2σ) and 19.7±1.6 (2σ), respectively, and these Hf/W ratios were established by core formation in the Moon and Earth. Using these estimates, the virtually identical ^{182}W/^{184}W ratios of the bulk lunar and terrestrial mantles require that core formation in the Moon and Earth were completed later than ~45 Ma, otherwise a ^{182}W excess would have

developed in the lunar compared to the terrestrial mantle. This new age constraint for core formation in the Moon also provides the earliest time the giant impact could have occurred and Earth's core could have completely been segregated. This new age constraint is inconsistent with termination of Earth's accretion at ~30 Myr [11] and also difficult to reconcile with the <30 Myr ^{146}Sm-^{142}Nd model age for differentiation of Earth's mantle [12]. Our new age constraint, however, is consistent with most U-Pb model ages for the Earth [13].

All successful simulations of the giant impact predict that ~80% of the Moon is derived from impactor material [14], such that any W isotope differences between the proto-Earth and impactor should be apparent in the composition of the Moon. The difference in initial ^{182}W/^{184}W between the lunar and terrestrial mantles, however, is smaller than ~0.5 ε units. Similarly, the identical O isotopic compositions of the Earth and Moon in spite of widespread O isotopic heterogeneity among all other inner solar system objects are unexpected. This has been interpreted to reflect accretion of the Earth and Moon at the same heliocentric distance [15] but this scenario cannot account for the identical W isotope compositions of the lunar and terrestrial mantles. Hence, unless the Moon is almost entirely derived from terrestrial material, lunar and terrestrial materials equilibrated in the aftermath of the giant impact. It has been shown that such equilibration is possible for O isotopes [16] but its effectiveness in equilibrating W isotopes remains to be investigated.

Reference: [1] Kleine T. et al. (2005), *Science*, *310*, 1671-1674. [2] Lee D.C. et al. (2002), *EPSL*, *198*, 267-274. [3] Shearer C.K. and Newsom H.E. (2000), *GCA*, *64*, 3599-3613. [4] Lee D.C. et al. (1997), *Science*, *278*, 1098-1103. [5] Nyquist L.E. et al. (1995), *GCA*, *59*, 2817-2837. [6] Rankenburg K. et al. (2006), *Science*, *312*, 1369-1372. [7] Leya I. et al. (2000), *EPSL*, *175*, 1-12. [8] Righter K. and Shearer C.K. (2003), *GCA*, *67*, 2497-2507. [9] Borg L.E. et al. (1999), *GCA*, *63*, 2679-2691. [10] Carlson R.W. and Lugmair G.W. (1988), *EPSL*, *90*, 119-130. [11] Jacobsen S.B. (2005), *AREPS*, *33*, 531-570. [12] Boyet M. and Carlson R.W. (2005), *Science*, *309*, 576-581. [13] Allegre C.J. et al. (1995), *GCA*, *59*, 1445-1456. [14] Canup R.M. and Asphaug E. (2001), *Nature*, *412*, 708-712. [15] Wiechert U. et al. (2001), *Science*, *294*, 345-348. [16] Palhevan K. and Stevenson D.J. (2007), *EPSL*, in press.

^{26}AL-^{26}MG DATING CALCIUM-ALUMINIUM-RICH INCLUSIONS

[1]Chris C. Town, [1]Martin Schiller, [2]Martin Bizzarro and [1]Joel A. Baker. [1]School of Geography, Environment and Earth Sciences, Victoria University of Wellington, P.O. Box 600, Wellington, New Zealand (townchri@student.vuw.ac.nz, joel.baker@vuw.ac.nz); [2]Axiom Laboratory, Geological Institute, University of Copenhagen, 1350 Copenhagen, Denmark (bizzarro@geol.ku.dk).

Introduction: Refractory inclusions in meteorites include calcium-aluminium-rich inclusions (CAIs) and amoeboid olivine aggregates (AOAs). These solids are of particular interest because both long- and short-lived chronometers have shown that they are the oldest material that formed in the Solar System [1,2]. Thus, high-precision dating, petrographic, chemical and isotopic studies of refractory inclusions can offer insights into the chemical and astrophysical environment present in the solar nebula and/or proto-planetary disc during formation of our Solar System.

A particularly important aspect of refractory inclusions is the clearly demonstrated evidence of the former presence of the short-lived isotope ^{26}Al (mean age = 1.05 Myr) in most normal CAIs [1] with an initial abundance > 5 x 10^{-5}. For more than 30 years it has been possible to measure this initial abundance of ^{26}Al in CAIs with a relative precision of < ca. 10%. This makes it possible to determine ^{26}Al-^{26}Mg ages of other meteoritic material relative to CAIs with little significant uncertainty (ca. < 0.4 My) introduced from the initial ^{26}Al abundance measurement of CAIs.

Recent application of multiple-collector inductively coupled plasma mass spectrometry (MC-ICPMS) techniques to Mg isotope analysis of bulk CAIs [3,4] has produced two important results. Firstly, both solution-based and *in situ* studies have suggested that the initial ^{26}Al abundance of CAIs (^{26}Al/^{27}Al$_0$) is higher than the "canonical" value of ca. 5 x 10^{-5} i.e., 5.9 x 10^{-5}. Secondly, the precision of this measurement has been improved by almost an order of magnitude meaning that it is possible to determine ages of other meteoritic material relative to CAIs with uncertainties as low as 0.1 Myr. Given the variety of nebula (condensation/evaporation) and planetary processes (partial melting, crystallization) that were able to fractionate Al/Mg ratios in the young Solar System this should make the ^{26}Al-^{26}Mg system the method of choice for high-resolution dating a wide range of meteorite material.

However, recent reinvestigation of the ^{26}Al-^{26}Mg systematics of six CAIs from Allende [5] has questioned the revision of the initial abundance of ^{26}Al in CAIs to the "super-canonical" abundance of 5.9 x 10^{-5}. Here we report on a petrographic, chemical and isotopic study of a number (n = 9) of refractory inclusions from CV and CK chondrites, as well as a interlaboratory comparison of the six CAIs analysed in [5].

Analytical Techniques: Refractory inclusions were removed from meteorite slices using a diamond saw. After removal of most matrix material each refractory inclusion was either broken or sawn into two parts. One part was mounted in epoxy and polished for electron microprobe and laser ablation ICPMS analysis of major and trace elements, and any future *in situ* analytical study. The remaining fragment was used to obtain samples for ^{26}Al-^{26}Mg dating.

Petrographic and major and trace element analysis. Each polished sample was imaged and the major mineral phases analysed for major element compositions using a JEOL Superprobe 733 electron microprobe at Victoria University of Wellington. After major element analysis, minerals in each inclusion were analysed for >30 trace elements with a 193 nm laser ablation system coupled to an Agilent 7500 ICPMS at Victoria University of Wellington. BCR-2G was used as a standard to correct for trace element fractionation during the analysis and ^{43}Ca from the electron microprobe analysis was used as an internal standard.

Al/Mg ratio and Mg isotope analysis. Bulk pieces of refractory inclusions or handpicked mineral separates (pyroxene or mellilite/anorthite mixtures) were taken fully into solution using standard HF-HNO_3 digestion techniques. A small aliquot of this solution was used for Al/Mg determination by solution ICPMS. The remaining aliquot was then processed through several steps of ion exchange separation involving anion, Eichrom DGA and cation exchange resins to produce a Mg separate of > 99% purity. Ultra-pure Seastar acids were used for sample digestion and chemistry. Al/Mg ratios were determined on an Agilent 7500 ICPMS using gravimetrically prepared Al/Mg standards and BCR2 as an internal standard. Replicate analyses of BCR2 reproduce to better than 1% (2 sd) and are within 0.3% of the recommended value of this standard. Mg isotope ratios were determined using a Nu Plasma MC-ICPMS at Victoria University of Wellington and methods described more fully in [6]. The ^{26}Mg excess (δ^{26}Mg*) of each CAI is measured to a precision of < ±0.015‰. We use a kinetic law to calculate δ^{26}Mg* as high-precision Mg isotope studies of CAIs have shown that this approach produces tightly defined isochrons that would not exist if δ^{26}Mg* was calculated using an equilibrium law.

Samples: Refractory inclusions were extracted from the following meteorites:

- NWA2364 (CV3 chondrite) = CAI0, CAI1, CAI2, CAI3 and CAI4
- NWA 1559 (CK3-anomolous chondrite) = CAI8, AOA1 and AOA2
- NWA 760 (CV3 chondrite) = CAI5

In addition we carried out Al/Mg and Mg isotope measurements on aliquots of six CAIs from the CV3 chondrite Allende (A33, A39, A43, A44A, A60 and AJEF) generously provided to us by Dr Qing-zhu Yin and Benjamin Jacobsen from UC Davis by way of a interlaboratory comparison.

In all, a total of 15 refractory inclusions will be ^{26}Al-^{26}Mg dated. CAI0, CAI1, CAI2, CAI8, A39, A43, A44A and AJEF are coarse-grained type B CAIs. A33 and CAI3 are compact type A CAIs and CAI4 is a fluffy type A CAI.

Results: To-date we have reanalyzed the Al/Mg ratios for the six Allende CAIs studied by [5] as well as the Mg isotope composition of an aliquot of A44A processed through our Mg chemical separation procedures. While we obtain some minor differences in Al/Mg ratios measured in New Zealand as compared to UC Davis these are not large enough to account for the discrepancy in initial ^{26}Al abundance of Allende CAIs reported by [3,4,5]. Our Al/Mg and Mg isotope measurement of Allende CAI A44A produces a model initial $^{26}Al/^{27}Al_0 = (4.98 \pm 0.14) \times 10^{-5}$, which is essentially within error of the value reported by [5].

We have also analysed a bulk fragment of a coarse-grained Type B CAI from NWA2364 (CAI0) illustrated in Figure 1. This fragment of CAI0 defines a very precise model initial $^{26}Al/^{27}Al_0 = (5.04 \pm 0.07) \times 10^{-5}$.

Discussion: The preliminary results of this study confirm that the "canonical" initial $^{26}Al/^{27}Al_0$ values reported by [5] for six Allende CAIs are unlikely to be the result of analytical artifacts. Moreover, the one CAI we have analysed from NWA2364 also has a "canonical" initial $^{26}Al/^{27}Al_0$ value that is significantly lower than the "super-canonical" $^{26}Al/^{27}Al_0$ values reported for CAIs in [3,4]. A critical evaluation of the reason for this discrepancy will be more appropriate when the remaining CAIs in this study have been analysed. In particular, a series of mineral separates and bulk fragments from a large Type B CAI (CAI1) have been prepared in order to precisely determine if CAIs with $^{26}Al/^{27}Al_0$ values of 5×10^{-5} have elevated initial ^{26}Mg abundances that are consistent with them recording a later thermal event ca. 300,000 years after primary CAI formation as represented by an initial $^{26}Al/^{27}Al_0 = 5.9 \times 10^{-5}$. One possible explanation to account for the discrepancy between the different initial $^{26}Al/^{27}Al_0$ values being measured in the studies of [3,4,5] and also here relates to the scale of the sampling. The study of [3] involved sampling of nearly entire CAIs (i.e. true analyses of bulk CAIs), whereas the study of [5] and herein (thus far) involves sampling of rather small parts of bulk CAIs, which may result in the obtained $^{26}Al/^{27}Al_0$ values representing younger thermal events associated with internal redistribution of ^{26}Mg some time after primary CAI formation.

Figure 1 Plain-light and back-scattered electron image of CAI0 from NWA2364. This coarse grained CAI is composed of mellilite, fassaitic pyroxene, anorthite and spinel.

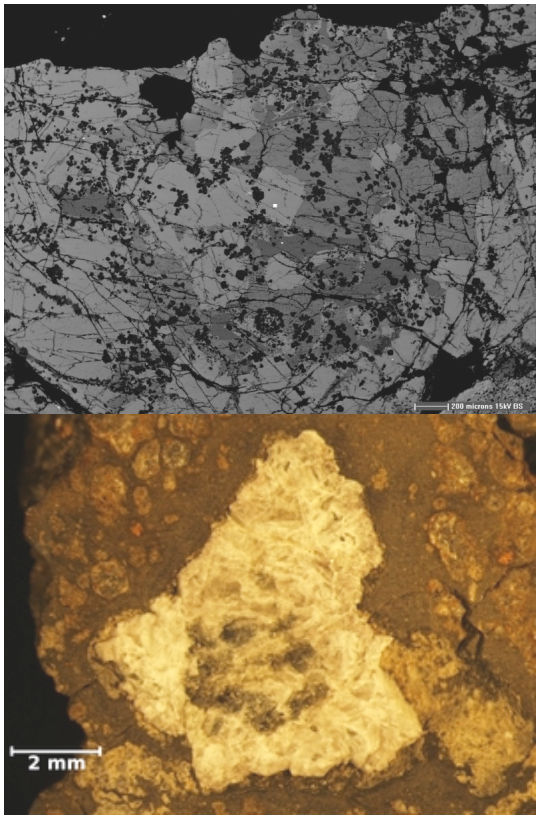

References: [1] Lee T. et al. (1976) *GRL, 3*, 41-44 [2] Amelin Y. et al. (2002) *Science, 297*, 1678-1683 [3] Thrane K. et al. (2006) *ApJ, 646*, L159-L162 [4] Young E. D. et al. (2005) *Science, 308*, 223-227. [5] Jacobson B. et al. (2007) *LPS XXXVIII,* Abstract #1491 [6] Schiller M. et al. (2007) *this conference.*

ORIGIN OF TITANIUM ISOTOPE HETEROGENEITY IN THE PROTOPLANETARY DISK

A. Trinquier[1], M. Bizzarro[1], D. Ulfbeck[1], A.N. Krot[2], J.N. Connelly[1,3]. [1] Geological Institute, University of Copenhagen, Denmark (trinquier@geol.ku.dk), [2] Hawaii Institute of Geophysics and Planetology, University of Hawaii at Manoa, Honolulu, USA, [3] The Jackson School of Geosciences, The University of Texas at Austin, USA.

Introduction: Nucleosynthetic isotopic anomalies in meteorites and their components preserve a record of the various stellar sources that have contributed material to the solar system's parental molecular cloud. These residual heterogeneities are commonly believed to reflect inefficient thermal processing of presolar dust during the earliest evolutionary stages of the protoplanetary disk and, as such, provide a means to explore potential genetic relationships between early solar system condensates, meteorite groups and the terrestrial planets. Titanium is the 21st most abundant element in the universe and, owing to its refractory nature, exists primarily in solid phases in the interstellar medium. Therefore, it can be used as a tracer to monitor the isotopic evolution of solids in the protoplanetary disk. Titanium has five stable isotopes – ^{46}Ti, ^{47}Ti, ^{48}Ti, ^{49}Ti and ^{50}Ti – with the following respective abundances, 8.0%, 7.3%, 73.8%, 5.5% and 5.4% [1]. The nucleosynthesis of ^{46}Ti, ^{47}Ti, ^{48}Ti and ^{49}Ti is believed to result mainly from explosive and hydrostatic oxygen- and silicon-burning in massive stars [1]. On the other hand, the neutron-rich ^{50}Ti nuclide is most efficiently produced by the rare type Ia supernova close to the Chandrasekhar mass limit, together with other neutron-rich isotopes of iron-group elements such as ^{48}Ca, ^{54}Cr, ^{58}Fe, ^{62}Ni and ^{64}Ni [1]. Anomalous Ti isotopic compositions have been reported in primitive meteorites and their components, including Ca,Al-rich refractory inclusions (CAIs), hibonites and presolar grains [2-9]. In material of solar origin, the anomalies are typically restricted to ^{50}Ti, where both deficits and excesses have been observed, ranging from ~0.1‰ in bulk chondrites to ~300‰ in hibonite grains. Taking advantage of improved methods for high-precision measurements of Ti isotopes by multiple-collector inductively coupled plasma source mass spectrometry (MC-ICPMS), we analyzed the Ti isotope composition of various inner solar system objects, including primitive and differentiated meteorites, to assess the extent of Ti isotope heterogeneity that may have been present in the protoplanetary disk.

Chemical purification of Ti: Terrestrial and meteoritic samples were digested with HF-HNO_3 acid mixtures in Teflon beakers on a hot plate at 150°C. Following complete dissolution, the residue is fluxed in 29M HF to bring the maximum amount of Ti in solution, while precipitating major elements in a fluoride salt. The solid is centrifuged out and leached additional times with HF. Ti is further purified from the decanted supernatant following a procedure adapted from Makishima et al. [10]. Remaining impurities are eluted in low molarity HF/HCl acids on anion exchange resin, and this is normally repeated 2-3 times to ensure adequate separation of Cr. An additional Zr and Ca clean-up step is achieved using TODGA resin [11]. This chemical separation procedure ensures yields of >90%, with total procedural blanks of 10 ng, which is negligible compared to the typical amounts of Ti analyzed (10-100 μg).

Mass spectrometry: Ti isotope data was obtained by MC-ICPMS (VG-Axiom, University of Copenhagen) using the sample-standard bracketing technique. Samples were introduced in the plasma source in 1M HNO_3/0.05M HF via an Aridus desolvating nebuliser using only Ar as sweep gas. Data was acquired in static mode measuring ^{47}Ti, ^{48}Ti, ^{49}Ti, ^{50}Ti and ^{52}Cr simultaneously with typical ion beam currents of 5×10^{-10} A on ^{48}Ti. Following a 120 s half-mass baseline, data was collected for 600 s with 10 s integration times. Prior to analysis, samples were scanned for matrix contaminants and, especially, for species potentially interfering on the Ti mass array. These include ^{50}Cr, ^{50}V, ^{48}Ca as well as doubly-charged Zr, Mo and Ru species. Interference from ^{50}Cr on ^{50}Ti was corrected for by monitoring ^{52}Cr, and the magnitude of this correction was typically <20 ppm. Other potential interfering species were not detected above background levels. Results are reported in the ε notation (per ten thousand deviation) relative to the mean mass bias-corrected ^{48,49,50}Ti/^{47}Ti obtained on a bracketing in-house Ti standard. Our preferred normalization scheme uses the ^{49}Ti/^{47}Ti ratio (^{49}Ti/^{47}Ti = 0.749766, [2]) to correct for instrumental mass bias, although all other correction schemes are monitored to ensure data integrity. The reproducibility and accuracy of our approach was evaluated by analyzing terrestrial rock samples, as well as by doping a pure Ti standard solution and the BCR-2 rock standard with a ^{48}Ti spike (99% pure) to create gravimetrically determined ^{48}Ti excesses. These experiments allow us to estimate an accuracy and reproducibility of ~20 ppm for all Ti isotope ratios.

Results: Terrestrial rock standards (n=4) yielded a Ti isotope composition identical to the standard solution. Except for the enstatite chondrite Qingzhen, the enstatite achondrite Itqiy and the lunar meteorite NWA479, all bulk meteorites analyzed in this study

displayed variable anomalies in ^{50}Ti. However, no anomalies in ^{47}Ti, ^{48}Ti and ^{49}Ti were detected at the ± 20 ppm level. Carbonaceous chondrites (CC) display variable excesses in ^{50}Ti ranging from 1.8 to 5.0 ε-unit, whereas ordinary chondrites (OC) record a uniform deficit in ε_{50Ti} of -0.69±09. Except for NWA2976, which displays a ^{50}Ti excess similar to that present in CCs, all meteorite samples originating from differentiated planetesimals (that is, angrites, eucrites, mesosiderites and ureilites) display variable deficits of up to ~2 ε-units. Similarly, martian meteorites analyzed in this study have a small, but resolvable, deficit in ε_{50Ti} of -0.30±09. In an attempt to identify the carrier of the ^{50}Ti in primitive materials, we have subjected samples of bulk CCs and OCs to a stepwise leaching procedure using acids of increasing strengths [12]. Our preliminary results for Orgueil, a CI1 chondrite, show that the ^{50}Ti carrier is most likely a non-refractory silicate phase. The enrichment and depletion in ^{50}Ti amongst the various leaches relative to the bulk-rock analysis are correlated with that of ^{54}Cr [13], indicating a common carrier for both ^{54}Cr and ^{50}Ti. In constrast, stepwise leaching of the DAG313 (LL3) ordinary chondrite did not reveal significant variations in the ε_{50Ti} value compared to our mean OC average of -0.69±09ε. This suggets that the ^{50}Ti carrier may be mostly absent in OCs.

Discussion: The ^{50}Ti anomalies in bulk OCs and most differentiated meteorites are correlated with previously published ^{54}Cr data for the same meteorite group, but not for CCs (Fig. 1). Given that the abundance of refractory inclusions contribute strongly to the Ti (but not the Cr) budget of CC, we have re-calculated the CAI-free ^{50}Ti isotope composition of CC using mass balance equations and published abundances of CAIs in the diverse CC groups [14]. Once this CAI-component is removed, we observe a linear ^{54}Cr-^{50}Ti correlation amongst all meteorite groups (Fig. 1), with CAIs as the enriched endmember. Therefore, the ^{54}Cr-^{50}Ti carrier is most enriched in the CAI precursor material, but depleted in the accretion region of differentiated meteorites, OCs and the terrestial planets. A further important point is that the precursor material of the terrestrial planets, most differentiated planetesimals and OCs did not contain CAIs. In contrast, the NWA2976 basaltic meteorite plots above the correlation line (Fig. 1), probably reflecting the presence of CAIs in its precusor material. The magnitude of the ^{50}Ti and ^{54}Cr excesses in CCs correlates positively with the matrix-normalized concentration of presolar diamonds for the same meteorites [18]. It is unlikely that presolar diamonds are the ^{50}Ti-^{54}Cr carrier, given that our chemical dissolution procedures are not expected to attack and dissolve such refractory phases. Instead, the observed correlation may reflect the selective preservation of a less refractory presolar phase, most likely presolar silicates, in CC matrices. This is supported by the observation that the ^{50}Ti and ^{54}Cr excesses in CCs also correlate with the inferred degree of thermal processing of CC matrices [18]. If correct, this would suggest that preservation of isotopic anomalies in early solar system objects may not be related to primordial heterogeneity, but to the degree of thermal processing of their precursor material in the protoplanetary disk.

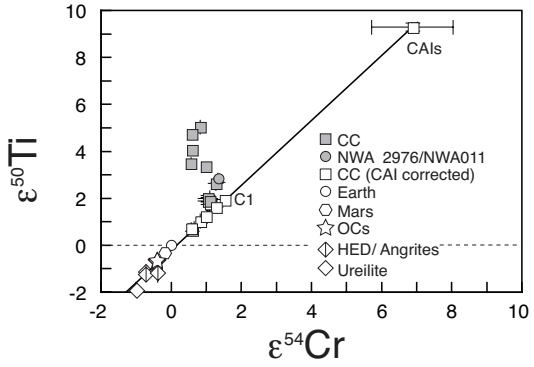

Figure 1: ε_{50Ti} -ε_{54Cr} correlation amongst inner solar system solids, planetesimals and planets. ^{54}Cr data are from [13, 15-17].

References: [1] Clayton D.D. (2003) *Handbook of isotopes in the cosmos. Cambridge Univ. Press.* [2] Niederer F.R. et al. (1981) *GCA, 45,* 1017 [3] Niemeyer S. and Lugmair G.W. (1984) *GCA, 48,* 1401 [4] Fahey A. J. et al. (1987) *GCA, 51,* 329 [5] Ireland T. R. (1990) *GCA, 54,* 3219 [6] Amari S. et al. (2001) *ApJ, 546,* 248 [7] Zinner E. et al. (2005) *LPS XXXVI,* Abstract #1691 [8] Choi B. J. (1998) *Science, 13,* 1284 [9] Hoppe P. and Besmehn A. (2002) *ApJ, 576,* L69-L72. [10] Makishima A. et al. (2002) *JAAS, 17,* 1290 [11] Connelly J. N. et al. (2006) *Chem. Geol., 233,* 126 [12] Rotaru M. et al. (1992) *Nature, 358,* 465 [13] Trinquier A. et al. (2007) *ApJ, 655,* 117 [14] Scott E.R.D. and Krot A.N. (2003) *in Treatise on Geochemistry,* 143 [15] Papanastassiou D.A. et al. (2005) *LPS XXXVI,* Abstract #2198. [16] Bogdanovski O. and Lugmair G.W. (2003) *Met. Planet. Sci.,* 38, Abstract #5094. [17] Yamashita K. et al. (2005) *Antarctic Meteorites XXIX*, 100 [18] Huss, G. et al. (2003) *GCA, 67,* 4823.

COMPARISON OF SHORT-LIVED AND LONG-LIVED CHRONOMETERS: TOWARDS A CONSISTENT CHRONOLOGY OF THE EARLY SOLAR SYSTEM. M. Wadhwa[1], Y. Amelin[2], M. Bizzarro[3], N. Kita[4], T. Kleine[5], G. W. Lugmair[6], and Q. Yin[7], [1]Center for Meteorite Studies, School of Earth and Space Exploration, Arizona State University, Tempe, AZ 85287, USA, [2]Geological Survey of Canada, Ottawa, Ontario K1A 0E8, Canada, [3]Geological Institute, University of Copenhagen, Copenahgen, Denmark, [4]Dept. Geology and Geophysics, University of Wisconsin, Madison, WI, USA, [5]Inst. Isotope Geochemistry and Mineral Resources, ETH Zurich, Switzerland, [6]Scripps Institution of Oceanography, University of California, San Diego, La Jolla, CA 92093, USA, [7]Department of Geology, University of California at Davis, One Shields Avenue, Davis, CA 95616, USA.

In the last few decades, chronometers based on both long- and short-lived radionuclides have been applied extensively to a variety of meteoritic materials with the goal of determining the timing of events that occurred in the early solar system, including the formation of the first solids in the solar nebula, as well as the accretion and differentiation of asteroidal and planetary bodies. Long-lived chronometers typically do not have the time resolution required to resolve events occurring within the first tens of millions of years of solar system history. In contrast, short-lived chronometers can provide high time resolution (i.e., a million years or less); however, an isochron from such a chronometer provides not an age but a measure of the abundance of the radionuclide at the time of last isotopic closure, and comparison of the isochron slopes for two separate events can provide only a relative time difference (ΔT) between these events. Therefore, for the high-resolution relative ages obtained from short-lived chronometers to be mapped on to an absolute time scale, they need to be "anchored" to an absolute age. This absolute age is usually provided by the U-Pb chronometer which is capable of providing ages with the sub-My precision comparable to that of short-lived chronometers. Furthermore, application of a high resolution chronometer based on a short-lived radionuclide requires that the initial abundance of this radionuclide be uniform in the region of the solar system where rocky bodies were forming, a condition that may not necessarily have been met.

Analytical advances over the last several decades have allowed dramatic improvements in the precision and accuracy of isotope ratio measurements for a wide range of elements in meteoritic and planetary materials. As a result, since the first evidence for the former presence of a short-lived radioncuclide, i.e., ^{129}I (t1/2 ~15.7 My) in the Richardton chondrite [1], there have been numerous other such radionuclides with half lives <100 My whose former presence in the early solar system has been unambiguously established (primarily through detection of small variations in the abundance of the daughter isotope that correlate with parent/daughter element ratios) [2-4]. Furthermore, these analytical advances have also made it increasingly feasible to analyze multiple isotope systematics in the same meteoritic objects, thereby making it possible to compare ages from several short-lived chronometers. Here we provide a review of ages obtained primarily from three short-lived chronometers (i.e., ^{26}Al-^{26}Mg, ^{53}Mn-^{53}Cr and ^{182}Hf-^{182}W; Table 1) that have thus far been most extensively applied towards obtaining chronological constraints on a variety of meteorites and their components and evaluate whether these chronometers provide time scales consistent with each other and with the absolute Pb-Pb chronometer. For all three of these chronometers, the D'Orbigny angrite is chosen as the time anchor since this is a rapidly cooled, relatively unmetamorphosed basaltic sample [5] in which the Pb-Pb, Al-Mg, Mn-Cr and Hf-W systems are likely to have closed contemporaneously.

Table 2 provides a comparison of ^{207}Pb-^{206}Pb absolute ages with the ^{26}Al-^{26}Mg, ^{53}Mn-^{53}Cr and ^{182}Hf-^{182}W ages (calculated relative to the D'Orbigny angrite time anchor; Table 1) for several types of meteorites and their components. With a few exceptions, the three short-lived chronometers appear to yield ages that are generally consistent with each other and with the absolute Pb-Pb ages, implying that the initial distributions of ^{26}Al, ^{53}Mn and ^{182}Hf were uniform in the meteorite-forming region of the protoplanetary disk.

Calcium-aluminum-rich inclusions (CAIs) in chondritic meteorites have the oldest absolute (Pb-Pb [6-9]) and relative (Al-Mg [10]; Hf-W [11,12]) ages. The most precise absolute age of 4567.11±0.16 Ma is defined by the Efremovka E60 CAI [7,8]. Chondrules from unequilibrated chondrites have Pb-Pb [7], Al-Mg [10] and Mn-Cr [13] ages that are typically ~1-3 My younger than CAIs. Silicate differentiation on the parent body of the Howardites-Eucrites-Diogenites (HED) group, as dated by ^{26}Al-^{26}Mg, ^{53}Mn-^{53}Cr and ^{182}Hf-^{182}W systematics in whole rock samples of these meteorites, occurred essentially contemporaneously with chondrule formation [14-16]. Igneous activity and basalt formation on early-accreted planetesimals also began within a few My after CAI formation [17-19].

In the cases where there is discordancy between chronometers (indicated in red in Table 2), there are several possibilities that may explain the lack of concordance. For example, the discordant ages may be a reflection of the different closure temperatures of the different isotope systems in a slowly-cooled sample. This may be the case for the Asuka 881394 eucrite, which shows textural evidence for slow cooling at near-solidus temperatures, and in which the Pb-Pb system may have closed earlier than the Al-Mg and Mn-Cr systems. Differences in closure temperatures may also account for discordant ages obtained for some H chondrites. While the Pb-Pb, Mn-Cr and Hf-W systems

closed simultaneously in silicates in the Ste Marguerite (H4) chondrite at relatively high (near-solidus) temperatures, the Al-Mg system probably reflects slow cooling below 400-500°C [20] (Table 2). This is supported by the fact that the Pb-Pb age of phosphates in Ste Marguerite [21] (which also dates cooling below ~480°C) is identical within errors to this Al-Mg age. Secondary alteration processes, such as shock and thermal metamorphism, may also have affected different isotope systems to different degrees in a given sample.

References: [1] Reynolds J. H. (1960) *PRL, 4,* 351–354. [2] Wasserburg G. J. (1985) In *Protostars and Planets II,* Eds. D. C. Black and M. S. Matthews, pp. 703-737. [3] McKeegan K. D. and A. M. Davis (2004) In *Treatise on Geochemistry Vol. I,* Ed. A. M. Davis, pp. 431-460. [4] Wadhwa M. et al. (2007) In *Protostars and Planets V,* Eds. B. Reipurth, D. Jewitt, and K. Keil, pp. 835-848. [5] Mittlefehldt D. W. et al. (2002) *MAPS, 37,* 345-369. [6] Allègre C. J. et al. (1995) *GCA, 59,* 1445-1456. [7] Amelin Y. et al. (2002) *Science, 297,* 1678-1683. [8] Amelin Y. et al. (2006) *LPS XXXVII,* #1970. [9] Bouvier A. et al. (2007) *GCA, 71,* 1583-1604. [10] Kita N. et al. (2005) In *Chondrites and the Protoplanetary Disk,* Eds. A. N. Krot, E. R. D. Scott and B. Reipurth, pp. 558-587; and references therein. [11] Kleine T et al. (2005) *GCA, 69,* 5805-5818. [12] Burkhardt C. et al. (2007) *MAPS, 42,* #5189. [13] Yin Q. et al. (2007) *ApJ, 662,* L43-L46. [14] Lugmair G. W. and Shukolyukov A. (1998) *GCA, 62,* 2863-2886. [15] Kleine T. et al. (2004) *GCA, 68,* 2935-2946. [16] Bizzarro M. et al. (2005) *ApJ, 632,* L41-L44. [17] Baker J. et al. (2005) *Nature, 436,* 1127-1131. [18] Wadhwa M. et al. (2005) *LPS XXXVI,* #2126. [19] Amelin Y. (2007) *LPS XXXVIII,* #1669. [20] LaTourette and Wasserburg (1998) EPSL, 158,91-108. [21] Göpel C. et al. (1994) *EPSL, 121,* 153-171. [22] Spivak-Birndorf L. et al. (2005) *MAPS, 40,* A145. [23] Glavin D. P. et al. (2004) *MAPS, 39,* 655-783. [24] Markowski A. et al. (2007) *EPSL,* in press. [25] Polnau E. and Lugmair G. W. (2001) *LPS XXXII,* #1527. [26] Zinner E. and Göpel C. (2002) *MAPS, 37,* 1001-1013. [27] Kleine T. et al. (2002) *Nature, 418,* 952-955. [28] Amelin Y. et al. (2005) *GCA, 69,* 505-518. [29] Kleine T. et al. (2007) in prep. [30] Amelin Y. (2005) *Science, 310,* 839-841. [31] Zipfel J. et al. (1996) *MAPS, 31,* A160. [32] Goodrich C. et al. (2002) *MAPS, 37,* A54. [33] Kita N. et al. (2003) *LPS XXXIV,* #1557. [34] Connelly J. C. et al. (2007) *GCA,* submitted. [35] Sugiura N. et al. (2005) *EPS 57,* e13-e16. [36] Lugmair G. W. and Galer S. J. G. (1992) *GCA, 56,* 1673-1694. [37] Wadhwa M. et al. (2004) *LPS XXXV,* #1843.

Table 1. Short-lived radioisotopes applied extensively towards refining the chronology of the early solar system events.

Radioisotope (R*)	$T_{1/2}$ (My)	Daughter Isotope (D*)	Reference Isotope (R)	Solar System Initial Ratio $(R^*/R)_0$	Time Anchor
^{26}Al	0.72	^{26}Mg	^{27}Al	$\sim 5 \times 10^{-5}$	D'Orbigny Angrite $(R^*/R)_T = 5.06 \times 10^{-7}$ [22] at 4564.5±0.2 Ma [19]
^{53}Mn	3.7	^{53}Cr	^{55}Mn	$\sim 10^{-5}$	D'Orbigny Angrite $(R^*/R)_T = 3.23 \times 10^{-6}$ [23] at 4564.5±0.2 Ma [19]
^{182}Hf	8.9	^{182}W	^{180}Hf	$\sim 10^{-4}$	D'Orbigny Angrite $(R^*/R)_T = 7.4 \times 10^{-5}$ [24] at 4564.5±0.2 Ma [19]

Table 2. Comparison of ^{207}Pb-^{206}Pb absolute ages with those based on the ^{26}Al-^{26}Mg, ^{53}Mn-^{53}Cr, and ^{182}Hf-^{182}W chronometers.

Sample	^{207}Pb-^{206}Pb age (Ma)	^{53}Mn-^{53}Cr age (Ma)	^{26}Al-^{26}Mg age (Ma)	^{182}Hf-^{182}W age (Ma)
E60 CAI	4567.11±0.16 [7,8]		4569.2±0.2 [7]	
Allende CAI	4566±2 [6]			4568.4±0.7 [11,12]
	4568.1±9.4 [9]			
Chondrules	4564.7±0.6 [7]	4566.9±2.0 [13]	~4566-4568 [10]	
Ste Marguerite (H4) silicates	4566.7±1.6 [21]	4566.6±0.5 [25]	4563.9±0.3 [26]	4566.2±0.7 [27]
Richardton (H5) silicates	4562.7±1.7 [28]	4557.8±1.6 [25]		4562.8±1.0 [29]
HED silicate differentiation		4566.5±0.7 [14]	4565.1-4566.6 [16]	4564.2±1.0 [15]
Acapulco (acapulcoite)	4556.5±0.8 [30]	4556.6±1.1 [31]		
Ureilite feldspathic clasts		4563.9±0.4 [32]	4564.2±0.3 [33]	
Sahara 99555 (angrite)	4564.4±0.7 [19]	4563.8±0.8 [35]	4564.5±0.2 [22]	4564.1±0.6 [24]
	4564.6±0.2 [34]		4564.4±0.3 [17]	
D'Orbigny (angrite)	**4564.5±0.2 [19]**	**≡4564.5±0.2**	**≡4564.5±0.2**	**≡4564.5±0.2**
LEW 86010 (angrite)	4557.8±0.5 [36]	4559.4±0.4 [14]		
	4558.6±0.2 [19]			
Asuka 881394 (eucrite)	4566.5±0.3 [8]	4565.4±0.4 [18]	4565.5±0.2 [18]	
Ibitira (eucrite)	4557.4±0.6 [8]	4558.6+2/-3 [14]	<4562.8 [37]	

For a given sample, ages indicated in red are discordant with the ages determined from other chronometers for the same sample (within ±3σ). The ^{207}Pb-^{206}Pb age for the D'Orbigny serves as the anchor for the ^{26}Al-^{26}Mg, ^{53}Mn-^{53}Cr snd ^{182}Hf-^{182}W systems (indicated in black bolded letters). Errors in the ^{26}Al-^{26}Mg, ^{53}Mn-^{53}Cr and ^{182}Hf-^{182}W ages include the errors in the ^{26}Al/^{27}Al, ^{53}Mn/^{55}Mn and ^{182}Hf/^{180}Hf ratios, respectively, and the uncertainty in the absolute age of the anchor; all errors shown in the table are ±2σ.

SEDIMENTATION, MINERALZATION, PLANET FORMATION AND DISSIPATION IN PROTOPLANETARY DISKS

D. M. Watson, University of Rochester (dmw@pas.rochester.edu)

Recent observations with the NASA Spitzer Space Telescope offer the interesting possibility of synchronizing the work of astronomers and meteoriticists: of finding long-sought details of how the evolution of protoplanetary disks corresponds to the chronology of the Solar system's early stages of development. Here we review the present state of several large Spitzer mid-infrared spectroscopic and imaging surveys of protoplanetary systems in nearby young stellar clusters. We present determinations of several important time scales:: those for the crystallization and growth of dust grains, the settling of the dust to disk midplane, the development of radial structure in disks caused by giant-planet formation, the duration of protostellar accretion, and the dissipation of disks. We will also describe the effects these strong constraints have on models of giant-planetary formation and disk dissipation.

Compound chondrule formation in the shock-wave heating model: three-dimensional hydrodynamic simulation of disruption of the molten dust particle. S.Yasuda[1,3,4], H. Miura[2,4], T. Nakamoto[3]. 1. Pure and Applied Sciences, University of Tsukuba, Tsukuba, Ibaraki 305-8577, Japan, yasuda@geo.titech.ac.jp, 2. Department of Physics, Kyoto University, Sakyo, Kyoto 606-8502, Japan, 3. Department of Earth and Planetary Sciences, Tokyo Institute of Technology, Meguro, Tokyo 152-8551, Japan, 4. Research Fellow of the Japan Society for the promotion of Science.

Introduction:

Chondorules are mm-sized, spherical-shaped, once-molten particles that are the main inclusion of chondritic meteorites. They are thought to have formed by flash heating events in the early solar nebula. There also exist compound chondrules. The fraction of compound chondrules is about 4% in all the chondrules. Some compound chondrules seemed to be formed by collisions of two independent particles. However, It seems difficult to form compound chondrules, because the collision frequency of two dust particles in the solar nebula is expected to be very low.

Shock-wave heating model is one of the plausible models for chondrule formation. We notice the heating mechanism of this model. In this model, dust particles are exposed to the high-speed gas flow behind the shock front and heated by the gas frictional heating. Since the gas frictional heating works only at the surface of the dust particle, the surface of the dust particle is expected to be molten at first, then the inside to be molten later due to the thermal conduction [1]. In that case, the ram pressure of the gas flow may split and/or strip off the molten part [2, 3]. Since the local number density of ejectors behind the stripped dust particle (we call it "parent dust particle") is increased, the mutual collisions between these ejectors are likely to occur frequently. It is strongly suggested that this mechanism accounts for the compound chondrule formation.

The collision frequency F_{coll} can be estimated by $F_{coll} = (72\rho_{mat} r_e^7 R_{eject}^3 / r_p^4 \Delta v P_{fm})^{1/3}$,where R_{eject}, r_e, and Δv are the ejection rate, radius, and velocity dispersion of ejectors, respectively, and ρ_{mat}, r_p , and P_{fm} are the material density of dust particle (=3 g/cm^3), radius of parent particle, and gas ram pressure, respectively (see a paper presented by Miura et al. in this meeting). Using above formula, we can confirm whether our new model for compound chondrule formation is possible or not if we obtain information of ejectors (R_{eject}, r_e, Δv). The purpose of this study is (1) to numerically simulate hydrodynamical evolution of the molten dust particle in the shock-wave heating model and estimate the collision frequency and (2) to discuss whether compound chondrules can form by collisions among ejectors or not.

Numerical model:

Fig 1(A) represents initial setup of our simulation. A spherical molten dust particle is expressed by a green-object. The gas flows from the left hand side, and the dust particle is exposed to the gas flow. In order to express the molten surface facing to the gas flow directly, the left hemisphere of the dust particle is assumed to be low-viscous fluid (μ =1 poise), in contrast, the right one to be high-viscous fluid (μ =10^6 poise). We numerically solve the hydrodynamics equations using a new code recently we developed based on the CIP method [4].

Disruption of molten dust particle:

Numerical results: One of the results of our simulation is showed in Figure 1(B)-(D). The radius of parent particle r_p is 5 mm, ram pressure of gas flow $P_{fm}$is 20000 dyn/cm^2, and surface tension coefficient σ is 400 dyn/cm. Corresponding Weber number *We* is 25. These panels in figure1 represent hydrodynamical evolution of the molten particle. The time is (B) 0.0050 sec, (C) 0.0109 sec, and (D) 0.0136 sec after initial settings shown in (A). At first the liquid part is tore away from the parent particle due to the gas flow (B). Then the blown fluids are disrupted into small pieces by the effect of the surface tension (C). As a results, many ejectors scatter behind the parent particle (D).

Identification of each ejector: In order to examine the radius and velocity of each ejector, and total number of ejectors, we use *Clump Find* method, which is used in the field of information technology to identify isolated clumps. After the identification of clumps, we identify 26 ejectors in the panel (C). In addition, we also obtain the radius of each ejector assuming a spherical shape and its velocity of mass center. From information of ejectors we can obtain the mean ejector radius is 0.82mm and radial velocity dispersion Δv is 20.4cm/s. The ejection rate R_{eject} is 1.2x10^4 s^{-1} calculated from ejection duration and number of ejectors.

Collision frequency: From our numerical simulation, we can estimate the collision frequency. Its values are 7.01 (r_p = 5 mm, P_{fm}= 20000 dyn/cm^2), 4.03 (r_p = 10 mm, P_{fm}= 20000 dyn/cm^2), and 4.85 (r_p = 5 mm, P_{fm}= 80000 dyn/cm^2) respectively. Therefore each ejector will experience about 1-10 times of collisions in average per one disruption event. Since these values are large enough, it seems possible to form compound chondrules in the shock-wave heating model.

Collision of ejectors:

Shadow effect: Though we discussed collision frequency of ejectors statistically, we can examine the

the collision of ejectors directly using our numerical simulation. Indeed, we observed in our simulations that some ejectors are colliding each other (see Figs 1(C) and (D)). We examine velocity evolutions of z-direction (the direction of gas flow) of two ejectors, named *ejector1* [ejected earlier] and *ejector2* [ejected later] (Figure 2). While *ejector2* is accelerated by gas flow, *ejector1* is not accelerated (almost uniform velocity motion) because *ejector2* blocks out the gas flow. We call it "*shadow effect*". Thanks to the *shadow effect*, *ejector2* catches up *ejector1*.

Compound chondrule formation: It is required for two component chondrules of a set of compound to have temperature (viscosity) difference because if the viscosities of both components are too low to keep their external shapes during collision, they must fuse together and we may not observe them as compound chondrules. If we assume that *ejector2* does not cool because the gas frictional heating takes place, in contrast, *ejector1* can cool rapidly by the radiative cooling because the gas flow is blocked by *ejector2*. Assuming that the temperatures of these two ejectors are the same at the time when *ejector2* blocks the gas flow toward *ejector1*, the variation in temperature of *ejector2* from ejection to collision (~0.004 sec), that is, temperature diffrence between two ejectors is

$$T_{\mathrm{dif}} = \frac{3\varepsilon\sigma T^4}{4 r_{\mathrm{e}} \rho_{\mathrm{mat}} C} t = 0.52 \left(\frac{\varepsilon}{1}\right)\left(\frac{t}{0.004\mathrm{sec}}\right)\left(\frac{T}{1900\mathrm{K}}\right)\left(\frac{r_{\mathrm{e}}}{1\mathrm{mm}}\right) \mathrm{K},$$

where σ, ε, T, and C are Stefan-Boltzmann constant, emissivity of ejector, temperature, and heat capacity of the dust particle, respectively. The value of heat capacity is set as 1.4×10^{7} erg g^{-1} K^{-1}. The calculated temperature difference may be too low to generate enough viscosity difference. It might be difficult to form compound chondrule from this collision (*ejector1* and *ejector2*). We can consider two possibilities to get over this difficulty. First, ejectors would cool more as they go away from the parent dust particle. If they collide at t~1sec after ejection, they cool by about 100K due to the radiative cooling. This might result into stiff collision to form compound chondrule. However, the number density of ejectors far from the parent particle is much smaller than beside it. We have to examine the orbit of each ejector in order to confirm whether collisions occur at such low-density region or not. Second, there can be an initial temperature (viscosity) difference between two ejectors at the time when they are ejected. In this case, the collisions immediately after the ejection account for the compound chondrule formation because one ejector has been already stiffer than another. In order to confirm this idea, we have to improve our code involving the energy equation taking into account heat conduction, gas drag heating, and radiative cooling. This is challenging, but very important to elucidate the compound chondrule formation. We are planning to develop such code and carry out the thermo-hydrodynamical simulation in the future.

Summary:

We performed three-dimensional hydrodynamicssimulations to examine disruption of the molten dust particle exposed to high-velocity gas flow and estimated the collision frequency among ejectors in the framework of shock-wave heating model. We found that the collision frequency is much higher than the observational frequency of compound chondrules. In addition, we confirmed collision of ejectors in our numerical simulation. These results strongly suggest that the disruption of large molten dust particle in the gas flow account for the compound chondrule formation and support the scenario of chondrule formation by nebula shocks.

References:

[1] Yasuda S. and Nakamoto T. (2005) *LPSC XXXI,* #1252. [2] Kato, T. et al. (2006) *Meteorite. Planet. Sci.*, **41**, 49-65. [3] Kadono, T. and Arakawa, M. (2005) *Icarus,* **173**, 295-299. [4] Miura, H and Nakamoto, T.(2007) Icarus, **188,** 246-265.

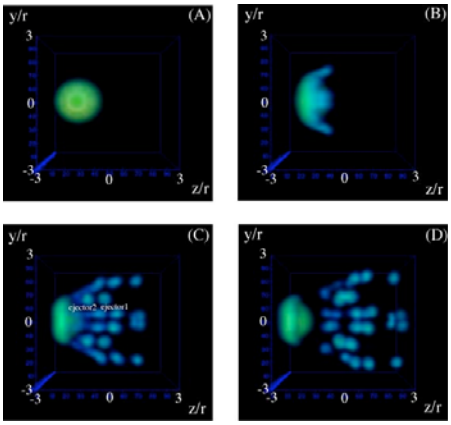

Figure1: Hydrodynamics simulation of molten dust particle.

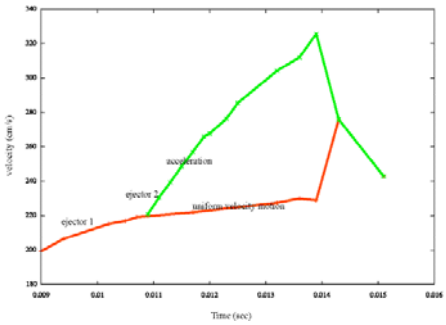

Figure2: Time evolution of two ejectors. Red line represents *ejector1* and green line represents *ejector2*. Horizontal axis is progress time and vertical axis is z-directional velocity.

TOWARD CONSISTENT CHRONOLOGY IN THE EARLY SOLAR SYSTEM: HIGH RESOLUTION ^{53}Mn-^{53}Cr CHRONOMETRY APPLIED TO CHONDURLES IN PRIMITIVE ORDINARY CHONDRITE.

Qing-zhu Yin[1], Benjamin Jacobsen[1], Frederic Moynier[1] and Ian D. Hutcheon[2], [1]Department of Geology, University of California at Davis, One Shields Avenue, Davis, CA 95616 (yin@geology.ucdavis.edu) [2]Glenn T. Seaborg Institute, Lawrence Livermore National Laboratory, Livermore, CA 94551.

Introduction: The use of short-lived radio nuclides as robust high-resolution chronometers in the early Solar System is based on the fundamental assumption that all these radio nuclides were initially homogeneously distributed throughout the early solar nebula. This assumption can be rigorously tested by cross calibrating the different chronometers through acquisition of high-precision isotope data in a suite of early solar system materials suitable for this purpose. Classically, the short-lived ^{53}Mn-^{53}Cr chronometer ($T_{1/2}$=3.7 Ma) is anchored to the absolute Pb-Pb age of 4557.8±0.5 Ma [1] for angrites LEW 86010 (LEW) and Angra dos Reis (ADOR) with the ^{53}Mn/^{55}Mn ratio of (1.25±0.07)x10^{-6} [2]. A growing number of new high-precision data suggests that short lived relative chronometers such as the ^{26}Al-^{26}Mg system ($T_{1/2}$= 0.73 Ma) are broadly consistent with the high-precision long-lived ^{207}Pb-^{206}Pb chronometer (see [3]). It has been recognized for some time, however, that there are some inconsistencies in the ^{53}Mn-^{53}Cr chronometry (cf. [4]). For example, when using the angrite age anchor of [3] based on the ^{53}Mn/^{55}Mn ratios, the chondrules of ordinary chondrites [5] are older than that of CAIs, the oldest known solid objects of our solar system [6]. This is opposite to what one would conclude based on ^{26}Al-^{26}Mg and U-Pb chronometers, where most chondrules appear to be ≈2 Ma younger than the CAIs (cf. [7] for a recent review). Such results could be interpreted prematurely as an argument against a chronological interpretation for short-lived radioactivity in the early solar system and instead as favoring arguments for production of ^{53}Mn within the solar nebula and/or heterogeneous distribution of ^{53}Mn and ^{26}Al within the early solar system. The importance of this problem prompted us to revisit this issue using MC-ICP-MS to obtain high-precision ^{53}Mn-^{53}Cr data in a suite of chondrules from a primitive ordinary chondrite, Chainpur (LL3.4).

New results from UC Davis: Our new results show that the initial ^{53}Mn/^{55}Mn in Chainpur chondrules is (5.1±1.6)x10^{-6} (Fig. 1). Including the Chainpur whole rock data point of [5] with our new chondrule data, changes the regressed slope only imperceptibly (from 5.11x10^{-6} to 5.07x10^{-6}), with the same uncertainty of ±1.59x10^{-6} (Fig. 2). Our initial ^{53}Mn/^{55}Mn ratio for Chainpur is similar to the new value for Semarkona (LL3.0) chondrules, (5.8±1.9)x10^{-6}, obtained at the Johnson Space Center (JSC) [7]. If we regress only the chondrule data of [5] for Chainpur, we obtain ^{53}Mn/^{55}Mn = (6.9±2.0)x10^{-6}, consistent within error with our new data. However, the latter value for the initial ^{53}Mn/^{55}Mn ratio is substantially lower than that reported by [5] for Chainpur chondrules (LL3.4), ^{53}Mn/^{55}Mn = (9.4±1.7)x10^{-6} and barely overlaps with that obtained for Bishunpur chondrules (LL3.1), ^{53}Mn/^{55}Mn = (9.5±3.1) x10^{-6}.

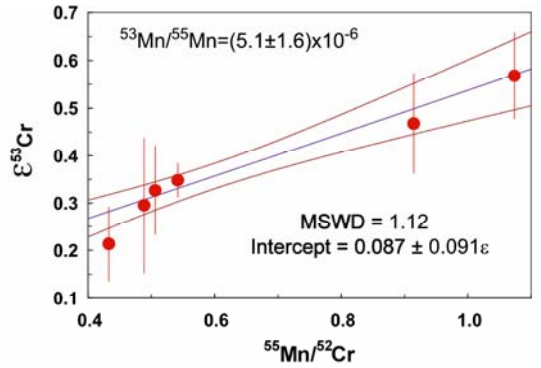

Fig. 1. New UC Davis ^{53}Mn-^{53}Cr isochron for six chondrules from Chainpur (LL3.4) ordinary chondrites.

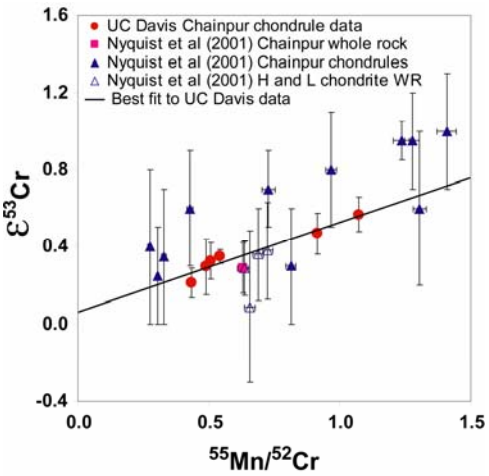

Fig. 2. New UC Davis ^{53}Mn-^{53}Cr data compared with the literature data [5] for Chainpur LL3.4 chondrules.

Solution to the inconsistent ^{53}Mn/^{55}Mn ratios: We have closely reexamined the data in [5] and found that the high initial ^{53}Mn/^{55}Mn value of (9.4±1.7)x10^{-6} for Chainpur was obtained by regression of all the chondrule data together with data from five bulk chondrites, including one whole rock Chainpur chondrite and four additional ordinary chondrites. The data for Bishunpur were treated by [5] consistently.

We note that there are no Bishunpur whole rock data reported in [5]. Applying the Ludwig Isoplot 3 program to the Nyquist et al. (2001) data, we obtain $^{53}Mn/^{55}Mn$ = (9.08±2.95)x10^{-6} for Chainpur and (9.53±3.97)x10^{-6} for Bishunpur, respectively, consistent within error to the values obtained by [5] using the Williamson program. This agreement precludes the different data reduction algorithms as being the cause of the differences in the regressed slopes. Thus, the differences between the initial $^{53}Mn/^{55}Mn$ ratios in our study and that of [5] are primarily due to the inclusion of data for four other whole rock ordinary chondrites. We suggest that the approach used here by including data only for one meteorite (Chainpur) provides a more accurate assessment of the initial abundance of ^{53}Mn during Chainpur chondrule formation.

Comparative chronology in the early Solar System: We use two absolute age anchors in Fig. 3, the high precision Pb-Pb ages of CAIs (*filled circle*, 4567.2_0.6 Ma; [6]) and LEW (*filled square*, 4557.8±0.5 Ma; [1]), respectively; the offset between the two ages is 9.4±0.8 Ma. If we use instead the recently updated LEW 86010 Pb-Pb age of 4558.62±0.18 Ma [8], the age difference between the two age anchors is 8.58±0.63 Ma, identical within error to the previous value. The line joining the two age-anchor points shall be called the "early solar system equiline." The ^{53}Mn-^{53}Cr systematics in CAIs are complex and not well understood [9]. The solar system's initial abundance of ^{53}Mn is instead obtained from bulk carbonaceous chondrites, which give a $^{53}Mn/^{55}Mn$ ratio of (8.5±1.5)x10^{-6} [10]. We have also obtained a similar result for carbonaceous chondrites (8.5±1.2)x10^{-6} [11]. Relative to this value, our Chainpur chondrules are calculated to be 2.73 Ma younger than the CAIs (Fig. 3, *filled circle*). Relative to the LEW/ADOR age anchor with $^{53}Mn/^{55}Mn$ = (1.25±0.07)x10^{-6} [2], our Chainpur chondrules are 7.51 Ma older (*filled green square*). Because of the common Pb problem, there is no high precision Pb-Pb age available for the Chainpur chondrules (Y. Amelin 2007, private communication). Plotted instead on the *x*-axis in Figure 3 is the widely accepted younger ^{26}Al-^{26}Mg age for chondrules (Kita et al. 2005), 2.5±1.0 Ma, relative to the CAI age anchor at 4567.2±0.6 Ma [6]. Our new Chainpur data plot on the equiline within the analytical uncertainty. The new JSC Semarkona chondrule data with a $^{53}Mn/^{55}Mn$ ratio of (5.8±1.9)x10^{-6} give a ^{53}Mn-^{53}Cr age of 7.5±2.1 Ma older than the LEW/ADOR anchor, consistent with the ^{26}Al-^{26}Mg ages of chondrules [7]. In contrast, the earlier Chainpur data [5] with an initial $^{53}Mn/^{55}Mn$ ratio of (9.4±1.7)x10^{-6} would correspond to an age of 10 Ma older than LEW 86010 with an uncertainty of 1–2 Ma, very similar to the time of CAI formation, but inconsistent with the ^{26}Al-^{26}Mg age of chondrules [7]. Based on the collective ^{53}Mn-^{53}Cr, ^{26}Al-^{26}Mg, and ^{207}Pb-^{206}Pb systematics [12-13], the Asuka 881394 eucrite also plots on the equiline; the filled circle is an ^{26}Al-^{26}Mg age relative to the CAI anchor, while the open square behind it is a ^{53}Mn-^{53}Cr age relative to the LEW/ADOR anchor. Two quenched angrites (D'Orbigny and Asuka 881371) are also plotted in Figure 3 based on literature data [14-17]. Using the latest ^{207}Pb-^{206}Pb age of 4564.65±0.65 Ma [8] and $^{53}Mn/^{55}Mn$ initial ratio of (3.40±0.14)x10^{-6} [18] relative to the new ^{207}Pb-^{206}Pb age anchor of 4558.62±0.18 Ma [8] and respective $^{53}Mn/^{55}Mn$= (1.25±0.07)x10^{-6} for LEW [2], the angrite Sahara 99555 also plots on the equiline. The very old age of 4566.18±0.14 Ma reported by [19] for this angrite would plot off the equiline significantly.

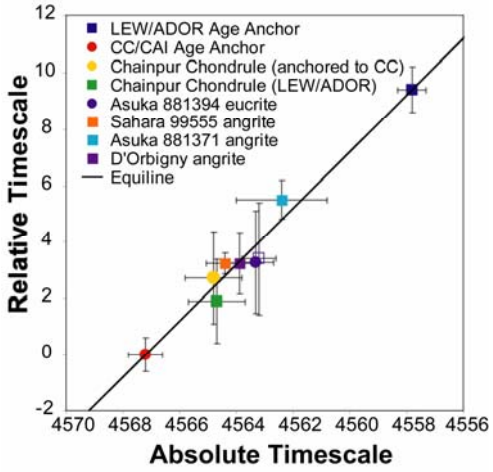

Fig. 3. Consistent chronology of Chainpur chondrule plotting on the *E*arly *S*olar *S*ystem *E*quiline (ESSE). *Equiline* is drawn through the two age anchors commonly used in the early Solar System chronology (LEW86010 /Angra dos Reis and carbonaceous chondrite CAIs).

References: [1] Lugmair, G. W., & Galer, S. J. G. 1992, GCA, 56, 1673 [2] Lugmair, G. W., & Shukolyukov, A. 1998, GCA, 62, 2863 [3] Sanders, I. S., & Taylor, G. J. 2005, ASP, 341, 915 [4] McKeegan, K. D., & Davis, A. M. 2003, TOG, 431 [5] Nyquist, L. et al. 2001, MAPS, 36, 911 [6] Amelin, Y. et al., 2002, Science, 297, 1678 [7] Kita, N. et al., 2005, ASPC. 341, 558 [8] Amelin, Y. 2007, LPSC, 38, 1669 [9] Papanastassiou, D. A., et al., 2002, MAPS, 37, A114 [10] Shukolyukov, A. & Lugmair, G. W. 2006, EPSL, 250, 200 [11] Moynier, F., et al., 2007, LPSC., 38, 1401 [12] Nyquist, L. E et al., 2003, EPSL, 214, 11 [13] Wadhwa, M., et al., 2005, LPSC., 36, 2126 [14] Glavin, D. P., et al., 2004, MAPS, 39, 693 [15] Spivak-Birndorf, L., et al., 2005, MAPS, 40, 5097 [16] Sugiura, N., et al., 2005, EPSL, 57, 13 [17] Zartman, R. E., et al., 2006, LPSC., 37, 1580 [18] Shukolyukov, A. & Lugmair, G. W. 2007 LPSC, 38, 1423 [19] Baker, J et al, 2005, Nature, 436, 1127

THE TIMING OF OXYGEN ISOTOPE VARIATIONS IN THE EARLY SOLAR SYSTEM: A MEASURE OF RADIAL TRANSPORT IN THE SOLAR PROTOPLANETARY DISK?. E. D. Young[1], [1]Department of Earth and Space Sciences and Institute of Geophysics and Planetary Physics, University of California Los Angeles, 595 Charles Young Drive East, 2676 Geology Building, Los Angeles, CA 90095 (Email: eyoung@ess.ucla.edu).

Introduction: When considered in the context of realisitic models for disk chemistry and transport, the oxygen isotopic compositions of meteoritical materials may serve as indicators of timescales of large-scale processes in the solar circumstellar disk. Optically thin surfaces of the disk were likely sites for generating ^{16}O isotope variability in the early Solar System. Astrochemical reaction network calculations predict that a robust feature of these photoactive horizons of the disk was conversion of CO gas to ^{16}O-poor (high $\Delta^{17}O$) H_2O ice on a timescale of 10^5 years [1]. Because far ultraviolet (FUV) fluxes were so great within 5 AU of the nascent Sun, the CO self shielding oxygen isotopic effect was an outer disk phenomen [2] transferred to the inner disk. Calculations depicting transport in the disk suggest that CO photodissociation at disk surfaces triggered a wave of high-$\Delta^{17}O$ H_2O that passed from surface regions through the outer disk and into the rocky planet-forming region on a timescale of 10^5 to 10^6 years. The scenario deduced from such models can be compared with the meteoritical evidence for the timing of changes in $\Delta^{17}O$ in differentiated meteorites, calcium aluminum-rich inclusions (CAIs), chondrules, and chondrite matrix.

CO Self Shielding: Within a few AU of the central star FUV fluxes were too great to permit trapping of the oxygen isotopic effects of CO photodissociation in H_2O, or in any other oxygen-bearing molecule, unless CO was added from outside the disk at unrealistically high rates. Trapping of the CO self shielding isotopic effect must therefore have been an outer disk phenomenon, necessitating inward transport of the ^{16}O-poor, high- $\Delta^{17}O$ signal into the region of terrestrial planet formation in the inner disk (Fig. 1). Simple box models that incorporate timescales of transport within accretion disks can be used to predict the timescale of transfer of high- $\Delta^{17}O$ H_2O produced by CO photochemistry in the outer disk to the inner disk. Inward radial transfer of high-$\Delta^{17}O$ water would have taken place either continuously during the infall phase of disk evolution or by virtue of a wave of high-$\Delta^{17}O$ H_2O that passed from disk surfaces through the outer disk and into the rocky planet-forming region on a timescale of 10^5 to 10^6 years post infall (Fig. 2).

Many observations are consistent with photodissociation of CO in the diffuse regions of the solar nebula as an explanation for the slope-1 line in oxygen three-isotope space. It accounts for the fact

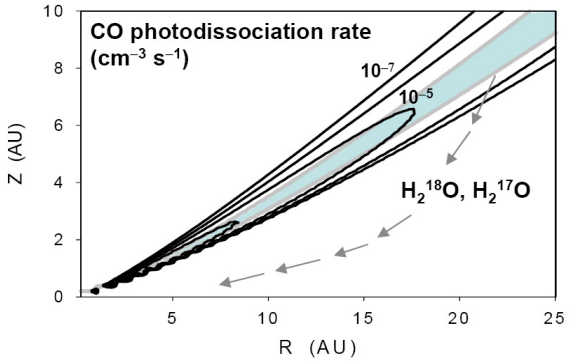

Fig. 1 Disk model showing contours of CO dissociation rate and the region between optical depth τ =1 and 4 for CO (grey) where self shielding by CO obtains. Arrows show transport of high-$\Delta^{17}O$ H_2O required by such a model.

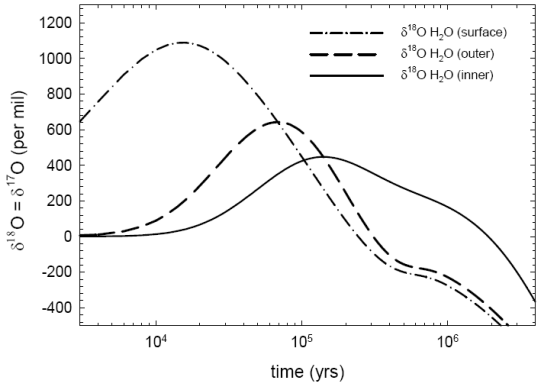

Fig. 2 Result of box model calculation for the oxygen isotopic evolution of H_2O in surficial, outer, and inner regions of the solar circumstellar disk. The result shows the timescale required to transport a high-$\Delta^{17}O$ signal as water into the region of terrestrial planet formation.

isotope space. It accounts for the fact that H_2O was almost certainly depleted in ^{16}O (enriched in ^{18}O and ^{17}O, i.e., enriched in H_2Q) relative to silicates and other metal oxides in the Solar System [1, 3, 4]. Production in the outer solar nebula also provides a natural explanation for the correlation between ^{16}O and the refractory nature of solids; many refractory minerals

such as those found in CAIs should have retained their original ^{16}O-rich compositions because they would have had limited opportunity for reaction with H_2Q during transit through the nebula despite numerous heating events. Less refractory materials like Fe-bearing olivine and glass that comprise chondrite matrix, materials that are generally ^{16}O poor, had greater opportunity for exchange.

Solid-state exchange of oxygen isotopes and H_2O gas: The assertion that exchange with H_2O is consistent with the oxygen isotope data for meteorites can be examined quantitatively with reference to self diffusion coefficients for oxygen in various pertinent mineral phases that comprised dust, chondrules, and CAIs in the early Solar System. The overall picture deduced from diffusivities of oxygen is one in which Fe-bearing dust and chondrules made from that dust acquired their oxygen isotope ratios by exchange with H_2O while important constituents of igneous CAIs could not exchange. If Δ^{17}O of exchangeable gas in the inner solar system rose with time (Fig. 2), Δ^{17}O in various minerals provides a record of processing in the disk.

Self diffusion coefficients for Fe-bearing olivine, representing the less refractory dust in the solar nebula, and spinel, pyroxene and melilite, representing the more refractory CAIs, are known [5, 6]. These diffusivities are compared by converting them into maximum radii of mineral grains that will experience complete oxygen isotope exchange for a given temperature and time. These maximum radii r_{max} are given by the expression

$$r_{\max} = \pi \left(\frac{-t\left(D_0 \exp(-E_a/(kT))\right)}{\ln(C/C_s)} \right)^{1/2}$$

where D_o is the preexponential for the diffusion coefficient, E_a is the activation energy for the diffusion coefficient, t is the duration for diffusion, and C/C_s is the ratio of concentration to the concentration imposed externally on the surface of the grain. Integrated heating times are thought to have been on the order of 10^2 to 10^3 years in the nebula [7-9]. For t = 500 years, C/C_s = 0.1, and T = 1600 K (a subsolidus temperature for both CAIs and olivine at nebular pressures) r_{max} values are 0.3 μm for olivine at appropriate fugacities of O_2, 22 μm for spinel, 3607 μm for melilite, and 130 μm for pyroxene. The r_{max} values can be compared with typical grain sizes of << 1 μm for olivine in matrix, ~ 30 to 50 μm for spinel in igneous CAIs, ≥1000 μm or larger for melilite in igneous CAIs, and ≥500 μm for pyroxene in igneous CAIs. The comparison suggests that fine-grained sub-micron sized dust comprising matrix and precursors to CAIs both could have equilibrated with H_2O given the opportunity. Matrix dust is ^{16}O poor, allowing for the interpretation that dust comprising matrix was indeed heated in the inner disk during passage of the ^{16}O-poor H_2O wave. CAIs, however, are generally ^{16}O rich and yet must have spent some time in the inner solar nebula where temperatures were high, suggesting that dust precursors to CAIs avoided being heated in the presence of ^{16}O-poor H_2O. This interpretation is consistent with early formation of CAIs prior to passage of the H_2O wave in the inner nebula (i.e., at $t \leq 10^5$ years). In the case of igneous CAIs crystallized from melts and subsequently heated, the r_{max} values predict that spinel and pyroxene in these CAIs should have retained their ^{16}O-rich compositions while melilite would not. Spinel will not have entered the melt during partial melting events because it is the liquidus phase (the last solid phase to remain on the liquidus with heating), further insulating it from exchange [10]. As a consequence, one would predict that spinels should have remained ^{16}O rich even after numerous partial melting events and indeed spinels in igneous CAIs are generally ^{16}O rich. Pyroxenes in CAIs will have melted near the CAI eutectic and preservation of ^{16}O-rich compositions in many, but not all, pyroxenes could imply some melting prior to (or after) the passage of the ^{16}O-poor wave of H_2O in the inner nebula.

These predictions are consistent with observations [6]; igneous CAI spinel and pyroxene tend to be ^{16}O rich while igneous CAI melilite and the matrix of the meteorites are generally ^{16}O poor. The ^{16}O-poor compositions of chondrules are also consistent with this scenario because dust similar to matrix was likely the precursor to chondrules. Melting of chondrules would have facilitated their exchange with H_2O gas due to the rapid self diffusion of O in silicate melt.

References: [1] Lyons J. R. and Young E. D. (2005) *Nature 435*, 317-320. [2] Young E. D. (2007) *Earth and Planetary Science Letters* (in press). [3] Sakamoto N. *et al.* (2007) *Science 317*, 231-233. [4] Yurimoto H. and Kuramoto K. (2004) *Science 305*, 1763-1766. [5] Ryerson F. J. *et al.* (1989) *Journal of Geophyhsical Research 94*, 4105-4118. [6] Ryerson F. J. and McKeegan K. D. (1994) *Geochimica et Cosmochimica Acta 58*, 3713-3734. [7] Shahar A. and Young E. D. (2007) *Earth and Planetary Science Letters 257*, 497-510. [8] Simon J. I. *et al.* (2005) *Earth and Planetary Science Letters 238*, 272-283. [9] Young E. D. *et al.* (2005) *Science 308*, 223-227. [10] Stolper E. M. and Paque J. M. (1986) *Geochimica et Cosmochimica Acta 50*, 1785-1806.

THE INITIAL ^{26}AL/^{27}AL OF THE SOLAR SYSTEM AND IMPLICATIONS FOR THE DURATION OF THE ACTIVE SOLAR PROTOPLANETARY DISK. E. D. Young[1] and A. Shahar[1], [1]Department of Earth and Space Sciences and Institute of Geophysics and Planetary Physics, University of California Los Angeles, 595 Charles Young Drive East, 2676 Geology Building, Los Angeles, CA, 90095 (Email: eyoung@ess.ucla.edu).

Introduction: Key questions surrounding the development of a robust chronology for the early Solar System are whether or not there was a uniform initial $^{26}Al/^{27}Al$ for the Solar System as a whole ($(^{26}Al/^{27}Al)_o$) and if so, what was this uniform value? Soon after discovery of the decay product of ^{26}Al, excess ^{26}Mg, in calcium aluminum-rich inclusions (CAIs) [1] it seemed clear that CAIs recorded a Solar System-wide $(^{26}Al/^{27}Al)_o$ of $5x10^{-5}$ (the canonical $(^{26}Al/^{27}Al)_o$) [2]. Since that time, however, new measurements using new technologies have complicated this simple interpretation.

It was suggested recently that $(^{26}Al/^{27}Al)_o$ was considerably higher than the canonical value, with new estimates varying from $6x10^{-5}$ to $7x10^{-5}$ [3, 4]. These "supracanonical" values for $(^{26}Al/^{27}Al)_o$ represent either final closure of CAIs to Mg isotope redistribution over a rapid timescale of ~50,000 yrs [5, 6] or an original $(^{26}Al/^{27}Al)_o$ value that was followed by ~300,000 yrs of subsequent thermal resetting of the ^{26}Al clock in the protoplanetary disk [3] . If the latter interpretation is correct, it is possible that the canonical $(^{26}Al/^{27}Al)_o$ represents the cessation of the most turmoltuous period of disk evoluition during which CAIs were heated relentlessly in numerous short-lived events (e.g., shock waves); the significance of the canonical $(^{26}Al/^{27}Al)_o$ for CAIs lies at the heart of any Solar System chronology.

The existence of supracanonical $(^{26}Al/^{27}Al)_o$ values has been questioned recently on the basis of more high-precision measurements showing the prevalance of canonical $(^{26}Al/^{27}Al)_o$ values among "whole rock" CAIs [7].

Consideration of all published data thus far suggests a disparity between results obtained by in-situ techniques (laser ablation MC-ICPMS and SIMS) [3, 8] and those obtained by acid digestion of fragments of CAIs [3, 6, 7]. Here we suggest that the apparent inconsistencies are the result of the evaporation history of CAIs. The implication is that the Solar System $(^{26}Al/^{27}Al)_o$ was at least $6.5x10^{-5}$ and that CAIs suffered ~300,000 to 400,000 yrs of thermal processing in an active protoplanetar disk. The inference is that the canonical $(^{26}Al/^{27}Al)_o$ indeed marked the cessation of the most turbulent phase of disk evolution.

Evaporation of CAIs: The high $^{25}Mg/^{24}Mg$ and $^{29}Si/^{28}Si$ of igneous CAIs is prima facie evidence that these objects evaporated as molten objects in space.

The pressure regime in which the CAIs evaporated bears on the tractability of their durations of melting. If CAIs melted with partial pressures of evaporating species (P', e.g., Mg, SiO) approaching equilibrium (P_{sat}), then their durations of melting are uncertain. Conversely, if molten CAIs evaporated into an environment with $P' << P_{sat}$, timescales of evaporation are well constrained and can be ascertained uniquely using stable isotope fractionation. A calculation of partial pressures as a function of number density of CAIs shows that the regime between no evaporation ($P' = P_{sat}$) and free evaporation ($P' << P_{sat}$) is separated by a narrow range of number densities (Fig. 1).

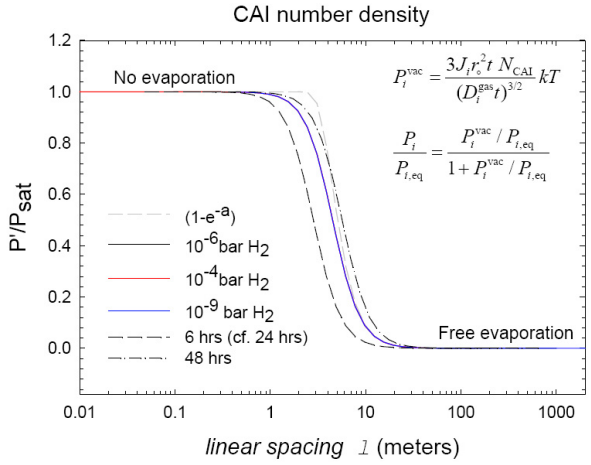

Fig. 1 Plot of ratio of partial pressure of Mg (P′) to equilibrium vapor pressure of Mg (Psat) as a function of number density of molten CAIs. Curves represent different total pressures and durations of melting. Equations used to derive curve are shown at upper right (J_i=flux of i, r = radius, N = number of molten CAIs, D_{gas}=diffusivity of i in gas, i =Mg).

As a result, it is safe to assume that CAIs most likely evaporated into vacuum. The degree of fractionation of both Mg and Si can therefore be used to obtain unique estimates of the durations of melting of CAIs. Results show that CAIs were molten for cumulative timescale of days to several weeks [9]. The duration of melting was almost certainly the cumulative effect of several tens of melting events since single episodes of melting lasted no more than a day [10].

Measurements of Mg and Al concentrations in whole-rock samples of unmelted CAIs (fluffy type A CAIs) and modeling of Mg and Si isotopic effects of evaporation show that a robust feature of igneous CAI history was an increase in $^{27}Al/^{24}Mg$ ratios from about 1.6 prior to evaporation to greater values following evaporation. CAIs were therefore open systems with evolving Al/Mg, complicating their $^{26}Al \rightarrow {}^{26}Mg^*$ decay history.

Open-system decay of ^{26}Al: Application of the decay equation to CAIs with thermal histories involving ~30 melting events over a period of 300,000 to 400,000 yrs results in $^{26}Mg^*$-Al/Mg systematics resembling the data for CAIs if these objects had an initial $^{26}Al/^{27}Al$ of $6.5x10^{-5}$ to $6.8x10^{-5}$. The open-system evolution of the igneous CAIs results in whole rocks (Fig. 2) that define an "errorchron" (whole-rock isochron) with an apparent $(^{26}Al/^{27}Al)_o$ of $5.7x10^{-5}$ to $5.9x10^{-5}$, similar to some whole-rock CAI data [3, 6]. Mineral isochrons for these same CAIs record apparent canonical initial $(^{26}Al/^{27}Al)_o$ values near 4.5 to $5.0x10^{-5}$ (Fig. 2). Minerals in CAIs that escaped resetting would record model $(^{26}Al/^{27}Al)_o$ values of 6.5 to $6.8x10^{-5}$ (the true initial). To the extent that many reported "whole rock" CAI data are actually fragments of CAIs, and so essentially points on a mineral isochron for the object, one expects a prevalence of canonical $(^{26}Al/^{27}Al)_o$ values like that observed.

A key consequence of open system evolution of CAIs is that true whole-rock isochrons record a minimum $(^{26}Al/^{27}Al)_o$, and that the true $(^{26}Al/^{27}Al)_o$ value must have been greater than that recorded by the whole rocks (Fig. 2).

Conclusion: Both *in-situ* and "whole-rock" CAI data are explained if it is recognized that CAIs evolved as open systems due to evaporation at low partial pressures of Mg, SiO and other rock-forming gas species. In this case, evaporation over hundreds of thousands of years attended decay of ^{26}Al to $^{26}Mg^*$. The true Solar System initial $^{26}Al/^{27}Al$ will have been recorded by minerals that escaped resetting while many isochrons composed of minerals and CAI fragments will record a canonical $(^{26}Al/^{27}Al)_o$. It is suggested that this canonical value marks the cessation of thermal resetting and waning of the most active phase of protoplanetary disk evolution.

References: [1] Lee T. *et al.* (1974) *Geophysical Research Letters 1*, 225-228. [2] MacPherson G. J. *et al.* (1995) *Meteoritics 30*, 365-386. [3] Young E. D. *et al.* (2005) *Science 308*, 223-227. [4] Galy A. *et al.* (2000) *Science 290*, 1751-1753. [5] Bizzarro M. *et al.* (2004) *Nature 431*, 275-278. [6] Bizzarro M. *et al.* (2005) *Nature 435*, 1280. [7] Jacobsen B. *et al.* (2007) *Lunar and Planetary Science Conference XXXVIII*, . [8] Taylor D. J. *et al.* (2005) *Meteoritical Society 2005, Meteoritics & Planetary Science, 40*, 40, 5282. [9] Shahar A. and Young E. D. (2007) *Earth and Planetary Science Letters 257*, 497-510. [10] Desch S. J. and Connolly H. C. (2002) *Meteoritics 37*, 183-202.

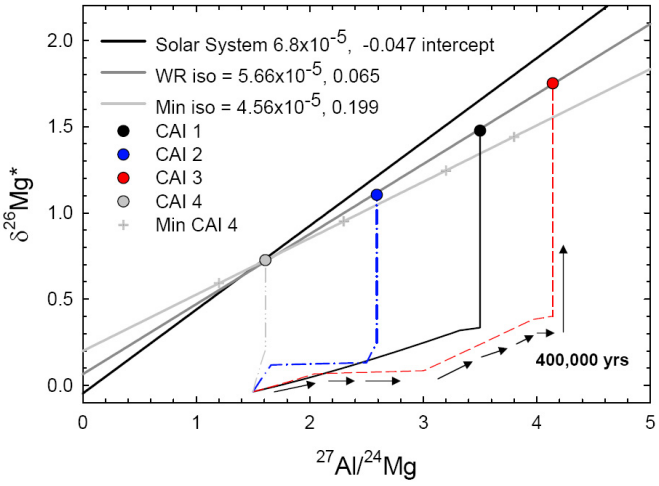

Fig. 2 ^{26}Al-$^{26}Mg^*$ evolution diagram showing results of simultaneous ^{26}Al decay and evaporation for four fictive igneous CAIs. The evaporation history of each CAI is shown by the lines leading up to the final datum (circles) for each CAI. Isochrons representing the model initial $^{26}Al/^{27}Al$, the apparent initial $^{26}Al/^{27}Al$ recorded by the whole rocks, and a mineral isochron for CAI 4 are shown for comparison. The whole-rock isochron and mineral isochron resemble analyses of CAIs obtained by MC-ICPMS and acid digestion. Minerals that escaped resetting by melting (e.g., some spinels, Al-rich melilite) will record the true initial $^{26}Al/^{27}Al$ and would lie on the uppermost isochron in the diagram. These points would be consistent with some in-situ analyses of igneous CAIs.

NOTES